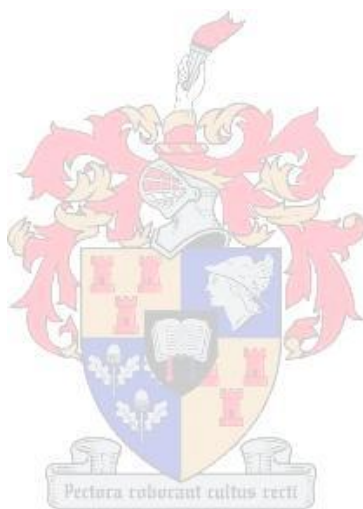


Cation- π induced association and nano-structured aggregate formation of water-soluble $[\text{Pt}^{\text{II}}(\text{diimine})(\text{L}^{\text{n}}-\text{S},\text{O})]^+$ complexes examined with high-resolution ^1H and DOSY NMR: Towards understanding their potential antimalarial activity

By

Izak Aldert Kotzé



*Dissertation presented for the degree of Doctor of Chemistry in the
Faculty of Science at
Stellenbosch University*

Promoter: Prof. Klaus R. Koch

December 2013

Declaration

By submitting this thesis electronically, I declare that the entirety of the work contained therein is my own, original work, that I am the owner of the copyright thereof (unless to the extent explicitly otherwise stated) and that I have not previously in its entirety or in part submitted it for obtaining any qualification.

Signed:

Izak Aldert Kotzé

August 2013

Acknowledgements

I would sincerely like to thank:

My supervisor, Prof. Klaus Koch, for his motivation, enthusiasm and guidance throughout my studies.

Dr. Wilhelmus Gerber for his time, effort and knowledgeable insight.

Elsa Malherbe and Dr. Jaco Brand from the NMR lab for their friendship and technical assistance.

Dr. Vincent Smith for the SCXRD analysis.

Mr. Mohammed Jaffer from UCT for the TEM analysis.

Prof. Tim Egan for making his lab available for the β -haematin inhibition studies.

The technical staff at the Analytical Chemistry section, Shafiek Mohammed, Deidre Davids and Roger Lawrence.

All the present and past PGM group members for their friendship and creating a memorable working environment.

My wife Lize, friends and family for their love and support throughout the course of this work.

The University of Stellenbosch, Anglo Platinum and the National Research Foundation for financial support.

Publications

Izak A. Kotzé, Wilhelmus J. Gerber, Yu-Shan Wu and Klaus R. Koch, *Dalton Transactions*, **2013**,42, 3791-3801. (*Dalton Trans. cover feature*)

Izak A. Kotzé, Wilhelmus J. Gerber, Jean M. Mckenzie, and Klaus R. Koch, *European Journal of Inorganic Chemistry*, **2009**, 12, 1626–1633.

Conference Proceedings

2011	Euromar Conference (Frankfurt, Germany) European Magnetic Resonance Meeting	Poster Presented
	SACI 11 (South African Chemical Institute) Johannesburg	Poster Presented
2009	South African PhD Project Conference Johannesburg	Invited Delegate
	RSC SACI-Inorganic Conference Bloemfontein	Poster Presented
2008	Cape Organometallic Symposium Cape Town	Delegate
	SACI 08 (South African Chemical Institute) Stellenbosch	Poster Presented

Abstract

A series of mixed ligand $[\text{Pt}^{\text{II}}(\text{diimine})(\text{L}^n\text{-S},\text{O})]\text{Cl}$ complexes (where diimine is 1,10-phenanthroline (phen) or 2,2'-bipyridyl (bipy) and $\text{L}^n\text{-S},\text{O}$ represents various chelating N,N -di(alkyl)- N' -acylthioureas) have been synthesized and characterized. The ^1H NMR spectrum of $[\text{Pt}^{\text{II}}(\text{phen})(\text{L}^1\text{-S},\text{O})]\text{Cl}$ was unambiguously assigned using 1D NOESY experiments which confirms previous assignments of this complex. The effect of changing the metal centre from Pt^{II} to Pd^{II} in the $[\text{M}^{\text{II}}(\text{phen})(\text{L}^1\text{-S},\text{O})]\text{Cl}$ complex on its antimalarial activity has been investigated.

The first crystal structure of $\text{Pt}^{\text{II}}(\text{bipy})\text{Cl}_2$ which co-crystallized with a solvent molecule (acetonitrile) has been obtained. The crystal packing of the yellow $\text{Pt}^{\text{II}}(\text{bipy})\text{Cl}_2 \cdot \text{CH}_3\text{CN}$ crystals show close contact between the Pt centers of adjacent molecules. This interaction is similar to the $\text{Pt}^{\text{II}} \cdots \text{Pt}^{\text{II}}$ interaction observed for the red polymorph of $\text{Pt}^{\text{II}}(\text{bipy})\text{Cl}_2$, which displays significant d_{z^2} -orbital overlap and the reason for the bathochromic or red-shift observed for this polymorph.

The synthesis of $[\text{Pt}^{\text{II}}(\text{phen})(\text{L}^2\text{-S},\text{O})]\text{Cl}$ yielded significant quantities of novel *bis*-monodentate coordinated- L^2 complex, $\text{Pt}^{\text{II}}(\text{phen})(\text{L}^2\text{-S})_2$ which could be synthesised in high yields after optimisation. The crystal structure of $\text{Pt}^{\text{II}}(\text{phen})(\text{L}^2\text{-S})_2$ shows *intra*-molecular aromatic π -stacking interactions between the naphthoyl moiety of the coordinated L^2 and the coordinated phen ligand. This π -stacking interaction was found to be present in methanol- d_4 solutions using 1D NOESY experiments, which could account for the presence of $\text{Pt}^{\text{II}}(\text{phen})(\text{L}^2\text{-S})_2$ in the synthesis of $[\text{Pt}^{\text{II}}(\text{phen})(\text{L}^2\text{-S},\text{O})]\text{Cl}$. This monodentate- S coordination was also observed for other N,N -di(alkyl)- N' -acylthioureas which form monodentate $\text{Pt}^{\text{II}}(\text{phen})(\text{L}^n\text{-S})_2$ complexes in high yields, especially those with aroylthiourea ligands. The crystal structure of $\text{Pt}^{\text{II}}(\text{phen})(\text{L}^4\text{-S})_2$ revealed *inter*-molecular π -stacking between the 1,10-phenanthroline ligands of two adjacent complexes, similar to the interaction postulated for the self-association $\text{Pt}^{\text{II}}(\text{phen})(\text{L}^2\text{-S})_2$ in chloroform. The versatility of N,N -di(alkyl)- N' -acylthiourea ligands to coordinate in a monodentate fashion *via* the sulphur donor atom or as a chelate *via* the oxygen- and sulphur donor atoms have been shown by the relatively high yields obtained for the synthesis of both cationic $[\text{Pt}^{\text{II}}(\text{phen})(\text{L}^n\text{-S},\text{O})]\text{Cl}$ and neutral $\text{Pt}^{\text{II}}(\text{phen})(\text{L}^n\text{-S})_2$ complexes.

The outer-sphere self-association of $[\text{Pt}^{\text{II}}(\text{phen})(\text{L}^1\text{-S},\text{O})]^+$ in 0 - 100 % (v/v) $\text{D}_2\text{O}:\text{CD}_3\text{CN}$ solutions has been investigated by means of significant concentration dependence of ^1H NMR chemical shifts as well as Diffusion Ordered Spectroscopy (DOSY NMR). $[\text{Pt}^{\text{II}}(\text{phen})(\text{L}^1\text{-S},\text{O})]^+$ forms regiospecific non-covalent dimers, $2\text{M}^+ \rightleftharpoons \{\text{M}^+\}_2$, in 0 to 30 % (v/v) $\text{D}_2\text{O}:\text{CD}_3\text{CN}$ solutions. The extent of dimerisation increases significantly as the D_2O content is increased, with the dimerisation constant (K_{D}) increasing from $17 \pm 2 \text{ M}^{-1}$ in CD_3CN to $71 \pm 8 \text{ M}^{-1}$ in 30% (v/v) $\text{D}_2\text{O}:\text{CD}_3\text{CN}$ at 299.3K, presumably *via* non-covalent cation- π interactions ($\Delta_r G_{\text{CD}_3\text{CN}}^0 = -7.0 \text{ kJ}\cdot\text{mol}^{-1}$; $\Delta_r G_{30\% \text{D}_2\text{O}:\text{CD}_3\text{CN}}^0 = -10.4 \text{ kJ}\cdot\text{mol}^{-1}$). Experimental data are consistent with an 'offset' face-to-face cation- π stacking arrangement of the planar cationic complexes. However, in water-rich solvent mixtures from >30%

(v/v) D₂O:CD₃CN to pure D₂O, the extent of aggregation significantly increases until a critical aggregation concentration (CAC) is reached, estimated to be 9.6 and 10.3 mM from ¹H NMR chemical shift concentration dependence and DOSY NMR measurements respectively. Above the CAC the formation of spaghetti-like nano-structures formulated as $\{[\text{Pt}^{\text{II}}(\text{phen})(\text{L}^1\text{-S},\text{O})]^+\}_n\text{Cl}_y^-$ ($n, y > 2$) is indicated. DOSY studies show a significant decrease of the average diffusion coefficient D_{obs} as a function of increasing concentration of $[\text{Pt}^{\text{II}}(\text{phen})(\text{L}^1\text{-S},\text{O})]\text{Cl}$ in D₂O. The *aggregation number* (N) estimated from hydrodynamic volumes of the mononuclear $[\text{Pt}^{\text{II}}(\text{phen})(\text{L}^1\text{-S},\text{O})]^+$ cation (V_{H}^0), and those V_{H} estimated from D_{obs} ($N = V_{\text{H}}/V_{\text{H}}^0$) as a function of total complex concentration, ranges from ~2 to ~735 in pure D₂O. Above the CAC the well defined nano-structures, which may be loosely termed “metallogels”, could be characterized by means of Transmission Electron Microscopy. As expected, the addition of NaCl appears to increase the extent of aggregation formation, presumably by stabilizing the formation of a nano-sized $\{[\text{Pt}^{\text{II}}(\text{phen})(\text{L}^1\text{-S},\text{O})]^+\}_n\text{Cl}_y^-$ aggregates thus preventing excessive positive electrostatic charge build-up.

The $[\text{Pt}^{\text{II}}(\text{phen})(\text{L}^1\text{-S},\text{O})]^+$ cation forms relatively strong non-covalent 1:1 outer-sphere complexes with pyrene (C₁₆H₁₀), with association constants (37.9 M⁻¹) similar to that observed for the fluoranthene (39.7 M⁻¹) at 298.15 K. Pyrene was found to form a tighter 1:1 aggregate with $[\text{Pt}^{\text{II}}(\text{phen})(\text{L}^1\text{-S},\text{O})]^+$ with the corresponding $\Delta_{\text{r}}H_{(\text{M/P})} = -18.1 \pm 3 \text{ kJ}\cdot\text{mol}^{-1}$ compared to fluoranthene ($\Delta_{\text{r}}H_{(\text{M/F})} = -13.3 \pm 3 \text{ kJ}\cdot\text{mol}^{-1}$), which is postulated to be due to the larger aromatic π -surface of pyrene potentially forming a stronger cation- π interaction with the $[\text{Pt}^{\text{II}}(\text{phen})(\text{L}^1\text{-S},\text{O})]^+$ cation.

A β -haematin (synthetic crystalline ferriprotoporphyrin, Fe(III)PPIX) inhibition assay has been performed on the series of $[\text{Pt}^{\text{II}}(\text{diimine})(\text{L}^n\text{-S},\text{O})]^+$ complexes, $[\text{Pd}^{\text{II}}(\text{phen})(\text{L}^1\text{-S},\text{O})]^+$ and $[\text{Pt}^{\text{II}}\text{Cl}(\text{dmsO})(\text{en})]^+$ to establish their potential for antimalarial activity. The series of $[\text{Pt}^{\text{II}}(\text{diimine})(\text{L}^n\text{-S},\text{O})]^+$ complexes was found to significantly inhibit β -haematin formation, while the respective ligands were inactive. $[\text{Pt}^{\text{II}}(\text{phen})(\text{L}^n\text{-S},\text{O})]^+$ complexes were found to be significantly better β -haematin inhibitors compared to the $[\text{Pt}^{\text{II}}(\text{bipy})(\text{L}^n\text{-S},\text{O})]^+$ and $[\text{Pd}^{\text{II}}(\text{phen})(\text{L}^1\text{-S},\text{O})]^+$ variations. $[\text{Pt}^{\text{II}}_2(\text{phen})_2(\text{L}^9\text{-S},\text{O})]^{2+}$, where $\text{L}^9 = \text{bis-}(N,N\text{-diethyl})\text{-}N'\text{-adipoylthiourea}$ consisting of two S,O -coordination sites, was found to be the most efficient β -haematin inhibitor tested with a corresponding $\text{IC}_{50} = 8 \pm 1 \mu\text{M}$; roughly half the IC_{50} of the mono-functional complexes $[\text{Pt}^{\text{II}}(\text{phen})(\text{L}^n\text{-S},\text{O})]^+$ and more efficient than the known antimalarials chloroquine ($34 \pm 2 \mu\text{M}$) and amodiaquine ($13 \pm 1 \mu\text{M}$). The interactions between $[\text{Pt}^{\text{II}}(\text{diimine})(\text{L}^n\text{-S},\text{O})]^+$ complexes and the solution species of haematin are postulated to be mainly cation- π interactions while other possible contributing non-covalent interactions include ion-pairing, π -stacking, cation- π interactions and potential coordination of the acyl group of L^n and the Fe(III) metal centre.

Samevatting

’n Reeks gemengde-ligand $[\text{Pt}^{\text{II}}(\text{di-imien})(\text{L}^n\text{-S},\text{O})]\text{Cl}$ komplekse (waar di-imien 1,10-fenantrilien (phen) of 2,2'-bipiridiel (bipy) is en $\text{L}^n\text{-S},\text{O}$ verskeie chelerende N,N -di(alkiel)- N' -asielthiureas verteenwoordig) was gesintetiseer en gekarakteriseer. Die ^1H KMR spektrum van $[\text{Pt}^{\text{II}}(\text{phen})(\text{L}^1\text{-S},\text{O})]\text{Cl}$ was eenduidig toegedeel deur gebruik te maak van 1D NOESY eksperimente en het vorige toedelings van hierdie kompleks bevestig. Die effek wat die verandering van die sentrale metaal in die $[\text{M}^{\text{II}}(\text{phen})(\text{L}^1\text{-S},\text{O})]\text{Cl}$ kompleks, van Pt^{II} na Pd^{II} , op die anti-malaria aktiwiteit daarvan het, word in hierdie studie ondersoek.

Die eerste kristalstruktuur van $\text{Pt}^{\text{II}}(\text{bipy})\text{Cl}_2$, wat mede-kristalle met die oplosmiddel molekule (asetonitriël) gevorm het, is verkry. Die kristalpakking van die geel $\text{Pt}^{\text{II}}(\text{bipy})\text{Cl}_2 \cdot \text{CH}_3\text{CN}$ kristalle toon dat daar noue kontak tussen die sentrale Pt-atome van aangrensende molekules is. Hierdie interaksie is soortgelyk aan die Pt...Pt interaksie wat vir die rooi polimorf van $\text{Pt}^{\text{II}}(\text{bipy})\text{Cl}_2$ waargeneem is. Die rooi polimorf toon beduidende dz^2 -orbitaal oorvleueling wat die batochromiese of rooi-verskuiwing wat waargeneem is, teweeg gebring het.

Tydens die sintese van die $[\text{Pt}^{\text{II}}(\text{phen})(\text{L}^2\text{-S},\text{O})]\text{Cl}$ kompleks is beduidende hoeveelhede van die nuutontdekte *bis*-monodentaat gekoördineerde- L^2 kompleks, $\text{Pt}^{\text{II}}(\text{phen})(\text{L}^2\text{-S})_2$, gevorm en na verdere optimalisering kon laasgenoemde kompleks in hoë opbrengste gesintetiseer geword het. Die kristalstruktuur van $\text{Pt}^{\text{II}}(\text{phen})(\text{L}^2\text{-S})_2$ toon *intra*-molekulêre aromatiese π -stapel interaksies tussen die naftoiël groep van die gekoördineerde L^2 en die gekoördineerde phen ligand. 1D NOESY KMR eksperimente het gewys dat hierdie π -stapel interaksie in die metanol- d_4 oplossings plaasvind, wat dus die vorming van $\text{Pt}^{\text{II}}(\text{phen})(\text{L}^2\text{-S})_2$ tydens die sintese van $[\text{Pt}^{\text{II}}(\text{phen})(\text{L}^2\text{-S},\text{O})]\text{Cl}$ kan verduidelik. Soortgelyk was hierdie monodentaat- S koördinasie ook vir ander N,N -di(alkiel)- N' -asielthiureas wat monodentaat- $\text{Pt}^{\text{II}}(\text{phen})(\text{L}^n\text{-S})_2$ komplekse in hoë opbrengste lewer, veral die met aroiëlthiurea ligande, waargeneem. Die kristalstruktuur van $\text{Pt}^{\text{II}}(\text{phen})(\text{L}^4\text{-S})_2$ het verder getoon dat daar *inter*-molekulêre π -stapel interaksies tussen die 1,10-fenantrilien ligande van die twee aangrensende komplekse is, soortgelyk aan die interaksie wat vir die self-assosiasie van $\text{Pt}^{\text{II}}(\text{phen})(\text{L}^2\text{-S})_2$ in chloroform gepostuleer is. Die veelsydigheid van N,N -di(alkiel)- N' -asielthiurea ligande om of in ’n monodentate wyse *via* die swael donoraatom of as ’n chelaat *via* beide die suurstof en swael donoraatome te kan koördineer, is getoon deur die relatiewe hoë opbrengste wat behaal is tydens die sintese van beide die kationiese $[\text{Pt}^{\text{II}}(\text{phen})(\text{L}^n\text{-S},\text{O})]\text{Cl}$ en neutrale $\text{Pt}^{\text{II}}(\text{phen})(\text{L}^n\text{-S})_2$ komplekse.

Die buite-sfeer self-assosiasie van $[\text{Pt}^{\text{II}}(\text{phen})(\text{L}^1\text{-S},\text{O})]^+$ in 0 - 100 % (v/v) $\text{D}_2\text{O}:\text{CD}_3\text{CN}$ oplossings is ondersoek deur die beduidende konsentrasie-afhanklikheid van die ^1H KMR chemiese verskuiwings te bestudeer, sowel as om van Diffusie Geordende Spektroskopie (DOSY KMR) gebruik te maak. $[\text{Pt}^{\text{II}}(\text{phen})(\text{L}^1\text{-S},\text{O})]^+$ vorm regio-spesifieke nie-kovalente dimere, $2\text{M}^+ \rightleftharpoons \{\text{M}^+\}_2$, in 0 to 30 % (v/v) $\text{D}_2\text{O}:\text{CD}_3\text{CN}$ oplossings. Die graad van dimerisasie neem aansienlik toe soos die persentasie D_2O verhoog, met die dimerisasiekonstante (K_D) wat van $17 \pm 2 \text{ M}^{-1}$ in CD_3CN tot $71 \pm 8 \text{ M}^{-1}$ in 30% (v/v) $\text{D}_2\text{O}:\text{CD}_3\text{CN}$ by 299.3K toeneem, vermoedelik *via* nie-kovalente katioon- π interaksies ($\Delta_r G_{\text{CD}_3\text{CN}}^0 = -7.0 \text{ kJ}\cdot\text{mol}^{-1}$; $\Delta_r G_{30\%\text{D}_2\text{O}:\text{CD}_3\text{CN}}^0 = -10.4 \text{ kJ}\cdot\text{mol}^{-1}$). Die eksperimentele data wat verkry is stem ooreen met ’n “offset”

aangesig-tot-aangesig kation- π stapel rangskikking van die planêre kationiese komplekse. Terwyl in wateryke mengsels van oplosmiddels waar die D_2O konsentrasie toeneem vanaf >30% (v/v) $D_2O:CD_3CN$ tot suiwer D_2O , neem die graad van samebondeling (“aggregation”) aansienlik toe totdat ’n kritiese samebondeling konsentrasie (CAC) bereik word, wat deur middel van 1H NMR chemiese verskuiwing konsentrasie-afhanklikheid en DOSY KMR metings as 9.6 en 10.3 mM onderskeidelik, bepaal is. Bo die CAC is spaghetti-agtige nanostrukture waargeneem wat as $\{[Pt^{II}(\text{phen})(L^1-S,O)]^+\}_n Cl^-_y$ ($n, y > 2$) geformuleer is. DOSY KMR studies het gewys dat daar ’n beduidende afname in die gemiddelde diffusie koëffisiënt, D_{obs} , is soos wat die konsentrasie van $[Pt^{II}(\text{phen})(L^1-S,O)]Cl$ in D_2O toeneem. Die *samebondeling nommer* (N), wat vanaf die hidrodinamiese volumes van die mononukleêre $[Pt^{II}(\text{phen})(L^1-S,O)]^+$ kation (V_H^0) en die V_H afgelei van die D_{obs} , bereken kan word ($N = V_H/V_H^0$), wissel van ~ 2 to ~ 735 in suiwer D_2O as ’n funksie van die totale konsentrasie van die kompleks. Bo die CAC is goed-gedefinieerde nanostrukture, wat losweg “metallogele” genoem kan word, met Transmissie Elektronmikroskopie gekarakteriseer. Soos verwag, het die toevoeging van NaCl die graad van samebondeling verhoog, vermoedelik deur die stabilisering van die vorming van ’n nano-grootte $\{[Pt^{II}(\text{phen})(L^1-S,O)]^+\}_n Cl^-_y$ bundel, wat die opbou van oortollige positiewe elektrostatische lading voorkom.

Die $[Pt^{II}(\text{phen})(L^1-S,O)]^+$ kation vorm relatief sterk nie-kovalente 1:1 buite-sfeer komplekse met piren ($C_{16}H_{10}$), en het ’n assosiasie konstante van $37.9 M^{-1}$ wat soortgelyk is aan die wat vir fluorantheen ($39.7 M^{-1}$) by 298.15 K bepaal is. Verder is gevind dat piren ’n nouer 1:1 aggregraat met $Pt^{II}(\text{phen})(L^1-S,O)^+$ vorm ($\Delta_r H_{(M/P)} = -18.1 \pm 3 \text{ kJ.mol}^{-1}$) as fluorantheen ($\Delta_r H_{(M/F)} = -13.3 \pm 3 \text{ kJ.mol}^{-1}$). Daar word gepostuleer dat die rede hiervoor is dat die groter aromatische π -oppervlak van pyreen waarskynlikheid ’n sterker kationiese π -interaksie met die $Pt^{II}(\text{phen})(L^1-S,O)^+$ kation vorm.

’n β -haematin (sintetiese kristallyn ferriprotoporpien, Fe(III)PPIX) inhibisie toets is op die reeks $[Pt^{II}(\text{diimine})(L^n-S,O)]^+$ komplekse, sowel as op $[Pd^{II}(\text{phen})(L^1-S,O)]^+$ en $[Pt^{II}Cl(\text{dmsO})(\text{en})]^+$ uitgevoer om hul potensiaal vir anti-malaria aktiwiteit vas te stel. Daar is gevind dat die $[Pt^{II}(\text{di-imien})(L^n-S,O)]^+$ komplekse β -haematin formasie beduidend belemmer het, terwyl die onderskeie ligande onaktief was. $[Pt^{II}(\text{phen})(L^n-S,O)]^+$ komplekse is gevind om aansienlik beter β -haematin inhibitors as die $[Pt^{II}(\text{bipy})(L^n-S,O)]^+$ en $[Pd^{II}(\text{phen})(L^1-S,O)]^+$ variasies te wees. $[Pt^{II}_2(\text{phen})_2(L^9-S,O)]^{2+}$, waar $L^9 = \text{bis}(N,N\text{-dietetiel})\text{-}N'$ -adipoylthiourea bestaande uit twee S,O -koördinasie posisies, is bevind as die mees doeltreffende β -haematin inhibitor met toetse wat bewys het dat $IC_{50} = 8 \pm 1 \mu M$ verkry is; sowat die helfte van die IC_{50} van die mono-funksionele $[Pt^{II}(\text{phen})(L^n-S,O)]^+$ komplekse en meer doeltreffend as die welbekende anti-malaria middels chloroquine ($34 \pm 2 \mu M$) en amodiaquine ($13 \pm 1 \mu M$). Die interaksie tussen $[Pt^{II}(\text{diimine})(L^n-S,O)]^+$ komplekse en die spesies van haematin wat in oplossing is, word gepostuleer om hoofsaaklik kation- π interaksies te wees, terwyl ander nie-kovalente interaksies soos ion-paring, π -stapel, kation- π interaksies en potensiële koördinering van die asiel groep van L^n en die sentrale Fe(III) metaal ook moontlike bydraes kan lewer.

Table of Content

Declaration	ii
Acknowledgements	iii
Publications	iv
Abstract	v
Samevatting	vii
Table of Contents	ix

Chapter 1 – General Introduction and Background

1.1	Biological activity of square planar platinum complexes	1
1.2	Antimalarial drug discovery	2
1.2.1	The life cycle of <i>Plasmodium falciparum</i>	4
1.2.2	Malaria treatment and Drug design	5
1.3	Non-covalent drug interactions	8
1.3.1	Hydrogen bonding	9
1.3.2	Ion-pairing	10
1.3.3	Cation- π interactions	11
1.3.4	Aromatic π -stacking interactions	13
1.3.5	Hydrophobic interactions	15
1.4	Objectives of this study	17
1.5	References	19

Chapter 2 – Ligand and Complex Synthesis, Characterization and Experimental

2.1	Introduction	24
2.2	Synthesis of mixed ligand $[\text{Pt}^{\text{II}}(\text{diimine})(N,N\text{-di(alkyl)-}N'\text{-acylthiourea)}]\text{Cl}$ complexes and precursor	26
2.2.1	Nomenclature for the ligands and complexes used in this study	26
2.2.2	Synthesis of the $N,N\text{-di(alkyl)-}N'\text{-acylthiourea}$ ligands	26
2.2.3	Synthesis of $\text{Pt}^{\text{II}}\text{Cl}_2(1,10\text{-phenanthroline})$	30
2.2.4	Synthesis of $[\text{Pt}^{\text{II}}(1,10\text{-phenanthroline})(N,N\text{-di(alkyl)-}N'\text{-acylthiourea)}]\text{Cl}$ complexes	31
2.3	Detailed characterization of $[\text{Pt}^{\text{II}}(\text{phen})(L^1\text{-}S,O)]\text{Cl}$ by ^1H , COSY, HMBC and NOESY NMR	36
2.4	Synthesis of mixed ligand $[\text{Pt}^{\text{II}}(2,2'\text{-bipyridyl})(N,N\text{-di(alkyl)-}N'\text{-acylthiourea)}]\text{Cl}$ complexes and their precursors	42
2.4.1	Synthesis of $\text{Pt}^{\text{II}}(2,2'\text{-bipyridyl})\text{Cl}_2$	42
2.4.2	Synthesis of mixed ligand $[\text{Pt}^{\text{II}}(2,2'\text{-bipyridyl})(N,N\text{-di(alkyl)-}N'\text{-acylthiourea)}]\text{Cl}$ complexes	48
2.5	Synthesis of the mixed ligand $[\text{Pd}^{\text{II}}(\text{phen})(L^1\text{-}S,O)]\text{Cl}$ complex and its precursors	51
2.5.1	Synthesis of $\text{Pd}^{\text{II}}\text{Cl}_2(1,10\text{-phenanthroline})$	51

2.5.2	Synthesis of Pd ^{II} ₃ (OAc) ₆	52
2.5.3	Synthesis of Pd ^{II} (1,10-phenanthroline)(CH ₃ CO ₂) ₂	54
2.5.4	Synthesis of the mixed ligand [Pd ^{II} (1,10-phenanthroline)(<i>N,N</i> -pyrrolidyl- <i>N'</i> -pivaloylthiourea)]Cl complex	55
2.6	Synthesis of [Pt ^{II} Cl(DMSO)(en)]Cl	56
2.6.1	Synthesis of <i>cis</i> -[Pt ^{II} Cl ₂ (DMSO) ₂]	56
2.6.2	Synthesis of [Pt ^{II} Cl(DMSO)(en)]Cl	57
2.7	Interesting features of the ¹ H NMR spectra of platinum(II) diimine complexes	58
2.7.1	¹⁹⁵ Pt coupling in the ¹ H NMR of square planar Pt ^{II} (diimine) complexes and the effect of chemical shift anisotropy and quadrupolar coupling	58
2.7.2	The second-order “roof” effect observed in the ¹ H NMR of Pt ^{II} (phen) complexes	62
2.8	Experimental Section	64
2.8.1	Instrumentation	64
2.8.2	Crystal and Structure Refinement Data for Pt ^{II} (bipy)Cl ₂ ·CH ₃ CN and <i>cis</i> -[Pt ^{II} (L ⁿ - <i>S,O</i>) ₂]	65
2.8.3	Synthetic procedures of Pt ^{II} complexes and precursors	65
2.8.3.1	Preparation of <i>N,N</i> -di(alkyl)- <i>N'</i> -acylthiourea	65
2.8.3.2	Preparation of Pt ^{II} (diimine)Cl ₂	66
2.8.3.3	Preparation of ([Pt ^{II} (phen)(L ⁿ - <i>S,O</i>)]Cl	67
2.8.3.4	Preparation of [Pt ^{II} (bipy)(L ⁿ - <i>S,O</i>)]Cl	70
2.8.3.5	Preparation of <i>cis</i> -[Pt ^{II} Cl ₂ (DMSO) ₂]	70
2.8.3.6	Preparation of [Pt ^{II} Cl(DMSO)(en)]Cl	71
2.8.4	Synthetic procedures of Pd ^{II} complexes and precursors	71
2.8.4.1	Preparation of Pd ^{II} Cl ₂ (phen)	71
2.8.4.2	Preparation of Pd ^{II} ₃ (OAc) ₆	72
2.8.4.3	Preparation of Pd ^{II} (phen)(OAc) ₂	72
2.8.4.4	Preparation of ([Pd ^{II} (phen)(L ⁿ - <i>S,O</i>)]Cl	73
2.9	References	74

Chapter 3 – Understanding the synthesis and properties of the novel Pt^{II}(phen)(*N,N*-di(alkyl)-*N'*-acylthiourea)₂ complexes, an unusual coordination of *N,N*-dialkyl-*N'*-acylthiourea

3.1	Introduction	77
3.2	Results and discussion	79
3.2.1	The first evidence of the formation of Pt ^{II} (phen)(<i>N,N</i> -dibutyl- <i>N'</i> -naphthoylthiourea) ₂	79
3.2.2	Synthesis and characterization of Pt ^{II} (phen)(<i>N,N</i> -dibutyl- <i>N'</i> -naphthoylthiourea) ₂	81
3.2.2.1	Assignment of the ¹ H NMR spectrum of Pt ^{II} (phen)(<i>N,N</i> -dibutyl- <i>N'</i> -naphthoylthiourea) ₂	84
3.2.2.2	Assignment of the ¹³ C{ ¹ H} NMR spectrum of Pt ^{II} (phen)(<i>N,N</i> -dibutyl- <i>N'</i> -naphthoylthiourea) ₂	87
3.2.3	Temperature and Concentration dependence of the ¹ H NMR of Pt ^{II} (phen)(<i>N,N</i> -dibutyl- <i>N'</i> -naphthoylthiourea) ₂	92

3.2.3.1	The effect of increasing the temperature on the ^1H NMR of $\text{Pt}^{\text{II}}(\text{phen})(N,N\text{-dibutyl-}N'\text{-naphthoylthiourea})_2$	92
3.2.3.2	The concentration dependence of the ^1H NMR of $\text{Pt}^{\text{II}}(\text{phen})(N,N\text{-dibutyl-}N'\text{-naphthoylthiourea})_2$	96
3.2.3.3	The effect of lower temperature on the ^1H NMR of $\text{Pt}^{\text{II}}(\text{phen})(N,N\text{-dibutyl-}N'\text{-naphthoylthiourea})_2$ in CDCl_3	98
3.2.4	Crystal structure of $\text{Pt}^{\text{II}}(\text{phen})(N,N\text{-dibutyl-}N'\text{-naphthoylthiourea})_2$	103
3.2.5	Probing solution interactions using the Nuclear Overhauser Effect	108
3.2.6	Comparison of HL^n structure on the preparation of various $\text{Pt}^{\text{II}}(\text{phen})(N,N\text{-dialkyl-}N'\text{-acylthiourea})_2$	111
3.2.7	Ligand characteristics/effect on synthesis and stability	119
3.3	Conclusions	122
3.4	Crystal and Structure Refinement Data for $\text{Pt}^{\text{II}}(\text{phen})(\text{L}^2\text{-S})_2$ and $\text{Pt}^{\text{II}}(\text{phen})(\text{L}^4\text{-S})_2$	124
3.5	References	124

Chapter 4 – Cation- π induced aggregation of water-soluble $[\text{Pt}^{\text{II}}(\text{diimine})(\text{L}^n\text{-S},\text{O})]^+$ complexes studied by ^1H DOSY NMR and TEM: from ‘dimer aggregates’ in acetonitrile to nano-aggregates (‘metallogeles’) in water

4.1	Introduction	127
4.2	Results and discussion	129
4.2.1	The effect of solvent composition (0-30% (v/v) $\text{D}_2\text{O}:\text{CD}_3\text{CN}$) on aggregation of $[\text{Pt}^{\text{II}}(\text{phen})(\text{L}^1\text{-S},\text{O})]\text{Cl}$	129
4.2.2	Aggregation behaviour of $[\text{Pt}^{\text{II}}(\text{phen})(\text{L}^1\text{-S},\text{O})]\text{Cl}$ in water-rich mixtures >30% (v/v) $\text{D}_2\text{O}:\text{CD}_3\text{CN}$	133
4.2.2.1	Effect of chloride ion concentration on $[\text{Pt}^{\text{II}}(\text{phen})(\text{L}^1\text{-S},\text{O})]^+$ aggregation in water	139
4.2.2.2	Diffusion Ordered NMR Spectroscopy	141
4.2.2.3	Transmission Electron Microscopy (TEM)	148
4.3	Hetero-association of $[\text{Pt}^{\text{II}}(\text{phen})(\text{L}^1\text{-S},\text{O})]^+$ and pyrene	152
4.4	Conclusions	163
4.5	Experimental Section	164
4.5.1.1	Computational Methods	164
4.5.2	Analytical Instrumentation	165
4.5.3	Synthesis of Complexes	166
4.6	References	166

Chapter 5 – Preliminary assessment of potential antimalarial activity of a series of $[\text{Pt}^{\text{II}}(\text{diimine})(\text{L}^n\text{-S},\text{O})]^+$ complexes using a surfactant mediated β -haematin inhibition assay

5.1	Introduction	169
5.2	β -haematin Inhibition Assay	171
5.3	Results and Discussion	171
5.4	Conclusions	179
5.5	Experimental Section	180

5.6	References	185
	Chapter 6 – Conclusions	186
	Appendix A – Additional Tables and Figures	191
	Appendix B – Publication from work from parts of Chapter 4	217
	Appendix C – Electronic Crystal data Files	CD

1

General Introduction and Background

1.1 Biological activity of square planar platinum complexes

The use of metal complexes as pharmaceuticals has great potential for development of drugs with novel/unique mechanisms of action.¹ Apart from the potential of the metal to take part in the binding to specific target sites, metal complexes have the advantage of large degree of structural variability, induced by numerous ligands and substituents on such ligands. Furthermore, complexes can be neutral or formally charged, depending on the oxidation state of the metal and the ligand system utilised. Cationic complexes for example interact more readily with a range of negatively charged biomolecules such as the negatively charged backbone of DNA.¹ Metal complexes also have the advantage of retaining their formal charge over a range of pH values in the matrix, provided the ligands themselves are not pH sensitive.

Platinum complexes have great potential for this application since the metal is almost kinetically inert compared to some other transition metals. The use of platinum complexes as bioactive agents escalated from the discovery of the famous anticancer drug *cisplatin* (*cis*-diaminedichloroplatinum(II)), by Rosenberg in 1965.² Platinum-based anticancer drugs are still being used over three decades after the discovery of *cisplatin*, with annual sales in the order of two billion U.S. dollars worldwide.³

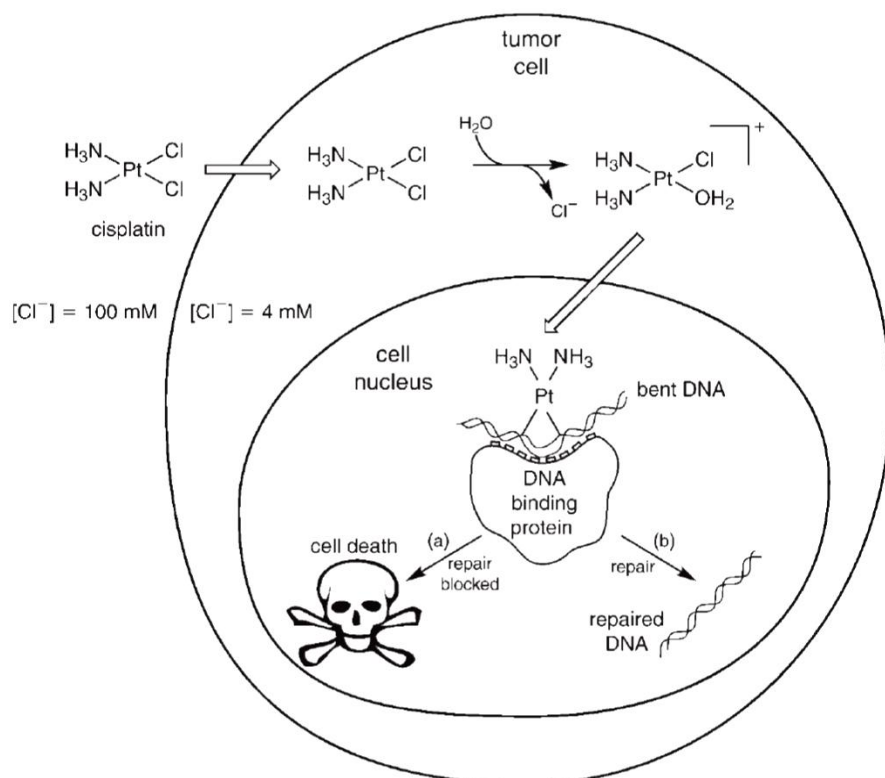


Figure 1.1 Schematic showing the cytotoxic pathway for *cisplatin*.³

Following the determination/elucidation of the mechanism of complex interaction with DNA (Figure 1.1), extensive research has been conducted to develop complexes with the ability to bind/associate with DNA *via* a range of interactions such as direct coordination to DNA.³ Moreover, non-covalent interactions between transition metal complexes and DNA occur by intercalation (π -stacking), groove binding or electrostatic interactions (hydrogen bonding and ion-pairing).¹

Charged platinum(II) diimine complexes, where the diimine is 1,10-phenanthroline or substituted variations thereof, have been shown to have a range of antimicrobial⁴ and even antiviral⁵ activity, presumably as a result of DNA intercalation. Egan and Koch have shown that the cationic complexes, $[\text{Pt}^{\text{II}}(\text{diimine})(N,N\text{-di(alkyl)-}N'\text{-acylthiourea})]^+\text{X}^-$, display significant antimalarial activity in the chloroquine resistant strains of *Plasmodium falciparum*.⁶

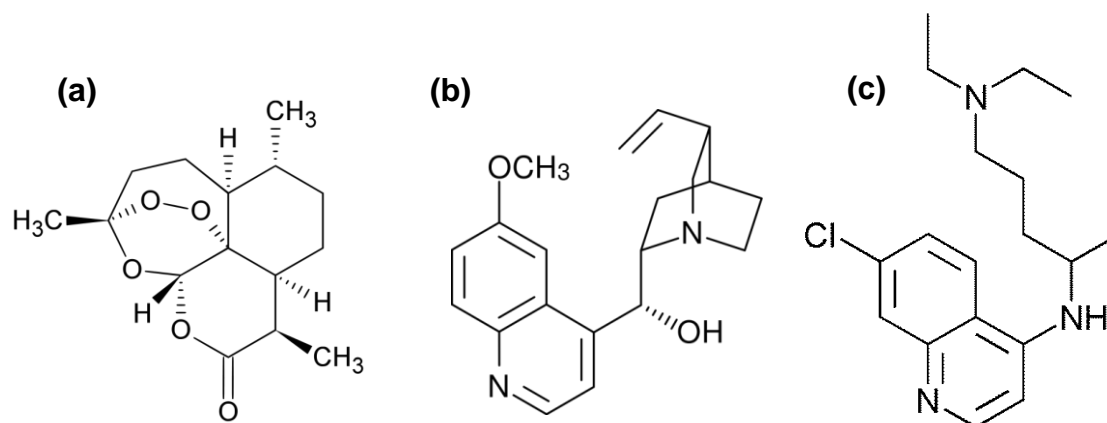
The advantage of using platinum(II) complexes for medicinal applications is the unique chemistry associated with this metal centre, forming stable complexes with generally slow ligand exchange kinetics. This potentially allows for the drug molecule to reach the intended target site unaltered. Furthermore, the square planar geometry allows for direct non-covalent interactions such as intercalation with the metal centre while a wide variety of ligands with specific functionality for the required properties can be incorporated in the complex structure.⁷⁻⁹

1.2 Antimalarial drug discovery

Malaria is the fifth most lethal infectious disease in the world.¹⁰ According to the World Health Organisation, worldwide there are more than 1 million deaths and 250 - 500 million infections of malaria annually.¹¹ The most affected areas are sub-Saharan Africa where the effective control of the disease is almost impossible due to additional economical and socio-economical challenges apart from the tropical environmental factors. The fight against malaria includes therapeutics, large scale pesticide applications as well as the distribution of mosquito nets.¹²

Malaria is caused by the *Plasmodium* (*P.*) parasite of which five strains are pathogenic to humans, *P. falciparum*, *P. vivax*, *P. ovale*, *P. malariae* and occasionally, *P. knowlesi*. The *Plasmodium falciparum* strain is the most studied parasite since it can be cultured and is believed to be responsible for 90% of the mortalities worldwide and also exhibits a significant increase in drug resistance.¹³

The two active compounds used against malaria before the time of modern pharmaceuticals were artemisinin and quinine (Scheme 1.1a and b), extracted from natural sources.



Scheme 1.1 The two ancient antimalarials, (a) artemisinin and (b) quinine extracted from the barks of the *Artemisia annua* and *Cinchona* trees respectively. (c) The well known synthetic antimalarial, chloroquine.

Artemisinin was initially extracted from the bark of the sweet wormwood tree (*Artemisia annua*) known from ancient Chinese medicine which makes it probably the oldest antimalarial.^{14,15} In 1979, artemisinin was scientifically proven to be an effective antimalarial drug and is currently still being used in the treatment of malaria, often in combination with other antimalarials.¹⁶

Quinine on the other hand, was extracted from the bark of the *Cinchona* tree and was used by the Incas and other Quechua people in South America as a treatment for fever and unknowingly for malaria, since fever is a symptom of malaria infection. Various synthetic derivatives of quinine became available in the last century with chloroquine (a 4-aminoquinoline compound) being the first clinically available synthetic antimalarial drug in 1947 (Scheme 1.1c) which were less toxic and easier to produce than quinine.¹⁶ Furthermore, chloroquine is considered one of the most successful drugs ever produced because it is safe, cheap and has saved millions of lives to date.¹⁶

However, the effectiveness of the current treatment of malaria has drastically been compromised by the manifestation of drug resistance.¹⁷ The global distribution of malaria as well as the reported drug resistance to the two commonly used chloroquine and sulphadoxine-pyrimethamine drugs is shown in Figure 1.2.

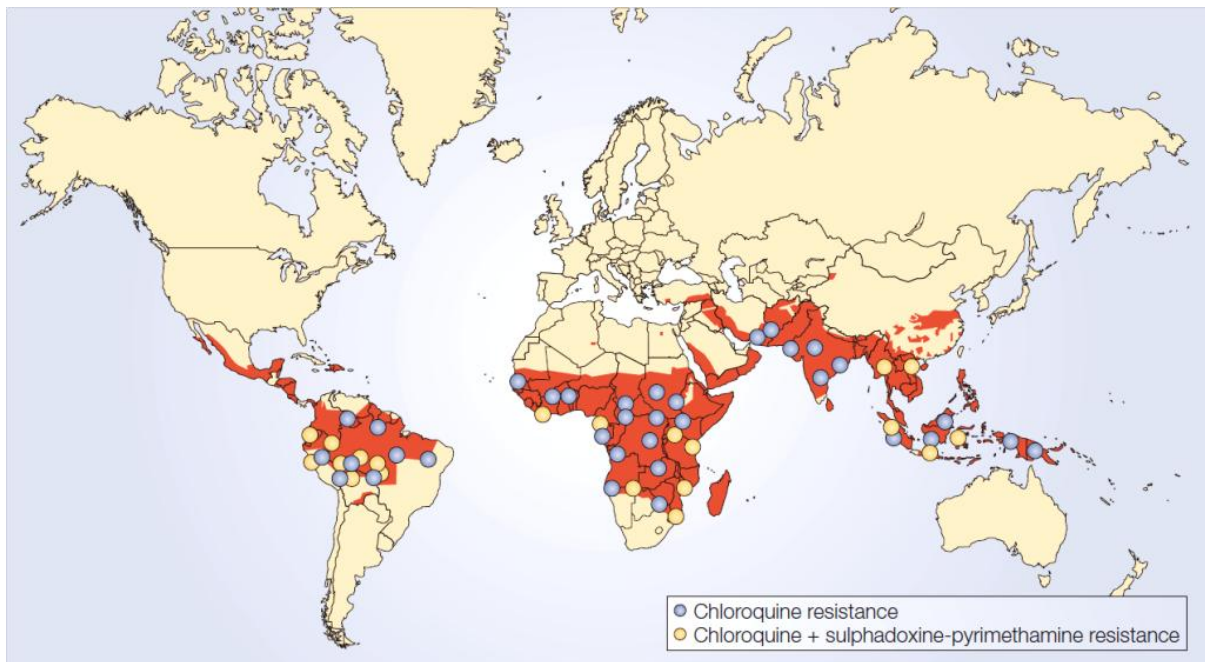


Figure 1.2 The global malaria-endemic regions (in red) with reported drug resistance to commonly used antimalarial drugs, chloroquine and sulphadoxine-pyrimethamine, as indicated on the map.^{10,17}

1.2.1 The life cycle of *Plasmodium falciparum*

The life cycle of the malaria parasite consists of three major stages, which take place across two different hosts: the female mosquito and humans (Figure 1.3).¹⁸

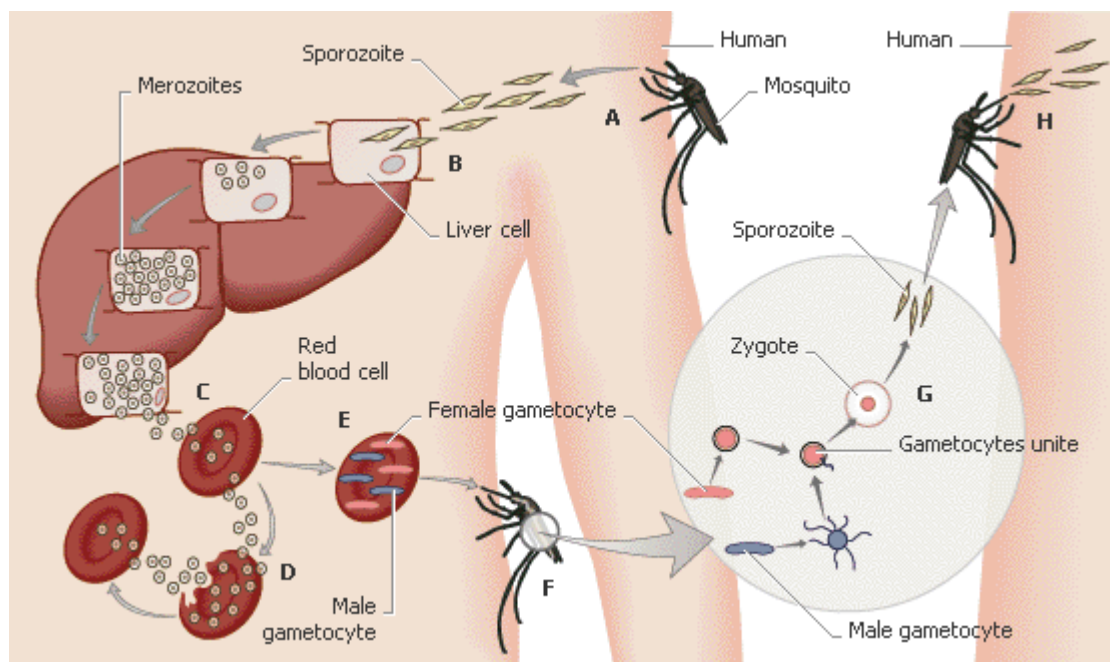


Figure 1.3 The life cycle of the malaria parasite *Plasmodium* showing the stages of development of the parasite in the two hosts. (picture reproduced from MSN Encarta)¹⁸

The first stage involves transfer of sporozoites from the mosquito on biting of the human host, where they enter the blood stream (**A** on Figure 1.3). The sporozoites infect the liver (**B**) in which they multiply asexually for ~10 days to become merozoites. These merozoites subsequently enter the blood stream (**C**) and invade the red blood cells. This marks the onset of the second stage of the life cycle. The parasite matures further and reproduces asexually results in a drastic increase in the number of parasites in the host, which is cause of the symptoms presented in an infected human (**D**). The merozoites form sexual gamatocytes (**E**) which are transferred to the mosquito upon feeding on an infected human host (**F**) and is the onset of the third stage of the life cycle.

Sexual reproduction takes place in the gut of the mosquito resulting in zygotes which are ultimately responsible for the release of sporozoites in the salivary glands of the mosquito (**G**), completing the life cycle of the malaria parasite. The disease spreads by the transfer of sporozoites into another human host (**H**) where the whole cycle repeats itself. The disease spreads rapidly, since the life cycle of *Plasmodium falciparum* is so short (10-14 days). Current attempts to control the disease include minimising human exposure to mosquitos in general by spraying large areas with pesticides and using mosquito poison and nets in housing areas.

1.2.2 Malaria treatment and Drug design

Various drug targets have been identified in the fight against malaria over the past decade.^{10,16} The majority of antimalarial drugs target the parasite while it resides in the blood of the human host (the blood stage), since it is during this stage that the typical fever-like symptoms are observed and from which the disease is diagnosed.¹² The exact mechanism of action of most antimalarial drugs is still contentious, although most drugs target the blood stage of the life cycle of the parasite.¹⁹

During the blood stage when the parasite resides in the red blood cell (RBC), the haemoglobin of the host is used as a food source for the parasite. Haemoglobin (Hb) from the human red blood cell (Figure 1.4) is endocytosed into the cytoplasm (cyt; blue) of the parasite and is transported in the transport vecicle to the food vacuole (FV; white) where digestion takes place.

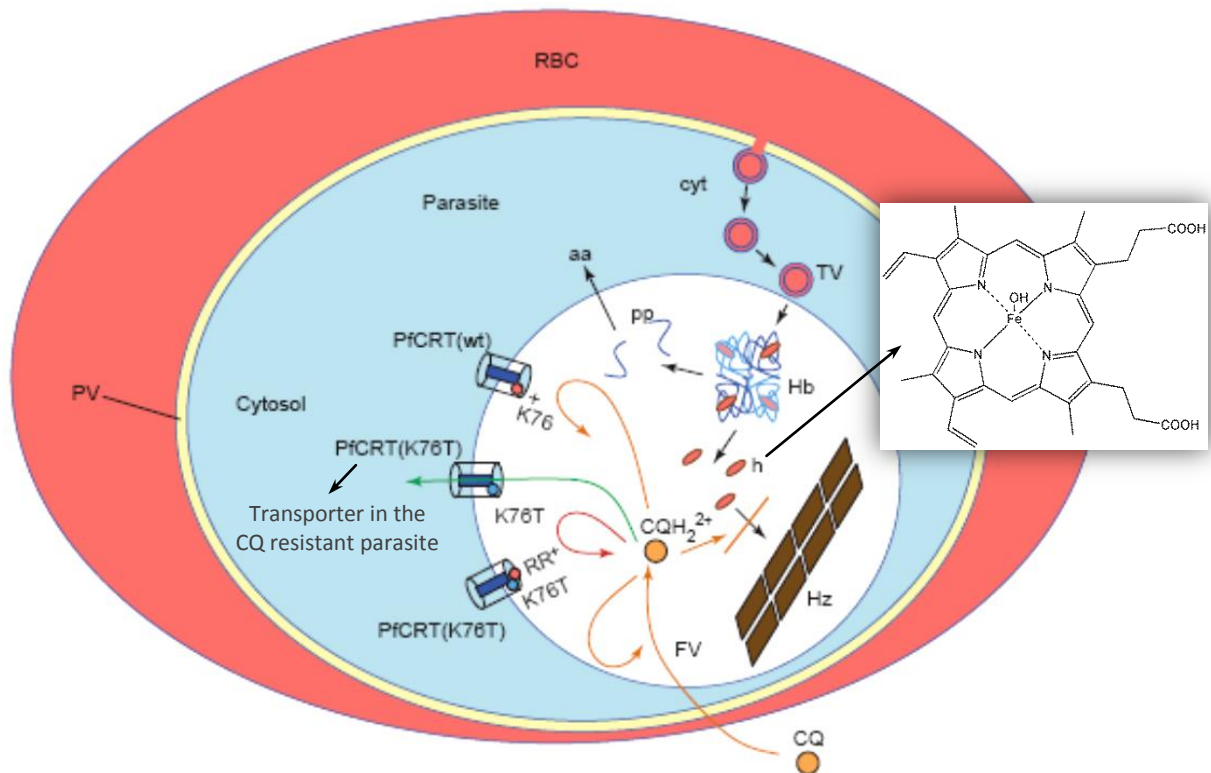


Figure 1.4 Representation from Egan *et al.* of the mode of action of chloroquine (CQ) in the malaria parasite in the human red blood cell which shows the transport of CQ to the food vacuole of the parasite where CQ accumulates as a result of the protonation of CQ to form CQH_2^{2+} to effectively inhibit haemozoin formation.¹⁹

Haemoglobin consists of protein and 4 prosthetic haem groups. The protein is digested to polypeptides (pp) and finally amino acids (aa) which are used as an energy source. Upon release, haem is oxidised to haematin (h) (ferriprotoporphyryn) which is a toxic by-product which causes the death of the parasite from its accumulation in the food vacuole. To prevent toxic levels of haematin, Fe(III)PPIX biomineralise through dimerisation to form the insoluble crystalline haemozoin (Hz) (Figure 1.5), that appears as black spots under a microscope and is commonly known as malaria pigment.^{12,20}

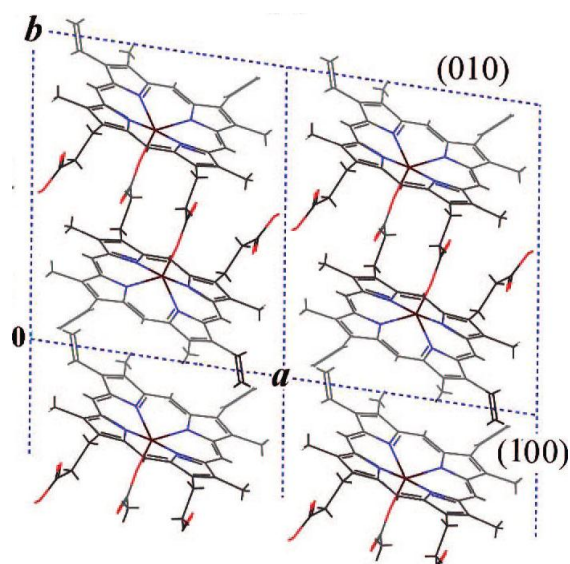


Figure 1.5 The packing arrangement of synthetic haemozoin or β -haematin which consists of cyclic dimers of haematin viewed along the c -axis.²¹ (Picture reproduced from reference 12)

Chloroquine (CQ) and other antimalarials are believed to be effective by inhibiting this detoxification step. Chloroquine for example, accumulates in the food vacuole of the parasite in the protonated (CQH_2^{2+}) form through pH-trapping, which leads high concentrations of CQH_2^{2+} to effectively inhibit haemozoin formation, leading to the death of the malaria parasite due to toxic levels haematin.¹⁹ However, in chloroquine resistant strains, the PfCRT transporter protein in the membrane of the food vacuole has mutated to decrease the protonated chloroquine concentration, leading to ineffective haemozoin inhibition due to low concentrations of the drug molecule in the food vacuole.^{22,23}

The effective treatment of malaria in the future will ultimately rely on new anti-malarials to be discovered and these will have to be modified constantly to treat resistant strains of malaria. Egan and co-workers based on the above model of drug action proposed some essential properties for future potential drug compounds acting in the food vacuole of the parasite during the blood stage; these include effective accumulation of the drug in the food vacuole and strong association/complexation with haematin to effectively inhibit haemozoin formation as being of paramount importance.⁶

Antimalarial drugs acting as haemozoin inhibitors have the ability to strongly associates/interacts with haematin mainly through non-covalent interactions while covalent bonding are often the mode of interaction.²⁴

1.3 Non-covalent drug interactions

Non-covalent interactions play a central role in many chemical and biological systems.²³⁻²⁹ They are 'weak' ($1-5 \text{ kcal.mol}^{-1}$)²⁵ relative to covalent bonding and complex in nature, which makes them especially difficult to study.²⁶ Nevertheless, these weak interactions are extremely important in biological processes and are essential for the functioning of living organisms which includes protein folding²⁷, enzyme catalysis, the function of DNA and RNA,²⁸ drug binding and molecular recognition.²⁹⁻³² Furthermore, non-covalent interactions are also responsible for self-association of molecules in solution and they play an important role in many chemical reactions.³³⁻³⁵ Physical properties of compounds and mixtures are also determined by non-covalent interactions as seen in melting and boiling points, viscosity, solvation, adsorption, condensation and crystallization.²⁸

The most common non-covalent interaction is the hydrogen bond, which holds our DNA double helix in place and gives water its unique properties, enabling it to be the 'solvent' of life. The structure of the DNA double helix is determined by hydrogen-bonding between the complementary nucleobases to keep the two strands together, while π -stacking interactions between the stacked bases is believed to be responsible for the helical structure of this macromolecule (Figure 1.6).

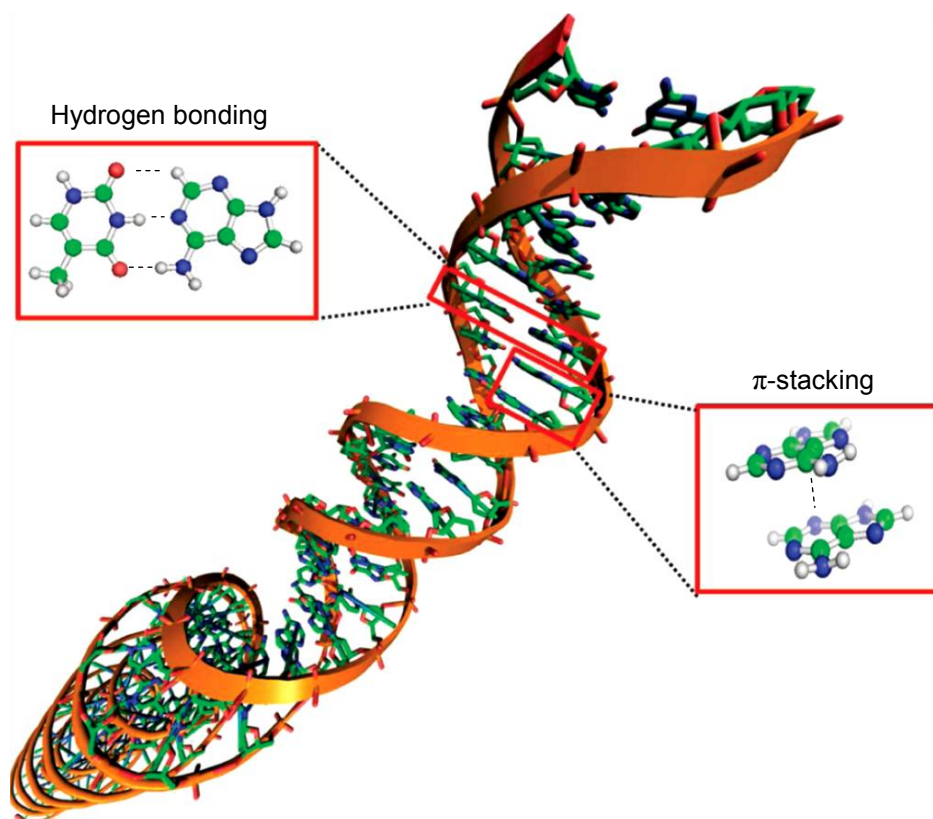
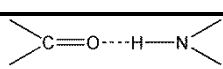
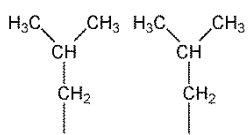
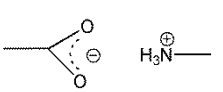
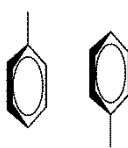
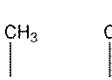
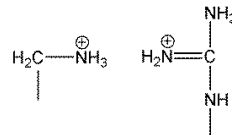


Figure 1.6 The importance of hydrogen bonding and π -stacking for the structural integrity of the double helix of DNA.²⁸

Most weak interactions in molecular assemblies are a combination of a range of weak non-covalent interactions which complicates the identification/characterization and contributions of the respective interactions.²⁶ The stabilisation energies of some non-covalent bonding interactions in proteins are shown in Table 1.1 as an example.

Table 1.1 Approximate stabilization energies of typical non-covalent bonding/interactions in proteins.³⁶

Interaction	Stabilization Energy kcal.mol ⁻¹	Interaction	Stabilization Energy kcal.mol ⁻¹
	2-5		1.5
	< 10		1.5
	0.3		< -5

The remarkably complex structure and behaviour of proteins can to some extent be ascribed to the relatively weak stabilization energies associated with the non-covalent interactions shown in Table 1.1. Other common non-covalent interactions relevant to our study include ion-pairing, aromatic- π stacking, cation- π interactions and hydrophobic effects which will be discussed in more detail.

1.3.1 Hydrogen bonding

The first mention of a hydrogen bond dates back to 1912 with Moore and Winmill ascribing the weaker basicity of trimethylammonium hydroxide compared to tetramethylammonium hydroxide to hydrogen bonding interactions.³⁷ Perhaps the most famous molecule with regards to hydrogen bonding is water, due to its unique properties resulting from extensive hydrogen bonding. Wilson Bentley was first to photograph various snowflake crystals back in 1885 with a total of 15 distinct polymorphs of ice known to date, due to variation in hydrogen bonding.³⁸

Hydrogen bonding entails the electrostatic dipole-dipole interaction between a hydrogen atom and the lone pair of electrons of a more electronegative atom. Hydrogen bonding is difficult to define explicitly and several types of hydrogen bonds are known.³⁹ The most elementary hydrogen bond of the type $D-H\cdots A$, is formed by the interaction of an electronegative donor atom (D) and a neighbouring proton acceptor with lone-pair electrons (A). Hydrogen bonds depend on the electronegativity of the acceptor atom and their strength ranges from very weak ($1-2 \text{ kJ}\cdot\text{mol}^{-1}$) to extremely strong ($161.5 \text{ kJ}\cdot\text{mol}^{-1}$) for $[\text{HF}_2]^-$.⁴⁰

The energetically favoured orientation of the hydrogen bonding in water is shown in Figure 1.7a with the electrostatic potential surface of two hydrogen-bonded water molecules also shown (Figure 1.7b).⁴¹

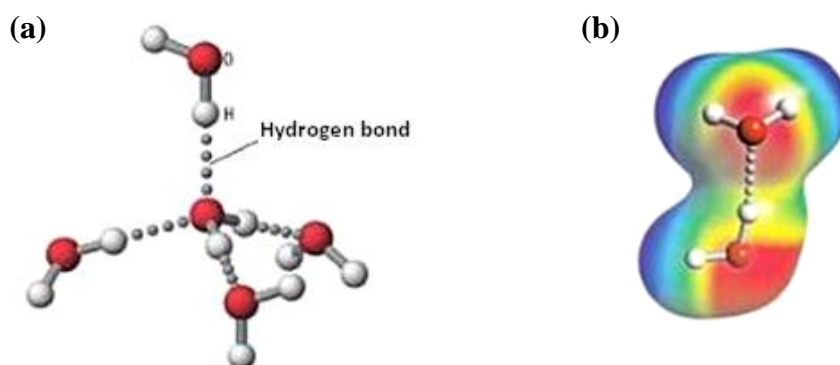


Figure 1.7 Hydrogen bonding between water molecules with (a) the energetically stable 'tetrahedral' geometry and (b) the electrostatic surface of two hydrogen bonded water molecules.⁴¹

Hydrogen bonds can exist between atoms in the same molecule (intramolecular H-bonding) or between different molecules (intermolecular H-bonding). The particular structural conformations of molecules and complexes are often a result of hydrogen bonding as seen in the case of thermochromism of $[\text{NH}_3(\text{CH}_2)_2\text{NH}_3][\text{CuCl}_4]$, with the coordination geometry of $[\text{CuCl}_4]^{2-}$ changing from distorted square planar to tetrahedral as the temperature increases, which is ascribed to the decrease in hydrogen bonding as the temperature increases.⁴²

Hydrogen bonding often dictates molecular conformation and aggregation in chemical systems ranging from inorganic⁴³ to biological systems⁴⁴⁻⁴⁷ (i.e. protein folding and DNA base pairing).

1.3.2 Ion-pairing

An ion pair is formed when oppositely charged ions are held together by Coulombic/electrostatic interaction without the formation of a covalent bond.⁴⁸ The degree and type of ion pairing is largely dependent on the magnitude of the charges, size of the ions and the polarity of the solvent. Ion pairs can be classified into two groups, contact/intimate ion pairs and loose ion-pairs, based on the extent of solvation of the respective ions. Contact ion pairs are solvated as one entity; solvent shared ion pair has only one solvent molecule separating the ions while solvent separated ion-pairs have more than one solvent molecule separating the ions in solution.

The nature of the solvation shell is generally not known with any certainty. Direct measurement of solvent-separated ion-pairs is not possible since the spectroscopic properties of such ion pairs are indistinguishable from those of the free ions, and indirect spectroscopic and conductivity measurements are generally used for their identification/characterization.⁴⁹ There is much interest in the effect of ion pairing on chemical and physical properties especially in the areas of marine chemistry⁵⁰, biology⁵¹ and pharmaceuticals⁵². Furthermore, outer-sphere coordination is in essence a contact ion pair between a ligand and a complex ion. For example, Westra and co-workers found strong interaction between the protonated amine ligand and the face of 3 chlorido-ligands in the $[\text{PtCl}_6]^{2-}$ octahedral anion.⁵³

The use of ion-pairing is also exploited as in phase-transfer agents like Aliquat 336, a quaternary ammonium salt used to extract $[\text{Pt}(\text{SNCl}_3)_5]^{3-}$ anions into an organic phase.⁵⁴ Furthermore, the importance of outer-sphere ion-pairing in catalysts has also gained significant interest since it has been shown that the contribution of this interaction to the exceptional superiority of enzymes over some synthetic transition metal-based catalyst, in terms of rate and selectivity.⁵⁵

1.3.3 Cation- π interactions

The attractive interaction between a formal cation and an aromatic moiety is known as a cation- π interaction. The cation- π interaction is believed to be of electrostatic nature since the positively charged cation interacts with the negative π -electron cloud of the π -system.⁵⁶⁻⁵⁸ Benzene for example, has no net dipole moment, but a substantial quadrupole moment ($-29 \times 10^{-40} \text{C.m}^2$) which allows for the electrostatic interaction with ions (Figure 1.8a).⁵⁹

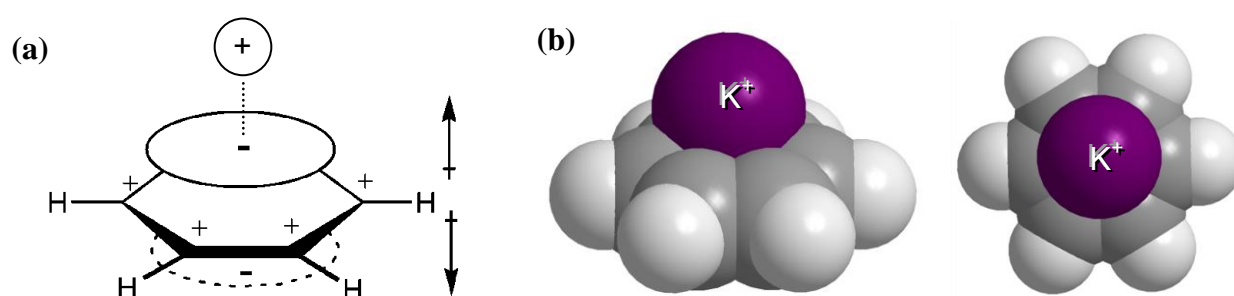
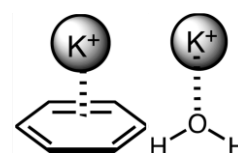


Figure 1.8 (a) Schematic drawing of the charge distribution of benzene showing the positively charged σ -framework and negatively charged π -electron cloud forming a quadrupole moment and (b) the cation- π interactions showing the contact of the potassium cation (K^+) and benzene.⁵⁹

Kebarle and co-workers were the first to study the interaction between the potassium cation (K^+) and benzene experimentally using mass spectrometry and found K^+ to have a slight preference to bind to benzene ($\Delta G = -19$ kcal.mol⁻¹) compared to water ($\Delta G = -18$ kcal.mol⁻¹) in the gas phase.⁶⁰



Dougherty and co-workers investigated cation- π interactions using theoretical calculations and emphasised the importance of this interaction experimentally in biological processes.⁶¹ The cation- π interaction has been widely exploited and utilised due to its occurrence in structural biology and fundamental importance in supramolecular chemistry. Moreover, its pivotal role in host-guest chemistry and molecular recognition has gained significant interest.⁶² Multinuclear NMR has been shown to be an excellent tool in establishing the presence of cation- π interactions in solution as marked shielding was observed for various NMR active nuclides upon addition of aromatic molecules.⁵⁹

Generally the π -stacking interactions between aromatic moieties (which will be discussed in the next section) are weaker compared to hydrogen bonding while cation- π interactions tend to be stronger.^{63,64} The combination of cation- π and aromatic π -stacking enhances the strength of both interactions and they are commonly observed together.⁵⁹ An example of this can be seen in the host-guest complex of the enzyme acetylcholinesterase and the Alzheimer drug Aricept[®] (Figure 1.9), where both OH- π and π - π -stacking are observed.

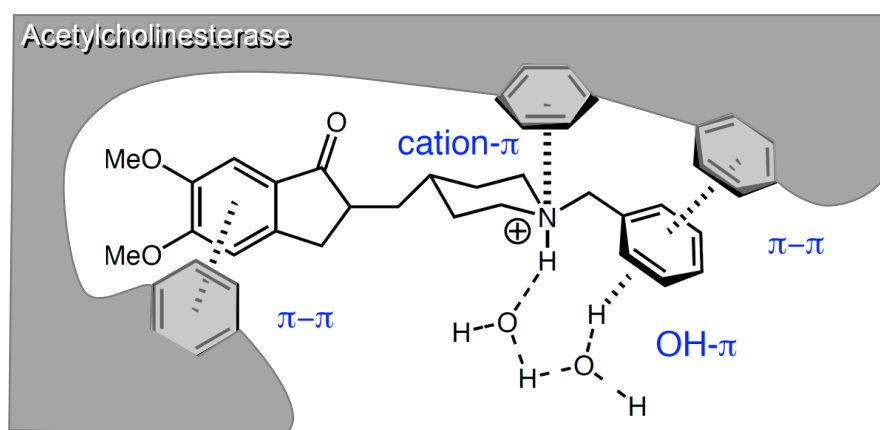
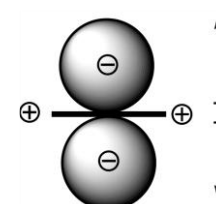


Figure 1.9 Combination of cation- π and aromatic π -stacking interactions observed in enzyme-drug complex of Aricept[®] and acetylcholinesterase from *Torpedo californica*.⁶⁵

1.3.4 Aromatic π -stacking interactions

The self-association or non-covalent 'dimer' formation of benzene has been central in the understanding the aromatic π -stacking interaction between aromatic moieties.²⁹ This aromatic interaction is believed to be a combination of dispersion, hydrophobic and electrostatic forces.^{29,66} The interaction between aromatic moieties plays a major role in determining structure and properties of molecular assemblies in biology and general chemistry prevalent in molecular recognition and crystal packing.²⁷⁻³¹

Hunter and Sanders developed an electrostatic model to describe aromatic π -stacking interactions by considering the π - and σ -systems separately as shown in the accompanying figure.⁶⁷ Aromatic molecules attract one another when the π -system of one arene interacts more strongly with the σ system of the other, rather than the destabilizing π - π repulsion. The energy of the interaction between two π -system molecules is a combination of electrostatic, dispersion, induction and repulsion:



$$E_{\text{Total}} = E_{\text{Electrostatic}} + E_{\text{Dispersion}} + E_{\text{Induction}} + E_{\text{Repulsion}}$$

The electrostatic, induction and dispersion terms are normally attractive while the repulsion term destabilizes the interaction and becomes significant when the distance between the molecules is reduced beyond a certain point. This model of aromatic π -interactions between uncharged aromatic and/or quasi-aromatic molecules can take several conformations, as shown in Figure 1.10 for benzene as an example.⁶⁷

The three common conformations of two interacting benzene molecules include face-to-face, edge-to-face and offset conformations with the electrostatic potential surfaces of the molecules also shown.⁶⁸

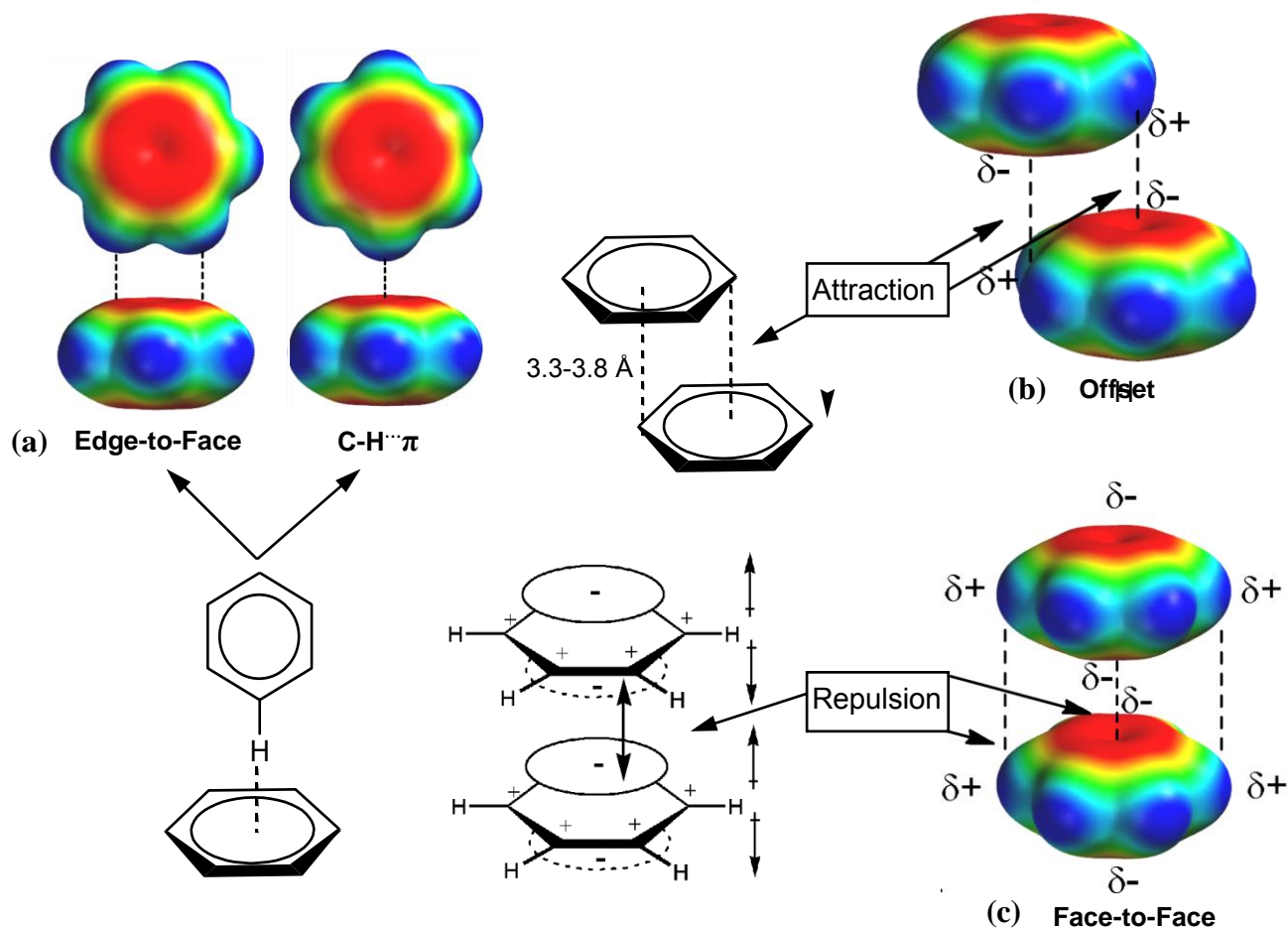


Figure 1.10 The common types of aromatic π -stacking interactions which includes (a) edge-to-face, (b) offset and (c) face-to-face interactions.^{67,68}

The potential of aromatic moieties like benzene to π -stack is a result of electrostatic attraction between opposite charges, evident from its electric quadrupole moment as shown for the cation- π interaction (Figure 1.8), visually expressed by the electrostatic potential surfaces as shown in Figure 1.10. The red colour indicates electron rich environments while blue represents quasi-positive environments.⁶⁸

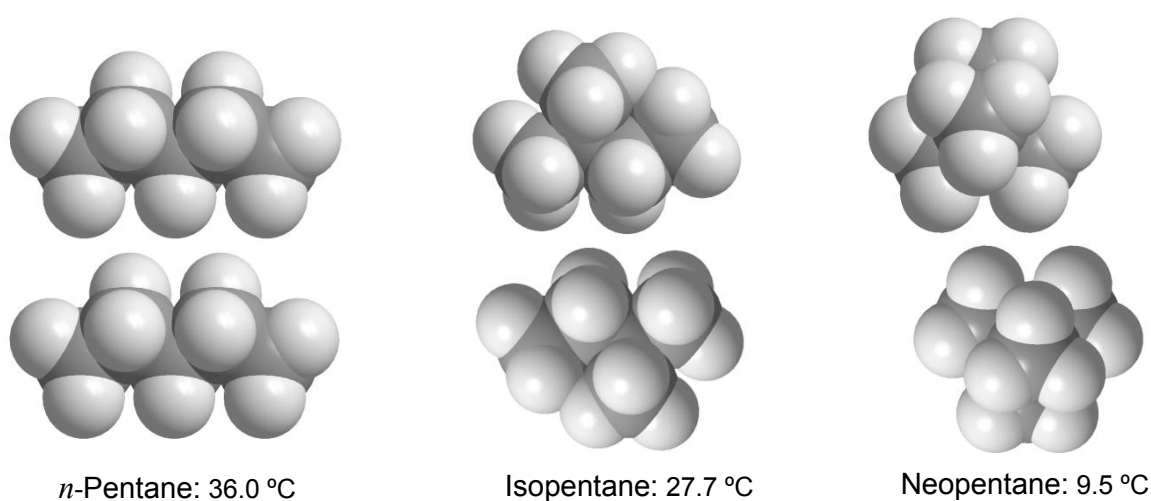
The aromatic π -stacking interaction manifests itself when the attraction between the π -electron cloud and the positive σ -framework outweighs the unfavourable π - π electron repulsion. The offset aromatic π -stacking (Figure 1.10b) and edge-to-face stacking geometries (Figure 1.10a) are energetically more favourable in general, while the face-to-face geometry (Figure 1.10c) is sometimes favoured in polar environments where hydrophobic effects also

contribute to the total stability of the aggregate. Therefore, the interpretation of aromatic π -stacking interactions in polar environments, as observed for protein folding²⁷ and drug intercalation into DNA,⁶⁹ should include the hydrophobic effect since aromatic molecules/moieties are hydrophobic by nature.

1.3.5 Hydrophobic interactions

Hydrophobic interactions involve the interaction of non-polar (hydrophobic) molecules, typically when they are mixed with water or polar solvents.⁷⁰ The two major contributions to the stabilization of this interaction are the increase in entropy as ordered water molecules are "released" upon association, and attractive London dispersion forces between the non-polar groups.⁷⁰

London dispersion forces are a result of polarization of the electron clouds of at least two non-polar groups which allows for attractive electrostatic interaction. The different physical properties of the structural isomers of pentane roughly illustrate the degree of this attractive interaction.⁷¹



Scheme 1.2 Structural isomers of pentane with markedly different boiling points.⁷¹

It is clear from Scheme 1.2 that *n*-pentane has a larger interaction surface with a neighbouring pentane compared to the other two isomers which results in larger total area of dispersion interaction between *n*-pentane molecules, which reasonably accounts for the higher boiling point of this isomer.

These weak hydrophobic interactions are very important; they are responsible for the formation of membranes, vesicles and micelles in aqueous solutions.⁷⁰

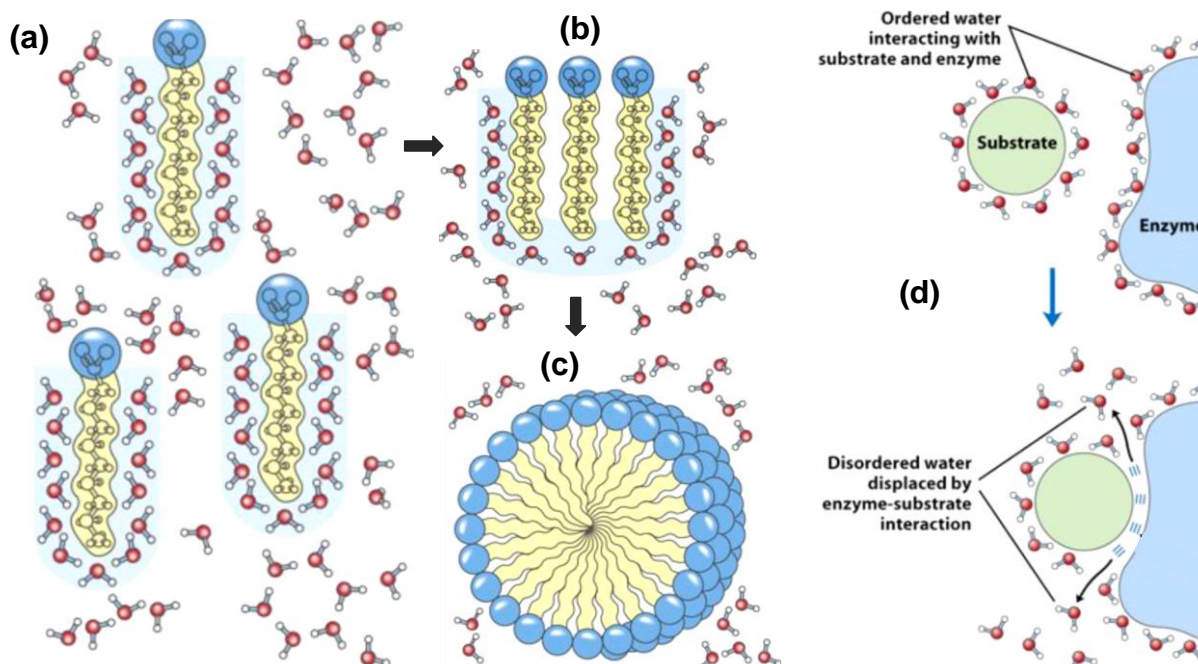


Figure 1.11 Illustration of hydrophobic interactions in the formation of micelles. The process involves (a) the solvation of lipid molecules in water which forms (b) aggregates which ultimately forms (c) ordered micelles. (d) The importance of hydrophobic interactions in molecular recognition.⁷⁰

Lipid molecules consist of a hydrophilic/polar 'head' and a non-polar hydrocarbon 'tail'. When these lipid molecules are solvated by water molecules in aqueous solutions, water does not readily interact with the tail, but rather forms a network of highly ordered hydrogen bonding (H-O-H \cdots H-O-H) surrounding the tail (Figure 1.11a).⁵⁵

The aggregation/interaction of lipid tails results in the 'release' of ordered water molecules (Figure 1.11b), which is energetically favoured from an entropy point of view. This aggregation of lipid molecules can result in highly sophisticated supramolecular structures such as micelles (Figure 1.11c), membranes and vesicles. Furthermore, hydrophobic interactions/bonding can be observed in the recognition of substrates (*e.g.* steroid hormones) and receptors (*e.g.* enzymes) as shown (Figure 1.11d).⁷⁰ Many drugs are designed to take advantage of this type of hydrophobic effect.

Other well known examples of hydrophobic interactions are the workings of surfactants. Lipids and surfactants are all ambiphilic molecules, widely used in detergents, wetting agents, emulsifiers, foaming agents and dispersants.⁷²

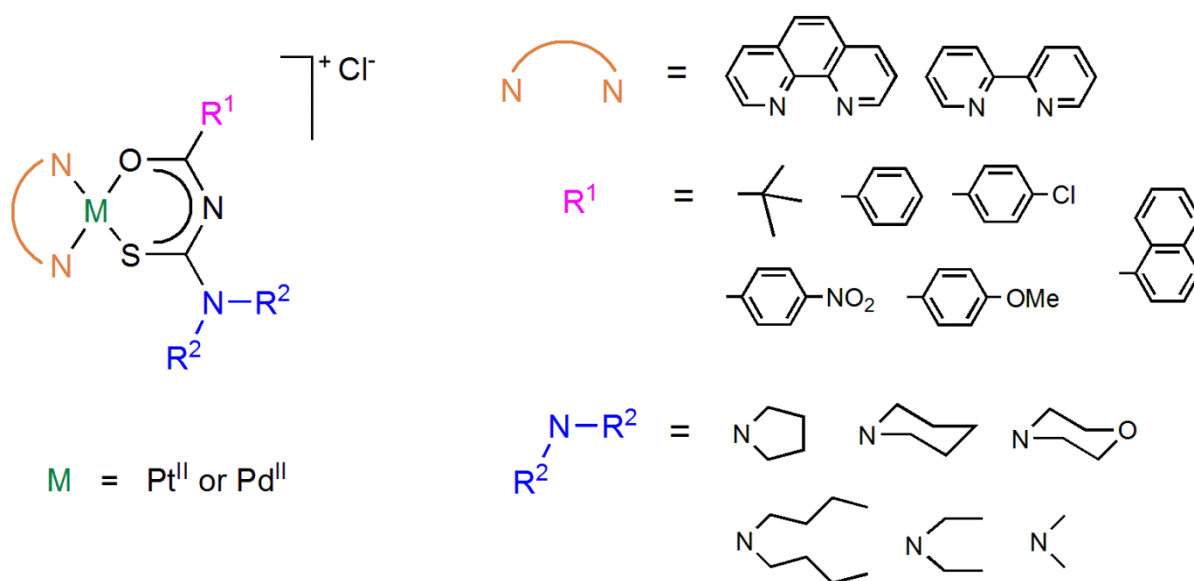
1.4 Objectives of this study

Koch and Egan have shown that mixed-ligand platinum(II) complexes with the general structure $[\text{Pt}^{\text{II}}(\text{diimine})(\text{L}^{\text{n}}-\text{S},\text{O})]\text{X}$, where diimine is 1,10-phenanthroline (phen) or 2,2'-bipyridyl (bipy), L^{n} indicates various *N,N*-di(alkyl)-*N'*-acylthiourea ligands and $\text{X} = \text{PF}_6^-$ or Cl^- , display significant antimalarial activity.⁶ The *in vitro* anti-malarial activity of $[\text{Pt}^{\text{II}}(\text{diimine})(\text{L}^{\text{n}}-\text{S},\text{O})]^+$ is postulated to arise by inhibition of haemozoin formation (blocking parasite's detoxification of haematin), presumably as a result of the cationic planar complex $[\text{Pt}^{\text{II}}(\text{diimine})(\text{L}^{\text{n}}-\text{S},\text{O})]^+$ forming moderately strong outer-sphere aggregates with ferriprotoporphyrin IX (haematin). This hetero-association was demonstrated in 40% aqueous dimethyl sulfoxide (DMSO) solution, and is thought to be through a combination of cation- π and aromatic π -stacking interactions.⁶ It has also been shown previously that such planar $[\text{Pt}^{\text{II}}(\text{diimine})(\text{L}^{\text{n}}-\text{S},\text{O})]^+$ complexes have a tendency to self-associate in solution as well as to form relatively strong outer-sphere complex aggregates with the polyaromatic hydrocarbon fluoranthene.⁷³⁻⁷⁵

However, the mechanism of antimalarial activity of $[\text{Pt}^{\text{II}}(\text{diimine})(\text{L}^{\text{n}}-\text{S},\text{O})]\text{X}$ is still contentious although it is thought to be a result from relatively strong non-covalent interaction between $[\text{Pt}^{\text{II}}(\text{diimine})(\text{L}^{\text{n}}-\text{S},\text{O})]^+$ and haematin. A detailed investigation of the non-covalent interactions and solution behaviour of these complexes is therefore important.¹⁹

In this context, the current study involves:

- the synthesis of a series of novel square planar $[\text{Pt}^{\text{II}}(\text{phen})(\text{L}^{\text{n}}-\text{S},\text{O})]^+$ complexes. The main structural variation is the *N,N*-dialkyl-*N'*-acylthiourea while 1,10-phenanthroline will be substituted for 2,2'-bipyridine and platinum(II) for palladium(II) (Scheme 1.3).



Scheme 1.3 Structural variations of the series of $[\text{M}^{\text{II}}(\text{diimine})(\text{L}^n\text{-S,O})]\text{Cl}$ complexes synthesised.

A thorough investigation of the synthesis of this class of complexes will be conducted. The effect of the acylthiourea ligand on the characteristics of the complex will be investigated, since these ligands have been shown to have significantly different solution behaviour with small changes in the molecular structure⁷⁶ and have several coordination modes⁷⁷ which will also be investigated. The monodentate coordination of selected *N,N*-dialkyl-*N'*-acylthioureas which forms novel $\text{Pt}^{\text{II}}(\text{phen})(\text{L}^n\text{-S})_2$ complexes will be investigated in detail which could potentially be a new class of biological active compounds.

- the investigation of the behaviour of these complexes in aqueous solutions (self-association) since self-association (from a series of non-covalent interactions) will have a drastic effect on the association of $[\text{Pt}^{\text{II}}(\text{phen})(\text{L}^n\text{-S,O})]^+$ with haematin which is expected to effect the potential for antimalarial activity. These complexes showed interesting aggregation behaviour in water, which will be studied in detail using ^1H NMR, Diffusion Ordered spectroscopy (DOSY) and Transmission Electron Microscopy.
- the investigation of the outer-sphere complex formation of $[\text{Pt}^{\text{II}}(\text{phen})(\text{L}^1\text{-S,O})]^+$ and pyrene as a model for the postulated coplanar stacking with haematin, using NMR spectroscopy. Pyrene was used as a model since haematin is paramagnetic and could not be used in the NMR study. These results will be compared to the previously studied hetero-association of $[\text{Pt}^{\text{II}}(\text{phen})(\text{L}^1\text{-S,O})]^+$ with fluoranthene in acetonitrile.

- the investigation of potential haemozoin inhibition of the series of $[\text{Pt}^{\text{II}}(\text{phen})(\text{L}^{\text{n}}-\text{S},\text{O})]^+$ complexes, since complexes of this class have been shown to display significant *in vitro* antimalarial activity.⁶ Haemozoin inhibition specifically will be considered as a potential antimalarial mechanism in this work and not DNA intercalation, since this class of complexes is already known to be significant DNA intercalators.⁴ Therefore, the series of complexes will be tested for β -haematin (synthetic haemozoin) inhibition using a surfactant-mediated β -haematin assay, to shed light on the postulated *in vitro* mechanism of antimalarial activity of this class of complexes to be haemozoin inhibition.\

1.5 References

1. J. Aldrich-Wright, *Metallointercalators: Synthesis and Techniques to Probe Their Interactions with Biomolecules*, Springer-Verlag/Wien, Germany, **2011**, 28-30.
2. B. Rosenberg, L. Van Camp, T. Krigas, *Nature*, 1965, **205**, 698-699.
3. R. A. Alderden, M. D. Hall, T. W. Hambley, *J. Chem. Ed.*, 2006, **83**, 728-734.
4. Y. S. Wu, K. R. Koch, V. R. Abratt, H. H. Klump, *Arch. Biochem. Biophys.*, 2005, **440**, 28-37.
5. N. Margiotta, A. Bergamo, G. Sava, G. Padovano, E. de Clercq, G. Natile, *J. Inorg. Biochem.*, 2004, **98**, 1385-1390.
6. T. J. Egan, K. R. Koch, P. L. Swan, C. Clarkson, D. A. Van Schalkwyk, P. J. Smith, *J. Med. Chem.*, 2004, **47**, 2926-2934.
7. D. A. Dougherty, *Science*, 1996, **271**, 163-168.
8. D. Cuc, D. Canet, J. P. Morel, N. Morel-Desrosiers, P. Mutzenhardt, *ChemPhysChem*, 2007, **8**, 643-645.
9. M. Howe-Grant K. C. Wu, W. R. Bauer, S. J. Lippard, *Biochem.*, 1976, **15**, 4339-46.
10. D. A. Fidock, P. J. Rosenthal, S. L. Croft, R. Brun, S. Nwaka, *Nature Rev.*, 2004, **3**, 509-520.
11. <http://www.who.int/health-topics/malaria.htm>.
12. I. Weissbuch, L. Leiserowitz, *Chem. Rev.*, 2008, **108**, 4899-4914.
13. S. I. Hay, C. A. Guerra, A. J. Tatem, A. M. Noor, R. W. Snow, *Lancet Infect. Dis.*, 2004, **4**, 327-336.
14. N. J. White, *Science*, 2008, **320**, 330-334.
15. L. W. Cui, X. Z. Su, *Expert Rev. Anti-Inf. Ther.*, 2009, **7**, 999-1013.
16. I. B. Müller, J. E. Hyde, *Future Microbiol.*, 2010, **5**, 1857-1873.
17. B. Greenwood, T. Mutabingwa, *Nature*, 2002, **415**, 670-672.

18. <http://encarta.msn.com/malaria.html>
19. T. J. Egan, *Trends Parasitol.*, 2006, **22**, 235-237.
20. T. J. Egan, *Drug Des. Rev.*, 2004, **1**, 93-110.
21. S. Pagola, W. P. Stephens, D. S. Bohle, A. D. Kosar, S. K. Madsen, *Nature*, 2000, **404**, 307-310.
22. D. A. Fidock, T. Nomura, A. K. Talley, R. A. Cooper, S. M. Dzekunov, M. T. Ferdig, L. M. B. Ursos, A. B. S. Sidhu, B. Naude, K. W. Deitsch, *Mol. Cell*, 2000, **6**, 861-871.
23. R. A. Cooper, M. T. Ferdig, X. Su, L. M. B. Ursos, J. Mu, T. Nomura, H. Fujioka, D. A. Fidock, P. D. Roepe, T. E. Wellems, *Mol. Pharmacol.*, 2002, **61**, 35-42.
24. A. Leed, K. DuBay, D. Sears, A.C. de Dios, P. D. Roepe, *Biochem.*, 2002, **41**, 10245-10255.
25. H. Lodish, A. Berk, S. L. Zipursky, *Molecular Cell Biology 4th Ed.*, New York: W. H. Freeman, 2000.
26. K. Mueller-Dethlefs, P. Hobza, *Chem. Rev.*, 2000, **100**, 143-167.
27. C. R. Matthews, *Annu. Rev. Biochem.*, 1993, **62**, 653-683.
28. D. Ghosh, D. Kosenkov, V. Vanovschi, C. F. Williams, J. M. Herbert, M. S. Gordon, M. W. Schmidt, L. V. Slipchenko, A. I. Krylov, *J. Phys. Chem. A*, 2010, **114**, 12739-12754.
29. E. A. Meyer, R. K. Castellano, F. Diederich, *Angew. Chem. Int. Ed.*, 2003, **42**, 1210-1250.
30. B. Askew, P. Ballester, C. Buhr, K. S. Jeong, S. Jones, K. Parris, K. Williams, J. Rebek, *J. Am. Chem. Soc.*, 1989, **111**, 1082-1090.
31. C. A. Hunter, *Chem. Soc. Rev.*, 1994, **23**, 101-109.
32. H.-J. Schneider, *Angew. Chem. Int. Ed. Engl.*, 1991, **30**, 1417-1436.
33. P. Wu, R. Chaudret, X. Hu, W. Yang, *J. Chem. Theory Comput.*, 2013, **9**, 2226-2234.
34. S. S. Sheiko, F. C. Sun, A. Randall, D. Shirvanyants, M. Rubinstein, H. Lee, K. Matyjaszewski, *Nature*, 2006, **440**, 191-194.
35. G. A. DiLabio, P. G. Piva, P. Kruse, R. A. Wolkow, *J. Am. Chem. Soc.*, 2004, **126**, 16048-16050.
36. R. Barker, *Organic Chemistry of Biological Compounds*, Prentice Hall, Englewood Cliffs, N. J. **1971**, 103-110.
37. T. S. Moore, T. F. Winmill, *J. Chem. Soc., Trans.*, 1912, **101**, 1635-1676
38. C. G. Salzmann, P. G. Radaelli, B. Slater, J. L. Finney, *Phys. Chem. Chem. Phys.*, 2011, **13**, 18468-18480.
39. T. Steiner, *Angew. Chem. Int. Ed.*, 2002, **41**, 48-76.
40. J. Emsley, *Chem. Soc. Rev.*, 1980, **9**, 91-124.
41. <http://chemistry.tutorvista.com/physical-chemistry/hydrogen-bonding.html>
42. R. D. Willet, J. A. Haugen, J. Lebsack, J. Morrey, *J. Inorg. Chem.*, 1974, **12**, 2510-2513
43. R. J. Warr, A. N. Westra, K. J. Bell, J. Chartres, R. Ellis, C. Tong, T. G. Simmance, A. Gadzhieva, A. J. Blake, P. A. Tasker, *Chem. Eur. J.*, 2009, **15**, 4836-4850.

44. N. J. Wheate, P. G. Anil Kumar, A. M. Torres, J. R. Aldrich-Wright, W. S. Price, *J. Phys. Chem. B*, 2008, **112**, 2311-2314.
45. A. M. Krause-Heuer, N. J. Wheate, M. J. Tilby, D. G. Pearson, C. J. Ottley, J. R. Aldrich-Wright, *Inorg. Chem.*, 2008, **47**, 6880-6888.
46. W Lu, D. A. Vicic, J. K. Barton, *Inorg. Chem.*, 2005, **44**, 7970-7980.
47. M. Cusumano, M. L. Di Pietro, A. Giannetto, *Inorg. Chem.*, 2006, **45**, 230-235.
48. A. D. McNaught, A. Wilkinson, *IUPAC. Compendium of Chemical Terminology, 2nd ed. (the "Gold Book")*. Blackwell Scientific Publications, Oxford, **1997**.
49. K. Miyoshi, *Bul. Chem. Soc. Japan*, 1973, **46**, 426-430.
50. P.M. May, *Mar. Chem.*, 2006, **99**, 62-69.
51. P. Sipos, M. Schibeci, G. Peintler, P.M. May, G. Hefter, *Dalton Trans.*, 2006, 1858-1866.
52. J. Irungu, D.S. Dalpathado, E.P. Go, H. Jiang, H.V. Ha, G.R. Bousfield, H. Desaire, *Anal. Chem.*, 2006, **78**, 1181-1190.
53. K.J. Bell, A.N. Westra, R.J. Warr, J. Chartres, R. Ellis, C.C. Tong, A.J. Blake, P.A. Tasker, M. Schröder, *Angew. Chem. Int. Ed.*, 2008, **47**, 1745-1748
54. K. R. Koch, *Mag. Res. Chem.*, 1992, **30**, 158-162
55. W. J. Shaw, *Cat. Rev. Sci. Eng.*, 2012, **54**, 489-550.
56. A. S. Reddy, G. N. Sastry, *J. Phys. Chem. A*, 2005, **109**, 8893-8903.
57. G. W. Gokel, S. L. De Wall, E. S. Meadows, *Eur. J. Org. Chem.*, 2000, **17**, 2967-2978.
58. G. W. Gokel, L. J. Barbour, S. L. De Wall, E. S. Meadows, *Coord. Chem. Rev.*, 2001, **222**, 127-154.
59. A. S. Mahadevi, G. N. Sastry, *Chem. Rev.*, 2013, **113**, 2100-2138.
60. J. Sunner, K. Nishizawa, P. J. Kebarle, *J. Phys. Chem.*, 1981, **85**, 1814-1820.
61. P. J. Gallivan, D. A. Dougherty, *Proc. Nat. Acad. Sci. U.S.A.*, 1999, **96**, 9459-9464.
62. S. Yamada J. S. Fossey, *Org. Biomol. Chem.*, 2011, **9**, 7275-7281
63. C. A. Hunter, J. K. M. Sanders, *J. Am. Chem. Soc.*, 1990, **112**, 5525.
64. M. O. Sinnokrot, E. F. Valeev, C. D. Sherrill, *J. Am. Chem. Soc.*, 2002, **124**, 10887-10893.
65. G. Kryger, I. Silman, J. L. Sussman, *J. Phys. Paris*, 1998, **92**, 191-194.
66. C.A Hunter, K. R. Lawson, J. Perkins, C. J. Urch, *J. Chem. Soc., Perkin Trans.*, 2001, **2**, 651-669.
67. C. A. Hunter, J. K. M. Sanders, *J. Am. Chem. Soc.*, 1990, **112**, 5525-5534.
68. D. W. Oxtoby, H. P. Gillis, A. Campion, *Principles of Modern Chemistry, 7th Ed.*, Brookes/Cole, Cengage Learning, Belmont, **2012**, 284-285.
69. L. S. Lerman, *J. Mol. Biol.*, 1961, **3**, 18-30.

70. D. L. Nelson, M. M. Cox, *Lehninger Principles of Biochemistry 5th Ed.*, W. H. Freeman and Company, New York. **2008**.
71. J. Wei, *Ind. Eng. Chem. Res.*, 1999, **38**, 5019-5027.
72. M. J. Rosen, *Surfactants and Interfacial Phenomena 2nd Ed.*, Wiley, New York, **1989**.
73. I. A. Kotzé, MSc. Thesis, *University of Stellenbosch*, 2009.
74. K. R. Koch, C. Sacht, C. Lawrence, *Dalton Trans.*, 1998, **4**, 689-695.
75. I. A. Kotzé, W. J. Gerber, J. M. Mckenzie, K. R. Koch, *Eur. J. Inorg. Chem.*, 2009, **12**, 1626-1633.
76. A. N. Mautjana, J. D. S. Miller, A. Gie, S. A. Bourne, K. R. Koch, *Dalton Trans.*, 2003, 1952-1960.
77. K. R. Koch, *Coord. Chem. Rev.*, 2001, **216–217**, 473-488.

2

Synthesis and Characterization of $[\text{Pt}^{\text{II}}(\text{diimine})(\text{L}^{\text{n}}-\text{S},\text{O})]\text{Cl}$ and $[\text{Pd}^{\text{II}}(\text{phen})(\text{L}^1-\text{S},\text{O})]\text{Cl}$ complexes

This chapter describes the synthetic procedures, detailed characterization and interesting features of the ^1H NMR spectra of a series of $[\text{M}^{\text{II}}(\text{diimine})(\text{L}^{\text{n}}-\text{S},\text{O})]\text{Cl}$ complexes and $\text{Pt}^{\text{II}}\text{Cl}_2(\text{diimine})$ precursors, with M = platinum(II) or palladium(II), diimine = 1,10-phenanthroline (phen) or 2,2-bipyridyl (bipy) and $\text{L}^{\text{n}}-\text{S},\text{O}$ represents various N,N -di(alkyl)- N' -acylthioureas. More specifically, the synthesis $[\text{Pt}^{\text{II}}(\text{phen})(\text{L}^{\text{n}}-\text{S},\text{O})]\text{Cl}$ complexes and their precursors will be discussed followed by the detailed characterization of one of these complexes, $[\text{Pt}^{\text{II}}(\text{phen})(\text{L}^1-\text{S},\text{O})]\text{Cl}$, where $\text{L}^1 = N$ -pyrrolidyl- N' -pivaloylthiourea. Thereafter, the synthesis of $[\text{Pt}^{\text{II}}(\text{bipy})(\text{L}^{\text{n}}-\text{S},\text{O})]^+$ complexes and precursors will be described and the crystal structure of a new form (polymorph) of $\text{Pt}^{\text{II}}(\text{bipy})\text{Cl}_2$ as an acetonitrile solvate, will be discussed. The synthesis and characterisation of $[\text{Pd}^{\text{II}}(\text{phen})(\text{L}^1-\text{S},\text{O})]^+$ and its precursors, $\text{Pd}^{\text{II}}_3(\text{OAc})_6$, $\text{Pd}^{\text{II}}\text{Cl}_2(\text{phen})$ and $\text{Pd}^{\text{II}}(\text{OAc})_2(\text{phen})$ will be presented followed by the synthesis and characterisation of $[\text{Pt}^{\text{II}}\text{Cl}(\text{DMSO})(\text{en})]\text{Cl}$, a cation platinum(II) complex without a ligand containing a π -surface. A number of interesting features of the ^1H NMR spectra of these $[\text{M}^{\text{II}}(\text{diimine})(\text{L}^{\text{n}}-\text{S},\text{O})]^+$ complexes will be presented and discussed. The last section of this chapter is the experimental section and contains the detailed synthetic procedures and characterization data. All these complexes will be tested for β -haematin inhibition, with the results shown in Chapter 5.

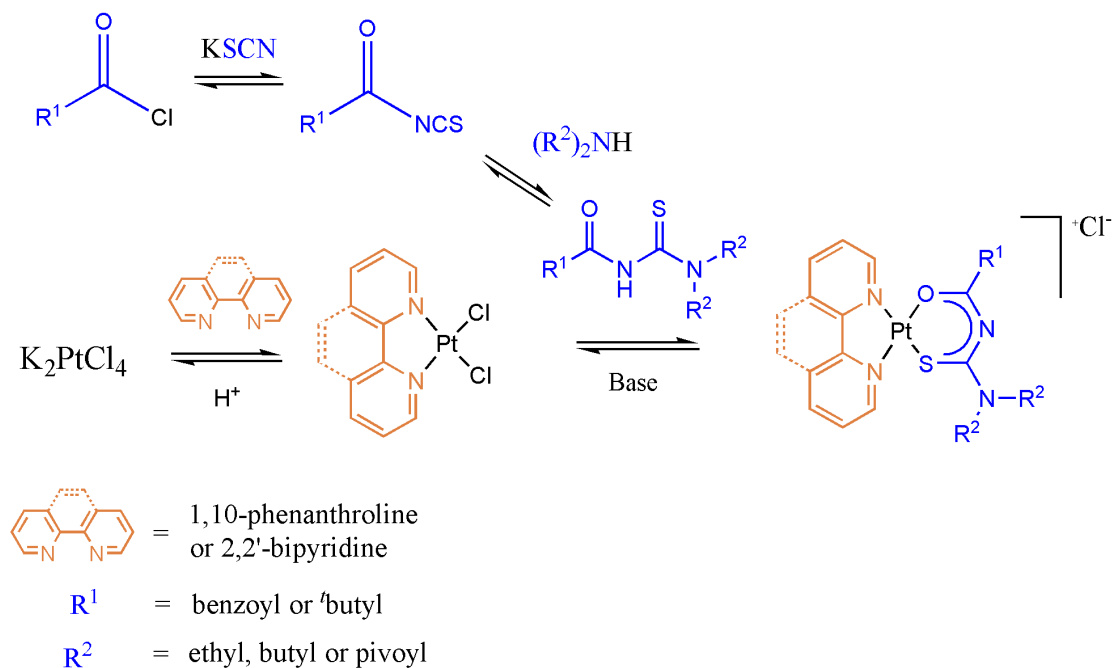
2.1 Introduction

The overall method of synthesis of platinum(II) complexes with the general structure $[\text{Pt}^{\text{II}}(\text{diimine})(\text{L}^{\text{n}}-\text{S},\text{O})]\text{X}$, where diimine is 1,10-phenanthroline or 2,2'-bipyridyl, L^{n} various *N,N*-di(alkyl)-*N'*-acylthiourea and $\text{X} = \text{PF}_6^-$ or Cl^- is well documented.¹⁻⁵ The potential anti-malarial activity of these mixed ligand complexes is thought to result from the combination of a electron-rich aromatic surface and cationic metal centre in one plane as a result of the coordination of the aromatic diimine moiety resulting in a preferred square-planar geometry of the platinum(II) complex.^{1,4} The diimine ligands are therefore thought to be the 'functional' ligand and the various *N,N*-di(alkyl)-*N'*-acylthiourea the ancillary ligand. Although it has recently been shown that some *bis-N,N*-di(alkyl)-*N'*-acylthiourea platinum complexes exhibit significant anti-bacterial activity,⁶ such uncharged *bis-N,N*-di(alkyl)-*N'*-acylthiourea platinum complexes are not expected to have any anti-malarial activity, which has been confirmed previously.²

The central postulate in this thesis is that the antimalarial activity of $[\text{Pt}^{\text{II}}(\text{diimine})(\text{L}^{\text{n}}-\text{S},\text{O})]\text{X}$ complexes arises from the non-covalent association of the square planar complex with haematin (iron porphyrin complex), a toxin present in the parasite from the digestion of haemoglobin.² Since it is known that the malaria parasite decreases the toxic levels of haematin by converting the haematin to insoluble haemozoin,⁷ any association of potential drug molecules to haematin to prevent this detoxification step is thought to ultimately lead to the death of the parasite. It was previously shown that $\text{Pt}^{\text{II}}(\text{diimine})(\text{L}^{\text{n}}-\text{S},\text{O})\text{X}$ complexes self-aggregate and associate to aromatic model compounds, which supports the potential cation- π binding of $\text{Pt}^{\text{II}}(\text{diimine})(\text{L}^{\text{n}}-\text{S},\text{O})\text{X}$ complexes with haematin.⁵ In this context, the interaction between $[\text{Pt}^{\text{II}}(\text{diimine})(\text{L}^{\text{n}}-\text{S},\text{O})]^+$ and haematin is believed to be a combination of cation- π and aromatic π -stacking interactions.¹⁻³

Koch and co-workers found that the 1,10-phenanthroline variation of $\text{Pt}^{\text{II}}(\text{diimine})(\text{L}^{\text{n}}-\text{S},\text{O})\text{X}$ exhibit significantly stronger binding affinities to the synthetic polynucleotide, polydA-PolydT, and also has larger self-association constants in 50% (v/v) water:acetonitrile solutions.⁸ The Gibbs energy (ΔG) of the self-association of these complexes in acetonitrile increases with increments of $2.4 \pm 0.4 \text{ kJ}\cdot\text{mol}^{-1}$ per aromatic ring of the diimine moiety coordinated to the complexes.¹

In this work, focus was placed mainly on 1,10-phenanthroline as the diimine moiety and the nature of *N'*-acyl-*N,N*-dialkylthiourea ligand was varied. A series of $\text{Pt}^{\text{II}}(1,10\text{-phenanthroline})(\text{L}^{\text{n}}\text{-S},\text{O})\text{Cl}$ complexes with the addition of two $\text{Pt}^{\text{II}}(2,2\text{-bipyridine})(\text{L}^{\text{n}}\text{-S},\text{O})\text{Cl}$ variations were synthesised as well as $\text{Pd}^{\text{II}}(\text{phen})(\text{L}^{\text{n}}\text{-S},\text{O})^+$ for comparison. The general reaction scheme for the synthesis of the series of platinum(II) complexes and precursors is shown in Scheme 2.1.



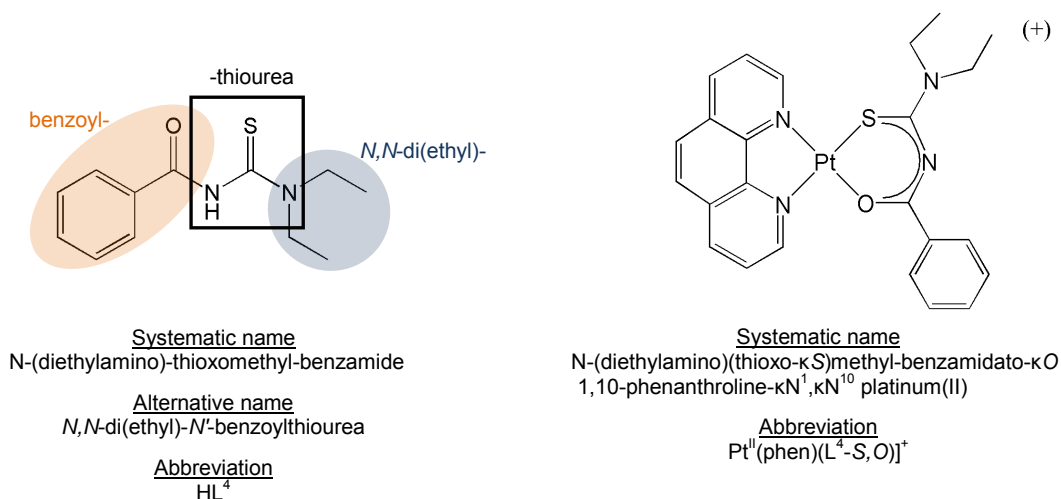
Scheme 2.1 General synthetic procedure for the synthesis of various $[\text{Pt}^{\text{II}}(\text{diimine})(\text{L}^{\text{n}}\text{-S},\text{O})\text{Cl}]$ complexes, where L^{n} represents various acyl-dialkylthioureas.

The first step in the synthesis involves the addition of the appropriate diimine as a solid to an acidic aqueous solution of $\text{K}_2[\text{Pt}^{\text{II}}\text{Cl}_4]$ to yield an insoluble $\text{Pt}^{\text{II}}(\text{diimine})\text{Cl}_2$ complex. The second step involves the reaction of the purified $\text{Pt}^{\text{II}}(\text{diimine})\text{Cl}_2$ from suspension with the appropriate *N,N*-di(alkyl)-*N'*-acylthiourea, previously prepared, to yield the desired mixed ligand platinum(II) complex (Scheme 2.1).

2.2 Synthesis of mixed ligand $[\text{Pt}^{\text{II}}(\text{diimine})(N,N\text{-di(alkyl)-}N'\text{-acylthiourea})]\text{Cl}$ complexes and precursors

2.2.1 Nomenclature for the ligands and complexes used in this study

In this study, the literature accepted common names or similar naming strategies for the ligands and complexes were used. For example, the ligand *N*-(diethylamino)-thioxomethyl-benzamide, which are called *N,N*-di(ethyl)-*N'*-benzoylthiourea, and the corresponding $[\text{Pt}^{\text{II}}(1,10\text{-phenanthroline})(N\text{-}(\text{diethylamino})\text{-thioxomethyl-benzamidato})]^+$ complex are shown in Scheme 2.2 together with their correct systematic names.



Scheme 2.2 Alternative naming of the ligands and complexes used in this study.

The alternative naming of the acylthiourea ligands comprise of an acyl-part (benzoyl in this case), *N*-bound dialkyl- (*N,N*-di(ethyl)-) and a thiourea-part as highlighted in Scheme 2.2. The abbreviation of this ligand is HL^4 in this study with HL indicating the protonated ligand and 4 an arbitrary number. Upon chelation/coordination of the deprotonated ligand *via* the sulphur and oxygen donor atoms, the notation becomes $\text{L}^4\text{-S,O}$ as shown for the $\text{Pt}^{\text{II}}(\text{phen})(\text{L}^4\text{-S,O})^+$ complex (Scheme 2.2).

2.2.2 Synthesis of the *N,N*-di(alkyl)-*N'*-acylthiourea ligands

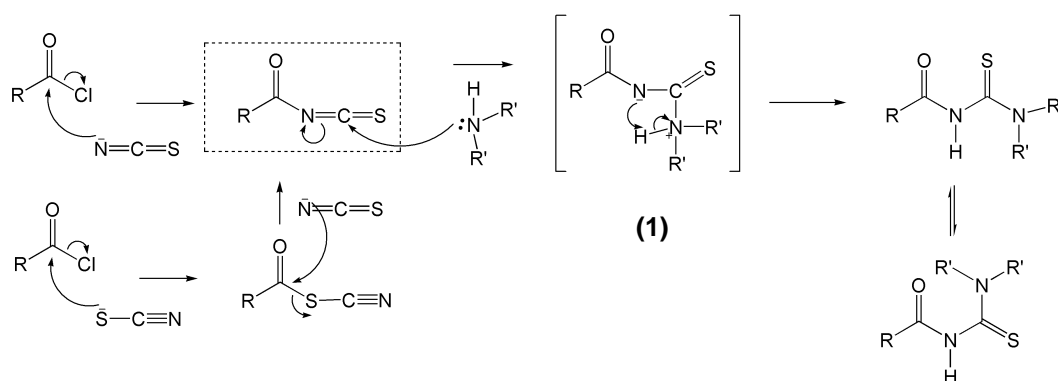
The synthesis of *N,N*-di(alkyl)-*N'*-acylthioureas was almost 90 years ago described by Douglas and Dains.⁹ This synthesis involves reaction of potassium thiocyanate with an acyl

chloride in which thiocyanate acts as a nucleophile, attacking the acyl chloride to release a chloride ion which precipitates with the K^+ in anhydrous acetone. Thiocyanate undergoes thermal isomerisation to form the isothiocyanate anion which is thought to be the 'active' form of the nucleophile for the synthesis of acylthiourea ligands.¹⁰



Scheme 2.3 Thermal isomerisation of thiocyanate and isothiocyanate¹⁰

The reaction of the thiocyanate isomer with acyl chloride yields an unstable product which rapidly reacts with the preferred isothiocyanate isomer to form mainly the acylisothiocyanate intermediate (Scheme 2.4).¹⁰



Scheme 2.4 Proposed reaction mechanism for the synthesis of *N,N*-di(alkyl)-*N'*-acylthiourea ligands. The dashed rectangle shows the desired product of the first step of the reaction. This product reacts with an amine to form the donor-acceptor intermediate indicated by **(1)**.

The acylisothiocyanate intermediate can react with an amine which acts as a nucleophile and mainly attacks the thiocarbonyl carbon of acylisothiocyanate in polar solvents to yield the elusive donor-acceptor intermediate **(1)** (Scheme 2.4).¹¹ It has been suggested by Elmore and co-workers that the proton transfer takes place after the unstable donor-acceptor complex has been formed to yield the desired *N,N*-di(alkyl)-*N'*-acylthiourea ligand.¹¹

The ligand *N*-pyrrolidyl-*N'*-pivaloylthiourea (HL^1) was synthesised by the reaction of isothiocyanate with pivaloyl chloride to yield the crude pivaloylisothiocyanate intermediate to which pyrrolidine was added to yield a crude HL^1 which was obtained by re-crystallization (yield 76%). The 1H and ^{13}C NMR spectra of HL^1 in chloroform- d_1 are shown in Figure 2.1.

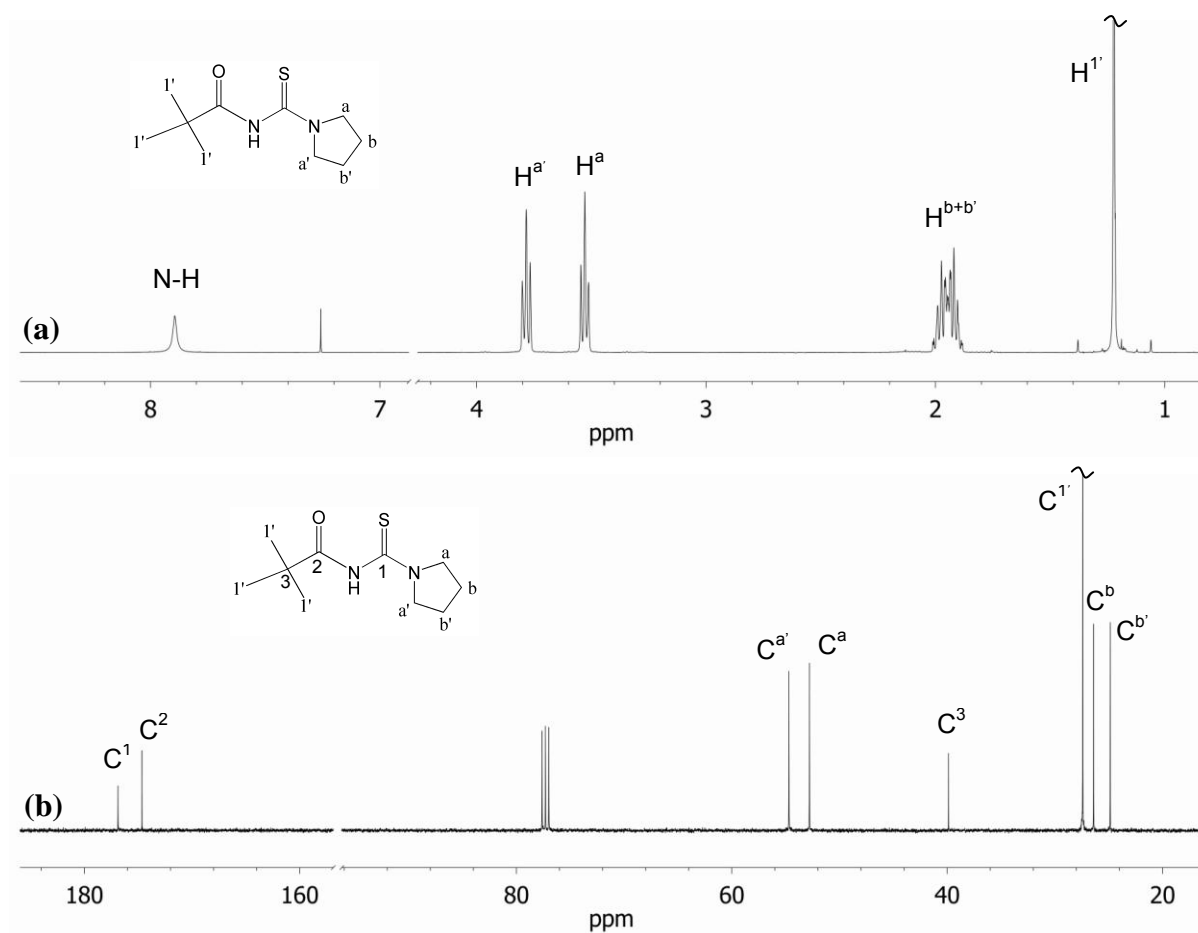
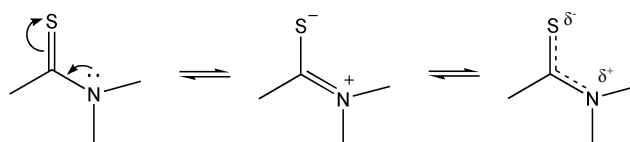


Figure 2.1 (a) ^1H NMR spectrum and assignments and (b) ^{13}C NMR spectrum and assignments of *N*-pyrrolidyl-*N'*-pivaloylthiourea (HL^1) in CDCl_3 .

The N-H proton could be easily assigned to the broad singlet observed at 7.88 ppm which is in the typical downfield chemical shift range of N-H protons of this type. The singlet at 1.23 ppm was assigned to $\text{H}^{1'}$ as it integrates for 9 H's. Interestingly, all the $-\text{CH}_2-$ groups are magnetically inequivalent and 4 sets of signals are observed for the pyrrolidyl part of the molecule. This suggests significant restricted rotation around the bond between the thiocarbonyl carbon and the pyrrolidyl nitrogen as illustrated by Scheme 2.5.

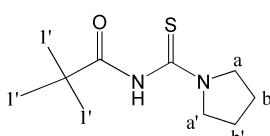
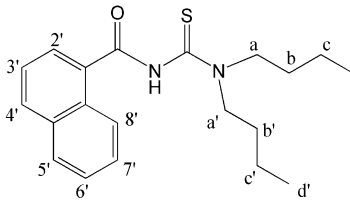
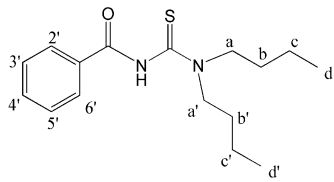
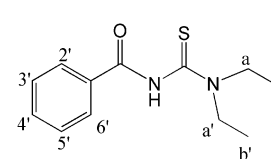
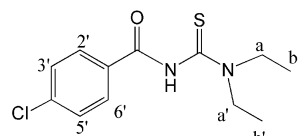
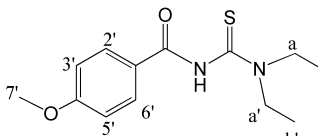
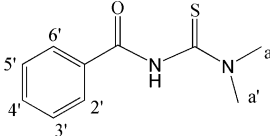
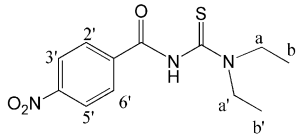
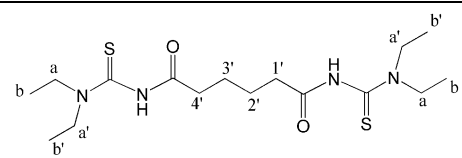
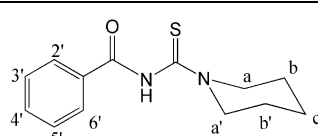
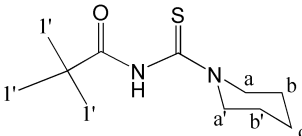
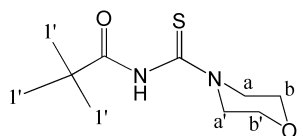
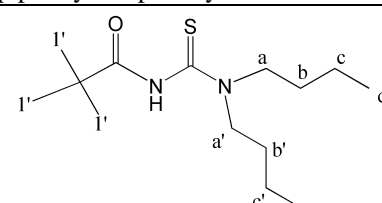
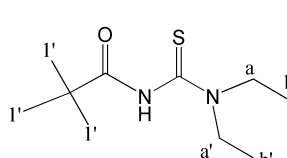


Scheme 2.5 Restricted rotation in *N,N*-di(alkyl)-*N'*-acylthiourea ligands.

Therefore the 4 sets of resonance signals integrate for two protons each with the two more downfield quasi-triplets assigned to $\text{H}^{a'}$ and H^a respectively and the two overlapping pentets assigned to H^b and $\text{H}^{b'}$ as suggested previously by Koch and co-workers.¹²

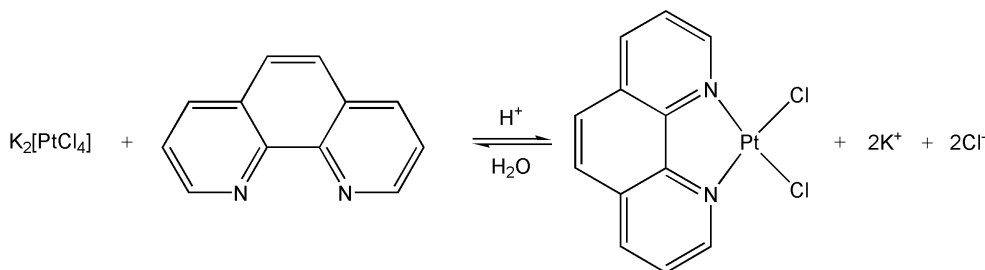
Table 2.1 lists the *N,N*-di(alkyl)-*N'*-acylthioureas used in this study, together with their alternative names and numbering schemes.

Table 2.1 Ligands numbering, alternative names and abbreviations used in this study

Ligand name, numbering and abbreviation	Ligand name, numbering and abbreviation
 HL^1 <i>N</i> -pyrrolydyl- <i>N'</i> -pivaloylthiourea	 HL^2 <i>N,N</i> -di(<i>n</i> -butyl)- <i>N'</i> -1-naphthoylthiourea
 HL^3 <i>N,N</i> -di(<i>n</i> -butyl)- <i>N'</i> -benzoylthiourea	 HL^4 <i>N,N</i> -diethyl- <i>N'</i> -benzoylthiourea
 HL^5 <i>N,N</i> -diethyl- <i>N'</i> -4-chlorobenzoylthiourea	 HL^6 <i>N,N</i> -diethyl- <i>N'</i> -4-methoxybenzoylthiourea
 HL^7 <i>N,N</i> -dimethyl- <i>N'</i> -benzoylthiourea	 HL^8 <i>N,N</i> -diethyl- <i>N'</i> -4-nitrobenzoylthiourea
 HL^9 <i>bis</i> -(<i>N,N</i> -diethyl)- <i>N'</i> -adipoylthiourea	 HL^{10} <i>N</i> -piperidyl- <i>N'</i> -benzoylthiourea
 HL^{11} <i>N</i> -piperidyl- <i>N'</i> -pivaloylthiourea	 HL^{12} <i>N</i> -morpholinyl- <i>N'</i> -pivaloylthiourea
 HL^{13} <i>N,N</i> -di(<i>n</i> -butyl)- <i>N'</i> -pivaloylthiourea	 HL^{14} <i>N,N</i> -diethyl- <i>N'</i> -pivaloylthiourea

2.2.3 Synthesis of $\text{Pt}^{\text{II}}\text{Cl}_2(1,10\text{-phenanthroline})$

The $\text{Pt}^{\text{II}}\text{Cl}_2(\text{phen})$ precursor was synthesised according to the method described by Morgan and Burstall¹³ in which 1 equivalent of 1,10-phenanthroline was added to $\text{K}_2[\text{Pt}^{\text{II}}\text{Cl}_4]$ in acidic (HCl) aqueous solution and heated to reflux for two hours, during which time the pure product precipitated (Scheme 2.4).



Scheme 2.6 Reaction between $[\text{Pt}^{\text{II}}\text{Cl}_4]^{2-}$ and 1,10-phenanthroline in acidified water to yield the yellow $\text{Pt}^{\text{II}}\text{Cl}_2(\text{phen})$ as a precipitate.

The reaction time was extended to an overnight reaction (~14 hours) to ensure complete conversion with yields almost quantitative (90-98%). The role of the acid (HCl) in the synthesis of $\text{Pt}^{\text{II}}\text{Cl}_2(\text{phen})$ was investigated since it seemed unnecessary, apart from suppressing the hydrolysis of $[\text{Pt}^{\text{II}}\text{Cl}_4]^{2-}$. In acidic solution the protonation of phen is expected to compete with the coordination reaction and consequently NaCl was used instead of HCl to minimize the hydrolysis of $[\text{Pt}^{\text{II}}\text{Cl}_4]^{2-}$ with no compromise to the reaction yield. In the absence of any additional Cl^- in solution (1,10-phenanthroline and $[\text{Pt}^{\text{II}}\text{Cl}_4]^{2-}$ only), the reaction also yielded the desired product with the typical yield (>90%). However, the presence of HCl significantly increases the solubility of the 1,10-phenanthroline ligand in water which shortens the reaction time slightly. The $\text{Pt}^{\text{II}}\text{Cl}_2(\text{phen})$ product was characterized using ^1H NMR in dimethylsulfoxide- d_6 (Figure 2.2) and elemental analysis.

The ^1H NMR spectra of $\text{Pt}^{\text{II}}\text{Cl}_2(\text{phen})$ and 1,10-phenanthroline monohydrate in dimethyl sulfoxide- d_6 reveals a retention of the symmetry of the ^1H signals of the ligand upon coordination while a large downfield shift of all the ^1H resonances is observed. This downfield shift is indicative of the change in the electronic structure of the ligand as a result of the nitrogens donating their unpaired electrons into the empty d-orbitals of the platinum metal centre.

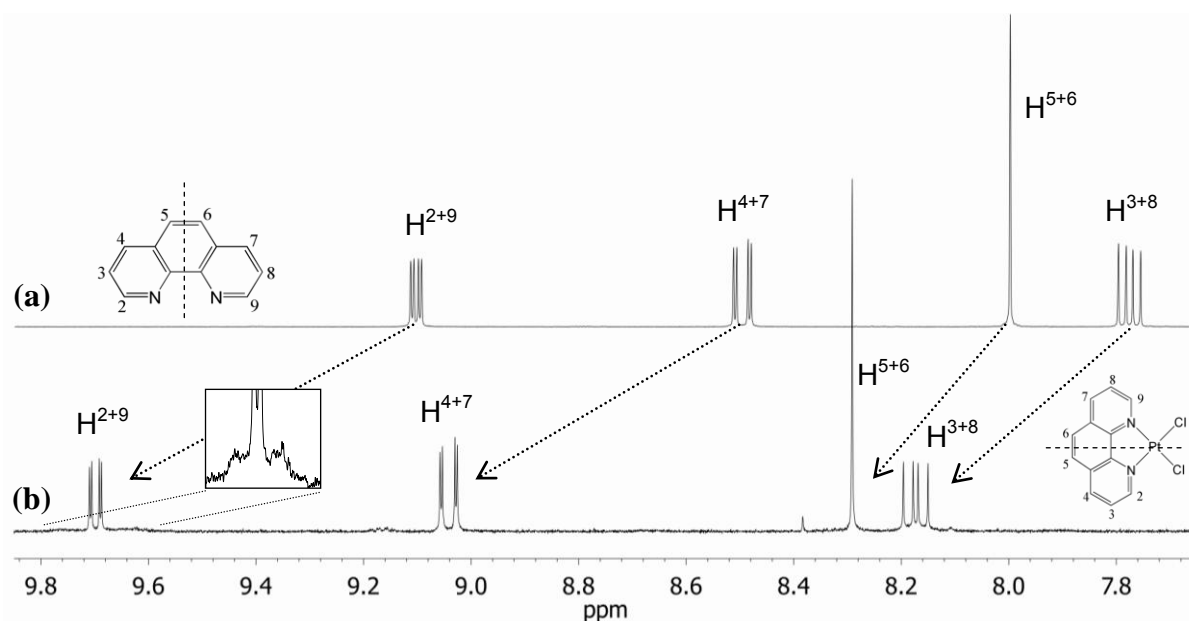


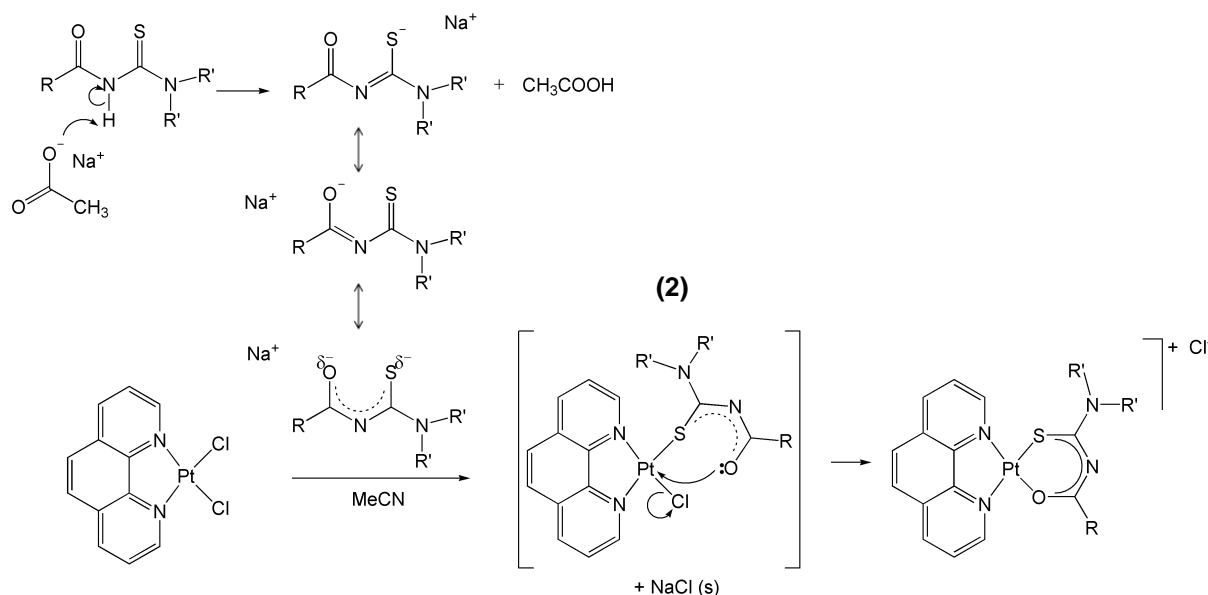
Figure 2.2 The changes in the ¹H NMR resonances of the 1-10-phenanthroline moiety (a) in dimethyl sulfoxide-d₆ upon coordination to form the Pt^{II}Cl₂(phen) precursor (b) ${}^3J({}^{195}\text{Pt}-{}^1\text{H}) = 38 \text{ Hz}$.

Considering the ¹H NMR spectrum of Pt^{II}Cl₂(phen) in dimethyl sulfoxide-d₆ (Figure 2.2b), the singlet resonance at 8.29 ppm could be assigned to H⁵⁺⁶ since no ${}^3J({}^1\text{H}-{}^1\text{H})$ coupling was observed. The doublet of doublets at 8.17 ppm which is made up of two relatively large coupling constants (${}^3J = 8.2 \text{ Hz}$ and 5.5 Hz) could be assigned to H³⁺⁸. The resonance at 9.70 ppm is also a doublet of doublets with small unresolved platinum satellites, ${}^3J({}^{195}\text{Pt}-{}^1\text{H}) = 38\text{Hz}$, as highlighted in the inset in Figure 2.2b and could be assigned to H²⁺⁹, which is 3 bonds from the platinum metal centre. The remaining doublet of doublets at 9.04 ppm was assigned to H⁴⁺⁷.

2.2.4 Synthesis of [Pt^{II}(1,10-phenanthroline)(*N,N*-di(alkyl)-*N'*-acylthiourea)]Cl complexes

A series of [Pt^{II}(phen)(*N,N*-di(alkyl)-*N'*-acylthiourea)]Cl complexes and precursors have been synthesized and characterized with the abbreviations and numbering of the ligands and respective complexes used in this study summarised in Table 2.2. The metal precursor, Pt^{II}Cl₂(phen), is used since the 1,10-phenanthroline coordinates strongly to the Pt(II) metal centre and remains coordinated to prevent more than one *N,N*-di(alkyl)-*N'*-acylthiourea (HLⁿ) to coordinate to Pt as happens for [PtCl₄]²⁻.

The synthesis of $[\text{Pt}^{\text{II}}(\text{phen})(\text{L}^{\text{n}}-\text{S},\text{O})]\text{Cl}$ involves the reaction of $\text{Pt}^{\text{II}}\text{Cl}_2(\text{phen})$ from suspension in acetonitrile with the N,N -di(alkyl)- N' -acylthiourea (L^{n}) to form the desirable soluble $[\text{Pt}^{\text{II}}(\text{phen})(\text{L}^{\text{n}}-\text{S},\text{O})]\text{Cl}$ complex (typical yields >70%). The proposed reaction pathway is shown in Scheme 2.7.



Scheme 2.7 Proposed reaction details for the synthesis of $[\text{Pt}^{\text{II}}(\text{phen})(N,N\text{-di(alkyl)-}N'\text{-acylthiourea})]\text{Cl}$ complexes from $\text{Pt}^{\text{II}}\text{Cl}_2(\text{phen})$ and the appropriate N,N -di(alkyl)- N' -acylthiourea in acetonitrile with NaOAc as base.

It has been suggested that the sulphur atom of the acylthiourea replaces one of the chlorides of the $\text{Pt}^{\text{II}}\text{Cl}_2(\text{phen})$ (see intermediate **(2)** in Scheme 2.7) since sulphur is known to be more nucleophilic and has a strong affinity for platinum(II), which is considered a ‘soft’ metal according to Pearson’s HSAB theory.¹⁴ The chelate is formed by the coordination of a lone pair of electrons of the oxygen after deprotonation of the ligand ($\text{HL}^{\text{n}} \rightarrow \text{L}^{\text{n}}$) using sodium acetate (NaOAc). The displaced Cl^- forms insoluble NaCl , which precipitates as a fine white powder from the reaction mixture. After the completion of reaction, NaCl(s) , traces of unreacted $\text{Pt}^{\text{II}}\text{Cl}_2(\text{phen})$ and excess NaOAc are filtered off. The $[\text{Pt}^{\text{II}}(\text{phen})(\text{L}^{\text{n}}-\text{S},\text{O})]\text{Cl}$ complex can be precipitated from solution by the addition of cold diethyl ether. Excess ligand and conjugate acid (AcOH) formed during the reaction were removed by extensive washing with cold diethyl ether.

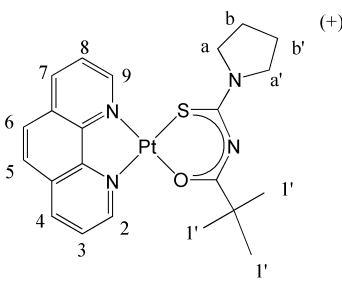
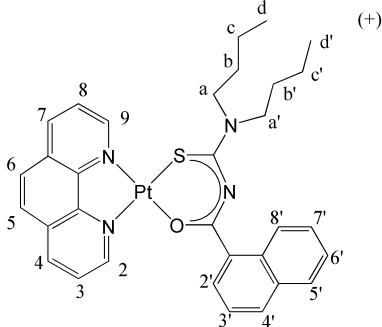
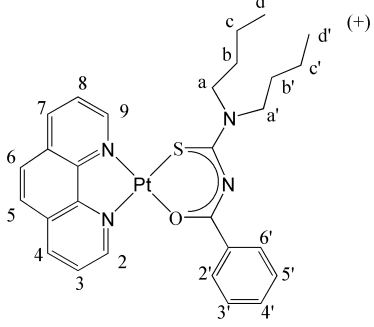
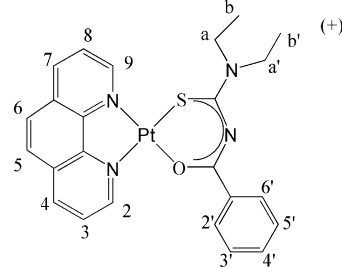
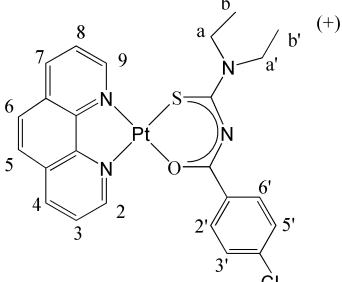
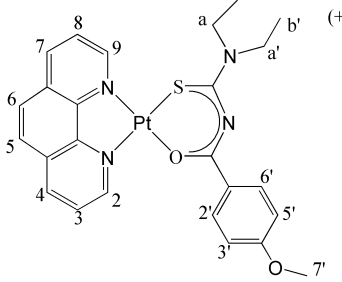
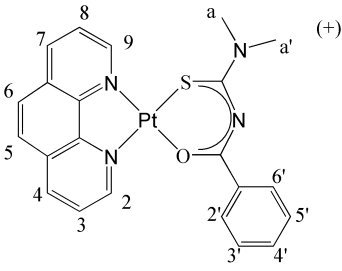
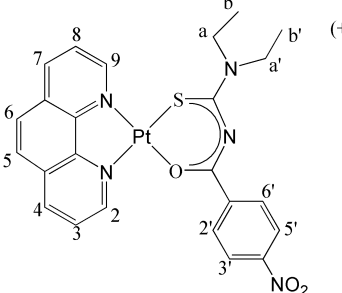
Variation of the solvent in which this preparation is carried out, from acetonitrile, methanol and dichloromethane as well as substituting the base (NaOAc) with triethylamine results in no significant changes in the yields.

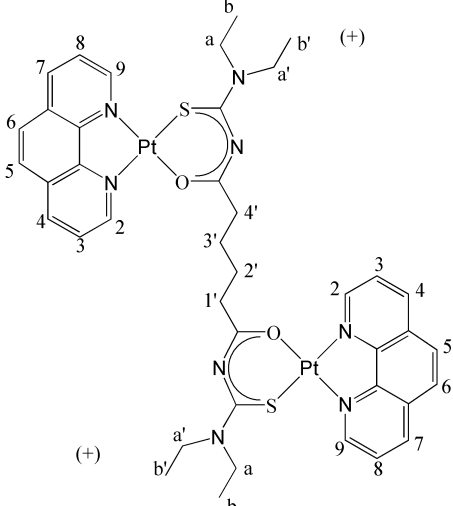
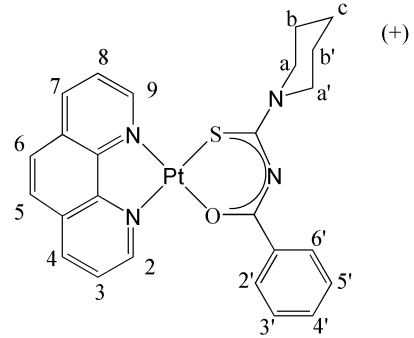
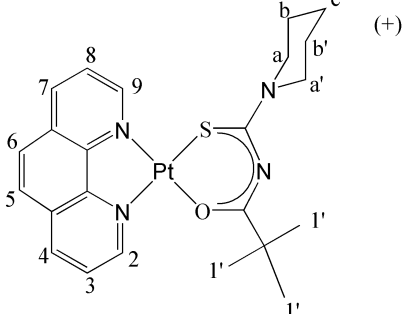
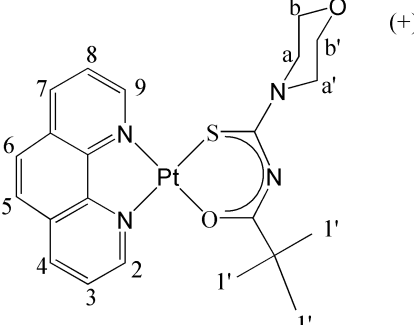
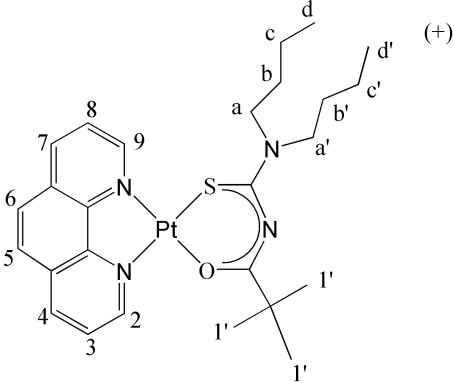
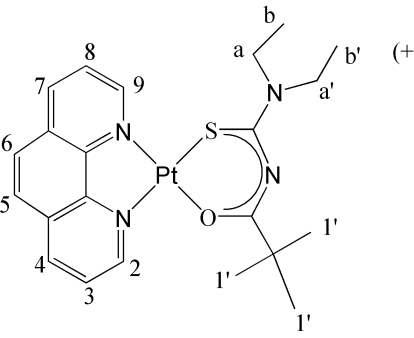
In this study the purification of this class of complexes proved to be difficult for the complexes with Cl^- as counter-ion, as compared to the PF_6^- salt as reported previously.⁸ Purification by column chromatography with Silica gel (SiO_2) as stationary phase failed since the $[\text{Pt}^{\text{II}}(\text{phen})(\text{L}^n\text{-S},\text{O})]^+$ has such a strong affinity for the silica that neither methanol nor acidic water were able to elute the product. However, it was found that neutral to basic chromatographic aluminium oxide (Al_2O_3) works well with small amounts of methanol in the mixed eluents (methanol/dichloromethane or methanol/acetonitrile) to elute the desired complex from the column.

In some cases the acetonitrile of the reaction mixture is polar enough to elute the product with the starting materials and by-products, in which case the acetonitrile was evaporated by heating under reduced pressure, and redissolving the reaction mixture in less polar dichloromethane. The precipitate consisting of mainly NaOAc and NaCl was filtered off and the sample in dichloromethane was introduced onto the column. The pure $\text{Pt}^{\text{II}}(\text{phen})(\text{L}^n\text{-S},\text{O})\text{Cl}$ was obtained by eluting any unreacted $\text{Pt}^{\text{II}}\text{Cl}_2(\text{phen})$ and HL^n together with unwanted $\text{Pt}^{\text{II}}(\text{phen})(\text{L}^n\text{-S})_2$ with dichloromethane while $[\text{Pt}^{\text{II}}(\text{phen})(\text{L}^n\text{-S},\text{O})\text{Cl}]$ was retained. The pure $[\text{Pt}^{\text{II}}(\text{phen})(\text{L}^n\text{-S},\text{O})\text{Cl}]$ was eluted by the addition of methanol to the eluent. The $[\text{Pt}^{\text{II}}(\text{phen})(\text{L}^n\text{-S},\text{O})\text{Cl}]$ complex was isolated by removing the solvent with heating under reduced pressure and dried in a vacuum desiccator. Characterization of the complexes was done using various one- and two-dimensional NMR techniques (see Section 2.3) as well as Mass Spectrometry and Elemental Analysis. All $[\text{Pt}^{\text{II}}(\text{phen})(\text{L}^n\text{-S},\text{O})\text{Cl}]$ complexes synthesised are listed in Table 2.2 with all corresponding names and abbreviations used.

However, for a few of the HL^n ligands, the yields were significantly lower, especially for HL^2 , HL^3 (40-50%) and the reactions in methanol which was attributed to the formation of *bis*-monodentate-*N,N*-di(alkyl)-*N'*-acylthiourea 1,10-phenanthroline platinum(II) complexes ($\text{Pt}^{\text{II}}(\text{phen})(\text{L}^n\text{-S})_2$); these reactions will be discussed in Chapter 3.

Table 2.2 Complexes numbering and abbreviated names used in this work.

Complex name numbering and abbreviation	Complex name numbering and abbreviation
 <p data-bbox="375 638 598 672">$[\text{Pt}^{\text{II}}(\text{phen})(\text{L}^1\text{-S},\text{O})]^+$</p> <p data-bbox="255 683 726 739">$[\text{Pt}^{\text{II}}(1,10\text{-phenanthroline})(N\text{-pyrrolidyl-}N'\text{-pivaloylthiourea})]^+$</p>	 <p data-bbox="997 638 1220 672">$[\text{Pt}^{\text{II}}(\text{phen})(\text{L}^2\text{-S},\text{O})]^+$</p> <p data-bbox="861 683 1356 739">$[\text{Pt}^{\text{II}}(1,10\text{-phenanthroline})(N,N\text{-di}(n\text{-butyl})\text{-}N'\text{-naphthoylthiourea})]^+$</p>
 <p data-bbox="375 1086 598 1120">$[\text{Pt}^{\text{II}}(\text{phen})(\text{L}^3\text{-S},\text{O})]^+$</p> <p data-bbox="239 1131 742 1187">$[\text{Pt}^{\text{II}}(1,10\text{-phenanthroline})(N,N\text{-di}(n\text{-butyl})\text{-}N'\text{-benzoylthiourea})]^+$</p>	 <p data-bbox="997 1086 1220 1120">$[\text{Pt}^{\text{II}}(\text{phen})(\text{L}^4\text{-S},\text{O})]^+$</p> <p data-bbox="877 1131 1340 1187">$[\text{Pt}^{\text{II}}(1,10\text{-phenanthroline})(N,N\text{-diethyl-}N'\text{-benzoylthiourea})]^+$</p>
 <p data-bbox="375 1500 598 1534">$[\text{Pt}^{\text{II}}(\text{phen})(\text{L}^5\text{-S},\text{O})]^+$</p> <p data-bbox="247 1545 734 1601">$[\text{Pt}^{\text{II}}(1,10\text{-phenanthroline})(N,N\text{-diethyl-}N'\text{-4-chlorobenzoylthiourea})]^+$</p>	 <p data-bbox="997 1500 1220 1534">$[\text{Pt}^{\text{II}}(\text{phen})(\text{L}^6\text{-S},\text{O})]^+$</p> <p data-bbox="869 1545 1348 1601">$[\text{Pt}^{\text{II}}(1,10\text{-phenanthroline})(N,N\text{-diethyl-}N'\text{-4-methoxybenzoylthiourea})]^+$</p>
 <p data-bbox="375 1926 598 1960">$[\text{Pt}^{\text{II}}(\text{phen})(\text{L}^7\text{-S},\text{O})]^+$</p> <p data-bbox="247 1971 734 2027">$[\text{Pt}^{\text{II}}(1,10\text{-phenanthroline})(N,N\text{-dimethyl-}N'\text{-benzoylthiourea})]^+$</p>	 <p data-bbox="997 1926 1220 1960">$[\text{Pt}^{\text{II}}(\text{phen})(\text{L}^8\text{-S},\text{O})]^+$</p> <p data-bbox="869 1971 1348 2027">$[\text{Pt}^{\text{II}}(1,10\text{-phenanthroline})(N,N\text{-diethyl-}N'\text{-4-nitrobenzoylthiourea})]^+$</p>

Complex name numbering and abbreviation	Complex name numbering and abbreviation
 <p data-bbox="236 779 746 880"> $\text{Pt}^{\text{II}}_2(\text{phen})_2(\text{L}^9\text{-S},\text{O})^{2+}$ <i>[bis-Pt^{II}(1,10-phenanthroline)(N,N-diethyl)-N'-adipoylthiourea]²⁺</i> </p>	 <p data-bbox="877 779 1337 880"> $[\text{Pt}^{\text{II}}(\text{phen})(\text{L}^{10}\text{-S},\text{O})]^+$ <i>[Pt^{II}(1,10-phenanthroline)(N-piperidyl)-N'-benzoylthiourea]⁺</i> </p>
 <p data-bbox="258 1243 718 1339"> $[\text{Pt}^{\text{II}}(\text{phen})(\text{L}^{11}\text{-S},\text{O})]^+$ <i>[Pt^{II}(1,10-phenanthroline)(N-piperidyl)-N'-pivaloylthiourea]⁺</i> </p>	 <p data-bbox="858 1243 1353 1339"> $[\text{Pt}^{\text{II}}(\text{phen})(\text{L}^{12}\text{-S},\text{O})]^+$ <i>[Pt^{II}(1,10-phenanthroline)(N-morpholinyl)-N'-pivaloylthiourea]⁺</i> </p>
 <p data-bbox="236 1747 742 1843"> $[\text{Pt}^{\text{II}}(\text{phen})(\text{L}^{13}\text{-S},\text{O})]^+$ <i>[Pt^{II}(1,10-phenanthroline)(N,N-di(n-butyl)-N'-pivaloylthiourea]⁺</i> </p>	 <p data-bbox="877 1747 1337 1843"> $[\text{Pt}^{\text{II}}(\text{phen})(\text{L}^{14}\text{-S},\text{O})]^+$ <i>[Pt^{II}(1,10-phenanthroline)(N,N-diethyl)-N'-pivaloylthiourea]⁺</i> </p>

2.3 Detailed characterization of $[\text{Pt}^{\text{II}}(\text{phen})(\text{L}^1\text{-S,O})]\text{Cl}$ by ^1H , COSY, HMBC, and NOESY NMR

The ^1H NMR spectrum of $[\text{Pt}^{\text{II}}(\text{phen})(\text{L}^1\text{-S,O})]\text{Cl}$ (Figure 2.3) is relatively uncomplicated compared to those of the other $[\text{Pt}^{\text{II}}(\text{phen})(\text{L}^{2-14}\text{-S,O})]\text{Cl}$ complexes since the 1,10-phenanthroline (phen) and *N*-pirrolidyl-*N'*-pivaloylthiourea (L^1) ^1H peak appear in different regions of the ^1H NMR spectrum. (see Appendix Figure A.1 to A.13).

The ^1H NMR spectrum of $\text{Pt}^{\text{II}}\text{Cl}_2(\text{phen})$ (Figure 2.3a) was used as a starting point in assigning the aromatic protons in the ^1H NMR spectrum of $[\text{Pt}^{\text{II}}(\text{phen})(\text{L}^1\text{-S,O})]\text{Cl}$ Figure 2.3b. The ^1H NMR spectrum of $\text{Pt}^{\text{II}}\text{Cl}_2(\text{phen})$ consist of only 4 sets of signals which accounts for the 8 H's as assigned previously (Figure 2.2b). In the $[\text{Pt}^{\text{II}}(\text{phen})(\text{L}^1\text{-S,O})]\text{Cl}$ complex the symmetry of the 1,10-phenanthroline ligand is lifted and one expects to see at least 8 sets of ^1H peaks in the aromatic region.

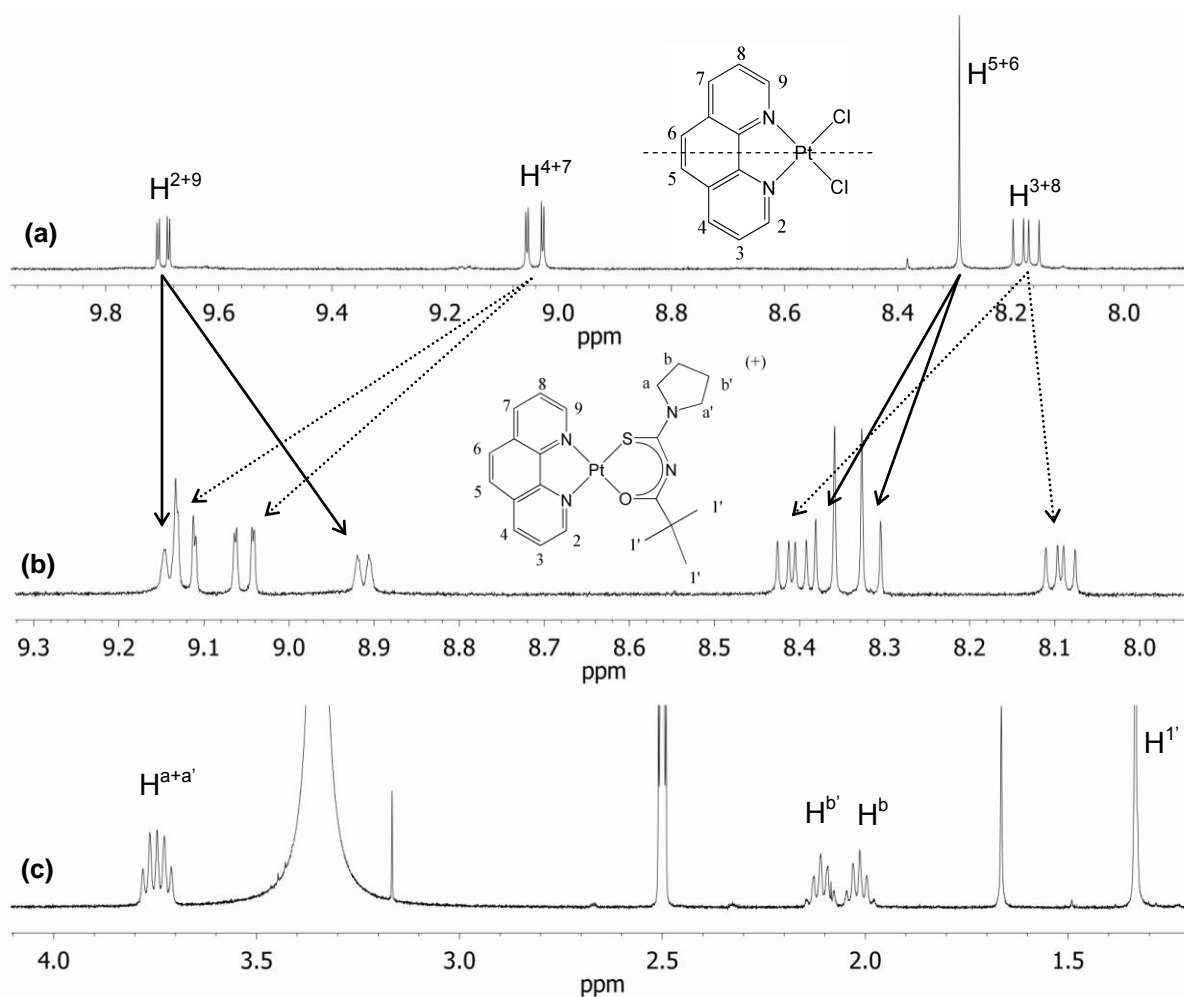


Figure 2.3 The ^1H NMR spectra of (a) the precursor $\text{Pt}^{\text{II}}\text{Cl}_2(\text{phen})$, (b) the aromatic region (c) the aliphatic region of $[\text{Pt}^{\text{II}}(\text{phen})(\text{L}^1\text{-S,O})]\text{Cl}$ in dimethyl sulfoxide- d_6 .

Using the features of the ^1H NMR spectrum of $\text{Pt}^{\text{II}}\text{Cl}_2(\text{phen})$, two possible assignments for each set of 1,10-phenanthroline resonances in the $[\text{Pt}^{\text{II}}(\text{phen})(\text{L}^1\text{-S,O})]\text{Cl}$ complex could be considered (Figure 2.3b). The most downfield singlet at 1.33 ppm integrates for 9 H's and could be unambiguously assigned as the pivaloyl protons, $\text{H}^{\text{I}'}$. The multiplicities of the other aliphatic ^1H resonances were used to make assignments, with the resonances at 3.73 and 3.78 ppm either H^{a} or $\text{H}^{\text{a}'}$ while the pentets at 2.12 and 2.03 ppm are H^{b} or $\text{H}^{\text{b}'}$. The $J(^1\text{H}\text{-}^1\text{H})$ coupling constants of these multiplets could not be used to further distinguish between the similar H's since these coupling constants are more or less of the same magnitude. Therefore, two-dimensional NMR techniques which give coupling information were required of which COSY (Homonuclear Correlation Spectroscopy) is commonly used for this purpose. This technique gives a two-dimensional plot with the ^1H NMR spectra on each dimension; cross-peaks off the diagonal (indicated by line in Figure 2.4) indicate relatively strong (e.g. $^3J > 5.0$ Hz) scalar coupling between the protons on the vertical and horizontal shown in Figure 2.4.

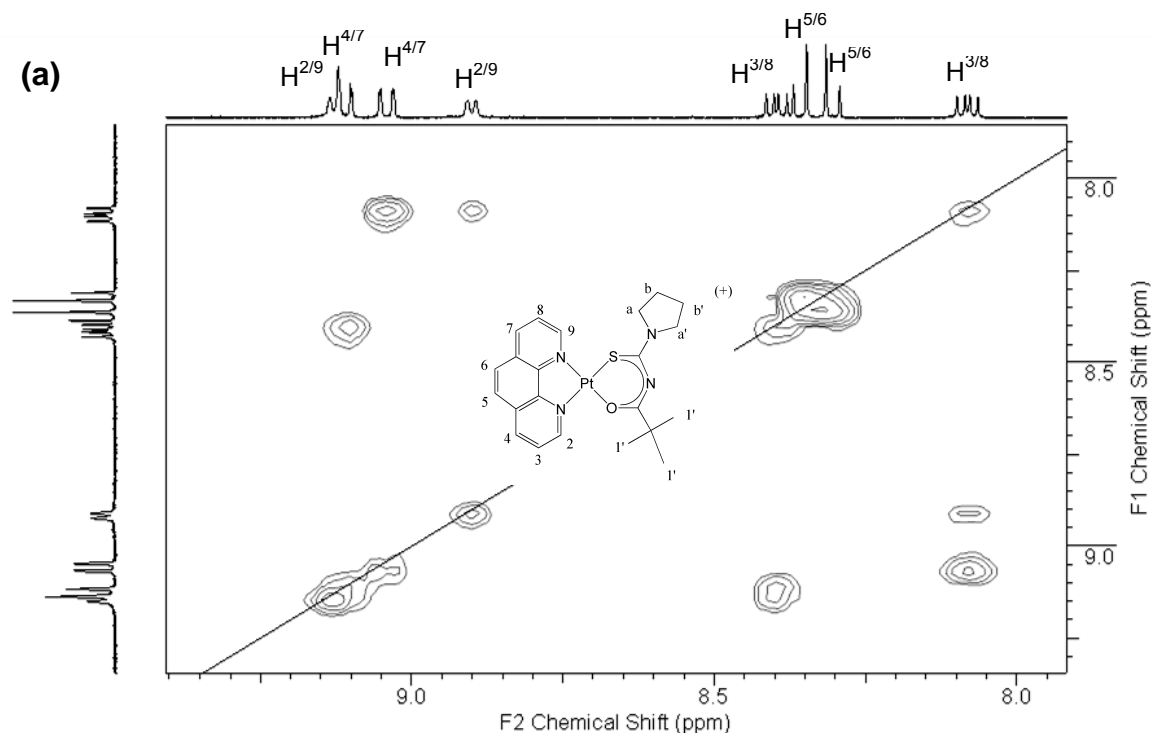


Figure 2.4 $^1\text{H}, ^1\text{H}$ COSY spectrum of $\text{Pt}^{\text{II}}(\text{phen})(\text{L}^1\text{-S,O})\text{Cl}$ in acetonitrile- d_3 where (a) is the COSY spectrum of the aromatic region and (b) the aliphatic region of the spectrum.

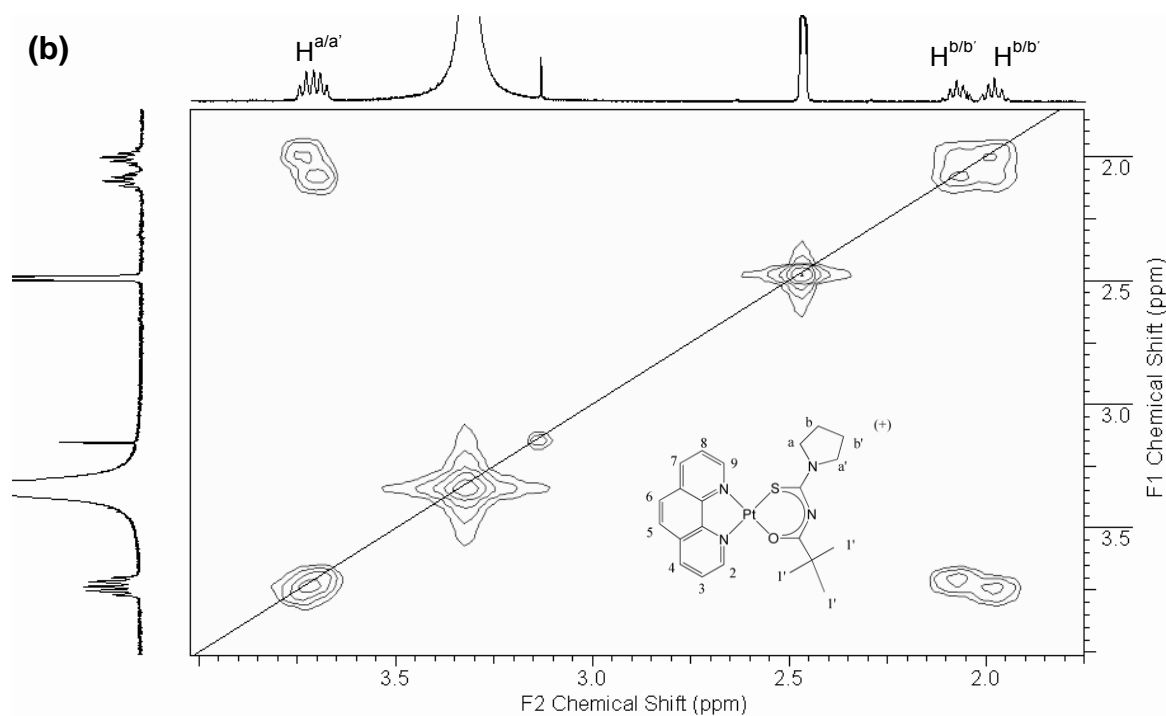


Figure 2.4 ^1H , ^1H COSY spectrum of $\text{Pt}^{\text{II}}(\text{phen})(\text{L}^1\text{-S},\text{O})\text{Cl}$ in acetonitrile- d_3 where (a) is the COSY spectrum of the aromatic region and (b) the aliphatic region of the spectrum.

The COSY experiment was optimised for the typical 3J proton couplings, with the result that all expected coupling correlations are observed. However, the unambiguous assignment of the ^1H NMR spectrum is not possible without an initial assignment. Previously the initial assignment was made based on the ^{15}N chemical shift of N^1 and N^2 and its correlation (scalar coupling) with the nearby H's in the phen moiety.⁵ This information was obtained using the ^1H , ^{15}N indirect detected HMBC (Heteronuclear Multiple Bond Correlation) NMR experiment which gives the chemical shift of the ^{15}N as well as the coupling correlation to the protons which could be optimised for 2J coupling between $\text{N}^1\text{-H}^2$ and $\text{N}^{10}\text{-H}^9$ respectively. The indirect detected HMBC method is preferred for obtaining ^{15}N chemical shifts due to the indirect detection of ^{15}N via the sensitive ^1H nuclide which makes it more sensitive than conventional ^{15}N NMR. The ^1H , ^{15}N HMBC plot obtained for $[\text{Pt}^{\text{II}}(\text{phen})(\text{L}^1\text{-S},\text{O})\text{Cl}]$ in acetonitrile- d_3 (Figure 2.5) shows positive correlation peaks for 3 nitrogens.

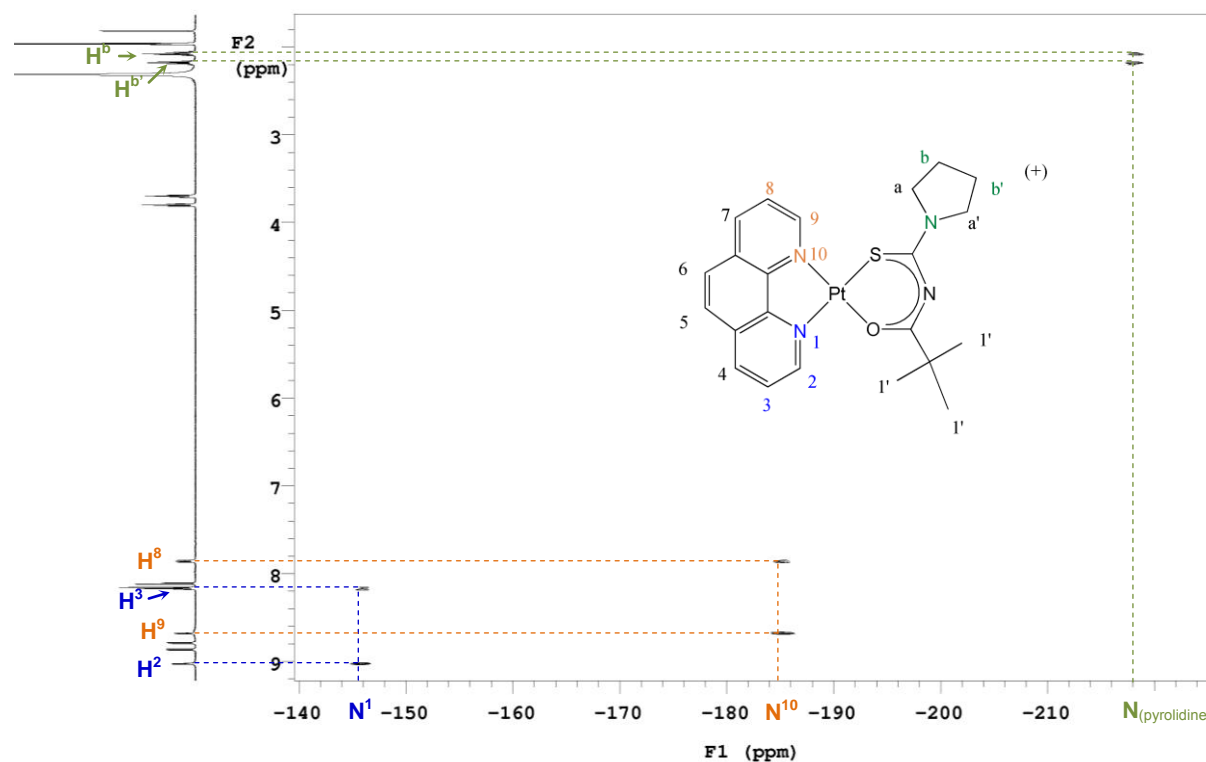


Figure 2.5 $^1\text{H},^{15}\text{N}$ HMBC plot of $[\text{Pt}^{\text{II}}(\text{phen})(\text{L}^1\text{-O,S})]\text{Cl}$ showing the ^1H and ^{15}N correlations in acetonitrile- d_6 . Nitrogen chemical shifts are reported relative to nitromethane.

The ^{15}N and corresponding ^1H NMR chemical shifts obtained from the $^1\text{H},^{15}\text{N}$ HMBC experiment are summarised in Table 2.3.

Table 2.3 Summary of the ^{15}N and ^1H NMR chemical shifts obtained $[\text{Pt}^{\text{II}}(\text{phen})(\text{L}^1\text{-S,O})]\text{Cl}$ from the $^1\text{H},^{15}\text{N}$ HMBC experiments and preliminary assignments.

	N^1	H^2	H^3	N^{10}	H^9	H^8	N	$\text{H}^{\text{b}+\text{b}'}$
δ / ppm	-145.80*	9.01	8.15	-185.27*	8.66	7.84	-218.15*	2.16, 2.05

*Chemical shifts relative to nitromethane.

The initial assignments of the nitrogen atoms to the various observed ^{15}N signals in Table 2.3 were on the basis that the nitrogen trans to the sulphur atom is the most deshielded and consequently labelled N^1 which needs to be confirmed by NOESY spectroscopy (Nuclear Overhauser Enhancement Spectroscopy). The sulphur is a soft donor atom according to Pearson's HSAB principle compared to oxygen which is a typical hard donor atom due to its relatively high electronegativity.¹⁴ It may be expected that the sulphur atom would form a 'stronger' bond with the relatively soft platinum(II) metal centre compared to oxygen.

Therefore, the nitrogen *trans* to the sulphur is expected to be more deshielded. The relatively large chemical shift difference between $N^1 - N^{10}$ (37.47 ppm) and $H^2 - H^9$ (0.35 ppm) reflects the significantly different electronic environments of the atoms *trans* to the Pt-S and Pt-O bonds. However, the unambiguous assignment of the 1H spectrum of $[Pt^{II}(\text{phen})(L^1-O,S)]Cl$ requires NOE (Nuclear Overhauser Effect) data which will yield the through space correlation between nuclei in close proximity, i.e. due to cross-relaxation between the nuclei.¹⁵ Several attempts using 2D NOESY experiments failed possibly due to low complex concentrations and a relatively large distance between the nuclei of interest (small NOE). Furthermore, 2D NOESY is better for large slowly tumbling molecules such as proteins and peptides.

However, the one-dimensional gradient NOESY pulse is sufficient for small molecules (<700 daltons) with relatively long distant (4-6Å) NOE's and was consequently used to unambiguously assign the 1H NMR spectra of $[Pt^{II}(\text{phen})(L^1-S,O)]Cl$. Positive NOE was observed between the protons of the 1,10-phenanthroline and *N*-pyrrolidyl-*N'*-pivaloylthiourea ligand as shown in Figure 2.6.

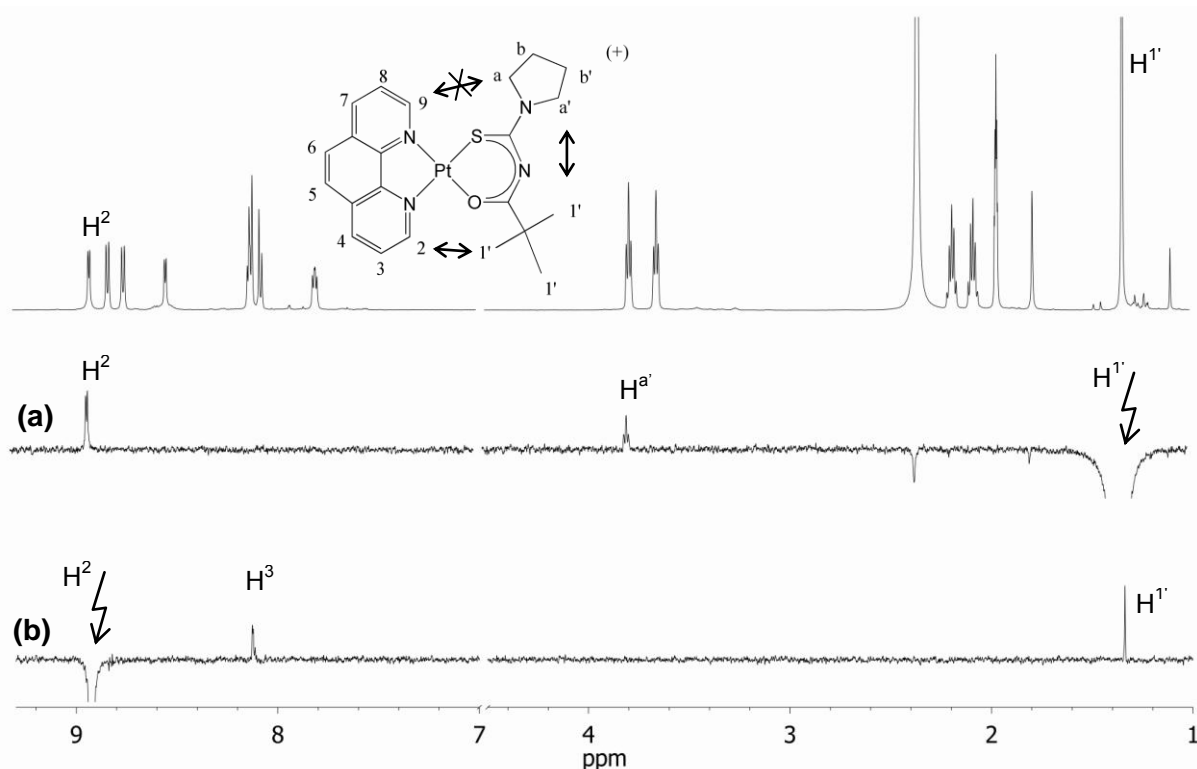


Figure 2.6 1H NMR signal NOE enhancements in a 1D gNOESY (gradient NOESY) experiment upon the irradiation of (a) the $H^{1'}$ and (b) H^2 protons of $[Pt^{II}(\text{phen})(L^1-S,O)]Cl$ respectively. This confirms the assignment of H^2 and $H^{a'}$ unambiguously.

The 1D NOESY data shows two NOE enhancements observed upon selective irradiation of the pivaloyl protons ($H^{1'}$) which allows for the assignment of the most downfield proton to H^2 since it is closest to $H^{1'}$. Furthermore, the peak at 3.78 ppm is a result of a positive NOE effect upon radiation of $H^{1'}$ and could be labelled $H^{a'}$.

The 1D NOESY data in conjunction with the COSY results presented earlier allows for the first unambiguous 1H NMR assignments of $[Pt^{II}(\text{phen})(L^n-S,O)]X$ complexes and validates the previous assignments of $[Pt^{II}(\text{phen})(L^n-S,O)]X$.^{1,4}

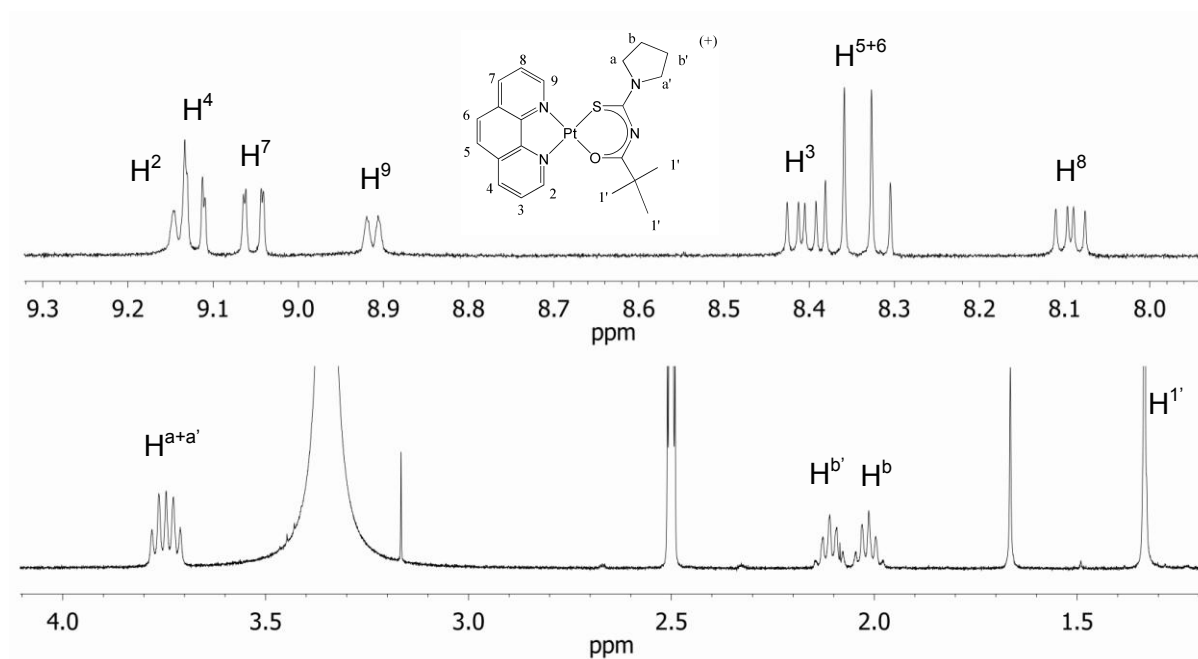
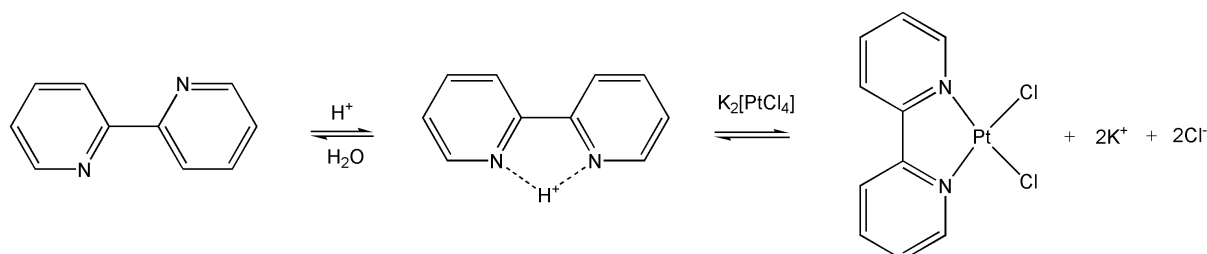


Figure 2.7 Full 1H NMR assignment of $[Pt^{II}(\text{phen})(L^1-S,O)]Cl$ in dimethyl sulfoxide- d_6 .

2.4 Synthesis of mixed ligand $[\text{Pt}^{\text{II}}(2,2'\text{-bipyridyl})(N,N\text{-di(alkyl)-}N'\text{-acylthiourea)]\text{Cl}$ complexes and their precursors

2.4.1 Synthesis of $\text{Pt}^{\text{II}}(2,2'\text{-bipyridyl})\text{Cl}_2$

The $\text{Pt}^{\text{II}}(\text{bipy})\text{Cl}_2$ precursor was synthesised by a similar method as for $\text{Pt}^{\text{II}}\text{Cl}_2(\text{phen})$, described by Morgan and Burstall,¹³ in which 1 mole equivalent of 2,2'-bipyridine (bipy) was added to 1 mole $\text{K}_2[\text{Pt}^{\text{II}}\text{Cl}_4]$ in HCl solution and heated to reflux for two hours whereby $\text{Pt}^{\text{II}}(\text{bipy})\text{Cl}_2$ precipitated. As was shown for the reaction of 1,10-phenanthroline (phen) and $\text{K}_2[\text{Pt}^{\text{II}}\text{Cl}_4]$ in water, the addition of HCl increases the solubility of the diimine ligand. However, the reactions of 2,2'-bipyridine and $\text{K}_2[\text{Pt}^{\text{II}}\text{Cl}_4]$ in the absence of HCl resulted in a highly insoluble orange-yellow precipitate, possibly a series of cluster complexes and/or coordination polymers with 2,2'-bipyridine and chlorides as bridging ligands.¹³ It is known that uncoordinated bipy adopts the 'trans' conformation where the nitrogen donor atoms are anti relative to the linking C-C bond. In slightly acidic aqueous solutions however, bipy readily forms the 'cis' conformation which is required to form the corresponding *cis*-chelated $\text{Pt}^{\text{II}}(\text{bipy})\text{Cl}_2$ (Scheme 2.8).¹⁶



Scheme 2.8 The change from the *trans*- to the *cis*-conformation of 2,2'-bipyridine in acidic aqueous solutions to form only the chelate complex with $[\text{Pt}^{\text{II}}\text{Cl}_4]^{2-}$.

The acidic medium was not needed for 1,10-phenanthroline since it does not have the conformational flexibility and usually more readily forms metal chelated complexes compared to bipy.¹⁶

The $\text{Pt}^{\text{II}}(\text{bipy})\text{Cl}_2$ product was characterized using ¹H NMR in dimethyl sulfoxide-d₆ (Figure 2.8b), Elemental Analysis and Single Crystal X-Ray Diffraction (SCXRD). The ¹H NMR spectra of $\text{Pt}^{\text{II}}(\text{bipy})\text{Cl}_2$ (Figure 2.8a) and bipy (Figure 2.8b) in dimethyl sulfoxide-d₆ show the large shift of all ¹H resonances which confirms the coordination to the Pt^{II}. Further proof for the coordination is the unresolved broad platinum satellites, ³J(¹⁹⁵Pt-¹H) = 24 Hz, visible at the base of the proton signal at 9.50 ppm, which could be assigned to H²⁺⁹ since these

protons are three bonds from the platinum centre and would exhibit scalar coupling to the ^{195}Pt . The doublet (d) observed at 8.58 ppm is assigned to H^{5+6} due to its multiplicity while the triplet of doublets (td) (8.42 ppm) and doublet of doublet of doublets (ddd) (7.84 ppm) were labelled H^{4+7} and H^{3+8} respectively.

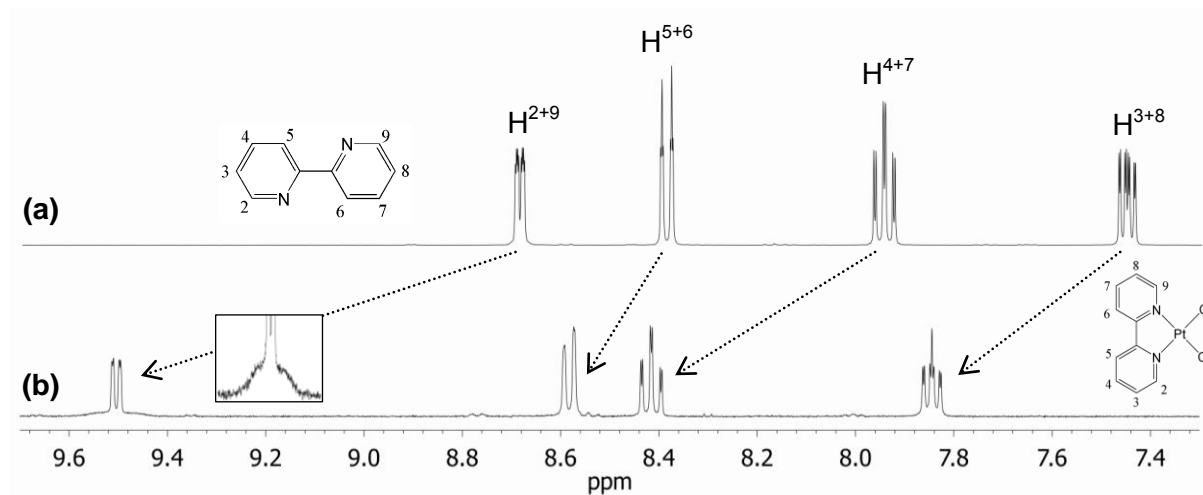


Figure 2.8 ^1H NMR spectrum and assignment of (a) bipy and (b) $\text{Pt}^{\text{II}}(\text{bipy})\text{Cl}_2$ in dimethyl sulfoxide- d_6 at 25°C

Single crystals suitable for SCXRD were obtained after overnight heating (14 hours) of $\text{Pt}^{\text{II}}(\text{bipy})\text{Cl}_2$ in acetonitrile, after which the solution was allowed to cool to room temperature, and left in a fume hood to allow the acetonitrile to evaporate. Small yellow crystals were obtained of which SCXRD data were collected. The molecular structure is shown in Figure 2.9. The crystal and structure refinement data is shown in Section 2.8.2 and the CIF file is given on the electronic Appendix C, accompanying this thesis.

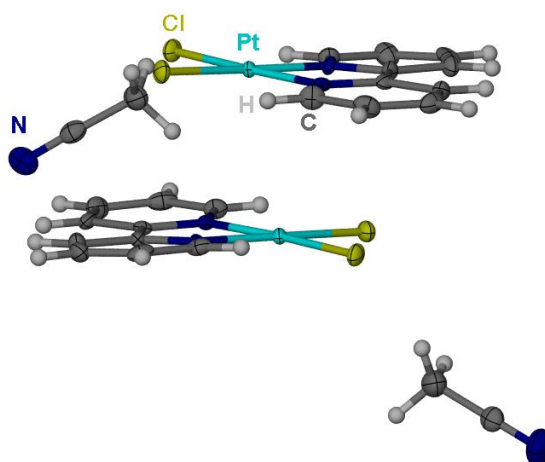


Figure 2.9 The molecular structure of $\text{Pt}^{\text{II}}(\text{bipy})\text{Cl}_2$ with an acetonitrile solvent molecule.

Two polymorphs of $\text{Pt}^{\text{II}}(\text{bipy})\text{Cl}_2$ are known which differ in colour as a result of the difference in crystal packing of the two polymorphs.^{17,18} The yellow polymorph is known to be significantly less stable compared to the red polymorph of $\text{Pt}^{\text{II}}(\text{bipy})\text{Cl}_2$. Interestingly, our crystal structure shown in Figure 2.9 is novel with two molecules of acetonitrile included in the structure with two molecules of $\text{Pt}^{\text{II}}(\text{bipy})\text{Cl}_2$; this is the first known crystal structure of $\text{Pt}^{\text{II}}(\text{bipy})\text{Cl}_2$ containing a solvate molecule in the crystal lattice. Furthermore, the stacking motifs of the crystals containing the acetonitrile solvate and the two polymorphs of $\text{Pt}^{\text{II}}(\text{bipy})\text{Cl}_2$ are shown in Figure 2.10.

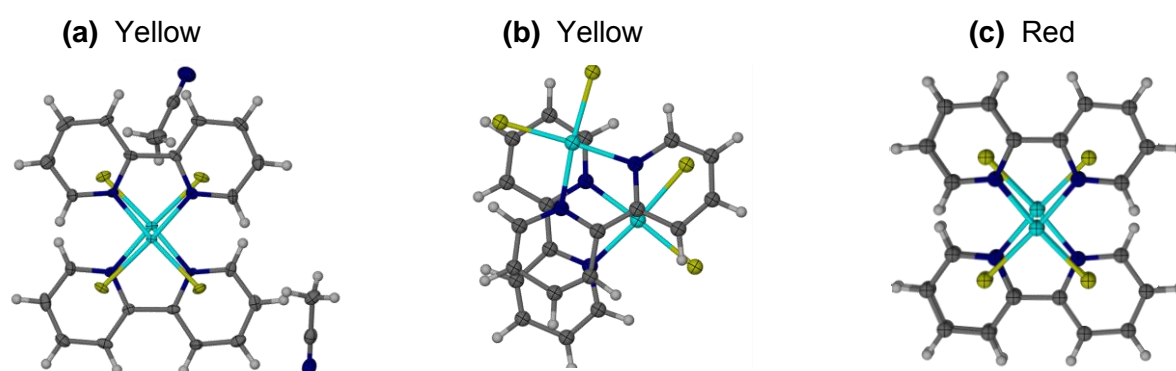


Figure 2.10 The three forms of $\text{Pt}^{\text{II}}(\text{bipy})\text{Cl}_2$ in the solid state with (a) yellow crystals with an acetonitrile solvate, (b) the yellow polymorph¹⁷ and (c) the red polymorph.¹⁸

Interestingly, the molecular packing in the yellow crystals isolated in this work shows a close resemblance to that of the red polymorph. This is interesting since this difference in colour of the two well known isomers was extensively studied previously and the red colour is believed to arise from the overlap of the d_{z^2} orbitals and the empty p_z of the platinum metal centres in the close packing arrangement which is thought to lead to a bathochromic shift.^{19,20} Attempts were made to convert the yellow polymorph (Figure 2.10b) to the red polymorph by pressurising the crystals with the yellow crystals turning red at high pressure.²⁰ However, after pressure is applied, the crystals were no longer single and further crystal data could not be collected.

The crystal packing of the well studied yellow and red polymorphs is shown in Figure 2.11.^{17,18}

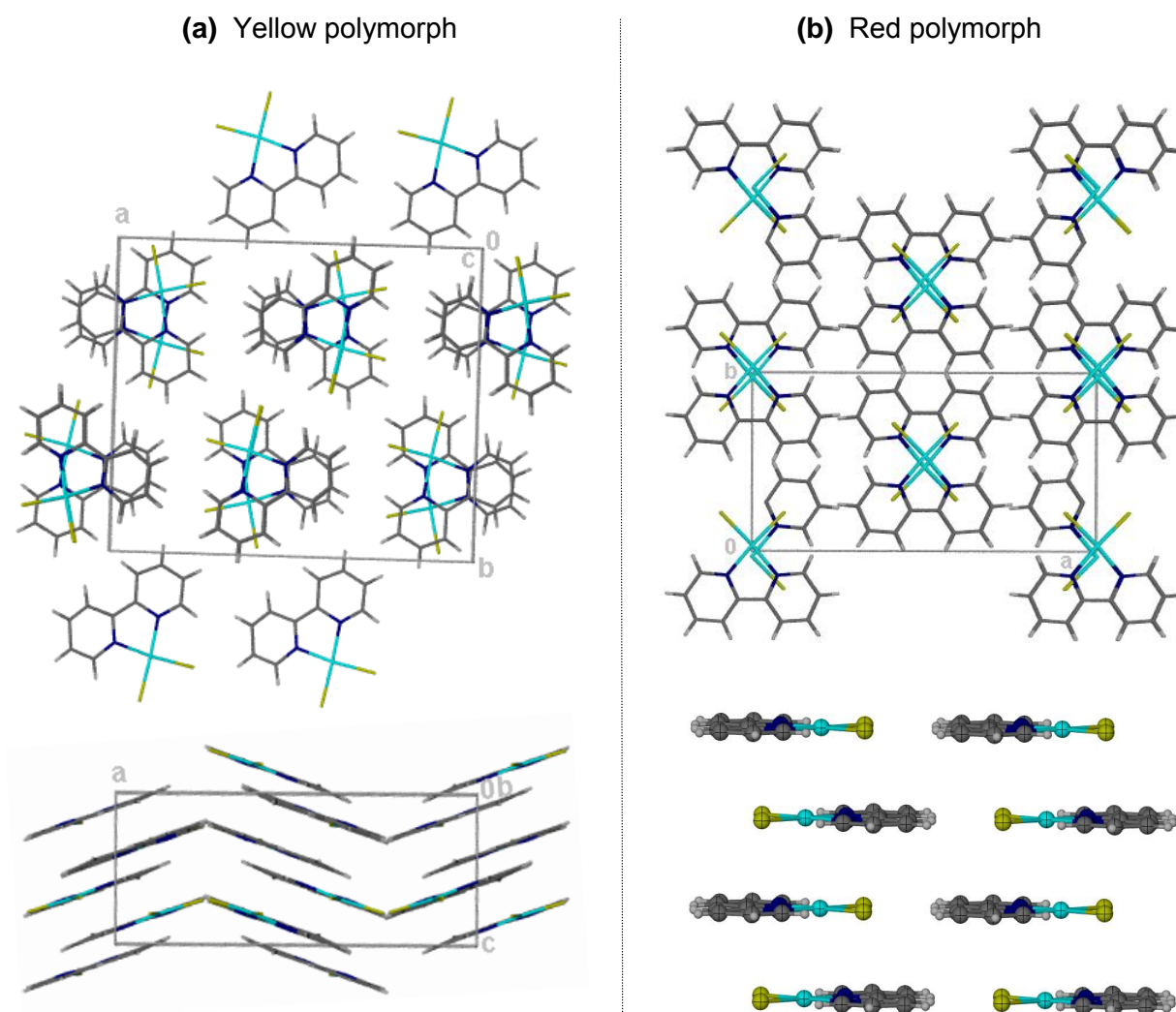


Figure 2.11 (a) The yellow polymorph¹⁷ of $\text{Pt}^{\text{II}}(\text{bipy})\text{Cl}_2$ viewed along the *c*-axis (top) and *b*-axis (bottom). (b) The red polymorph¹⁸ of $\text{Pt}^{\text{II}}(\text{bipy})\text{Cl}_2$ along the *c*-axis (top) and *b*-axis (bottom).

The yellow polymorph of $\text{Pt}^{\text{II}}(\text{bipy})\text{Cl}_2$ (Figure 2.11a) shows the individual molecules to exhibit aromatic- π stacking interactions of the 2-2-bipyridine ligand of complexes above and below each other to form an 'infinite' π -stack along the *c*-axis of the unit cell. The red polymorph similarly exhibits an 'infinite' stacking motif, however with the non-covalent interaction being $\text{Cl}\cdots\pi$ type rather than aromatic- π type. This packing arrangement allows for overlap of the d_{z^2} orbitals of the Pt centres leading to a bathochromic shift observed when going from solution to this specific red crystalline form of $\text{Pt}^{\text{II}}(\text{bipy})\text{Cl}_2$.

The crystal packing arrangement of the $\text{Pt}^{\text{II}}(\text{bipy})\text{Cl}_2\cdot\text{CH}_3\text{CN}$ isolated complex in this work is shown in Figure 2.12 viewed along the three axes of the unit cell. Two $\text{Pt}^{\text{II}}(\text{bipy})\text{Cl}_2$

molecules stack in a similar fashion to the red polymorph of $\text{Pt}^{\text{II}}(\text{bipy})\text{Cl}_2$ with CH_3CN separating/isolating these non-covalent 'dimer' pairs.

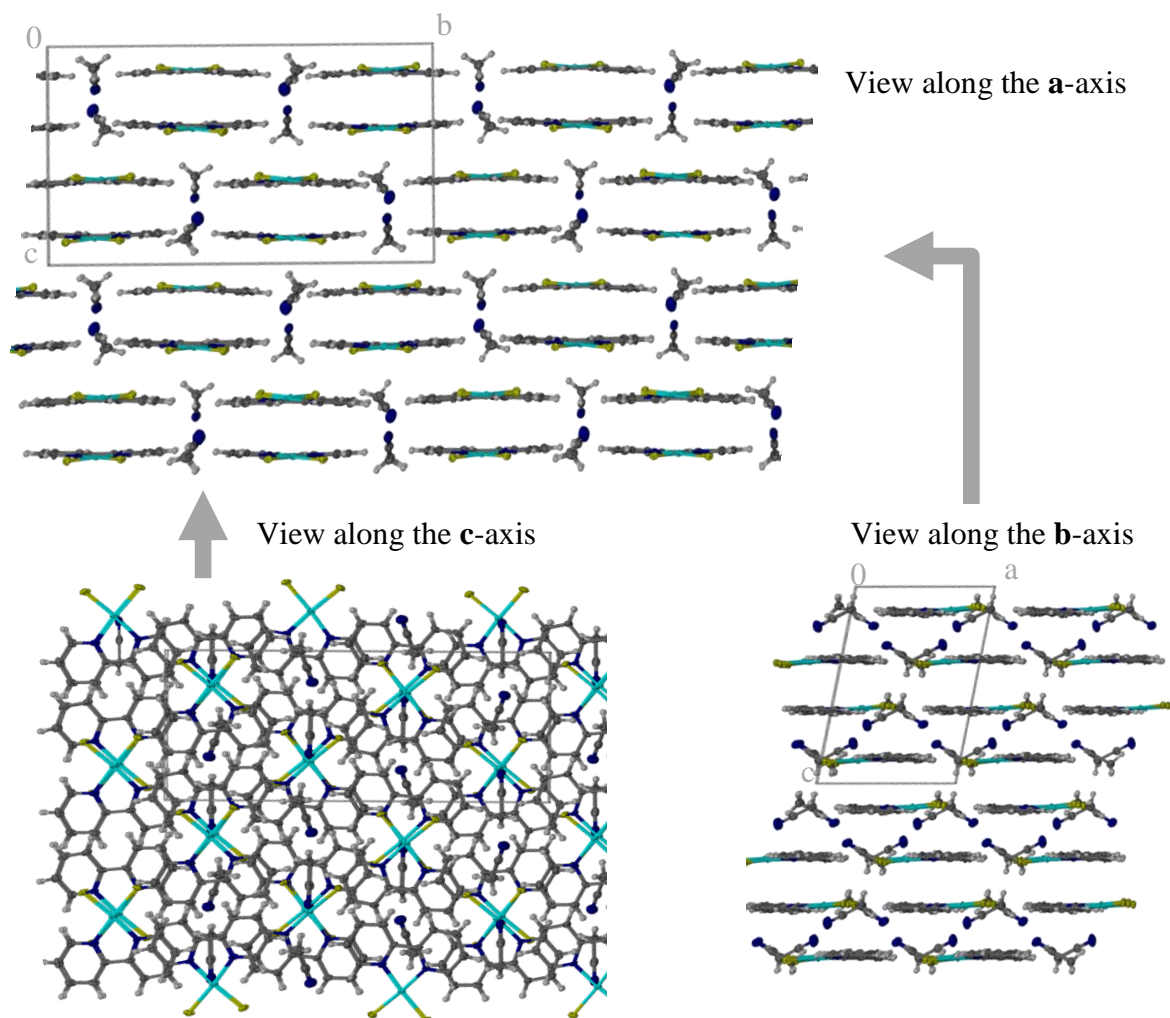


Figure 2.12 Crystal packing of the yellow $\text{Pt}^{\text{II}}(\text{bipy})\text{Cl}_2 \cdot \text{CH}_3\text{CN}$ form in the crystal lattice.

From this structure significant overlap of the d_{z^2} orbitals of the Pt metal centres might be expected for $\text{Pt}^{\text{II}}(\text{bipy})\text{Cl}_2 \cdot \text{CH}_3\text{CN}$. The three crystal structures will be compared and discussed using the Pt··Pt distances and angles defined by Figure 2.13. The difference between selected bond lengths and angles of the three forms of $\text{Pt}^{\text{II}}(\text{bipy})\text{Cl}_2$ in discussion are summarised in Table 2.4 with the atom numbers as in Figure 2.13.

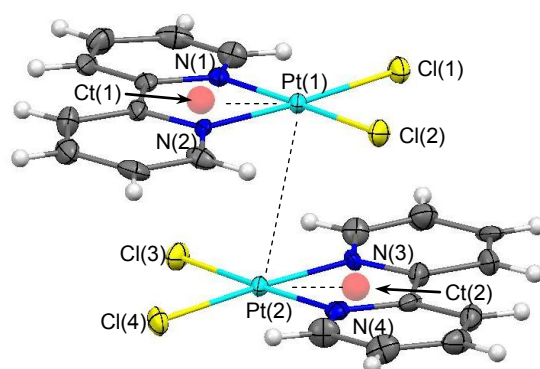


Figure 2.13 Atom labels and centroids (Ct) used to compare the crystal structures of $\text{Pt}^{\text{II}}(\text{bipy})\text{Cl}_2$ as listed in Table 2.4.

Table 2.4 Selected bond lengths, distances, angles and torsion angles for three crystal structures of $\text{Pt}^{\text{II}}(\text{bipy})\text{Cl}_2$.

	$\text{Pt}^{\text{II}}(\text{bipy})\text{Cl}_2 \cdot \text{MeCN}$	$\text{Pt}^{\text{II}}(\text{bipy})\text{Cl}_2$ (red) ¹⁸	$\text{Pt}^{\text{II}}(\text{bipy})\text{Cl}_2$ (yellow) ¹⁷
<i>Bonds:</i>	Å	Å	Å
Pt(1)-Cl(1)	2.2999	2.3017(4)	2.3017(4)
Pt(1)-Cl(2)	2.3073	2.3017(4)	2.2762(4)
Pt(2)-Cl(3)	2.3048	2.3017(4)	2.3017(4)
Pt(2)-Cl(4)	2.2992	2.3017(4)	2.2762(4)
Pt(1)-N(1)	2.0074	2.0091(4)	2.0247(4)
Pt(1)-N(2)	2.0097	2.0091(4)	2.0565(4)
Pt(2)-N(3)	2.0286	2.0091(4)	2.0247(4)
Pt(2)-N(4)	2.0206	2.0091(4)	2.0565(4)
Pt(1)-Pt(2)	3.4439(1)	3.449(1)	4.524(1)
<i>Angles:</i>			
Ct(1)-Pt(1)-Pt(2)	77.28°	80.51°	71.31°
Ct(2)-Pt(2)-Pt(1)	78.88°	80.51°	50.40°
*N(1)-Pt(1)-Cl(2)	2.15°	2.40°	3.56°
*N(2)-Pt(1)-Cl(1)	2.21°	2.09°	1.45°
*N(3)-Pt(2)-Cl(4)	2.53°	2.40°	3.56°
*N(4)-Pt(2)-Cl(3)	2.50°	2.09°	1.45°
<i>Torsion Angles:</i>			
Ct(1)-Pt(1)-Pt(2)-Ct(2)	179.70°	180.00°	108.22°

* The 'out of plane' angle of N-Pt-Cl which is expected to be 0° in a perfect square planar geometry.

The bond lengths and angles of $\text{Pt}^{\text{II}}(\text{bipy})\text{Cl}_2 \cdot \text{CH}_3\text{CN}$ show close resemblance to the red $\text{Pt}^{\text{II}}(\text{bipy})\text{Cl}_2$ polymorph as shown in Table 2.4. The only significant difference between these two structures is the Pt(2)-N(3) and Pt(2)-N(4) bond lengths. Interestingly, the Pt(1)-Pt(2) distance is almost identical within the error for $\text{Pt}^{\text{II}}(\text{bipy})\text{Cl}_2 \cdot \text{CH}_3\text{CN}$ compared to the red- $\text{Pt}^{\text{II}}(\text{bipy})\text{Cl}_2$ (3.444 and 3.449 Å respectively). These Pt...Pt distances are significantly shorter than of the yellow polymorph 4.524 Å and no d_{z^2} orbital is possible for the yellow polymorph. Furthermore, it is expected that $\text{Pt}^{\text{II}}(\text{bipy})\text{Cl}_2 \cdot \text{CH}_3\text{CN}$ should show a similar bathochromic shift upon crystallization as the red polymorph which is not observed. Therefore, it is reasonable to postulate that the bathochromic shift is only observed for $\text{Pt}^{\text{II}}(\text{bipy})\text{Cl}_2$ when the overlap of the d_{z^2} orbitals of the Pt metal centre is from both 'sides' and the metal centre is 'sandwiched' between two other $\text{Pt}^{\text{II}}(\text{bipy})\text{Cl}_2$ molecules to form an infinite stack of complexes with all the Pt d_{z^2} orbital overlapping to from both sides. In our $\text{Pt}^{\text{II}}(\text{bipy})\text{Cl}_2 \cdot \text{CH}_3\text{CN}$ crystal structure, d_{z^2} orbitals overlap only occur at one 'side' of the metal centre and the effect is apparently not sufficient to cause a visible change in colour.

Hot stage microscopy was done on a crystal of $\text{Pt}^{\text{II}}(\text{bipy})\text{Cl}_2 \cdot \text{CH}_3\text{CN}$ in order to release CH_3CN from the crystal lattice with an expected colour change as the crystals are heated. However, up to 260 °C no acetonitrile loss was observed prior to decomposition of the crystals > 260 °C.

2.4.2 Synthesis of mixed ligand $[\text{Pt}^{\text{II}}(2,2'\text{-bipyridyl})(N,N\text{-di(alkyl)-}N'\text{-acylthiourea})]\text{Cl}$ complexes

The synthesis of $[\text{Pt}^{\text{II}}(\text{bipy})(\text{L}^{1,2}\text{-}S,O)]\text{Cl}$ was accomplished using a similar method as described in Section 2.2.4 for $[\text{Pt}^{\text{II}}(\text{phen})(\text{L}^n\text{-}S,O)]\text{Cl}$. Although the reaction was allowed to proceed up to 14 hours, yields were significantly lower (typically 40-60%) compared to the synthesis of $[\text{Pt}^{\text{II}}(\text{phen})(\text{L}^n\text{-}S,O)]\text{Cl}$. Purification of $[\text{Pt}^{\text{II}}(2,2'\text{-bipyridyl})(N,N\text{-dibutyl-}N'\text{-naphthoyl-thiourea})]\text{Cl}$ ($[\text{Pt}^{\text{II}}(\text{bipy})(\text{L}^2\text{-}S,O)]\text{Cl}$) was difficult as observed for the corresponding 1,10-phenanthroline complexes, and the pure product could be obtained by the addition of water to a solution of the crude product in acetonitrile and diethyl ether which resulted in the formation of a third phase which contained the pure complex. Upon addition of water, an ether layer separates from the aqueous phase while the product extracted into a new third phase which formed at the bottom of the flask below the water phase. The third phase was collected and ^1H NMR revealed that this phase consisted of only $[\text{Pt}^{\text{II}}(\text{bipy})(\text{L}^2\text{-}S,O)]\text{Cl}$ and acetonitrile. Hence, for repeated reactions the diethyl ether was omitted and it

was found that the third phase still formed, containing essentially a concentrated pure product. The ^1H NMR spectrum of $[\text{Pt}^{\text{II}}(\text{bipy})(\text{L}^2\text{-S},\text{O})]\text{Cl}$ shows (Figure 2.14) the purity of this crude product obtained, together with the ^1H NMR assignments of the various proton resonances labelled on the spectrum.

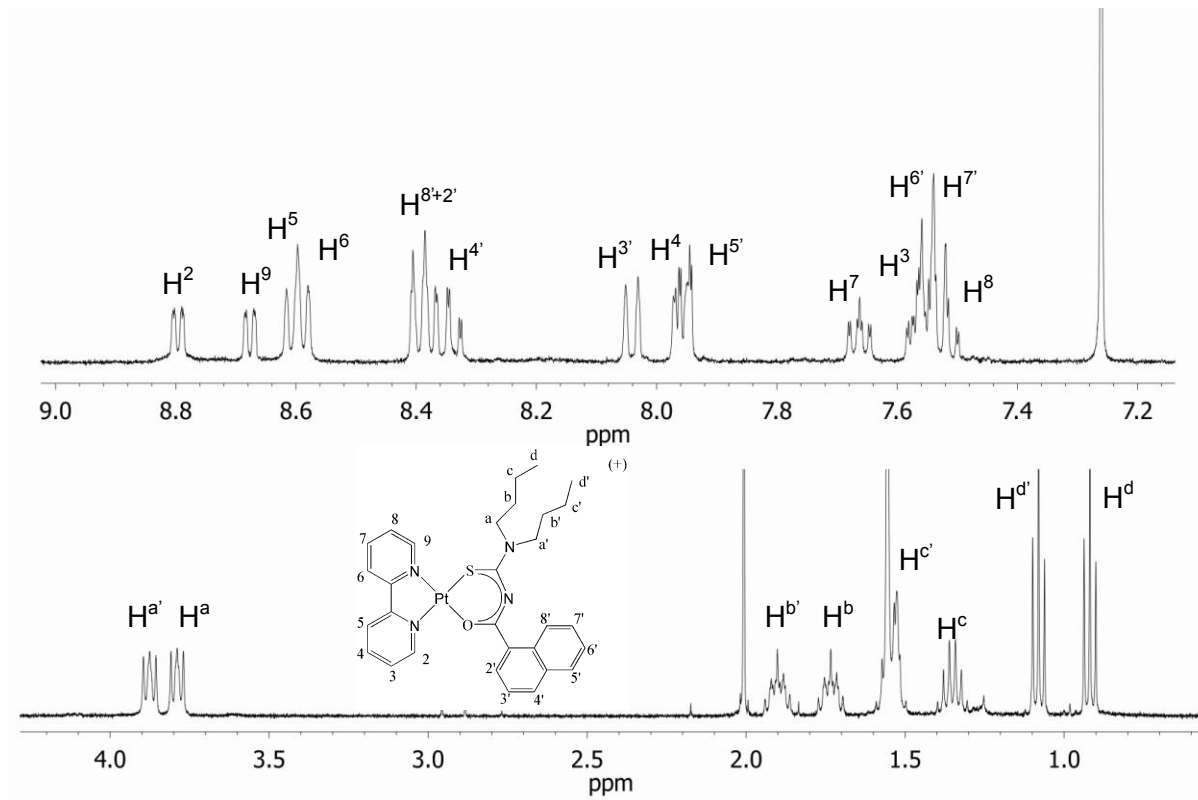


Figure 2.14 ^1H NMR spectrum of $[\text{Pt}^{\text{II}}(\text{bipy})(\text{L}^2\text{-S},\text{O})]\text{Cl}$ in chloroform- d_1 at 25°C .

The peaks assigned here are consistent with similar complexes previously made by Lawrence *et al.* for $[\text{Pt}^{\text{II}}(\text{bipy})(\text{N},\text{N}\text{-dibutyl-}\text{N}'\text{-naphthoylthiourea})]\text{PF}_6$ in chloroform- d_1 .¹ The ^1H NMR spectrum and assignments of the $[\text{Pt}^{\text{II}}(\text{bipy})(\text{N}\text{-pyrrolidyl-}\text{N}'\text{-pivaloylthiourea})]\text{Cl}$ variation are shown in **Error! Reference source not found.** in the Experimental Section **Error! Reference source not found.**

Attempts were made to synthesise $[\text{Pt}^{\text{II}}(\text{bipy})(\text{N},\text{N}\text{-dibutyl-}\text{N}'\text{-naphthoylthiourea})]^+$ in higher yields by changing the counter ion from Cl^- to PF_6^- , as found by Lawrence *et al.*¹ The reaction mixture was cooled to -18°C in an attempt to crystallize the pure $[\text{Pt}^{\text{II}}(\text{bipy})(\text{N},\text{N}\text{-dibutyl-}\text{N}'\text{-naphthoylthiourea})]\text{PF}_6$ complex. Interestingly, bright yellow crystals formed after 5 days at -18°C . The SCXRD however, revealed this to be the *cis*-(*N,N*-di(*n*-butyl)-*N'*-naphthoylthiourea platinum(II) complex or *cis*- $[\text{Pt}^{\text{II}}(\text{L}^2\text{-S},\text{O})_2]$ in short, as shown in Figure 2.15.

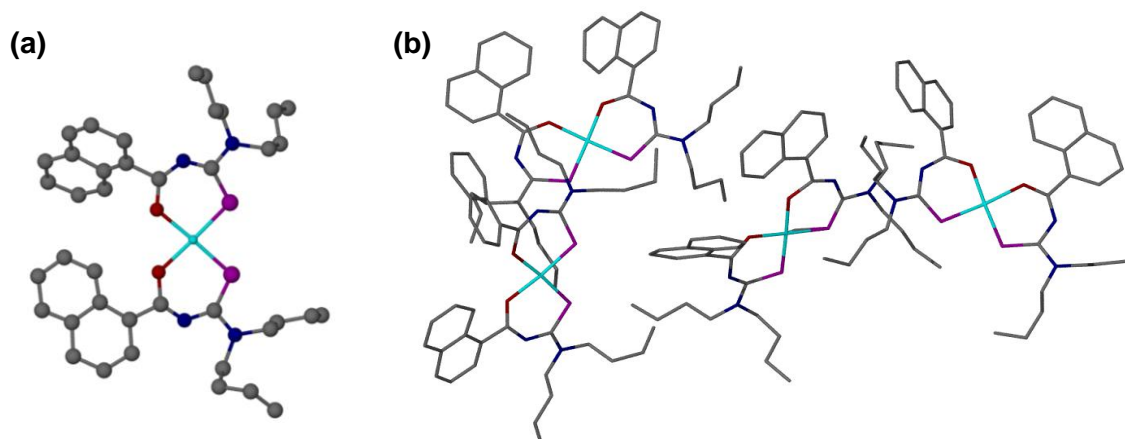


Figure 2.15 Crystal structure of $\text{Pt}^{\text{II}}(\text{L}^2\text{-S},\text{O})_2$ collected at 100K with (a) the molecular structure and (b) the asymmetric unit.

This complex is the *cis*-isomer, which is the most common form in which these *N,N*-di(alkyl)-*N'*-acylthiourea ligands coordinate.²¹ The *cis*- $[\text{Pt}^{\text{II}}(\text{L}^n\text{-S},\text{O})_2]$ complexes are predominantly formed while the *trans*- $[\text{Pt}^{\text{II}}(\text{L}^n\text{-S},\text{O})_2]$ complexes are rare. Only very few authenticated *trans*- $[\text{Pt}^{\text{II}}(\text{L}^n\text{-S},\text{O})_2]$ complexes have been characterised.²² Koch and co-workers managed to crystallize *trans*- $[\text{Pt}^{\text{II}}(\text{N,N}$ -dibutyl-*N'*-naphthoylthiourea)₂] several years ago and were the first to report a *trans*-complex of acylthioureas.²² They later discovered that the *cis*↔*trans* interconversion is a photo-chemical process with the more common *cis*-isomer abundant at ambient conditions.²¹ Furthermore, Koch and co-workers studied this *cis*↔*trans* isomerisation of various complexes of *N,N*-di(alkyl)-*N'*-acylthioureas with Pt(II) and Pd(II) using a light source and separating the two isomers using HPLC.²¹ The *trans*- $[\text{Pt}^{\text{II}}(\text{L}^2\text{-S},\text{O})_2]$ complex crystallised by Koch and co-workers was crystallized in the presence of strong sunlight which was found to be the reason for the crystals forming.

In our case, the crystals of the *cis*- $[\text{Pt}^{\text{II}}(\text{L}^2\text{-S},\text{O})_2]$ formed in the dark, and crystallized at -18°C. The repeating unit or unit-cell is comprised of 4 molecules of $\text{Pt}^{\text{II}}(\text{L}^2\text{-S},\text{O})_2$ and is highly unsymmetrical. Unfortunately, the error in the fit of the model to the experimental diffraction spots is rather large (R factor = 11) and unacceptable for publication. For our purpose of characterization however, it is clear that the *cis*-*N,N*-dibutyl-*N'*-naphthoylthiourea platinate complex was crystallized.

2.5 Synthesis of the mixed ligand $[\text{Pd}^{\text{II}}(\text{phen})(\text{L}^{1-S,O})]\text{Cl}$ complex and its precursors

2.5.1 Synthesis of $\text{Pd}^{\text{II}}\text{Cl}_2(1,10\text{-phenanthroline})$

The synthesis of $\text{Pd}^{\text{II}}\text{Cl}_2(\text{phen})$ was carried out using a similar method as described for the platinum analogue, $\text{Pt}^{\text{II}}\text{Cl}_2(\text{phen})$, by the reaction of $\text{K}_2[\text{Pd}^{\text{II}}\text{Cl}_4]$ and 1,10-phenanthroline in acidic (HCl) aqueous solutions. The complex formation reaction is significantly faster for $\text{Pd}^{\text{II}}\text{Cl}_2(\text{phen})$ compared to $\text{Pt}^{\text{II}}\text{Cl}_2(\text{phen})$ as expected for the generally kinetically labile Pd(II) coordination chemistry.¹⁴ On addition of equimolar quantities of reagents, the reaction was typically complete at room temperature after 1 hour resulting in a yield of 95-98%. The reaction mixture changed colour from a dark brown solution to a pale pink-yellow suspension within 5-7 minutes. This fast kinetics is characteristic of palladium(II) reactions since it is known that ligands coordinated to palladium are much more labile than its inert platinum(II) counterpart.¹⁴ The ^1H NMR spectrum of $\text{Pd}^{\text{II}}\text{Cl}_2(\text{phen})$ is similar to the spectrum observed for $\text{Pt}^{\text{II}}\text{Cl}_2(\text{phen})$ and ^1H resonances and assignments are shown in Figure 2.16.

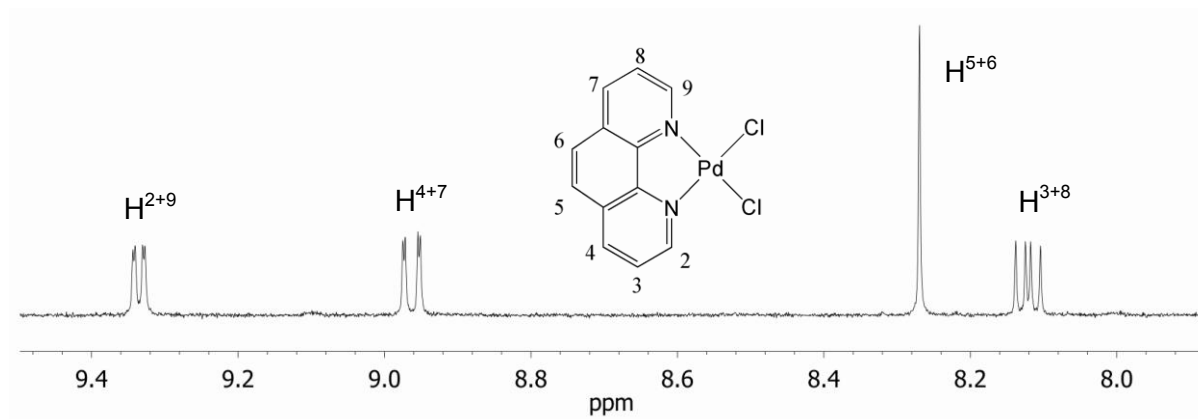


Figure 2.16 ^1H NMR spectrum of $\text{Pd}^{\text{II}}\text{Cl}_2(\text{phen})$ in dimethyl sulfoxide- d_6 at $25\text{ }^\circ\text{C}$.

As expected, the proton resonance at 9.35 ppm (Figure 2.16) shows no satellites resulting from coupling to the Pd centre, as was observed for Pt complexes ($^3J(^{195}\text{Pt}-^1\text{H})$) observed for $\text{Pt}^{\text{II}}\text{Cl}_2(\text{phen})$. While Pd has one NMR active isotope (^{105}Pd at 22,2% natural abundance), this isotope is a quadrupolar nucleus with a quantum number $I = 5/2$, and would result in broad unresolved multiple splitting if these are observable at all, in view of the probably rapid quadrupolar relaxation induced by the $I = 5/2$ nucleus.²³

2.5.2 Synthesis of $\text{Pd}^{\text{II}}_3(\text{OAc})_6$

The low solubility of $\text{Pd}^{\text{II}}\text{Cl}_2(\text{phen})$ in organic solvents made the synthesis of $[\text{Pd}^{\text{II}}(\text{phen})(\text{L}^{1-S,O})]^+$ difficult in organic solvents. Therefore, the more soluble precursor $\text{Pd}^{\text{II}}(1,10\text{-phenanthroline})(\text{CH}_3\text{CO}_2)_2$ or $\text{Pd}^{\text{II}}(\text{phen})(\text{OAc})_2$, was synthesized. The $\text{Pd}^{\text{II}}(\text{phen})(\text{OAc})_2$ complex is normally synthesised from $\text{Pd}^{\text{II}}_3(\text{OAc})_6$. However, the successful and reproducible synthesis of $\text{Pd}^{\text{II}}_3(\text{OAc})_6$ in high yields has been contentious in the literature for some methods suggested and the yields could not be easily reproduced.²⁴ Murillo and co-workers have carefully studied the synthesis according to common literature methods and have presented a reproducible method to synthesise $\text{Pd}^{\text{II}}_3(\text{OAc})_6$ in high yields.²⁵ Their improved synthesis involves the reaction of $\text{Pd}^{\text{II}}\text{Cl}_2$ with NaHCO_2 to reduce the Pd^{II} complex to Pd^0 . The Pd^0 is then filtered off and washed with water. The Pd^0 is re-oxidised to Pd^{II} with HNO_3 in glacial acetic acid to form the crude $\text{Pd}_3(\text{OAc})_6$ with the ^1H NMR shown in Figure 2.17b for our synthesis according to the method described by Murillo and co-workers.²⁵ For comparison, the ^1H NMR spectrum of the commercially available $\text{Pd}_3(\text{OAc})_6$ is also shown in Figure 2.17a.

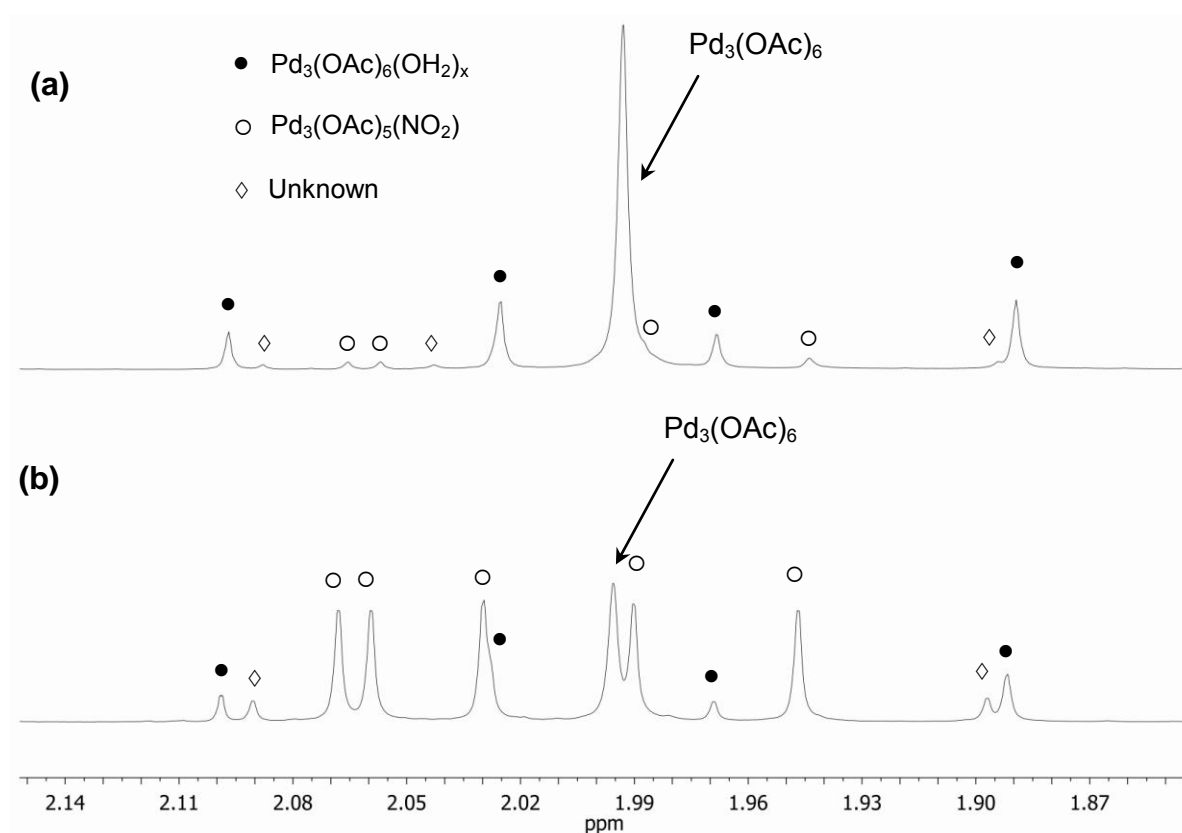


Figure 2.17 ^1H NMR spectra of $\text{Pd}_3(\text{OAc})_6$ in chloroform- d_1 . The material was (a) obtained commercially and (b) synthesised according to the method of Murillo and co-workers.²⁵ The species assignments are shown.

The assignments of ^1H NMR spectrum of $\text{Pd}_3(\text{OAc})_6$ from this synthesis method were made previously by Murillo and Cotton.²⁵ The ^1H NMR spectrum of our prepared " $\text{Pd}_3(\text{OAc})_6$ " clearly show significant amount of $\text{Pd}_3(\text{OAc})_5(\text{NO}_2)$ compared to the commercial sample, according to the assignments made by Murillo and Cotton. However, the 'unknown' peaks labelled in Figure 2.17 observed in our sample as well as the commercial sample were not assigned by Murillo and Cotton. A recent publication on the speciation of $\text{Pd}_3(\text{OAc})_6$ by Hii and co-workers suggest three structures in solution as shown in Figure 2.18, which may account for the additional peaks observed.²⁶

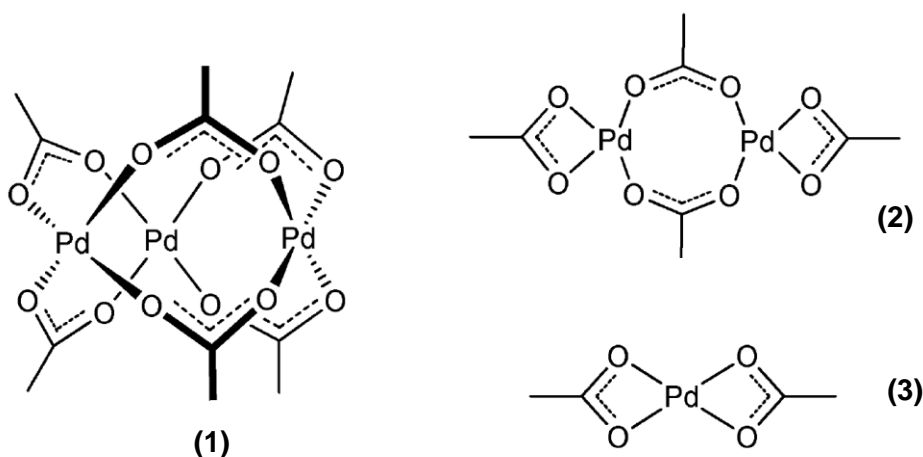


Figure 2.18 Suggested structures of $\text{Pd}(\text{OAc})_2$ in solution.²⁶

The trinuclear complex (1) is the major species in solution while the dinuclear (2) and mononuclear (3) complexes are present in lower quantities.²⁶ However, the presence of these two additional species (2) and (3), is not discussed by Murillo and Cotton and could account for the three additional signals observed in the ^1H NMR spectrum of our samples (Figure 2.17). The dinuclear complex (2) should show two singlets with equal intensity as a result of the acetate ligands being in two different chemical environments. One singlet ^1H resonance is expected for the mononuclear *bis*-acetonato complex (3). If both of these products are in solution, two signals are expected of equal intensity and a single peak with the total being three additional peaks. This is indeed what was observed and this two additional species (2) and (3) may account for the previously un-assigned peaks in the ^1H NMR spectrum of commercially available $\text{Pd}_3(\text{OAc})_6$ and synthesised " $\text{Pd}_3(\text{OAc})_6$ ".

2.5.3 Synthesis of Pd^{II}(1,10-phenanthroline)(CH₃CO₂)₂

The Pd^{II}(phen)(OAc)₂ complex was synthesised as a more soluble precursor for the synthesis of [Pd^{II}(phen)(L^{1-S,O})]⁺. An improved synthesis described by Milani and co-workers was used for the preparation of Pd^{II}(phen)(OAc)₂.²⁷ The synthesis involves the reaction of Pd^{II}₃(OAc)₆ in acetone with 1,10-phenanthroline at room temperature. The product precipitated as a yellow crystalline material in high yields (87%). Pd^{II}(phen)(OAc)₂ was characterised using ¹H NMR, with assignments based on the comparison with the assignments of the Pd^{II}(phen)Cl₂ complex in dimethyl sulfoxide-*d*₆ with the addition of a singlet at 1.97 ppm integrating for 6 protons and consequently labelled H^{1'} (Figure 2.19).

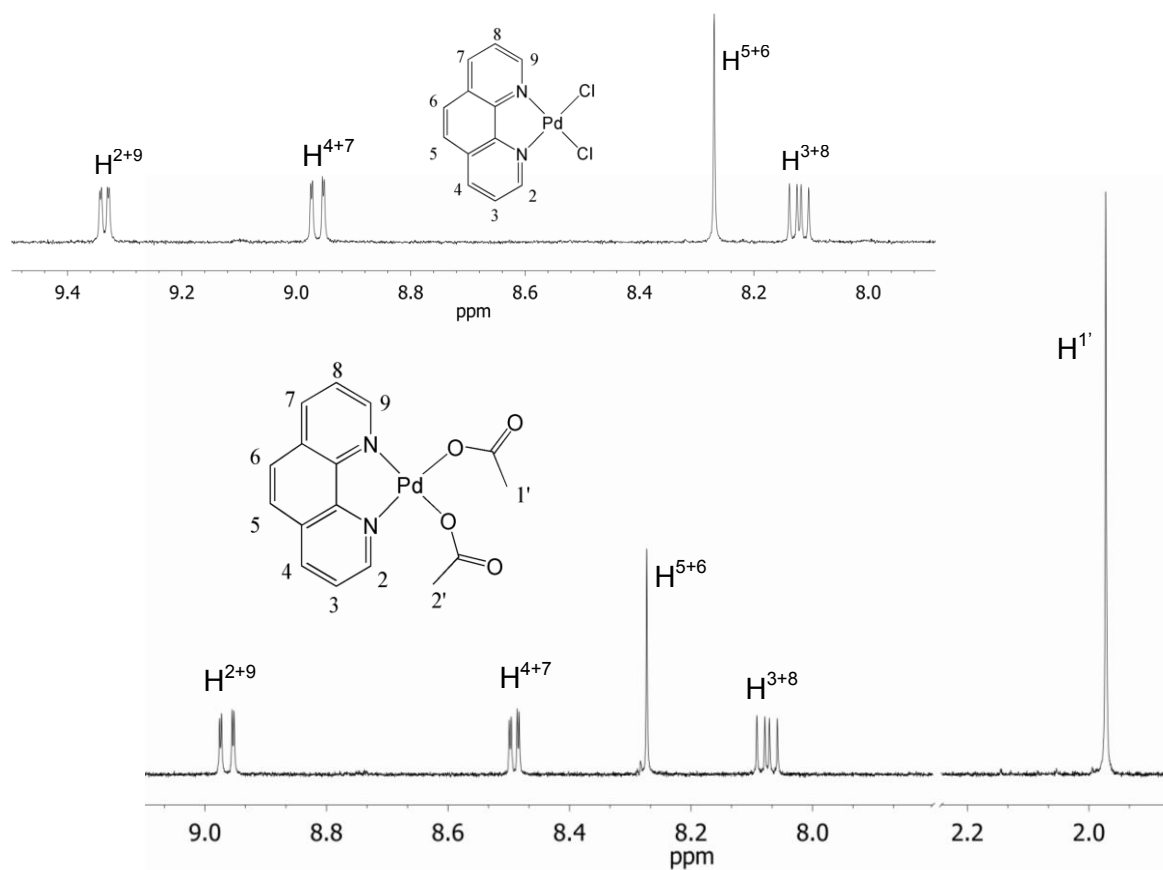


Figure 2.19 ¹H NMR spectrum of Pd^{II}(phen)(OAc)₂ in dimethyl sulfoxide-*d*₆ at 25 °C.

2.5.4 Synthesis of the mixed ligand $[\text{Pd}^{\text{II}}(1,10\text{-phenanthroline})(N,N\text{-pyrrolidyl-}N'\text{-pivaloylthiourea})]\text{Cl}$ complex

The synthesis of $[\text{Pd}^{\text{II}}(1,10\text{-phenanthroline})(N,N\text{-pyrrolidyl-}N'\text{-pivaloylthiourea})]^+$ or $[\text{Pd}^{\text{II}}(\text{phen})(L^1\text{-}S,O)]^+$ was carried out either using $\text{Pd}^{\text{II}}(\text{phen})(\text{OAc})_2$ and $\text{Pd}^{\text{II}}\text{Cl}_2(\text{phen})$ as precursors. Initially a synthesis route in acetonitrile, similar to the $[\text{Pt}^{\text{II}}(\text{Phen})(L^1\text{-}S,O)]^+$ was attempted using $\text{Pd}^{\text{II}}\text{Cl}_2(\text{phen})$ as precursor which was unsuccessful. However, using $\text{Pd}^{\text{II}}(\text{phen})(\text{OAc})_2$ as precursor it was possible to prepare the desired complex in reasonable to good yields (70%). However, a crude synthesis product consisted of a mixture of $[\text{Pd}^{\text{II}}(\text{phen})(L^1\text{-}S,O)]^+$ and $\text{Pd}^{\text{II}}(\text{phen})(\text{OAc})_2$ required the separation of $[\text{Pd}^{\text{II}}(\text{phen})(L^1\text{-}S,O)]^+$ from the precursor using column chromatography with Al_2O_3 stationary phase and a dichloromethane/acetone mobile phase, with the pure $[\text{Pd}^{\text{II}}(\text{phen})(L^1\text{-}S,O)]^+$ complex eluting with an 80/20 (v/v) acetone/water mixture (70% yield). The ^1H NMR spectrum and assignments of pure $[\text{Pd}^{\text{II}}(\text{phen})(L^1\text{-}S,O)]^+$ in chloroform is shown in Figure 2.20.

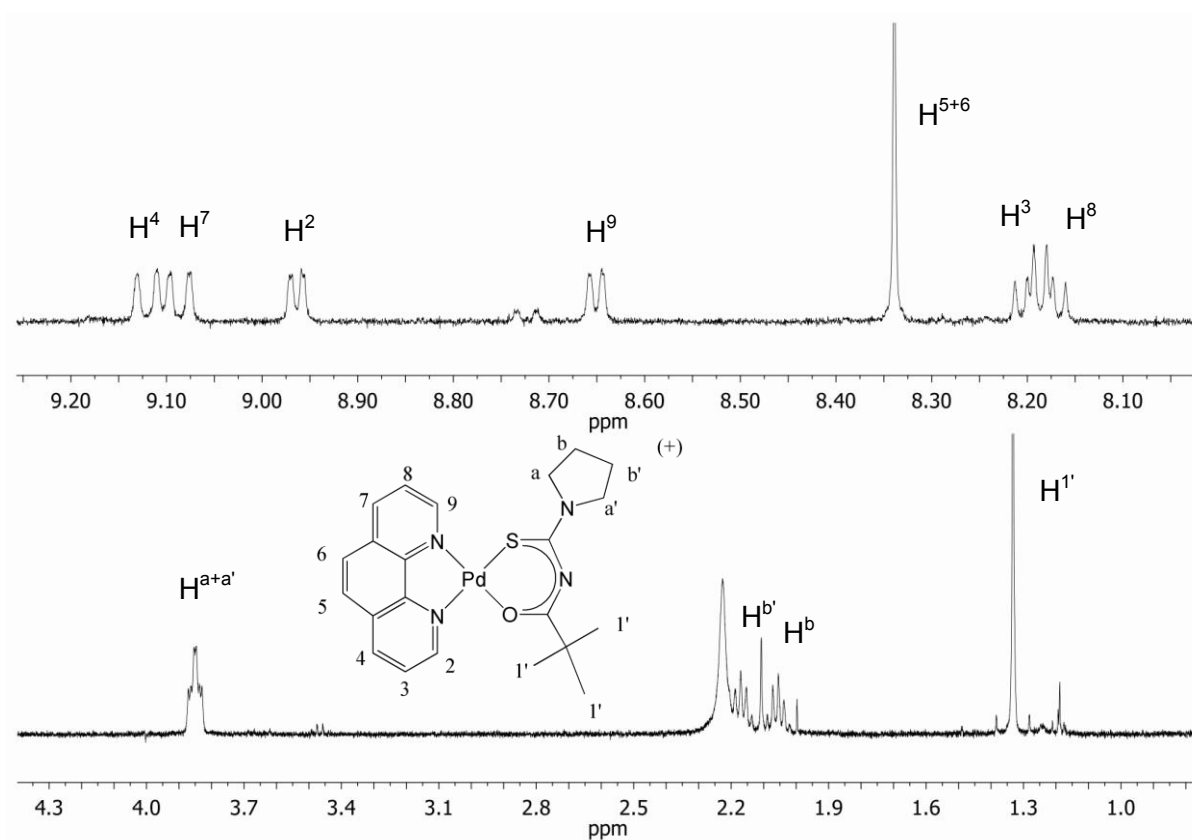


Figure 2.20 ^1H NMR spectrum of $[\text{Pd}^{\text{II}}(\text{phen})(L^1\text{-}S,O)]\text{Cl}$ in chloroform- d_1 at 25°C .

The ^1H NMR spectrum of $[\text{Pd}^{\text{II}}(\text{phen})(\text{L}^1\text{-S},\text{O})]\text{Cl}$ shows the expected H^2 and H^9 resonances with no coupling to Pd. The synthesis of $[\text{Pd}^{\text{II}}(\text{phen})(\text{L}^1\text{-S},\text{O})]\text{Cl}$ from the $\text{Pd}^{\text{II}}\text{Cl}_2(\text{phen})$ precursor which was found to be unsuccessful in acetonitrile was possible by the reaction of $\text{Pd}^{\text{II}}\text{Cl}_2(\text{phen})$ and HL^1 in a dichloromethane/water mixture containing NaOAc. A bright yellow precipitate of $[\text{Pd}^{\text{II}}(\text{phen})(\text{L}^1\text{-S},\text{O})]\text{Cl}$ accumulated at the interface which dissolves with the addition of acetonitrile to the mixture. The bottom acetonitrile/dichloromethane layer containing the $[\text{Pd}^{\text{II}}(\text{phen})(\text{L}^1\text{-S},\text{O})]\text{Cl}$ complex was separated from the aqueous phase, filtered and the $[\text{Pd}^{\text{II}}(\text{phen})(\text{L}^1\text{-S},\text{O})]\text{Cl}$ complex precipitated from solution by the addition of ether. Typical yields of 60-70% were obtained using this novel synthetic method. Furthermore, the water was found to be essential for the reaction to take place and postulate that water is required to solvate the Cl^- in solution. The solvation of Cl^- in water would be energetically more favourable than in organic solvents and may account for the reaction to occurring in the presence of water.

2.6 Synthesis of $[\text{Pt}^{\text{II}}\text{Cl}(\text{DMSO})(\text{en})]\text{Cl}$

2.6.1 Synthesis of *cis*- $[\text{Pt}^{\text{II}}\text{Cl}_2(\text{DMSO})_2]$

The synthesis of *cis*- $\text{Pt}^{\text{II}}\text{Cl}_2(\text{DMSO})_2$ precursor was done using the method described by Price and co-workers.²⁸ The pure product precipitates as a pale yellow crystalline material from a solution containing $\text{K}_2[\text{Pt}^{\text{II}}\text{Cl}_4]$ and dimethyl sulfoxide in water at room temperature (2hrs). $\text{Pt}^{\text{II}}\text{Cl}_2(\text{DMSO})_2$ was characterized by ^1H NMR (Figure 2.21).

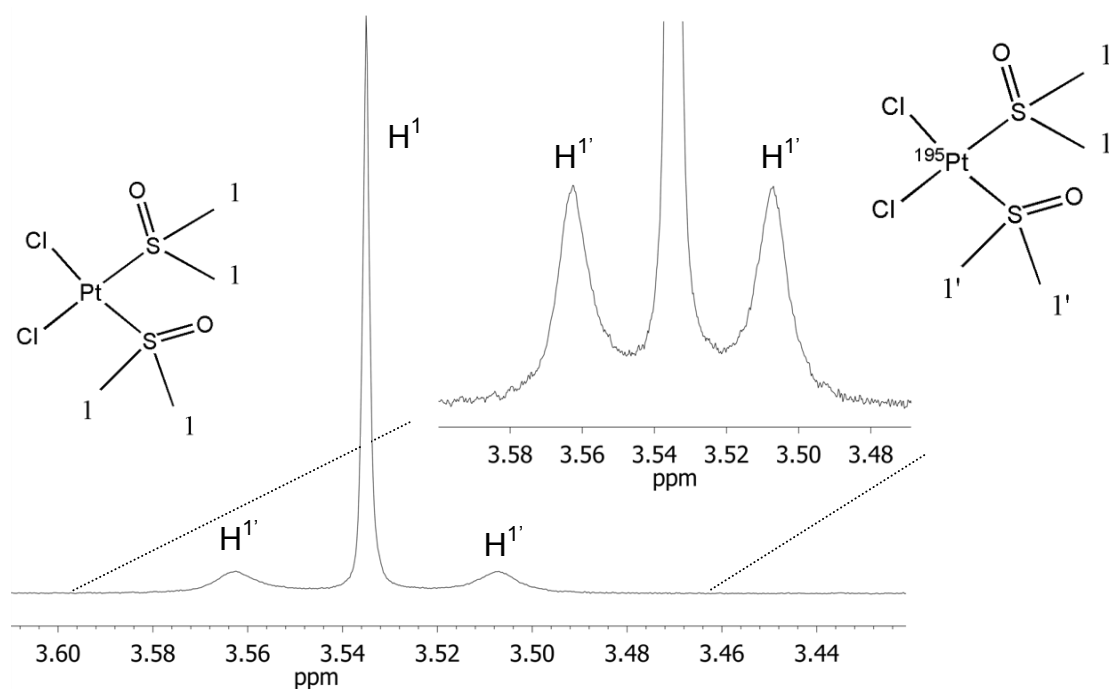


Figure 2.21 ^1H NMR spectrum of $\text{Pt}^{\text{II}}\text{Cl}_2(\text{DMSO})_2$ in chloroform- d_1 at 25°C .

Interestingly the ^1H NMR spectrum show coupling between the $-\text{CH}_3$ protons of the coordinated dimethyl sulfoxide (DMSO) and the ^{195}Pt metal centre as the broad doublet ($\text{H}^{1'}$) around the main singlet at 3.54 ppm with a coupling constant $^3J(^{195}\text{Pt}-^1\text{H}) = 22.5$ Hz in CDCl_3 . The singlet at 3.54 ppm corresponds to the DMSO coordinated to the NMR inactive Pt isotopes (*ca.* 67% natural abundance) and is labelled (H^1).

2.6.2 Synthesis of $[\text{Pt}^{\text{II}}\text{Cl}(\text{DMSO})(\text{en})]\text{Cl}$

$[\text{Pt}^{\text{II}}\text{Cl}(\text{DMSO})(\text{en})]\text{Cl}$ was synthesised as an analogue to $[\text{Pt}^{\text{II}}(\text{phen})(\text{L}^n\text{-S},\text{O})]\text{Cl}$ with the distinct difference of not having any aromatic groups. Therefore, this cationic complex could possibly form cation- π interactions with aromatic moieties without the capability of forming additional aromatic- π stacking interactions, as expected for $[\text{Pt}^{\text{II}}(\text{phen})(\text{L}^n\text{-S},\text{O})]\text{Cl}$. Moreover, cation- π interaction with aromatic moieties (pyrene or benzene) is thought to be of greater importance compared to aromatic- π stacking interactions in this case.

The synthesis of $[\text{Pt}^{\text{II}}\text{Cl}(\text{DMSO})(\text{en})]\text{Cl}$ involves the reaction of $\text{Pt}^{\text{II}}\text{Cl}_2(\text{DMSO})_2$ with ethylenediamine (en) in methanol.²⁹ However, acetonitrile was used instead of methanol with the product precipitated as a white powder-like material. The ^1H NMR spectrum of $[\text{Pt}^{\text{II}}\text{Cl}(\text{DMSO})(\text{en})]\text{Cl}$ in D_2O (Figure 2.22) shows the presence of $[\text{Pt}^{\text{II}}(\text{en})_2]^{2+}$ (*ca.* 10%) which is a side product which is always present for this synthesis.²⁹

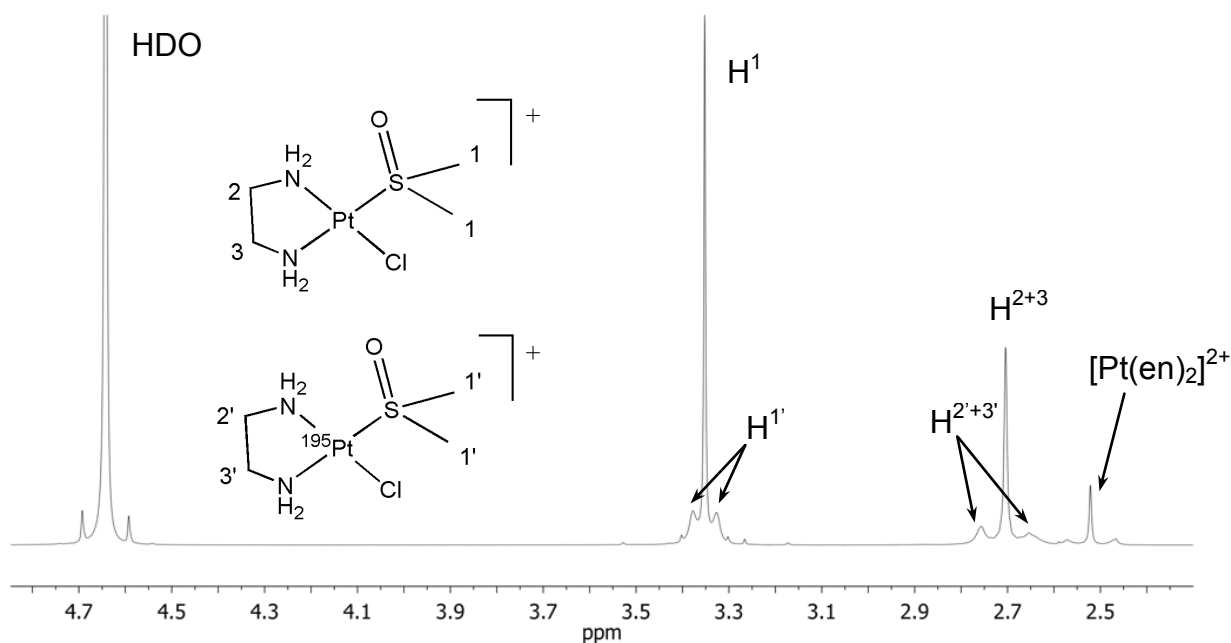


Figure 2.22 ^1H NMR spectrum of $[\text{Pt}^{\text{II}}\text{Cl}(\text{DMSO})(\text{en})]\text{Cl}$ in D_2O at 25°C .

Interestingly, isotopologues of $[\text{Pt}^{\text{II}}\text{Cl}(\text{DMSO})(\text{en})]^+$ could be observed with the complex containing the NMR active ^{195}Pt as broad doublets for H^1 and H^{2+3} while the NMR inactive isotopes exhibit no coupling and singlets are observed for H^1 and H^{2+3} . the $^3J(^{195}\text{Pt}-^1\text{H})$ coupling to H^1 and H^{2+3} is 20.3 and 42.3 Hz respectively and compares well with values of 23 and 42 Hz obtained by Tobe and co-workers.²⁹

2.7 Interesting features of the ^1H NMR spectra of platinum(II) diimine complexes

2.7.1 ^{195}Pt coupling in the ^1H NMR spectrum of square planar Pt^{II} (diimine) complexes and the effect of chemical shift anisotropy and quadrupolar coupling

The ^1H NMR spectra of the various Pt^{II} complexes exhibit scalar-coupling to the NMR active ^{195}Pt nuclei. The ability to observe the so-called platinum satellites in ^1H NMR depends largely on the spin-relaxation of the ^{195}Pt nuclei. If the relaxation rate is relatively slow, the ^1H lines of the ^{195}Pt -containing isotopic analogues are well resolved and split by the NMR active nucleus and coupling is observed. However, in the cases of fast relaxation of the ^{195}Pt nucleus, the satellites are expected to be broad and unresolved. In the case of extremely fast

relaxation of the J -coupling nucleus, no coupling is observed, a phenomenon known as self-decoupling.³⁰ This effect is indeed visible for the Pd complexes (Figure 2.16-Figure 2.20), where no ^{105}Pd coupling is observed due to the extremely fast relaxation of the ^{105}Pd quadrupolar nucleus.³⁰ However, in the case of ^{105}Pd , the quadrupolar relaxation mechanism is dominant, while for ^{195}Pt in square planar complexes, chemical shift anisotropy (CSA) is believed to be the major relaxation mechanism which is dependent on the magnetic field strength (B_0).³¹

Chemical shift anisotropy refers the dependence of the local magnetic field experienced by a nucleus on the orientation of the molecule relative to the direction of the applied magnetic field B_0 , since the molecules are not spherical. Reorientation (tumbling) of the molecule in the applied field results in a change, or fluctuation, of the local field which result in spin-lattice relaxation of the ^{195}Pt nucleus.

This motion can be expressed as a function of the rotational correlation time, τ_c , which is loosely defined as the average time it takes a molecule to change its orientation or rotate by 1 radian.²³ Furthermore, as the viscosity of the solution increases, the τ_c becomes longer, which result in an increase in the importance of the CSA mechanism which results in reduced relaxation times.

This effect is observed in the ^1H NMR spectrum of $\text{Pt}^{\text{II}}(\text{bipy})\text{Cl}_2$ in dimethyl sulfoxide- d_6 and acetonitrile- d_3 in which the ^{195}Pt satellites are significantly broader in dimethyl sulfoxide compared to the less viscous acetonitrile (Figure 2.23) at the same temperature and B_0 . This broadening due to CSA relaxation can also be observed in the ^1H NMR spectrum of the square-planar $\text{Pt}^{\text{II}}\text{Cl}_2(\text{DMSO})_2$ complex (Figure 2.21). A marked difference in the line width of the ^{195}Pt satellites of $\text{Pt}^{\text{II}}\text{Cl}_2(\text{DMSO})_2$ and the parent line is observed with the peak width at half-height $\Delta\nu_{1/2} \approx 4.0$ Hz for the ^{195}Pt satellites compared to 0.6 Hz for the parent line.

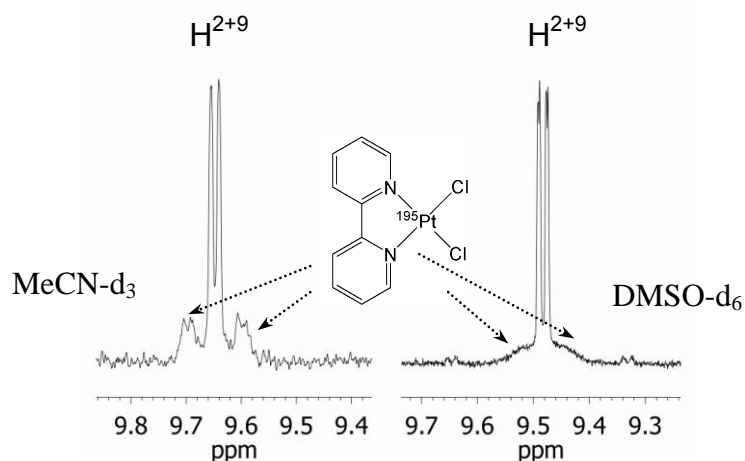


Figure 2.23 The effect of solvent on the CSA relaxation due to the change in correlation time, τ_c , displayed in the broadness of the platinum satellites of H^2 observed in the 1H NMR spectra of $Pt^{II}(bipy)Cl_2$ in acetonitrile- d_3 and dimethyl sulfoxide- d_6 at the same field (600 MHz).

However, broadening of the ^{195}Pt satellites is not only due to the increase in correlation time i.e. slow tumbling, τ_c , but also the strength of the external magnetic field, B_0 . CSA effects decrease at lower magnetic field strength since the CSA relaxation is directly dependant on the square of the applied field (B_0^2).^{23,31} The relationship between the spin lattice relaxation time due to CSA is given by equation 2.1:³¹

$$T_1^{-1}(CSA) \propto \gamma B_0^2 (\Delta\sigma)^2 \tau_c \quad (2.1)$$

Where, $T_1^{-1}(CSA)$ is the spin lattice relaxation due to CSA, γ the gyromagnetic ratio of the observed nucleus and $\Delta\sigma$ the anisotropy term. The dependence of the CSA relaxation on the square of the magnetic fields strength (B_0^2) can be clearly seen by the broad ^{195}Pt satellites observed for $Pt^{II}(phen)(L^1-S,O)Cl$ at 600MHz compared to the 400 MHz 1H NMR spectrum (Figure 2.24).

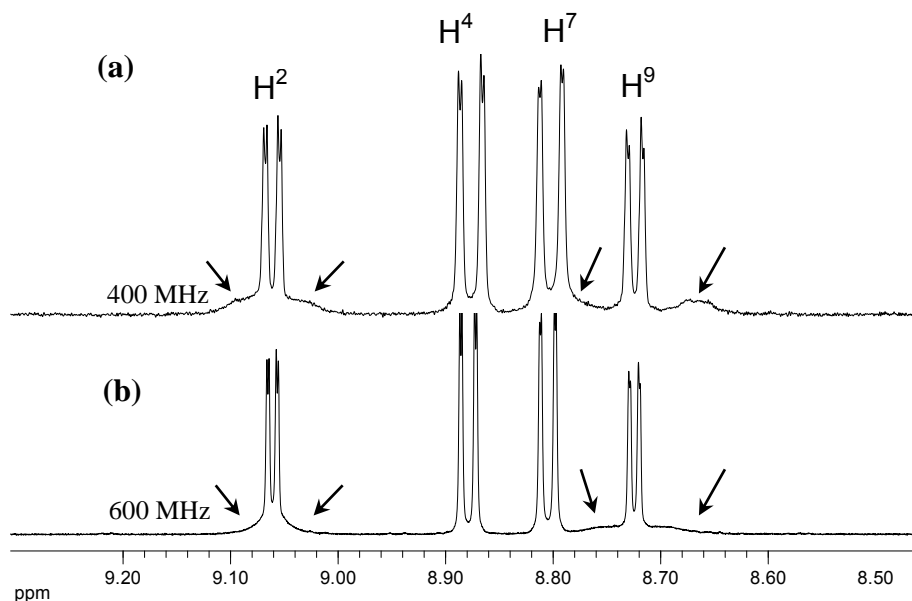


Figure 2.24 The ^1H NMR spectrum of $\text{Pt}^{\text{II}}(\text{phen})(\text{L}^1\text{-S},\text{O})\text{Cl}$ showing broad unresolved ^{195}Pt satellites that are more visible (a) at 400 MHz (9.4 T) than (b) at a higher magnetic field of 600 MHz (14.1 T).

The ^{195}Pt J -coupling constant to H^2 and H^9 in the $\text{Pt}^{\text{II}}(\text{phen})(\text{L}^1\text{-S},\text{O})\text{Cl}$ complex is significantly different in magnitude and the signals are broad (Figure 2.24b). The platinum satellites of H^2 and H^9 in the $[\text{Pt}^{\text{II}}(\text{bipy})(\text{L}^1\text{-S},\text{O})]\text{Cl}$ complex however, was significantly more resolved with the corresponding coupling constants $^3J(^{195}\text{Pt}\text{-H}^2) = 23 \text{ Hz}$ and $^3J(^{195}\text{Pt}\text{-H}^9) = 46 \text{ Hz}$. (Figure 2.25)

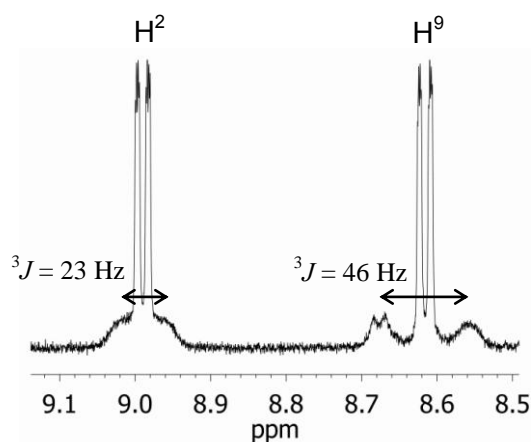


Figure 2.25 ^1H NMR peaks of H^2 and H^9 showing $^3J(^{195}\text{Pt}\text{-}^1\text{H})$ coupling for (a) $[\text{Pt}^{\text{II}}(\text{bipy})(\text{L}^1\text{-S},\text{O})]\text{Cl}$.

The difference in the magnitude of the ^1H - ^{195}Pt coupling constants observed for H^2 and H^9 can be rationalised on the basis of electron density in the Pt-N bonds *trans* to the donor atoms of the *N,N*-di(alkyl)-*N'*-acylthiourea. The Pt-S bond is thought to be the strongest and withdraws more electrons from the Pt-N bond *trans* to the sulphur atom. This leads to a loss of electron density in the region *trans* to the sulphur causing N^1 and H^2 to be the most deshielded. Less electron density implies that the coupling constant must decrease because of the 'through-bond' coupling nature of scalar J-coupling.³² The relationship between the J-coupling and the nature of the bonding between two atoms A and B is given by the Ramsey formula (equation 2.2):³³

$$J(A, B) \propto -\gamma_A \gamma_B |\psi_{ns}(O)_A|^2 |\psi_{ns}(O)_B|^2 \pi_{A,B} \quad (2.2)$$

where, γ is the gyromagnetic ratios of nucleus A and B, the $|\psi_{ns}(O)|^2$ term represents the valence *s* electron density at the nucleus and π_{AB} the mutual polarizability.

2.7.2 The second-order “roof” effect observed in the ^1H NMR spectrum of $\text{Pt}^{\text{II}}(\text{phen})$ complexes

The ^1H NMR spectra of all the $\text{Pt}^{\text{II}}(\text{phen})$ complexes showed an interesting second-order spin-spin coupling effect commonly known as the ‘roof’ effect, especially for protons H^5 and H^6 . The doublets of H^5 and H^6 are distorted due to strong coupling between two nuclei which alters the transitional probabilities of the four NMR lines reflected in the intensity of the lines of the multiplets. The probabilities of the transitions corresponding to the inner lines are increased by this strong coupling, while those corresponding to the outer lines become less probable, as seen from the difference in intensities observed (Figure 2.26).³⁴ This effect is more pronounced for a smaller gap or difference in frequency ($\delta\nu$) between $\alpha_A\beta$ and $\beta_A\alpha_B$ relative to the scalar coupling (J) between the two nuclei A and B, where α and β are the two spin states ($m = +1/2$ and $-1/2$) of the respective nuclei (spin quantum number $I = 1/2$ i.e. ^1H).

The two cases of weak- and strong coupling are displayed as conventional- and distorted doublets shown in Figure 2.26a with the corresponding energy level diagrams.

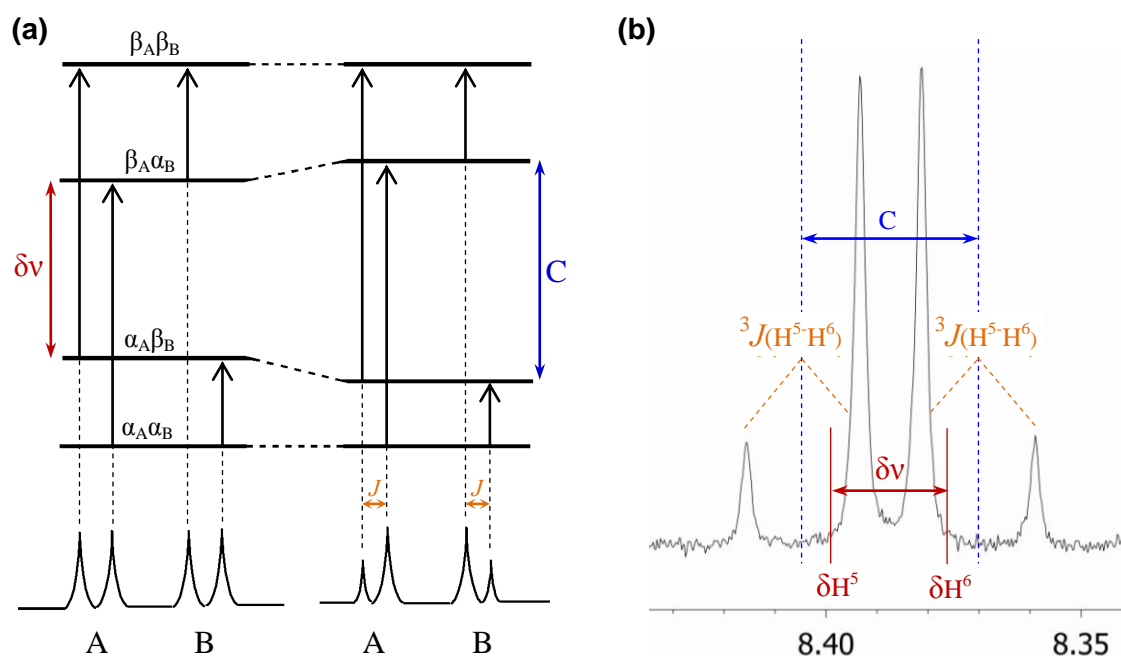


Figure 2.26 (a) Energy levels and the predicted spectra of two ${}^1\text{H}$'s in a weakly coupled system (left of diagram) and in the case of strong coupling to the right.³⁴ (b) The 'roof' effect observed of the strongly coupled H^5 and H^6 of $\text{Pt}^{\text{II}}(\text{phen})(\text{L}^1\text{-S},\text{O})\text{Cl}$ in chloroform- d_1 , where $\delta\nu$ is the chemical shift difference between H^5 and H^6 and C denotes the separation of the two central states.

In the presence of strong coupling as observed for H^5 and H^6 , the separation of the two states increases from $\delta\nu$ to $C = [(\delta\nu)^2 + J^2]^{1/2}$, while the doublets are no longer centred at the chemical shift positions ($\delta\text{H}^{5/6}$) as shown by the red lines in Figure 2.26b and Figure 2.27.

The effect of the magnitude of the coupling constant relative to the chemical shift difference ($\delta\nu$) on the ${}^1\text{H}$ NMR spectra of various $\text{Pt}^{\text{II}}(\text{phen})$ complexes are shown in Figure 2.27 with $\delta\nu$ ranging from $8.8J$ to 0. The coupling constant between H^5 and H^6 is constant at ${}^3J = 8.9$ Hz with the inner lines of the two doublets increase in intensity while the outer lines become weaker in intensity as the chemical shift differences ($\delta\nu$) decreases until $\delta\nu = 0$, where only a single line is observed for H^5 and H^6 .

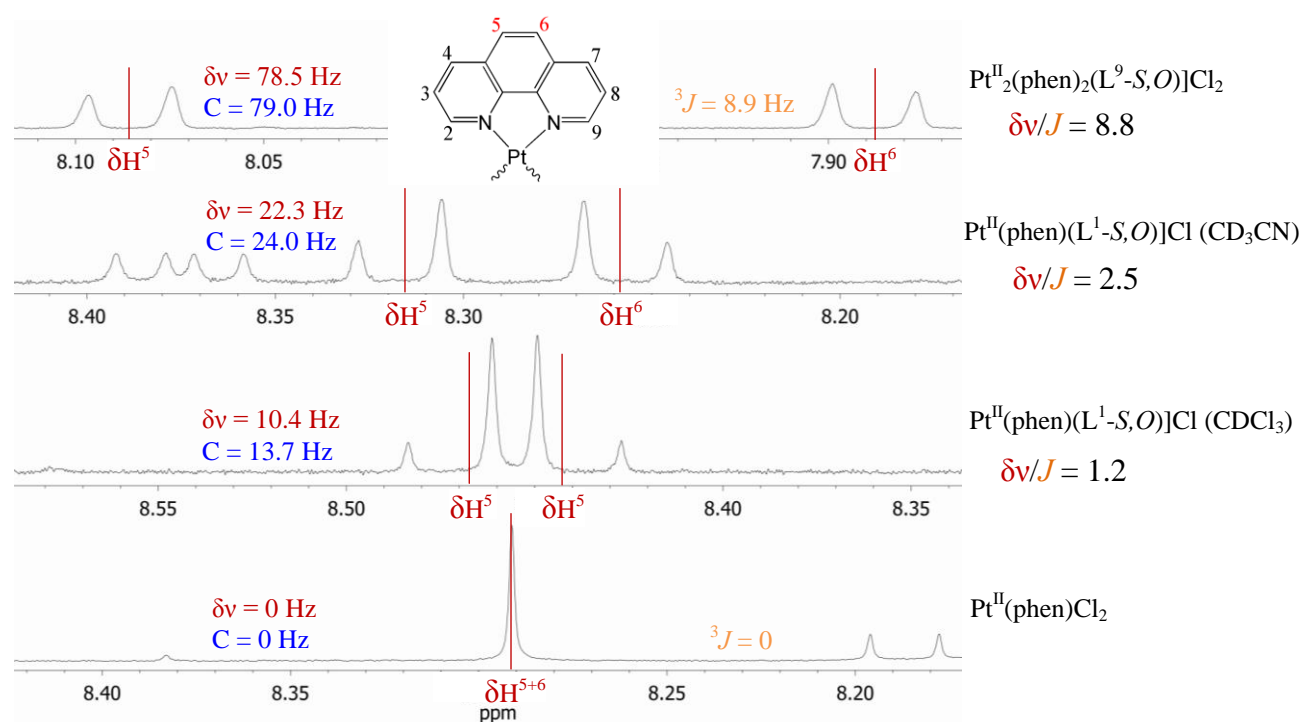


Figure 2.27 ^1H NMR spectra of various $\text{Pt}^{\text{II}}(\text{phen})$ complexes showing a range of $\delta\nu/J$ values between 8.8 and zero for the strongly coupled protons H^5 and H^6 .

Interestingly, the difference between $\delta\nu$ and C increases significantly from 0.5 Hz for weakly coupled $\text{Pt}^{\text{II}}_2(\text{phen})_2(\text{L}^9\text{-S},\text{O})\text{Cl}_2$ complex to 3.2 Hz for the strongly coupled $\text{Pt}^{\text{II}}(\text{phen})(\text{L}^1\text{-S},\text{O})\text{Cl}$. Therefore, the chemical shift of strongly coupled nuclei such as H^5 and H^6 in $\text{Pt}^{\text{II}}(\text{phen})(\text{L}^1\text{-S},\text{O})\text{Cl}$ is shifted from the ‘centre’ of the distorted doublets (blue dashed lines in Figure 2.26b) towards the more intense inner NMR lines of the doublets with the actual chemical shift of H^5 and H^6 (δH^5 and δH^6 indicated by the red lines) shifted by a value $\frac{1}{2}(C - \delta\nu) = 1.9$ Hz.

Therefore, for characterisation purposes, the chemical shifts of H^5 and H^6 are reported as a single value at the centre of the two distorted doublets since the actual chemical shift can only be obtained by the calculations discussed above.

2.8 Experimental Section

2.8.1 Instrumentation

^1H NMR and 2D NMR experiments were done in 5mm tubes using a Varian Unity Inova 400 MHz spectrometer operating at 399.95 MHz or a Varian Unity Inova 600 MHz spectrometer equipped with an inverse detection pulsed field gradient (idpfg) probe operating at 599.99

MHz. Melting points were determined using an Electrothermal IA9300 Digital Melting Point Apparatus. UV-VIS spectra were recorded on a single beam Agilent 8253E UV-visible spectrophotometer. The IR absorbance spectra were recorded on a Thermo Nicolet Nexus FT-IR spectrometer fitted with a Smart-ATR adaptor. Elemental analysis for C, H and N was done on an EA Euro 3000 Elemental Analyser. Electron spray mass spectra were obtained using a Waters Synapt G2 Mass Spectrometer with leucine enkephalin as lock mass.

2.8.2 Crystal and Structure Refinement Data for Pt^{II}(bipy)Cl₂·CH₃CN

	Pt ^{II} (bipy)Cl ₂ ·CH ₃ CN	
Empirical formula	C ₁₀ H ₈ Cl ₂ N ₂ Pt, 2(C ₂ H ₃ N)	
Formula weight	463.23	
Temperature (K)	100	
Wavelength (Å)	0.71073	
Crystal system	Monoclinic	
Space group	P21/n	
Unit cell dimensions (Å, °)	$a = 9.1069(2)$	$\alpha = 90$
	$b = 22.7965(6)$	$\beta = 101.342(1)$
	$c = 13.1246(4)$	$\gamma = 90$
Volume (Å ³)	2671.53(12)	
Z	8	
Calculated density (g cm ⁻³)	2.303	
Absorption coefficient (mm ⁻¹)	10.888	
F_{000}	1728	
Crystal size (mm ³)	0.08 x 0.10 x 0.33	
θ range for data collection (°)	1.8 to 26.4	
Reflections collected	20604	
Independent reflections	5473 [$R_{\text{int}} = 0.052$]	
Data / restraints / parameters	4557 / 0 / 327	
Goodness-of-fit on F^2	1.04	
Final R indices [$I > 2\sigma(I)$]	$R1 = 0.0318$, $wR2 = 0.0666$	
Largest diff. peak and hole (e Å ⁻³)	-0.98, 2.12	

2.8.3 Synthetic procedures of Pt^{II} complexes and precursors

2.8.3.1 Preparation of N,N-di(alkyl)-N'-acylthiourea

The synthesis of *N*-pyrrolidyl-*N'*-pivaloylthiourea (HL¹) was done using the method described by Douglas and Dains.⁹ The ligands HL² – HL¹⁴ were previously synthesised and purified by co-workers and were used with their permission. The synthesis of HL¹ was carried out in anhydrous acetone which was collected from an acetone still with 4Å molecular

sieves. Vacuum oven dried KSCN (16 mmol) was dissolved in acetone (25 ml) to which pivaloyl chloride (15 mmol) was added drop-wise. The reaction mixture was heated to reflux for 45 minutes and cooled to room temperature before pyrrolidine (15 mmol) was drop-wise added. The reaction mixture was then heated to reflux for an additional 2 hours before it was poured into a beaker containing 50ml water at room temperature. The evaporation of the acetone over the course of 2 days in the fume hood resulted in the white crystalline product.

***N*-pyrrolidyl-*N'*-pivaloylthiourea (HL¹):** 2.44 g, Yield 76 %, m.p. 136-137°C; ¹H NMR (399.95 MHz, DMSO-d₆, 25°C), δ=9.74 (s, 1H: NH), 3.63 (m, 2H: H^a), 3.42 (m, 2H: H^a), 1.90 (m, 4H: H^b, H^b), 1.16 (s, 9H: H¹); ¹³C NMR (50.31 MHz, CDCl₃, 25°C), δ=27.16 (C^{3''}), 39.62 (C^{2''}), 54.43 (C^{3'}), 52.52 (C³), 26.16 (C^{4'}), 24.59 (C⁴), 176.66 (C^S), 174.38 ppm (C^O); UV/Vis: λ_{max} (ε) 216(13 399), 276 nm (14 792 dm³mol⁻¹cm⁻¹); Elemental analysis calculated (%) for C₁₀H₁₈N₂OS: C 57.8, H 8.5, N 13.1, S 14.96; found: C 57.0, H 8.8, N 13.3, S 14.8.

2.8.3.2 Preparation of Pt^{II}(diimine)Cl₂

The general method of Morgan and Burstall was used to prepare Pt^{II}Cl₂(phen) and Pt^{II}(bipy)Cl₂.¹³ K₂[Pt^{II}Cl₄] (0.95g, 2.3 mmol) was dissolved in water (50ml) containing 6 ml of a 4M HCl solution. The diimine (phen/bipy) was added in a slight excess (2.32 mmol) and the solution heated to a gentle reflux for 2 to 14 hours. The yellow product precipitated from solution upon cooling to 4°C, was recovered by filtration and washed with cold deionized water followed by an acetonitrile and ether wash to remove unreacted [Pt^{II}Cl₄]²⁻ and diimine respectively and dried under vacuum. The product was obtained in high yields (87-96%).

Pt^{II}Cl₂(1,10-phenanthroline): 980 mg, Yield 96 %, m.p. > 350°C. ¹H NMR (399.95 MHz, DMSO-d₆, 25°C), δ=9.70 (dd, ⁴J(H,H)=1.3 Hz, ³J(H,H)=5.5 Hz, 2H; H⁹, H²), 9.04 (dd, ⁴J(H,H)=1.3Hz, ³J(H,H)=8.2 Hz, 2H; H⁴, H⁷), 8.29 (s, 2H; H⁵, H⁶), 8.17 ppm (dd, ³J(H,H)=5.5 Hz, ³J(H,H)=8.2 Hz, 2H; H³, H⁸). IR (ATR): ν (cm⁻¹), 3083 (arom. C-H stretch), 3059 (arom. C-H stretch), 1427 (arom. C-C stretch), 1220 (asym. C-N stretch) 1208 (sym. C-N stretch); Elemental analysis calculated (%) for C₁₂H₈N₂Pt: C 32.30, N 6.28; found: C 32.6, N 6.0.

Pt^{II}(2,2-bipyridyl)Cl₂: 197 mg, Yield 90.6 %, m.p. > 350°C. ¹H NMR (399.95 MHz, DMSO-d₆, 25°C), δ=9.50 (dd, 2H; H⁹, H²), 8.58 (d, 2H; H⁵, H⁶), 8.42 (td, 2H; H⁴, H⁷), 7.84 ppm (ddd, H³, H⁸). Elemental analysis calculated (%) for C₁₀H₈N₂Pt: C 28.45, H 1.91, N 6.64; found (%): C 29.0, H 2.4, N 7.0.

2.8.3.3 Preparation of ([Pt^{II}(phen)(Lⁿ-S,O)]Cl

The general method for the synthesis of mixed-ligand [Pt^{II}(diimine)(Lⁿ-S,O)]PF₆ complexes, described by Koch *et al.*¹ was modified for the preparation of [Pt^{II}(phen)(L¹-S,O)]Cl. A suspension of Pt^{II}Cl₂(phen) (0.045 g, 0.1 mmol) in 10 ml of acetonitrile was heated under reflux for 10 min, after which *N*-pyrrolidyl-*N'*-pivaloylthiourea (0.022 g, 0.101 mmol) in 2 ml acetonitrile was added dropwise and the mixture heated under reflux for 15 min. A suspension of sodium acetate (NaOAc) (0.028 g, 0.15 mmol) in acetonitrile was added and the mixture was heated under reflux *ca.* 14 hrs. The mixture was allowed to cool to room temperature and filtered through Celite to remove any NaCl precipitate formed. The filtrate was concentrated by evaporation to a volume of *ca.* 2 ml. Diethyl ether (100 ml) was added to precipitate the product and this precipitate was collected by centrifugation, resuspended several times with cold diethyl ether and centrifuged again. The yellow product was dried overnight under vacuum.

In some cases dichloromethane was used as solvent instead of acetonitrile while the NaOAc was replaced by triethylamine. The use of methanol as solvent was also investigated with NaOAc which is soluble in methanol. Reaction yields varied significantly for this series of complexes; these details will be discussed in the next chapter.

[Pt^{II}(phen)(L¹-S,O)]Cl: 58 mg, Yield 93%, m.p. 134 – 135 °C ¹H NMR (599.99 MHz, CD₃CN), δ=9.01 (dd, ⁴J(H,H)=0.9 Hz, ³J(H,H)=4.5 Hz, 1H: H²), 8.85 (dd, ⁴J(H,H)=0.9 Hz, ³J(H,H)=7.7 Hz, 1H: H⁴), 8.77 (dd, ⁴J(H,H)=0.6 Hz, ³J = 7.8 Hz, 1H: H⁷), 8.66 (d, ³J(H,H)=5.3 Hz, 1H: H⁹), 8.15 (dd, ³J(H,H)=4.5 Hz, ³J(H,H)=7.7 Hz 1H: H³), 8.12 (m, 2H: H⁵, H⁶), 7.84 (dd, ³J(H,H)=5.3 Hz, ³J(H,H)=7.3 Hz, 1H: H⁸) 3.76 (t, 2H: H^a), 3.74 (t, 2H: H^a), 2.11 (p, 2H: H^b), 2.02 (p, 2H: H^b), 1.33 ppm (s, 9H: H¹). IR (ATR): ν (cm⁻¹), 3086 (arom. C-H stretch), 3059 (arom. C-H stretch), 2969 (C-H stretch), 2927 (C-H stretch), 1482

(C-O stretch), 1380 (CH₃ umbrella deformation), 1434 (arom. C-C stretch) 1264 (asym. C-N stretch) 1228 (sym. C-N stretch); (+) ESI MS: *m/z* 588.141 (*M*⁺)

[Pt^{II}(phen)(L²-S,O)]Cl: 46 mg, Yield 41%, m.p. 121 - 123 °C ¹H NMR (399.95 MHz, DMSO-d₆), δ=9.06 (d, 2H: H⁴⁺⁷), 9.01 (d, 1H: H²), 8.93 (d, 1H: H⁹), 8.42 (d, 1H: H⁸), 8.33 (m, 2H: H⁵, H⁶), 8.19 (d, 1H: H^{2'}), 8.14 (m, 2H: H³, H⁸), 8.08 (m, 2H: H^{4'}, H^{5'}), 7.63 (m, 2H: H^{6'}, H^{3'}), 7.56 (m, 1H: H^{7'}), 3.92 (t, 2H: H^{a'}), 3.80 (t, 2H: H^a), 1.85 (p, 2H: H^{b'}), 1.68 (p, 2H: H^b), 1.50 (s, 2H: H^{c'}), 1.27 (s, 2H: H^c), 1.03 (t, 3H: H^{d'}), 0.83 ppm (t, 3H: H^d); (+) ESI MS: *m/z* 716.204 (*M*⁺)

[Pt^{II}(phen)(L³-S,O)]Cl: 20 mg, Yield 20%, m.p. 151 - 154 °C ¹H NMR (399.95 MHz, DMSO-d₆), δ=9.10 (dd, 1H: H²), 8.78 (dd, 1H: H⁴), 8.69 (m, 2H: H⁷, H⁹), 8.14 (dd, 1H: H³), 8.07 (m, 2H: H^{2'}, H^{6'}), 8.04 (m, 2H: H⁵, H⁶), 7.80 (dd, H: H⁸), 7.67 (t, 1H: H^{4'}) 7.52 (t, 2H: H^{3'}, H^{5'}), 3.76 (m, 4H: H^{a'}, H^a), 1.83 (p, 2H: H^{b'}), 1.70 (p, 2H: H^b), 1.52 (s, 2H: H^{c'}), 1.43 (s, 2H: H^c), 1.09 (t, 3H: H^{d'}), 0.98 ppm (t, 3H: H^d); (+) ESI MS: *m/z* 666.187 (*M*⁺)

[Pt^{II}(phen)(L⁴-S,O)]Cl: 43 mg, Yield 75%, m.p. 218 - 221 °C ¹H NMR (399.95 MHz, DMSO-d₆), δ=9.34 (dd, 1H: H²), 9.13 (d, 1H: H⁴), 9.06 (d, 1H: H⁷), 9.06 (d, 1H: H⁹), 8.43 (dd, 1H: H³), 8.35 (m, 2H: H⁵, H⁶), 8.26 (d, 2H: H^{2'}, H^{6'}), 8.11 (dd H: H⁸), 7.70 (m, 1H: H^{4'}) 7.58 (t, 2H: H^{3'}, H^{5'}), 3.97 (q, 2H: H^{a'}), 3.93 (q, 2H: H^a) 1.42 (t, 3H: H^{b'}), 1.29 ppm (t, 3H: H^b); (+) ESI MS: *m/z* 610.124 (*M*⁺)

[Pt^{II}(phen)(L⁵-S,O)]Cl: 50 mg, Yield 45 %, m.p. 208 - 209 °C ¹H NMR (399.95 MHz, DMSO-d₆), δ=9.38 (dd, 1H: H²), 9.16 (d, 1H: H⁴), 9.11 (d, 1H: H⁹), 9.09 (d, 1H: H⁷), 8.45 (dd, 1H: H³), 8.38 (m, 2H: H⁵, H⁶), 8.29 (d, 2H: H^{2'}, H^{6'}), 8.15 (dd H: H⁸), 7.63 (t, 2H: H^{3'}, H^{5'}), 4.00 (q, 2H: H^{a'}), 3.94 (q, 2H: H^a), 1.44 (t, 3H: H^{b'}), 1.30 ppm (t, 3H: H^b); (+) ESI MS: *m/z* 644.085 (*M*⁺)

[Pt^{II}(phen)(L⁶-S,O)]Cl: 104 mg, Yield 95%, m.p. 239 - 240 °C ¹H NMR (399.95 MHz, DMSO-d₆), δ=9.40 (dd, 1H: H²), 9.15 (d, 1H: H⁴), 9.09 (d, 1H: H⁹), 9.07 (d, 1H: H⁷), 8.43 (dd, 1H: H³), 8.37 (m, 2H: H⁵, H⁶), 8.27 (d, 2H: H^{2'}, H^{6'}), 8.15 (dd H: H⁸), 7.12 (t, 2H: H^{3'}, H^{5'}), 3.99 (q, 2H: H^{a'}), 3.93 (q, 2H: H^a), 3.89 (s, 3H: H^{7'}), 1.44 (t, 3H: H^{b'}), 1.30 ppm (t, 3H: H^b); (+) ESI MS: *m/z* 640.136 (*M*⁺)

[Pt^{II}(phen)(L⁷-S,O)]Cl: 103 mg, Yield 95%, m.p. 235 - 236 °C ¹H NMR (399.95 MHz, DMSO-d₆), δ=9.29 (dd, 1H: H²), 9.07 (d, 1H: H⁴), 9.00 (d, 1H: H⁷), 8.94 (d, 1H: H⁹), 8.39 (dd, 1H: H³), 8.30 (m, 2H: H⁵, H⁶), 8.20 (d, 2H: H^{2'}, H^{6'}), 8.05 (dd H: H⁸), 7.71 (m, 1H: H^{4'}) 7.57 (m, 2H: H^{3'}, H^{5'}), 3.44 (s, 3H: H^{a'}), 3.42 ppm (s, 3H: H^a); (+) ESI MS: *m/z* 582.092 (*M*⁺)

[Pt^{II}(phen)(L⁸-S,O)]Cl: 90 mg, Yield 84%, m.p.158 - 160 °C ¹H NMR (399.95 MHz, DMSO-d₆), δ=9.26 (dd, 1H: H²), 9.09 (d, 1H: H⁴), 9.00 (d, 1H: H⁷), 8.94 (d, 1H: H⁹), 8.38 (dd, 1H: H³), 8.29 (d, 2H: H⁵, H⁶), 8.14 (d, 2H: H^{2'}, H^{6'}), 8.07 (dd H: H⁸), 7.07 (t, 2H: H^{3'}, H^{5'}), 3.92 (q, 2H: H^{a'}), 3.86 (q, 2H: H^a), 1.42 (t, 3H: H^{b'}), 1.29 ppm (t, 3H: H^b); (+) ESI MS: *m/z* 640.137 (*M*⁺)

[Pt^{II}(phen)(L⁹-S,O)]Cl: 93 mg, Yield 70%, m.p. 169 - 171 °C ¹H NMR (399.95 MHz, DMSO-d₆), δ=9.16 (dd, 1H: H²), 8.99 (dd, 1H: H⁴), 8.57 (dd, 1H: H⁷), 8.26 (dd, 1H: H³), 8.09 (d, 1H: H⁵), 7.96 (d, 1H: H⁹), 6.89 (s, 1H: H⁶), 7.55 ppm (dd, 1H: H⁸), 3.84 (q, 2H: H^{a'}), 3.82 (q, 2H: H^a), 1.38 (t, 2H: H^{b'}), 1.32 ppm (t, 2H: H^b); (+) ESI MS: *m/z* 561.117 (*M*²⁺)

[Pt^{II}(phen)(L¹⁰-S,O)]Cl: 87 mg, Yield 88%, m.p. 198 - 201 °C ¹H NMR (399.95 MHz, DMSO-d₆), δ=9.33 (dd, 1H: H²), 9.11 (dd, 1H: H⁴), 9.06 (dd, H: H⁹), 9.04 (dd, 1H: H⁷), 8.40 (dd, 1H: H³), 8.33 (m, 2H: H⁵, H⁶), 8.22 (m, 2H: H^{2'}, H^{6'}), 8.07 (dd, H: H⁸), 7.70 (m, 1H: H^{4'}) 7.57 (m, 2H: H^{3'}, H^{5'}), 4.18 (m, 4H: H^{a'}, H^a), 1.76 (m, 4H: H^{b'}, H^b), 1.69 ppm (m, 2H: H^c); (+) ESI MS: *m/z* 622.124 (*M*⁺)

[Pt^{II}(phen)(L¹¹-S,O)]Cl: 93 mg, Yield 96%, m.p. 128-132 °C ¹H NMR (399.95 MHz, DMSO-d₆), δ=9.23 (dd, 1H: H²), 9.15 (dd, 1H: H⁴), 9.09 (dd, H: H⁹), 9.07 (dd, 1H: H⁷), 8.44 (dd, 1H: H³), 8.37 (m, 2H: H⁵, H⁶), 8.11 (dd, H: H⁸), 4.17 (m, 2H: H^{a'}), 4.09 (m, 2H: H^a), 1.75 (m, 4H: H^{b'}, H^b), 1.65 (m, 2H: H^c), 1.35 ppm (s, 9H: H¹); (+) ESI MS: *m/z* 602.155 (*M*⁺)

[Pt^{II}(phen)(L¹²-S,O)]Cl: 79 mg, Yield 82%, m.p. 130 - 133 °C ¹H NMR (399.95 MHz, DMSO-d₆), δ=9.19 (dd, 1H: H²), 9.15 (dd, 1H: H⁴), 9.07 (dd, 1H: H⁷), 9.05 (dd, H: H⁹), 8.43 (dd, 1H: H³), 8.36 (m, 2H: H⁵, H⁶), 8.10 (dd, H: H⁸), 4.20 (m, 2H: H^{a'}), 4.12 (m, 2H: H^a), 3.85 (m, 2H: H^{b'}), 3.75 (m, 2H: H^b), 1.34 ppm (s, 9H: H¹); (+) ESI MS: *m/z* 604.134 (*M*⁺)

[Pt^{II}(phen)(L¹³-S,O)]Cl: 73 mg, Yield 70%, m.p. 132 - 135 °C ¹H NMR (399.95 MHz, MeCN-d₃), δ=9.06 (dd, 1H: H²), 8.86 (dd, 1H: H⁴), 8.79 (dd, 1H: H⁷), 8.78 (dd, H: H⁹), 8.16 (dd, 1H: H³), 8.13 (m, 2H: H⁵, H⁶), 7.88 (dd, H: H⁸), 3.82 (t, 2H: H^a), 3.76 (t, 2H: H^a), 1.85 (p, 2H: H^b), 1.70 (p, 2H: H^b), 1.52 (s, 2H: H^c), 1.39 (s, 2H: H^c), 1.06 (t, 3H: H^d), 0.98 (t, 3H: H^d), 1.35 ppm (s, 9H: H¹); (+) ESI MS: *m/z* 646.219 (*M*⁺)

[Pt^{II}(phen)(L¹⁴-S,O)]Cl: 66 mg, Yield 67%, m.p. 125 - 130 °C ¹H NMR (399.95 MHz, DMSO-d₆), δ=9.23 (dd, 1H: H²), 9.15 (dd, 1H: H⁴), 9.07 (dd, 1H: H⁷), 9.05 (dd, H: H⁹), 8.44 (dd, 1H: H³), 8.37 (m, 2H: H⁵, H⁶), 8.13 (dd, H: H⁸), 3.93 (q, 2H: H^a), 3.81 (q, 2H: H^a), 1.40 (t, 2H: H^b), 1.35 (s, 9H: H¹), 1.24 ppm (t, 2H: H^b); (+) ESI MS: *m/z* 590.154 (*M*⁺)

2.8.3.4 Preparation of [Pt^{II}(bipy)(Lⁿ-S,O)]Cl

The preparation of [Pt^{II}(bipy)(Lⁿ-S,O)]Cl complexes were done using the method described in Section 2.8.3.3 for the synthesis of [Pt^{II}(phen)(Lⁿ-S,O)]Cl.

[Pt^{II}(bipy)(L¹-S,O)]Cl: 180 mg, Yield 98%, m.p. 132 - 134 °C ¹H NMR (399.95 MHz, MeCN-d₃), δ=8.97 (ddd, 1H: H²), 8.60 (ddd, 1H: H⁹), 8.43 (m, 2H: H⁵, H⁶), 8.37 (td, 1H: H⁴), 8.28 (td, 1H: H⁷), 7.29 (ddd, 1H: H³), 7.61 ddd, 1H: H⁸), 3.75 (t, 2H: H^a), 3.71 (t, 2H: H^a), 2.12 (p, 2H: H^b), 2.01 (p, 2H: H^b), 1.31 ppm (s, 9H: H¹).; (+) ESI MS: *m/z* 564.140 (*M*⁺)

[Pt^{II}(bipy)(L²-S,O)]Cl: 170 mg, Yield 78%, m.p. 88 - 90 °C ¹H NMR (399.95 MHz, CHCl₃-d₁), δ=8.80 (ddd, 1H: H²), 8.68 (ddd, 1H: H⁹), 8.60 (m, 2H: H⁵, H⁶), 8.40 (m, 2H: H⁸, H²), 8.35 (ddd, 1H: H⁴), 8.04 (d, 1H: H³), 7.96 (m, 2H: H⁴, H⁵), 7.66 (dd, 1H: H⁷), 7.54 (m, 4H: H³, H⁶, H⁷, H⁸), 3.88 (t, 2H: H^a), 3.79 (t, 2H: H^a), 1.90 (p, 2H: H^b), 1.73 (p, 2H: H^b), 1.55 (s, 2H: H^c), 1.35 (s, 2H: H^c), 1.08 (t, 3H: H^d), 0.92 ppm (t, 3H: H^d); (+) ESI MS: *m/z* 692.205 (*M*⁺)

2.8.3.5 Preparation of *cis*-[Pt^{II}Cl₂(DMSO)₂]

The neural *cis*-platinum dimethyl sulfoxide complex was prepared using the method of Price *et al.*²⁸ K₂[Pt^{II}Cl₄] (0.5 mmol) was dissolved in a minimum volume of deionized water (2 ml); to this solution dimethyl sulfoxide (1.5 mmol) was added and the solution stirred at room temperature for 2 hours. Upon addition of DMSO the colour of the solution changed instantly

from red to orange with a yellow precipitate. This $\text{Pt}^{\text{II}}\text{Cl}_2(\text{DMSO})_2$ precipitate was filtered off and washed with water, ethanol and ether and was dried under vacuum to obtain a yield of 60%.

$\text{Pt}^{\text{II}}\text{Cl}_2(\text{DMSO})_2$: 126 mg, Yield 60 %, m.p. 225 - 227 °C. ^1H NMR (399.95 MHz, chloroform- d_1 , 25°C), $\delta=3.54$ (s, 6H, H^1), 3.54 ppm (d, $^3J(^{195}\text{Pt}-^1\text{H}) = 22.5$ Hz, $\text{H}^{1'}$).

2.8.3.6 Preparation of $[\text{Pt}^{\text{II}}\text{Cl}(\text{DMSO})(\text{en})]\text{Cl}$

The cationic $[\text{Pt}^{\text{II}}\text{Cl}(\text{DMSO})(\text{en})]\text{Cl}$ was prepared by the method described by Tobe and co-workers.²⁹ However, acetonitrile was used as solvent instead of methanol. Ethylenediamine (8.4 mg) was added to $\text{Pt}^{\text{II}}\text{Cl}_2(\text{DMSO})_2$ (58.7 mg) in acetonitrile (5ml). The solution was stirred at room temperature for ~14 hrs. The white product precipitated immediately after addition of ethylenediamine. The precipitate was washed with ether and dried under vacuum.

$[\text{Pt}^{\text{II}}\text{Cl}(\text{DMSO})(\text{en})]\text{Cl}$: 232 mg, Yield 97.8 %, m.p. > 350°C. ^1H NMR (399.95 MHz, D_2O , 25°C), $\delta=3.50$ (s, 6H, H^1), 3.50 (d, $^3J(^{195}\text{Pt}-^1\text{H}) = 20.3$ Hz, H^2 , H^3), 2.85 (s, 4H, H^2 , H^3), 2.85 ppm (d, $^3J(^{195}\text{Pt}-^1\text{H}) = 42.3$ Hz, $\text{H}^{2'}$, $\text{H}^{3'}$).

2.8.4 Synthetic procedures for Pd^{II} complexes and precursors

2.8.4.1 Preparation of $\text{Pd}^{\text{II}}\text{Cl}_2(\text{phen})$

A method similar to that used for the synthesis of $\text{Pt}^{\text{II}}\text{Cl}_2(\text{diimine})$ described in Section 2.8.3.2 was used for the synthesis of $\text{Pd}^{\text{II}}\text{Cl}_2(\text{phen})$. However, the reaction time and temperature was decreased from over night (~14 hours at 95°C) to 1 hour at room temperature. $\text{K}_2[\text{Pd}^{\text{II}}\text{Cl}_4]$ (216.5 mg) was dissolved in water (50ml) containing 6 ml of a 2M HCl solution. The ligand, 1,10-phenanthroline was then added in a slight excess (132.6 mg) and the solution shaken for 1 hour. The pale yellow-pink product precipitated almost

immediately from solution when cooled to 4°C, filtered off and washed with cold deionized water followed by an acetone and ether wash to remove unreacted $[\text{Pt}^{\text{II}}\text{Cl}_4]^{2-}$ and diimine respectively and dried under vacuum. The product was obtained in high yields (95-98%).

Pd^{II}Cl₂(1,10-phenanthroline): 232 mg, Yield 97.8 %, m.p. > 350°C. ¹H NMR (399.95 MHz, DMSO-d₆, 25°C), δ=9.35 (dd, 2H; H⁹, H²), 8.98 (dd, 2H; H⁴, H⁷), 8.29 (s, 2H; H⁵, H⁶), 8.14 ppm (dd, 2H; H³, H⁸).

2.8.4.2 Preparation of Pd^{II}₃(OAc)₆

The method described by Murillo and Cotton was used to synthesise Pd₃(OAc)₆ from PdCl₂.²⁵ A solution of NaOH (3.02 g) and CH₃OONa (2.40 g) was added to a solution of PdCl₂ (1.57 g) in water (150 ml). The solution was stirred for 30 min while Pd⁰ precipitated. The Pd⁰ was collected by filtration and washed with water and acetone and dried under vacuum. The black Pd⁰ powder was then suspended in glacial acetic acid (60 ml) and concentrated HNO₃ was added slowly to oxidize the metal to Pd^{II}. The mixture was heated to reflux for 30 min while N₂ gas was bubbled through the solution. The volume was reduced by slow evaporation with heating to a third of the volume after which the mixture was cooled to room temperature. The orange-brown crystalline material was isolated by filtration and washed with cold acetone.

Pd^{II}₃(MeCO₂)₆: 1.57 mg, Yield 76 %, m.p. 205 -208°C. ¹H NMR 399.95 MHz, Chloroform-d₁, 25°C), δ=2.00 (s, 18H; H¹).

2.8.4.3 Preparation of Pd^{II}(phen)(OAc)₂

Pd^{II}(phen)(OAc)₂ was synthesised according to the method described by Milani and co-workers.²⁷ Pd^{II}₃(OAc)₆ (102 mg) was dissolved in acetone (9 ml) and two drops of glacial acetic acid were added. The 1,10-phenanthroline ligand was dissolved in acetone (2 ml) and added to the Pd^{II}₃(OAc)₆ solution and stirred for ~1 hr at room temperature with the brown solution turning to yellow after which the product precipitated. The Pd^{II}(phen)(OAc)₂ was filtered off, washed with cold acetone and dried under vacuum.

Pd^{II}(1,10-phenanthroline)(MeCO₂)₂: 157 mg, Yield 87 %, decomposition temperature: 240 - 250 °C. ¹H NMR 399.95 MHz, DMSO-d₆, 25°C), δ=8.96 (dd, 2H; H⁹, H²), 8.49 (dd, 2H; H⁴, H⁷), 8.27 (s, 2H; H⁵, H⁶), 8.08 (dd, 2H; H³, H⁸), 1.97 ppm (s, 2H; H¹).

2.8.4.4 Preparation of $[\text{Pd}^{\text{II}}(\text{phen})(\text{L}^{\text{n}}-\text{S},\text{O})]\text{Cl}$

$[\text{Pd}^{\text{II}}(\text{phen})(\text{L}^{\text{n}}-\text{S},\text{O})]\text{X}$ was synthesised using two different Pd precursors, namely $\text{Pd}^{\text{II}}(\text{phen})(\text{OAc})_2$ and $\text{Pd}^{\text{II}}\text{Cl}_2(\text{phen})$. In both synthetic procedures the product was further purified using column chromatography as discussed in Section 2.5.4 if the purity was not desirable.

Synthesis from $\text{Pd}^{\text{II}}(\text{phen})(\text{OAc})_2$:

Several methods were attempted to synthesise $\text{Pd}^{\text{II}}(\text{phen})(\text{OAc})_2$ with the use of acetone as solvent being the preferred method. $\text{Pd}^{\text{II}}(\text{phen})(\text{OAc})_2$ (25 mg) and NaOAc (8 mg) was suspended in acetone. HL^1 (19 mg) was added dropwise while the solution turned bright yellow as the reaction proceeded. After 1 hour the solution was filtered to remove the excess NaOAc and unreacted $\text{Pd}^{\text{II}}(\text{phen})(\text{OAc})_2$. The solvent was removed under reduced pressure and the precipitate washed with ether. Isolated yields were typically 60 - 70 %.

Synthesis from $\text{Pd}^{\text{II}}\text{Cl}_2(\text{phen})$:

$\text{Pd}^{\text{II}}\text{Cl}_2(\text{phen})$ (50 mg) and HL^1 (26 mg) were suspended in dichloromethane (10 ml). To this mixture was added NaOAc dissolved in water (5 ml). The mixture was shaken at room temperature for 30 min while the dichloromethane phase turned yellow while a bright yellow product precipitated at the water/dichloromethane interface. Acetonitrile was added (15ml) and the precipitate dissolved with the organic phase being bright yellow. The organic phase was separated and filtered and the solvent volume was reduced until the product precipitated. The isolated yields were in the range of 60 - 70%.

$[\text{Pd}^{\text{II}}(\text{phen})(\text{L}^1-\text{S},\text{O})]\text{Cl}$: Yield 60 - 70%, m.p. 126 - 128°C ^1H NMR (399.95 MHz, Chloroform- d_1 , 25°C), δ =9.13 (d, 1H: H^4), 9.09 (d, 1H: H^7), 8.97 (d, 1H: H^2), 8.65 (d, 1H: H^9), 8.34 (s, 2H: H^5 , H^6), 8.20 (dd, 1H: H^3), 8.18 (dd, 1H: H^8), 3.85 (m, 4H, H^{a} , $\text{H}^{\text{a}'}$), 2.18 (p, 2H, H^{b}), 2.07 (p, 2H, H^{b}), 1.33 ppm (s, 9H, H^1).; (+) ESI MS: m/z 499.079 (M^+)

2.9 References

1. K. R. Koch, C. Sacht, C. Lawrence, *Dalton Trans.*, **4**, 1998, 689-695.
2. T. J. Egan, K. R. Koch, P. L. Swan, C. Clarkson, D. A. Van Schalkwyk, P. J. Smith, *J. Med. Chem.*, 2004, **47**, 2926-2934.
3. Y. S. Wu, K. R. Koch, V. R. Abratt, H. H. Klump, *Arch Biochem Biophys.*, 2005, **440**, 28-37.
4. I. A. Kotzé, W. J. Gerber, J. M. Mckenzie, K. R. Koch, *Eur. J. Inorg. Chem.*, 2009, **12**, 1626-1633.
5. I. A. Kotzé, MSc. Thesis, *University of Stellenbosch*, 2009.
6. S. Saeeda, N. Rashida, M. Alib, R. Hussain, *Eur. J. Chem.*, **3**, 2010, 200-205.
7. T. J. Egan, *Drug Design Rev. Online*, 2004, **1**, 93-110.
8. Yu-Shan Wu, PhD Thesis, *University of Cape Town*, 2002.
9. I. B. Douglass, F. B. Dains, *J Am. Chem. Soc.*, 1934, **56**, 719-721.
10. A. Takamizawa, K. Hira, K. Matsui, *Bull. Chem. Soc. Japan.*, **36**, 1963, 1214.
11. D.T Elmore, R. J. Ogle, *J. Chem. Soc.* 1958, 1141-1145.
12. A. N. Mautjana, J. D. S. Miller, A. Gie, S. A. Bourne, K. R. Koch, *Dalton Trans.*, **10**, 2003, 1952-1960.
13. G. T. Morgan, F. H. Burstall, *J. Chem. Soc.*, 1934, 965-971.
14. J. E. Huheey, E. A. Keiter, R. L. Keiter, *Inorganic Chemistry-Principals of Structure and Reactivity 4th Edition*, HarperCollins, New York, 2003, **4**, 344-348.
15. T. Brand, E. J. Cabrita, S. Berger, *Prog. NMR Spectr.*, 2005, **46**, 159-196.
16. A. Göller, U.-W. Grummt, *Chem. Phys. Lett.* **321**, 2000, 399-405.
17. A. J. Canty, M. G. Gardiner, R. C. Jones, Ma. Sharma, *Aus. J. Chem.*, **64**, 2011, 1355-1359.
18. R. S. Osborn, D. Rogers, *Dalton Trans.*, 1974, 1002-1004.
19. V. H. Houlding, V. M. Miskowskib, *Coord. Chem. Rev.*, **111**, 1991, 145-152.
20. R. Valiente, J. M. García-Lastra, P. García-Fernández, S. García-Revilla, O. S. Wenger, *Eur. J. Inorg. Chem.* **36**, 2007, 5735-5742.
21. K. R. Koch, *Coord. Chem. Rev.*, **216-217**, 2001, 473-488.
22. K. R. Koch, J. du Toit, M. R. Caira, C. Sacht, *Dalton Trans.*, 1994, 185-786.
23. T. D. W. Claridge, *High-Resolution NMR Techniques in Organic Chemistry, Tetrahedron Organic Chemistry Series*, Pergamon, Oxford, **19**, 1999.
24. I. P. Stolyarov, L. I. Demina, N. V. Cherkashina, *Rus. J. Inorg. Chem.*, 2011, **56**, 1611-1616.
25. V. I. Bakhmutov, J. F. Berry, F. A. Cotton, S. Ibragimov, C. A. Murillo, *Dalton Trans.*, **11**, 2005, 1989-1992.

26. L. A. Adrio, B. N. Nguyen, G. Guilera, A. G. Livingston, K. K. Hii, *Catal. Sci. Technol.*, 2012, **2**, 316-323.
27. B. Milani, E. Alessio, G. Mestroni, A. Sommazzi, F. Garbassi, E. Zangrando, N. Bresciani-Pahora, L. Randaccio, *Dalton Trans.*, **1**, 1994, 1903-1911.
28. J.H. Price, A.S. Williamson, R.S. Schramm, B.B. Wayland, *Inorg. Chem.*, **11**, 1972, 1280-1284.
29. R. Romeo, D. Minniti, S. Lanza, M. L. Tobe, *Inorg. Chim. Acta*, **22**, 1977, 87-91.
30. V.I. Bakhmutov, *Practical NMR Relaxation for Chemists*, John Wiley & Sons Ltd., Chichester, U. K., 2004.
31. J. Y. Lallemand, J. Soulie, J. C. Chottard, *Chem. Comm.*, 1980, **10**, 436-438.
32. S. J. Wilkens, W. M. Westler, J. L. Markley, F. Weinhold, *J. Am. Chem. Soc.*, 2001, **123**, 12026-12036.
33. J.A. Pople, D. P. Santry, *Mol. Phys.*, 1964, **8**, 1-18.
34. P.J Hore, *Nuclear Magnetic Resonance*, Oxford, New York, 1995, 32-33.

3

Understanding the synthesis and properties of the novel $\text{Pt}^{\text{II}}(\text{phen})(N,N\text{-di(alkyl)-}N'\text{-acylthiourea})_2$ complexes, an unusual coordination of $N,N\text{-dialkyl-}N'\text{-acylthiourea}$

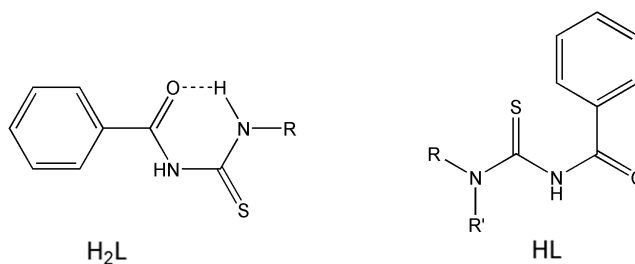
The synthesis of a series of $[\text{Pt}^{\text{II}}(\text{phen})(\text{L}^n\text{-}S,O)]^+$ complexes (as described in chapter 2) revealed the presence of an unknown compound forming in significant amounts. This chapter describes the full characterization of this coordination product. It was found that the $N,N\text{-dialkyl-}N'\text{-acylthiourea}$ ligands (HL^n) tend to coordinate to the platinum (II) metal centre in the rare monodentate fashion *via* the sulphur atom to form neutral $\text{Pt}^{\text{II}}(\text{phen})(\text{L}^n\text{-}S)_2$ complexes with a sulphur bound L^n denoted as $\text{L}^n\text{-}S$. This phenomenon will be discussed together with the Single Crystal X-ray Diffraction data, which reveals the postulated $\text{Pt}^{\text{II}}(\text{phen})(\text{L}^n\text{-}S)_2$ complexes for $N,N\text{-dibutyl-}N'\text{-naphthoylthiourea}$ (HL^2) and $N,N\text{-diethyl-}N'\text{-benzoylthiourea}$ (HL^4). The relative tendencies of the $N,N\text{-dialkyl-}N'\text{-acylthioureas}$ to form monodentate sulphur-coordinated complexes with Pt^{II} depends on the structure of the $N,N\text{-dialkyl-}N'\text{-acylthiourea}$. Therefore, a series of selected $N,N\text{-dialkyl-}N'\text{-acylthioureas}$ with specific structural variations will be discussed. $\text{Pt}^{\text{II}}(\text{phen})(\text{L}^2\text{-}S)_2$ in particular forms in high yields (>90%) and will be tested for β -haematin inhibition capabilities, since no bioactivity of this novel class of complexes are known (shown in chapter 5). These novel complexes could be a new class of bioactive compounds and opens the door for a new class of complexes to be studied.

3.1 Introduction

In the past large variation in isolated yields were observed for the synthesis of various $[Pt^{II}(\text{diimine})(L^n-S,O)]^+$ complexes, where "diimine" refers to 2,2-bipyridine, 1,10-phenanthroline or substituted variations thereof and L^n-S,O various N,N -dialkyl- N' -acylthioureas.¹⁻³ More specifically, the complexes of $[Pt^{II}(\text{phen})(L^2-S,O)]^+$ and $[Pt^{II}(\text{bipy})(L^2-S,O)]^+$ were found to have significant lower yields compared to the other acylthioureas (>80%) for the deceptively simple synthetic procedure.^{1,2}

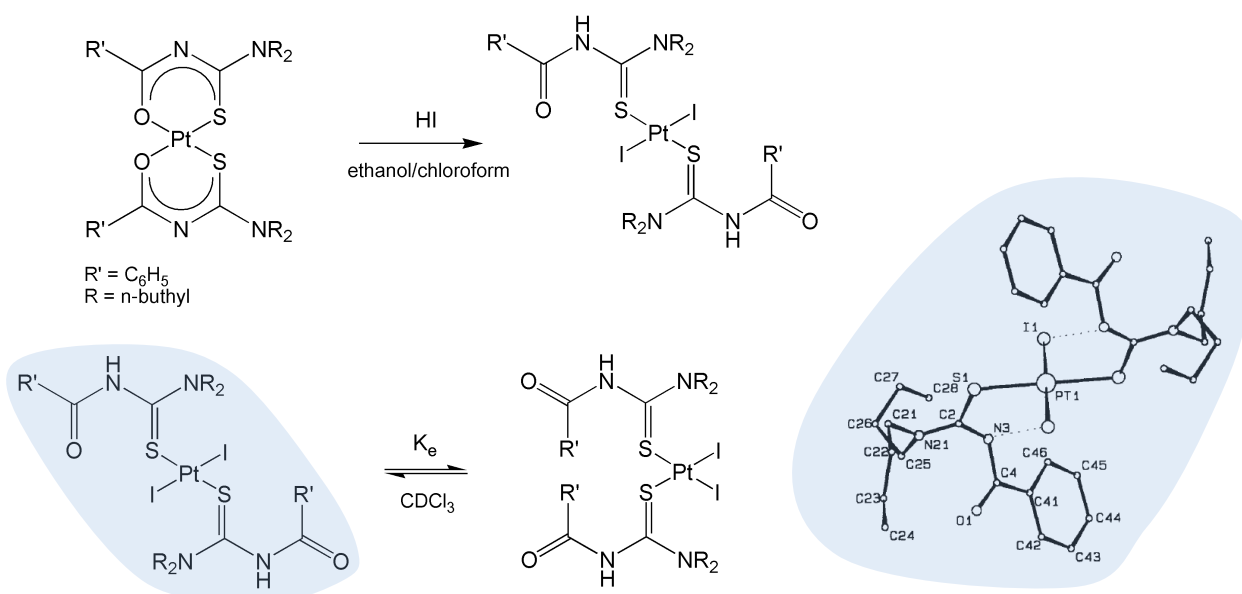
The usual mode of coordination of N,N -dialkyl- N' -acylthioureas (L^n) to transition metals is a chelate *via* sulphur and oxygen.⁴ The mechanism of coordination to Pt^{II} and Pd^{II} in particular is thought to be a two step mechanism whereby the 'soft' sulphur atom coordinates to the metal centre due to its affinity for Pt^{II} and Pd^{II} .^{5,6} The second step involves the coordination of the oxygen donor atom, after deprotonation of the NH group, which increases the nucleophilicity of the O^- donor resulting in coordination to the metal.⁶ However, evidence of this chelate forming in acidic solutions suggests that the chelation effect drives the coordination even though the oxygen is considered as a 'hard' donor in the protonated ligand.⁷

Koch and co-workers have observed an interesting monodentate (through the sulphur donor atom) mode of coordination of mono-alkyl-acylthioureas in acidic aqueous solutions.^{8,9} This is ascribed to *intra*-molecular $O\cdots H$ hydrogen bonding as shown in Scheme 3.1.



Scheme 3.1 *Intra*-molecular hydrogen bonding in mono-alkyl-acylthioureas (H_2L) which exposes the sulphur for potential coordination to the metal (M). The dialkyl-acylthiourea ligands (HL) do not exhibit this hydrogen bonding.^{8,9}

Therefore, the mode of coordination of the acylthiourea to the platinum group metals can be separated into monodentate coordination through the sulphur donor atom for mono-alkyl-substituted acylthioureas and chelation for the N,N -dialkyl- N' -acylthiourea ligands.⁴ Monodentate coordination of N,N -dialkyl- N' -acylthioureas to Pt^{II} and Pd^{II} has been observed but only in strongly acidic solutions in the presence of Cl^- or I^- ions (Scheme 3.2).¹⁰



Scheme 3.2 Coordination modes of acylthiourea complexes as a result of *intra*-molecular hydrogen bonding and deprotonation of the amido-proton with the molecular structure of *trans*- $Pt^{II}(L^3)_2$ highlighted.¹⁰

Initial ‘activation’ of ligand for coordination occurs by deprotonation of the acylthiourea ligand by the shift of electron density towards the oxygen and sulphur which significantly increases the nucleophilicity of the donor atoms, ensuring a relatively strong chelating capability of the acylthiourea ligands. However, the possibility of monodentate coordination of deprotonated *N,N*-dialkyl-*N'*-acylthiourea ligands does exist but is rare as observed for Cu(I) and Cu(II) cluster complexes being the only known examples as shown in Figure 3.1.^{11,12}

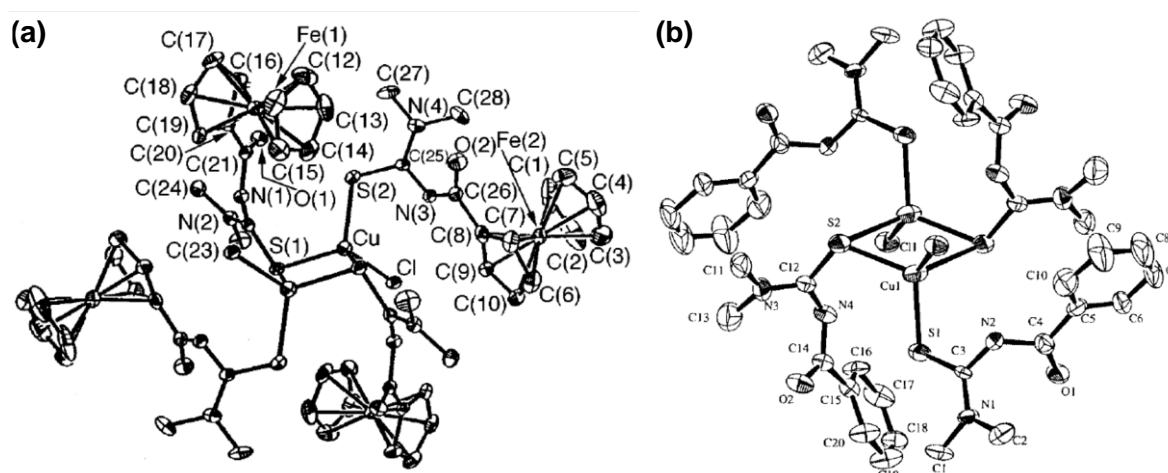


Figure 3.1 Two crystal structures showing (a) monodentate $\mu\text{-S}$ bridging of a deprotonated *N,N*-dimethyl-*N'*-ferrocenylthiourea in a Cu(I) cluster and (b) monodentate coordination and $\mu\text{-S}$ bridging of *N,N*-dimethyl-*N'*-benzoylthiourea in Cu(II) cluster of $[\{CuL(HL)Cl\}_2]$.^{11,12} (Images reproduced from reference 12 and 13)

Nevertheless a monodentate mode of coordination of deprotonated *N,N*-dialkyl-*N'*-acylthiourea to Pt^{II} has not been observed or studied to date. This relatively rare monodentate-*S* coordination of *N,N*-dialkyl-*N'*-acylthioureas to platinum(II)(1,10-phenanthroline) complexes was therefore investigated.

3.2 Results and discussion

3.2.1 The first evidence of the formation of $Pt^{II}(phen)(N,N\text{-dibutyl-}N'\text{-naphthoylthiourea})_2$

The synthesis of $[Pt^{II}(phen)(L^2-S,O)]Cl$ and $[Pt^{II}(bipy)(L^2-S,O)]Cl$ as described in Chapter 2 yielded a crude product, the purification of which was challenging (Figure 3.2). Extensive washing with ether and extraction from $CHCl_3$ into an aqueous phase failed to yield the pure product since $[Pt^{II}(bipy)(L^2-S,O)]Cl$ in particular is only slightly soluble in water. The purification of $[Pt^{II}(bipy)(L^2-S,O)]Cl$ was ultimately accomplished by an interesting third phase formation with an attempt by solvent extraction as discussed in Chapter 2 (Section 2.4.3). Upon addition of water to the organic phase consisting of the crude product in acetonitrile and ether, a dark red/orange third phase formed at the bottom of the flask. The 1H NMR spectrum of such highly concentrated droplet reveals that the emulsion consists of only acetonitrile and the pure $[Pt^{II}(bipy)(L^2-S,O)]Cl$ complex. This method of purification was also successful for $[Pt^{II}(phen)(L^2-S,O)]Cl$ which was obtained by the formation of a third phase emulsion with the addition of water to an ether-acetonitrile solution of the crude product. This deep orange-red product separates as a droplet at the bottom of the vial while a yellow precipitate is left in the aqueous phase as a suspension; this precipitate contains the 'unknown' products in the synthesis. The 1H NMR spectrum of the crude product reveals "unknown" peaks indicated by the * in Figure 3.2, which correspond to the yellow precipitate in the aqueous phase since the 1H NMR spectrum of the pure $[Pt^{II}(phen)(L^2-S,O)]Cl$ is known (Figure 2.28).

The 1H NMR spectrum of the 'unknown' product exhibits a doublet at 9.26 ppm, two doublets of doublets at 8.46 and 7.55 ppm, and singlet at 7.51 ppm in the aromatic region while broad unresolved peaks are observed more upfield (0.800 - 4.00 ppm). These 'unknown' peaks, which were also observed by others¹, cannot be uncoordinated 1,10-phenanthroline or L^2 since the chemical shifts do not correspond to those known for these

ligands, but should be a complex in which 1,10-phenanthroline is bound symmetrically to the metal Pt^{II} . This ‘product’ was not identified by others, since only trace amount was obtained as a by-product with no aliphatic proton resonances observable in the 1H NMR spectrum. The symmetrically bound 1,10-phenanthroline peaks are not consistent with the $Pt^{II}Cl_2(phen)$ starting material and the solubility of $Pt^{II}Cl_2(phen)$ in chloroform is very low. This complex could potentially correspond to a symmetrically bound 1,10-phenanthroline complex with two monodentate coordinated *N,N*-dibutyl-*N'*-naphthoylthiourea ligands, resulting in broad peaks observed in the aliphatic region, with relatively sharp naphthoyl 1H peaks observed in the aromatic region. The integration of these peaks suggests two L^2 ligands to one symmetrical 1,10-phenanthroline in this complex.

In fact, it was found that the conventional synthesis of $[Pt^{II}(phen)(L^2-S,O)]Cl$ in acetonitrile (Chapter 2) yields the two coordination products, even when the ligand HL^2 is not in excess. The synthesis of this postulated $Pt^{II}(phen)(L^2-S)_2$ complex was attempted after which the possibility of other *N,N*-dialkyl-*N'*-acylthioureas to coordinate in a similar fashion was investigated.

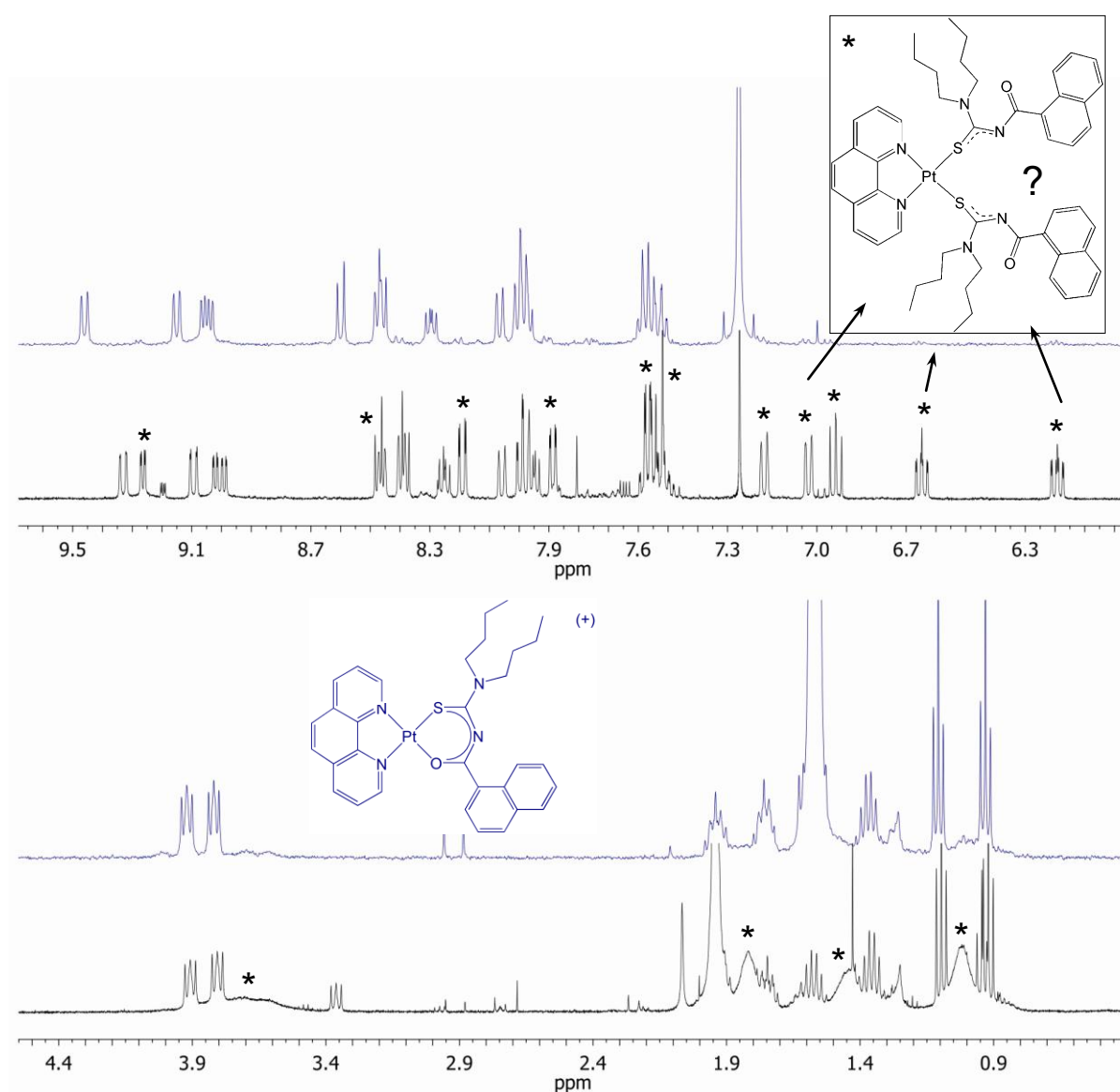
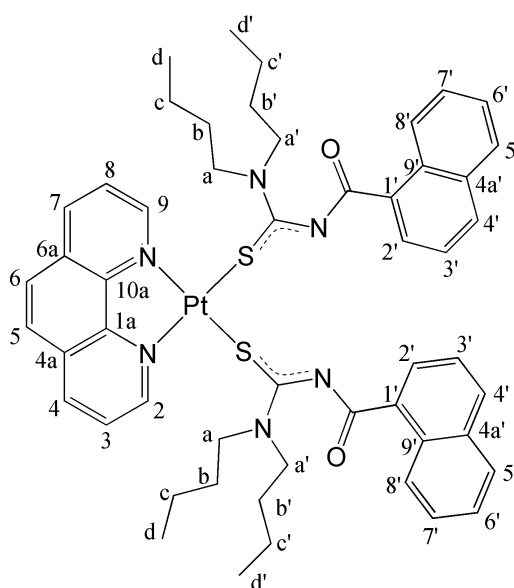


Figure 3.2 ^1H NMR spectra of the reaction mixture obtained for the synthesis of $[\text{Pt}^{\text{II}}(\text{phen})(\text{L}^2\text{-S},\text{O})]^+$ containing a significant amount of the previously 'unknown' $\text{Pt}(\text{phen})(\text{L}^2\text{-S})_2$ with the ^1H NMR spectrum of the pure $[\text{Pt}^{\text{II}}(\text{phen})(\text{L}^2\text{-S},\text{O})]^+$ in blue.

3.2.2 Synthesis and characterization of $\text{Pt}^{\text{II}}(\text{phen})(\text{N},\text{N}\text{-dibutyl-}N'\text{-naphthoylthiourea})_2$

The synthesis of the postulated $\text{Pt}^{\text{II}}(\text{phen})(\text{L}^2\text{-S})_2$ was accomplished by the addition of a suspension of $\text{Pt}^{\text{II}}\text{Cl}_2(\text{phen})$ in acetonitrile dropwise to 2.5eq. of HL^2 and 3.5eq. NaOAc in acetonitrile, after which the mixture was heated to reflux for 1 hour. An orange powder was obtained by the removal of the unreacted NaOAc and NaCl formed during the reaction by filtration and removal of the solvent under reduced pressure. The crude product was dissolved in dichloromethane and hexane was added (50:50 v/v). The products were separated chromatographically using neutral aluminium oxide (Al_2O_3) as stationary phase and

dichloromethane/hexane and acetonitrile as mobile phases. The unreacted L^2 and acetic acid formed in the reaction eluted with the 50:50 v/v dichloromethane:hexane mixture $Pt^{II}(phen)(L^2-S)_2$ eluted with 10:90 v/v acetonitrile:dichloromethane. From the 1H NMR spectra (Figure 3.3) it is clear that the product obtained is similar to the complex of which the 1H NMR resonances are labelled by the * in Figure 3.2. The numbering scheme of such a sulphur-coordinated $Pt^{II}(phen)(L^2)_2$ product is shown in Scheme 3.3 with the nomenclature for a sulphur bound L^2 denoted as L^2-S .



Scheme 3.3 Structure and numbering scheme for $Pt^{II}(phen)(L^2-S)_2$.

Interestingly, the 1H resonances of the N,N -dibutyl naphthoylthiourea are extremely broad ($\nu_{1/2}$ of $H^{a+a'} = 107$ Hz) and these would probably not be observable in the 1H NMR spectra if the complex was only present in small quantities. This may explain the previous oversight by others.^{6,13} The broad 1H resonances of the alkyl substituents in 1-5 ppm range suggest slow to intermediate rotation of the dibutyl groups of the N,N -dibutyl- N' -naphthoylthiourea due to the partial double bond character of the N-C bond between the amino nitrogen and the thiocarbonyl carbon, and should resolve with an increase in temperature (Figure 3.3).

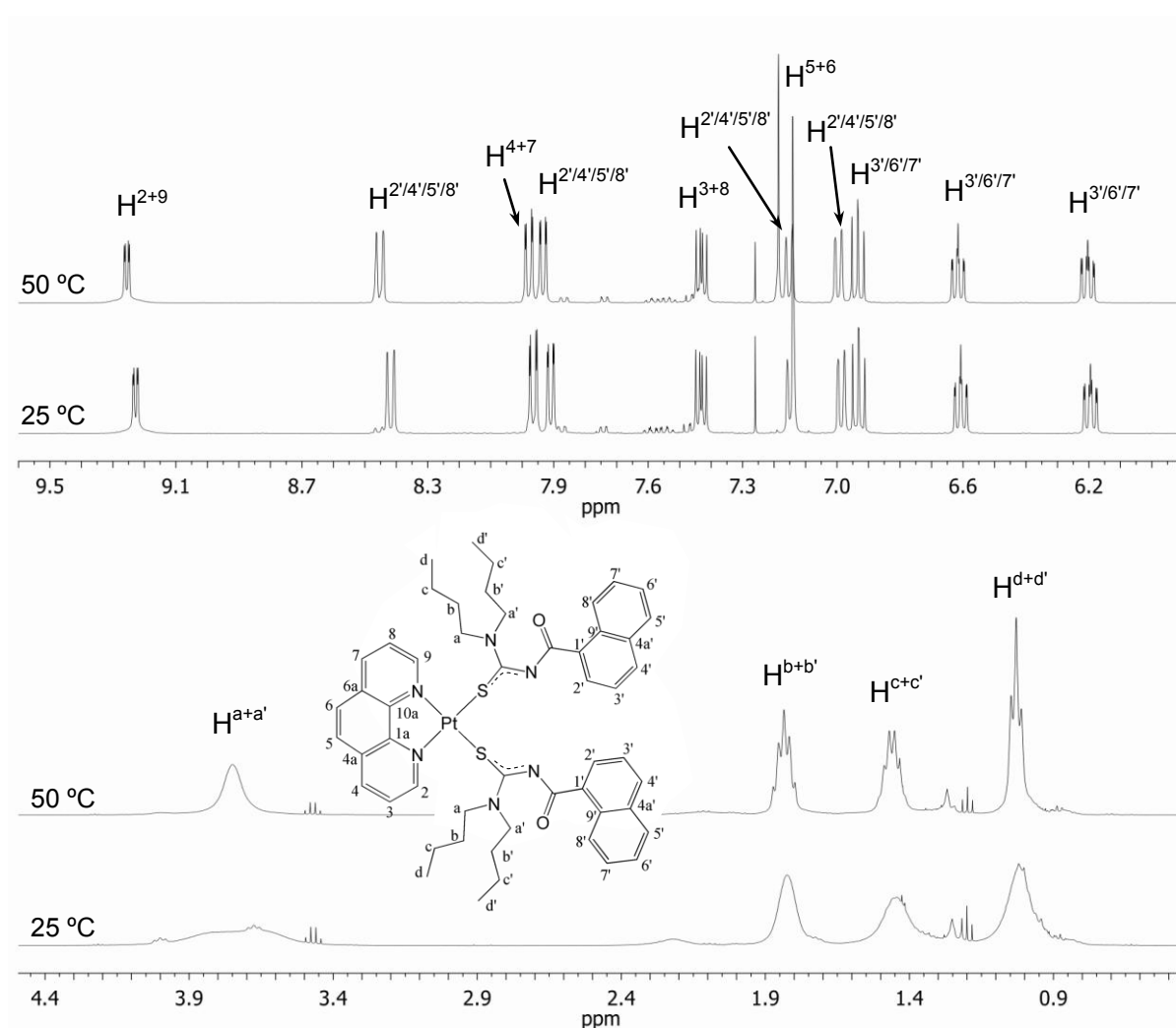


Figure 3.3 ^1H NMR spectra of $\text{Pt}^{\text{II}}(\text{phen})(\text{L}^2\text{-S})_2$ at 25°C and 50°C in chloroform- d_1 .

The well resolved ^1H NMR resonances of the latter region obtained at 50 °C integrate for a 2:1 L^2 to 1,10-phenanthroline and suggest monodentate coordination of a deprotonated L^2 ligand most probably *via* the S-donor atom. It is reasonable to argue that the coordination would be through the thiocarbonyl rather than the carbonyl since platinum is considered a ‘soft’ metal according to Pearson’s HSAB theory and would prefer the ‘softer’ sulphur atom compared to oxygen.⁵ Therefore a tentative assignment of the previously “unknown” ^1H resonance signals to the monodentate *bis*-acythiourea 1,10-phenanthroline platinum(II) complex, $\text{Pt}^{\text{II}}(\text{phen})(\text{L}^2\text{-S})_2$, where, $\text{L}^2\text{-S}$ refers to a monodentate sulphur-coordinated *N,N*-dibutyl-*N'*-naphthoyl-thiourea ligand is reasonable, and as will be seen below is confirmed.

3.2.2.1 Assignment of the 1H NMR spectrum of $Pt^{II}(phen)(N,N\text{-dibutyl-}N'\text{-naphthoyl-thiourea})_2$

The 1H NMR resonances in the 5-12 ppm spectral region corresponding to a symmetrically coordinated 1,10-phenanthroline were identified by comparison of the relevant coupling constants and were labelled H^{2+9} , H^{4+7} , H^{3+8} and H^{5+6} consecutively. Interestingly, the base of the signal assigned to H^{2+9} is significantly broadened, suggestive of unresolved ^{195}Pt satellites as a result of the CSA relaxation at this high magnetic field strength (14 Tesla) as discussed in Chapter 2 for other $Pt^{II}(phen)$ complexes.

By inspection one of the three triplet-like resonances represented as $H^{3'/6'/7'}$ could be assigned to H^3 (6.94 ppm) since it shows resolved coupling to $H^{2'}$ and $H^{4'}$. The complete assignment of the L^2 protons could not be done without 1H correlation spectroscopy (COSY) to obtain the necessary coupling partners. The COSY experiment was optimised for the typical 3J proton couplings (5-8 Hz) and only cross-peaks were observed for the aromatic protons with no correlations in the latter because of dynamic motion (Figure 3.4).

The 1H NMR assignment of a symmetrically bound 1,10-phenanthroline is confirmed by the COSY spectra (Figure 3.4), with the most downfield proton previously assigned as H^{2+9} showing a strong correlation to the resonance assigned H^{3+8} and a weak cross-peak observed to the protons labelled H^{4+7} . Furthermore, the resonance H^{4+7} shows a strong correlation to H^{3+8} , while the correlation to H^{2+9} is weak due to the 4 bond distance between the nuclei. As expected from the singlet resonance labelled H^{5+6} , no coupling is observed in the 1H NMR. The aromatic protons of the coordinated L^2 clearly show two separate ring systems, with the most upfield proton (6.19 ppm) showing strong coupling to the two protons at 8.41 (doublet) and 6.60 ppm (triplet-like multiplet) and additional weak coupling to the doublet at 7.00 ppm. This coupling pattern suggests a coupling system of 4 non-equivalent protons which should correspond to the protons labelled $H^{5'-8'}$ in the naphthoyl moiety.

The *ChemDraw Ultra Edition* software was used to aid the complete assignment of the 1H NMR spectrum; while these calculations are not always accurate, large difference in the chemical shift of $H^{5'}$ and $H^{8'}$ due to their very different position in the ring system is expected (Figure A.16). The calculations are based on empirically estimated effects of various substituents on the chemical shift of basic fragments/skeleton structures. The most downfield doublet in this set of H's could be assigned to $H^{8'}$ with the calculated chemical shift of $H^{5'}$ and $H^{8'}$ 9.19 and 7.73 ppm respectively. The experimental chemical shift of both $H^{5'}$ and $H^{8'}$ is overestimated by roughly 0.75 ppm with the predicted chemical shift difference between $H^{8'}$ and $H^{5'}$ (1.46 ppm) is almost identical to the experimentally obtained value (1.41 ppm).

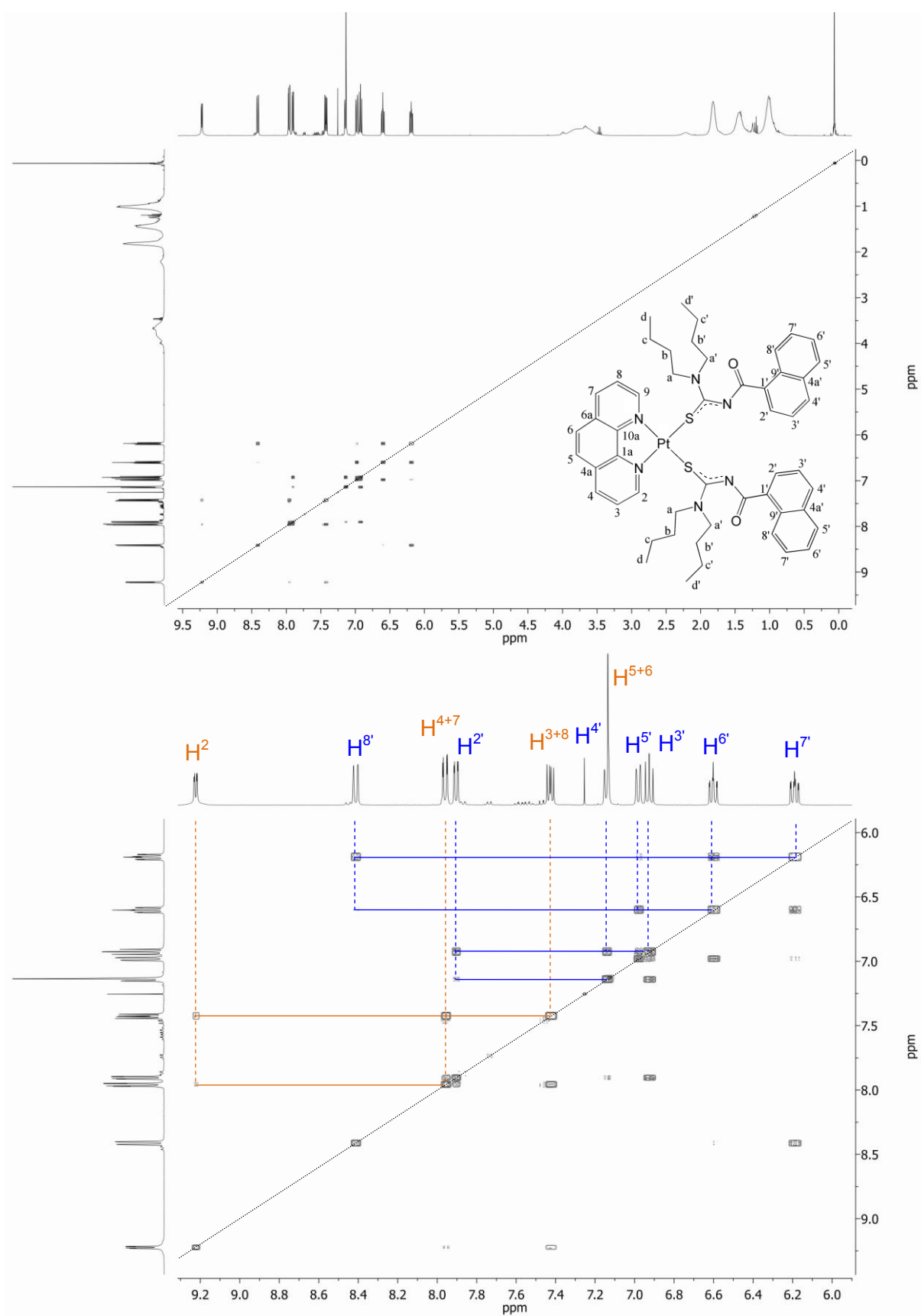


Figure 3.4 $^1\text{H},^1\text{H}$ COSY spectrum of $Pt^{II}(\text{phen})(L^2-S)_2$ in chloroform- d_1 with only the aromatic protons exhibiting cross-peaks.

The cross-peaks observed in the COSY of $Pt^{II}(\text{phen})(L^2-S)_2$ in chloroform allowed for the assignments of all aromatic protons while the broad aliphatic protons could be assigned using the multiplicity (J -coupling) and integration of the ^1H resonances of $Pt^{II}(\text{phen})(L^2-S)_2$ at 50°C (Figure 3.3). The integration of the broad resonances observed indicate that the peaks at 3.76, 1.82 and 1.44 ppm correspond to 8 H's each, with the resonance at 1.01 ppm integrating for 12 H's. The most downfield resonance is significantly separated from the others as a result of the electron withdrawing effect of the amino-nitrogen and is assigned to $H^{a+a'}$. The resonance integrating for 12 H's could be unambiguously assigned to $H^{d+d'}$. These assignments were consistent with the calculated values and assignment shown in Figure A.16. However, the assignment of the remaining two resonances at 1.82 and 1.44 ppm could not be made with confidence using the calculated chemical shifts since the difference is predicted to be only 0.08 ppm. However, the multiplicities of the signals of $H^{b+b'}$ and $H^{c+c'}$ are expected to be a pentet and a sextet respectively if only first order coupling is observed. The broad peaks were well resolved when the temperature was increased from 25 to 50°C , as shown in Figure 3.3. This allowed for the unambiguous assignment of the resonances at 1.82 and 1.44 ppm to $H^{b+b'}$ and $H^{c+c'}$ respectively. Figure 3.5 shows the full assignment of the ^1H NMR spectrum of $Pt^{II}(\text{phen})(L^2-S)_2$ in chloroform- d_1 .

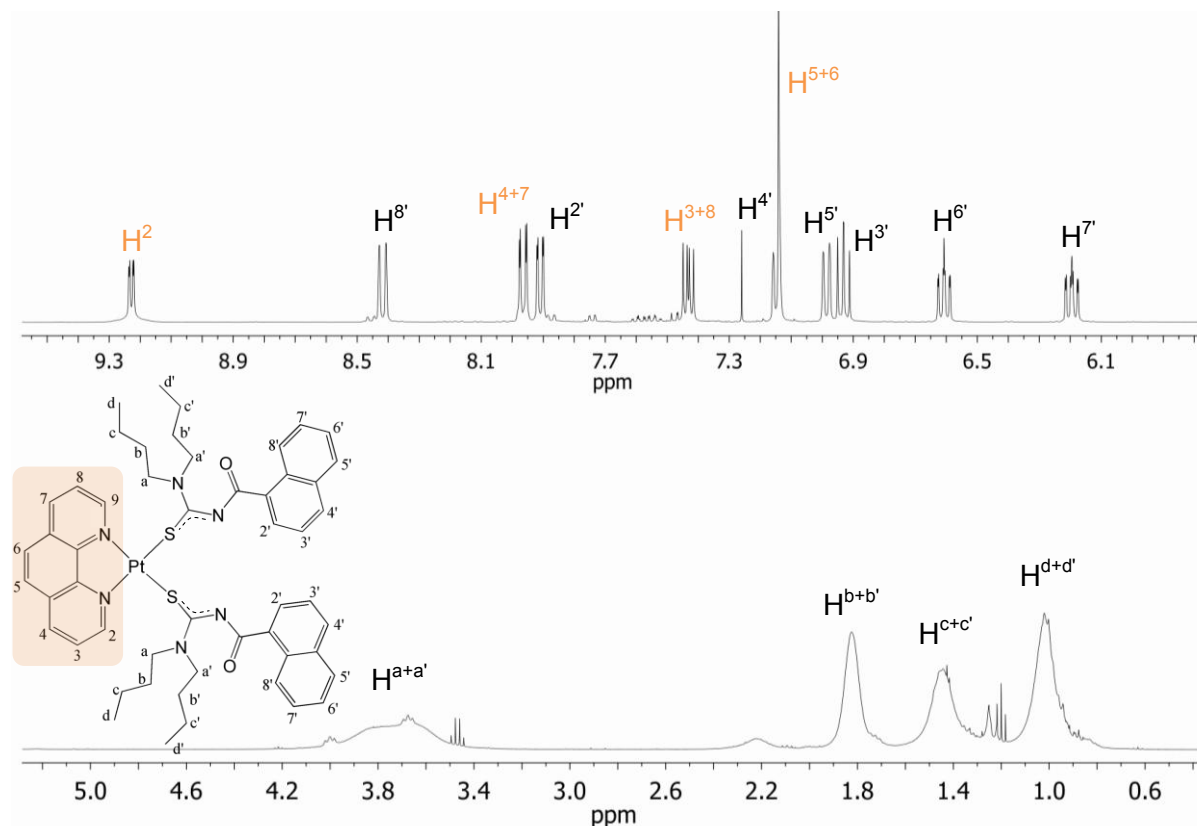


Figure 3.5 ^1H NMR spectrum of $Pt^{II}(\text{phen})(L^2-S)_2$ in chloroform- d_1 with complete assignment.

3.2.2.2 Assignment of the $^{13}C\{^1H\}$ NMR spectrum of $Pt^{II}(phen)(N,N\text{-dibutyl-}N'\text{-naphthoylthiourea})_2$

The ^{13}C APT (attached proton test) was run in an attempt to assign the $^{13}C\{^1H\}$ NMR spectrum of $Pt^{II}(phen)(L^2-S)_2$ in chloroform. Figure 3.6 shows the APT obtained with the methine (CH) and methyl (CH_3) signals positive and the quaternary (C) and methylene (CH_2) signals negative. The information from the ^{13}C APT spectrum leads to the assignment of the $-CH_3$ group of the butyl moieties ($C^{d+d'}$), the most downfield $-CH_2-$ to $C^{a+a'}$ and differentiate between C^2 and C^{1a} of the phenanthroline ring.

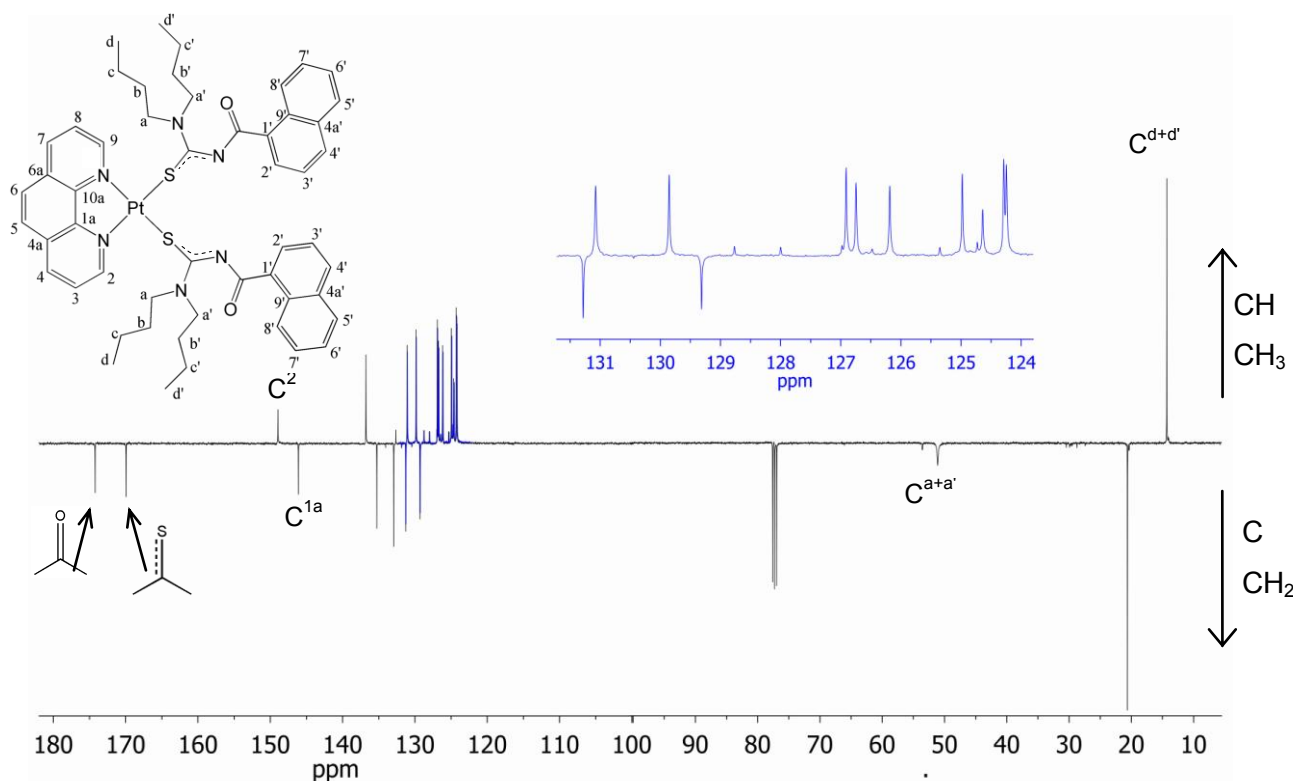


Figure 3.6 ^{13}C APT of $Pt^{II}(phen)(L^2-S)_2$ with the methine (CH) and (CH_3) signals positive and the quaternary (C) and (CH_2) signals negative. The part of the spectrum highlighted in blue is expanded to clearly show all peaks in this region.

In addition the use of the $^{13}C\{^1H\}$ NMR spectrum of the uncoordinated HL^2 in chloroform to aid the assignment of $Pt^{II}(phen)(L^2-S)_2$ as shown in Figure 3.7 is helpful to understand the ^{13}C NMR spectrum of the complex. With the assignments of HL^2 known from literature,¹ it is possible to identify the minor impurity to be uncoordinated L^2 in the $^{13}C\{^1H\}$ NMR spectrum of the complex shown in Figure 3.7. Furthermore, the known assignment of HL^2 was used to assign the aliphatic carbons of $Pt^{II}(phen)(L^2-S)_2$ as shown in Figure 3.7. The two isolated peaks at 149 and 146 ppm could be assigned to C^2 and C^{1a} using the $^{13}C\{^1H\}$ NMR spectrum of HL^2 and the ^{13}C APT spectrum of $Pt^{II}(phen)(L^2-S)_2$.

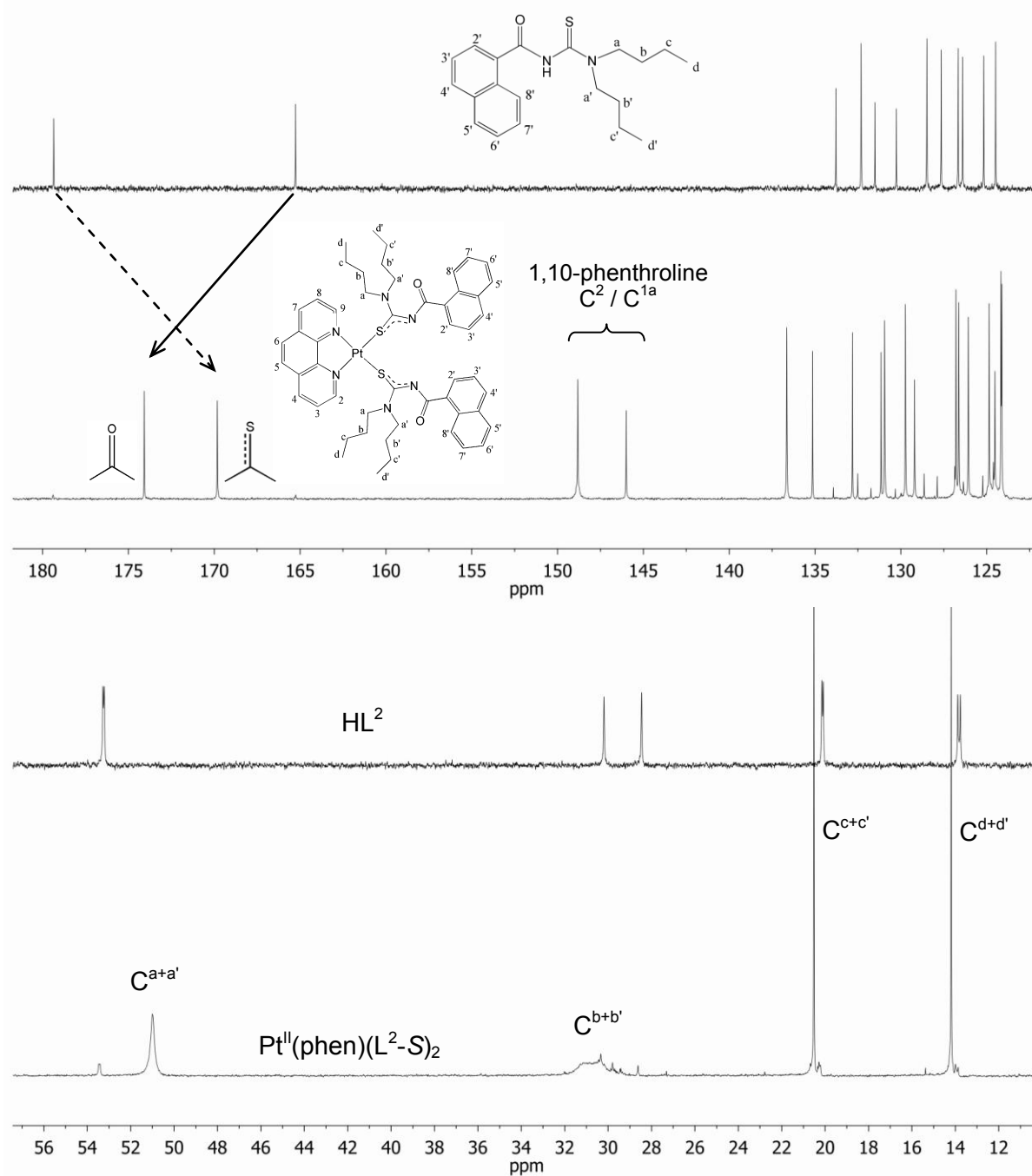


Figure 3.7 $^{13}\text{C}\{^1\text{H}\}$ NMR spectra of HL^2 and $\text{Pt}^{\text{II}}(\text{phen})(\text{L}^2\text{-S})_2$ in chloroform- d_1 .

The carbonyl and thiocarbonyl were assigned based on the line width of the resonances, difference in hybridisation of the two groups in the monodentate complex as well literature assignments of acylthioureas Pt^{II} complexes.¹⁴ The line width of the thiocarbonyl is greater than the carbonyl as a result of two quadrupolar nitrogens bonded to the thiocarbonyl carbon which shortens the relaxation time and results in broadening. Furthermore, this broader peak shifts downfield relative to the ligand while the carbonyl shifts upfield. This is consistent

with the change in hybridization from sp^2 to sp^3 upon coordination of the sulphur which would result in shielding of the thiocarbonyl carbon. The carbonyl carbon exhibits significant deshielding which suggests more double bond character of the carbonyl and greater chemical shift anisotropy.

However, there are some ^{13}C peaks which could not be assigned with only the ^{13}C APT of $Pt^{II}(phen)(L^2-S)_2$ and $^{13}C\{^1H\}$ NMR assignments of HL^2 necessitating the use of heteronuclear two-dimensional NMR spectroscopy. The widely used sequences to obtain 1H - ^{13}C short bond coupling information are the 1H , ^{13}C HETCOR (Heteronuclear Correlation) and 1H , ^{13}C HSQC (Heteronuclear Single Quantum Coherence) sequences.

The HSQC sequence has to a large extent replaced the earlier HETCOR sequence due to its superior sensitivity. The HETCOR sequence is also known as C,H COSY (Correlation Spectroscopy) and is weak in sensitivity due to the observed nuclei being ^{13}C with a very low natural abundance (1.1%) and a receptivity 5870 times lower than that of 1H . In contrast, the HSQC or H,C COSY is the reverse of HETCOR by first generating phase coherence in the channel corresponding to the insensitive nuclide (^{13}C) and then transferring the coherence to the sensitive nuclide (1H) which is then observed.¹⁵ The enhancement gained from the polarisation transfer during the experiment is proportional to the ratio of the gyromagnetic ratios of the nuclide from which the polarisation is transferred over the gyromagnetic ratio of the observed nuclide (γ_C/γ_H). However, for the preferred HSQC experiment the enhancement is significantly lower with the enhancement 0.25 compared to 4 times for the 'normal' ^{13}C detected HETCOR. The advantage of detecting the more sensitive nuclide together with the lower enhancement effect due to the effect of the gyromagnetic ratios of the two nuclides results in a total sensitivity gain of a factor of 2 for the HSQC (reverse) experiment over the HETCOR (normal) experiment with the corresponding time shortening of a factor of 4.¹⁵ The information gathered from the two experiments is similar with the advantage of higher sensitivity and thus shorter acquisition times.

The GHSQC (gradient-HSQC) sequence was used to obtain 1H - ^{13}C correlations to assign all the resonances in the $^{13}C\{^1H\}$ NMR spectrum of $Pt^{II}(phen)(L^2-S)_2$ (Figure 3.8). With all the assignments of the 1H NMR spectrum of $Pt^{II}(phen)(L^2-S)_2$ known, all the carbon atoms directly bonded to one or more hydrogen atoms could be readily assigned by correlating the 1H resonance to the corresponding ^{13}C resonance cross-peaks. Cross-peaks were observed for all 1H resonances, indicating that the GHSQC experimental were correctly optimised and that enough transients were collected. The correlations between the butyl H's and C's of L^2 could be observed (Figure 3.8), which confirmed the previous assignments of these carbons.

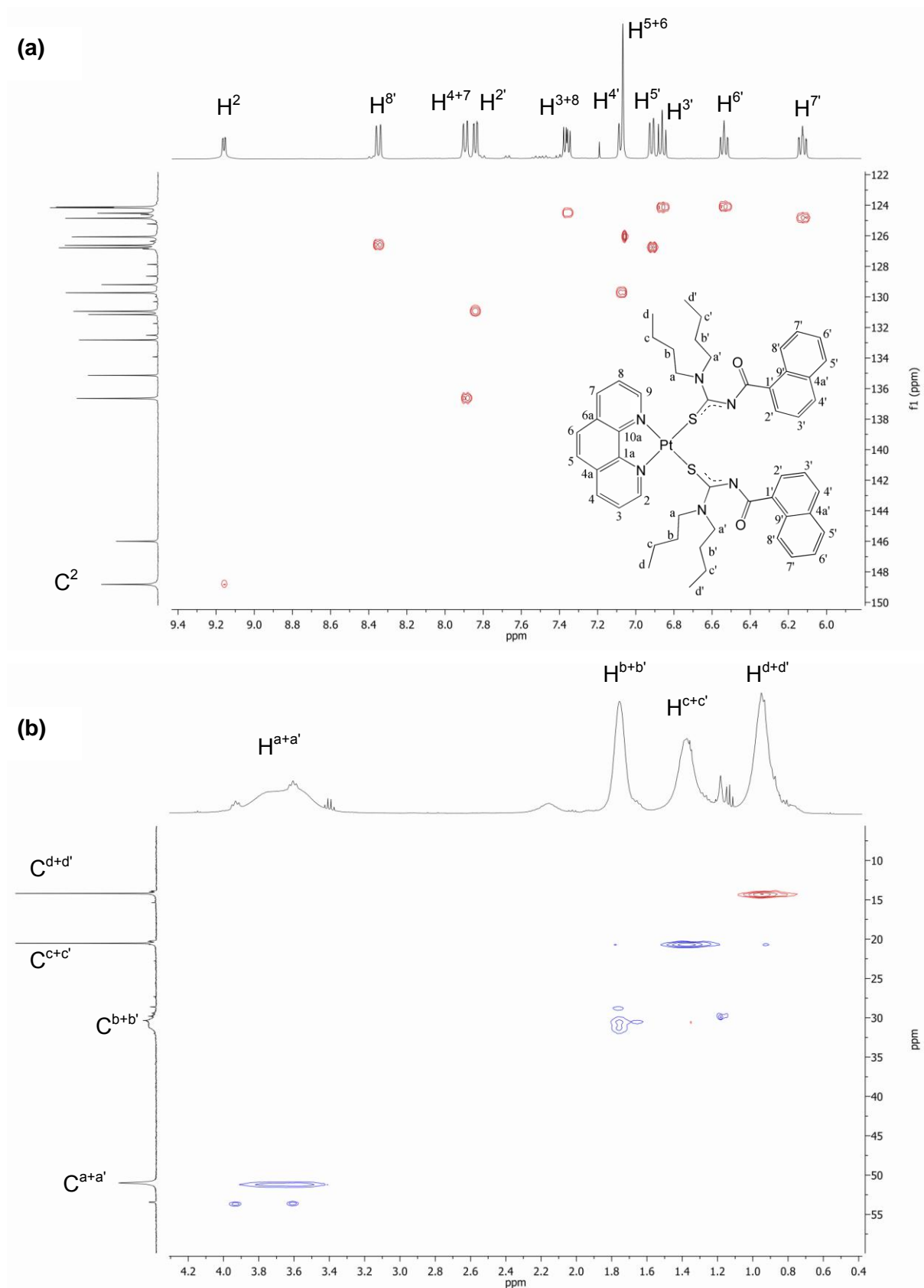


Figure 3.8 1H , ^{13}C GHSQC plot of $Pt^{II}(phen)(L^2-S)_2$ showing the 1H and ^{13}C correlations in chloroform- d_1 with (a) the aromatic region and the aliphatic region of the plot.

Furthermore, the negative cross-peaks (in blue) observed for the CH_2 carbons and positive cross-peaks (in red) observed for the CH_3 and CH groups is indicative of the evolution period in the experiment set as the inverse of the scalar (J) coupling constant.

With the assignments from the $^1H, ^{13}C$ GHSQC, ^{13}C APT experiments and the known assignments of HL^2 , the $^{13}C\{^1H\}$ NMR spectrum of $Pt^{II}(phen)(L^2-S)_2$ could be completely assigned. The full assignment of all ^{13}C resonances is shown in Figure 3.9 while the minor additional peaks in the $^{13}C\{^1H\}$ NMR spectrum correspond to unreacted L^2 . A list of all ^{13}C NMR chemical shifts and their assignments are shown in Table 3.1.

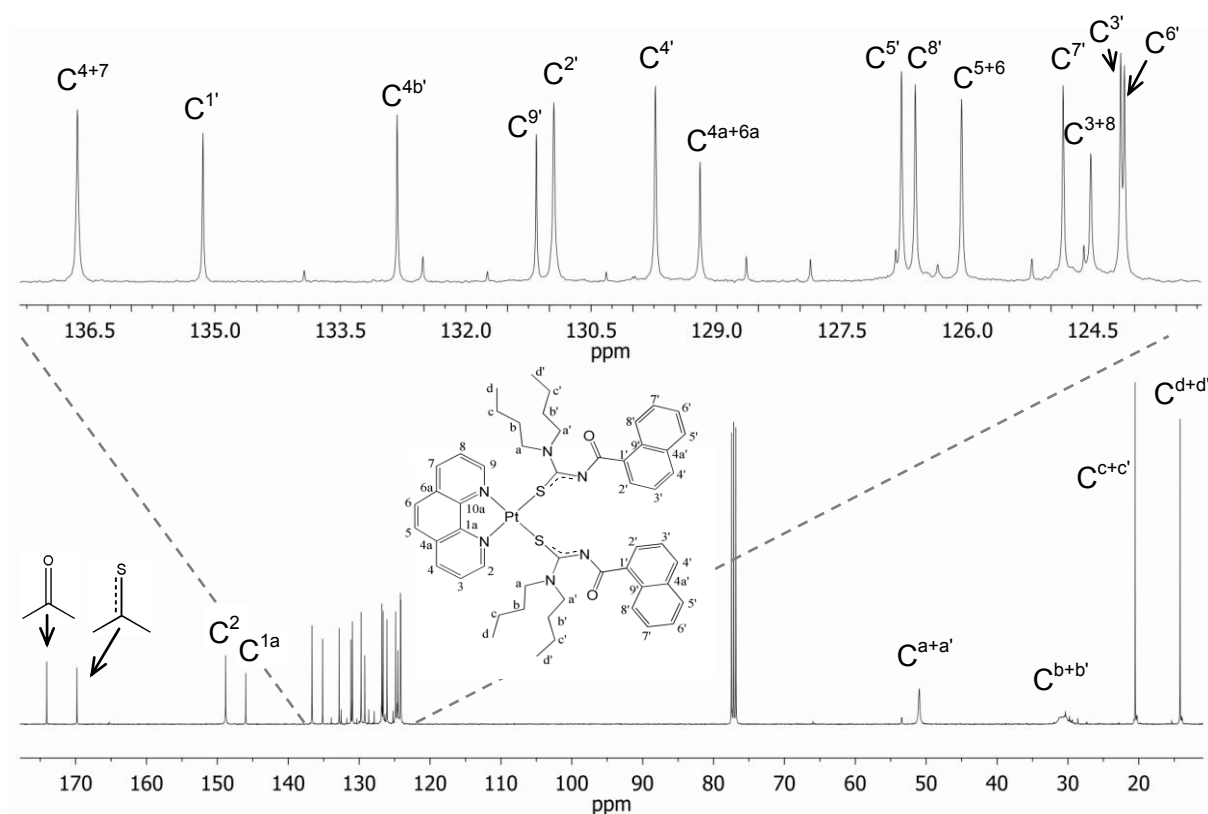


Figure 3.9 $^{13}C\{^1H\}$ NMR spectrum and assignments of $Pt^{II}(phen)(L^2-S)_2$ in chloroform- d_1 at 25°C.

Table 3.1 ^{13}C NMR chemical shift assignments of $Pt^{II}(phen)(L^2-S)_2$ in chloroform- d_1 .

Assignment	Chemical Shift (ppm)	Assignment	Chemical Shift (ppm)	Assignment	Chemical Shift (ppm)
C=O	173.921	C ^{2'}	130.785	C ^{3'}	124.004
C-S	169.661	C ^{4'}	129.571	C ^{6'}	123.960
C ²	148.666	C ^{4a+6a}	129.036	C ^{a+a'}	50.834
C ^{1a}	145.843	C ^{5'}	126.627	C ^{b+b'}	30.591
C ⁴⁺⁷	136.485	C ^{8'}	126.461	C ^{c+c'}	20.354
C ^{1'}	134.984	C ⁵⁺⁶	125.908	C ^{d+d'}	14.027
C ^{4b'}	132.659	C ^{7'}	124.693		
C ^{9'}	130.995	C ³⁺⁸	124.362		

3.2.3 Temperature and Concentration Dependence of the 1H NMR Spectrum of $Pt^{II}(phen)(N,N\text{-dibutyl-}N'\text{-naphthoylthiourea})_2$

3.2.3.1 The effect of increasing the temperature on the 1H NMR spectrum of $Pt^{II}(phen)(N,N\text{-dibutyl-}N'\text{-naphthoylthiourea})_2$

The effect of an increase in temperature on the 1H NMR spectrum of $Pt^{II}(phen)(L^2-S)_2$ was investigated from 25 to 109°C. For this temperature investigation the solvent system was changed from the chloroform- d_1 used in the characterization to dimethyl sulfoxide- d_6 since the boiling point of chloroform- d_1 is only 61°C while dimethyl sulfoxide d_6 is a liquid between 20 and 190 °C. The 1H NMR spectrum of $Pt^{II}(phen)(L^2-S)_2$ in dimethyl sulfoxide- d_6 (Figure 3.10) exhibits a similar intermediate exchange phenomenon for the butyl H's of L^2 as observed in chloroform- d_1 (Figure 3.3). The temperature was increased systematically, with the corresponding 1H NMR spectra stacked in Figure 3.10.

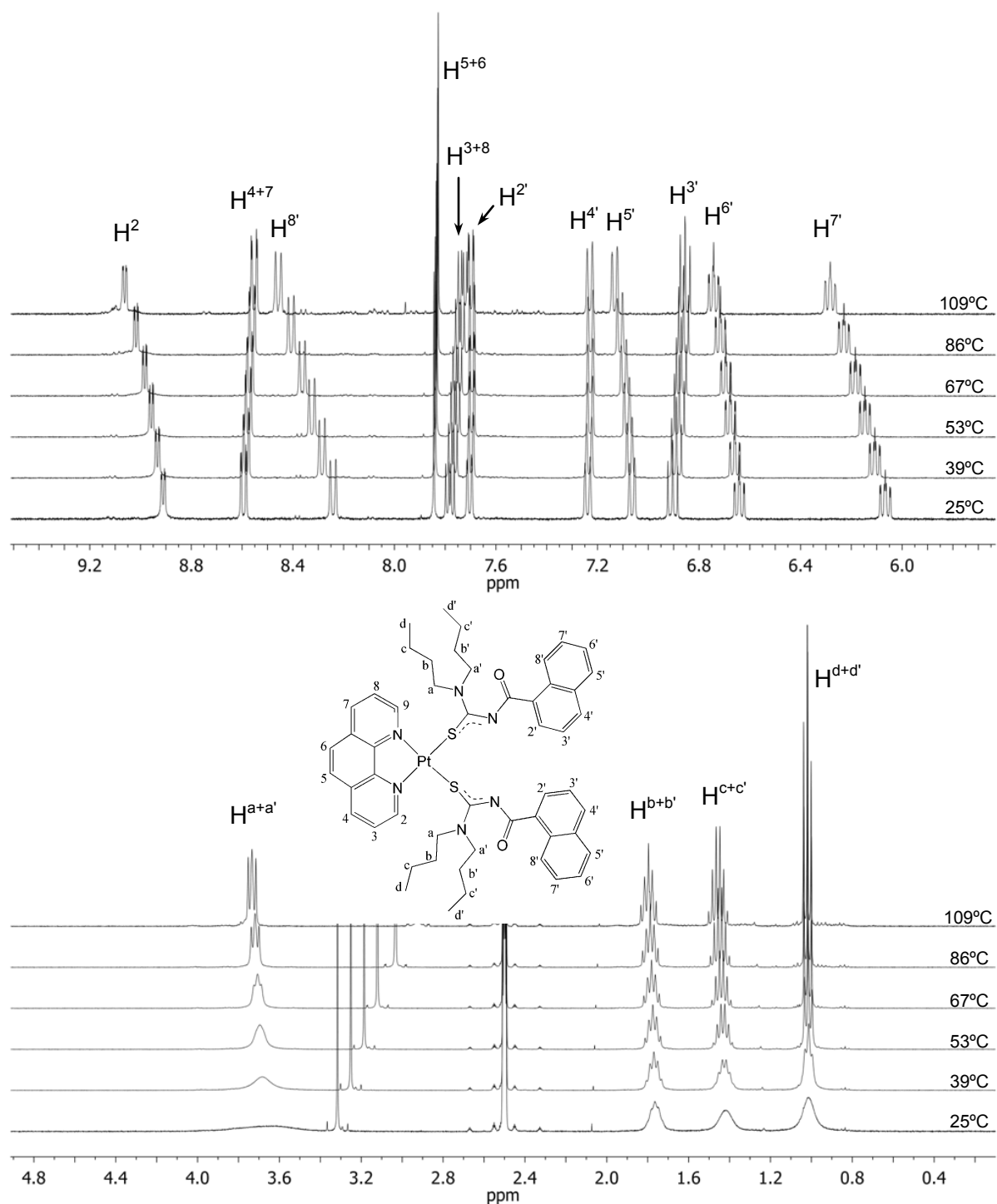


Figure 3.10 ^1H NMR spectra of $\text{Pt}^{\text{II}}(\text{phen})(\text{L}^2\text{-S})_2$ as a function of temperature in dimethyl sulfoxide- d_6 .

Interestingly, the ^1H NMR resonances of the butyl chains of L^2 sharpen significantly as the temperature increases, while the aromatic protons display no significant change in line-shape. This is indicative of the change from an intermediate exchange process to a fast exchange system with respect to restricted rotation around the C-N bond of the carbon of the thiocarbonyl and the butylamino nitrogen (Figure 3.11). The sharpening of the resonances of

$H^{a+a'}$ and $H^{d+d'}$ were carefully studied by a line-fitting procedure using the Line Fitting capabilities of the MestreNova NMR processing software to obtain accurate line widths for the broad/unresolved 1H multiplets at low temperatures. The fits to the experimental data as well as the errors and fitting parameters are shown in Figure A.17 and A.18 in the appendix.

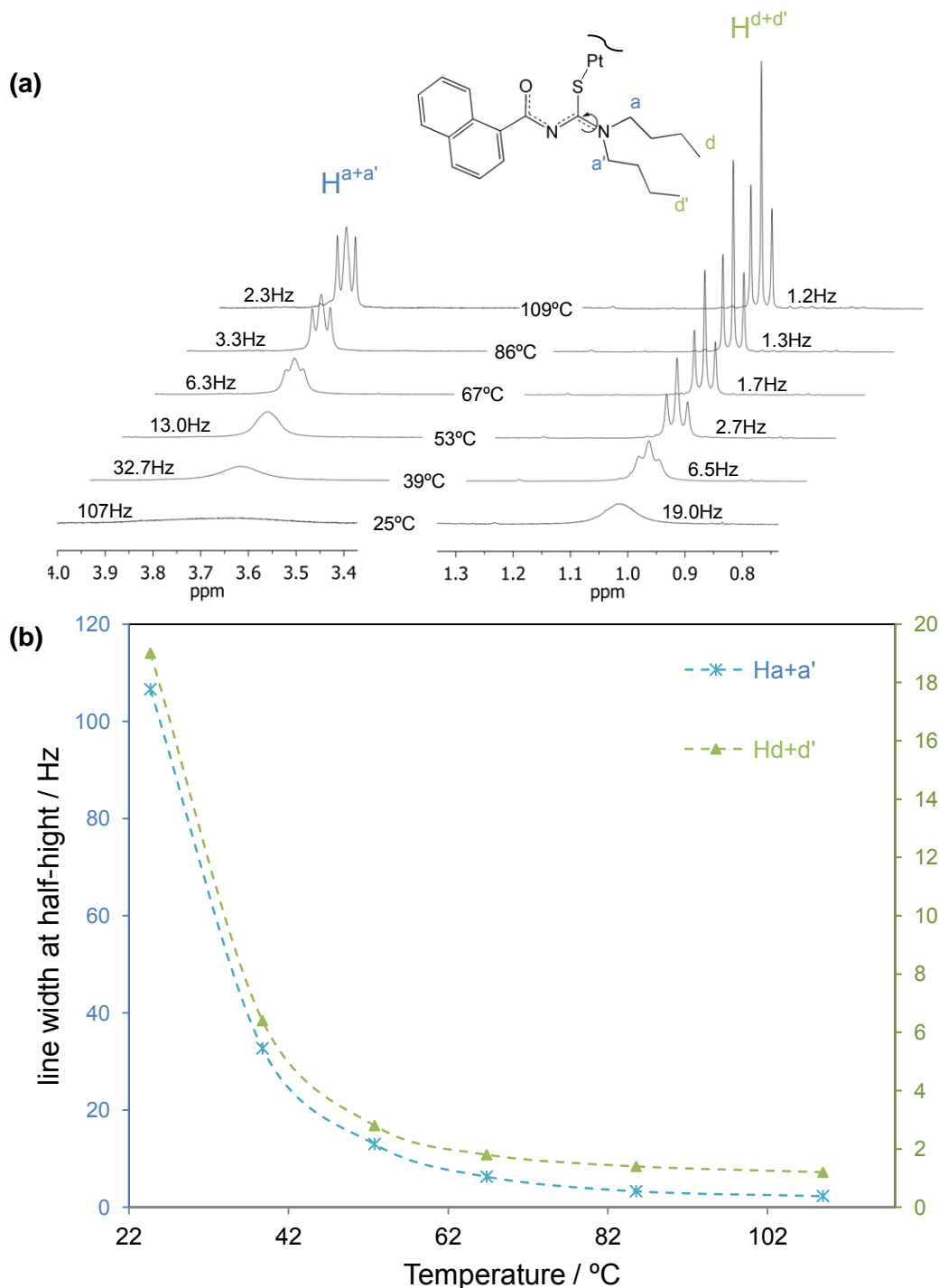


Figure 3.11 Temperature dependence of $H^{a+a'}$ and $H^{d+d'}$ showing (a) sharpening of the resonances with an increase in temperature for $Pt^{II}(phen)(L^2-S)_2$ in dimethyl sulfoxide- d_6 displayed using a stack angle of 35° and (b) the line-width at half-peak height ($\Delta v_{1/2}$) of $H^{a+a'}$ and $H^{d+d'}$ as a function of temperature.

Interestingly the line width at 25°C is significantly lower for $H^{d+d'}$ (19 Hz) compared to $H^{a+a'}$ (107 Hz). This marked difference in line-width can be rationalised on the basis of $H^{a+a'}$ being close to the site where rotation is restricted (Figure 3.11) whereas $H^{d+d'}$ is 5 bonds away. This restricted rotation is presumably the result of π -back donation of the amino-nitrogen into the π -antibonding orbitals (π^*) of the thiocarbonyl.

The 1H NMR spectrum of $Pt^{II}(phen)(L^2-S)_2$ in dimethyl sulfoxide- d_6 (Figure 3.10) exhibits significant temperature dependence of the chemical shifts of the aromatic protons, while those of the aliphatic protons are less affected. Moreover $\delta(^1H)$ of H^2 , $H^{7'}$ and $H^{8'}$ were the most sensitive towards a change in temperature with the chemical shift difference ($\Delta\delta$) for temperatures 25 and 109°C being $\Delta\delta H^2 = 0.152$ ppm, $\Delta\delta H^{7'} = 0.217$ ppm and $\Delta\delta H^{8'} = 0.216$ ppm. The chemical shift temperature dependence of all aromatic protons is shown in Figure 3.12.

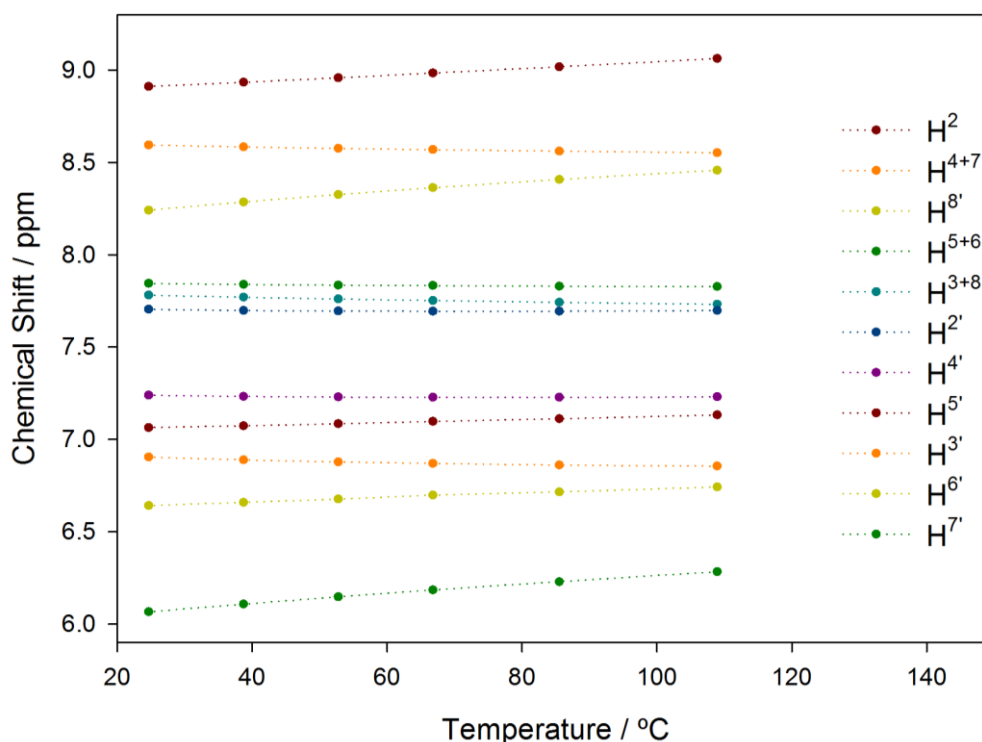


Figure 3.12 1H chemical shift temperature dependence of $Pt^{II}(phen)(L^2-S)_2$ in dimethyl sulfoxide- d_6 .

While 1H chemical shifts are normally affected by changes in solvent polarity and density/viscosity with temperature, the significant temperature dependence observed cannot be accounted for solely by changes in solvent characteristics. This could suggest self-aggregation or possible *intra*-molecular association/interactions in dimethyl sulfoxide

solutions. Chemical shift temperature and concentration dependence previously observed for the cationic $[Pt^{II}(phen)(L^n-,S,O)]^+$ complexes in acetonitrile solutions were postulated to be due to non-covalent dimer formation.¹ It was shown previously that $[Pt^{II}(phen)(L^1-S,O)]^+$ self-associates and forms non-covalent outer sphere complexes with the polyaromatic hydrocarbon fluoranthene ($C_{16}H_{10}$) in acetonitrile, presumably through cation- π and aromatic π -stacking interactions.¹⁶ Furthermore, the self-association of $[Pt^{II}(phen)(L^1-S,O)]^+$ increases drastically with the addition of D_2O to the solution and ultimately results in the formation of nano-aggregates in pure D_2O ; this will be discussed in detail in Chapter 4. The polarity of the solvent has a drastic effect on the possibility and the extent of aggregation of charged or uncharged aromatic moieties as hydrophobic forces becomes more dominant with an increase in solvent polarity.¹⁷

Since the $Pt^{II}(phen)(L^2-S)_2$ complex is formally uncharged it may be capable of inter- or *intra*-molecular aromatic- π stacking interactions in polar solutions since the complex consist of a 1,10-phenantroline ligand and two naphthoyl moieties of L^2 which amounts to a total of 7 aromatic rings. It is expected that the inter- or *intra*-molecular hydrophobic interactions would decrease significantly in less polar solvents. Indeed, the chemical shift temperature dependence for $Pt^{II}(phen)(L^2-S)_2$ is significantly less in chloroform- d_1 solutions (Figure 3.3) compared to dimethyl sulfoxide- d_6 solutions for the temperatures 25 and 50°C.

The 1H NMR spectra of $Pt^{II}(phen)(L^2-S)_2$ at 4 different concentrations in chloroform- d_1 was obtained during the course of the study and set out to examine the extent/possibility of self-association of this complex.

3.2.3.2 The concentration dependence of the 1H NMR spectrum of $Pt^{II}(phen)(N,N$ -dibutyl- N' -naphthoylthiourea) $_2$

The change in 1H chemical shift is found to be almost negligible when the concentration of $Pt^{II}(phen)(L^2-S)_2$ is 2.58 times higher (~3.4 mM) than the lowest concentration (~1.3 mM), but is significant for a concentration 87 times (~112 mM) the lowest concentration (Figure 3.13). However, the stacked spectra in Figure 3.13 are from different synthesis batches and were obtained over a period of months and were not obtained from serial dilution as seen from the impurities present in the 1H NMR spectrum of $N = 2.58$.

The overall chemical shift concentration dependence of H^{5+6} , H^{4+7} and H^{3+8} is 0.396, 0.232 and 0.136 ppm over this concentration range respectively while the other protons exhibit

significantly less chemical shift concentration dependence with $\Delta\delta < 0.05$ ppm. Interestingly, the aliphatic protons of L^2 exhibit no significant change in chemical shift with an increase in concentration. This is consistent with a postulated self-association of $Pt^{II}(phen)(L^2-S)_2$ by π -stacking in solution (*i.e.* aliphatic chains not directly involved).

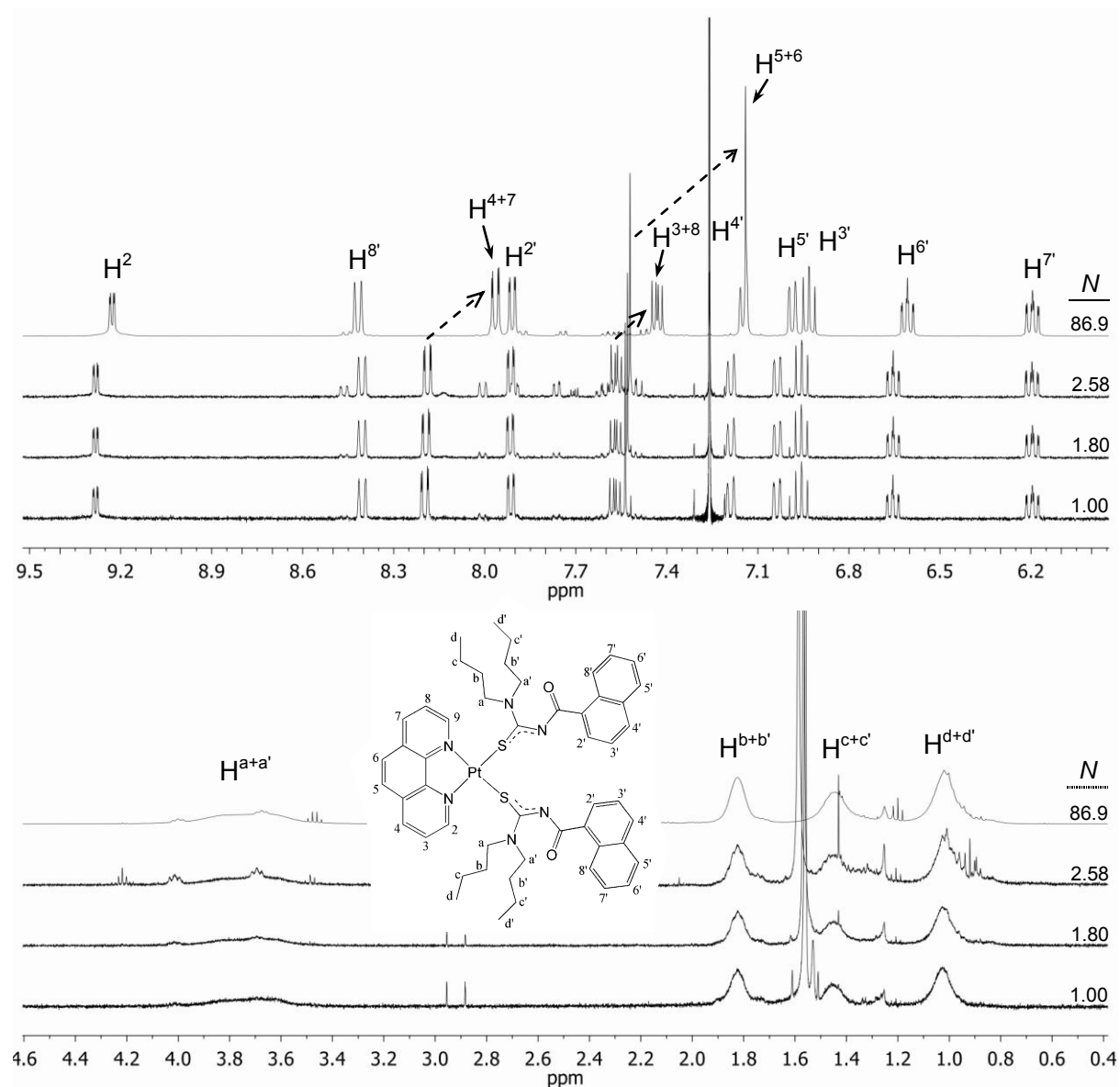
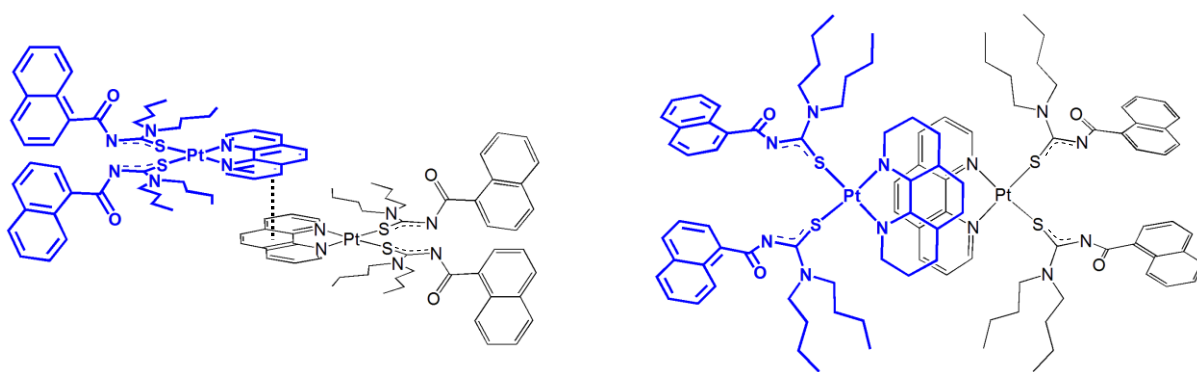


Figure 3.13 1H NMR spectra of $Pt^{II}(phen)(L^2-S)_2$ of different concentrations in chloroform- d_1 with N the normalized concentration relative to the lowest concentration (~ 1.3 mM).

With the chemical shift trends observed it is reasonable to postulate an average aggregate structure which could account for the marked difference in chemical shift concentration dependence observed for the various protons. It is expected that the extent of self-association of $Pt^{II}(phen)(L^2-S)_2$ would be limited to dimer aggregates in chloroform and higher-order

aggregation is unlikely in this less polar solvent compared to acetonitrile where $[Pt^{II}(\text{phen})(L^2-S,O)]^+$ is known to form only dimer aggregates in solution. Scheme 3.4 shows the proposed non-covalent dimers in solution which could account for the chemical shift trends observed, in which the protons of the 1,10-phenanthroline exhibit marked chemical shift concentration dependence compared to the protons of L^2 .



Scheme 3.4 Proposed dimer structures of $Pt^{II}(\text{phen})(L^2-S)_2$ in chloroform which could account for the chemical shift concentration dependence observed.

The overlap of the 1,10-phenanthroline moieties in the proposed average dimer structure of $Pt^{II}(\text{phen})(L^2-S)_2$ in chloroform (Scheme 3.4), is expected to result in increased shielding of the corresponding phen H's from the external magnetic field resulting in an upfield shift in the 1H NMR resonances as the equilibrium shifts toward more dimer formation. The driving force for such a postulated aggregation would be a favourable offset aromatic- π stacking interaction proposed by Hunter and Sanders in their study of porphyrin aggregation.¹⁸

However, with the limited experimental evidence, the formation of dimer aggregates is only speculative at present. A detailed study of the chemical shift and diffusion coefficient concentration dependence at various temperatures is required to which the appropriate aggregation models could be fitted to account for the experimental trend observed and is subject for future study.

3.2.3.3 The effect of lower temperature on the 1H NMR spectrum of $Pt^{II}(\text{phen})(N,N\text{-dibutyl-}N'\text{-naphthoylthiourea})_2$ in $CDCl_3$

The effect of temperature on the 1H NMR resonances of $Pt^{II}(\text{phen})(L^2-S)_2$ in chloroform- d_1 was investigated (Figure 3.14). Interestingly, the broad aliphatic protons separate into two sets of signals while the multiplicity becomes better resolved with a decrease in temperature,

contrary to the aromatic protons which exhibit broadening as the temperature was decreased. The increase in the line-width of the aromatic protons could be due to previously proposed aggregation/*intra*-molecular interactions and/or as a result of an increase in the relaxation time of the respective protons due to slow molecular tumbling (long τ_c) at lower temperatures. Aggregation of phen H's is expected to result in an increase in τ_c , while the butyl H's probably are more freely rotating. This then accounts for the observed line-widths, assuming a dipole-dipole mechanism under these conditions.

The narrowing of the butyl 1H resonances as the temperature decrease (Figure 3.14) is a result of the previously discussed restricted rotation around the thiocarbonyl carbon and the amino nitrogen (discussion of Figure 3.11). The transition from one broad signal to two well resolved multiplets as the temperature decreased is indicative of the transition from an intermediate- to a slow exchange system. Estimation of the rotational energy barrier is typically done using approximations by Gasparro and Kolodny and commonly used in dynamic NMR studies.¹⁹ Gasparro and Kolodny have used these approximations in the determination of the rotational barrier in N,N-dimethylacetamide with results for the energy of activation, $E_a = 17 \text{ kcal.mol}^{-1}$, closely comparable to the results obtained by Reeves *et al.* who simulated the spectra from the Bloch equations.²⁰

With two exchanging resonance frequencies ν_A and ν_B merging into one single peak and the decrease in line-width, the rate constant of the exchange/rotation, k , could be approximated several ways (Scheme 3.5).¹⁹ The distinct features of an exchanging process on the NMR spectra are a change in chemical shift ($\Delta\delta$) and a change in line width of the resonances. The line width at half-peak height, $(\Delta\nu)_{1/2}$, is easy to measure if the resonance signals are simple singlets or perfect first-order multiplets. However, this is rarely the case and the extraction of reliable $(\Delta\nu)_{1/2}$ values from real NMR data remains challenging. The use of the intensity (I) to calculate the rate constants in accordance with equation 2 in Scheme 3.5, was not desirable since baseline correction drastically influenced the results obtained.

In contrast to the difficulty in accurate determination of $(\Delta\nu)_{1/2}$ and I , the chemical shift can easily be obtained accurately and the peak separation was consequently used to calculate the rate constants (k) using equation (1) in Scheme 3.5.

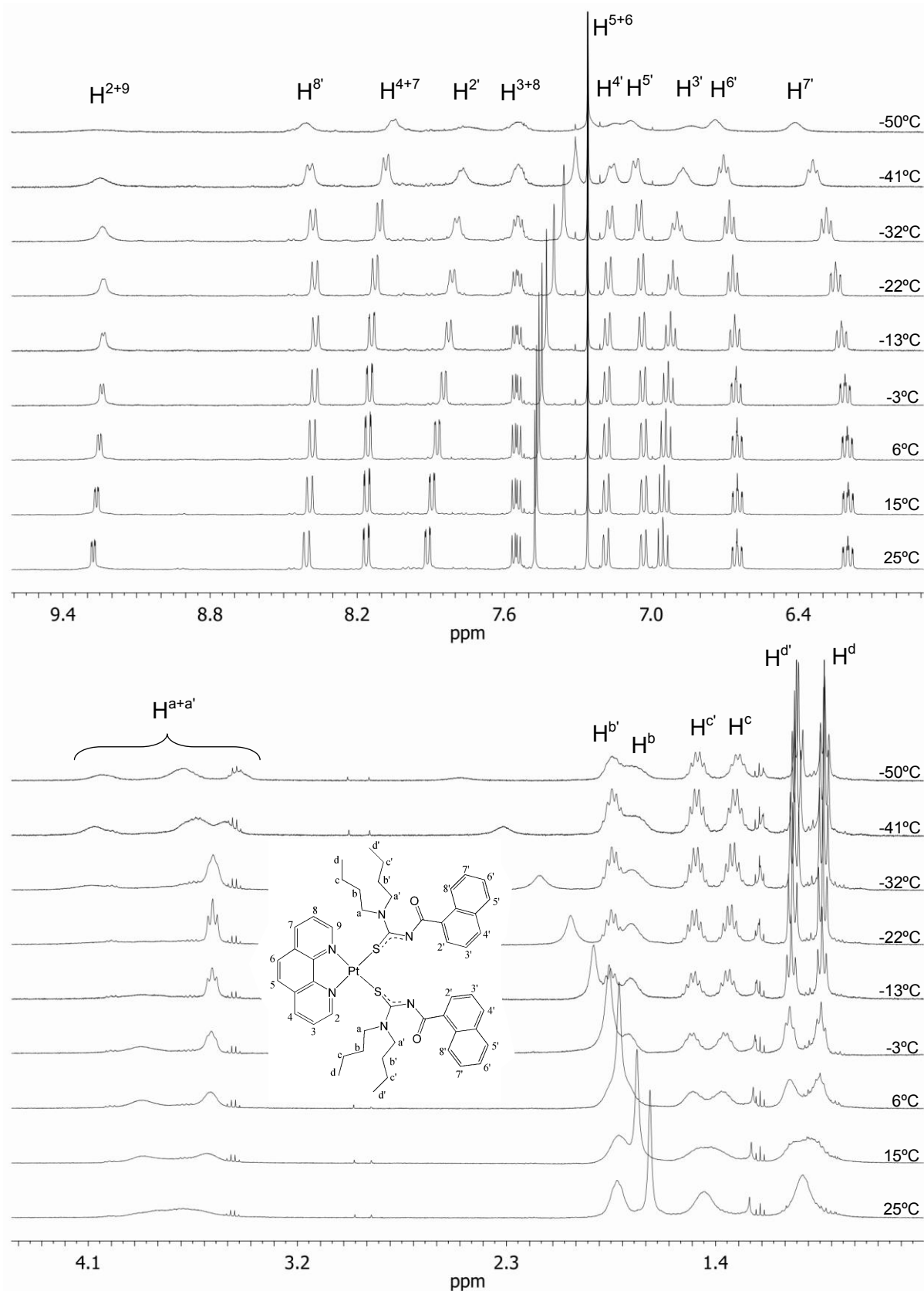
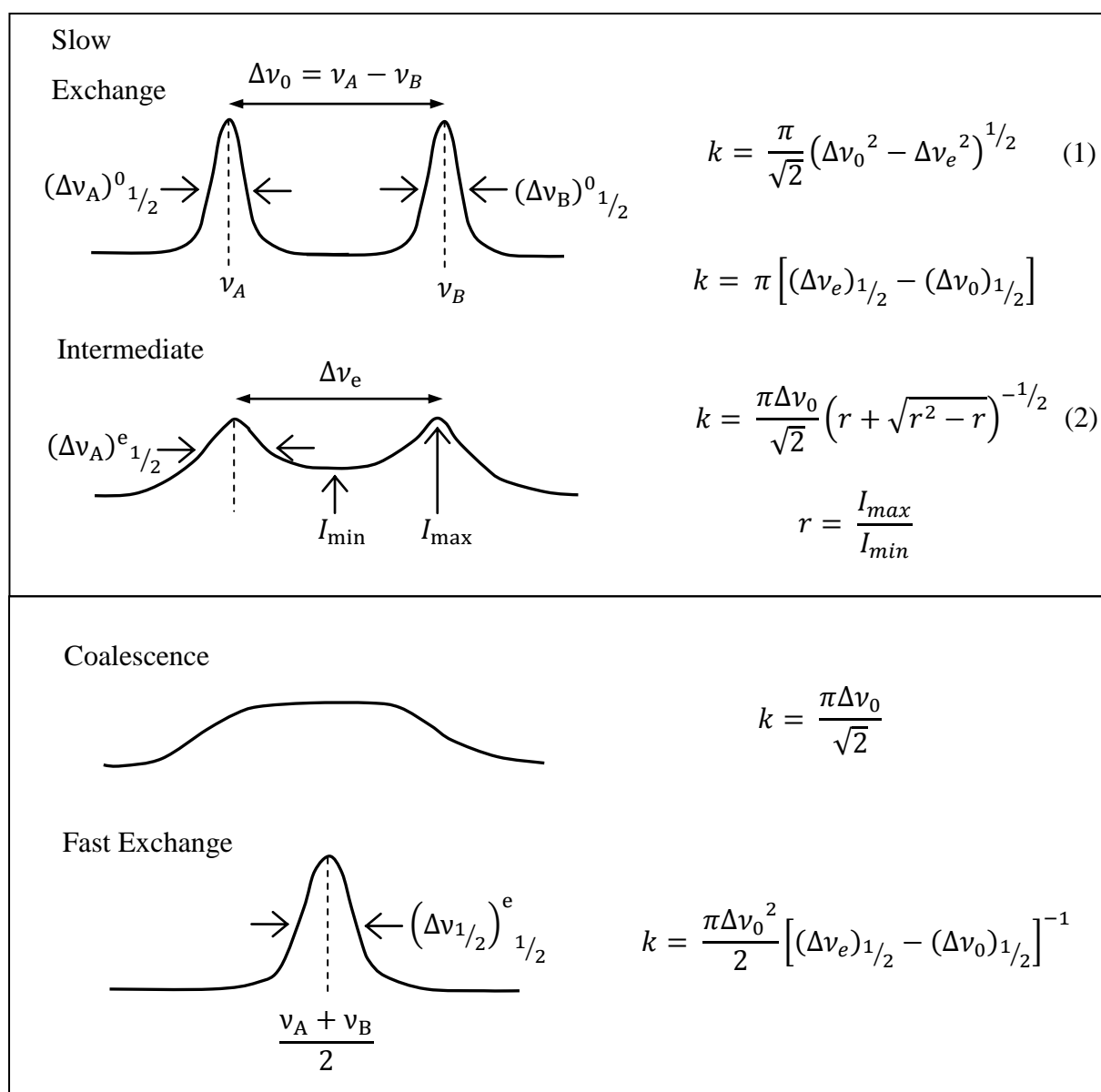


Figure 3.14 ^1H NMR spectra of $Pt^{II}(phen)(L^2-S)_2$ as a function of temperature in chloroform- d_1 .



Scheme 3.5 Representation of the approximations for calculating the rate constant in a dynamic NMR experiment with $\Delta\nu_0$ the difference in the frequency of A (ν_A) and B (ν_B) with no exchange, $\Delta\nu_e$ the difference in the frequency with exchange, $(\Delta\nu)_{1/2}^0$ the peak width at half-height of resonance A/B in the absence of exchange and $(\Delta\nu)_{1/2}^e$ with exchange.¹⁹

Equation (1) of Scheme 3.5 is only valid for slow to intermediate exchange (peak overlap < 20%) and was used to calculate the rate constants for the rotation around the bond between the thiocarbonyl carbon and the amino-nitrogen for the temperature range 5.9 to -50.2 °C using resonances H^c and H^{c'} with the k -values reported in Table 3.2.

Table 3.2 Calculated restricted rotation rate constants at various temperatures (T) using resonances H^c and H^{c'} and Equation (1) in Scheme 3.5.

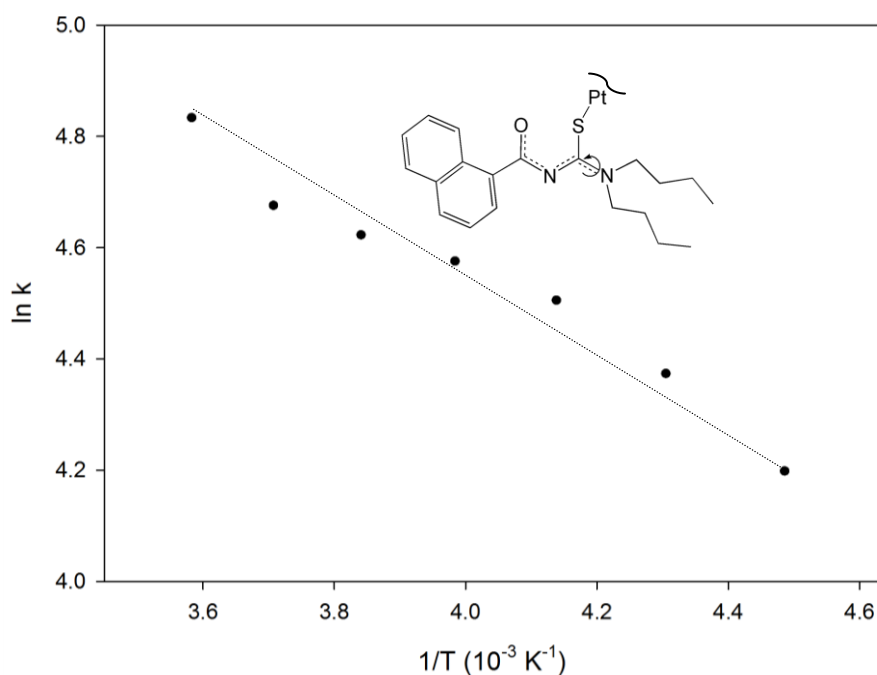
T (°C)	T (K)	$\Delta\nu_e$ (Hz)	k (s ⁻¹)	1/T (x10 ⁻³ K ⁻¹)	ln(k)
5.9	279.1	49.7	125.7	3.58	4.834
-3.4	269.7	57.8	107.3	3.71	4.676
-12.8	260.4	59.8	101.8	3.84	4.623
-22.1	251.0	61.3	97.1	3.98	4.576
-31.5	241.7	63.4	90.5	4.14	4.505
-40.9	232.3	66.3	79.3	4.31	4.373
-50.2	222.9	69.1	66.6	4.49	4.198

The Arrhenius plot of $\ln(k)$ vs T^{-1} can be used to estimate the activation energy (E_a) of the process from the derivation of the Arrhenius Equation:

$$k = Ae^{-E_a/k_B T}$$

$$\ln(k) = \ln(A) - \frac{E_a}{R} \left(\frac{1}{T} \right)$$

where, A denotes a pre-exponential factor which represents the total number of collisions per second, k_B Boltzmann constant and R the universal gas constant.

**Figure 3.15** Arrhenius plot for the rotation around the thiocarbonyl and amino nitrogen bond estimated from the chemical shift temperature dependence of H^c and H^{c'}.

If a linear trend is fitted to the data shown in Figure 3.15, the $R^2 = 0.966$ with the corresponding energy of activation $E_a = 5.2 \text{ kJ}\cdot\text{mol}^{-1}$, which is significantly less than the rotational barrier in N,N-demethylacetamide ($E_a = 71 \text{ kJ}\cdot\text{mol}^{-1}$). This is expected since the deprotonated coordinated ligand (L^2) of $Pt^{II}(phen)(L^2-S)_2$ should display significantly less π -back-donation from the amino nitrogen to the thiocarbonyl since the thiocarbonyl changed to a single C-S bond or at most a partial C-S double bond. Therefore, with the single bond character of the C-S bond, the π anti-bonding orbitals of the 'thiocarbonyl' are absent in the monodentate coordinated ligand. However, the newly formed double bond between the amino nitrogen to the C(S) carbon would have π anti-bonding orbitals into which the amino-nitrogen could to some extent donate its lone pair of electrons.

The Arrhenius plot clearly deviates from linearity in a specific manner which suggests that the rotation about the bond between the thiocarbonyl carbon and the amino-nitrogen is not the only process that influences the chemical shift and line-width of $H^{c+c'}$. It is reasonable to postulate additional reactions/processes in solutions to account for the deviation in the Arrhenius plot which could be possible self-association and/or *intra*-molecular interactions suggested earlier for the concentration and temperature dependence of $Pt^{II}(phen)(L^2-S)_2$. The 1H resonances of H^a and H^a' (Figure 3.14) also exhibit additional 'separation' of the broad signals into 3 broad peaks, with an integral ratio roughly integrates for 2:4:2. Details of the self-association of $Pt^{II}(phen)(L^2-S)_2$ and the proposed *intra*-molecular association interactions are required to completely understand the behaviour of $Pt^{II}(phen)(L^2-S)_2$ in solution but were out of the scope of this study.

3.2.4 Crystal structure of $Pt^{II}(phen)(N,N\text{-dibutyl-}N'\text{-naphthoylthiourea})_2$

Crystals suitable for single crystal X-ray diffraction analysis were obtained for a column purified fraction of $Pt^{II}(phen)(L^2-S)_2$ in acetonitrile confirming the previously proposed mode of coordination of L^2 (Figure 3.16). The crystal and structure refinement data are shown in Section 3.4, and the CIF file is given on the electronic Appendix C, accompanying this thesis.

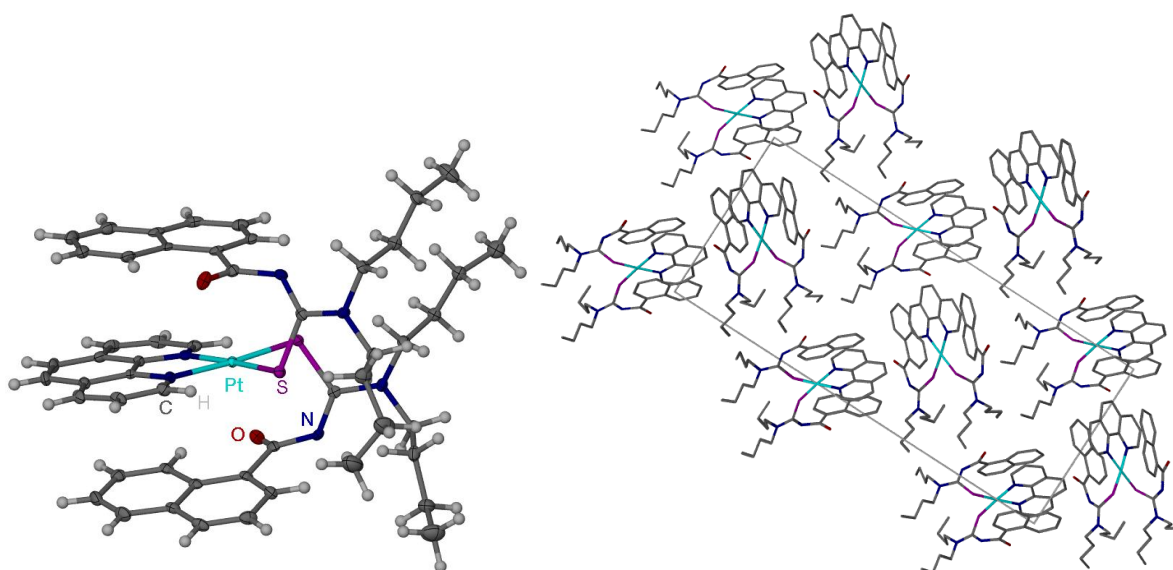


Figure 3.16 $Pt^{II}(phen)(L^2-S)_2$ and the stacking of $Pt^{II}(phen)(L^2-S)_2$ in the crystal lattice along the c axis.

The crystal structure reveals interesting *intra*-molecular interactions where two monodentate coordinated L^2 ligands are bent in such a way that the naphthoyl moieties 'sandwich' the chelated phen ligand of the square planar complex (Figure 3.17).

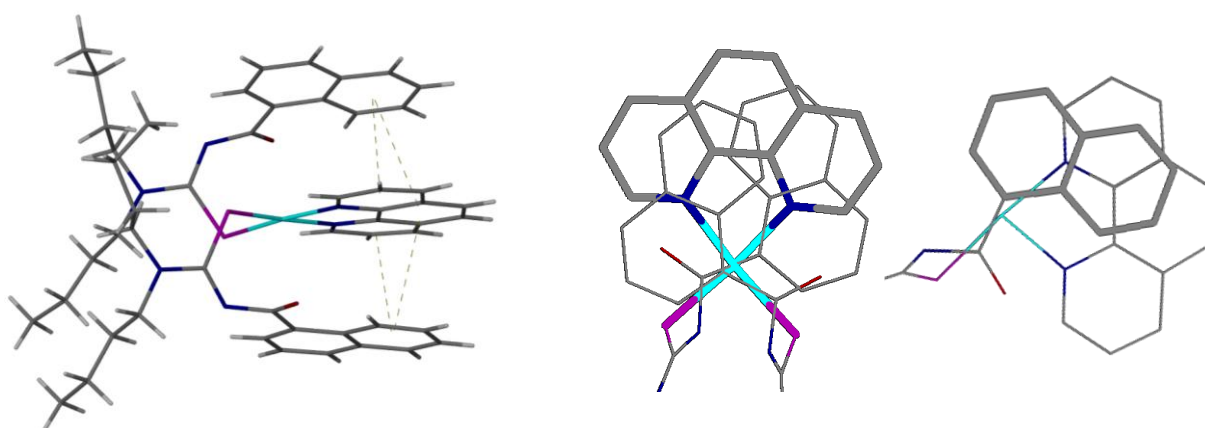


Figure 3.17 Offset aromatic- π stacking between the 1,10-phenanthroline ligands in the crystal structure of $Pt^{II}(phen)(L^2-S)_2$.

The naphthoyl moieties exhibit aromatic- π stacking interactions with the phen ligand in the characteristic offset manner proposed by Hunter and Sanders.¹⁸ Furthermore, it is evident from the crystal packing arrangement (Figure 3.16), the individual *intra*-molecular ' π -stacked' complexes do not π -stack to adjacent molecules to form linear chains of π -stacking but rather form individual *intra*-molecular associated complexes perpendicular to one another.

Table 3.3 Selected bond lengths, angles, torsion angles, plane angles and distances in the crystal structure of $Pt^{II}(phen)(L^2-S)_2$

<i>Bonds:</i>	Å	<i>Distances:</i>	Å
PT1-S3	2.2837(2)	C21 ... phen-pl	3.244
PT1-N9	2.0566(2)	C24 ... phen-pl	3.225
PT1-N10	2.0554(2)	* Ct1 ... phen-pl	3.374
PT1-S1	2.3002(2)	* Ct2 ... phen-pl	3.500
S3-C18	1.7783(2)	* Ct3 ... phen-pl	3.604
C18-N26	1.2962(1)	* Ct4 ... phen-pl	3.445
S1-C47	1.7809(2)	<i>Torsion angles:</i>	
N8-C18	1.3522(1)	O4-C3-C21-C14	-6.97°
C3-O4	1.2246(1)	O5-C49-C24-C6	-17.36°
C24-C49	1.520(2)	<i>Plane angles:</i>	
C3-C21	1.5285(2)	O4=C3-N26 < S1-Pt-S4	13.48°
C3-N26	1.3741(2)	O5=C49-N1 < S1-Pt-S4	11.55°
O5-C49	1.2334(1)	N9-Pt-N10 < S1-Pt-S4	2.42°
N1-C47	1.2874(1)	* Ct1-Ct2 < phen-pl	5.5°
N1-C49	1.3596(2)	* Ct3-Ct4 < phen-pl	15.2°
C47-N3	1.3623(1)		

**Ct* is centroids generated from the following carbons: *Ct1*=(C12,14,21,17,20,1), *Ct2*=(C13,14,12,19,33,42) *Ct3*=(C6,24,36,35,40,50) and *Ct4*=(C6,11,39,44,45,50).

Interestingly, the two sulphur-coordinated L^2 ligands exhibit similar interactions with the phen ligand with a marked difference in the angle of the π -stacking of the naphthoyl moieties with phen. The naphthoyl with centroids Ct1 and Ct2 is nearly parallel to the plane created by the atoms of the phenantrolone (Ct1-Ct2 < phen-pl = 5.5°) compared to the naphthoyl ligand with centroids Ct3 and Ct4, which π -stacks with an angle of 15.2°. The distances between the aromatic moieties are 3.374 and 3.44Å measured from Ct1...phen-plane and Ct4...phen-plane respectively. These two significantly different π -stacking modes are stable interactions as suggested by a theoretical study of various modes of π -stacking of benzene with fluoranthene by Kobayashi and co-workers.²¹

They have calculated the optimum angle for π -stacking for this system to be 4°; one of the naphthoyl groups displays a 5.5° angle. Furthermore, they have calculated the offset geometry to be the energy minimum configuration of π -stacking which is also consistent with our findings. The bond lengths of the two ligands do not differ substantially (< 0.015 Å) with the only other major difference being the orientation of the naphthyl relative to the carbonyl measured as a torsion angle of O=C to the naphthyl group. The in-plane geometry of the

aroyl group is commonly known to be the stable and more common conformer if no sterical interference/effects change the free energy of this conformation.²² However, the L^2 exhibiting a more parallel stacking interaction displays a smaller torsion angle between the naphthyl and the carbonyl groups (-6.97°) compared to -17.36° for the other π -stacked naphthyl group. The geometry of the Pt coordination sphere is slightly distorted from the ideal square planar geometry with 2.42° difference in the angle between two planes created by the phen nitrogens to platinum (N-Pt-N) and the two sulphur atoms to platinum (S-Pt-S). The important bond lengths of $Pt^{II}(phen)(L^2-S)_2$, $trans-Pt^{II}(L^2-S,O)_2$ ²³ and HL^2 are shown in Table 3.4.

Table 3.4 Comparison of relevant bond lengths of $Pt^{II}(phen)(L^2-S)_2$, $trans-Pt^{II}(L^2-S,O)_2$ and HL^2 with the average bond lengths reported for $Pt^{II}(phen)(L^2-S)_2$.

<i>Bond:</i>	$Pt^{II}(phen)(L^2-S)_2$	$trans-Pt^{II}(L^2-S,O)_2$ [23]	HL^2 [24]
	Å	Å	Å
Pt-S	2.292(2)	1.75(2)	
C=O	1.229(1)	1.28(3)	1.215(3)
C-S	1.780(2)	1.75(2)	1.662(2)
N-C(O)	1.367(2)	1.30(2)	1.376(4)
N-C(S)	1.129(1)	1.36(1)	1.420(4)
(S)C-N(R₂)	1.357(2)	1.34(3)	1.320(4)

The Pt-S bond of the *trans* complex is significantly shorter (1.75(2) Å) compared to that of $Pt^{II}(phen)(L^2-S)_2$ (2.292(2) Å). This could be a result of the *trans*-complex having less electron density in the Pt-S bond since the complex is formally a cationic complex, while $Pt^{II}(phen)(L^2-S)_2$ is neutral. The C-O bond length is in the order $trans-Pt^{II}(L^2-S,O)_2 > Pt^{II}(phen)(L^2-S)_2 > HL^2$. This is expected since the C=O bond in the free ligand would be almost a formal double bond while the monodentate complex is expected to exhibit longer/weaker C-O bond resulting from deprotonation of the ligand. The $trans-Pt^{II}(L^2-S,O)_2$ complex on the other hand would have mainly single bond character for C-O upon coordination as reflected in the 0.065 Å increase in bond length compared to that of HL^2 .

Interestingly, the N-C(S) bond in $Pt^{II}(phen)(L^2-S)_2$ is very short (1.129(1) Å) indicating the double bond character expected for this bond from the monodentate S-coordination. This is significantly shorter than N-C(S) of $trans-Pt^{II}(L^2-S,O)_2$ and HL^2 (1.36(1) and 1.420(4) Å respectively). This order is reversed for the N-C(O) bond length with $trans-Pt^{II}(L^2-S,O)_2$ having the shortest N-C(O); consistent with a shift in electron density towards the O atom to allow for coordination to Pt.

3.2.5 Probing solution interactions using the Nuclear Overhauser Effect

The synthesis of $Pt^{II}(\text{phen})(L^2-S)_2$ is typically done in polar solvents. As discussed earlier, the synthesis was most successful in methanol. The *intra*-molecular aromatic π -stacking interactions found in the SCXRD structure of $Pt^{II}(\text{phen})(L^2-S)_2$ is expected to also be prevalent in polar solvents, as found for the self-association of $[Pt^{II}(\text{phen})(L^1-S,O)]^+$ in water/acetonitrile mixtures which will be discussed in the next chapter. Furthermore, if this aromatic π -stacking interaction occurs in solution, it is expected to contribute to the stability of the aroyl complexes which will be absent in the unstable pivaloyl complexes. NOE experiments were conducted to investigate this phenomenon. The information obtained from such an NOE experiment allows for the assignment of nuclei that are close in space.

ROESY and NOESY1D experiments were attempted, with the best results obtained using the NOESY1D setup. For the NOESY1D experiment, the resulting ^1H enhancements as a result of the NOE of another ^1H nucleus that is close in space are monitored. The off-resonance irradiated spectrum is subtracted from this NOE enhanced ^1H NMR spectrum and the resultant spectrum displays the saturated peak as a negative signal while the other peaks observed correspond to nuclei close in space, i.e. experiencing the NOE.

To have a better understanding of this phenomenon, consider a simple two spin system A and X which represents two ^1H resonances having no scalar (J) coupling interaction (Figure 3.19).

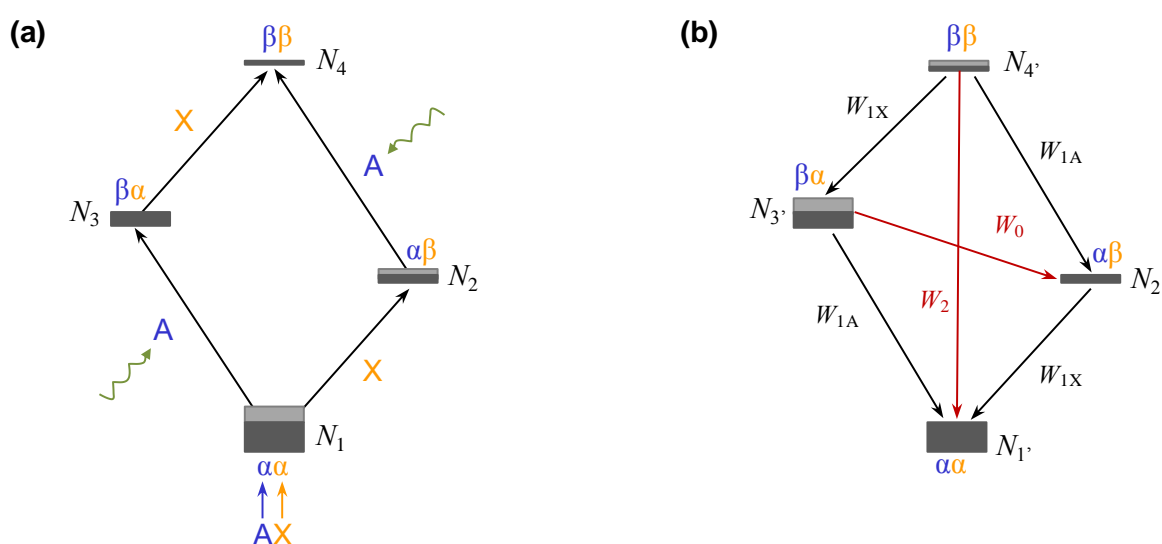


Figure 3.19 Changes in the population ratios in an NOE experiment. With (a) the initial equilibrium populations and (b) the populations when the two A transitions of equal energy are saturated.¹⁵ The different energy states are labelled N_{1-4} while α and β are the two spin state of the nuclei.

In general, A and X could be ^1H and ^{13}C or any other two nuclides, but in our case the basic principles of NOE will be discussed in terms of two non-coupled ^1H resonances which represents the NOESY1D experiment performed by us.¹⁵ When the nuclear spins A and X are close in space, they have a direct magnetic dipole-dipole interaction. This interaction affects the energies of the spin states of this two-spin system in a manner shown in Figure 3.2.

The transitions between states $N_1 \leftrightarrow N_3$ and $N_2 \leftrightarrow N_4$ are the spin transitions of nucleus A, while those between $N_1 \leftrightarrow N_2$ and $N_3 \leftrightarrow N_4$ are those of nucleus X. These transitions are spectroscopically allowed and are observed as singlets for the resonance of A and X in an NMR experiment.

In the NOE experiment the transition of spin A is saturated which alters the populations of the energy states, N_{1-4} in Figure 3.19b. The population of the spin states before (Figure 3.19a) and after selective excitation of A (Figure 3.19b) are indicated by the thickness of the bars; the thicker the bar (grey and black), the greater the population. The population contributions which have been transferred from $N_1 \rightarrow N_3$ and $N_2 \rightarrow N_4$ as a result of the selective excitation of A are indicated by light grey bars. At the stage immediately after the excitation of spin A, the population differences $N_{1'}$ - $N_{2'}$ and $N_{3'}$ - $N_{4'}$ are equal to the equilibrium differences N_1 - N_2 and N_3 - N_4 and the enhancement is not observed immediately. However, the system tries to restore the new populations (N_{1-4}) to the thermal equilibrium populations (N_{1-4}) through various relaxation processes indicated by W in Figure 3.19b with W_{1X} and W_{1A} the single quantum transition while W_0 and W_2 are zero and double quantum transitions respectively. W_{1X} and W_{1A} are observed spectroscopically and are typically a result of spin-lattice relaxation (T_1). W_0 and W_2 however, are spectroscopically forbidden but are allowed in relaxation and are typically related to dipole-dipole interactions.

The relaxation times of W_{1X} and W_{1A} (T_1 = several seconds) are much longer than the relaxation indicated by W_0 and W_2 (< 1 sec). The relaxation *via* W_2 results in a larger difference in $N_{1'}$ - $N_{2'}$ and $N_{3'}$ - $N_{4'}$ which determines the intensity of the X-transitions. It follows that W_2 leads to an enhancement effect while W_0 has the opposite effect by decreasing the population difference between the X-transitions. The mixing time which represents the time for the two coupled spins to interact, is optimised in a NOE experiment to have the maximum NOE effect with either W_0 or W_2 dominating in the specific conditions of the NOE experiment. The magnitude of the contributions of W_0 and W_2 determines whether the intensity increases, decreases or is zero ($W_0 = W_2$).

The relaxation through W_0 and W_2 is mostly dependent on the rotational correlation time, τ_c , (molecular tumbling) which is dependent on many factors including molecular size and

solvent viscosity. For small molecules and low viscosity solvents τ_c is short and W_2 dominates while W_0 dominates for macromolecules, resulting in negative NOEs.

NOESY1D experiments of $Pt^{II}(phen)(L^2-S)_2$ in methanol- d_4 were conducted to probe *intra*-molecular aromatic π -stacking interactions in solution. A temperature dependence study (-8.1 to 43.7 °C) of the 1H NMR spectrum of $Pt^{II}(phen)(L^2-S)_2$ in methanol (Figure A.21) was conducted to determine which temperature displays the appropriate interactions for the NOE experiment. No significant changes were observed for the temperature dependence and 25 °C was used for the NOESY1D experiments. The resulting 1H NMR spectra upon irradiation of H^2 , $H^{3'}$, $H^{5'}$, $H^{6'}$ and $H^{7'}$ are shown in Figure 3.20. Strong NOE enhancements were observed for the nuclei 3 bonds away from the saturated nuclei. However, we are interested in long range NOEs between nuclei that are close in space without J coupling to each other. A small NOE was observed for H^{5+6} upon irradiation of $H^{7'}$, $H^{6'}$, $H^{3'}$ and $H^{5'}$ as highlighted in Figure 3.20.

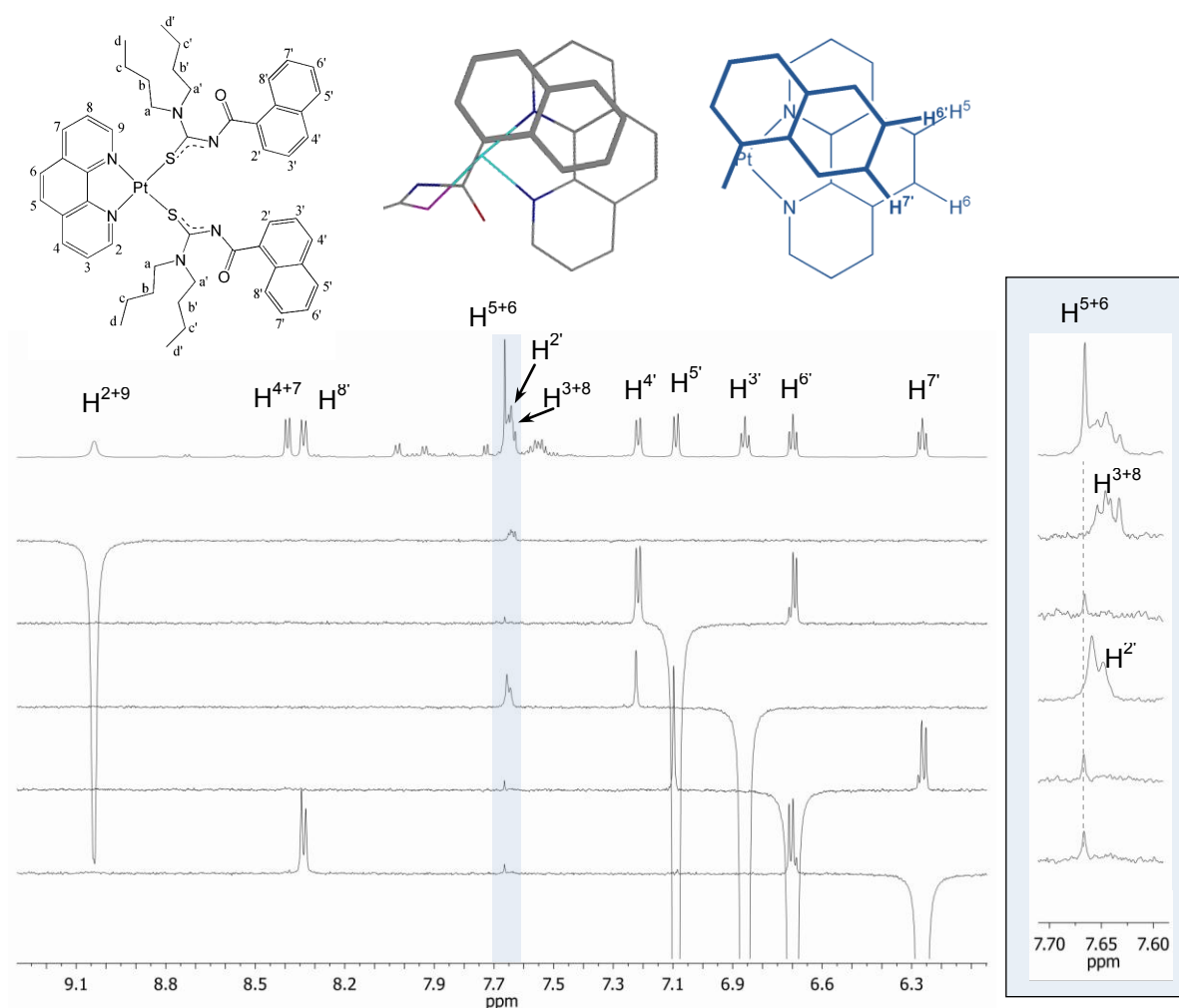
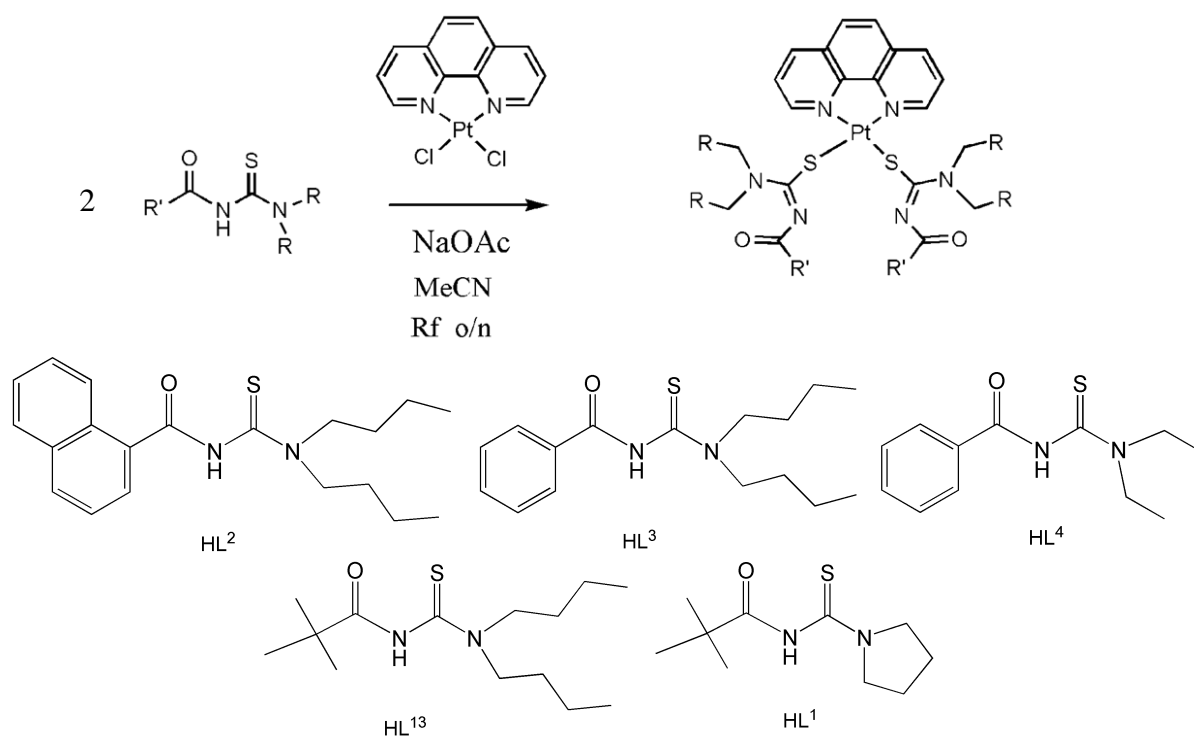


Figure 3.20 NOESY1D spectra of $Pt^{II}(phen)(L^2-S)_2$ in methanol- d_4 at 25°C. Mixing time was 500 ms, nt = 64, increments = 1024.

No NOE was observed for H^{5+6} upon irradiation of H^2 or H^3 which suggests that the small peak observed is not an artefact. The NOE correlations are proof of the naphthoyl and phen moieties to be close in space ($< 5 \text{ \AA}$) which can only be if they exhibit significant π -stacking interactions. Therefore, it is reasonable to argue that the aromatic- π stacking interaction does exist in methanol and could partially account for the marked stability and significant amounts of $Pt^{II}(phen)(L^2-S)_2$ present in the synthesis of $[Pt^{II}(phen)(L^2-S,O)]^+$.

3.2.6 Comparison of HL^n structure on the preparation of various $Pt^{II}(phen)(N,N\text{-dialkyl-}N'\text{-acylthiourea})_2$

The possibility of other N,N -dialkyl- N' -acylthiourea ligands to coordinate in a monodentate fashion *via* the sulphur atom was investigated. The effect of the different groups on the acylthiourea is believed to influence the coordination behaviour due to potential weak non-covalent interactions, steric and electronic structure effects. The following structural variations were chosen (Scheme 3.6).

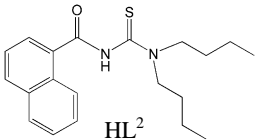
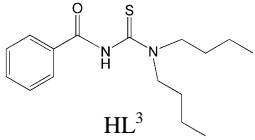
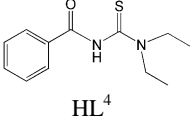
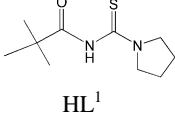
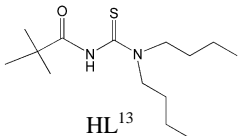


Scheme 3.6 Ligands used for the attempted synthesis of $Pt^{II}(phen)(L^n-S)_2$ complexes with the abbreviations from Chapter 2 used (Table 2.1).

With the ligands chosen, the difference in aroyl and pivaloyl functionality would be apparent as well as the effect of the N,N -dialkyl group with regard to coordination products and stability of $Pt^{II}(phen)(L^n-S)_2$.

The initial synthesis involved addition of 4 equivalents of ligand to platinum(II) precursor, $Pt^{II}(phen)Cl_2$, with 3.8 eq. NaOAc (sodium acetate) as base in acetonitrile (solvent). Significant amounts of $Pt^{II}(phen)(L^n-S)_2$ complexes were obtained for the aroylthioureas in Scheme 3.6. The reactions were repeated with a ligand ratio of 2.02eq relative to $Pt^{II}Cl_2(phen)$ with no significant effect on the yields. However, NaOAc is only sparingly soluble in acetonitrile and the reactions were also carried out in methanol which completely dissolves the NaOAc. The yields of the coordination products for the reaction of 2.02 eq HL^n in acetonitrile and methanol are shown in Table 3.5.

Table 3.5 Yields of the coordination products yields for the reaction of HL^n with $Pt^{II}Cl_2(phen)$ in acetonitrile and methanol.

Ligand	Acetonitrile Synthesis		Methanol Synthesis	
	$Pt^{II}(phen)(L^n-S)_2$	$[Pt^{II}(phen)(L^n-S,O)]^+$	$Pt^{II}(phen)(L^n-S)_2$	$[Pt^{II}(phen)(L^n-S,O)]^+$
 HL ²	90%	10%	100%	0%
 HL ³	75%	25%	99%	1%
 HL ⁴	60%	40%	100%	0%
 HL ¹	0%	100%	9%	91%
 HL ¹³	10%	90%	60%	40%

Yields were determined using 1H NMR spectrum of the reaction mixture in a mixed deuterated dimethyl sulfoxide/acetonitrile solvent system and are not isolated yields.

Interestingly, all the aroylthioureas in Scheme 3.6 have the *bis*-monodentate complexes as the major product. The pivaloylthioureas form little of this coordination product while the cationic complex is the only product for L^1 in acetonitrile. It is also clear that the formation of the *bis*-monodentate product is more favoured in methanol compared to acetonitrile.

Methanol is therefore the preferred solvent for the formation of the *bis*-monodentate complex which could be attributed to the high solubility of NaOAc in methanol.

The solubility of the base is postulated to be important since the conjugate acid (acetic acid in this case) is soluble in acetonitrile, presumably affecting the amount of ligand which will be deprotonated. However, changing the base to tri-ethylamine did not have a significant effect on the yield of the *bis*-monodentate thiourea complexes in acetonitrile. Therefore, the higher yields in methanol were attributed to the stronger hydrogen bonding capabilities of methanol which could stabilize the oxygen atom and prevent its coordination to the Pt.

Furthermore, the 1D NOESY experiments revealed the *intra*-molecular π -stacking present in methanol as shown in Figure 3.20. Such *intra*-molecular interactions could result in significant stabilisation of the monodentate $Pt^{II}(phen)(L^2-S)_2$ complex. All attempts to observe this *intra*-molecular interaction in chloroform using NOE experiments were unsuccessful. Therefore, a more polar solvent (like methanol) is believed to be necessary for the *intra*-molecular π -stacking. This is consistent with proposed aggregation behaviour of $Pt^{II}(phen)(L^2-S)_2$ in dimethyl sulfoxide- d_6 as well as the aggregation behaviour of $[Pt^{II}(phen)(L^1-S,O)]^+$ which will be discussed in the next chapter.

The synthesis for mono-substituted acylthioureas HL⁵ and HL⁶ was attempted which have a chlorine and methoxy group in the *para* position of the acylthiourea (respectively). The yields in acetonitrile revealed the *bis*-monodentate complex as the major product with yields 88% for $Pt^{II}(phen)(L^5-S)_2$ and 79% for $Pt^{II}(phen)(L^6-S)_2$. The acylthiourea mixtures are stable while the pivaloylthiourea samples were only stable for a few hours after which they turned dark brown. Figure 3.21 shows the ¹H NMR spectrum of a mixture of $[Pt^{II}(phen)(L^1-S,O)]^+$ and $Pt^{II}(phen)(L^1-S)_2$ from the synthesis in methanol.

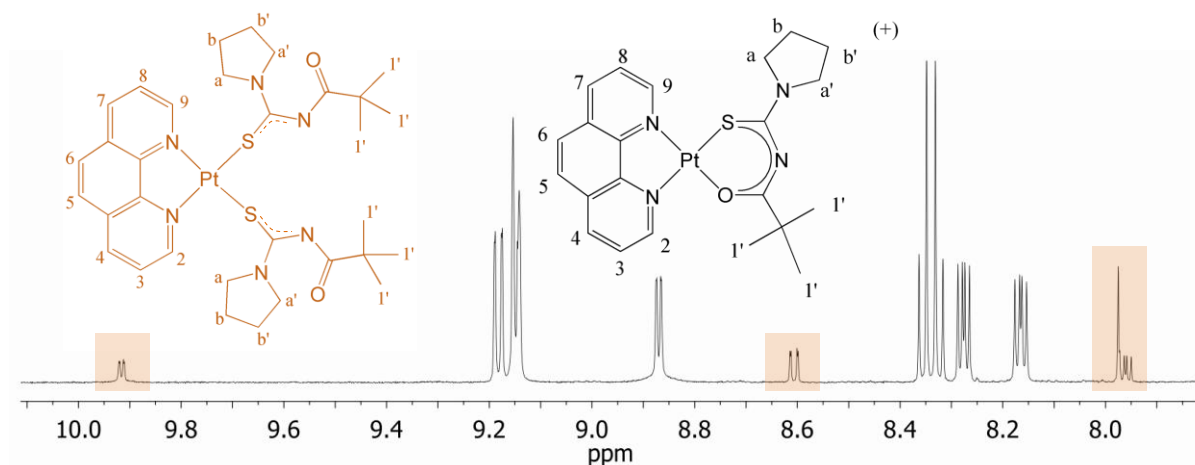


Figure 3.21 ¹H NMR spectrum of the reaction mixture of 2.02 eq. HL¹ and $Pt^{II}Cl_2(phen)$ after all $Pt^{II}Cl_2(phen)$ was reacted.

The $Pt^{II}(phen)(L^1-S)_2$ complex is very unstable and several attempts to isolate this product were unsuccessful. The stable $Pt^{II}(phen)(L^n-S)_2$ complexes of the aroylthioureas were isolated from the reaction mixtures. First attempts were made by extracting the monodentate complex in ether since the cationic chelate complex is only sparingly soluble in ether. However, this method proved to be inefficient since the cationic complex was always present and significant amounts of free ligand. The purification was ultimately done using chromatography with Al_2O_3 as stationary phase. The use of SiO_2 was abandoned since the cation complex is too strongly retained on the silica gel and could not be removed from the column. Neutral aluminium oxide was found to be an excellent choice for this purpose since less polar solvents eluted the monodentate complexes while the cationic complex elutes with the addition of methanol. The procedure for purification includes removal of the reaction solvents since these (acetonitrile/methanol) are too polar. The reaction solvent mixture was first removed using a rotavap. The solid mixture was then re-dissolved in dichloromethane and the insoluble NaCl and NaOAc filtered off. Petroleum ether was added before loading onto the column. The free ligand, conjugate acid (acetic acid/triethylammonium chloride) and unreacted $Pt(phen)Cl_2$ were eluted with a dichloromethane-petroleum ether mixture while $[Pt^{II}(phen)(L^n-S,O)_2]^+$ and the desired $Pt^{II}(phen)(L^n-S)_2$ were retained on the column. These were selectively eluted with dichloromethane-acetonitrile mixtures and methanol.

The 1H NMR spectrum of $Pt^{II}(phen)(L^4-S)_2$ is shown in Figure 3.23 with assignments. The aromatic region displays resonances of a symmetrically coordinated phen ligand similar to those observed for $Pt^{II}(phen)(L^2-S)_2$, and could be assigned based on the assignment of the $Pt^{II}(phen)(L^2-S)_2$ spectrum. The benzoyl protons could be assigned based on the relative integrals and multiplicities of the three sets of signals. Broad resonances are observed for the diethyl protons with the broad triplet assigned to $H^{b+b'}$ and broad peak at 3.75 ppm to $H^{a+a'}$. These assignments are consistent with the integrals of the resonances. Single crystals suitable for single crystal x-ray diffraction were obtained for $Pt^{II}(phen)(L^4-S)_2$. The $Pt^{II}(phen)(L^3-S)_2$ complex crystallised with the crystals obtained not being single. The molecular structure of $Pt^{II}(phen)(L^4-S)_2$ is shown in Figure 3.23.

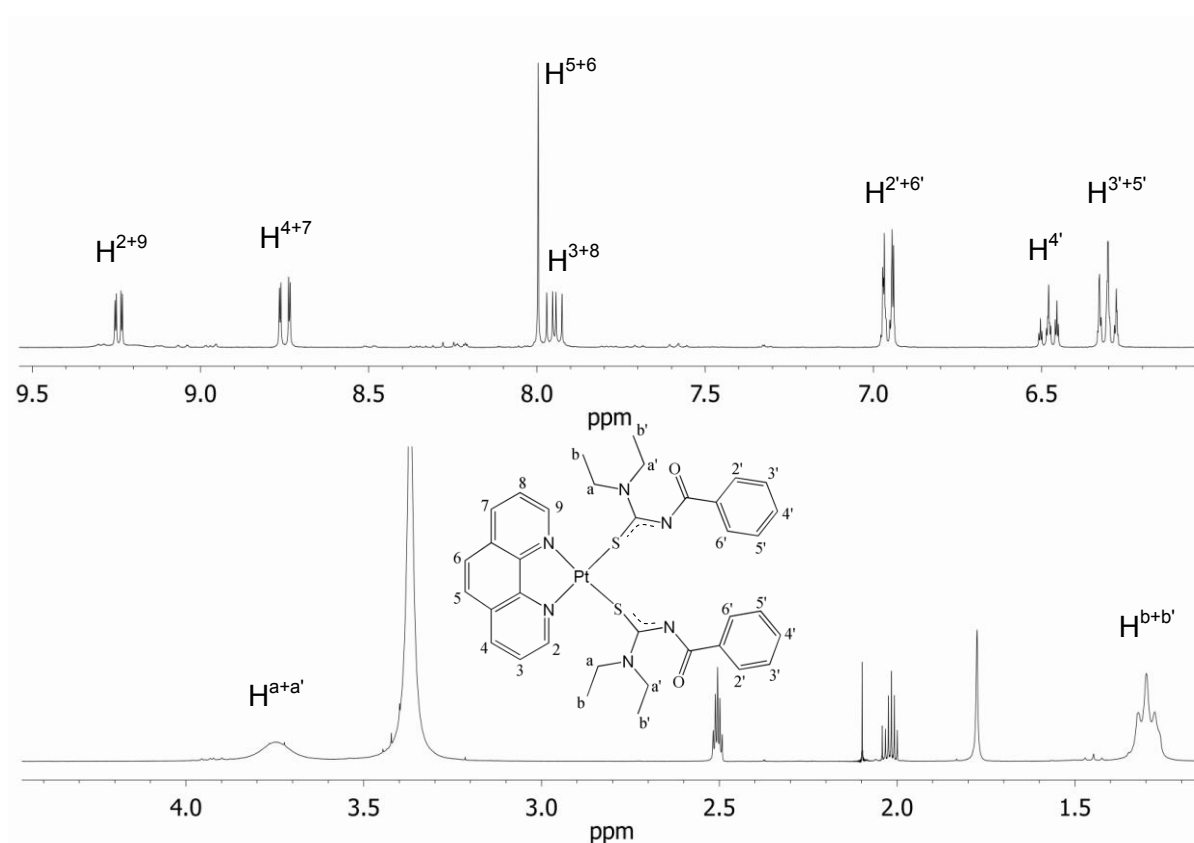


Figure 3.22 ^1H NMR spectrum of $\text{Pt}^{II}(\text{phen})(\text{L}^4\text{-S})_2$ in a mixture of deuterated dimethyl sulfoxide and acetonitrile.

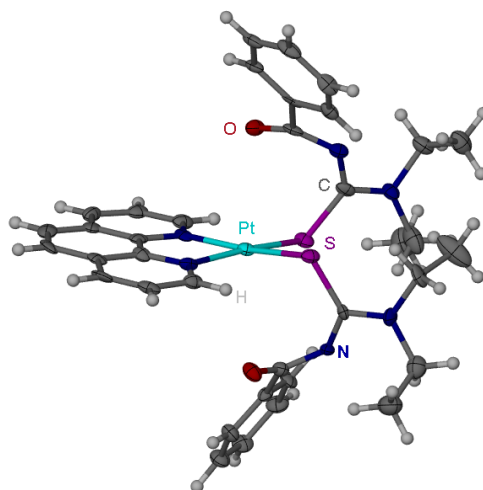


Figure 3.23 $\text{Pt}^{II}(\text{phen})(\text{L}^4\text{-S})_2$ and the asymmetric unit.

The structure postulated and deduced using ^1H NMR spectroscopy of $\text{Pt}^{II}(\text{phen})(\text{L}^4\text{-S})_2$ could be confirmed with the SCXRD data (Figure 3.23). The crystal and structure refinement data are shown in Section 3.4 and the CIF file is given on the electronic Appendix C, accompanying this thesis. Interestingly, one water molecule crystallizes with $\text{Pt}^{II}(\text{phen})(\text{L}^4\text{-S})_2$, hydrogen bonding with the acyl oxygen as shown in Figure 3.24b.

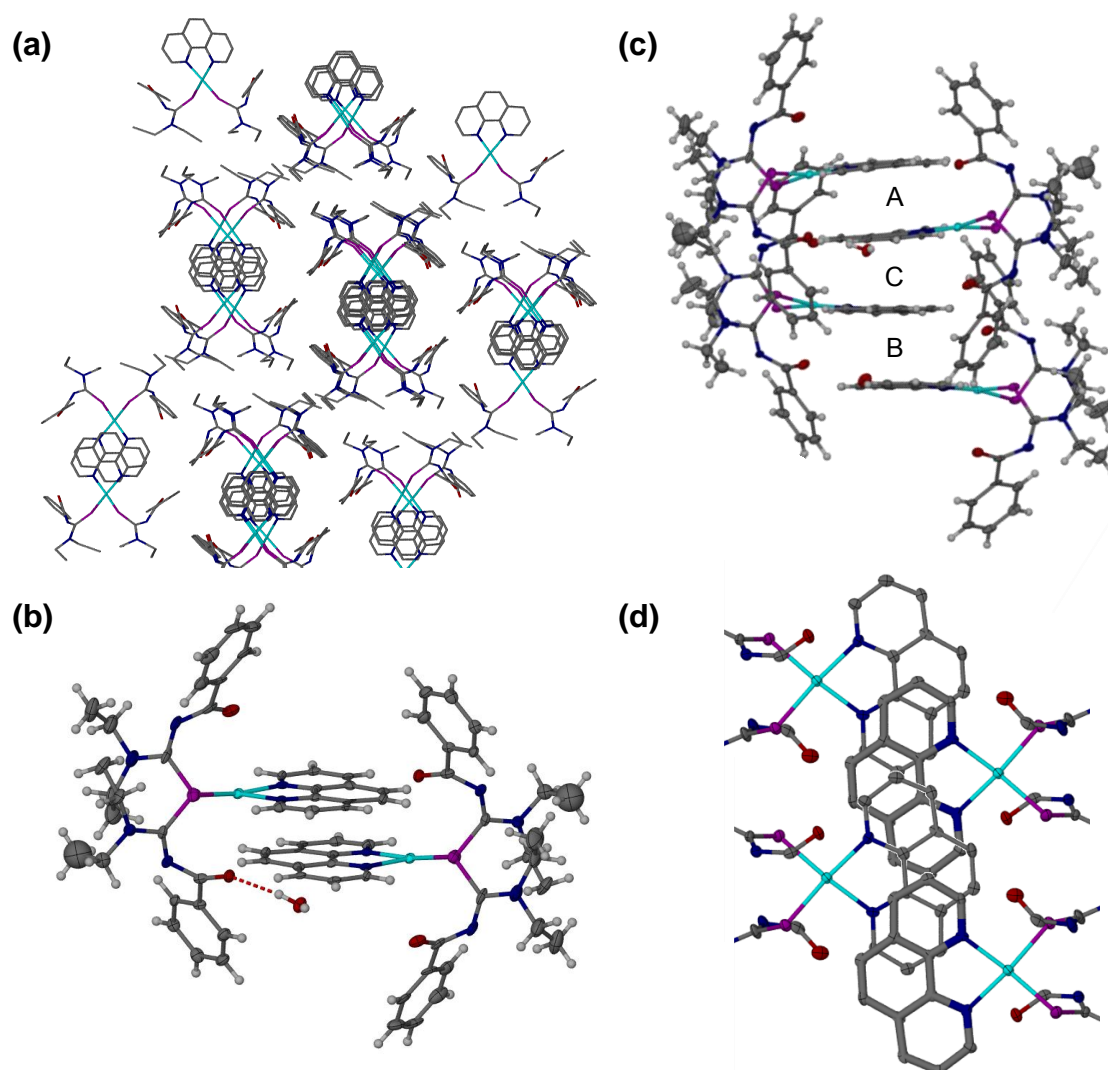


Figure 3.24 The stacking of $Pt^{II}(phen)(L^4-S)_2$ in the crystal lattice with (a) along the a axis and (c) the view along the c axis. The offset aromatic- π stacking between the 1,10-phenanthroline ligands in the crystal structure of $Pt^{II}(phen)(L^4-S)_2$ is shown in (b) and (d).

The crystal packing (Figure 3.24) shows interesting intermolecular aromatic π -stacking of the phen ligands of adjacent $Pt^{II}(phen)(L^4-S)_2$ complexes to form an infinite stack (Figure 3.24a) of two different sets of parallel stacked molecules (interaction indicated by A and B) with these sets π -stacking by interaction C (Figure 3.24c). The aromatic π -stacking is again in an offset manner with half of the phen associated on each sides of the planar ligand (Figure 3.24d). Similar aromatic stacking interactions have been postulated earlier to explain the concentration dependence of $Pt^{II}(phen)(L^2-S)_2$ in chloroform- d_1 (Scheme 3.4). Selected bond lengths, distances and angles for $Pt^{II}(phen)(L^4-S)_2 \cdot H_2O$ are summarized in Table 3.6.

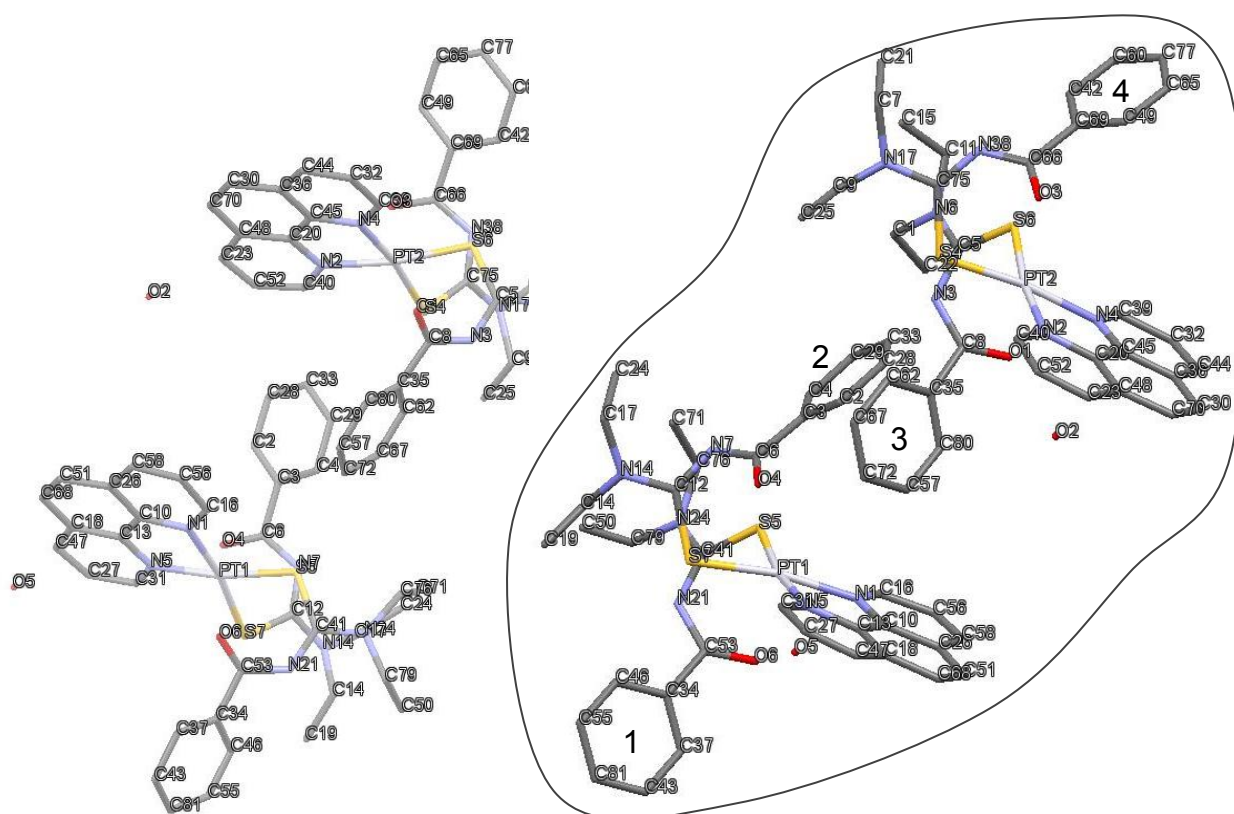


Figure 3.25 Atom numbering and phenyl group numbers of $Pt^{II}(phen)(L^4-S)_2$ for Table 3.6. The encircled structure is a different view of the adjacent molecular structure to show all atom numbering in the two views with the phenyl numbering 1-4 used Table 3.6.

Table 3.6 Selected bond lengths, angles, torsion angles, plane angles and distances in the crystal structure of $Pt^{II}(phen)(L^4-S)_2$

<i>Bonds:</i>	Å	<i>Bonds:</i>	Å	<i>Distances:</i>	Å
PT1-S5	2.2800(7)	N24-C41	1.3495(5)	C69 ... phen-pl	4.314
PT1-S7	2.2808(8)	C12-N14	1.3348(5)	C62 ... phen-pl	3.566
PT1-N1	2.0620(7)	N17-C75	1.3587(5)	* A phen-pl ... phen-pl	3.215
PT1-N5	2.0505(7)	N6-C5	1.3536(4)	* C phen-pl ... phen-pl	3.006**
PT2-S4	2.2836(7)	N21-C41	1.3187(5)	* B phen-pl ... phen-pl	3.333
PT2-S6	2.2790(6)	N21-C53	1.3608(5)	<i>Torsion angles:</i>	
PT2-N2	2.0633(6)	N7-C12	1.3118(4)	O1-C8-C35-C80	-20.84
PT2-N4	2.0528(6)	N7-C6	1.3409(6)	O3-C66-C69-C49	-14.11
S5-C41	1.7459(6)	N38-C66	1.3511(6)	O4-C6-C3-C2	-22.51
S7-C12	1.7551(8)	N38-C75	1.3165(4)	O6-C53-C34-C37	-17.54
S4-C75	1.7511(8)	N3-C8	1.3311(5)	<i>Plane angles:</i>	
S6-C5	1.7386(7)	N3-C5	1.3220(5)	N1-Pt1-N5 < S5-Pt1-S7	9.30°
O6-C53	1.2392(4)	C6-C3	1.5189(4)	N2-Pt2-N4 < S4-Pt2-S6	11.67°
O4-C6	1.2335(4)	C66-C69	1.5224(5)	* A phen-pl < phen-pl	0.00°
O3-C66	1.2399(4)	C34-C53	1.5068(5)		

O1-C8	1.2409(4)	C35-C8	1.4925(5)	*C phen-pl < phen-pl	5.57°
				*B phen-pl < phen-pl	0.00°
				Ph(1) < phen-pl (Pt1)	63.14°
				Ph(2) < phen-pl (Pt1)	61.88°
				Ph(3) < phen-pl (Pt2)	60.33°
				Ph(4) < phen-pl (Pt2)	50.81°

*A, B, and C indicates two 1,10-phenanthroline stacking as shown in Figure 3.24. ** The distance of the two closest atoms of the corresponding planes generated from all the atoms of the phen ligand. Figures A.24 and A.25 contain more images with measured angles and distances to clarify the nomenclature used.

The aromatic π -stacking of the 1,10-phenanthroline moieties show two parallel stacked interactions with gap A and B as shown in Figure 3.24c (0.00° angle with distances 3.215 and 3.333 Å for A and B respectively). The sets of parallel stacked molecules are connected by an π -stacking interaction with an angle of 5.57° and the closest point 3.006 Å. Interestingly, this angle is almost identical to the π -stacking angle of 5.50° observed for the naphthyl group and phen in the crystal structure of $Pt^{II}(phen)(L^2-S)_2$ and the 4° predicted by Kobayashi and co-workers for related systems.²¹ Selected bond lengths of $Pt^{II}(phen)(L^4-S)_2 \cdot H_2O$ are compared to $Pt^{II}(phen)(L^2-S)_2$ and their free ligands HL^4 and HL^2 (Table 3.7).

Table 3.7 Comparison of relevant bond lengths and angles of $Pt^{II}(phen)(L^4-S)_2 \cdot H_2O$, $Pt^{II}(phen)(L^2-S)_2$ and their ligands, HL^4 and HL^2 with the average bond lengths reported for $Pt^{II}(phen)(L^4-S)_2 \cdot H_2O$ and $Pt^{II}(phen)(L^2-S)_2$.

<i>Bond avg:</i> Å	$Pt^{II}(phen)(L^2-S)_2$	$Pt^{II}(phen)(L^4-S)_2 \cdot H_2O$	HL^2 [24]	HL^4 [25]
Pt-S	2.292(2)	2.281(8)		
Pt-N	2.056(2)	2.057(7)		
C-O	1.229(1)	1.238(4)	1.215(3)	1.219(1)
C-S	1.780(2)	1.748(8)	1.662(2)	1.677(1)
N-C(O)	1.367(2)	1.346(6)	1.376(4)	1.387(1)
N-C(S)	1.129(1)	1.317(6)	1.420(4)	1.418(2)
(S)C-N(R₂)	1.357(2)	1.349(5)	1.320(4)	1.326(1)
C(O)-Ar	1.524(2)	1.510(5)		1.495(2)
<i>Torsion angles:</i>				
O-C-C-[*]Ar1	-6.97°	-15.53°		
O-C-C-[*]Ar2	-17.36°	-21.68°		
<i>Plane angles:</i>				
N-Pt-N < S-Pt-S	2.42°	10.49°		
Ar < phen-pl	5.50°	56.35°		
Ar2 < phen-pl	15.20°	61.74°		

A marked increase in bond lengths of C-O and C-S is observed between the ligands HL² and HL⁴ and their corresponding complexes Pt^{II}(phen)(L²-S)₂ and Pt^{II}(phen)(L⁴-S)₂. This is expected since the bond character changes dramatically from carbonyl and thiocarbonyl in the ligands to more single bond character upon coordination to the metal centre. The average C-N bond length of the ligands and complexes shown in Table 3.7, consistent with a partial C-N double bond since all C-N bonds of the ligands are shorter than the average C-N single bond (1.472(5) Å).²⁶

The only significant difference between the two crystal structures of Pt^{II}(phen)(L²-S)₂ and Pt^{II}(phen)(L⁴-S)₂·H₂O, apart from the water of crystallization and the π -stacking of the phen, is the N-C(S) bond length, stacking angles of the aroyl to phen planes and the torsion angle of the aroyl group. The bond length of N-C(S) in Pt^{II}(phen)(L²-S)₂ is significantly shorter (1.129(1) Å) than the N-C(S) bond length in Pt^{II}(phen)(L⁴-S)₂ (1.317(6) Å). The square planar geometry of Pt^{II}(phen)(L⁴-S)₂ is more distorted (10.49°) compared to Pt^{II}(phen)(L²-S)₂ (2.42°) which is closer to the 0.00° ideal square planar angle between the planes created by N-Pt-N and S-Pt-S fragments. Furthermore, the aroyl groups of Pt^{II}(phen)(L²-S)₂ π -stack much more parallel with phen than in Pt^{II}(phen)(L⁴-S)₂ (Ar < phen-pl = 5.50° compared to 56.35°). The benzoyl groups also show a larger torsion angle between O-C-C-Ar1 (-15.53°) compared to the naphthoyl group (-6.97°).

3.2.7 Ligand characteristics/effect on synthesis and stability

Distinct variation in the yields and stabilities of Pt^{II}(phen)(Lⁿ-S)₂ complexes were observed. The complexes of the pivaloylthioureas (HL¹ and HL¹³) were found to be unstable while the aroylthioureas (HL², HL³ and HL⁴) formed stable *bis*-monodentate complexes as the only product in methanol. Therefore, the ligand characteristics were investigated using ¹³C{¹H} NMR, IR Spectroscopy and SCXRD data in an attempt to establish the relationship between stability and structure. It was previously mentioned that *intra*-molecular aromatic π -stacking interactions as a possible stabilizing factor for the stability observed for the aroylthioureas. Electronic effects due to the distinctly different properties of an aryl and the ^tbutyl functionality will also be considered.

The ¹³C{¹H} NMR spectrum is believed to give an indication of the different chemical environments of the carbonyl and thiocarbonyl, providing insight in the electronic structures of the various ligands. The ¹³C{¹H} NMR spectra of HL¹, HL², HL³ and HL¹³ are shown in Figure 3.26.

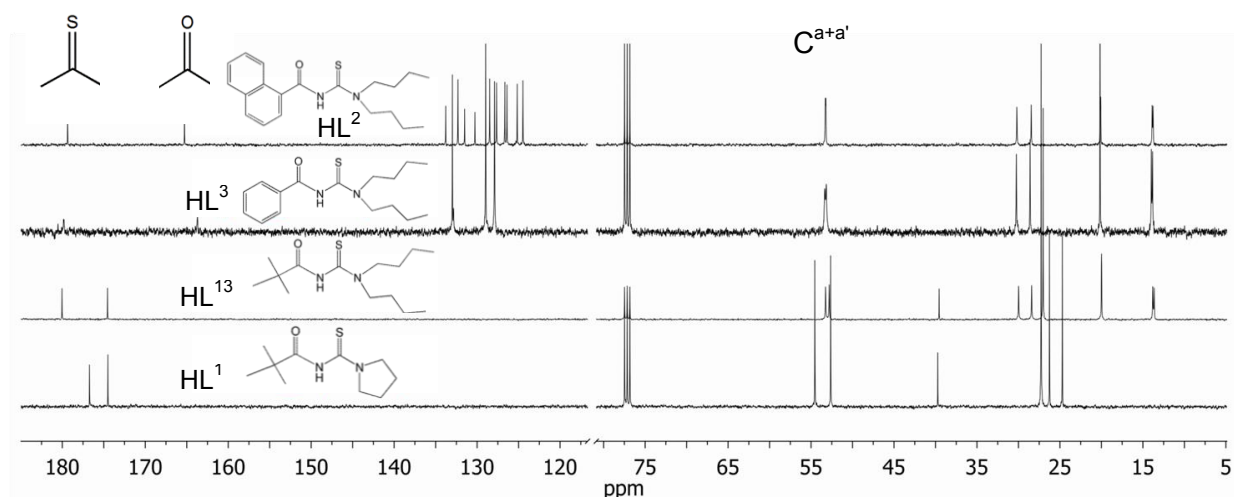
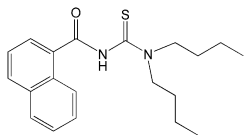
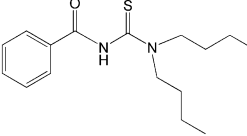
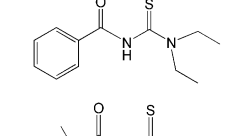
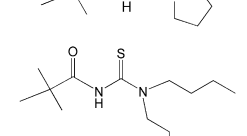
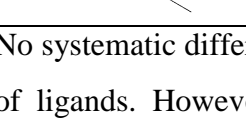


Figure 3.26 $^{13}\text{C}\{^1\text{H}\}$ NMR spectra of HL^1 , HL^2 , HL^3 and HL^{13} in chloroform- d_1 .

Interestingly, distinct differences are observed for the two groups of ligands (pivaloyl and aroyl). The resonance of the carbonyl carbons of the aroylthioureas are shifted more than 9 ppm upfield compared to those of HL^1 and HL^{13} . Furthermore, the carbons labelled C^a and $\text{C}^{a'}$ of the acylthioureas are almost equivalent while C^a and $\text{C}^{a'}$ of the pivaloylthioureas have significantly different chemical shifts. The $^{13}\text{C}\{^1\text{H}\}$ NMR chemical shifts as well as FT-IR data and bond lengths from crystal data are summarised in Table 3.8.

Table 3.8 Comparison to $^{13}\text{C}\{^1\text{H}\}$ NMR, FT-IR and SCXRD data of the series of ligands.

Ligand	^{13}C NMR (ppm)		FT-IR (cm^{-1})	bond lengths (\AA) ^[24,25,27,28,29]			
	C=O	C=S	C=O	C=O	C=S	C-C(O)	N-C(S)
 HL^2	165.3	179.3	1680	1.215	1.662	-	1.420
 HL^3	163.7	179.8	1684	1.214	1.684	1.492	1.326
 HL^4	-	-	1650	1.219	1.677	1.495	1.326
 HL^1	174.5	176.7	1678	1.221	1.677	1.523	1.320
 HL^{13}	174.5	180.0	1653	1.222	1.668	1.540	1.321

No systematic differences were observed for the carbonyl stretching frequencies for the series of ligands. However, the C=O bond length estimated from crystal data show a slightly

longer/weaker bond for the pivaloyl ligands. This is expected to be a result of the inductive effect (+I) of the ^tbutyl group which pushes the electron density towards the carbonyl carbon through the σ -bond C-C(O). Furthermore, this bond is also longer for the pivaloylthioureas which is consistent with the carbonyl carbon bonded to a sp^3 carbon compared to a sp^2 carbon for the acylthioureas. The N-C(S) bond on the other hand is shorter for the pivaloylthioureas which implies more double bond character which is also reflected in the two distinct signals observed for C^a and C^b in the $^{13}C\{^1H\}$ NMR spectra of the various ligands.

Interesting electronic resonance structures were calculated for various HL^n ligands by Mengstu and co-workers.³⁰ The probability of the mesomeric resonance structures of HL^1 and HL^2 involving a negative charge on the sulphur atom are shown in Figure 3.27, since HL^2 forms mainly $Pt^{II}(phen)(L^2-S)_2$ while HL^1 forms exclusively $[Pt^{II}(phen)(L^1-S,O)]^+$ in acetonitrile.

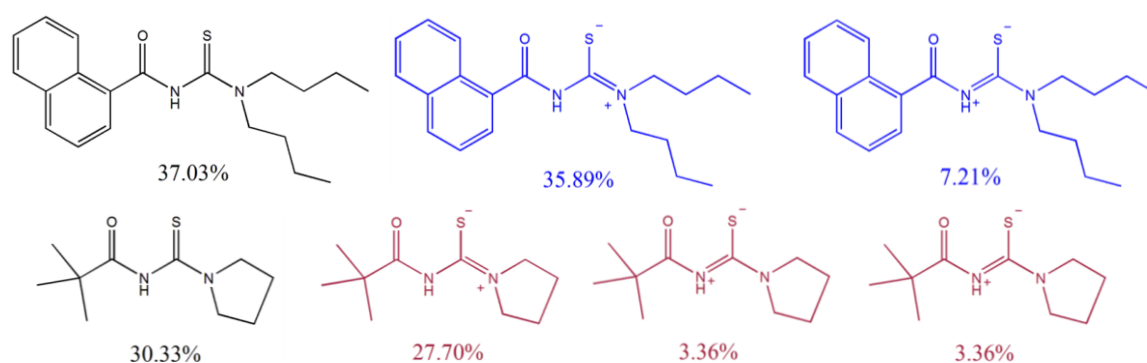


Figure 3.27 Three most significant resonance structures of HL^1 and HL^2 concerning the sulphur atom as calculated from Natural Resonance Theory Analysis.³⁰

The resonance is significantly more shifted towards the sulphur atom for HL^2 with a total of 43.1% compared to 31.1% for HL^1 .³⁰ The mesomeric effect of the aromatic substituent on the magnetic shielding of the carbonyl carbon needs to be considered since it is not possible for the ^tbutyl group. The pivaloyl group only exhibits an inductive effect which is positive, while the arylthioureas have a mesomeric as well as an inductive effect on the carbonyl functionality. The mesomeric structures of the aryl group are shown in Figure 3.28.

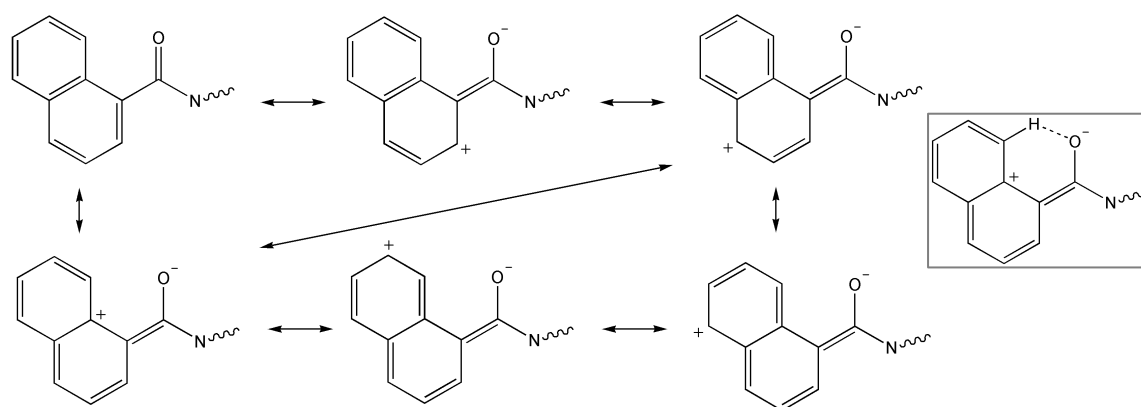


Figure 3.28 Proposed mesomeric effect of the naphthoyl moiety of HL^2 .

Pople and co-workers have shown that the planar configuration of substituted benzoyl is the most stable configuration as a result of a positive mesomeric (+M) effect while the sp^2 hybridization of the aromatic carbon leads to a negative inductive effect (-I).²² They have also concluded that the carbonyl is more stabilised by aromatic substituents compared to methyl and other sp^3 carbon groups. This is consistent with what was observed experimentally; the carbonyls are close to co-planar of the aromatic moieties which allows for extensive resonance of the conjugated π -electrons of the aryl and carbonyl in the aroyl functionality.

The steric effect of the relatively bulky naphyl group compared to ^tbutyl would significantly influence the chelation of the oxygen since the conformation drawn in Figure 3.28 is also observed in the crystal structures of HL^2 , $Pt^{II}(phen)(L^2-S)_2$ and $trans-Pt^{II}(L^2-S,O)_2$. The naphthoyl group is almost flat with the naphthyl pointing in the same direction as the carbonyl C=O bond which allows for a weak hydrogen bonding between $H^{\delta+}$ and the carbonyl oxygen to form a favourable six membered ring as shown in Figure 3.28.

3.3 Conclusions

In conclusion, monodentate $Pt^{II}(phen)(L^n-S)_2$ complexes was successfully synthesised, the first example of these types of complexes. The monodentate sulphur coordination of deprotonated *N,N*-dialkyl-*N'*-acylthioureas is extremely rare with only HL^4 known to coordinate in this fashion in two examples of Cu(I) and Cu(II) cluster complexes.¹¹ The $Pt^{II}(phen)(L^n-S)_2$ complexes could be synthesised in high yields (>90%) for complexes with aroylthioureas while the pivaloylthioureas seem to be unstable, formed in markedly lower yields <60%.

It was found that $Pt^{II}(phen)(L^2-S)_2$ exhibits significant chemical shift concentration dependence in chloroform- d_1 which is consistent with coplanar π -stacking of the 1,10-phenanthroline ligands of two complexes in solution. Furthermore, the temperature dependence of $Pt^{II}(phen)(L^2-S)_2$ in chloroform- d_1 and dimethyl sulfoxide- d_6 suggests a combination of self-association and/or *intra*-molecular π -stacking between the naphthoyl moiety of L^2 and 1,10-phenanthroline.

Crystal structures were obtained for $Pt^{II}(phen)(L^2-S)_2$ and $Pt^{II}(phen)(L^4-S)_2$ which showed interesting *intra*-molecular π -stacking interactions, consistent with the NMR concentration and temperature dependence data. The two naphthoyl moieties of the *S*-coordinated L^2 of the $Pt^{II}(phen)(L^2-S)_2$ complex are 'clipped' around the bound 1,10-phenanthroline ligand to form favourable offset π -stacking interactions. This *intra*-molecular π -stacking interaction between the ligands of $Pt^{II}(phen)(L^2-S)_2$ were attributed to the occurrence and stability of this complex. This complex in particular, forms in the synthesis of $[Pt^{II}(phen)(L^2-S,O)]Cl$ with only 1 mole equivalence of HL^2 to Pt. The existence of this *intra*-molecular π -stacking could be confirmed, which is believed to stabilise this complex significantly in methanol solutions, using 1D-NOESY data.

The crystal structure of $Pt^{II}(phen)(L^4-S)_2$ revealed the co-crystallization of one H_2O molecule per $Pt^{II}(phen)(L^4-S)_2$ which hydrogen bonds to the benzoyl-oxygen atom of one of the coordinated L^4 ligands. Furthermore, intermolecular π -stacking interactions between the bound 1,10-phenanthroline ligands of neighbouring complexes are observed which is similar to the π -stacking postulated for the self-association of $Pt^{II}(phen)(L^4-S)_2$ in chloroform.

The carbonyl and aromatic group of the acylthiourea in the crystal structures are co-planar, suggesting extensive delocalization of the electron density between the two groups. This is reflected in the $^{13}C\{^1H\}$ NMR chemical shifts of the ligands as well as the crystallographic C-O bond lengths.

The aromatic moiety withdraws electron density from the carbonyl group as a result of the inductive effect of the sp^2 hybridisation (*-I*) in contrast to the positive mesomeric effect (resonance) which results in shielding of the carbonyl carbon as the π -electrons is shifted towards the oxygen. This is consistent with the carbonyl chemical shifts in the free ligands which is significantly more upfield (164-169 ppm) compared to the pivaloylthioureas (177-180 ppm).

3.4 Crystal and Structure Refinement Data for $Pt^{II}(phen)(L^2-S)_2$ and $Pt^{II}(phen)(L^4-S)_2 \cdot H_2O$

	$Pt^{II}(phen)(L^2-S)_2$	$Pt^{II}(phen)(L^4-S)_2 \cdot H_2O$
Empirical formula	$C_{52} H_{58} N_6 O_2 Pt S_2$	$C_{36} H_{36} N_6 O_2 Pt S_2, C_{36} H_{38} N_6 O_2 Pt S_2, 2(H_2O)$
Formula weight	1058.25	1725.88
Temperature (K)	100	100
Wavelength (Å)	0.71073	0.71073
Crystal system	Orthorhombic	Triclinic
Space group	Pca21	P-1
Unit cell dimensions (Å, °)	$a = 32.089(5)$ $b = 10.5036(15)$ $c = 13.786(2)$	$13.203(6)$ $\alpha = 102.474(5)$ $14.849(7)$ $\beta = 108.801(5)$ $19.502(9)$ $\gamma = 94.644(5)$
Volume (Å ³)	4646.6(12)	3487(3)
Z	4	2
Calculated density (g cm ⁻³)	1.513	1.644
Absorption coefficient (mm ⁻¹)	3.158	4.189
F_{000}	2152	1724
Crystal size (mm ³)	0.12 × 0.17 × 0.28	0.08 x 0.12 x 0.28
θ range for data collection (°)	1.9 to 28.9	1.4 to 25.1
Reflections collected	28874	33590
Independent reflections	10255 [$R_{int} = 0.030$]	12306 [$R_{int} = 0.065$]
Data / restraints / parameters	9243 / 0 / 572	8821/0/901
Final R indices [$I > 2\sigma(I)$]	$R1 = 0.0222$, $wR2 = 0.0456$	$R1 = 0.0429$, $wR2 = 0.1006$
Largest diff. peak and hole (e Å ⁻³)	-0.52, 0.69	-2.05, 1.37

3.5 References

1. K. R. Koch, C. Sacht, C. Lawrence, *Dalton Trans.*, **4**, 1998, 689-695.
2. Y. S. Wu, K. R. Koch, V. R. Abratt, H. H. Klump, *Archives of Biochem. Biophys.*, 2005, **440**, 28-37.
3. T. J. Egan, K. R. Koch, P. L. Swan, C. Clarkson, D. A. Van Schalkwyk, P. J. Smith, *J. Med. Chem.*, 2004, **47**, 2926-2934.
4. K. R. Koch, *Coord. Chem. Rev.*, **216-217**, 2001, 473-488.
5. R. G. Pearson, *Science*, **151**, 1966, 172-177.

6. P. L. Swan, *MSc. thesis*, University of Cape Town, 2002
7. K.R. Koch, A. Irving, M. Matoetoe, *Inorg. Chim. Acta*, **206**, 1993, 193-199.
8. K. R. Koch, T. Grimmacher, C. Sacht, *Polyhedron*, **17**, 1998, 267-274.
9. K. R. Koch, Y. Wang, A. Coetzee, *J. Chem. Soc., Dalton Trans.*, 1999, 1013-1016.
10. K.R. Koch, S. Bourne, *J. Molecular Structure*, **441**, 1998, 11-16.
11. D. Che, X. Yao, G. Li, Y. Hong Li, *J. Chem. Soc., Dalton Trans.*, **11**, 1998, 1853-1856.
12. D. Che, G. Li, X. Yao, Y. Zhu, D. Zhou, *J. Chem. Soc., Dalton Trans.*, **16**, 1999, 2683-2687
13. C. J. Lawrence, *MSc. thesis*, University of Cape Town, 1997
14. M. C. Matoetoe, K. R Koch, *Mag. Res. Chem.*, **29**, 1991, 1158-1160.
15. H. Friebolin, *Basic One- and Two-Dimensional NMR Spectroscopy*, Wiley-VCH, Weinheim, 2005
16. I. A. Kotzé, W. J. Gerber, J. M. Mckenzie, K. R. Koch, *Eur. J. Inorg. Chem.*, 2009, **12**, 1626-1633.
17. T. Förster, *Pure Appl. Chem.*, **7**, 1963, 73-78.
18. C. A. Hunter, J. K. M. Sanders, *J. Am. Chem. Soc.* 1990, **112**, 5525-5534.
19. F. P. Gasparro, N. H. Kolodny, *J. Chem. Ed.*, **54**, 1977, 258-261
20. L. W. Reeves, R. C. Shaddick, K. N. Shaw, *Can. J. Chem.*, **49**, 1971, 3683-3691.
21. S. Enomoto, K. Kumagai, T. Tamura, M. Hasegawa, K. Nakada, T. Hoshi, M. Kobayashi, *Monatshefte fuer Chemie*, 2004, **135**, 471-481.
22. W. J. Hehre, L. Radom, J. A. Pople, *J. Am. Chem. Soc.*, **94**, 1972, 1496-1504.
23. K.R. Koch, J. du Toit, M.R. Caira, C. Sacht, *J. Chem. Soc. Dalton Trans.*, 1994, 785-786
24. K. R. Koch and C. Sacht, unpublished results.
25. L.R. Gomes, L.M.N.B.F. Santos, J.A.P. Coutinho, B.Schroder, J.N. Low, *Acta Crystallogr.,Sect.E*, 2010, **66**, 870
26. *CRC Handbook of Chemistry and Physics*, 64th edn., ed. R.C. Weast, CRC Press, Boca Raton, Florida, 1983, p. F-171.
27. N. Gunasekaran, R. Karvembu, Seik Weng Ng, E. R. T. Tiekink, *Acta Cryst.*, **E66**, 2010, 2601
28. J. Dillen, M. G. Woldu, K. R. Koch, *Acta Cryst.*, **E62**, 2006, 5228-5229
29. J. Dillen, M. G. Woldu, K. R. Koch, *Acta Cryst.*, **E62**, 2006, 4819-4820
30. Ghebreyesus Woldu Mengstu, *MSc. Thesis*, Stellenbosch University, 2004

4

Cation- π induced aggregation of water-soluble $[\text{Pt}^{\text{II}}(\text{diimine})(\text{L}^n\text{-S},\text{O})]^+$ complexes studied by ^1H DOSY NMR and TEM: from ‘dimer aggregates’ in acetonitrile to nano-aggregates (‘metallo gels’) in water

Results of this chapter have been published in Dalton Transactions 2013 (Appendix B)

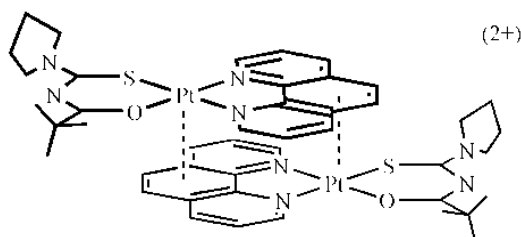
This chapter describes the interesting self-association behaviour of some $[\text{Pt}^{\text{II}}(\text{diimine})(\text{L}^n\text{-S},\text{O})]^+$ complexes in solution. This behaviour illustrates the tendency of these cationic complexes to form relatively strong non-covalent interactions in solution. Therefore, we propose $[\text{Pt}^{\text{II}}(\text{diimine})(\text{L}^n\text{-S},\text{O})]^+$ complexes to be β -haematin inhibitors *via* relatively strong non-covalent interactions between the complex cation and haematin. More specifically, the self-association of $[\text{Pt}^{\text{II}}(\text{phen})(\text{L}^1\text{-S},\text{O})]^+$ will be studied in $\text{D}_2\text{O}:\text{CD}_3\text{CN}$ mixtures ranging from pure CD_3CN to D_2O only, towards understanding the non-covalent self-association phenomenon in detail. The effect of NaCl to the extent of aggregation of $[\text{Pt}^{\text{II}}(\text{phen})(\text{L}^1\text{-S},\text{O})]^+$ in D_2O will also be shown. Finally, the hetero-association of $[\text{Pt}^{\text{II}}(\text{diimine})(\text{L}^n\text{-S},\text{O})]^+$ complexes with pyrene ($\text{C}_{16}\text{H}_{10}$), will be studied by ^1H and DOSY NMR spectroscopy, as a crude model for complex/haematin interaction, since haematin is paramagnetic and could not be studied by NMR spectroscopy.

4.1 Introduction

The ‘self-association’ of transition metal complexes, which display biological activity of potential pharmaceutical use, has been the subject of extensive interest in the last decade since their detailed physicochemical behaviour particularly in aqueous solution may have important implications on their mode of action.¹⁻⁵ Our interest in the chemistry of planar, cationic mixed-ligand Pt^{II} complexes of the general type $[\text{Pt}^{\text{II}}(\text{diimine})(\text{L}^n\text{-S,O})]^+$ (where diimine is 2,2-bipyridine or 1,10-phenanthroline and $\text{HL}^n\text{-S,O}$ are various chelating *N*-acyl-*N,N*-dialkylthioureas), arises from their interesting biological activity ranging from potential anti-malarial activity,⁶ to DNA-intercalation and demonstrable *in vivo* activity toward bacterial *E. coli* AB1886 (uvr A) cultures.⁷ It was previously shown that $[\text{Pt}^{\text{II}}(2,2\text{-bipyridyl})(\text{N,N-di}(2\text{-hydroxyethyl})\text{-N}'\text{-benzoylthiourea})]\text{Cl}$ undergo interesting DNA-templated ‘biomineralization’.⁸ The *in vitro* anti-malarial activity of $[\text{Pt}^{\text{II}}(\text{diimine})(\text{L}^n\text{-S,O})]^+$ is postulated to arise by inhibition of β -hematin formation (synthetic haemozoin or malaria pigment) presumably as a result of the cationic planar complex $[\text{Pt}^{\text{II}}(\text{diimine})(\text{L}^n\text{-S,O})]^+$ forming moderately strong outer-sphere aggregates with ferriprotoporphyrin IX, as can be demonstrated in 40% aqueous dimethyl sulfoxide (DMSO) solution, possibly through non-covalent cation- π interactions.⁶ Moreover the ¹H NMR spectra of the series of cationic $[\text{Pt}^{\text{II}}(\text{diimine})(\text{N,N-di}(n\text{-butyl})\text{-N}'\text{-benzoylthiourea})]^+$ complexes (as PF_6^- salts where diimine = 1,10-phenanthroline, 4,7-diphenyl-1,10-phenanthroline, 2,2-bipyridyl, 4,4-di-*tert*-butyl-2,2-bipyridyl and 4,4-dimethyl-2,2-bipyridyl) in acetonitrile at room temperature show significant concentration dependence, consistent with the formation of non-covalent dimer aggregates $2\text{M}^+ \rightleftharpoons \{\text{M}^+\}_2$ (where $\text{M}^+ = [\text{Pt}^{\text{II}}(\text{diimine})(\text{L}^n\text{-S,O})]^+$).⁹

This concentration dependence of the ¹H NMR chemical shifts can be used to estimate the association constants of such an aggregation process, while the relative spatial orientation of the molecules undergoing non-covalent association may be inferred from the extent of the relative changes in ¹H NMR chemical shifts induced as a function of concentration.⁹⁻¹² A recent, detailed study of the water-soluble $[\text{Pt}^{\text{II}}(1,10\text{-phenanthroline})(\text{N-pyrrolidyl-N-(2,2-dimethylpropanoyl)-thiourea})]\text{Cl}$ ($[\text{Pt}^{\text{II}}(\text{phen})(\text{L}^1\text{-S,O})]\text{Cl}$) in acetonitrile showed that in addition to the non-covalent aggregation of the cationic $[\text{Pt}^{\text{II}}(\text{phen})(\text{L}^1\text{-S,O})]^+$ complexes to result in dimer aggregates $2\text{M}^+ \rightleftharpoons \{\text{M}^+\}_2$ in solution (Scheme 4.1), the $[\text{Pt}^{\text{II}}(\text{phen})(\text{L}^1\text{-S,O})]^+$ cation certainly forms non-covalent *hetero*-aggregates with aromatic molecules such as

fluoranthene (F) corresponding to $\text{M}^+ + \text{F} \rightleftharpoons \text{M}^+\text{F}$ in acetonitrile, with an estimated association constant $K_{\text{B}} \sim 67 \pm 7 \text{ M}^{-1}$ at 273.4 K.¹³ Moreover, in water-rich acetonitrile solutions the ^1H NMR spectra of the $[\text{Pt}^{\text{II}}(\text{phen})(\text{L}^1-\text{S},\text{O})]^+$ become progressively broader as the relative amount of water increases. This corroborates observations of extremely broad, almost featureless ^1H NMR spectra obtained in D_2O at room temperature of the highly water-soluble complex $[\text{Pt}^{\text{II}}(\text{diimine})(\text{N},\text{N}-\text{di}(2\text{-hydroxyethyl})-\text{N}'\text{-benzoylthiourea})]\text{Cl}$ (Figure A.36).¹⁴ These interesting NMR spectra suggest formation of larger nano-scale aggregate structures in water of such cationic complexes,¹⁴ the detailed nature of which has not been established to date.



Scheme 4.1 Postulated ‘average’ structure of a $\{[\text{Pt}^{\text{II}}(\text{phen})(\text{L}^1-\text{S},\text{O})]^+\}_2$ dimer aggregate in solution based on ^1H NMR shielding trends as a function of concentration.

A study of the non-covalent aggregation behaviour of $[\text{Pt}^{\text{II}}(\text{phen})(\text{L}^1-\text{S},\text{O})]^+$ cations in acetonitrile/water mixtures ranging from pure acetonitrile to pure water by means of the concentration dependence of the ^1H NMR and Diffusion Ordered Spectroscopy (DOSY) techniques, supplemented by Transmission Electron Microscopy, to elucidate the nature of these phenomena and the structure of the nano-aggregates which appear to form in water is presented here. The hetero-association of $[\text{Pt}^{\text{II}}(\text{phen})(\text{L}^1-\text{S},\text{O})]^+$ and polyaromatic hydrocarbon pyrene was also investigated using ^1H and DOSY NMR.

^1H Diffusion Ordered Spectroscopy is a suitable technique for studying aggregation behaviour in solution since diffusion coefficients, which are very sensitive towards changes in the molecular/aggregate size, while the number of individual molecules which constitute an aggregate may be approximately estimated using the Stokes-Einstein equation.^{15,16} The aim is to mimic the biological media in which such complex cations may be active, particularly in the context to their potential anti-malarial activity *in vitro* and/or *in vivo*.¹⁷

4.2 Results and discussion

4.2.1 The effect of solvent composition (0-30% (v/v) $\text{D}_2\text{O}:\text{CD}_3\text{CN}$) on aggregation of $[\text{Pt}^{\text{II}}(\text{phen})(\text{L}^1-\text{S},\text{O})]\text{Cl}$.

The ^1H NMR chemical shift concentration dependence trends obtained in pure acetonitrile and 10% (v/v) $\text{D}_2\text{O}:\text{CD}_3\text{CN}$ (Figure 4.1a), as well as diffusion coefficients obtained by DOSY NMR (*vide infra*) of $[\text{Pt}^{\text{II}}(\text{phen})(\text{L}^1-\text{S},\text{O})]\text{Cl}$ can satisfactorily be accounted for by means of an aggregation model resulting in essentially exclusive formation of a $\{[\text{Pt}^{\text{II}}(\text{diimine})(\text{L}^{\text{n}}-\text{S},\text{O})]^+\}_2$ dimer, consistent with a non-covalent cation- π association of $[\text{Pt}^{\text{II}}(\text{phen})(\text{L}^1-\text{S},\text{O})]^+$ as demonstrated previously for related complexes.^{9,13} However, by increasing the water content in these solutions, the ^1H NMR resonances as a function of $[\text{Pt}^{\text{II}}(\text{phen})(\text{L}^1-\text{S},\text{O})]\text{Cl}$ concentration at 299.3 K become significantly broader as shown for 100% D_2O in Figure 4.1b.

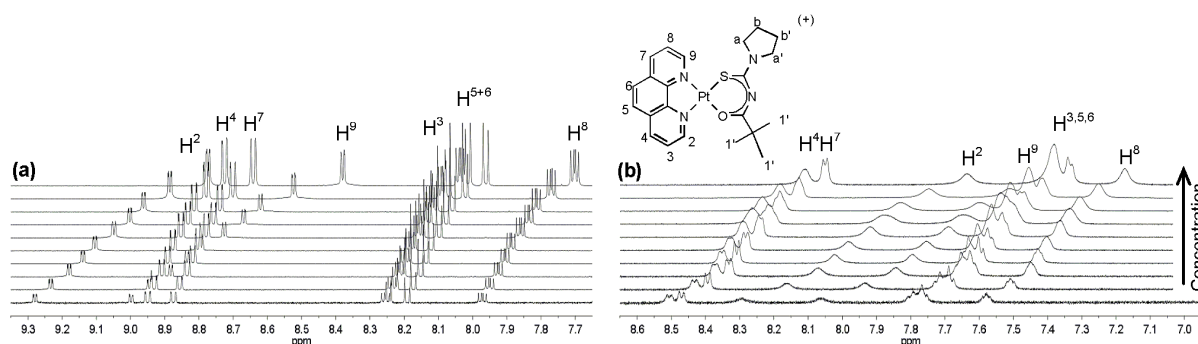


Figure 4.1 ^1H NMR spectra (599.99 MHz) of $[\text{Pt}^{\text{II}}(\text{phen})(\text{L}^1-\text{S},\text{O})]^+$ showing the chemical shift dependence of the 1,10-phenanthroline protons on the concentration of $[\text{Pt}^{\text{II}}(\text{phen})(\text{L}^1-\text{S},\text{O})]^+$ in solutions containing (a) 10% (v/v) $\text{D}_2\text{O}:\text{CD}_3\text{CN}$ (0.3 – 26.4 mM, 299.3K) and (b) D_2O (0.3 – 25.0 mM, 309.6K)

Moreover, all the ^1H NMR peaks of the diimine moiety of the platinum complex show relatively larger upfield chemical shift displacements (peaks become more shielded) as the water content of the solutions increases, as well as on increasing the concentration of $[\text{Pt}^{\text{II}}(\text{phen})(\text{L}^1-\text{S},\text{O})]^+$ for a given acetonitrile/water mixture. Since only one set of resonance signals is observed in the ^1H NMR spectra for the $[\text{Pt}^{\text{II}}(\text{phen})(\text{L}^1-\text{S},\text{O})]^+$ complex/aggregate under any conditions, these complexes are probably in fast to intermediate exchange on the NMR timescale for the temperature range of 267.1 to 309.6 K. The relative upfield displacements of the $\delta_{\text{obs}}(\text{H}^2)$ and $\delta_{\text{obs}}(\text{H}^9)$ resonances (δ/ppm) of the diimine moiety of the $[\text{Pt}^{\text{II}}(\text{phen})(\text{L}^1-\text{S},\text{O})]^+$ cation are significantly more pronounced compared to the ^1H NMR

signals of the *N*-acyl-*N,N*-dialkylthiourea moiety with increasing concentration (Figure 4.1a) and increasing water content of the solvent mixture (Figure 4.1b).

The relative changes of $\delta_{\text{obs}}(\text{H}^{2/9})/\text{ppm}$ induced as the concentration of $[\text{Pt}^{\text{II}}(\text{phen})(\text{L}^1\text{-S,O})]\text{Cl}$ increases from 0.34 - 10.3 mM are significantly larger in pure D_2O compared to acetonitrile ($\Delta^{\text{max}}\delta_{\text{MeCN}} = 0.28$ ppm to $\Delta^{\text{max}}\delta_{\text{D}_2\text{O}} = 0.41$ ppm). Similar trends have been reported for the related $[\text{Pt}^{\text{II}}(\text{diimine})(\text{N,N-di}(n\text{-butyl})\text{-N}'\text{-benzoylthiourea})]^+$ cation (Figure A.36).¹⁴ The experimental trends of $\delta_{\text{obs}}(\text{H}^2)$ as a function of $[\text{Pt}^{\text{II}}(\text{phen})(\text{L}^1\text{-S,O})]\text{Cl}$ concentration in solutions up to 30% (v/v) $\text{D}_2\text{O}:\text{CD}_3\text{CN}$ at various temperatures are shown in Figure 4.2. Non-linear least squares fitting of the experimental $\delta_{\text{obs}}(\text{H}^2)$ data to a dimer aggregate model $2\text{M}^+ \rightleftharpoons \{\text{M}^+\}_2$ ($\text{M}^+ = [\text{Pt}^{\text{II}}(\text{phen})(\text{L}^1\text{-S,O})]^+$) results in excellent agreement, allowing for estimated K_{D} ($\text{RSD}_{\text{max}} < 13\%$) values in 0, 10, 20 and 30% (v/v) $\text{D}_2\text{O}:\text{CD}_3\text{CN}$ shown in Table 4.1 in a temperature range 282.6-309.6 K.

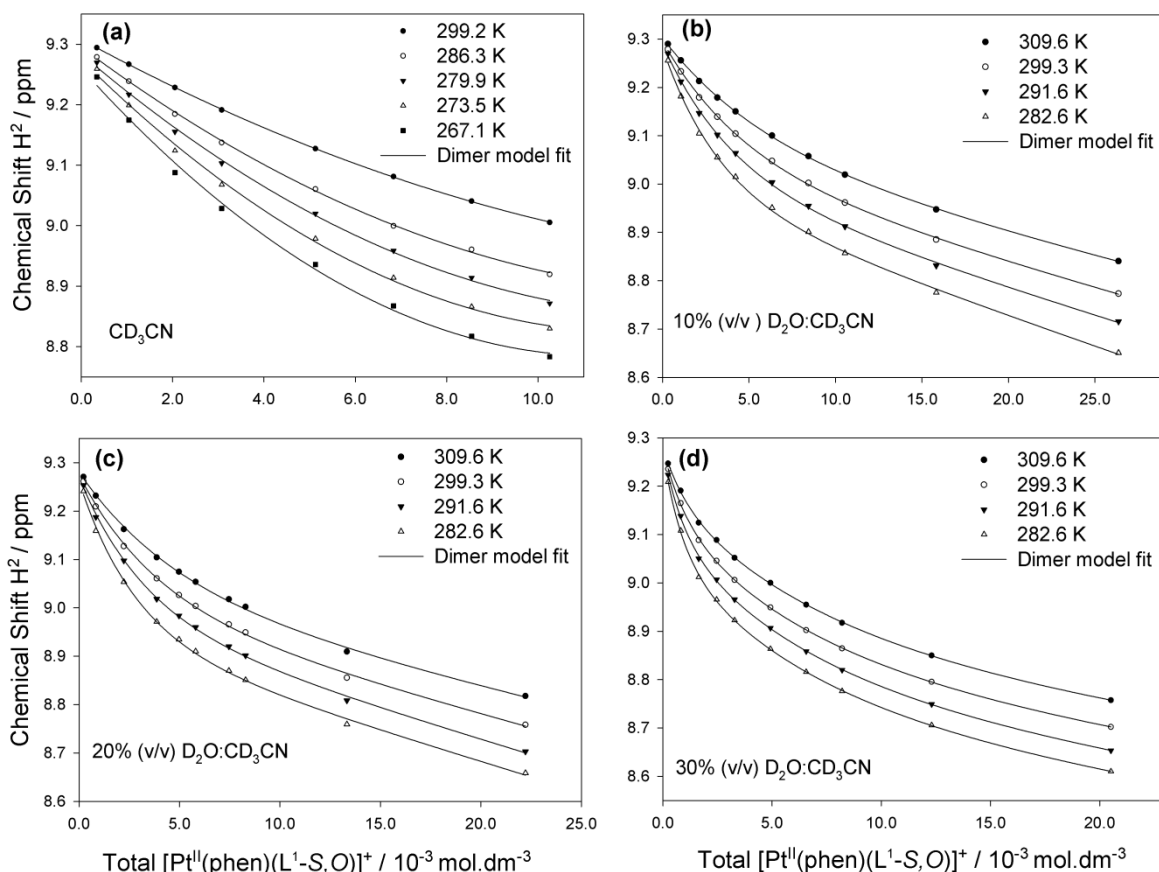


Figure 4.2 Excellent agreement between the dimer model least-squares fits and the experimental (symbols) chemical shift dependence of the 1,10-phenanthroline H^2 proton a concentration probe of $[\text{Pt}^{\text{II}}(\text{phen})(\text{L}^1\text{-S,O})]\text{Cl}$ in (a) 0:100 (b) 10:90, (c) 20:80 and (d) 30:70 (v/v) $\text{D}_2\text{O}:\text{CD}_3\text{CN}$ mixtures. (Calculated monomer and dimer chemical shifts available in Appendix A)

Standard reaction enthalpy ($\Delta_r H^0$) and entropy ($\Delta_r S^0$) values were estimated by fitting the Van't Hoff equation 4.1 to the temperature dependent K_D data resulting in the Van't Hoff plots shown in Figure 4.3; the good linear plots of $\ln K_D$ vs $1/T$ are consistent with only a dimer $2\text{M}^+ \rightleftharpoons \{\text{M}^+\}_2$ equilibrium and rule out other possible competing association processes or equilibria, such as ion-pairing and/or higher order aggregate formation for these solvent compositions ($\leq 30\%$ (v/v) $\text{D}_2\text{O}:\text{CD}_3\text{CN}$).

$$\ln(K_D) = -\frac{\Delta_r H^0}{RT} + \frac{\Delta_r S^0}{R} \quad (4.1)$$

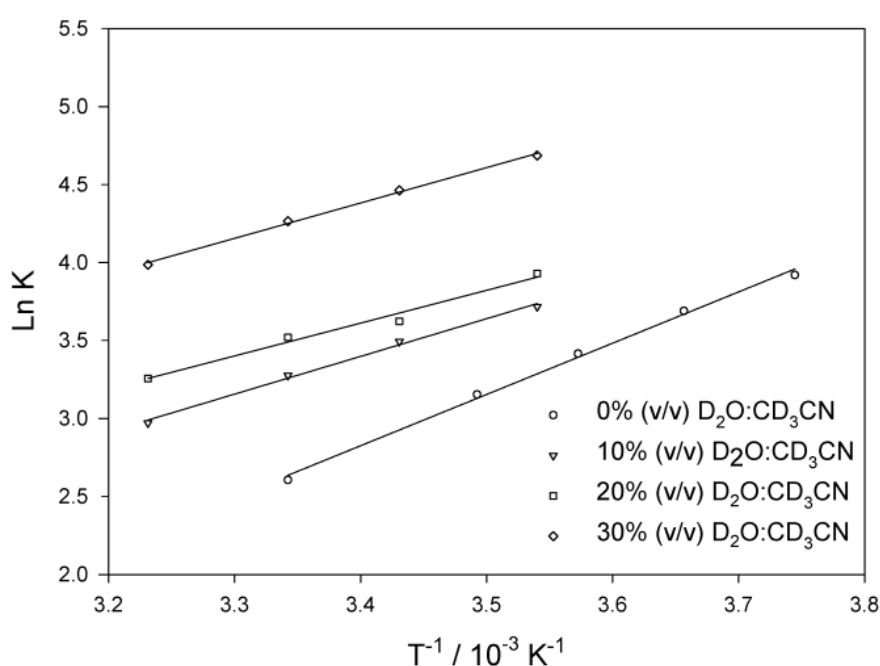


Figure 4.3 Van't Hoff Plots of the dimerization of $[\text{Pt}^{\text{II}}(\text{phen})(\text{L}^1\text{-S},\text{O})]^+$ in solutions 0-30% (v/v) $\text{D}_2\text{O}:\text{CD}_3\text{CN}$.

The increase in K_D by a factor of 4 - 5 as the solvent composition is changed from pure acetonitrile to 30% (v/v) $\text{D}_2\text{O}:\text{CD}_3\text{CN}$ mixtures indicates that the dimer aggregate $\{[\text{Pt}^{\text{II}}(\text{phen})(\text{L}^1\text{-S},\text{O})]^+\}_2$ is clearly favoured with increasing water (D_2O) content, as might be anticipated due to the expected hydrophobicity of such planar complex cations.

The process $2\text{M}^+ \rightleftharpoons \{\text{M}^+\}_2$, is clearly enthalpy driven ($\Delta_r H^0 < 0$) while a negative standard reaction entropy ($\Delta_r S^0 < 0$) is consistent with an aggregation/association process (Table 4.1).¹⁸ Interestingly the enthalpy of the dimer formation ($\Delta_r H^0$) decreases somewhat on passing from pure acetonitrile ($\Delta_r H^0 = -25.1 \text{ kJ}\cdot\text{mol}^{-1}$) to a 10% (v/v) $\text{D}_2\text{O}:\text{CD}_3\text{CN}$ ($\Delta_r H^0 = -$

19.7 kJ.mol⁻¹) mixture, after which the reaction enthalpy remains essentially constant within experimental error for 20 and 30% (v/v) D₂O:CD₃CN solutions.

By contrast the $\Delta_r S^0$ becomes systematically less negative as the D₂O content increases, Table 4.1. Doty and Myers attributed similar trends in $\Delta\Delta_r S^0$ for dimerization of protein moieties, to the dehydration of charged groups upon aggregation, while Kauzmann and Scheraga suggested that this trend may be due to non-covalent hydrophobic interaction of non-polar groups increasing the degree of freedom of the water molecules close to hydrophobic groups.¹⁹⁻²¹ It is thus reasonable to postulate that the trends in $\Delta\Delta_r S^0$ observed in this study may be attributed to the “hydrophobicity” of the coordinated 1,10-phenanthroline moiety, the effects of which become more significant as the solvent polarity increases with increasing water content of the solvent mixture (dielectric constant, $\epsilon_{\text{water}} = 78.5$ and $\epsilon_{\text{acetonitrile}} = 37.5$).^{22,23}

Table 4.1 Thermodynamic data for the self-association of $[Pt^{II}(\text{phen})(L^1-S,O)]^+$ in 0-30% (v/v) D₂O:CD₃CN solutions as calculated from ¹H NMR chemical shift concentration and temperature dependence.

% (v/v) D ₂ O:CD ₃ CN	Temperature (K)	K _D (M ⁻¹)	$\Delta_r H^0$ (kJ.mol ⁻¹)	$\Delta_r S^0$ (J.mol ⁻¹ .K ⁻¹)	$\Delta_r G^0$ (kJ.mol ⁻¹)
0	309.6	12 (± 1)	-25.1 (± 3.1)	-61 (± 11)	-7.0
	299.3	17 (± 2)			
	291.6	22 (± 2)			
	282.6	29 (± 3)			
10	309.6	20 (± 2)	-19.7 (± 2.4)	-40 (± 7)	-8.0
	299.3	27 (± 3)			
	291.6	33 (± 3)			
	282.6	41 (± 5)			
20	309.6	29 (± 3)	-20.1 (± 2.5)	-38 (± 7)	-8.6
	299.3	39 (± 4)			
	291.6	43 (± 4)			
	282.6	64 (± 7)			
30	309.6	54 (± 5)	-18.9 (± 2.3)	-27 (± 5)	-10.4
	299.3	71 (± 8)			
	291.6	87 (± 9)			
	282.6	109 (± 10)			

The $\delta(^1\text{H})$ trend differences for ^1H peaks of the 1,10-phenanthroline moiety as compared to butyl and *N*-pyrrolidyl ^1H signals of $[\text{Pt}^{\text{II}}(\text{phen})(\text{L}^1\text{-S},\text{O})]^+$ as a function of concentration and temperature are entirely consistent with a *regiospecific* face-to-face stacking arrangement of the $[\text{Pt}^{\text{II}}(\text{phen})(\text{L}^1\text{-S},\text{O})]^+$ cations in a dimer (Scheme 4.1) in these solutions up to 30% (v/v) $\text{D}_2\text{O}/\text{CD}_3\text{CN}$ as previously postulated in pure acetonitrile.^{9,13} The two planar complex cations interact with one another through cation- π interactions in a characteristic ‘offset’ stacking configuration consistent with the model proposed by Sanders *et al*²⁴ in their study on the nature of “ π -stacking interactions” based on porphyrin-porphyrin aggregation. The observed shielding trends as a function of concentration particularly of the H^2 and H^9 protons of the coordinated diimine moiety, clearly rule out a possible “T-shaped” cation- π interaction in these solutions.²⁴

4.2.2 Aggregation behaviour of $[\text{Pt}^{\text{II}}(\text{phen})(\text{L}^1\text{-S},\text{O})]\text{Cl}$ in water-rich mixtures >30% (v/v) $\text{D}_2\text{O}:\text{CD}_3\text{CN}$.

In water-rich acetonitrile mixtures (> 30% (v/v) $\text{D}_2\text{O}:\text{CD}_3\text{CN}$) significantly broader ^1H NMR resonances are observed for all the ^1H peaks associated with the diimine moiety in $[\text{Pt}^{\text{II}}(\text{phen})(\text{L}^1\text{-S},\text{O})]^+$ (Figure 4.1), eventually resulting in poorly resolved ^1H NMR spectra compared to solutions < 30% (v/v) $\text{D}_2\text{O}:\text{CD}_3\text{CN}$. Additionally, the even more pronounced shielding of the H^2 and H^9 protons of diimine moiety with increasing $[\text{Pt}^{\text{II}}(\text{phen})(\text{L}^1\text{-S},\text{O})]^+$ concentrations, suggests increased aggregation or large scale aggregates in solution. The application of a simple dimer $2\text{M}^+ \rightleftharpoons \{\text{M}^+\}_2$ model to the experimentally observed ^1H NMR shielding trends fails to account for these satisfactorily, particularly as the water content of the solvent increases to pure D_2O .

The significant line-broadening of ^1H NMR peaks in D_2O may be associated with a decrease in the T_2 relaxation times as estimated from ^1H NMR peak width at half-height ($\Delta\nu_{1/2}$) under optimum magnetic field homogeneities:^{25,26}

$$\Delta\nu_{1/2} = \pi \left(\frac{1}{T_2} + \frac{1}{T_{2(\Delta B_0)}} \right) \quad (4.2)$$

Where, $T_{2(\Delta B_0)}$ refers to the contribution of the magnetic field in homogeneity to the observed line-width. The measured ^1H NMR resonance half-height ($\Delta\nu_{1/2}$) of the $\text{H}^{2/9}$ resonances in

$[\text{Pt}^{\text{II}}(\text{phen})(\text{L}^1-\text{S},\text{O})]^+$ increases from 0.9Hz in pure CD_3CN to 18Hz in pure D_2O at constant temperature. The extremely pronounced ^1H NMR broadening observed for $[\text{Pt}^{\text{II}}(\text{diimine})(N,N\text{-di}(2\text{-hydroxyethyl})\text{-}N'\text{-benzoylthiourea})]\text{Cl}$ (Figure A.36) in D_2O , and an inverse dependence of line-width on temperature¹⁴, undoubtedly indicates that whatever the nature of the aggregate structure(s) formed in aqueous solution must have significantly larger average molecular weights.²⁷ The increase in line-width (fast T_2) observed with increasing D_2O content is postulated to be a result of the formation of nano-sized aggregates by non-covalent intermolecular interactions; these nano-sized aggregates are expected to have longer τ_c times, resulting in the observed decrease in T_2 an increase in $\Delta\nu_{1/2}$ commonly associated with macromolecules.²⁶⁻²⁸ The greater degree of shielding of *inter alia* H^{29} with increasing $[\text{Pt}^{\text{II}}(\text{phen})(\text{L}^1-\text{S},\text{O})]^+$ complex concentration in D_2O (due to the chemical shift anisotropy (CSA) phenomenon) illustrated by the data in Figure 4.4 for several temperatures due is consistent with more extensive cation- π aromatic-ring stacking expected for the planar quasi-aromatic $[\text{Pt}^{\text{II}}(\text{phen})(\text{L}^1-\text{S},\text{O})]^+$ cation.

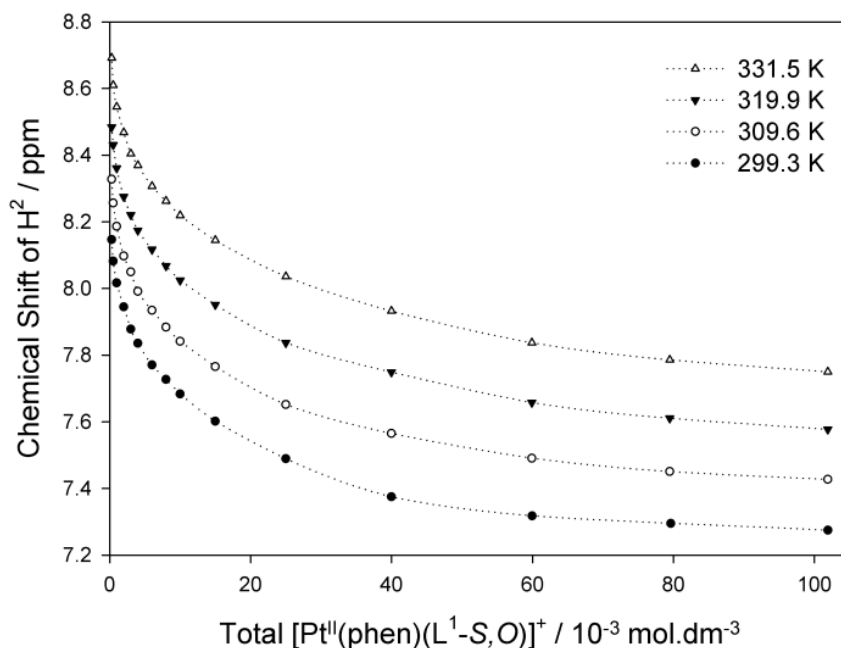
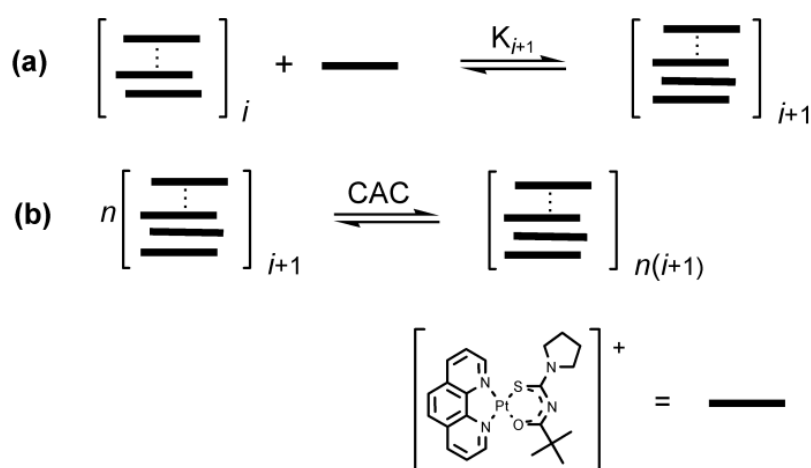


Figure 4.4 The ^1H NMR chemical shift dependence of H^2 on $[\text{Pt}^{\text{II}}(\text{phen})(\text{L}^1-\text{S},\text{O})]\text{Cl}$ concentration in D_2O at temperatures 299.3, 309.6, 319.9, and 331.5 K. (Note: The dotted lines are aids for trend visualization.)

Despite our best efforts, the ^1H shielding trends in D_2O and water rich solutions ($> 30\%$ (v/v) $\text{D}_2\text{O}:\text{CD}_3\text{CN}$) could also not be satisfactorily accounted for by a simple or even higher order aggregation models such as trimer-, tetramer formation *etc.* Therefore, a multiple aggregate formation model leading to the formation of structures formulated as $\{[\text{Pt}^{\text{II}}(\text{phen})(\text{L}^1\text{-S,O})]^+\}_n\text{Cl}^-_y$, (n and y variable but > 2) similar to a model proposed for procyanidin aggregation in a wine-like medium described by Pianet *et al* is proposed.²⁹ This aggregation model is illustrated in Scheme 4.2.



Scheme 4.2 Postulated aggregation model of $[\text{Pt}^{\text{II}}(\text{phen})(\text{L}^1\text{-S,O})]\text{Cl}$ in aqueous solutions consisting of two major equilibrium processes with (a) an accumulative aggregation with K_i the respective association constant corresponding to the i^{th} monomer associating to the aggregate and (b) the formation of nano-sized aggregates after a specific critical aggregation concentration (CAC).

The experimental NMR data in D_2O is consistent with the model described in Scheme 4.2, in which at initially relatively low total complex concentrations, (a) the self-association of $[\text{Pt}^{\text{II}}(\text{phen})(\text{L}^1\text{-S,O})]^+$ cations results in dimer aggregates, which however eventually lead to the formation of $\{[\text{Pt}^{\text{II}}(\text{phen})(\text{L}^1\text{-S,O})]^+\}_n\text{Cl}^-_y$ structures *via* an unspecified number of sequential equilibria (K_{i+1}), as the total complex concentration increases; (b) above a certain critical concentration of $[\text{Pt}^{\text{II}}(\text{phen})(\text{L}^1\text{-S,O})]^+$, which may for convenience be termed a ‘critical aggregation concentration’ (CAC), similar to the well-known critical micelle concentration (CMC), larger nano-sized aggregate structures appear to form with concomitant ion-pair formation by Cl^- ions to offset excessive positive charge build-up as a result of the formation of a highly charged ‘cation-aggregate’ (Scheme 4.2b).²⁹

In support of such a CAC model, a plot of $\delta_{\text{obs}}(\text{H}^2)$ of $[\text{Pt}^{\text{II}}(\text{phen})(\text{L}^1\text{-S},\text{O})]^+$ against $1/[\text{M}]_{\text{T}}$ ($[\text{M}]_{\text{T}}$ = total $[\text{Pt}^{\text{II}}(\text{phen})(\text{L}^1\text{-S},\text{O})]\text{Cl}$ concentration) results in two quasi-linear regions (Figure 4.5), the intercept of such lines gives an estimate of the critical aggregation concentration^{30,31} in D_2O for the $[\text{Pt}^{\text{II}}(\text{phen})(\text{L}^1\text{-S},\text{O})]^+$ complex as listed in Table 4.2. The estimated CAC for $[\text{Pt}^{\text{II}}(\text{phen})(\text{L}^1\text{-S},\text{O})]^+$ increases with temperature as may be expected given that the aggregation process is enthalpy driven ($\Delta_{\text{r}}H^0 < 0$), suggested by data in Table 4.1.

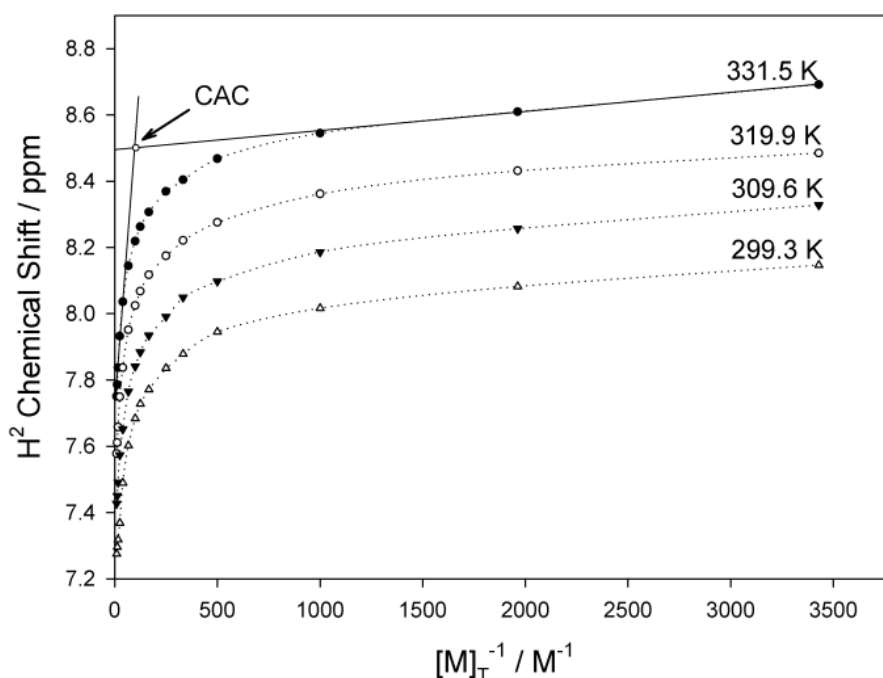
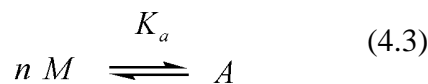


Figure 4.5 The observed ^1H chemical shift of H^2 at temperatures 299.3 - 331.5 K against $1/[\text{M}]_{\text{T}}$, where $[\text{M}]_{\text{T}}$ = Total $[\text{Pt}^{\text{II}}(\text{phen})(\text{L}^1\text{-S},\text{O})]\text{Cl}$ concentration in D_2O . The expansions and extrapolations of the ^1H NMR chemical shift concentration dependence of all temperatures are displayed in Figure A.37. (Note: The dotted lines are aids for trend visualization.)

Table 4.2 Estimated critical aggregation concentrations (CAC) in D_2O from concentration dependence $\delta_{\text{obs}}(\text{H}^2)$ data at various temperatures, as well as diffusion coefficient (D_{obs}) dependence on concentration at 299.3K.

Temperature (K)	299.3	309.6	319.9	331.5
δ , CAC mM	9.6 (± 0.6)	12.0 (± 0.7)	13.9 (± 0.9)	14.9 (± 0.9)
D , CAC mM	10.3 (± 1.5)			
δ log plot, CAC mM	11.5			

Luchetti and co-workers have determined CAC using the general mass action law model (relation 4.3) to describe the aggregation of surfactants in solution of unknown aggregation numbers.³⁰



$$K_a = \frac{[A]}{[M]^n} \quad (4.4)$$

where n is the aggregation number, K_a the equilibrium constant and M and A are the monomer and aggregate form of $[Pt^{II}(\text{phen})(L^1-S,O)]Cl$ respectively. The simplest expression for the observed chemical shift of an aggregating system which displays one set of signals due to fast exchange in chemical shift on the NMR time scale is given by equation 4.5. The chemical shift of nuclei in the monomer δ_M and aggregate δ_A can be estimated using δ_{obs} versus $[M]_T$ and δ_{obs} versus $1/[M]_T$ plots respectively where $[M]_T$ is the total $[Pt^{II}(\text{phen})(L^1-S,O)]Cl$ concentration. The aggregation number n , which represents the number of molecules in an aggregate can be determined from equation 4.6 obtained by combining equations 4.4 and 4.5:

$$\delta_{\text{obs}} = x_M \delta_M + x_A \delta_A \quad (4.5)$$

$$\log\{[M]_T(\delta_M - \delta_{\text{obs}})\} = n \log\{[M]_T(\delta_{\text{obs}} - \delta_A)\} + \log(n K_a) + (1 - n) \log(\delta_M - \delta_A) \quad (4.6)$$

where, X represents the mole fraction of the species. If the aggregation is correctly described by equation 4.6, a plot of $\log\{[M]_T(\delta_M - \delta_{\text{obs}})\}$ versus $\log\{[M]_T(\delta_{\text{obs}} - \delta_A)\}$ should exhibit a linear relationship with the slope equal to the aggregation number n . Interestingly, the plot of $\log\{[M]_T(\delta_M - \delta_{\text{obs}})\}$ versus $\log\{[M]_T(\delta_{\text{obs}} - \delta_A)\}$ with δ_{obs} the observed chemical shift of H^2 , displays *two* linear regions (see Figure 4.6).

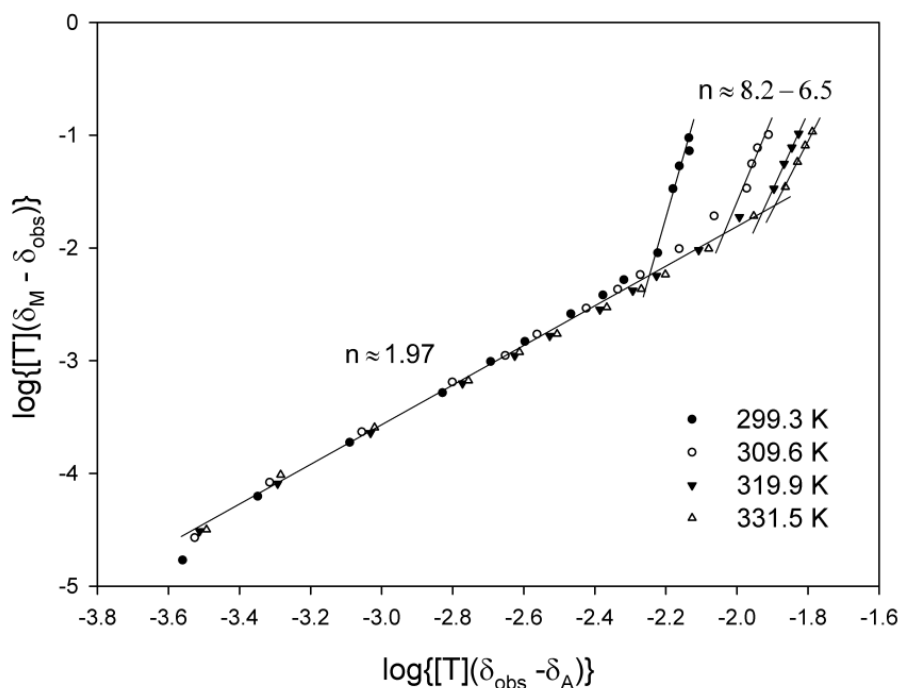


Figure 4.6 Plot of equation 4.6 of H^2 in acetonitrile- d_3 .

The presence of two linear portions is an indication of at least two aggregation equilibria in solution with the slopes of the two regression lines equal to the aggregation numbers of these equilibria. For the lower concentration range $n = 1.97$ and the higher concentration $n = 6.5 - 8.2$. The intersection of the two regression lines would be the concentration where the equilibrium changes from presumably dimerization to a higher aggregation equilibrium (*ca.* 8 molecules in an aggregate);³⁰ a reasonable critical aggregation concentration of 11.5 mM was obtained for the data at 299.3 K. However, the validity of using the simple aggregation model (eq. 4.3) is not evident since the chemical shift of H^2 in a dimer aggregate is not expected to be equivalent to the H^2 chemical shift of a higher aggregate and the aggregation process is not likely to be isodesmic as the electrostatic potential will increase with the addition of more monomers to the aggregate. Furthermore, equation 4.5 would need additional terms to compensate for the difference in chemical shift of the two or more aggregated states as shown by equation 4.7,

$$\delta_{\text{obs}} = x_M \delta_M + x_D \delta_D + x_A \delta_A + \dots + x_{A_i} \delta_{A_i} \quad (4.7)$$

where x_M , x_D and x_{A_i} are the mole fractions and δ_M , δ_D and δ_{A_i} the chemical shifts of molecules in the monomer, dimer and i^{th} aggregate form respectively. Since the number of aggregation equilibria in solution is unknown, the observed chemical shift δ_{obs} can

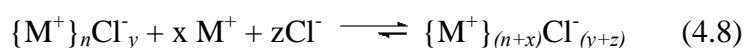
comprise of many terms making calculations extremely complicated and impractical at this stage.

4.2.2.1 Effect of chloride ion concentration on $[\text{Pt}^{\text{II}}(\text{phen})(\text{L}^{\text{1}}-\text{S},\text{O})]^+$ aggregation in water.

The extent of aggregation of cationic $[\text{Pt}^{\text{II}}(\text{phen})(\text{L}^{\text{1}}-\text{S},\text{O})]^+$ complexes to form dimer $\{\text{M}\}_2^{2+}$ type structures in mainly acetonitrile, and the postulated nano-scale aggregate structures $\{[\text{Pt}^{\text{II}}(\text{phen})(\text{L}^{\text{1}}-\text{S},\text{O})]^+\}_n$ in water is likely to result in electrostatic positive charge build-up. These highly charged structures are probably stabilised in solution by ion-pairing of Cl^- . Thus the effective Cl^- :cation ratio may be expected to stabilize and/or affect the formation of larger aggregate structures in D_2O . This is confirmed by the significant shielding induced in the $\delta_{\text{obs}}(\text{H}^2)$ peak of the 1,10-moiety of $[\text{Pt}^{\text{II}}(\text{phen})(\text{L}^{\text{1}}-\text{S},\text{O})]^+$ on a 4.54 mM solution of $[\text{Pt}^{\text{II}}(\text{phen})(\text{L}^{\text{1}}-\text{S},\text{O})]^+$ (below the CAC) with addition of NaCl, increasing the effective $[\text{Cl}^-]$ from 10.5 to 346.7 mM, as illustrated in Figure 4.7a, corresponding to a Cl^- : cation ratio of *ca.* 2 to 77. The dependence $\delta(^1\text{H})$ on NaCl concentration in D_2O is shown in Figure 4.7b.

Further increases to a Cl^- : cation ratio of > 80 , leads to precipitation of a yellow solid from solution. The upfield shift of $\delta_{\text{obs}}(\text{H}^{2/9})$ as a result of increasing the Cl^- : cation ratio cannot be solely due to ionic strength increases since the corresponding ^1H NMR chemical shifts of the butyl and *N*-pyrrolidyl protons are comparatively small compared to those of the diimine protons, while the residual solvent peak and the signals of any minor impurities in the ^1H NMR spectrum remain essentially unaffected over the titration range. These trends suggest that the nano-scale aggregates $\{[\text{Pt}^{\text{II}}(\text{phen})(\text{L}^{\text{1}}-\text{S},\text{O})]^+\}_n\text{Cl}_y^-$ become larger (n,y increase) or are at least stabilized with increasing Cl^- : cation ratio, until precipitation from solution occurs, akin to the well-known “salting-out” phenomenon.

Thus in water, or at least in water-rich acetonitrile mixtures above 30% (v/v) $\text{D}_2\text{O}/\text{CD}_3\text{CN}$, the proposed positively charged aggregate structures of the $[\text{Pt}^{\text{II}}(\text{phen})(\text{L}^{\text{1}}-\text{S},\text{O})]^+$ complex cation (M^+) as envisaged in Scheme 4.2, may be reasonably represented by the following equation:



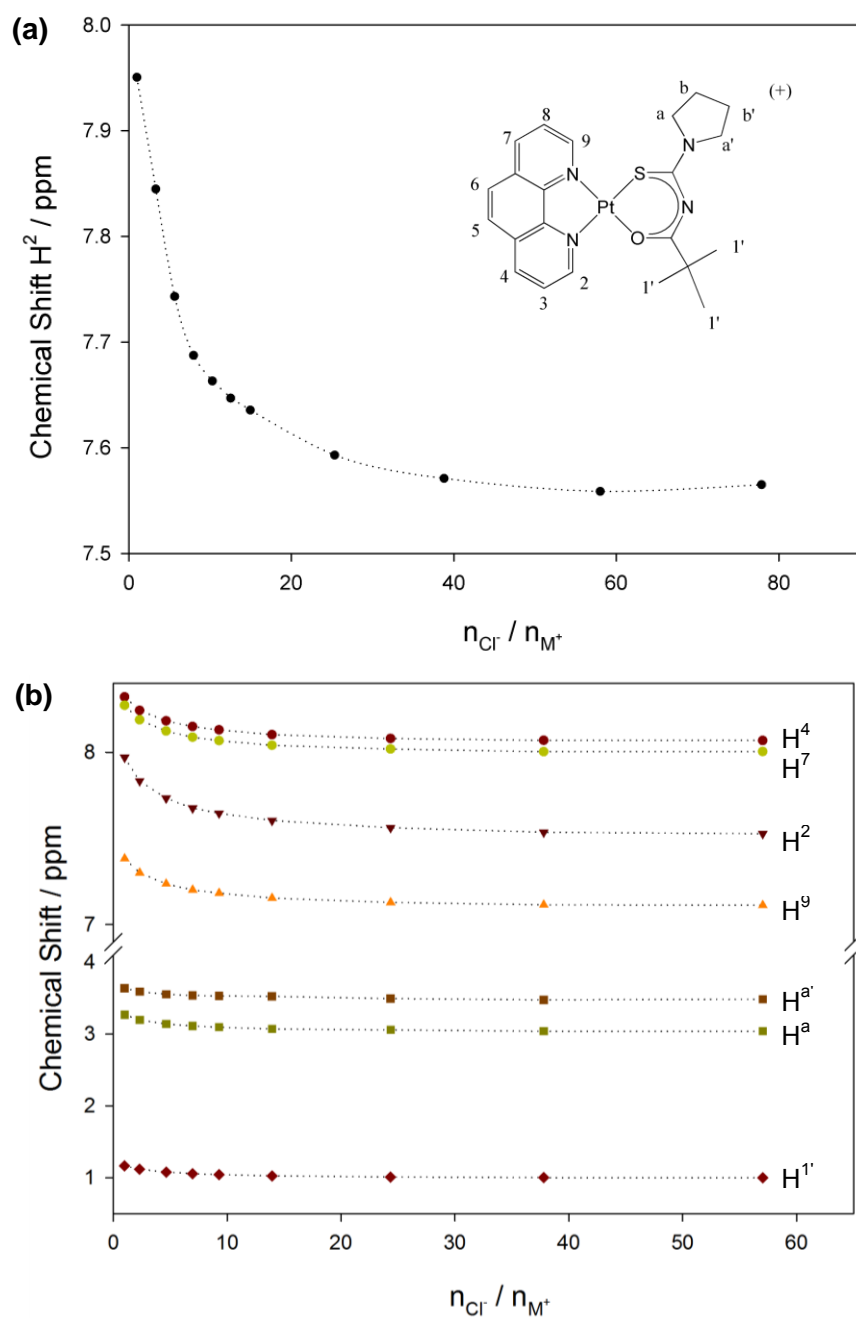


Figure 4.7 Variation of (a) $\delta_{\text{obs}}(\text{H}^2)$ and (b) all ^1H resonances as a function of Cl^- concentration using a total $[\text{Pt}^{\text{II}}(\text{phen})(\text{L}^1\text{-S,O})\text{Cl}]$ concentration $[\text{Z}] = 4.50 \text{ mM}$ and a final Cl^- concentration of 346.7 mM .

4.2.2.2 Diffusion Ordered NMR Spectroscopy

A semi-quantitative estimate of the effective number of complex cations (n) which constitute the proposed nano-sized aggregate structure, would lend convincing support to this model. The translational diffusion of such aggregates in solution should depend significantly on their effective 'size' as suggested by the concentration dependence of ^1H NMR shielding data.

The diffusion coefficient is a measure of the natural diffusion of a molecule in solution. This can be estimated by measuring the attenuation of the NMR signals in a pulsed field gradient experiment as shown in Figure 4.8.

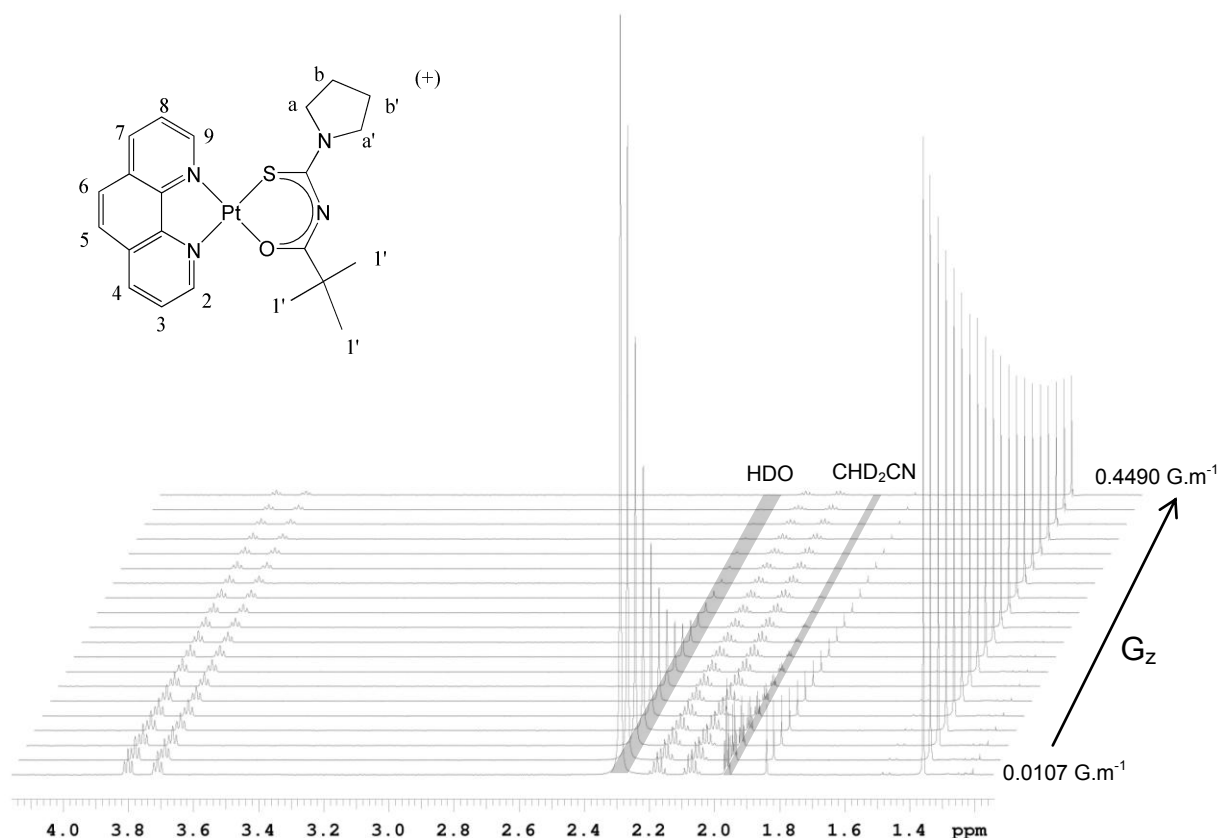
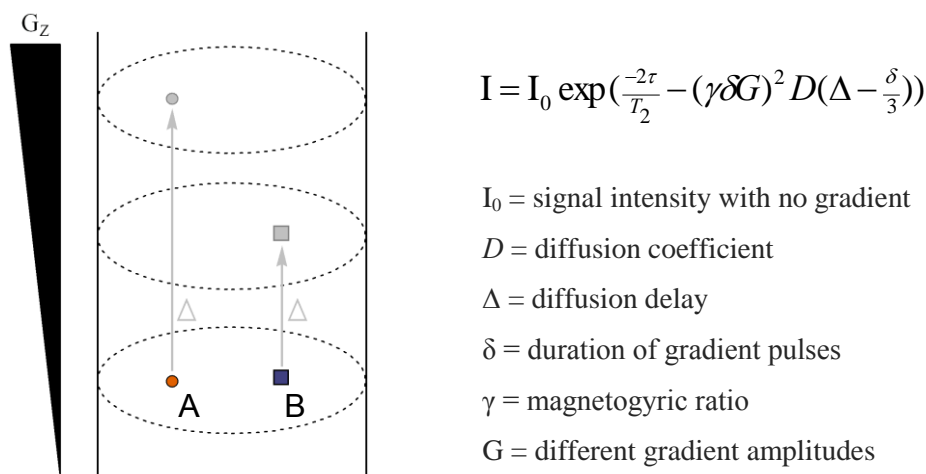


Figure 4.8 Attenuation of the ^1H NMR signals of $[Pt^{II}(\text{phen})(L^1-S,O)]\text{Cl}$ in acetonitrile- d_3 during a typical DOSY experiment with increasing gradient strength ($0.0107\text{--}0.449\text{ G}\cdot\text{m}^{-1}$).

The attenuation of the resonance signal can be explained by a derivation of the Stejskal-Tanner equation and the diagram shown in Scheme 4.3.²⁵ The pulsed-field gradient experiment (PFGE) can be explained by considering two molecules of different sizes A and B with A being the smaller of the two which diffuses faster (i.e. greater distance) than B during the same diffusion delay Δ . In the simplest case, the experiment consists of two pulsed field gradients (PFGs) which are the exact inverse of each other and the diffusion delay Δ separating these two opposing PFGs. These PFGs scramble the magnetisation in a specific

way and because the second PFG is the inverse of the first, the magnetisation will be completely refocused if the diffusion delay is zero.



Scheme 4.3 Graphical representation of the diffusion of two hypothetical molecules A and B during the diffusion delay Δ . The signal intensity during a PFG is defined by a derivation of the Stejskal-Tanner equation (right).

However, the local magnetic field is spatially dependent because of the field gradient (G_z) that is used. Therefore, a molecule that diffuses after the diffusion delay between the two gradient pulses will experience a different local magnetic field when the second PFG is applied which leads to only partial refocusing of the magnetization, resulting in the attenuation of the resonance signal. The signal attenuation follows an exponential decay as illustrated in Figure 4.8 and is a function of the magnetic gradient pulse amplitude/strength (G) and the diffusion coefficient (D) as shown by the equation in Scheme 4.3. A least-squares fit of this equation to the attenuation of the signal intensities allows for the calculation of the diffusion coefficients which is displayed as a two-dimensional plot with the 1H NMR spectrum on the one axis and the calculated diffusion coefficient on the other (Figure 4.9).

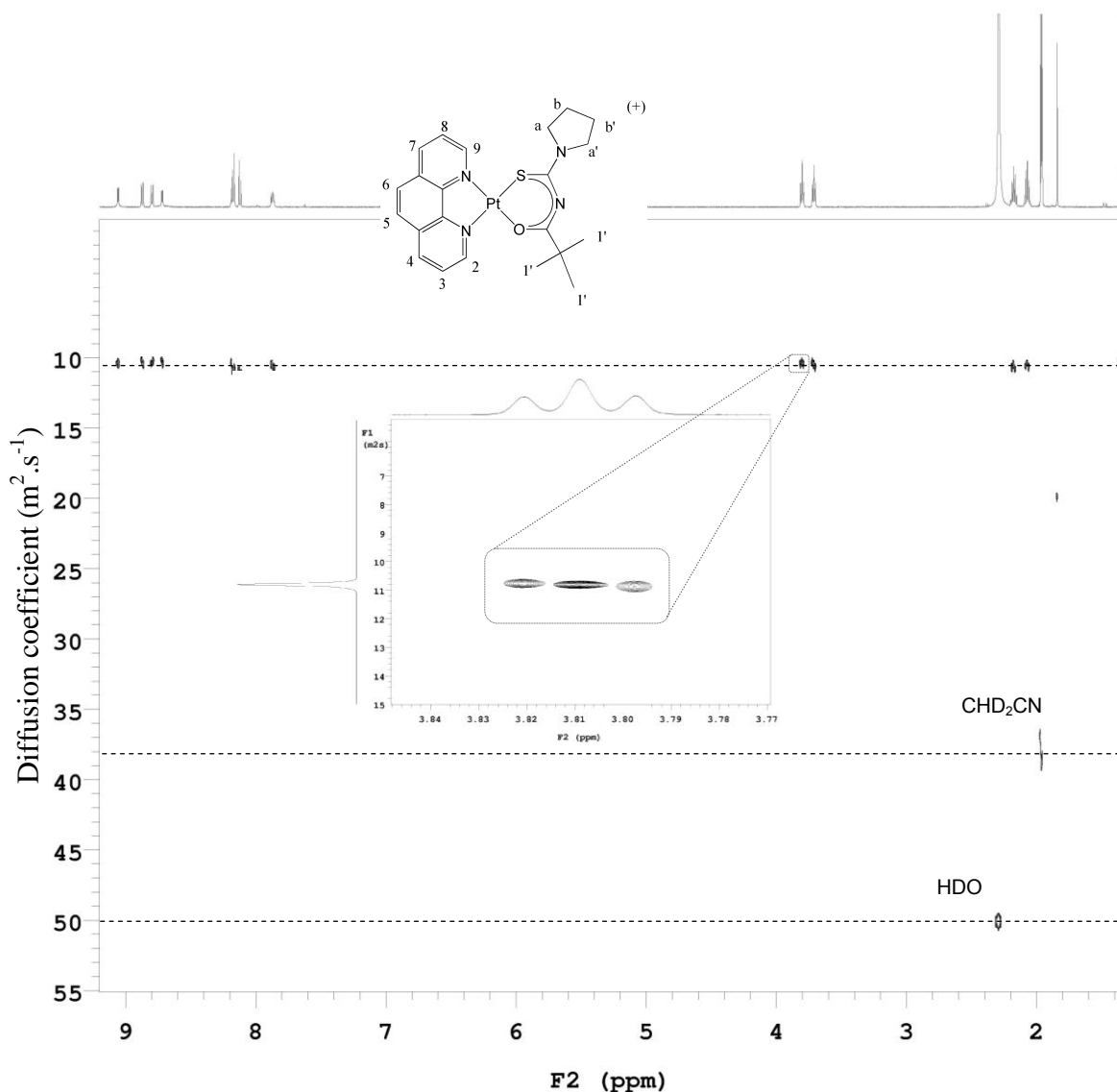


Figure 4.9 ^1H DOSY plot of $\text{Pt}^{\text{II}}(\text{phen})(\text{L}^1\text{-S},\text{O})\text{Cl}$ in acetonitrile- d_3 . ($\Delta = 30$ ms, $\delta = 2$ ms, $G = 0.0107\text{-}0.449$ $\text{G}\cdot\text{m}^{-1}$)

All resonance signals belonging to the same molecule exhibit diffusion coefficients that are similar. It is clear from Figure 4.9 that $\text{Pt}^{\text{II}}(\text{phen})(\text{L}^1\text{-S},\text{O})\text{Cl}$, HDO and CHD_2CN have significantly different diffusion coefficients with the order $\text{Pt}^{\text{II}}(\text{phen})(\text{L}^1\text{-S},\text{O})\text{Cl} < \text{CHD}_2\text{CN} < \text{HDO}$. This can also be intuitively seen from the attenuation spectra (Figure 4.8) where the water signal as well as acetonitrile resonance disappear when subjected to strong gradients while $\text{Pt}^{\text{II}}(\text{phen})(\text{L}^1\text{-S},\text{O})\text{Cl}$ is still observed.

Data from DOSY NMR experiments in the concentration range 0.34-76.08 mM $[\text{Pt}^{\text{II}}(\text{phen})(\text{L}^1\text{-S},\text{O})\text{Cl}]^+$ at 299.3 K in D_2O and the NaCl titration data are shown in Figure 4.10 and Table 4.4.

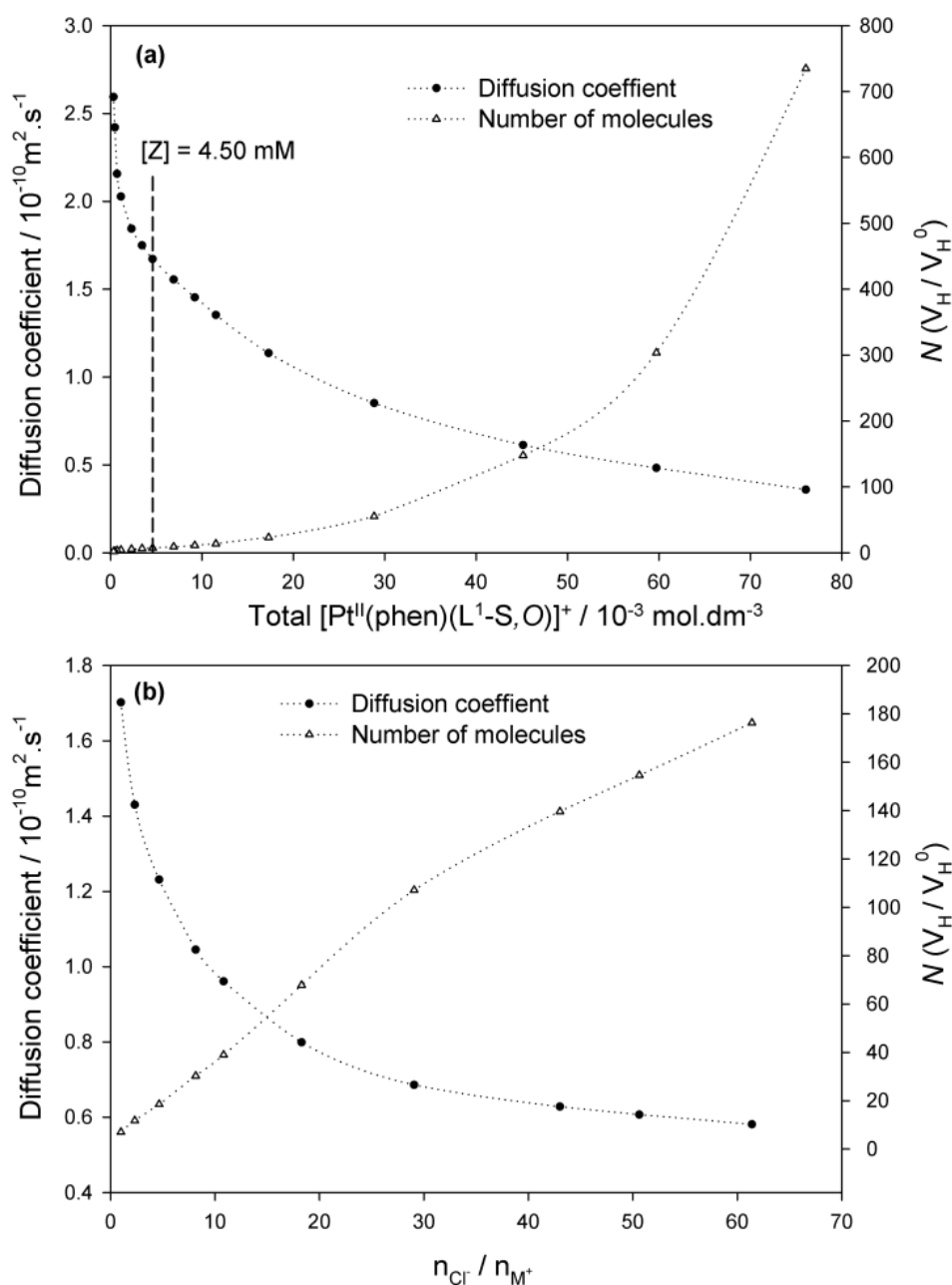


Figure 4.10(a) $[\text{Pt}^{\text{II}}(\text{phen})(\text{L}^1\text{-S},\text{O})]\text{Cl}$ diffusion coefficient (D_{obs}) and average aggregation number (N) ($N = V_{\text{H}}/V_{\text{H}}^0$) as a function of $[\text{Pt}^{\text{II}}(\text{phen})(\text{L}^1\text{-S},\text{O})]\text{Cl}$ concentration in pure D_2O . **(b)** The effect of Cl^- addition (NaCl) on the diffusion coefficient of $[\text{Pt}^{\text{II}}(\text{phen})(\text{L}^1\text{-S},\text{O})]\text{Cl}$ (concentration indicated as $[\text{Z}]$) and the calculated average number of molecules (N) with $n_{\text{Cl}^-}/n_{\text{M}^+}$ the mole ratio of Cl^- over $[\text{Pt}^{\text{II}}(\text{phen})(\text{L}^1\text{-S},\text{O})]^+$ in D_2O .

Table 4.3 Variation of $\delta_{\text{obs}}(\text{H}^2)$ and D_{obs} of a 4.5 mM $[\text{Pt}^{\text{II}}(\text{phen})(\text{L}^1\text{-S},\text{O})]\text{Cl}$ solution as a function of NaCl concentration with the calculated hydrodynamic radii (r_{H}), volumes (V_{H}) and aggregation numbers (N).

Mole Ratio $n_{Cl^-}:n_{M^+}$	$\delta_{obs}(H^2)$ (ppm)	Mole Ratio $n_{Cl^-}:n_{M^+}$	D ($10^{-10}m^2.s^{-1}$)	r_H (Å)	V_H (Å ³)	N (V_H/V_H^0)
1	7.95	1	1.70	11.9	7060	7.0
3.32	7.84	2.33	1.43	14.2	11904	11.8
5.65	7.74	4.66	1.23	16.5	18660	18.5
7.97	7.69	8.15	1.05	19.4	30503	30.3
10.30	7.69	10.8	0.96	21.1	39221	39.0
12.53	7.65	18.3	0.80	25.4	68242	67.8
14.94	7.64	29.1	0.69	29.5	107824	107
25.35	7.59	43.0	0.63	32.3	140543	140
38.80	7.57	50.6	0.61	33.4	155640	155
58.02	7.56	61.4	0.58	34.9	177484	176
77.88	7.57					

Table 4.4 Diffusion coefficient (D) concentration dependence data, calculated hydrodynamic radii (r_H) and average aggregation numbers (N), with $N = V_H/V_H^0$ where V_H is the volume calculated from r_H and V_H^0 the estimated volume of a monomer at infinite dilution.

Concentration ($10^{-3} mol.dm^{-3}$)	D ($10^{-10}m^2.s^{-1}$)	r_H (Å)	V_H (Å ³)	N (V_H/V_H^0)
76.08	0.36	56.1	739692	735
59.72	0.52	39.1	250561	304
45.14	0.61	32.9	148577	148
28.84	0.85	23.7	55532	55.2
17.31	1.14	17.7	23345	23.2
11.54	1.35	14.9	13818	13.7
9.230	1.47	13.7	10708	11.1
6.922	1.55	13.0	9120	9.06
4.615	1.67	12.1	7335	7.29
3.462	1.77	11.4	6182	6.35
2.307	1.84	10.9	5458	5.42
1.154	2.05	9.84	3990	4.08
0.721	2.16	9.34	3415	3.39
0.481	2.42	8.32	2415	2.40
0.337	2.59	7.76	1961	1.95
0a	3.24	6.22	1007	1

^a Extrapolated to infinite dilution using the D_{obs} vs. $1/[M]_T$ plot

A single exponential decay function fits the attenuation of the ^1H DOSY NMR data very well, and indicates that the observed diffusion coefficients (D_{obs}) is an average of that of the mononuclear $[\text{Pt}^{\text{II}}(\text{phen})(\text{L}^1\text{-S},\text{O})]^+$ and *all* aggregate species in solution.

$$D_{\text{obs}} = \alpha_m D_m + \dots + \alpha_i D_i \quad (4.9)$$

The D_{obs} for the $[\text{Pt}^{\text{II}}(\text{phen})(\text{L}^1\text{-S},\text{O})]^+$ in water shows a significant decrease as a function of concentration (Figure 4.10a), consistent with a higher order aggregate formation.

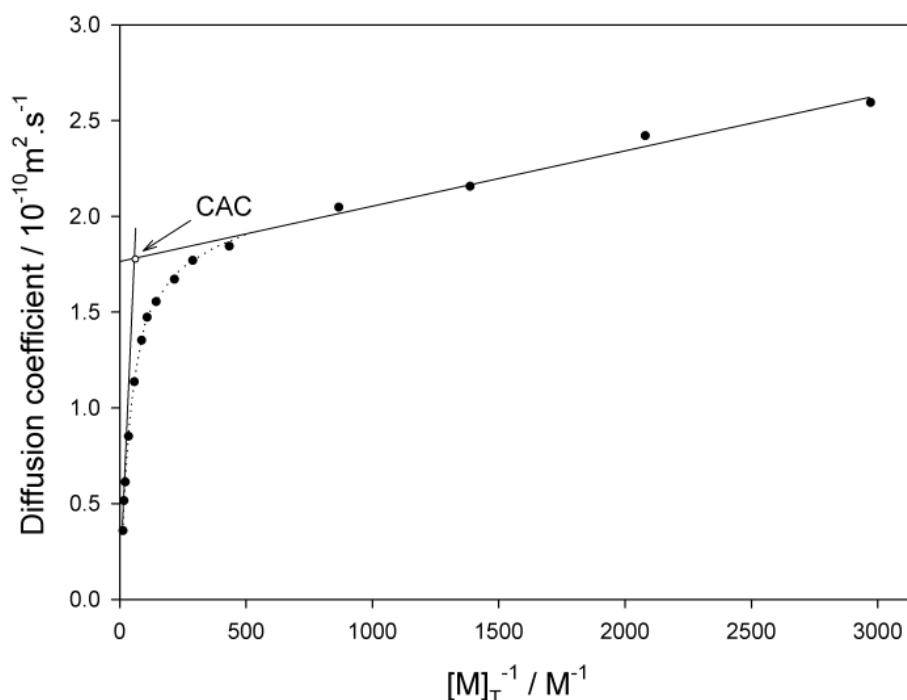


Figure 4.11 $[\text{Pt}^{\text{II}}(\text{phen})(\text{L}^1\text{-S},\text{O})]^+$ diffusion coefficient at 299.3 K against $1/[\text{M}]_{\text{T}}$, where $[\text{M}]_{\text{T}} = \text{Total } [\text{Pt}^{\text{II}}(\text{phen})(\text{L}^1\text{-S},\text{O})]\text{Cl}$ concentration. (Note: The dotted lines are aids for trend visualization.)

The Stokes-Einstein equation 4.9 may be used to estimate the hydrodynamic radii (r_{H}) of species from the measured diffusion coefficients (D),

$$D = \frac{kT}{6\pi\eta r_{\text{H}}} \quad (4.9)$$

where k is the Boltzmann constant, η the solvent viscosity, and r_{H} the hydrodynamic radius. Since the diffusion coefficient obtained for $[\text{Pt}^{\text{II}}(\text{phen})(\text{L}^1\text{-S},\text{O})]^+$ is the average between all

species in solution, the r_H is also an average value. Although the Stokes-Einstein equation is only a crude approximation for estimating the ‘size’ of a square planar $[Pt^{II}(\text{phen})(L^1-S,O)]^+$ complex, the changes in the average r_H as a function of concentration may provide support for the proposed aggregation model. The r_H of a single monomer (r_H^0) has been estimated by extrapolating the D_{obs} to infinite dilution from the plot of D_{obs} vs. $1/[M]_T$, Figure 4.11. An estimate of the CAC of *ca.* 10.3 ± 1.5 for this complex may also be obtained from this plot; this value is in satisfactory agreement with the CAC values obtained by the simple $\delta(H^2)$ concentration dependence data shown in Table 4.2.

The extent of aggregation can be estimated by considering the *aggregation number* (N) calculated using the hydrodynamic volumes of the monomer (V_H^0) and V_H estimated from D_{obs} ($N = V_H/V_H^0$).³² Table 4.4 lists the data obtained for this system from the ^1H DOSY NMR experiments at 299.3 K. The average aggregate number in solution increases from $N \sim 1.95$ at the lowest practically measureable concentration by DOSY NMR of 0.34 mM of $[Pt^{II}(\text{phen})(L^1-S,O)]^+$ with an estimated hydrodynamic radius of *ca.* 7.8 Å and V_H 1961 Å³, to a maximum $N \sim 735$ ($[M]_T = 76.1$ mM) corresponding to a ‘size’ of *ca.* 735 nm³ for the postulated nano-aggregate structure of $\{[Pt^{II}(\text{phen})(L^1-S,O)]^+\}_n\text{Cl}_y$ structure(s) in solution.

Significant changes in D_{obs} are seen in D₂O for a 4.5 mM $[Pt^{II}(\text{phen})(L^1-S,O)]^+$ solution ($[Z]$ dashed line in Figure 4.10a) upon increasing the Cl⁻ : cation ratio by means of ‘titration’ with NaCl. The 4.5mM concentration was chosen well below the CAC value of 9.6 mM to show maximum effect. In this way the calculated average aggregation number (N) of $[Pt^{II}(\text{phen})(L^1-S,O)]^+$ increased from 8 to a maximum of *ca.* 176 for the highest practical Cl⁻ : cation ratio ($n_{\text{Cl}^-}/n_{\text{M}^+}$), before precipitation occurs (Figure 4.10b). The increase in NaCl concentration up to a maximum of ~ 342 mM, might be expected to increase the viscosity of the solution significantly, although the estimated overall change in viscosity is at most *ca.* 0.02 mPa.s, which results in a difference of only *ca.* 1.8-2% in the calculated diffusion coefficients.³³ This data satisfactorily confirms the effect of increasing the Cl⁻ : cation ratio on the postulated nano-aggregate (“metallo-gel”) formation of $\{[Pt^{II}(\text{phen})(L^1-S,O)]^+\}_n\text{Cl}_y$ type structures in water, as summarized by the equilibrium (1) above. Such nano-aggregate structures are likely to be well within a nano-size range, thus possibly observable by means of Transmission Electron Microscopy (TEM).

4.2.2.3 Transmission Electron Microscopy (TEM)

TEM images obtained from 10-15 mM $[\text{Pt}^{\text{II}}(\text{phen})(\text{L}^1\text{-S,O})]\text{Cl}$ solutions in water and stained with uranyl acetate revealed the presence of well-defined ‘spaghetti-like’ aggregate structures with a diameter of *ca.* 20 nm, as shown in Figure 4.12a. Similar TEM images have been obtained for the series of related highly water-soluble complexes $[\text{Pt}^{\text{II}}(\text{diimine})(\text{N,N-di}(2\text{-hydroxyethyl})\text{-N}'\text{-benzoyl-thiourea})]\text{Cl}$ from unpublished studies¹⁴, of which a representative image is shown in Figure A.38.

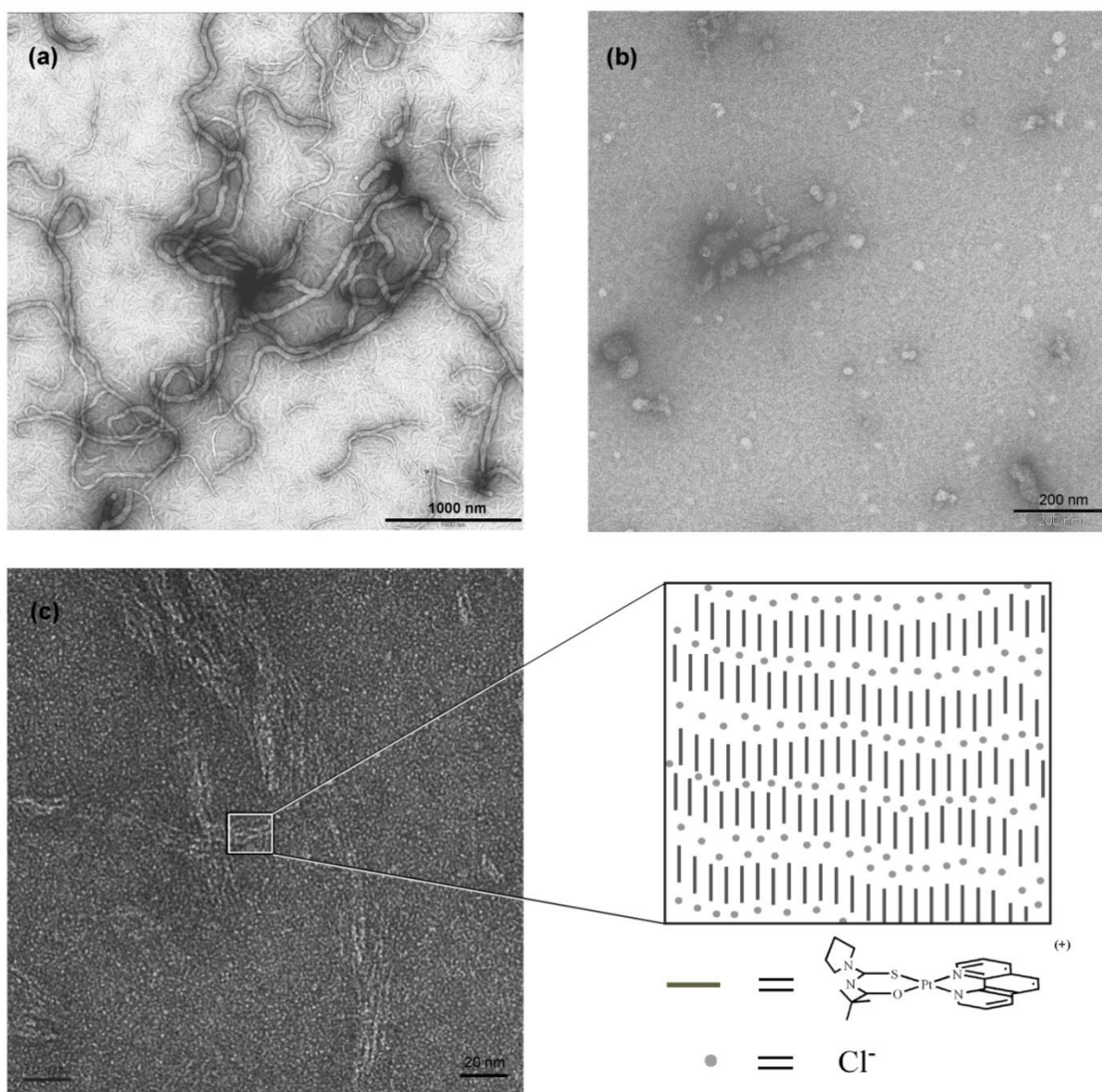


Figure 4.12 TEM image of $[\text{Pt}^{\text{II}}(\text{phen})(\text{L}^1\text{-S,O})]\text{Cl}$ in (a) water (b) acetonitrile* and (c) freshly diluted water with uranyl acetate as a stain. *Staining in acetonitrile was done with uranyl acetate in ethanol.

The maximum diameter of the spaghetti-like aggregates observed in the TEM images of $[Pt^{II}(\text{phen})(L^1-S,O)]Cl$ appears to be limited to *ca.* 20 nm, with the uranyl acetate stain accumulating at the surface/edges of these aggregates. Images obtained from $[Pt^{II}(\text{phen})(L^1-S,O)]Cl$ from pure acetonitrile solutions confirms that the extent of aggregation in such solutions is significantly less pronounced, resulting in only poorly defined irregular structures of variable and smaller average size (Figure 4.12b).

In keeping with the findings of Pianet and co-workers for the self-association of synthetic procyanidins,²⁹ solutions of $[Pt^{II}(\text{phen})(L^1-S,O)]^+$ in water also show a time dependent colloid formation process, resulting in micron-size structures from solutions of high $[Pt^{II}(\text{phen})(L^1-S,O)]^+$ concentration after aging > 7 days, as observed in TEM image shown in Figure 4.13.

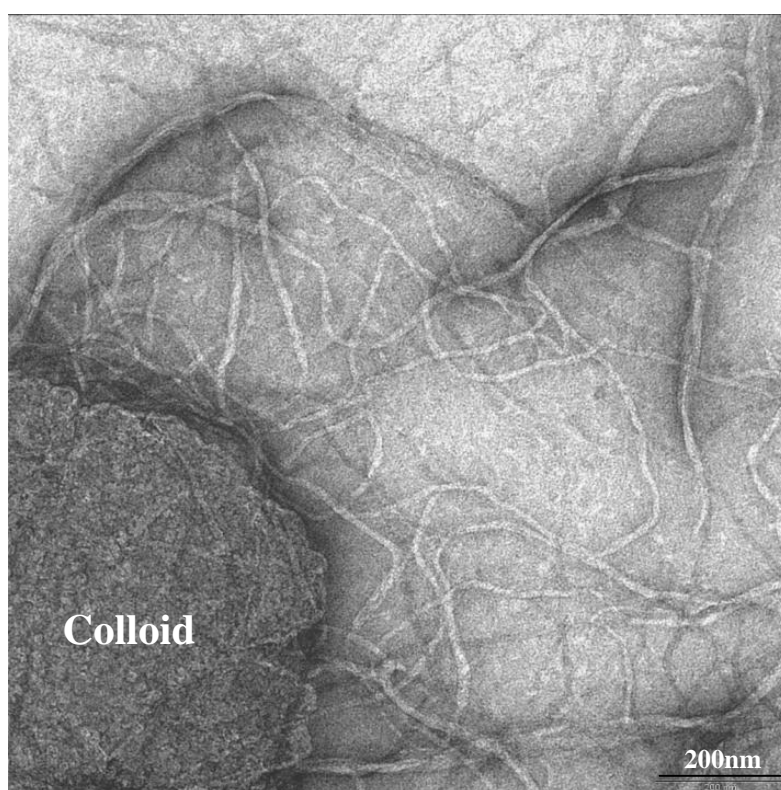


Figure 4.13 TEM images of $[Pt^{II}(\text{phen})(L^1-S,O)]Cl$ in water showing the presence of micron-size colloid particles in aged solutions (>7 days).

Preliminary Tyndall light-scattering experiments also confirm such an aging effect for concentrated solutions. Furthermore, Atomic Force Microscopy (AFM) images of a spin-

dried droplet of $[\text{Pt}^{\text{II}}(\text{phen})(\text{L}^{\text{I}}-\text{S},\text{O})]\text{Cl}$ dissolved in acetonitrile reveals the presence of micron-sized “spaghetti-like” structures, remarkably similar in overall appearance and morphology to those obtained from TEM images (Figure 4.14).

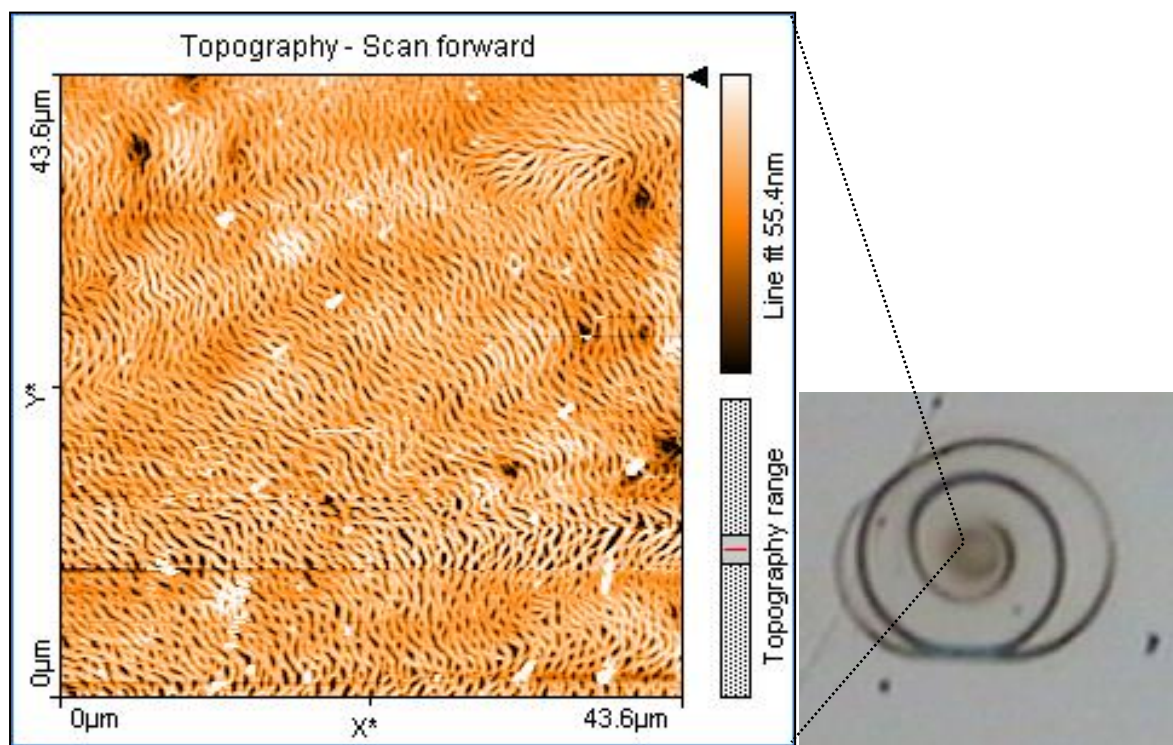


Figure 4.14 Atomic Force Microscopy (AFM) image of a spin-dried droplet of $[\text{Pt}^{\text{II}}(\text{phen})(\text{L}^{\text{I}}-\text{S},\text{O})]\text{Cl}$ in acetonitrile on a silicon oxide disk.

The possibility of a helical secondary structure was considered since the TEM images suggest that the aggregates have a distinct size and shape. High-resolution TEM of samples prepared on a carbon-coated grid immediately after dilution of a solution containing nano-aggregates at concentrations above the CAC, shows that the secondary structure appears to form from the agglomeration of ‘strands’ of $\{[\text{Pt}^{\text{II}}(\text{phen})(\text{L}^{\text{I}}-\text{S},\text{O})]^+\}_n\text{Cl}_y$ aligned parallel to one another, with a diameters of *ca.* 2 nm (Figure 4.12c and Figure 4.15). TEM images obtained for samples diluted and left to ‘age’ ($\pm 2\text{h}$) do not show any structures in the nano-range such as those that can be obtained from more concentrated freshly prepared samples. Evidently upon

dilution a type of dis-aggregation into presumably monomer and dimer species of $[\text{Pt}^{\text{II}}(\text{phen})(\text{L}^{\text{1}}-\text{S},\text{O})]\text{Cl}$ appears to take place.

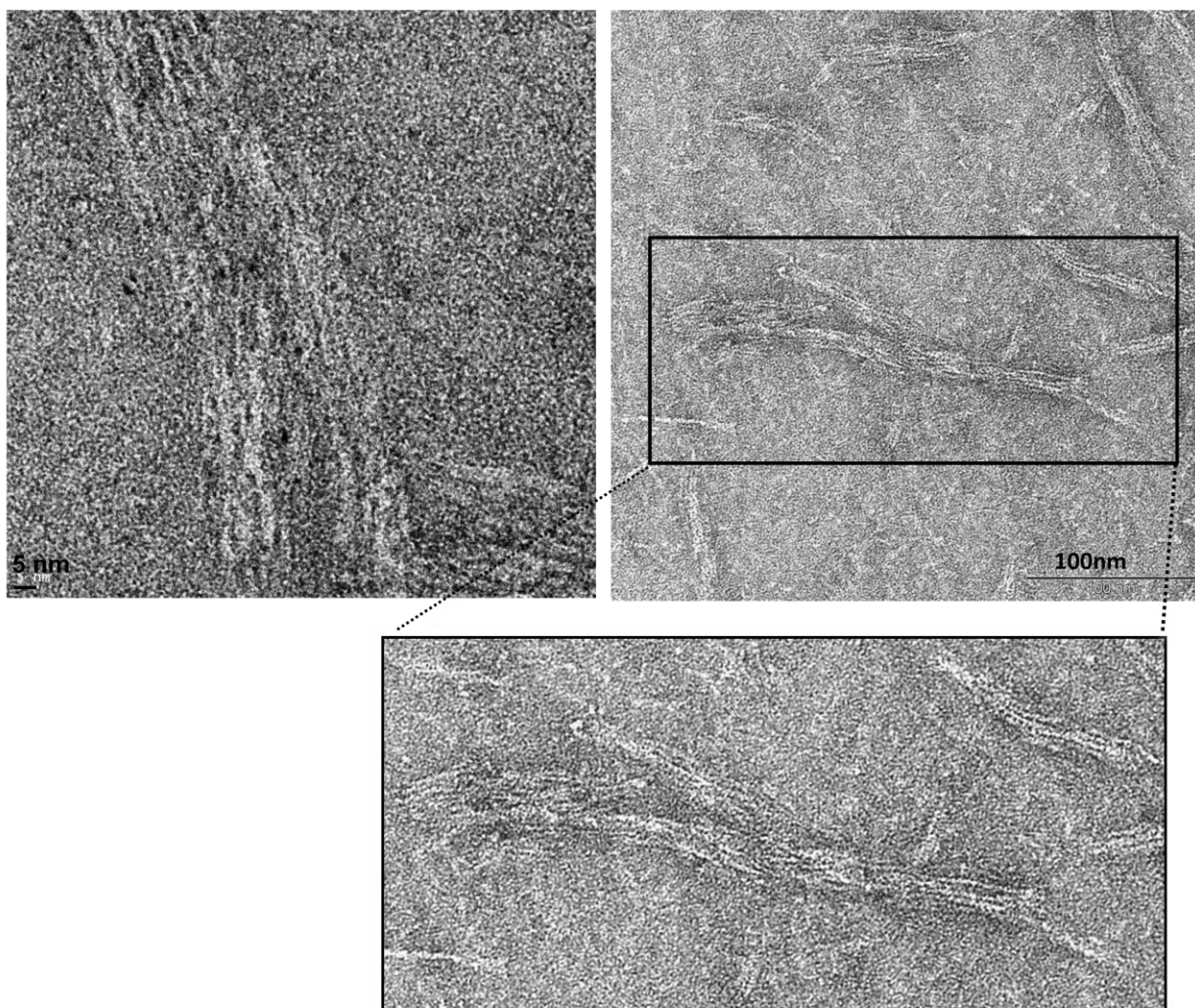


Figure 4.15 TEM images prepared from a freshly diluted sample of $[\text{Pt}^{\text{II}}(\text{phen})(\text{L}^{\text{1}}-\text{S},\text{O})]\text{Cl}$ water showing the agglomerated ‘strands’ arise from the secondary structure of the nano-sizes aggregates.

On the basis of all the experimental data, it is tempting to postulate a qualitative aggregate growth model for the non-covalent association of $[\text{Pt}^{\text{II}}(\text{phen})(\text{L}^{\text{1}}-\text{S},\text{O})]^+$ in water or water-rich solutions. The data is consistent with a *regio-specific* aggregation process of the hydrophobic planar $[\text{Pt}^{\text{II}}(\text{phen})(\text{L}^{\text{1}}-\text{S},\text{O})]^+$ cations postulated in Scheme 4.1, strongly indicating a preferred cation- π ”stacking” orientation, as also suggested in previous studies with related compounds.^{9,13} The driving force for the self-association or ”stacking” of $[\text{Pt}^{\text{II}}(\text{phen})(\text{L}^{\text{1}}-$

$\text{S},\text{O})]^+$ is most likely the result of a combination of cation- π interactions accentuated by hydrophobic effects. Despite numerous efforts, suitable single crystals for x-ray diffraction analysis could not be obtained.

An estimation of the approximate dimensions of the planar $[\text{Pt}^{\text{II}}(\text{phen})(\text{L}^1\text{-S},\text{O})]^+$ cation from data obtained from crystal structures of the related $[\text{Pt}^{\text{II}}(\text{en})(\text{phen})]\text{Cl}_2$ ³⁴ and *cis*- $[\text{Pt}^{\text{II}}(\text{L}^1\text{-S},\text{O})_2]$ ³⁵ complexes yields a diameter of *ca.* 1.5 ± 0.2 nm, suggesting that a single ‘strand’ of $[\text{Pt}^{\text{II}}(\text{phen})(\text{L}^1\text{-S},\text{O})]^+$ in a parallel co-planar stacking arrangement does not completely account for the *ca.* 20 nm nano-sized “spaghetti-like” structures observed in the TEM images. It is therefore postulated that the nano-aggregates form by means of agglomeration of single strands of presumably individually stacked $[\text{Pt}^{\text{II}}(\text{phen})(\text{L}^1\text{-S},\text{O})]^+$ cations in an offset cation- π arrangement, most probably stabilized by negatively charged chloride counter ions which may coil into the tube-like super-structures observed in Figure 4.12c and Figure 4.15. The aggregation of the individual strands of co-planar cation- π stacked complexes may be facilitated by the chloride counter ion layers around the strands to form a positively charged “core” and a negatively charged outer layer of chloride ions to which the next positively charged strand may align due to electrostatic attractions. The overall diameter of the observed tube-like structures in TEM images is limited to ± 20 nm in diameter. The apparent preferred accumulation of the cationic uranyl stain on the outer surface of the nano-structures in the TEM images is consistent with the aggregate formation model postulated here, in which the uranyl cations ion-pair with a negatively charged chloride ‘layer’ on the surface of the “stacked” cations $[\text{Pt}^{\text{II}}(\text{phen})(\text{L}^1\text{-S},\text{O})]^+$.

4.3 Hetero-association of $[\text{Pt}^{\text{II}}(\text{phen})(\text{L}^1\text{-S},\text{O})]^+$ and pyrene

The self-association of $[\text{Pt}^{\text{II}}(\text{phen})(\text{L}^n\text{-S},\text{O})]^+$ the hetero-association of $[\text{Pt}^{\text{II}}(\text{phen})(\text{L}^n\text{-S},\text{O})]^+$ with the polyaromatic hydrocarbon pyrene ($\text{C}_{16}\text{H}_{10}$) was investigated in view of the cation- π and aromatic- π stacking capabilities of the $[\text{Pt}^{\text{II}}(\text{phen})(\text{L}^1\text{-S},\text{O})]^+$ complex in acetonitrile. ^1H and DOSY NMR were used to probe this phenomenon and the results compared to a previous study of the hetero-association of $[\text{Pt}^{\text{II}}(\text{phen})(\text{L}^1\text{-S},\text{O})]^+$ with the fluoranthene studied only by ^1H NMR.^{13,36} The complexes $[\text{Pt}^{\text{II}}(\text{phen})(\text{L}^1\text{-S},\text{O})]^+$, $[\text{Pt}^{\text{II}}(\text{bipy})(\text{L}^1\text{-S},\text{O})]^+$ and $[\text{Pt}^{\text{II}}(\text{bipy})(\text{L}^2\text{-S},\text{O})]^+$ was considered but the hetero-association of $[\text{Pt}^{\text{II}}(\text{phen})(\text{L}^1\text{-S},\text{O})]^+$ and pyrene was chosen to be studied in some detail.

Preliminary work showed significant changes in the ^1H NMR chemical shifts of the three mentioned complexes upon addition of pyrene to an acetonitrile solution containing arbitrary concentrations of the Pt complexes. Interestingly, $[\text{Pt}^{\text{II}}(\text{bipy})(\text{L}^2\text{-S,O})]^+$ exhibits significant broadening of the ^1H NMR signals of the coordinated bipy immediately after the addition of pyrene as shown in Figure 4.16. This broadening was also observed for $[\text{Pt}^{\text{II}}(\text{bipy})(\text{L}^1\text{-S,O})]^+$, but to a lesser extent, while $[\text{Pt}^{\text{II}}(\text{phen})(\text{L}^1\text{-S,O})]^+$ exhibits only chemical shift changes. Therefore, the ^1H NMR spectrum of $[\text{Pt}^{\text{II}}(\text{bipy})(\text{L}^2\text{-S,O})]^+$ was acquired with a pre-acquisition delay after mixing $[\text{Pt}^{\text{II}}(\text{bipy})(\text{L}^2\text{-S,O})]^+$ and pyrene at -6°C (Figure 4.16).

The ^1H NMR spectrum of the mixture in acetonitrile- d_3 was acquired at time intervals of 5 minutes after the addition of pyrene to investigate possible kinetic effects or high-order aggregation (Figure 4.16).

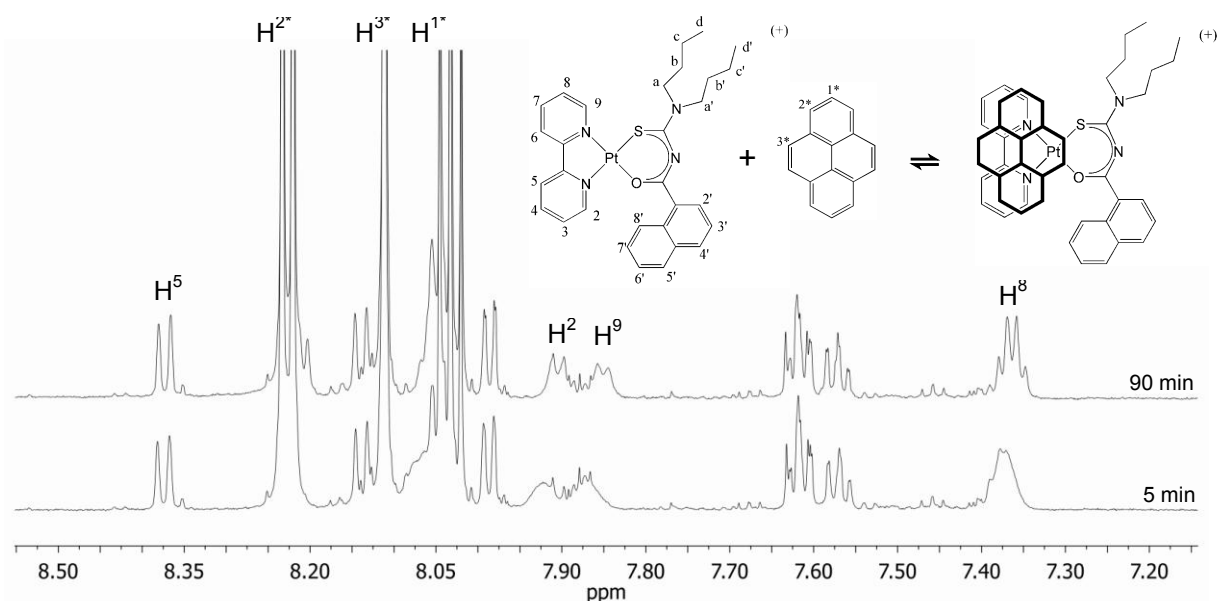


Figure 4.16 ^1H NMR spectra of $[\text{Pt}^{\text{II}}(\text{bipy})(\text{L}^2\text{-S,O})]\text{Cl}$ (6.5 mM, 0.7ml) in acetonitrile- d_3 upon addition of pyrene (3.9 mg). ^1H NMR of $[\text{Pt}^{\text{II}}(\text{phen})(\text{L}^1\text{-S,O})]^+$ and pyrene at -6°C in acetonitrile- d_3 straight after mixing (bottom) and 90 min after mixing (top). ($n_{\text{Pt}}:n_{\text{Pyr}} = 1:4.25$)

A significant increase in resolution of the ^1H NMR peaks was observed for the spectrum acquired 90 min after mixing, with no additional broadening thereafter. This broadening is clearly due to slow kinetics of the aggregation of $[\text{Pt}^{\text{II}}(\text{bipy})(\text{L}^2\text{-S,O})]^+$ and pyrene and not

large aggregate formation (with slow molecular correlation time) since the signals resolve with time.

However, even at $-6\text{ }^\circ\text{C}$ the line-broadening effect was too small to estimate reliable rate constants for the proposed hetero-association. It is reasonable to exclude insufficient mixing of the sample as a reason for the broad lines since this will affect all Hs of the same molecule and broadening was only observed for the 2,2'-bipyridyl protons and not for the coordinated L^2 . Furthermore, insufficient mixing would probably result in an oriented phase in the NMR experiment as shown in Figure A.35 for a freshly made sample of $[\text{Pt}^{\text{II}}(\text{phen})(\text{L}^1\text{-S,O})]^+$ which was not mixed sufficiently, which appears rather different.

The hetero-association was found to be significantly slower for $[\text{Pt}^{\text{II}}(\text{bipy})(\text{L}^2\text{-S,O})]^+$ and $[\text{Pt}^{\text{II}}(\text{bipy})(\text{L}^1\text{-S,O})]^+$ compared to $[\text{Pt}^{\text{II}}(\text{phen})(\text{L}^1\text{-S,O})]^+$. With the primary focus on the extent of aggregation and the additional complication with the slow kinetic phenomenon here, it was found to be more practical to investigate the reaction/association of $[\text{Pt}^{\text{II}}(\text{phen})(\text{L}^1\text{-S,O})]^+$ and pyrene at equilibrium in detail. The ^1H NMR spectra of a mixture of 5.0 mM $[\text{Pt}^{\text{II}}(\text{phen})(\text{L}^1\text{-S,O})]^+$ and various amounts of pyrene is shown in Figure 4.17.

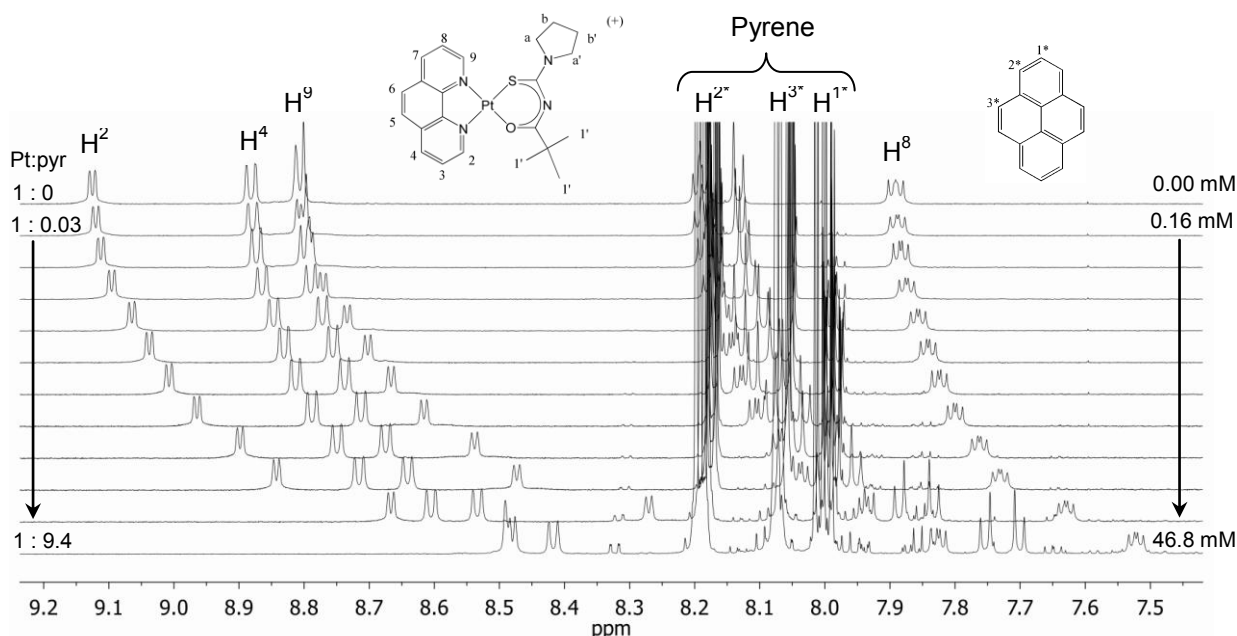


Figure 4.17 ^1H NMR spectra of a $[\text{Pt}^{\text{II}}(\text{phen})(\text{L}^1\text{-S,O})]\text{Cl}$ (5.0 mM) and pyrene mixture in acetonitrile- d_3 at 25°C as a function of the pyrene concentration.

The significant changes in the shielding as reflected by the chemical shift of the phen protons of $[\text{Pt}^{\text{II}}(\text{phen})(\text{L}^1-\text{S},\text{O})]^+$ are observed, in particular for H^2 and H^9 ($\Delta\delta = 0.63$ and 0.65 ppm respectively) are remarkable. The shielding of H^2 was used to 'probe' the proposed hetero-association between $[\text{Pt}^{\text{II}}(\text{phen})(\text{L}^1-\text{S},\text{O})]^+$ and pyrene, in view of its sensitivity to pyrene concentration and this resonance does not overlap with the pyrene ^1H resonances. A previous study of the hetero-association between $[\text{Pt}^{\text{II}}(\text{phen})(\text{L}^1-\text{S},\text{O})]^+$ and fluoranthene revealed a 1:1 aggregate of $[\text{Pt}^{\text{II}}(\text{phen})(\text{L}^1-\text{S},\text{O})]^+$ and fluoranthene in acetonitrile solutions which is expected to be similar for pyrene.^{13,36} an attempt was made to fit a 1:1 aggregation model to $\delta(\text{H}^2)$ data while taking the non-covalent dimerisation of $[\text{Pt}^{\text{II}}(\text{phen})(\text{L}^1-\text{S},\text{O})]^+$ into account. These simultaneous equilibria can be expressed by the following equations,



where, P = pyrene monomer, P_2 = pyrene 'dimer', M = $[\text{Pt}^{\text{II}}(\text{phen})(\text{L}^1-\text{S},\text{O})]^+$, MP = $[\text{Pt}^{\text{II}}(\text{phen})(\text{L}^1-\text{S},\text{O})]^+$ /pyrene dimer, $\text{M}_2 = \{[\text{Pt}^{\text{II}}(\text{phen})(\text{L}^1-\text{S},\text{O})]^+\}_2$ and K = the association constants of the respective reactions. The self-association of pyrene was taken to be negligible within the concentration range used since very small chemical shift and diffusion coefficient dependence on concentration were observed (Figure 4.18).

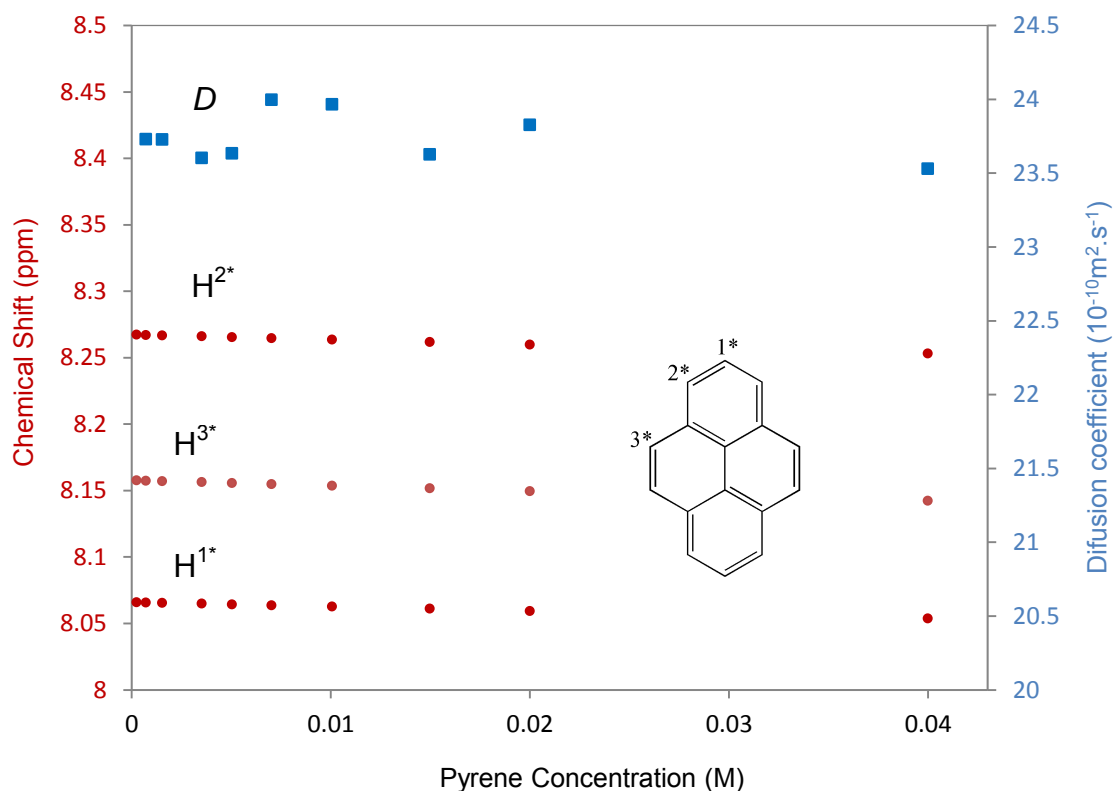


Figure 4.18 ^1H NMR chemical shifts and diffusion coefficient of pyrene in acetonitrile- d_3 as a function of pyrene concentration.

The diffusion coefficients obtained from the ^1H DOSY show large degree of scatter in the data. This was a result of the system struggling to lock properly during the pulsed field gradient experiment (PFGE) for all solutions containing pyrene. The peak shape was significantly compromised by this problem, especially with an increase in gradient strength; this problem could be an instrumental problem on the system, but has not been resolved. The problem was minimised using a maximum lock power with the best results shown in Figure 4.19.

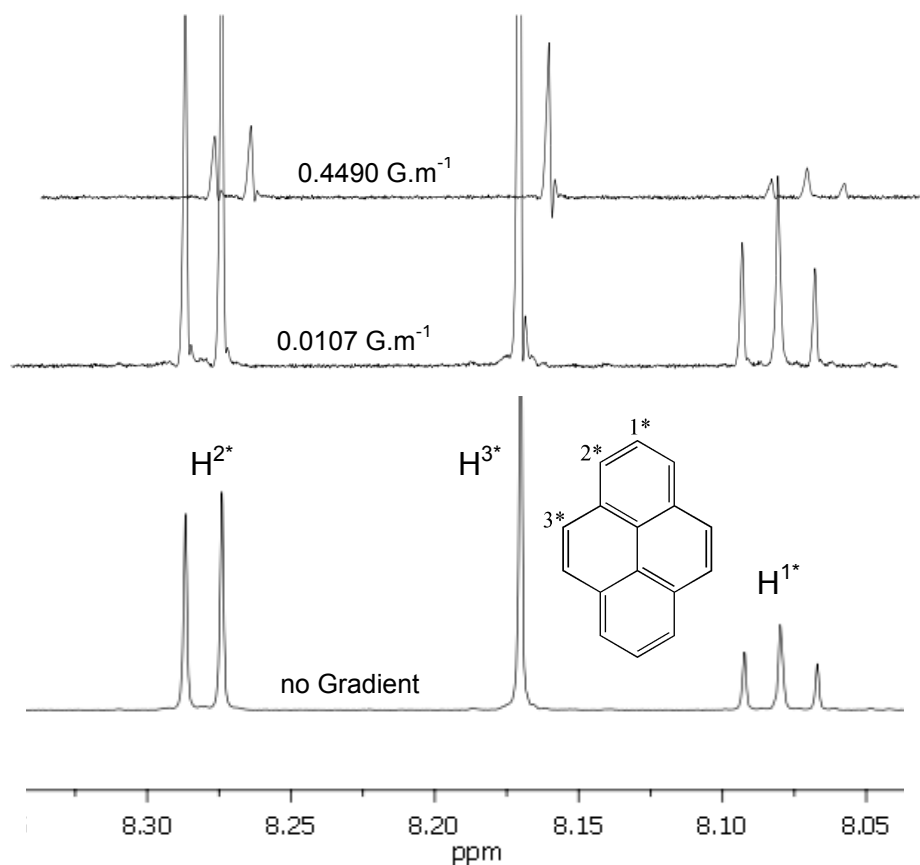


Figure 4.19 ^1H DOSY spectrum of pyrene with variation of gradient strength.

Various post acquisition processing methods were tried including line-broadening, FIDDLE (line-shape correction algorithm) and absolute value phasing without reliable diffusion coefficients measured. The diffusion coefficients obtained for $[\text{Pt}^{\text{II}}(\text{phen})(\text{L}^1\text{-S,O})]^+$ at various pyrene concentrations are shown in Figure 4.20. These data were obtained using absolute value phasing and an exponential line broadening of 1 Hz. Considerable scattering of the data suggests large errors in the measurements as a result of the lock problem discussed earlier. Notwithstanding these difficulties, a marked decrease in the diffusion coefficient of $[\text{Pt}^{\text{II}}(\text{phen})(\text{L}^1\text{-S,O})]^+$ is observed as the pyrene concentration increases. This is indicative of increase in molecular size as the equilibrium shifts towards more $[\text{Pt}^{\text{II}}(\text{phen})(\text{L}^1\text{-S,O})]^+$ /pyrene aggregate formation.

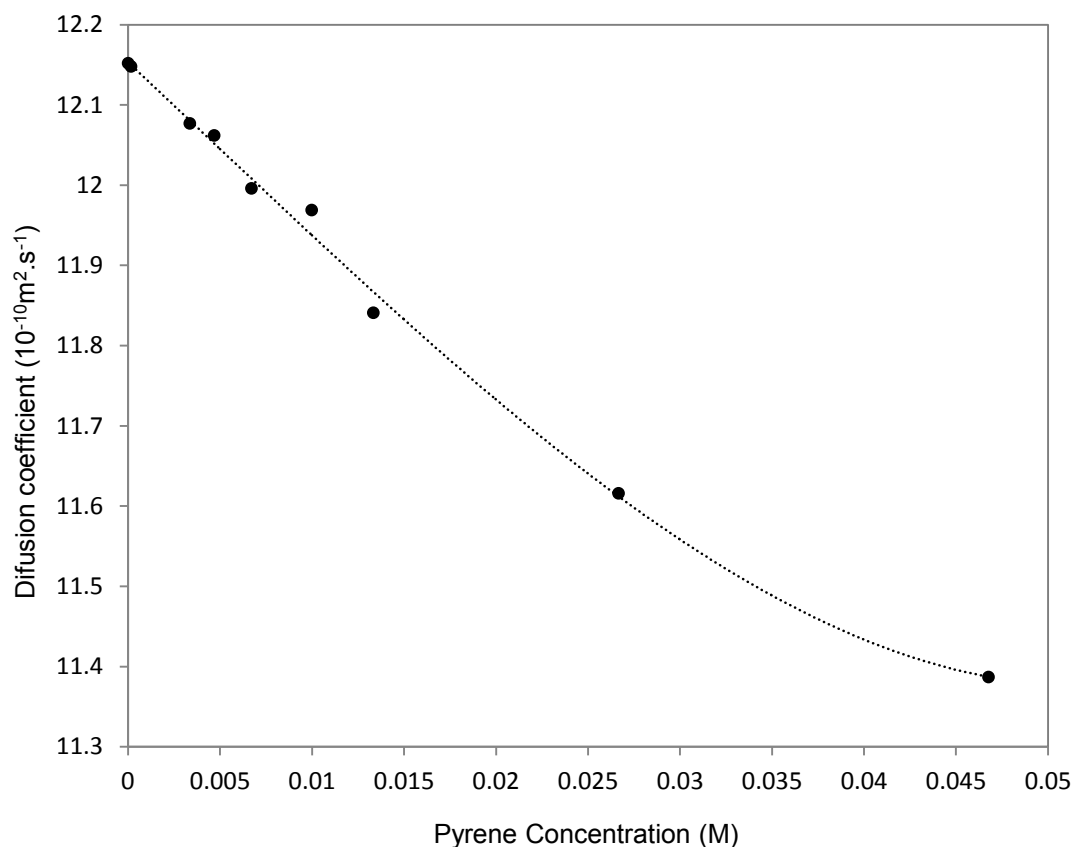


Figure 4.20 Diffusion coefficient of $[\text{Pt}^{\text{II}}(\text{phen})(\text{L}^1\text{-S,O})]^+$ (5.0 mM) as a function of pyrene concentration. (dashed line only aid in trend visualization)

Trends in diffusion coefficients were previously used to calculate the dimerisation constant of $[\text{Pt}^{\text{II}}(\text{phen})(\text{L}^1\text{-S,O})]^+$ in acetonitrile- d_3 with results close to the K_{D} calculated from the ^1H NMR chemical shift data ($\delta(^1\text{H})$).¹³ The large scatter in the diffusion data for $[\text{Pt}^{\text{II}}(\text{phen})(\text{L}^1\text{-S,O})]^+$ as a function of pyrene concentration does not allow for reliable calculation of the association constant of $[\text{Pt}^{\text{II}}(\text{phen})(\text{L}^1\text{-S,O})]^+$ and pyrene. Therefore, the dependence of the ^1H NMR chemical shift of H^2 , $\delta(\text{H}^2)$, on the concentration of pyrene was employed to probe the aggregation phenomenon. A series of solutions containing 5.0 mM $[\text{Pt}^{\text{II}}(\text{phen})(\text{L}^1\text{-S,O})]^+$ and various amounts of pyrene in acetonitrile- d_3 was prepared after which the ^1H NMR spectra were acquired at various temperatures. Excellent agreement between the experimental data and 1:1 $[\text{Pt}^{\text{II}}(\text{phen})(\text{L}^1\text{-S,O})]^+$ to pyrene model in conjunction with the known dimerisation of $[\text{Pt}^{\text{II}}(\text{phen})(\text{L}^1\text{-S,O})]^+$ was obtained (Figure 4.21).

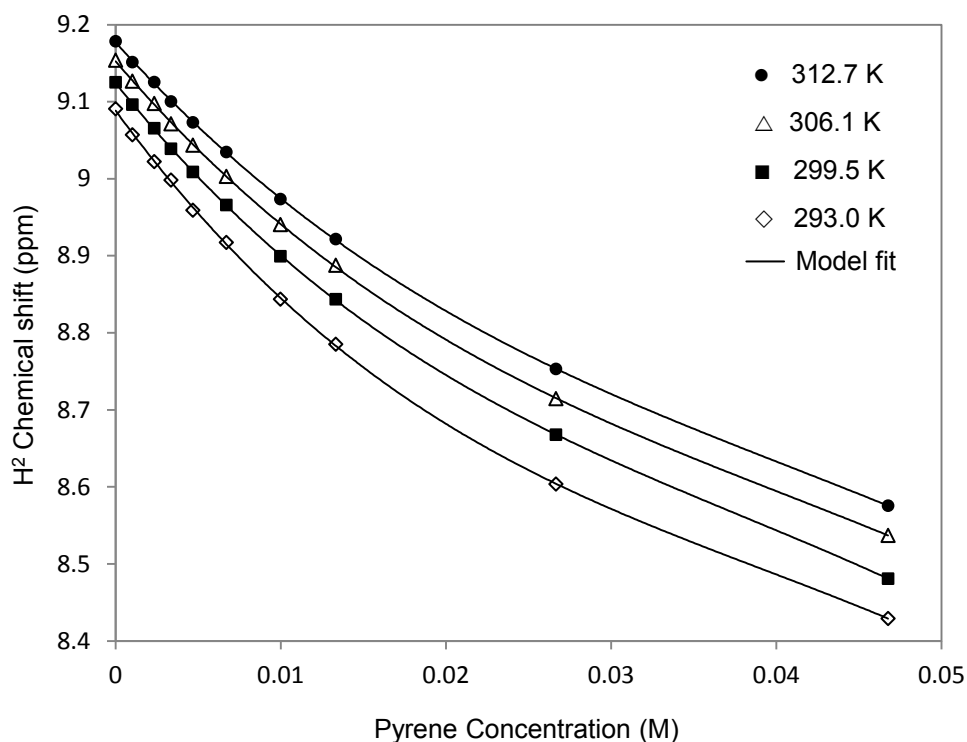


Figure 4.21 H^2 chemical shift dependence on pyrene concentration at temperatures 293.0 - 312.7 K.

The excellent fit of the multiple equilibria $2\text{M} \rightleftharpoons \text{M}_2$ (4.12) and $\text{M} + \text{P} \rightleftharpoons \text{MP}$ (4.13) to the chemical shift data of H^2 allows for the calculation of the association constant K_B . The calculated association constant for the 1:1 $[\text{Pt}^{\text{II}}(\text{phen})(\text{L}^1\text{-S,O})]^+$ /pyrene aggregation (K_B) at various temperatures could be used to calculate the reaction enthalpy ($\Delta_r\text{H}$), entropy ($\Delta_r\text{S}$) and the standard reaction Gibbs energy ($\Delta_r\text{G}$) using the Van't Hoff equation (4.1). The Van't Hoff plot will only be linear if the model used to calculate the equilibrium constants is accurate. Therefore, the linear trend observed in the Van't Hoff plot further validates the model used. The Van't Hoff plot of the two simultaneous reactions (4.12) and (4.13) as well as the hetero-association constant of $[\text{Pt}^{\text{II}}(\text{phen})(\text{L}^1\text{-S,O})]^+$ and fluoranthene ($\text{M} + \text{F} \rightleftharpoons \text{MF}$)¹³ are shown in Figure 4.22.

The linear relationship observed for the 1:1 $[\text{Pt}^{\text{II}}(\text{phen})(\text{L}^1\text{-S,O})]^+$ /pyrene aggregation model (4.13) validates the model used with close resemblance to the $[\text{Pt}^{\text{II}}(\text{phen})(\text{L}^1\text{-S,O})]^+$ /fluoranthene data. This is also reflected in the thermodynamic data calculated from the Van't Hoff plot as summarised in Table 4.5.

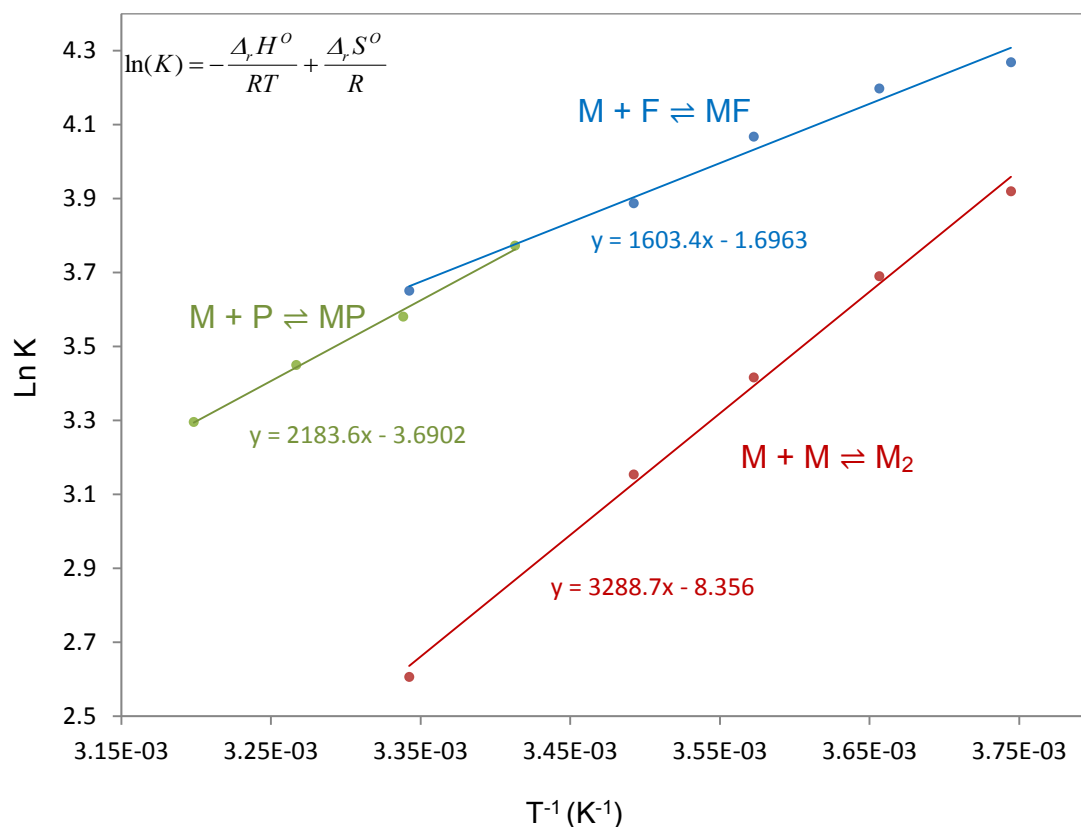


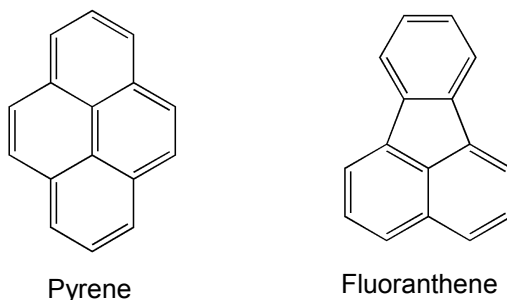
Figure 4.22 Van't Hoff plot for the self-association and hetero-association of $[\text{Pt}^{\text{II}}(\text{phen})(\text{L}^1\text{-S},\text{O})]^+$ with pyrene and fluoranthene¹³ in acetonitrile- d_3 .

Table 4.5 Thermodynamic data for the self- and hetero-association of $[\text{Pt}^{\text{II}}(\text{phen})(\text{L}^1\text{-S},\text{O})]^+$ (M) with pyrene (P) and fluoranthene (F) in acetonitrile- d_3 .

Temp / K	K_B / M^{-1}	$\Delta_r H^0 / \text{kJ}\cdot\text{mol}^{-1}$	$\Delta_r S^0 / \text{J}\cdot\text{mol}^{-1}\cdot\text{K}^{-1}$	$\Delta_r G^0 / \text{J}\cdot\text{mol}^{-1}$
293.0	43.5 (± 5)	-18.2 (± 3)	-31 (± 11)	-9166
299.5	35.9 (± 4)			-8965
306.1	31.5 (± 4)			-8764
312.7	27.0 (± 3)			-8562
M + M \rightleftharpoons M₂¹³				
298.15	14.5	-25.1 (± 3)	-69 (± 11)	-6630
M + P \rightleftharpoons MP				
298.15	37.9	-18.1 (± 3)	-31 (± 10)	-9008
M + F \rightleftharpoons MF¹³				
298.15	39.7	-13.3 (± 3)	-14 (± 9)	-9126

The $[\text{Pt}^{\text{II}}(\text{phen})(\text{L}^1\text{-S},\text{O})]^+$ /pyrene aggregation significantly increases as the temperature decreases. The aggregation reaction is spontaneous ($\Delta_r G < 0$) and clearly enthalpy driven

since $\Delta_r H \gg \Delta_r S$. Interestingly, the hetero-association is energetically more favourable ($\Delta_r G = -9.0 \text{ kJ}\cdot\text{mol}^{-1}$ at 25°C) compared to the self-association of $[Pt^{II}(\text{phen})(L^1-S,O)]^+$ ($\Delta_r G = -6.6 \text{ kJ}\cdot\text{mol}^{-1}$ at 25°C). It is reasonable to argue that the charge repulsion in the self-association of $[Pt^{II}(\text{phen})(L^1-S,O)]^+$ would be less favourable than the aggregation of the neutral pyrene and the cation complex. The association constant (K_B) estimated for the hetero-association of $[Pt^{II}(\text{phen})(L^1-S,O)]^+$ and pyrene are within experimental error of the constant obtained for the $[Pt^{II}(\text{phen})(L^1-S,O)]^+$ /fluoranthene aggregation. However, the reaction enthalpy ($\Delta_r H$) and entropy ($\Delta_r S$) is significantly different for the two hetero-association reactions. Pyrene forms a stronger 1:1 aggregate with $[Pt^{II}(\text{phen})(L^1-S,O)]^+$ with the corresponding $\Delta_r H_{(M/P)} = -18.1 \pm 3 \text{ kJ}\cdot\text{mol}^{-1}$ compared to $\Delta_r H_{(M/F)} = -13.3 \pm 3 \text{ kJ}\cdot\text{mol}^{-1}$ calculated for the $[Pt^{II}(\text{phen})(L^1-S,O)]^+$ /fluoranthene aggregation. This is expected since pyrene has a large aromatic π -surface while fluoranthene has two π -systems.



Scheme 4.4 The molecular structure of pyrene (with one π -system) and fluoranthene (two π -ring systems)

Pyrene with the larger π -surface is expected to form a 'stronger' aggregate *via* cation- π interaction with the Pt metal centre and has better π -stacking capabilities with the bound 1,10-phenanthroline ligand compared to fluoranthene. However, the reaction entropy for the $[Pt^{II}(\text{phen})(L^1-S,O)]^+$ /pyrene association is more negative $\Delta_r S_{(M/P)} = -31 \pm 10 \text{ J}\cdot\text{mol}^{-1}\cdot\text{K}^{-1}$ compared to fluoranthene, $\Delta_r S_{(M/F)} = -14 \pm 9 \text{ J}\cdot\text{mol}^{-1}\cdot\text{K}^{-1}$. This difference in reaction entropy is the reason for the similar association constants obtained for $M + P \rightleftharpoons MP$ and $M + F \rightleftharpoons MF$ although pyrene forms the stronger 1:1 aggregate with $[Pt^{II}(\text{phen})(L^1-S,O)]^+$. The negative reaction entropy ($\Delta_r S$) is indicative of an association reaction and the positive contribution ($\Delta\Delta_r S > 0$) to the $\Delta_r S$ of the association of $[Pt^{II}(\text{phen})(L^1-S,O)]^+$ and fluoranthene ($M + F \rightleftharpoons MF$) relative to $M + P \rightleftharpoons MP$, could be attributed to fluoranthene being more solvated than pyrene in acetonitrile. This would result in more solvent molecules being released upon aggregate formation for fluoranthene/ $[Pt^{II}(\text{phen})(L^1-S,O)]^+$ compared to pyrene/ $[Pt^{II}(\text{phen})(L^1-S,O)]^+$ which would be a positive contribution to the overall negative $\Delta_r S$.

The aggregate structure between pyrene and $[\text{Pt}^{\text{II}}(\text{phen})(\text{L}^1\text{-S,O})]^+$ could be elucidated using the variation in ^1H chemical shift concentration dependence observed for the $[\text{Pt}^{\text{II}}(\text{phen})(\text{L}^1\text{-S,O})]^+$ and pyrene. Figure 4.23 shows the ^1H chemical shift dependence of $[\text{Pt}^{\text{II}}(\text{phen})(\text{L}^1\text{-S,O})]^+$ and pyrene on pyrene concentration.

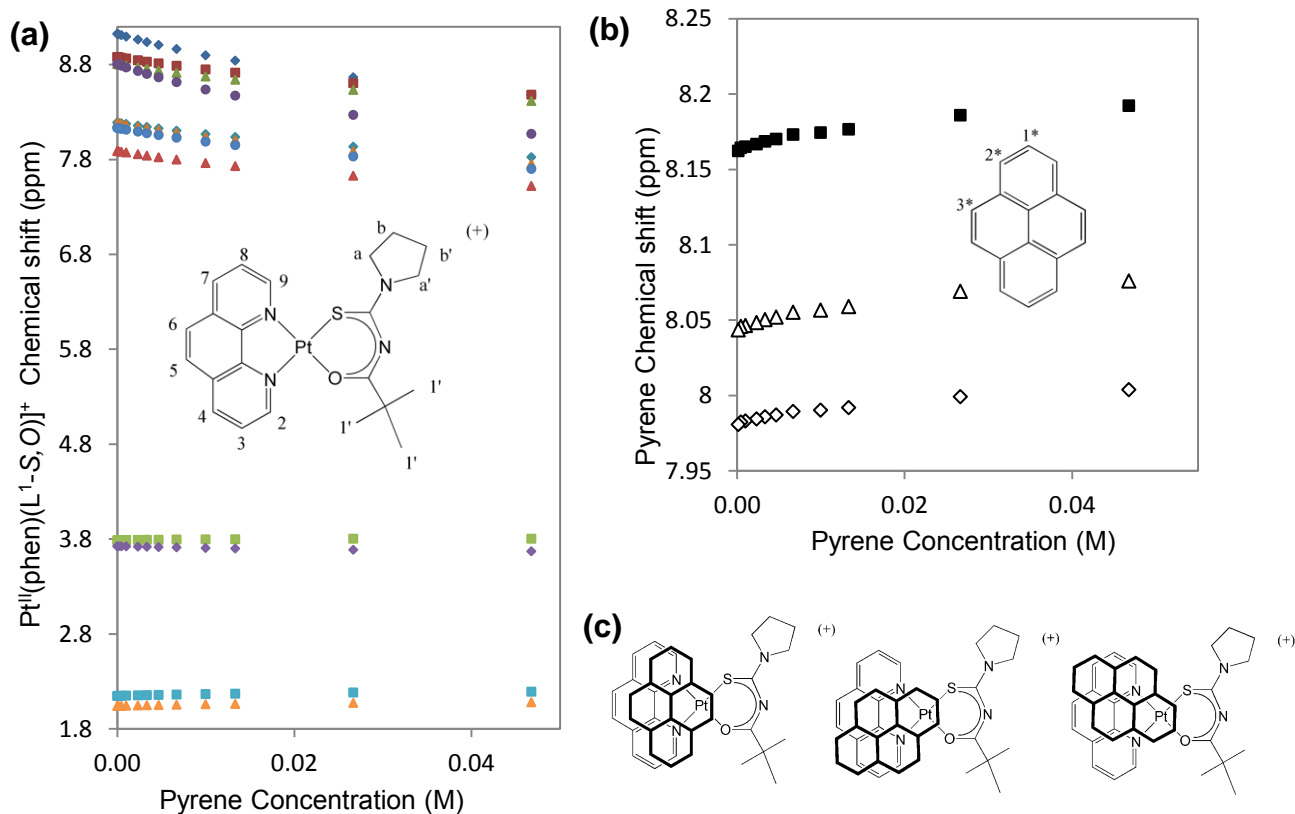


Figure 4.23 ^1H NMR chemical shift dependence of (a) $[\text{Pt}^{\text{II}}(\text{phen})(\text{L}^1\text{-S,O})]^+$ and (b) pyrene as a function of pyrene concentration in a 5.0 mM solution of $[\text{Pt}^{\text{II}}(\text{phen})(\text{L}^1\text{-S,O})]\text{Cl}$ at 25°C. (c) The proposed 1:1 aggregate structures of $[\text{Pt}^{\text{II}}(\text{phen})(\text{L}^1\text{-S,O})]^+$ /pyrene in solution.

Significant changes in the $\delta(^1\text{H})$ of phen protons are observed while the L^1 protons exhibit almost no dependence of $\delta(^1\text{H})$ on pyrene concentration. All the protons of pyrene show more or less the same degree of shift dependence, suggesting that the whole molecule π -stacks and/or form cation- π interactions with $[\text{Pt}^{\text{II}}(\text{phen})(\text{L}^1\text{-S,O})]^+$. The chemical shift concentration dependence of H^2 and H^9 shows that these protons are the most affected by the addition of pyrene to the solution which suggests that the pyrene interacts with $[\text{Pt}^{\text{II}}(\text{phen})(\text{L}^1\text{-S,O})]^+$ in such a way that these protons are the most shielded by the pyrene molecule with the proposed aggregate structures shown in Figure 4.23.

4.4 Conclusions

$[Pt^{II}(\text{phen})(L^1-S,O)]^+$ cations (M^+) ‘self-associate’ by non-covalent intermolecular cation- π interactions in acetonitrile solutions and water-acetonitrile mixtures of up to 30% (v/v) $D_2O:CD_3CN$ to form essentially dimer aggregates according to the $2M^+ \rightleftharpoons \{M^+\}_2$ model. This process is strongly favoured in more polar water-rich solutions ($\Delta_r G^0_{CD_3CN} = -7.0 \text{ kJ}\cdot\text{mol}^{-1}$; $\Delta_r G^0_{30\%D_2O:CD_3CN} = -10.4 \text{ kJ}\cdot\text{mol}^{-1}$), with the corresponding K_D increasing from 17 ± 2 to $72 \pm 8 \text{ M}^{-1}$ at 299.3 K from acetonitrile to 30% $D_2O:CD_3CN$ mixtures. The experimental data obtained suggest that the primary driving force for such phenomena is consistent with mainly cation- π stacking interactions, with the increase in the K_D attributed to a favourable contribution to a negative $\Delta_r S^0$ as a result of the “hydrophobicity” of the quasi-aromatic nature of these complex cations. Increasing the water content from > 30% to 100% (v/v) $D_2O:CD_3CN$, results in a significant increase in the extent of aggregation as a function of the $[Pt^{II}(\text{phen})(L^1-S,O)]Cl$ concentration, culminating in the formation of nano-sized structures (“metallogeles”) consisting of up to *ca.* 735 mononuclear cations, as estimated by diffusion coefficients obtained by means of DOSY NMR spectroscopy, above a critical aggregation concentration (9.6 - 10.3 mM at 299.3K). Experimental data suggests that in water, excessive positive electrostatic charge build-up in such structures may be partially offset by extensive cation- π interactions as well as by ion-pairing with Cl^- anions. Uranyl acetate stained TEM images from freshly prepared samples of $[Pt^{II}(\text{phen})(L^1-S,O)]Cl$ and the related $[Pt^{II}(\text{diimine})(N,N\text{-di}(n\text{-butyl})\text{-}N'\text{-benzoylthiourea})]Cl$ compounds,¹⁴ provides convincing visual confirmation of the formation of extensive spaghetti-like structures, *ca.* 20 nm in diameter.

The $[Pt^{II}(\text{diimine})(L^n-S,O)]^+$ complexes showed significant interaction with pyrene in acetonitrile. The $[Pt^{II}(\text{phen})(L^1-S,O)]^+$ cation in particular, forms non-covalent 1:1 aggregates with pyrene ($C_{16}H_{10}$) with association constants (37.9 M^{-1} at 298.15 K) similar to what was observed for fluoranthene (39.7 M^{-1} at 298.15 K). Pyrene was found to form a tighter 1:1 aggregate with $[Pt^{II}(\text{phen})(L^1-S,O)]^+$ with the corresponding $\Delta_r H_{(M/P)} = -18.1 \pm 3 \text{ kJ}\cdot\text{mol}^{-1}$ compared to fluoranthene ($\Delta_r H_{(M/F)} = -13.3 \pm 3 \text{ kJ}\cdot\text{mol}^{-1}$), which is postulated to be due to the larger aromatic π -surface of pyrene potentially forming a tighter cation- π interaction with the $[Pt^{II}(\text{phen})(L^1-S,O)]^+$ cation. This relatively strong association of $[Pt^{II}(\text{phen})(L^1-S,O)]^+$ with pyrene and fluoranthene suggests that this class of complexes may form non-covalent interactions with haematin, which has a significant π -surface from the porphyrin ligand. This interaction is expected to result in β -haematin inhibition as discussed in the next chapter.

4.5 Experimental Section

4.5.1.1 Computational Methods

1H NMR as well as 1H DOSY data were used to probe the solution behaviour of $[Pt^{II}(\text{phen})(L^1-S,O)]Cl$ and pyrene. Using the average observed 1H chemical shift (δ_{obs}) or diffusion coefficient (D_{obs}), equations 4.14 and 4.15 (where α_i = mole fraction of species i), the reactions defined in the text the equilibrium constant(s), K_i , and chemical shifts, δ_i , of individual species (monomers, dimer aggregates, trimer aggregates, ion-pairs, etc) were calculated.

$$D_{obs} = \sum_{i=n} \alpha_i D_i \quad (4.14)$$

$$\delta_{obs} = \sum_{i=n} \alpha_i \delta_i \quad (4.15)$$

This particular type of non-linear least squares optimisation calculation can be solved in several ways.³⁷ A program called, DIMER- K_D , written by Koch and co-workers was used to fit data with a dimerization model⁹ (the program utilizes the algorithm by Horman and co-workers¹⁰). When dealing with multiple equilibria, the program Dynafit version 3 was used.³⁸ However, Dynafit version 3 uses the concentration of the species, c_i and not mole fraction in the mass balance equations and signal response calculations. This can be corrected by multiplying equation 3.5 with the total concentration, C_T , of the reagent which results in equation 4.16:

$$C_T \delta_{obs} = \sum_{i=n} c_i \delta_i \quad (4.16)$$

With these signal responses, the association constants could be calculated. The dimer model fitted with the program DIMER- K_D can be explained as follows:

The dimerisation reaction with M the monomer and M_2 representing the dimer can be expressed by eq 4.17 with the dimerisation constant K_D defined by equation 4.18.



$$K_D = [M_2] / [M]^2 \quad (4.18)$$

where $[M]$ is monomer concentration, $[M_2]$ the dimer concentration, $[M]_0$ the total concentration. The total concentration, $[M]_0$, can be expressed by equation 4.19:

$$[M_0] = [M] + 2[M_2] \quad (4.19)$$

Combining and rearranging equations 4.18 and 4.19 result in an equation that is dependent on K_D and the mole fraction of M present as the dimer M_2 ($2[M_2] / [M]_0$):

$$\frac{1}{(2K_D[M]_0)^2} = \frac{2[M_2]}{[M]_0} + \frac{[M]_0}{2[M_2]} - 2 \quad (4.20)$$

The average signal position (δ) of the monomer and dimer due to fast exchange on the NMR time scale is the weighted average between the monomer (δ_m) and dimer chemical shifts (δ_d).

$$\delta_{obs} = \alpha_m \delta_m + \alpha_d \delta_d \quad (4.21)$$

The assumption is made that the fraction of M present as the dimer ($\alpha_d = 2[M_2] / [M]_0$) is related to the measured chemical shift δ_{obs}

$$\alpha_d = (\delta_m - \delta_{obs}) / (\delta_m - \delta_d) \quad (4.22)$$

or

$$\delta_{obs} = \delta_m - \alpha_d (\delta_m - \delta_d) \quad (4.23)$$

A straight line should be obtained for the observed chemical shift (δ_{obs}) versus the fraction of dimer present (α_d). For a series of concentrations, $[M_0]$, different sets of α_d are calculated for each K_D . The value of K_D is varied and the final K_D value is defined as the best straight line fit for δ_i vs α_d . K_D is calculated from equations 4.20 and 4.22 by iterating the K_D and α_d to best fit the experimental data.

4.5.2 Analytical Instrumentation

1H NMR and DOSY experiments were recorded in 5-mm tubes using a Varian Unity Inova 400 MHz spectrometer operating at 399.95 MHz or a Varian Unity Inova 600 MHz spectrometer equipped with an inverse-detection pulsed field gradient (idpfg) probe operating at 599.99 MHz. 1H NMR chemical shift referencing was done using the corresponding solvent peak with the HDO signal showing no chemical shift changes as a function of complex concentration. Diffusion coefficients were calculated using the Varian vnmrj software (version 2.1b) with a line broadening of 1.0 Hz. Experimental parameters: Pulse sequence: Dbppste_cc (Bipolar Pulse Pair Stimulated Echo with Convection Compensation),

1H spectral width: 11 ppm, number of acquisitions varied from sample, recycling delay: 2 s, diffusion delay 50 ms, Gradient-pulse duration 3.5 or 4.0 ms, 25 different values of G , the gradient magnitude, varying between 0.0107 and 0.449 Gm^{-1} calibrated using the diffusion coefficient of HDO in D_2O .³⁹ Transmission Electron Microscopy imaging was done on a Zeiss 912 OMEGA EFTEM with a resolution of 0.35nm and high resolution images were recorded with a High Resolution FEI/Tecnai F20 Cryo TWIN FEGTEM.

4.5.3 Synthesis of Complexes

The synthesis and detailed characterisation of the various complexes and ligands is discussed in Chapter 2.

4.6 References

1. J. A. A. W. Elemans, A. E. Rowan, R. J. M. Nolte, *J. Am. Chem. Soc.*, 2002, **124**, 1532-1540.
2. W. Lu, D. A. Vicic, J. K. Barton, *Inorg. Chem.*, 2005, **44**, 7970-7980.
3. A. M. Krause-Heuer, N. J. Wheate, M. J. Tilby, D. G. Pearson, C. J. Ottley, J. R. Aldrich-Wright, *Inorg. Chem.*, 2008, **47**, 6880-6888.
4. F. H. Stootman, D. M. Fisher, A. Rodgerc, J. R. Aldrich-Wright, *Analyst*, 2006, **131**, 1145-1151.
5. S. Rafique, M. Idrees, A. Nasim, H. Akbar, A. Amin, *Biotech. Mol. Bio. Rev.*, 2010, **5**, 38-45.
6. Egan, T. J.; Koch, K. R.; Swan, P. L.; Clarkson, C.; Van Schalkwyk, D. A.; Smith, P. J. *J. Med Chem.*, 2004, **47**, 2926-2934.
7. Y.-S. Wu, K. R. Koch, V. R. Abratt, H. H. Klump, *Arch. Biochem. Biophys.*, 2005, **440**, 28-37.
8. H. H. Klump, K. R. Koch, C. T. S. Lin, *Afr. J. Chem.*, 2006, **102**, 264-266.
9. K. R. Koch, C. Sacht, C. Lawrence, *Dalton Trans.* 1998, **4**, 689-695.
10. I. Horman, B. Dreux, *Helv. Chim. Acta*, 1984, **67**, 754-764.
11. L. Fielding, *Tetrahedron*, 2000, **56**, 6151-6170.
12. A. Macchioni, A. Romani, C. Zuccaccia, G. Guglielmetti, C. Querci, *Organometallics*, 2003, **22**, 1526-1533.
13. I. A. Kotzé, W. J. Gerber, J. M. Mckenzie, K. R. Koch, *Eur. J. Inorg. Chem.*, 2009, **12**, 1626-1633.
14. Y.-S. Wu, *PhD dissertation*, University of Cape Town, 2002
15. P. S. Pregosin, *Prog. Nucl. Magn. Reson. Spectrosc.*, 2006, **19**, 261-288.

16. F. Song, S. J. Lancaster, R. D. Cannon, M. Schormann, S. M. Humphrey, C. Zuccaccia, A. Macchioni, M. Bochmann, *Organometallics*, 2005, **24**, 1315-1328.
17. T. J. Egan, *Trends in Parasitology*, 2006, **22**, 235-237.
18. I. Z. Steinberg, A. H. Scheraga, *J. of Bio Chem.*, 1963, **238**, 172-181.
19. P. Doty, G. E. Myers, *Discussions Faraday Soc.*, 1953, **13**, 51-58.
20. W. Kauzmann; C. B. Anfinsen, M. L. Anson, K. Bailey, J. T. Edsall, *Advances in Protein Chem.*, 1959, **14**, 1-63.
21. H. A. Scheraga, *J. Phys. Chem.*, 1961, **66**, 1071-1072.
22. C. H. Wohlfarth, *Landolt-Börnstein - Group IV Physical Chemistry*, Springer, Berlin Heidelberg, 2008, **17**, 117-121.
23. H.-J. Schneider, *Angew. Chem., Int. Ed. Engl.*, 1991, **30**, 1417-1436.
24. C. A. Hunter, J. K. M. Sanders, *J. Am. Chem. Soc.* 1990, **112**, 5525-5534.
25. T. D. W. Claridge, *High-Resolution NMR Techniques in Organic Chemistry - Tetrahedron Organic Chemistry Series*, Pergamon, Oxford, 1999, **19**.
26. H. Friebolin, *Basic One- and Two-Dimensional NMR Spectroscopy*, Wiley-VCH, Weinheim, 2005
27. P. J. Hore, *Nuclear Magnetic Resonance*, Oxford, 1995
28. V. I. Bakhmutov, *Practical NMR Relaxation for Chemists*, John Wiley and Sons Ltd. London, 2004.
29. I. Pianet, Y. André, M. A. Ducasse, I. Tarascou, J. C. Lartigue, N. Pinaud, E. Fouquet, E. J. Dufourc, M. Laguerre, *Langmuir*, 2008, **24**, 11027-11035.
30. L. Luchetti, G. Mancini, *Langmuir*, 2000, **16**, 161-165.
31. H. J. Hwang, S. K. Lee, S. Lee, J. W. Park, *J. Chem. Soc. Perkin Trans. 2*, 1999, 6, 1081-1086.
32. G. Bellachioma, G. Ciancaleoni, C. Zuccaccia, D. Zuccaccia, A. Macchioni, *Coord. Chem. Rev.*, 2008, **252**, 2224-2238.
33. H.-L. Zhang, G.-H. S.-J. Chen, Han, *J. Chem. & Eng. Data*, 1997, **42**, 526-530.
34. M. Kato, J. Takahashi, *Acta Crystallogr. Sect. C: Cryst. Struct. Commun.*, 1999, **C55**, 1809-1812.
35. A. N. Mautjana, J. D. S. Miller, A. Gie, S. A. Bourne, K. R. Koch, *Dalton Trans.*, 2003, **10**, 1952-1960.
36. I. A. Kotzé, MSc. Thesis, *University of Stellenbosch*, 2009.
37. M. Meloun, J. Havel, E. Högfeltdt, *Computation of Solution Equilibria – A Guide to Methods in Potentiometry, Extraction, and Spectrophotometry*, Ellis Horwood, Chichester, 1987.
38. P. Kuzmic, *Anal. Biochem.* 1996, **237**, 260–273.
39. B. Antalek, *Concepts Magn. Reson.*, 2002, **14**, 225-258

5

Preliminary assessment of potential antimalarial activity of a series of $[\text{Pt}^{\text{II}}(\text{diimine})(\text{L}^{\text{n}}-\text{S},\text{O})]^+$ complexes using a surfactant mediated β -haematin inhibition assay

This chapter describes the testing of all the complexes synthesised in this study for β -haematin inhibition. This will be done using a surfactant (NP-40) mediated β -haematin inhibition assay and the results compared to two well known anti-malarials, chloroquine and amodiaquine. The β -haematin inhibition of $[\text{Pt}^{\text{II}}(\text{diimine})(\text{L}^{\text{n}}-\text{S},\text{O})]^+$ complexes is believed to be a result of strong interaction with haematin via non-covalent interactions in view of the observed self- and hetero-association of $[\text{Pt}^{\text{II}}(\text{diimine})(\text{L}^{\text{n}}-\text{S},\text{O})]^+$ cations with pyrene and fluoranthene.

5.1 Introduction

Plasmodium falciparum is responsible for 90% of all malaria mortalities reported annually. During its life cycle the parasite resides in the red blood cell (RBC) of the human host where it digests haemoglobin, leaving the toxic haem (ferroprotoporphyrin IX or Fe(II)PPIX) in its food vacuole as discussed in Chapter 1. This haem is rapidly oxidised to ferriprotoporphyrin (Fe(III)PPIX) which has several forms in solution which includes monomeric, μ -oxo dimers and mainly π - π dimers.^{1,2} The π - π dimers associate to form haemozoin crystals at the lipid interface through a biomineralization/crystallization process (Figure 5.1).²

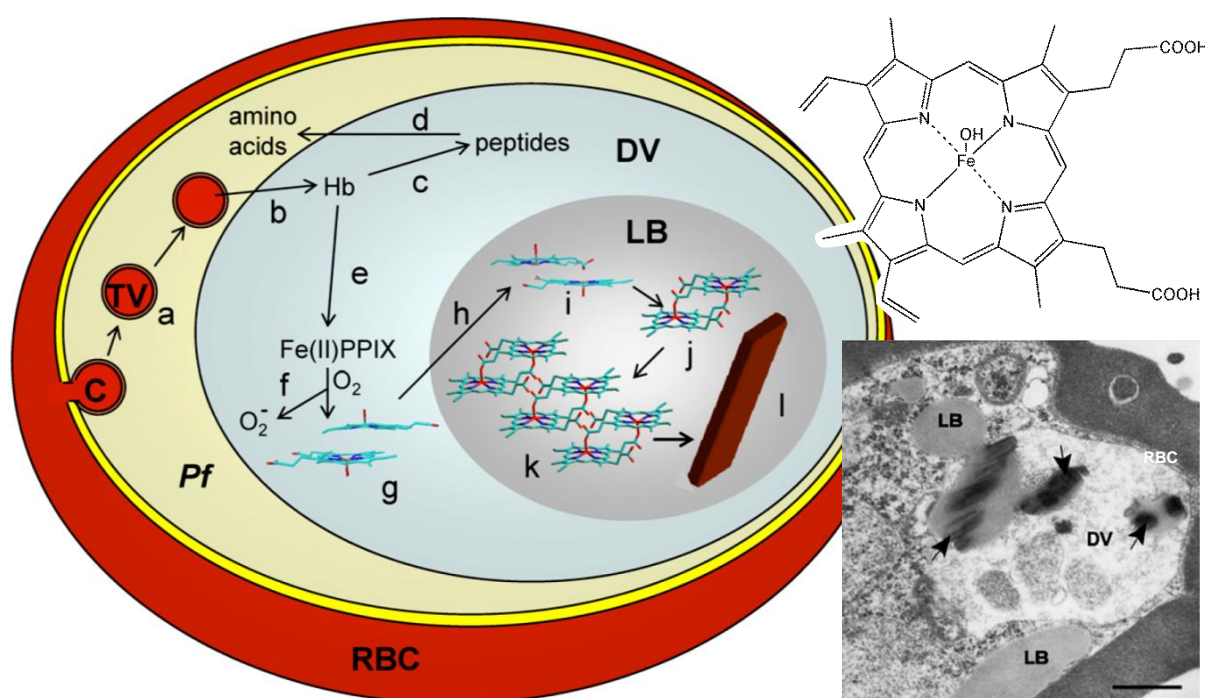


Figure 5.1 Proposed schematic representation of the processes involved in haemozoin formation in *Plasmodium falciparum* based on recent studies.^{2,3} In aqueous solution Fe(III)PPIX forms a π - π dimer (g) which is delivered (h) to a lipid body (LB) where it converts to the haemozoin dimer (j) by displacement of the axial water ligands of $\text{H}_2\text{O}-\text{Fe(III)PPIX}$ together with formation of the Fe(III)-propionate bonds. In the absence of competing hydrogen bonding to the lipid body, these dimers can start to nucleate haemozoin by hydrogen bonding to each other (k), finally assembling the haemozoin crystal (l). (*The TEM image was reproduced from reference 3*)

This process of haemozoin production is a critical vulnerability of the parasite, since free haematin build-up is highly toxic as discussed earlier. This detoxification step is the target of a number of antimalarial drugs. For example, chloroquine (CQ) inhibits haemozoin formation

by binding to the free haematin and/or to the haemozoin crystal surface to rapidly reduce the crystal growth.⁴ The repeating unit of the haemozoin crystal is shown in Figure 5.2.

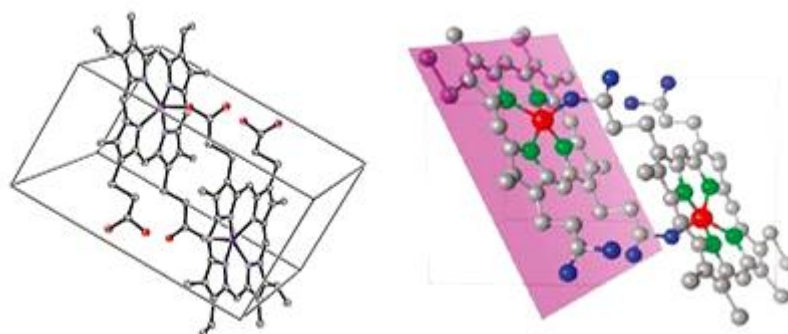


Figure 5.2 Molecular structure of the repeating unit of the haemozoin crystal. These units interact by means of hydrogen bonding between the free propionic groups.⁵ (*image reproduced from reference 6*)

Haemozoin inhibition is an attractive target for new antimalarials since symptoms of malaria infections manifest when the parasite is in the blood stage of its life cycle, and detection is easily done using a microscope (visible malaria pigment/haemozoin crystals). Furthermore, CQ and other quinolines have been shown to be highly effective drugs in targeting this detoxification process and are fast-acting and specific to the parasite. However, the wide occurrence of drug resistance (by decreasing CQ concentrations as discussed in Chapter 1) calls for new drugs to be discovered.

It has been shown that $[\text{Pt}^{\text{II}}(\text{diimine})(\text{benzoylthiourea})]^+$ exhibit significant *in vitro* antimalarial activity. The mechanism is however contentious since these complexes are also known to be DNA intercalators having demonstrable antibacterial properties.⁷ The $[\text{Pt}^{\text{II}}(\text{bipy})(N,N\text{-di}(2\text{-hydroxyethyl})\text{-}N'\text{-benzoylthiourea})]^+$ complex was shown to have the tendency to undergo DNA-mediated biomineralisation with nucleation/seed-crystal forming due to interaction with DNA.⁸ However, Egan and co-workers have shown that $[\text{Pt}^{\text{II}}(\text{diimine})(\text{benzoylthiourea})]^+$ associates with haematin in 40% aqueous dimethyl sulfoxide solution, which suggests haemozoin inhibition as the mechanism for the antimalarial activity.⁹ This mechanism was therefore investigated by testing a series of complexes $[\text{Pt}^{\text{II}}(\text{diimine})(\text{L}^n\text{-}S\text{-}O)]^+$ using a synthetic haemozoin (β -haematin) inhibition study.

It is expected that this class of $[\text{Pt}^{\text{II}}(\text{diimine})(\text{L}^n\text{-}S\text{-}O)]^+$ complexes to have the capability to bind/interact with these solution precursors of haemozoin, since the complexes also have the tendency to self-associate and form non-covalent complexes with poly aromatic

hydrocarbons through π - π stacking and cation- π interactions in solution. These complexes appear to engage in non-covalent interactions in solution, probably in a manner similar to that found for haematin.

5.2 β -haematin Inhibition Assay

The surfactant (NP-40) mediated β -haematin assay described by Carter and co-workers was used to investigate β -haematin inhibition potential of the series of $[\text{Pt}^{\text{II}}(\text{diimine})(\text{L}^{\text{n}}-\text{S}-\text{O})]^+$ complexes with synthesis described in Chapter 2.¹⁰

The well known antimalarials chloroquine (CQ) and amodiaquine (AQ) were used as positive controls in this assay. The experiments were carried out in 96-well plates consisting of 8 rows and 12 columns as shown in Figure 5.3 and all additions and serial dilutions were made by hand using a multi-channel pipette. The procedure and measurements were done in duplicate. Wells 2-12 contained solutions of test compound in various concentration; well 12 contained the highest concentration and wells 11 to 2 serial dilutions (50% of the previous well consecutively) while well 1 was the blank control.

To wells 1 to 11 was added 100 μL of a solution containing 70:20:10 (v/v) % H_2O :NP-40 solution (305.5 μM):dimethyl sulfoxide. To well 12 was added 140 μL H_2O and 40 μL NP-40 solution (305.5 μM). The test compounds were then added to wells 12 (20 μL of a 20 mM test compound in dimethyl sulfoxide) and mixed. From well 12, 100 μL of the mixture was drawn and added to well 11 as the start of the serial dilution. The solution in well 11 was mixed and 100 μL was drawn and added to well 10 and mixed and so on. The process was continued until well 2 where the 100 μL drawn was discarded since well 1 is the blank control. To all wells 100 μL of a suspension consisting of 178.8 μL haem solution (1mM in dimethyl sulfoxide) and 20 mL 1M acetate buffer (pH 4.75 - 4.90) was subsequently added. The plates were covered and placed in the incubator for 5 hours at 37°C.

Analysis of the assay was done using the colourimetric pyridine-complex method described by Ncokazi and Egan.¹¹ To all wells were added 32 μL of a solution containing 20:20:10:50 (v/v) % H_2O :Acetone:2M HEPES buffer:pyridine after which 60 μL acetone was added.

The solutions were mixed and the absorbances of the plate wells were measured at 405 nm on a SpectraMax plate reader.

5.3 Results and Discussion

The resultant plates of the compounds tested are shown in Figure 5.3. The orange/pink colour

(as observed for CQ and AQ in plate 1) indicates the pyridine-Fe(III)porphyrin complex which serves as a colourimetric indicator of the haematin not in the β -haematin crystalline state. This 'free' haematin which forms the pyridine-Fe(III)porphyrin complex is presumably not in the β -haematin crystalline state as a result of drug/haem interaction (β -haematin inhibition).

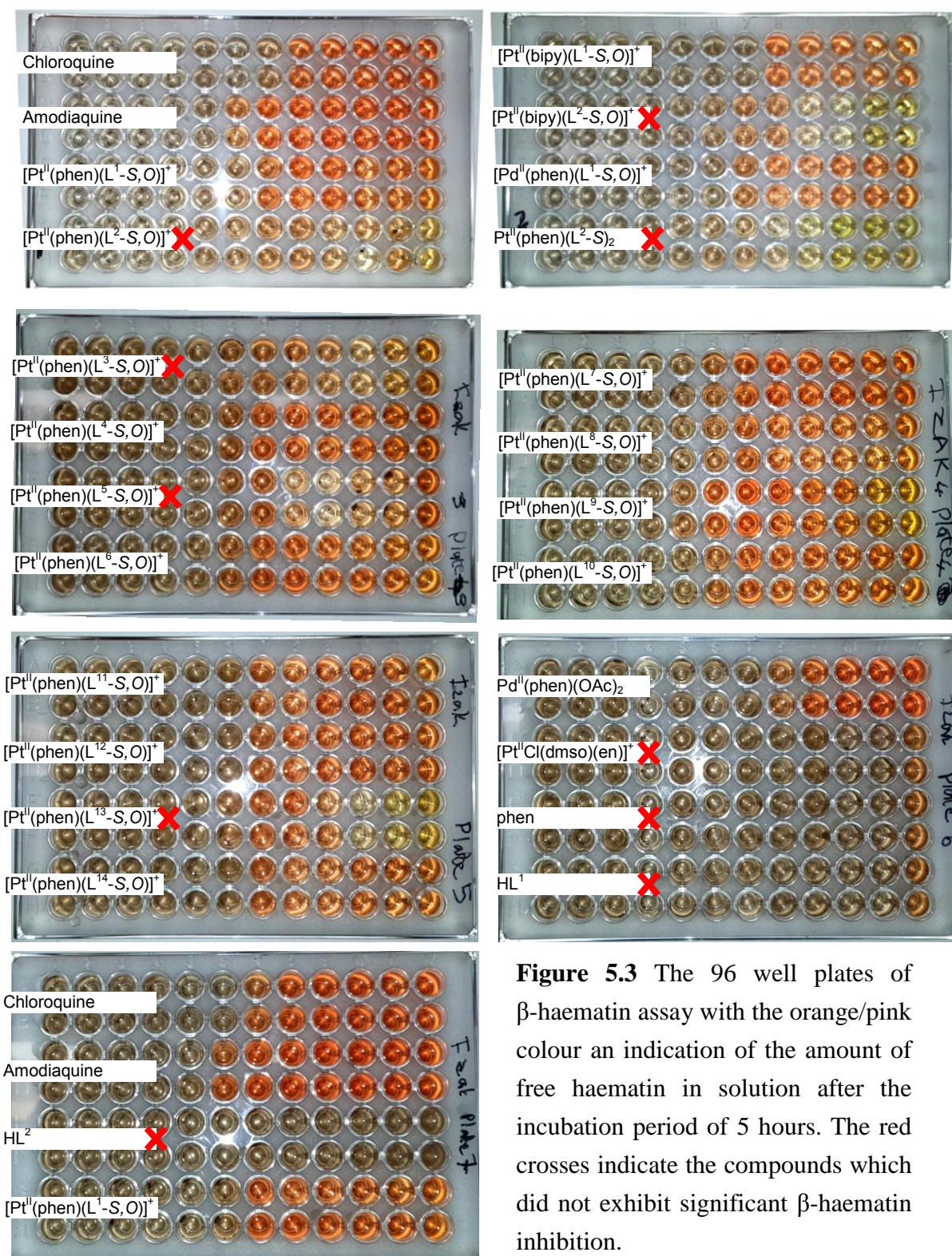


Figure 5.3 The 96 well plates of β -haematin assay with the orange/pink colour an indication of the amount of free haematin in solution after the incubation period of 5 hours. The red crosses indicate the compounds which did not exhibit significant β -haematin inhibition.

Crystalline β -haematin could be observed at all concentrations of inactive compounds (indicated by the red crosses) as well as for low concentrations of the active compounds. The sigmoidal dose response curves were fitted to the absorbance-concentration data using GraphPad Prism version 6.02, from which the half-maximal inhibitory concentration (IC_{50}) values were calculated. Selected dose-response curves are shown in Figure 5.4 with the IC_{50} values at the inflection point of each curve. All the raw data and fitting parameters are shown in Tables 5.2 and 5.3 of Section 5.5. The IC_{50} concentrations and chemical structures of all compounds tested are shown in Figure 5.5.

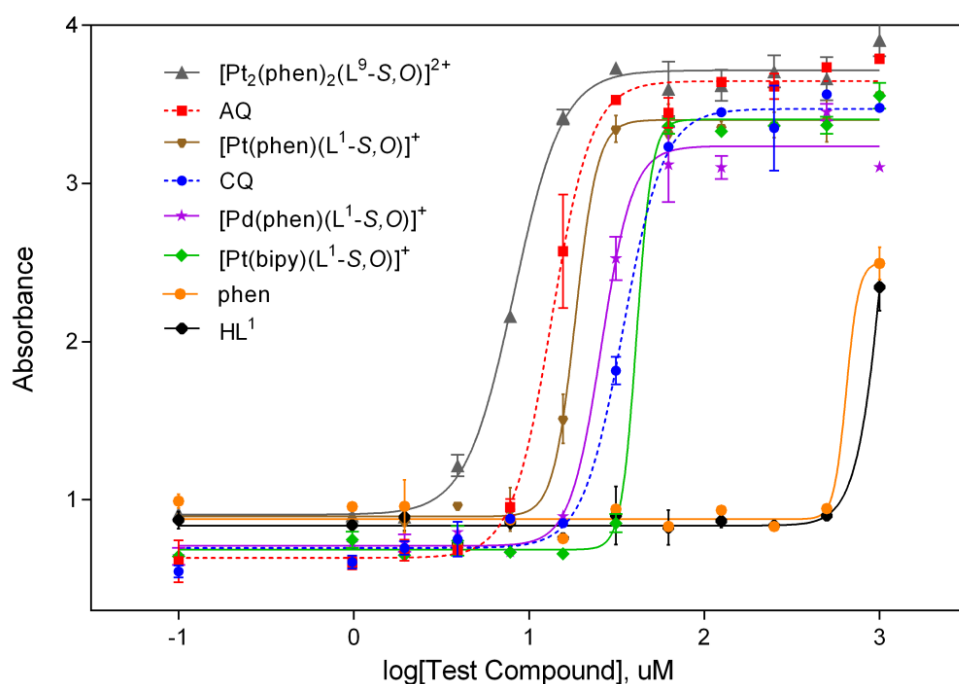
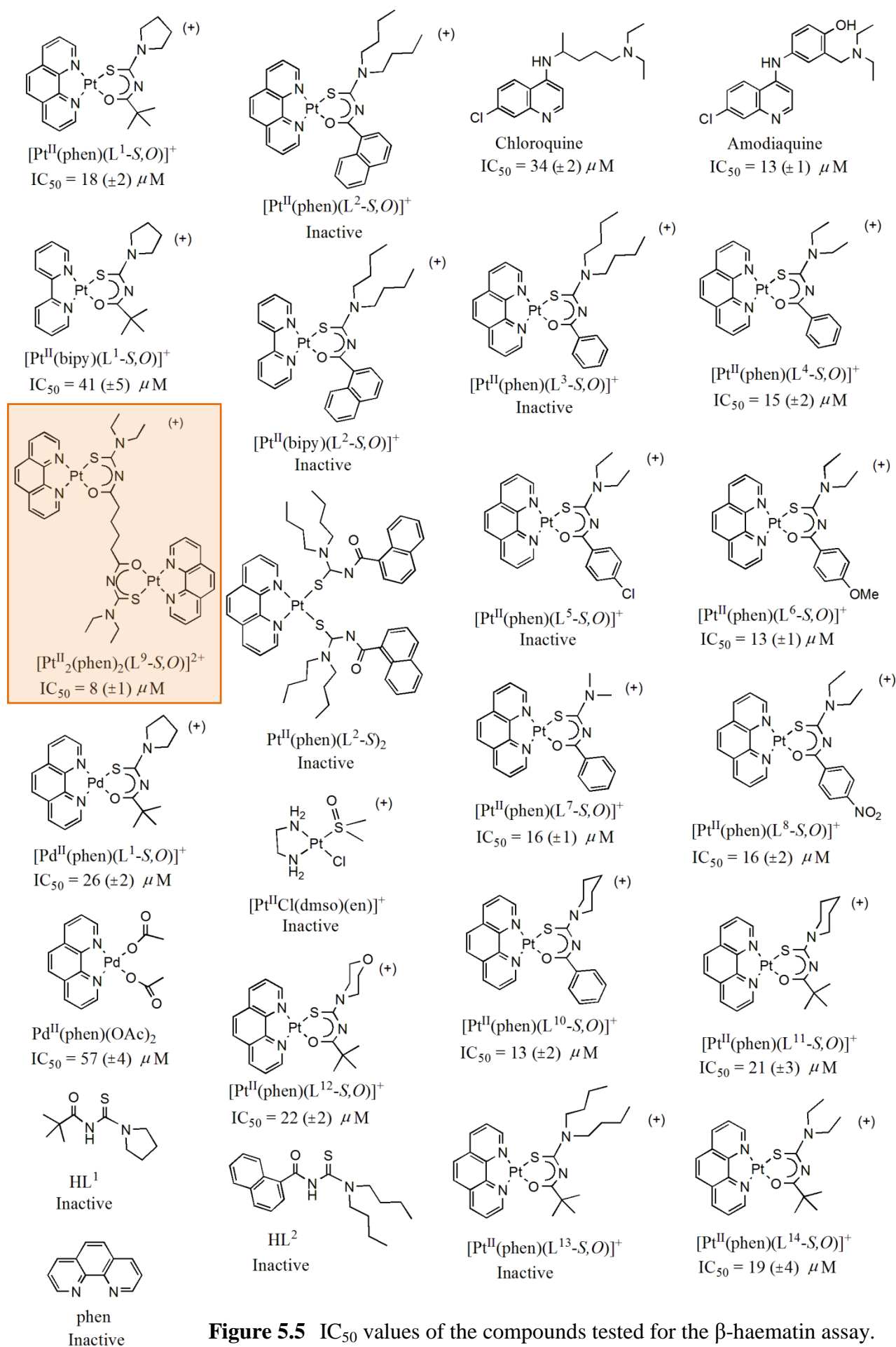


Figure 5.4 Selected test compounds concentration response curves of β -haematin assay.

The two well known antimalarials, chloroquine (CQ) and amodiaquine (AQ) (shown as dashed lines in Figure 5.4) were used as positive standards and are commonly used to determine the success of the assay as well as serving as standards to the IC_{50} values of the tested compounds. Interestingly, $[Pt^{II}(\text{phen})(L^1-S,O)]^+$ and its palladium analogue $[Pd^{II}(\text{phen})(L^1-S,O)]^+$ display IC_{50} values (activity) that are between those of CQ and AQ while the bipy variation $[Pt^{II}(\text{bipy})(L^1-S,O)]^+$ displays activity only at higher concentration ($IC_{50} = 41 \pm 5 \mu\text{M}$). By contrast, the ligands phen and HL^1 display only a slight absorbance at the highest concentration (1000 μM) and thus these are considered to be inactive for all practical purposes. The binuclear complex $[Pt^{II}_2(\text{phen})_2(L^9-S,O)]^{2+}$, on the other hand (highlighted in Figure 5.5), is highly active with an IC_{50} value of only $8 \pm 1 \mu\text{M}$, which is well below that of both known and commonly used antimalarials CQ ($34 \pm 2 \mu\text{M}$) and AQ ($13 \pm 1 \mu\text{M}$).

**Figure 5.5** IC_{50} values of the compounds tested for the β -haematin assay.

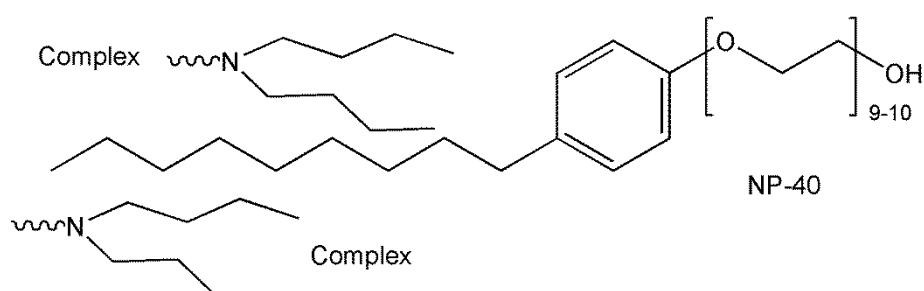
The binuclear complex $[\text{Pt}^{\text{II}}_2(\text{phen})_2(\text{L}^9\text{-S},\text{O})]^{2+}$ has two $\text{Pt}^{\text{II}}(\text{phen})$ moieties in addition to the (2+) charge so that it can be speculated that its low IC_{50} value may indicate that the complex interacts with haematin *via* two of the $\text{Pt}^{\text{II}}(\text{phen})$ groups of the complex. The IC_{50} values of all the complexes tested are summarised in Table 5.1 in order of most to least active.

Table 5.1 List of all active and inactive β -haematin inhibitor.

Active Compounds	IC_{50} (μM)	Inactive Compounds
$[\text{Pt}^{\text{II}}_2(\text{phen})_2(\text{L}^9\text{-S},\text{O})]^{2+}$	8 (± 1)	$[\text{Pt}^{\text{II}}(\text{phen})(\text{L}^2\text{-S},\text{O})]^+$
$[\text{Pt}^{\text{II}}(\text{phen})(\text{L}^{10}\text{-S},\text{O})]^+$	13 (± 2)	$[\text{Pt}^{\text{II}}(\text{bipy})(\text{L}^2\text{-S},\text{O})]^+$
$[\text{Pt}^{\text{II}}(\text{phen})(\text{L}^6\text{-S},\text{O})]^+$	13 (± 1)	$[\text{Pt}^{\text{II}}(\text{phen})(\text{L}^3\text{-S},\text{O})]^+$
AQ	13 (± 1)	$[\text{Pt}^{\text{II}}(\text{phen})(\text{L}^5\text{-S},\text{O})]^+$
$[\text{Pt}^{\text{II}}(\text{phen})(\text{L}^4\text{-S},\text{O})]^+$	15 (± 2)	$[\text{Pt}^{\text{II}}(\text{phen})(\text{L}^{13}\text{-S},\text{O})]^+$
$[\text{Pt}^{\text{II}}(\text{phen})(\text{L}^8\text{-S},\text{O})]^+$	16 (± 2)	$[\text{Pt}^{\text{II}}\text{Cl}(\text{dmso})(\text{en})]^+$
$[\text{Pt}^{\text{II}}(\text{phen})(\text{L}^7\text{-S},\text{O})]^+$	16 (± 1)	$\text{Pt}^{\text{II}}(\text{phen})(\text{L}^2\text{-S})_2$
$[\text{Pt}^{\text{II}}(\text{phen})(\text{L}^1\text{-S},\text{O})]^+$	18 (± 2)	phen
$[\text{Pt}^{\text{II}}(\text{phen})(\text{L}^{14}\text{-S},\text{O})]^+$	19 (± 4)	HL^2
$[\text{Pt}^{\text{II}}(\text{phen})(\text{L}^{11}\text{-S},\text{O})]^+$	21 (± 3)	HL^1
$[\text{Pt}^{\text{II}}(\text{phen})(\text{L}^{12}\text{-S},\text{O})]^+$	22 (± 2)	
$[\text{Pd}^{\text{II}}(\text{phen})(\text{L}^1\text{-S},\text{O})]^+$	26 (± 2)	
CQ	34 (± 2)	
$[\text{Pt}^{\text{II}}(\text{bipy})(\text{L}^1\text{-S},\text{O})]^+$	41 (± 5)	
$\text{Pd}^{\text{II}}(\text{phen})(\text{OAc})_2$	57 (± 4)	

Interestingly, in general almost all $[\text{Pt}^{\text{II}}(\text{phen})(\text{L}^n\text{-S},\text{O})]^+$ complexes were better β -haematin inhibitors than CQ except for the inactive complexes which contained *N,N*-dibutyl-*N*-acylthiourea ligands ($[\text{Pt}^{\text{II}}(\text{phen})(\text{L}^2\text{-S},\text{O})]^+$, $[\text{Pt}^{\text{II}}(\text{bipy})(\text{L}^2\text{-S},\text{O})]^+$, $[\text{Pt}^{\text{II}}(\text{phen})(\text{L}^3\text{-S},\text{O})]^+$ and $[\text{Pt}^{\text{II}}(\text{phen})(\text{L}^{13}\text{-S},\text{O})]^+$). The inactivity of $[\text{Pt}^{\text{II}}(\text{phen})(\text{L}^5\text{-S},\text{O})]^+$ may be attributed to its low solubility. The inactivity of all the complexes containing *N,N*-dibutyl-*N*-acylthioureas is probably due to the presence of the butyl groups. It is expected that these butyl groups could potentially interact with the nonyl group of the surfactant, which could be driven by hydrophobic effects (Scheme 5.1). It is tempting to postulate such hydrophobic interactions in view of the well known interaction in ion-pairing chromatography where the ion-pairing

reagent with hydrocarbon chain groups (i.e. tetrabutylammonium chloride) and the alkyl-functionalised reverse phase column (i.e. C₁₈ or C₉ etc.) result in a strong affinity for each other in polar/aqueous solutions. Indeed, the observed affinity of the β -haematin crystals for the walls of the plates at high concentration of complexes containing dibutyl groups, imply that the surfactant is not functioning as expected and this is consistent with the postulate above. Moreover, at low concentrations of complexes containing dibutyl-groups, the surfactant seems to be functioning as expected, since the precipitate (β -haematin) does not show an affinity for the walls of the plates and remains a homogeneous suspension.



Scheme 5.1 Postulated hydrophobic interaction between the nonyl group of NP-40 and the dibutyl groups of the complexes.

The neutral Pd^{II}(phen)(OAc)₂ complex shows activity only at a relatively high concentrations (IC₅₀ = 57 ± 4 μM), while the cationic [Pd^{II}(phen)(L¹-S,O)]⁺ is a much better β -haematin inhibitor (IC₅₀ = 26 ± 2 μM). It appears that the cationic nature (or protonatibility) of these complexes is a requirement for β -haematin inhibition activity since most of the cationic complexes shows activity, while similar but neutral complexes are found to be inactive. The activity of Pd^{II}(phen)(OAc)₂ could possibly result from being partially protonated in the slightly acidic solutions (pH = 4.7-4.9) or loss of acetate.

In general, the 1,10-phenanthroline complexes exhibit significantly higher activity compared to their 2,2-bipyridine analogues (IC₅₀ of [Pt^{II}(phen)(L¹-S,O)]⁺ = 18 ± 2 μM compared to IC₅₀ of [Pt^{II}(bipy)(L¹-S,O)]⁺ = 41 ± 5 μM). These results are therefore consistent with the effect of the diimine functionality postulated by Egan and Koch where diimines with more π -electrons display higher binding constants with haem.⁹ Furthermore, the aromatic diimine functionality appears to be a requirement for the antimalarial activity of these complexes since [Pt^{II}Cl(dmsO)(en)]⁺ displays no β -haematin inhibition.

The abovementioned findings, together with the interesting finding that the bipodal complex, $[\text{Pt}^{\text{II}}_2(\text{phen})_2(\text{L}^9\text{-S,O})]^{2+}$, displays more or less twice the activity of the other $[\text{Pt}^{\text{II}}(\text{phen})(\text{L}^n\text{-S,O})]^+$ complexes, we now propose that two structural properties are required for this class of complexes to interact with haematin. Firstly, the diimine ligands with π -electrons are required, with an increase in activity for $[\text{Pt}^{\text{II}}(\text{phen})(\text{L}^1\text{-S,O})]^+$ compared to $[\text{Pt}^{\text{II}}(\text{bipy})(\text{L}^1\text{-S,O})]^+$. Secondly, the ancillary ligand (dialkyl-acylthioureas in this case), should not contain any hydrophobic butyl or longer chain alkyl groups. It is also found that cationic complexes display significant activity compared to the similar neutral complexes.

It has been shown that haematin exist in various forms in solution, the 3 most common structures being monomeric haematin, μ -oxo dimers and the most abundant π - π dimers.^{1,2} The haemazoin inhibition of current antimalarials is thought to be a result of strong interaction with haem, haematin as observed by Cohen and co-workers or the seed crystals of haemazoin to hinder crystal growth shown by Hanscheid *et al.*^{4,12} It has also been proposed that AQ forms strong non-covalent π - π dimer complexes with the μ -oxo dimeric Fe(III)PPIX.¹³ Egan and co-workers have found a crystal structure in which the clinically used antimalarial halofantrine interacts with ferriprotoporphyrin IX (Fe(III)PPIX) as shown in Figure 5.6a.¹⁴ This crystal structure reveals the interaction of the alcohol functionality of halofantrine to the Fe(III)porphyrin centre in addition to π -stacking of the phenanthrene ring over the porphyrin. Furthermore, they have also proposed the formation of a salt bridge type hydrogen bond between the protonated tertiary amino group and the unprotonated haematin propionate group.¹⁴

Peyton and co-workers have established the nature of the interaction between 4,5-dihydroxyxanthone (45X2) and haem.¹⁵ These authors proposed a 1:2 45X2-Haem₂ stoichiometry with the coordination of the carbonyl oxygen atom, hydrogen bonding between the hydroxyl group of 45X2 and the propionate side chains of the haem, as well as π -stacking being the main interactions contributing to the stability of the drug/haem complex (Figure 5.6b). The importance of π -stacking in these interactions can also be seen from the proposed interaction of CQ and the μ -oxo dimer of Fe(III)PPIX (Figure 5.6c).

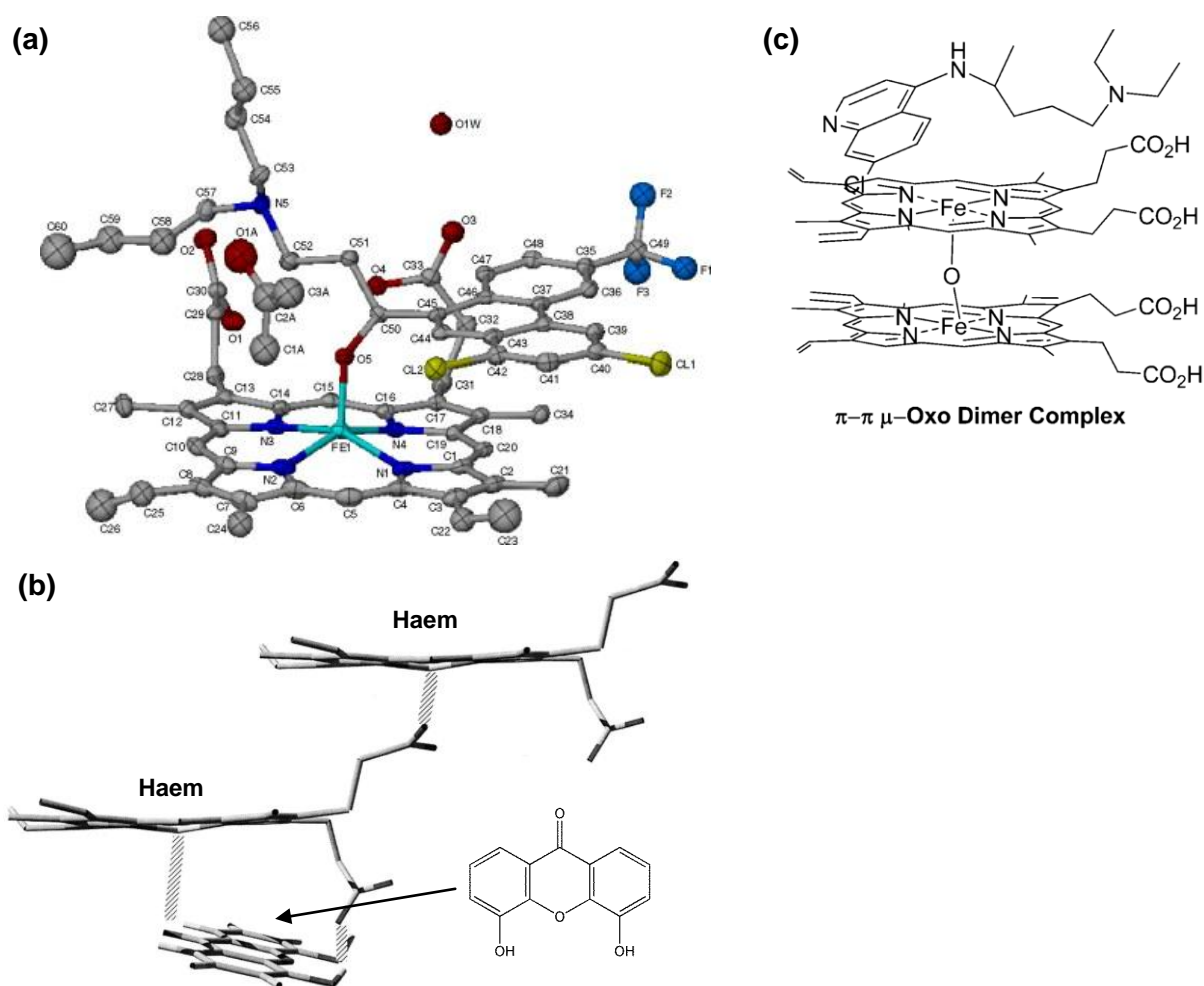
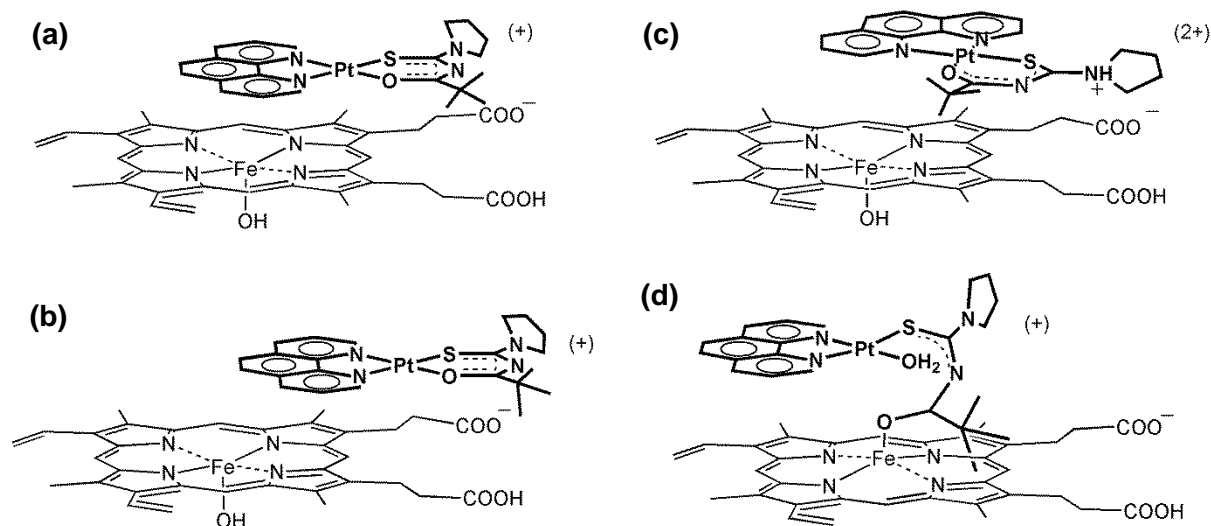


Figure 5.6 Proposed interaction of (a) halofantrine¹⁴ and (b) 4,5-dihydroxyxanthone (45X2)¹⁵ with haem. (c) The π -stacking interaction between chloroquine and the μ -oxo dimer of haematin.¹

Considering the nature of the interaction of common antimalarials with haematin species in solution described above, a mode of interaction of $[\text{Pt}^{\text{II}}(\text{diimine})(\text{L}^{\text{n}}-\text{S},\text{O})]^+$ complexes can be proposed. It was shown previously that the complexes of $[\text{Pt}^{\text{II}}(\text{diimine})(\text{L}^{\text{n}}-\text{S},\text{O})]^+$ are capable of engaging in non-covalent interactions from their self-association and relatively strong association with fluoranthene and pyrene. The inhibition of β -haematin formation by $[\text{Pt}^{\text{II}}(\text{diimine})(\text{L}^{\text{n}}-\text{S},\text{O})]^+$ is proposed to be a result of the interaction between these complexes and haematin in solution to form non-covalent hetero-dimers. Several intermolecular interactions may contribute to this association and these are illustrated in Scheme 5.2. Non-covalent π - π stacking between phenanthroline and porphyrin (b), cation- π interaction between Pt^{II} porphyrin and Fe^{II} phen (a) and ion-pairing of the cationic complex or protonated amino group of the complex with the propionate side chains of haematin (c). The possibility of coordination of the *N,N*-dialkyl-*N'*-acylthioureas ligand is also included (d).

The structures based on these interactions are shown in Scheme 5.2 with only one haematin complex representing all solution species of Fe(III)PPIX. Note that while only one possible geometry is shown for each set of interactions, the orientation of the $[\text{Pt}^{\text{II}}(\text{diimine})(\text{L}^{\text{n}}-\text{S},\text{O})]^+$ complex relative to Fe(III)PPIX will probably be an average interaction with the whole π -surface of the porphyrin.



Scheme 5.2 Postulated association of $[\text{Pt}^{\text{II}}(\text{phen})(\text{L}^{\text{n}}-\text{S},\text{O})]^+$ complexes with the various forms of haematin in solution to inhibit β -haematin formation. All structures are considered ion pairs with the additional interactions (a) cation- π , (b) π -stacking (c) a combination of cation- π , π -stacking and a salt bridge between the protonated amino group and the propionate and (d) coordination of the acyl group to Fe(III) with additional π -stacking interactions. Only one unit of haematin is shown while this represents monomeric haematin and/or μ -oxo dimeric haematin except for structure (d).

5.4 Conclusions

It was found that most of $[\text{Pt}^{\text{II}}(\text{diimine})(\text{L}^{\text{n}}-\text{S},\text{O})]^+$ complexes display significant β -haematin inhibition in the surfactant mediated β -haematin inhibition assay. This provides important information on the mechanism of the *in vitro* antimalarial activity observed previously for this class of complexes.⁹ It was also found that such complexes containing 1,10-phenanthroline ligands are more efficient (lower IC_{50}) β -haematin inhibitors than analogues containing 2,2-bipyridine ligands and that Pt^{II} complexes appear to be more active than the Pd^{II} variation. The complexes of *N,N*-dibutyl-*N'*-acylthioureas display no significant activity, possibly due to strong hydrophobic interaction with the surfactant (NP-40).

The binuclear complex $[\text{Pt}^{\text{II}}_2(\text{phen})_2(\text{L}^9\text{-S},\text{O})]^{2+}$ was found to be a very effective β -haematin inhibitor ($\text{IC}_{50} = 8 \pm 1 \mu\text{M}$) with IC_{50} value roughly half that of the other complexes and this can be speculated to be due to the two 'active' sites in the complex and the higher overall charge suggesting a higher degree of cation- π interactions. It is reasonable to postulate that β -haematin inhibition is mainly due to cation- π interaction between $[\text{Pt}^{\text{II}}(\text{diimine})(\text{L}^n\text{-S},\text{O})]^+$ complexes and solution precursors of haemozoin (Scheme 5.2). Other non-covalent interactions contributing to the effective binding of these complexes to haematin and haemozoin precursors include ion-pairing, π -stacking and hydrophobic interactions.

5.5 Experimental Section

All absorbances at 405nm of the plates shown in Figure 5.3 are given in Table 5.2. The corresponding least-squares fitting parameters and corresponding data for the dose response of the β -haematin assay are shown in Table 5.3.

Table 5.2 Absorbance at 405nm for the plates in the β -haematin assay.

Compound	Concentration μ M												
	0.00	0.98	1.95	3.91	7.81	15.63	31.25	62.50	125	250	500	1000	
CQ	0.607	0.613	0.741	0.817	0.838	0.879	1.644	3.278	3.410	3.485	3.593	3.561	Absorbance
CQ	0.561	0.591	1.036	0.738	0.903	0.803	1.780	3.375	3.466	3.570	3.565	3.591	
AQ	0.725	0.574	0.725	0.716	0.921	2.880	3.559	3.645	3.693	3.661	3.777	3.810	
AQ	0.510	0.641	0.872	0.710	0.860	2.383	3.551	3.484	3.699	3.604	3.746	3.858	
[Pt(phen)(L1-S,O)]+	0.631	0.698	0.666	0.742	1.184	1.323	3.085	3.539	3.511	2.818	3.468	3.756	
[Pt(phen)(L1-S,O)]+	0.720	0.689	1.000	0.739	0.855	1.367	3.302	3.260	3.547	3.195	3.363	3.796	
[Pt(phen)(L2-S,O)]+	0.747	0.679	0.780	0.897	1.292	1.692	2.251	2.352	1.724	2.212	2.218	2.293	
[Pt(phen)(L2-S,O)]+	0.835	0.709	0.838	0.890	1.283	1.689	2.204	2.298	1.918	0.808	2.861	2.234	
[Pt(bipy)(L1-S,O)]+	0.628	0.785	0.649	0.673	0.662	0.660	0.893	3.397	3.334	3.356	3.329	3.496	Absorbance
[Pt(bipy)(L1-S,O)]+	0.656	0.711	0.649	0.807	0.676	0.655	0.811	3.328	3.326	3.373	3.406	3.613	
[Pt(bipy)(L2-S,O)]+	0.648	0.857	0.657	0.877	0.969	1.525	2.497	2.646	1.724	1.305	1.577	1.266	
[Pt(bipy)(L2-S,O)]+	0.680	0.646	0.730	0.815	0.895	1.452	2.413	2.869	1.789	1.301	1.510	1.500	
[Pd(phen)(L1-S,O)]+	0.680	0.725	0.689	0.819	0.682	0.908	2.624	3.287	3.050	3.354	3.488	3.110	
[Pd(phen)(L1-S,O)]+	0.604	0.724	0.765	0.770	0.659	0.882	2.429	2.951	3.153	3.366	3.415	3.094	
Pt(phen)(L2-S)2	0.564	0.837	0.694	0.808	1.021	1.436	1.759	1.521	1.532	1.701	1.715	1.726	
Pt(phen)(L2-S)2	0.636	0.667	0.697	0.824	0.972	1.420	1.751	1.823	1.787	1.898	2.243	2.306	
[Pt(phen)(L3-S,O)]+	1.321	1.131	1.334	1.160	1.288	2.238	2.632	2.783	2.272	1.628	2.577	3.539	Absorbance
[Pt(phen)(L3-S,O)]+	1.491	1.090	1.227	1.141	1.250	2.146	2.679	2.487	1.956	1.682	2.099	4.000	
[Pt(phen)(L4-S,O)]+	1.328	1.051	1.119	1.014	1.198	2.494	3.352	3.429	3.429	3.373	3.692	4.000	
[Pt(phen)(L4-S,O)]+	1.409	1.068	1.124	1.050	1.172	2.578	3.469	3.355	3.462	3.629	3.755	4.000	
[Pt(phen)(L5-S,O)]+	1.281	1.075	1.052	1.037	1.242	2.258	2.927	1.768	1.499	2.231	2.367	3.920	
[Pt(phen)(L5-S,O)]+	1.283	1.146	1.044	1.137	1.331	2.318	3.151	1.892	1.348	2.203	2.511	3.895	
[Pt(phen)(L6-S,O)]+	1.257	0.967	1.023	1.052	1.307	2.600	3.324	3.338	3.339	3.097	3.204	3.649	
[Pt(phen)(L6-S,O)]+	1.151	1.148	1.061	1.070	1.449	2.779	3.416	3.402	3.250	3.320	3.430	3.530	
[Pt(phen)(L7-S,O)]+	1.035	1.074	0.994	1.145	1.274	2.429	3.434	3.580	3.551	3.627	3.756	4.000	Absorbance
[Pt(phen)(L7-S,O)]+	0.998	1.013	0.965	1.019	1.301	2.300	3.425	3.582	3.544	3.723	3.845	4.000	
[Pt(phen)(L8-S,O)]+	0.912	0.947	0.920	0.989	1.196	2.158	3.350	3.340	3.321	3.439	3.379	3.895	
[Pt(phen)(L8-S,O)]+	0.874	0.934	0.954	1.066	1.191	2.138	3.382	3.301	3.207	3.342	3.384	3.772	
[Pt(phen)(L9-S,O)]+	0.906	0.925	0.887	1.265	2.150	3.453	3.749	3.721	3.690	3.780	3.565	3.979	
[Pt(phen)(L9-S,O)]+	0.921	0.872	0.896	1.168	2.173	3.387	3.711	3.477	3.551	3.635	3.759	3.834	
[Pt(phen)(L10-S,O)]+	0.855	0.886	0.858	0.955	1.292	2.537	3.427	3.379	3.409	3.506	3.718	3.977	
[Pt(phen)(L10-S,O)]+	0.862	0.922	0.929	0.936	1.415	2.729	3.302	3.225	3.275	3.458	3.697	3.716	

Table 5.2 Continued..

Compound	Concentration μ M												Absorbance
	0.00	0.98	1.95	3.91	7.81	15.63	31.25	62.50	125	250	500	1000	
[Pt(phen)(L11-S,O)]+	0.982	1.065	1.024	1.001	0.997	1.509	3.110	2.975	3.094	3.389	3.365	3.397	Absorbance
[Pt(phen)(L11-S,O)]+	0.985	1.001	0.905	1.001	0.981	1.564	2.979	2.885	3.437	3.517	3.529	3.644	
[Pt(phen)(L12-S,O)]+	0.871	0.987	0.938	0.906	0.877	1.159	3.155	3.216	3.282	3.457	3.519	3.574	
[Pt(phen)(L12-S,O)]+	0.915	0.977	0.921	0.938	0.897	1.125	3.188	3.003	3.334	3.468	3.523	3.633	
[Pt(phen)(L13-S,O)]+	0.956	0.886	1.016	0.984	1.139	2.021	3.239	3.403	2.454	1.185	1.657	2.776	
[Pt(phen)(L13-S,O)]+	1.019	0.951	0.982	0.992	1.088	1.919	3.116	3.051	2.993	1.403	1.764	2.698	
[Pt(phen)(L14-S,O)]+	1.014	0.950	0.884	1.062	0.925	1.359	3.154	2.777	2.945	3.259	3.402	3.491	
[Pt(phen)(L14-S,O)]+	1.002	0.944	0.911	1.012	0.961	1.424	3.140	2.880	3.136	3.278	3.228	3.594	
Pd(phen)(OAc) ₂	1.000	0.899	1.054	0.709	0.961	0.923	1.262	2.570	3.326	3.488	3.599	3.652	Absorbance
Pd(phen)(OAc) ₂	1.034	1.097	1.048	0.732	0.943	0.860	1.296	2.405	3.450	3.545	3.638	3.693	
[PtCl(dmsO)(en)]+	0.962	0.974	0.974	0.699	0.933	0.852	0.941	0.927	1.095	0.834	0.999	2.547	
[PtCl(dmsO)(en)]+	1.047	0.987	1.023	0.672	0.986	0.815	0.956	0.926	0.994	0.900	1.019	2.634	
phen	1.023	0.949	0.838	0.743	0.864	0.766	0.953	0.852	0.950	0.833	0.943	2.567	
phen	0.961	0.963	1.077	0.668	0.882	0.742	0.928	0.810	0.919	0.830	0.947	2.422	
HL1	0.833	0.840	0.828	0.694	0.885	0.754	1.030	0.746	0.836	0.832	0.908	2.450	
HL1	0.909	0.840	0.952	0.748	0.830	0.762	0.770	0.902	0.895	0.842	0.892	2.239	
CQ	0.872	0.827	0.791	0.851	0.760	0.778	2.813	3.469	3.521	3.548	3.467	3.543	Absorbance
CQ	0.964	0.950	0.854	0.855	0.850	1.093	3.186	3.514	3.623	3.591	3.604	3.557	
AQ	0.869	0.873	0.763	0.782	0.947	2.932	3.552	3.703	3.688	3.754	3.779	3.818	
AQ	0.906	0.921	0.757	0.860	1.348	3.447	3.661	3.672	3.620	3.746	3.781	3.832	
HL2	0.875	0.825	0.811	0.873	0.851	0.748	0.871	0.828	1.033	0.961	1.075	1.440	
HL2	0.848	0.910	0.814	0.909	0.796	0.801	1.013	0.913	0.948	0.997	1.063	1.377	
[Pt(phen)(L1-S,O)]+	0.900	0.827	0.812	0.960	0.842	1.401	3.286	3.185	3.327	3.313	3.304	3.575	
[Pt(phen)(L1-S,O)]+	0.850	0.851	0.916	0.969	1.037	1.622	3.404	3.448	3.381	3.427	3.500	3.547	

Table 5.3 Least-squares fit of the dose response data of the β -haematin assay using GraphPad Prism.

	CQ	AQ	[Pt(phen)(L1-S,O)]+	[Pt(phen)(L2-S,O)]+	[Pt(bipy)(L1-S,O)]+
log(inhibitor) vs. response				Ambiguous	
Best-fit values					
Bottom	0.6954	0.6326	0.7567	0.01969	0.6842
Top	3.471	3.647	3.405	~ 6.010	3.404
LogIC50	1.537	1.129	1.267	~ 3.975	1.614
HillSlope	3.753	3.815	4.362	0.199	9.936
IC50	34.43	13.45	18.49	~ 9449	41.1
Span	2.776	3.014	2.649	~ 5.990	2.72
Std. Error					
Bottom	0.03604	0.04574	0.07863	3.147	0.02163
Top	0.04248	0.03799	0.07708	~ 39.30	0.02649
LogIC50	0.01492	0.01508	0.03165	~ 24.33	0.02679
HillSlope	0.491	0.4611	1.219	0.7936	2.136
Span	0.0577	0.06119	0.1126	~ 42.27	0.03421
95% Confidence Intervals					
Bottom	0.6203 to 0.7706	0.5372 to 0.7280	0.5927 to 0.9208	-6.545 to 6.585	0.6391 to 0.7293
Top	3.383 to 3.560	3.568 to 3.726	3.245 to 3.566	(Very wide)	3.349 to 3.460
LogIC50	1.506 to 1.568	1.097 to 1.160	1.201 to 1.333	(Very wide)	1.558 to 1.670
HillSlope	2.729 to 4.777	2.853 to 4.777	1.818 to 6.905	-1.456 to 1.854	5.480 to 14.39
IC50	32.05 to 36.99	12.51 to 14.46	15.88 to 21.53	(Very wide)	36.14 to 46.74
Span	2.655 to 2.896	2.887 to 3.142	2.414 to 2.884	(Very wide)	2.649 to 2.791
Goodness of Fit					
Degrees of Freedom	20	20	20	20	20
R square	0.9932	0.9934	0.9703	0.6569	0.9973
Absolute Sum of Squares	0.2734	0.312	1.144	3.51	0.1122
Sy.x	0.1169	0.1249	0.2392	0.4189	0.07489
Number of points					
Analyzed	24	24	24	24	24

	[Pt(bipy)(L2-S,O)]+	[Pd(phen)(L1-S,O)]+	Pt(phen)(L2-S)2	[Pt(phen)(L3-S,O)]+	[Pt(phen)(L4-S,O)]+
log(inhibitor) vs. response					
Best-fit values					
Bottom	0.7637	0.7081	0.6451	1.218	1.081
Top	1.862	3.235	1.871	2.622	3.6
LogIC50	1.126	1.413	1.078	1.137	1.172
HillSlope	5.603	4.869	1.586	5.826	4.347
IC50	13.36	25.87	11.97	13.7	14.85
Span	1.098	2.527	1.226	1.404	2.52
Std. Error					
Bottom	0.1555	0.04115	0.08999	0.1783	0.06493
Top	0.1276	0.04158	0.06832	0.1469	0.05622
LogIC50	0.152	0.01824	0.09939	0.1372	0.02247
HillSlope	10.02	0.7984	0.5087	11.35	1.266
Span	0.2045	0.05944	0.1227	0.2358	0.08934
95% Confidence Intervals					
Bottom	0.4393 to 1.088	0.6223 to 0.7939	0.4574 to 0.8328	0.8463 to 1.590	0.9454 to 1.216
Top	1.596 to 2.128	3.149 to 3.322	1.728 to 2.013	2.315 to 2.928	3.483 to 3.718
LogIC50	0.8088 to 1.443	1.375 to 1.451	0.8709 to 1.286	0.8505 to 1.423	1.125 to 1.218
HillSlope	-15.29 to 26.50	3.203 to 6.534	0.5252 to 2.648	-17.85 to 29.50	1.706 to 6.988
IC50	6.439 to 27.73	23.70 to 28.24	7.429 to 19.30	7.088 to 26.49	13.33 to 16.54
Span	0.6716 to 1.525	2.403 to 2.651	0.9696 to 1.482	0.9117 to 1.895	2.333 to 2.706
Goodness of Fit					
Degrees of Freedom	20	20	20	20	20
R square	0.6305	0.9905	0.9048	0.6783	0.9802
Absolute Sum of Squares	3.806	0.3295	0.6433	5.04	0.6744
Sy.x	0.4362	0.1284	0.1793	0.502	0.1836
Number of points					
Analyzed	24	24	24	24	24

Table 5.3 Continued..

	[Pt(phen)(L5-S,O)]+	[Pt(phen)(L6-S,O)]+	[Pt(phen)(L7-S,O)]+	[Pt(phen)(L8-S,O)]+	[Pt(phen)(L9-S,O)]+
log(inhibitor) vs. response	Ambiguous				
Best-fit values					
Bottom	1.078	1.063	1.011	0.9566	0.9056
Top	~ 1449	3.412	3.737	3.456	3.715
LogIC50	~ 10.39	1.114	1.199	1.197	0.9151
HillSlope	~ 0.3728	4.035	2.912	3.698	3.158
IC50	~ 2.441e+010	13	15.8	15.75	8.224
Span	~ 1448	2.349	2.726	2.499	2.809
Std. Error					
Bottom	0.6854	0.04379	0.0439	0.05445	0.04496
Top	~ 2.022e+006	0.036	0.03912	0.04896	0.03216
LogIC50	~ 1643	0.01861	0.01819	0.02123	0.01528
HillSlope	~ 0.7179	0.5876	0.3311	0.7411	0.3363
Span	~ 2.022e+006	0.058	0.0614	0.07629	0.05756
95% Confidence Intervals					
Bottom	-0.3520 to 2.508	0.9718 to 1.154	0.9195 to 1.103	0.8430 to 1.070	0.8118 to 0.9994
Top	(Very wide)	3.337 to 3.487	3.655 to 3.819	3.354 to 3.558	3.648 to 3.782
LogIC50	(Very wide)	1.075 to 1.153	1.161 to 1.237	1.153 to 1.242	0.8832 to 0.9469
HillSlope	(Very wide)	2.810 to 5.261	2.221 to 3.603	2.152 to 5.243	2.456 to 3.859
IC50	(Very wide)	11.89 to 14.21	14.48 to 17.25	14.23 to 17.44	7.642 to 8.850
Span	(Very wide)	2.228 to 2.470	2.598 to 2.854	2.340 to 2.658	2.689 to 2.929
Goodness of Fit					
Degrees of Freedom	20	20	20	20	20
R square	0.6637	0.9901	0.9924	0.9855	0.9938
Absolute Sum of Squares	6.732	0.2874	0.2819	0.4755	0.2338
Sy.x	0.5802	0.1199	0.1187	0.1542	0.1081
Number of points					
Analyzed	24	24	24	24	24
	[Pt(phen)(L10-S,O)]+	[Pt(phen)(L11-S,O)]+	[Pt(phen)(L12-S,O)]+	[Pt(phen)(L13-S,O)]+	[Pt(phen)(L14-S,O)]+
log(inhibitor) vs. response	Ambiguous				
Best-fit values					
Bottom	0.8737	0.9848	0.9216	1.001	0.9657
Top	3.544	3.337	3.403	2.478	3.2
LogIC50	1.105	1.313	1.347	~ 1.179	1.279
HillSlope	2.956	4.203	6.573	~ 18.35	7.37
IC50	12.73	20.55	22.22	~ 15.09	19.02
Span	2.67	2.352	2.481	1.477	2.234
Std. Error					
Bottom	0.06214	0.05539	0.04162	0.2021	0.0581
Top	0.0508	0.05505	0.04162	0.1675	0.05804
LogIC50	0.02562	0.02675	0.0227	~ 63.03	0.0468
HillSlope	0.4388	0.7448	0.9674	~ 75659	3.758
Span	0.08314	0.07918	0.05899	0.2692	0.08258
95% Confidence Intervals					
Bottom	0.7440 to 1.003	0.8692 to 1.100	0.8348 to 1.008	0.5797 to 1.423	0.8445 to 1.087
Top	3.438 to 3.650	3.222 to 3.452	3.316 to 3.490	2.129 to 2.828	3.079 to 3.321
LogIC50	1.051 to 1.158	1.257 to 1.369	1.299 to 1.394	(Very wide)	1.182 to 1.377
HillSlope	2.040 to 3.871	2.649 to 5.756	4.555 to 8.591	(Very wide)	-0.4707 to 15.21
IC50	11.26 to 14.40	18.07 to 23.37	19.92 to 24.78	(Very wide)	15.19 to 23.82
Span	2.497 to 2.844	2.187 to 2.517	2.358 to 2.604	0.9154 to 2.039	2.062 to 2.406
Goodness of Fit					
Degrees of Freedom	20	20	20	20	20
R square	0.9854	0.9809	0.9902	0.643	0.9767
Absolute Sum of Squares	0.5189	0.5743	0.3432	6.634	0.6706
Sy.x	0.1611	0.1695	0.131	0.5759	0.1831
Number of points					
Analyzed	24	24	24	24	24

Table 5.3 Continued..

	Pd(phen)(OAc) ₂	[PtCl(dmso)(en)] ⁺	phen	HL1	HL2
log(inhibitor) vs. response		Ambiguous	Ambiguous	Ambiguous	Ambiguous
Best-fit values					
Bottom	0.9312	0.9248	0.8775	0.8362	0.8526
Top	3.607	~ 2.595	~ 2.502	~ 5.543	~ 390.3
LogIC ₅₀	1.754	~ 2.798	~ 2.810	~ 3.064	~ 5.775
HillSlope	3.194	~ 12.83	~ 12.30	~ 5.112	1.03
IC ₅₀	56.74	~ 628.7	~ 645.3	~ 1158	~ 595529
Span	2.676	~ 1.670	~ 1.624	~ 4.706	~ 389.4
Std. Error					
Bottom	0.03156	0.02464	0.02413	0.01998	0.02059
Top	0.04309	~ 27.82	~ 40.58	~ 358.1	~ 321830
LogIC ₅₀	0.0156	~ 72.50	~ 71.96	~ 10.14	~ 350.9
HillSlope	0.343	~ 9278	~ 7888	~ 50.36	0.7167
Span	0.0555	~ 27.83	~ 40.59	~ 358.1	~ 321830
95% Confidence Intervals					
Bottom	0.8654 to 0.9970	0.8734 to 0.9762	0.8271 to 0.9278	0.7945 to 0.8779	0.8096 to 0.8955
Top	3.517 to 3.697	(Very wide)	(Very wide)	(Very wide)	(Very wide)
LogIC ₅₀	1.721 to 1.786	(Very wide)	(Very wide)	(Very wide)	(Very wide)
HillSlope	2.479 to 3.910	(Very wide)	(Very wide)	(Very wide)	-0.4654 to 2.525
IC ₅₀	52.64 to 61.15	(Very wide)	(Very wide)	(Very wide)	(Very wide)
Span	2.560 to 2.792	(Very wide)	(Very wide)	(Very wide)	(Very wide)
Goodness of Fit					
Degrees of Freedom	20	20	20	20	20
R square	0.9935	0.9585	0.9579	0.9669	0.8808
Absolute Sum of Squares	0.2227	0.2186	0.2096	0.1417	0.07867
Sy.x	0.1055	0.1045	0.1024	0.08418	0.06272

5.6 References

1. A. Leed, K. DuBay, D. Sears, A.C. de Dios, P. D. Roepe, *Biochem.*, 2002, **41**, 10245-10255.
2. T.J. Egan, *Mol. Biochem. Parasitol.*, 2008, **157**, 127-136.
3. T.J. Egan, *J. Inorg. Biochem.*, 2008, **102**, 1288-1299.
4. T. Hanscheid, T. J. Egan, M. P. Grobusch, *Lancet Infect. Dis.*, 2007, **7**, 675-685.
5. S. Pagola, W. P. Stephens, D. S. Bohle, A. D. Kosar, S. K. Madsen, *Nature*, 2000, **404**, 307-310.
6. Timothy J. Egan (2011). *Biomimetic Approaches to Understanding the Mechanism of Haemozoin Formation, On Biomimetics*, Dr. Lilyana Pramatarova (Ed.), ISBN: 978-953-307-271-5, InTech, DOI: 10.5772/18933.
7. Y. S. Wu, K. R. Koch, V. R. Abratt, H. H. Klump, *Arch. Biochem Biophys.*, 2005, **440**, 28-37.
8. H. H. Klump, K. R. Koch, C.T. Lin, *S. Afr. J. Sc.*, 2006, **102**, 264-266.
9. T. J. Egan, K. R. Koch, P. L. Swan, C. Clarkson, D. A. Van Schalkwyk, P. J. Smith, *J. Med. Chem.*, 2004, **47**, 2926-2934.
10. M. D. Carter, V. V. Phelan, R. D. Sandlin, B. O. Bachmann, D. W. Wright, *Comb. Chem. High T Scr.*, 2010, **13**, 285-292.
11. K. K. Ncokazi, T. J. Egan, *Anal. Biochem.* 2005, **338**, 306-319.
12. S. N. Cohen, K. O. Phifer, K. L. Yielding, *Nature*, 1964, **202**, 805-806.
13. A. P. Gorka, A. de Dios, P. D. Roepe. *J. Med. Chem.*, 2013, **56**, 5231-5246.
14. K. A. de Villiers, H. M. Marques, T. J. Egan, *J. Inorg. Biochem.*, 2008, **102**, 1660-1667.
15. J. X. Kelly, R. Winter, M. Riscoe, D. H. Peyton, *J. Inorg. Biochem.*, 2001, **86**, 617-625.

6

Conclusions

The synthesis and characterisation of a series of novel $[\text{Pt}^{\text{II}}(\text{diimine})(\text{L}^n\text{-S},\text{O})]\text{Cl}$ complexes (where diimine is 1,10-phenanthroline (phen) or 2,2'-bipyridyl (bipy), $\text{L}^n\text{-S},\text{O}$ various chelating N,N -di(alkyl)- N' -acylthiourea) has been completed. The ^1H NMR spectrum of $[\text{Pt}^{\text{II}}(\text{phen})(\text{L}^1\text{-S},\text{O})]\text{Cl}$ in particular was unambiguously assigned using COSY for J -coupling information and 1D NOESY for the through-space dipole-dipole coupling which allowed for the first direct spectroscopic evidence of the assignments which were previously postulated from ^1H - ^{195}Pt coupling constant information. Attempts to synthesise $[\text{Pt}^{\text{II}}(\text{phen})(\text{L}^2\text{-S},\text{O})]\text{Cl}$ resulted in the crystallization of a new polymorph of $\text{Pt}^{\text{II}}(\text{bipy})\text{Cl}_2$. The crystal structure of the yellow $\text{Pt}^{\text{II}}(\text{bipy})\text{Cl}_2$ revealed the co-crystallisation of acetonitrile while the data reveals a $\text{Pt}\cdots\text{Pt}$ interaction that is very similar to that reported for the red polymorph of this complex without having this red-shift from the d_{z^2} orbital overlap. This is to the best of our knowledge, the first example of a solvent molecule (acetonitrile) to co-crystallise with $\text{Pt}^{\text{II}}(\text{bipy})\text{Cl}_2$.

$[\text{Pd}^{\text{II}}(\text{phen})(\text{L}^1\text{-S},\text{O})]\text{Cl}$ was successfully synthesised from the precursors, $\text{Pd}^{\text{II}}(\text{phen})(\text{OAc})_2$ and $\text{Pd}^{\text{II}}\text{Cl}_2(\text{phen})$, as an analogue to the $[\text{Pt}^{\text{II}}(\text{phen})(\text{L}^1\text{-S},\text{O})]\text{Cl}$ complex in attempt to determine the effect of the metal to the extent of β -haematin inhibition. Interestingly, several attempts to synthesise $[\text{Pd}^{\text{II}}(\text{phen})(\text{L}^1\text{-S},\text{O})]\text{Cl}$ from $\text{Pd}^{\text{II}}\text{Cl}_2(\text{phen})$ in chloroform, dichloromethane, acetonitrile and methanol were unsuccessful, while the inclusion of water to the solvent as a mixture resulted in the formation of $[\text{Pd}^{\text{II}}(\text{phen})(\text{L}^1\text{-S},\text{O})]\text{Cl}$ in reasonable yields (60-70%). This was attributed to the solvation of Cl^- in water which would be energetically more favourable than in organic solvents and allows for the formation of the desired complex. $[\text{Pt}^{\text{II}}\text{Cl}(\text{DMSO})(\text{en})]\text{Cl}$ was also synthesised as a cationic complex of platinum(II) without any aromatic ligands, to see if ligands with significant π -electrons are a requirement for the complexes to be β -haematin inhibitors.

From the characterisation of the series of complexes mentioned above, interesting features of the ^1H NMR spectra of some of the complexes were observed. All diimine complexes display interesting second order coupling between H^5 and H^6 , while the resolution of the ^{195}Pt satellites, $^3J(^{195}\text{Pt}-^1\text{H})$, are highly dependent of the magnetic field strength and solvent viscosity due the increase in CSA (Chemical Shift Anisotropy) relaxation rate of the square planar platinum centre leading to line broadening.

Furthermore, the synthesis of $[\text{Pt}^{\text{II}}(\text{phen})(\text{L}^2\text{-S},\text{O})]\text{Cl}$ yielded significant quantities of a novel coordination product. Upon careful studying the ^1H NMR spectrum of the reaction mixture, a *bis*-monodentate coordinated- L^2 complex, $\text{Pt}^{\text{II}}(\text{phen})(\text{L}^2\text{-S})_2$ was proposed. Attempts

to synthesise $\text{Pt}^{\text{II}}(\text{phen})(\text{L}^2\text{-S})_2$ by adjusting the reaction conditions and ligand concentration proved that this compound could be synthesised in high yields and crystallised. The crystal structure proved the proposed structure and also revealed interesting *intra*-molecular aromatic π -stacking interaction between the naphthoyl group of the bound L^2 and the coordinated phenanthroline ligand. This *intra*-molecular π -stacking interactions could significantly stabilise the $\text{Pt}^{\text{II}}(\text{phen})(\text{L}^2\text{-S})_2$ complex in solution which could account for the presence of this product in the synthesis of $[\text{Pt}^{\text{II}}(\text{phen})(\text{L}^2\text{-S},\text{O})]\text{Cl}$. 1D NOESY data reveals the presence of this *intra*-molecular π -stacking interactions in methanol- d_4 with NOEs observed between H^{5+6} of the bound 1,10-phenanthroline and the protons of the naphthoyl moiety of the coordinated L^2 .

With this in mind, we attempted to synthesise other $\text{Pt}^{\text{II}}(\text{phen})(\text{L}^n\text{-S})_2$ complex using selected *N,N*-dialkyl-*N'*-acylthioureas with specific structural variations. It was found that these *N,N*-dialkyl-*N'*-acylthioureas also form monodentate $\text{Pt}^{\text{II}}(\text{phen})(\text{L}^n\text{-S})_2$ complexes in high yields, especially those with aroylthiourea ligands while the $\text{Pt}^{\text{II}}(\text{phen})(\text{L}^n\text{-S})_2$ complexes with pivaloylthiourea ligands seems to be unstable. This novel $\text{Pt}^{\text{II}}(\text{phen})(\text{L}^n\text{-S})_2$ complexes could potentially be a new class of complexes if they are found to have some bioactivity. Crystals was also obtained for $\text{Pt}^{\text{II}}(\text{phen})(\text{L}^4\text{-S})_2$ and the crystal structure data shows that the phenanthroline moieties of these complexes also interact *via* π -stacking, in a manner similar to that postulated for the self-association of $\text{Pt}^{\text{II}}(\text{phen})(\text{L}^2\text{-S})_2$ in chloroform. The formation of both $\text{Pt}^{\text{II}}(\text{phen})(\text{L}^n\text{-S})_2$ complexes and $[\text{Pt}^{\text{II}}(\text{phen})(\text{L}^n\text{-S},\text{O})]\text{Cl}$ in high yields depending on the reaction conditions, illustrates the versatility of the *N,N*-di(alkyl)-*N'*-acylthiourea ligands to coordinate in a monodentate fashion *via* the sulphur donor atom or as a chelate *via* the sulphur and oxygen donor atoms.

The $[\text{Pt}^{\text{II}}(\text{diimine})(\text{L}^n\text{-S},\text{O})]\text{Cl}$ complexes display interesting self-association behaviour in solution which was studied. The self-association of $[\text{Pt}^{\text{II}}(\text{diimine})(\text{L}^n\text{-S},\text{O})]\text{Cl}$ complexes *via* non-covalent interactions, is expected to influence the extent β -haematin inhibition and is therefore worthwhile studying. In particular, the aggregation of $[\text{Pt}^{\text{II}}(\text{phen})(\text{L}^1\text{-S},\text{O})]\text{Cl}$ was studied in detail for solutions 0 - 100 % (v/v) $\text{D}_2\text{O}:\text{CD}_3\text{CN}$. High resolution ^1H NMR as well as Diffusion Ordered Spectroscopy (DOSY NMR) were found to be particularly well suited for this type of investigation. ^1H NMR studies of $[\text{Pt}^{\text{II}}(\text{phen})(\text{L}^1\text{-S},\text{O})]\text{Cl}$ revealed that the complexes form regiospecific non-covalent dimers in 0 to 30 % (v/v) $\text{D}_2\text{O}:\text{CD}_3\text{CN}$ solutions (which are in fast exchange in chemical shift). The extent of dimerisation was found to

increase significantly as the D₂O content increases with the dimerisation constant (K_D) increasing from $17 \pm 2 \text{ M}^{-1}$ in CD₃CN to $71 \pm 8 \text{ M}^{-1}$ in 30% (v/v) D₂O:CD₃CN at 299.3K, presumably *via* non-covalent cation- π interactions ($\Delta_r G^0_{\text{CD}_3\text{CN}} = -7.0 \text{ kJ}\cdot\text{mol}^{-1}$; $\Delta_r G^0_{30\% \text{D}_2\text{O}:\text{CD}_3\text{CN}} = -10.4 \text{ kJ}\cdot\text{mol}^{-1}$). The increase in dimerisation constant was attributed to the stabilization of the doubly charged dimer by water molecules to a greater extent with the additional stabilization due to hydrophobic effects. This aggregation process was found to be enthalpy driven ($\Delta_r H^0_{\text{CD}_3\text{CN}} = -25.1 \text{ kJ}\cdot\text{mol}^{-1}$ and $\Delta_r H^0_{30\% \text{D}_2\text{O}:\text{CD}_3\text{CN}} = -18.9 \text{ kJ}\cdot\text{mol}^{-1}$) with a negative reaction entropy ($\Delta_r S^0_{\text{CD}_3\text{CN}} = -61 \text{ J}\cdot\text{mol}^{-1}\cdot\text{K}^{-1}$ and $\Delta_r S^0_{30\% \text{D}_2\text{O}:\text{CD}_3\text{CN}} = -27 \text{ J}\cdot\text{mol}^{-1}\cdot\text{K}^{-1}$), as expected for an association reaction. However, the entropy was found to become more positive (while still negative overall) as the D₂O content increase ($\Delta\Delta_r S^0 = 34 \text{ J}\cdot\text{mol}^{-1}\cdot\text{K}^{-1}$). This positive contribution was attributed to the well known hydrophobic effect, where ordered water molecules of solvation surrounding the non-polar groups are 'released' upon association of such groups.

For solutions of higher D₂O content, >30% (v/v) D₂O:CD₃CN, the ¹H NMR spectrum displays significantly broadened signals and a marked dependence of chemical shifts on D₂O content, which could not be accounted for by the dimerisation model or higher order aggregation models. The broad ¹H NMR signals and low DOSY diffusion coefficients of solutions of [Pt^{II}(phen)(L¹-S,O)]Cl in pure D₂O suggest that significant aggregation processes occur in these solutions, while TEM images reveal large well defined 'spaghetti-like' structures. The diffusion coefficients for these solutions obtained using DOSY NMR, suggests the formation of nano-sized structures ("metallo gels") consisting of up to *ca.* 735 mononuclear cations, above a critical aggregation concentration (9.6 - 10.3 mM at 299.3K). TEM images of freshly diluted samples reveals that the well defined 'spaghetti'-like structures (diameter = $\pm 20\text{nm}$) comprise of smaller parallel 'strands' ($\pm 2\text{nm}$), presumably linearly 'stacked' [Pt^{II}(phen)(L¹-S,O)]⁺ cations. The positive charge build-up that is expected to result from this association process is probably stabilized/offset by ion-pairing interactions with the chloride ions at the edges of such structures. This view is supported by the fact that the cationic uranyl acetate stain used in the TEM imaging accumulated at the edges of these nano-aggregates. The ¹H and DOSY NMR revealed significant shielding and slower diffusion coefficients with the addition of NaCl to the solutions which is consistent with an increase in the degree of aggregation. From these results it is clear that if [Pt^{II}(diimine)(Lⁿ-S,O)]Cl complexes will be considered as bioactive compounds in the future, the extensive self-

association behaviour these complexes cannot be ignored concerning the saline water content in biological systems.

The capability of $[\text{Pt}^{\text{II}}(\text{diimine})(\text{L}^{\text{n}}-\text{S},\text{O})]^+$ complexes to not only self-associate but also association with other molecules such as pyrene and haematin are of interest. However, since haematin is paramagnetic, it could not be used in the NMR study and pyrene was used. It was found that $[\text{Pt}^{\text{II}}(\text{phen})(\text{L}^1-\text{S},\text{O})]\text{Cl}$ forms relatively strong 1:1 outer-sphere complexes with pyrene. The equilibrium constant for the non-covalent 1:1 $[\text{Pt}^{\text{II}}(\text{phen})(\text{L}^1-\text{S},\text{O})]^+$ /pyrene aggregate formation was found to be 37.9 M^{-1} at 25°C from ^1H chemical shift data which is within experimental error to what was previously obtained for $[\text{Pt}^{\text{II}}(\text{phen})(\text{L}^1-\text{S},\text{O})]\text{Cl}$ /fluoranthene association (39.7 M^{-1}). Both these association constants are significantly higher than that of the self-association of $[\text{Pt}^{\text{II}}(\text{phen})(\text{L}^1-\text{S},\text{O})]^+$ ($K_{\text{D}} = 14.5 \text{ M}^{-1}$). Pyrene was found to form a stronger 1:1 aggregate with $[\text{Pt}^{\text{II}}(\text{phen})(\text{L}^1-\text{S},\text{O})]^+$ with the corresponding $\Delta_{\text{r}}H_{(\text{M/P})} = -18.1 \pm 3 \text{ kJ}\cdot\text{mol}^{-1}$ compared to fluoranthene ($\Delta_{\text{r}}H_{(\text{M/F})} = -13.3 \pm 3 \text{ kJ}\cdot\text{mol}^{-1}$) which is postulated to be due to the larger aromatic π -surface of pyrene forming a stronger cation- π interaction with the $[\text{Pt}^{\text{II}}(\text{phen})(\text{L}^1-\text{S},\text{O})]^+$ cation.

With the above mentioned findings it is reasonable to postulate that $[\text{Pt}^{\text{II}}(\text{diimine})(\text{L}^{\text{n}}-\text{S},\text{O})]^+$ complexes will have the capabilities to association to haematin to ultimately inhibit haemozoin formation in the malaria parasite, However, we have test this hypothesis using a synthetic haemozoin (β -haematin) inhibition study and the testing of the series of complexes of this study against the *Plasmodium falciparum* is subject of future study.

A β -haematin assay was performed for all complexes synthesized to establish their potential for antimalarial activity. The series of $[\text{Pt}^{\text{II}}(\text{diimine})(\text{L}^{\text{n}}-\text{S},\text{O})]^+$ complexes was found to significantly inhibit β -haematin formation, while the respective ligands were inactive. More specifically, $[\text{Pt}^{\text{II}}(\text{phen})(\text{L}^{\text{n}}-\text{S},\text{O})]^+$ complexes were found to be significantly better β -haematin inhibitors compared to the $[\text{Pt}^{\text{II}}(\text{bipy})(\text{L}^{\text{n}}-\text{S},\text{O})]^+$ and $[\text{Pd}^{\text{II}}(\text{phen})(\text{L}^{\text{n}}-\text{S},\text{O})]^+$ variations. The complexes with *N,N*-dibutyl-*N'*-acylthiourea ligands did not show significant activity, with large quantities of β -haematin precipitate adhering to the sides of the polypropylene wells. The inactivity of these complexes and the unusual behaviour of the β -haematin in these samples were attributed to a hydrophobic interaction of the butyl chains of these complexes with the surfactant (NP-40).

$[\text{Pt}^{\text{II}}_2(\text{phen})_2(\text{L}^{\text{g}}-\text{S},\text{O})]^{2+}$, a complex with an acylthiourea ligand with two *S,O*-coordination sites, was found to be the most efficient β -haematin inhibitor tested with the corresponding

$IC_{50} = 8 \pm 1 \mu\text{M}$. Remarkably, this value is roughly half the IC_{50} of the mono-functional complexes $[\text{Pt}^{\text{II}}(\text{phen})(\text{L}^{\text{n}}-\text{S},\text{O})]^+$ and is significantly more efficient than the two well known and commonly used antimalarials, chloroquine ($34 \pm 2 \mu\text{M}$) and amodiaquine ($13 \pm 1 \mu\text{M}$).

We have postulated 4 possible association/aggregate structures for the hetero-dimers of the solution species of haematin and the $[\text{Pt}^{\text{II}}(\text{phen})(\text{L}^{\text{n}}-\text{S},\text{O})]^+$ complexes. The cation- π interaction is believed to be responsible for the effectiveness of these complexes, while other contributing non-covalent interactions include ion-pairing, π -stacking while the coordination of the acyl group of L^{n} and the Fe(III) metal centre is also considered.

From this study significant insight is gained regarding the synthesis of this $[\text{Pt}^{\text{II}}(\text{diimine})(\text{L}^{\text{n}}-\text{S},\text{O})]^+$ complexes as bioactive molecules. Furthermore we have discovered a possible new class of $\text{Pt}^{\text{II}}(\text{phen})(\text{L}^{\text{n}}-\text{S})_2$ complexes which could have interesting bioactivity which is something of future study. We have also found a novel polymorph of $\text{Pt}^{\text{II}}(\text{bipy})\text{Cl}_2$ with acetonitrile and the possibility of other solvents to also co-crystallise with $\text{Pt}^{\text{II}}(\text{bipy})\text{Cl}_2$ would be interesting for future work. The self-association of $[\text{Pt}^{\text{II}}(\text{phen})(\text{L}^1-\text{S},\text{O})]^+$ was thoroughly being studied and the modelling of the aggregates (dimers and nano-aggregates) would be of great value in the future. Furthermore, other complexes could also be investigated in this manner to see if structural variation of the ligands influences the morphology of the aggregates in water.

More future recommendation includes the modelling of potential aggregate structures of $[\text{Pt}^{\text{II}}(\text{phen})(\text{L}^{\text{n}}-\text{S},\text{O})]^+/\text{Fe(III)PPIX}$ using quantum mechanical calculations to identify critical positions for structural variation/optimisation. In view of the excellent activity of $[\text{Pt}^{\text{II}}_2(\text{phen})_2(\text{L}^{\text{9}}-\text{S},\text{O})]^{2+}$, more complexes with bipodal ligands could be synthesised and their strengths of β -haematin inhibition could be compared together with the test results for the activity against real parasites. This ligand architecture could potentially be incorporated in macro-molecules with large amounts of functional groups, like polymers, dendrimers or functionalised nanoparticles which may increase the effectiveness and/or decrease cytotoxicity of these agents.

A.

Appendix A - Additional Figures and Tables

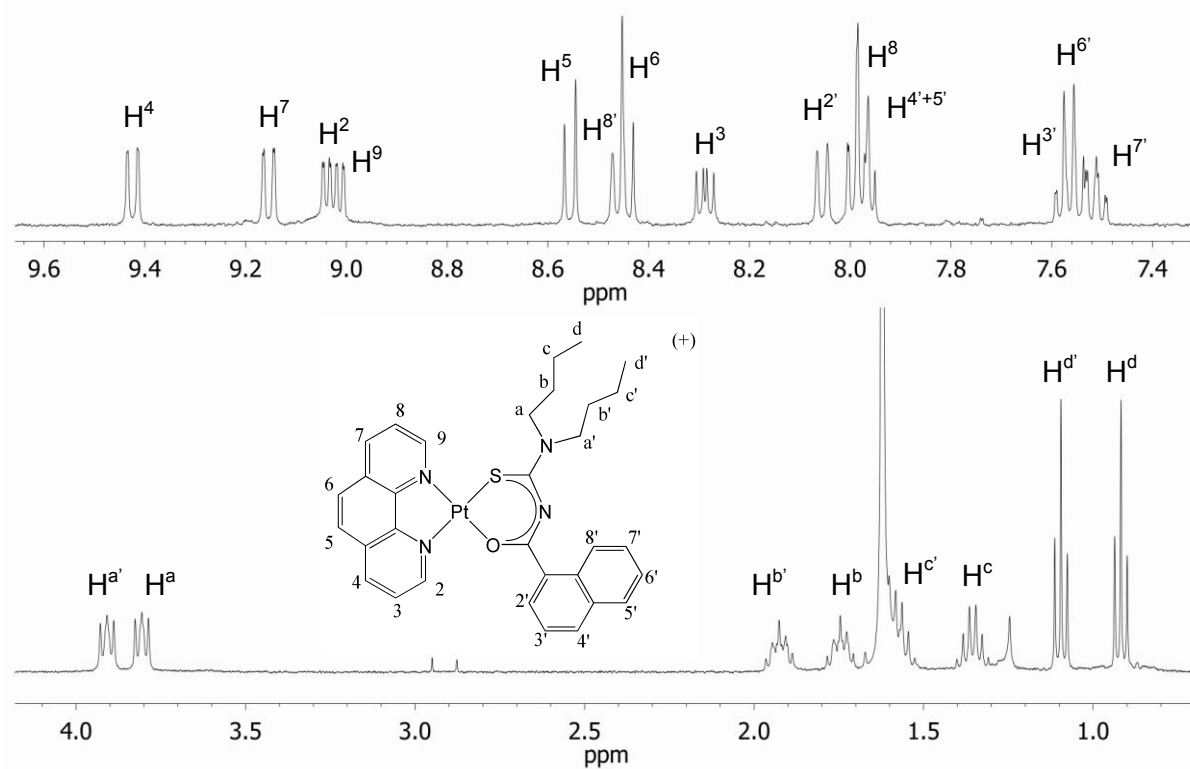


Figure A.1 ^1H NMR spectrum of $[\text{Pt}^{\text{II}}(\text{phen})(\text{L}^2\text{-S},\text{O})]\text{Cl}$ in chloroform- d_1 at 25°C .

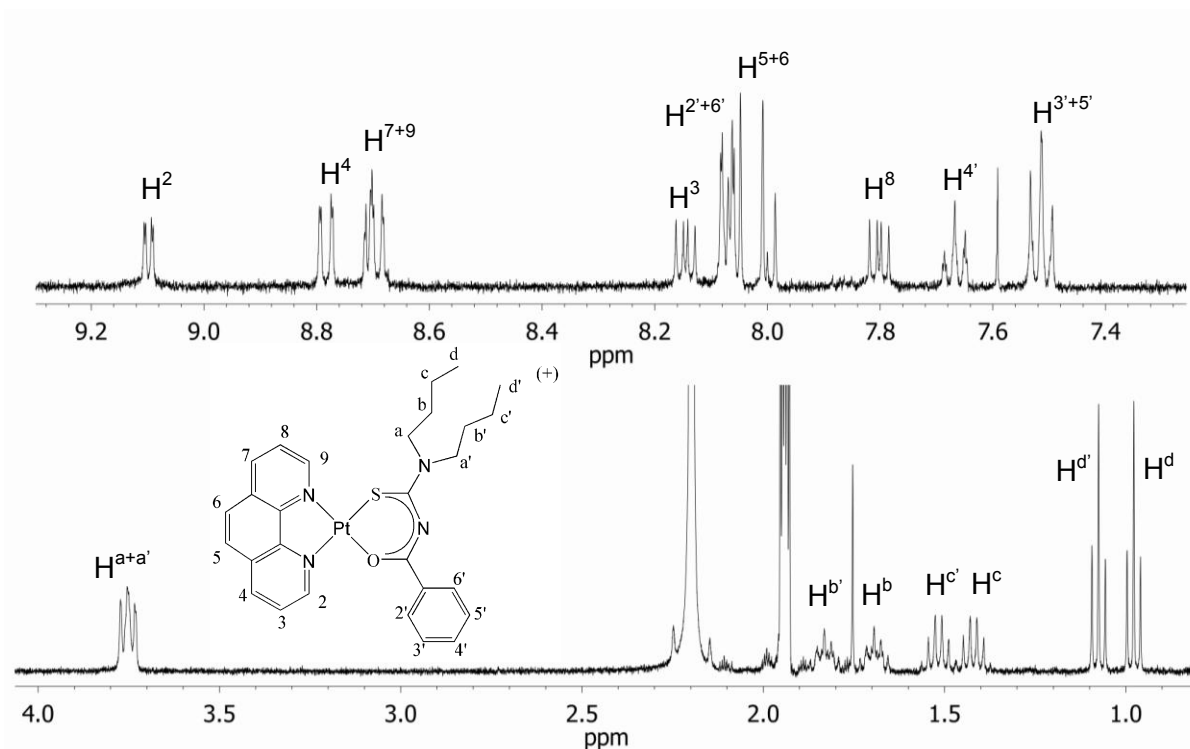


Figure A.2 ^1H NMR spectrum of $[\text{Pt}^{\text{II}}(\text{phen})(\text{L}^3\text{-S},\text{O})]\text{Cl}$ in acetonitrile- d_3 at 25°C .

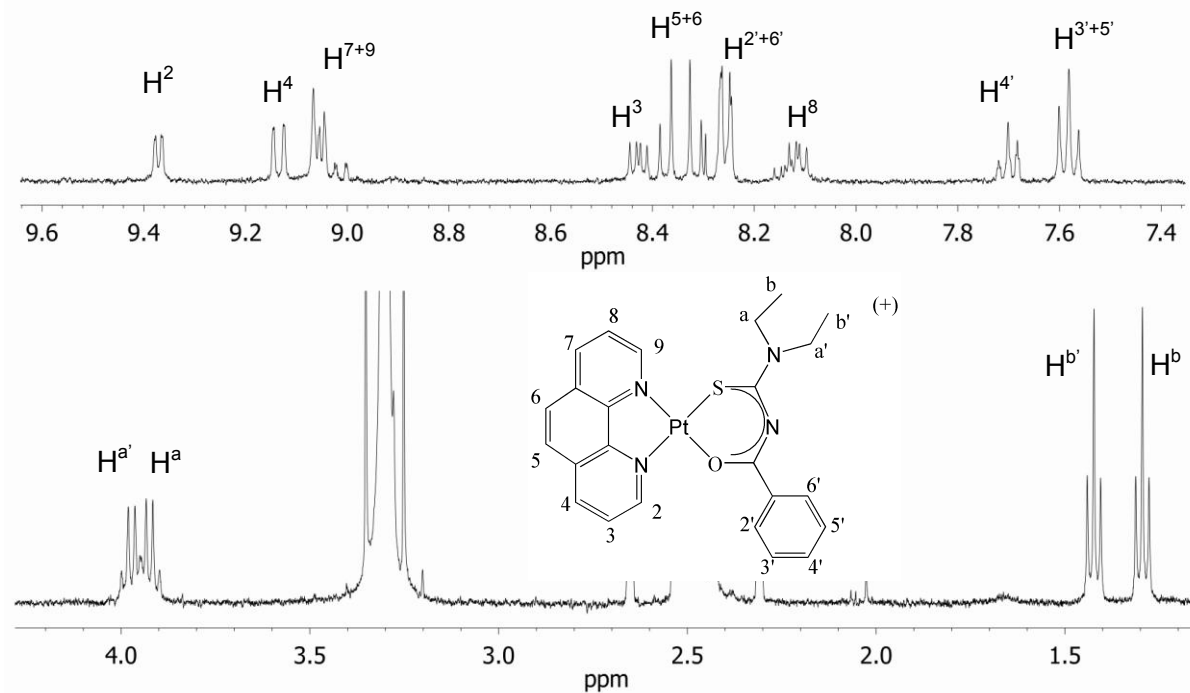


Figure A.3 ^1H NMR spectrum of $[\text{Pt}^{\text{II}}(\text{phen})(\text{L}^4\text{-S},\text{O})]\text{Cl}$ in dimethyl sulfoxide- d_6 at 25°C .

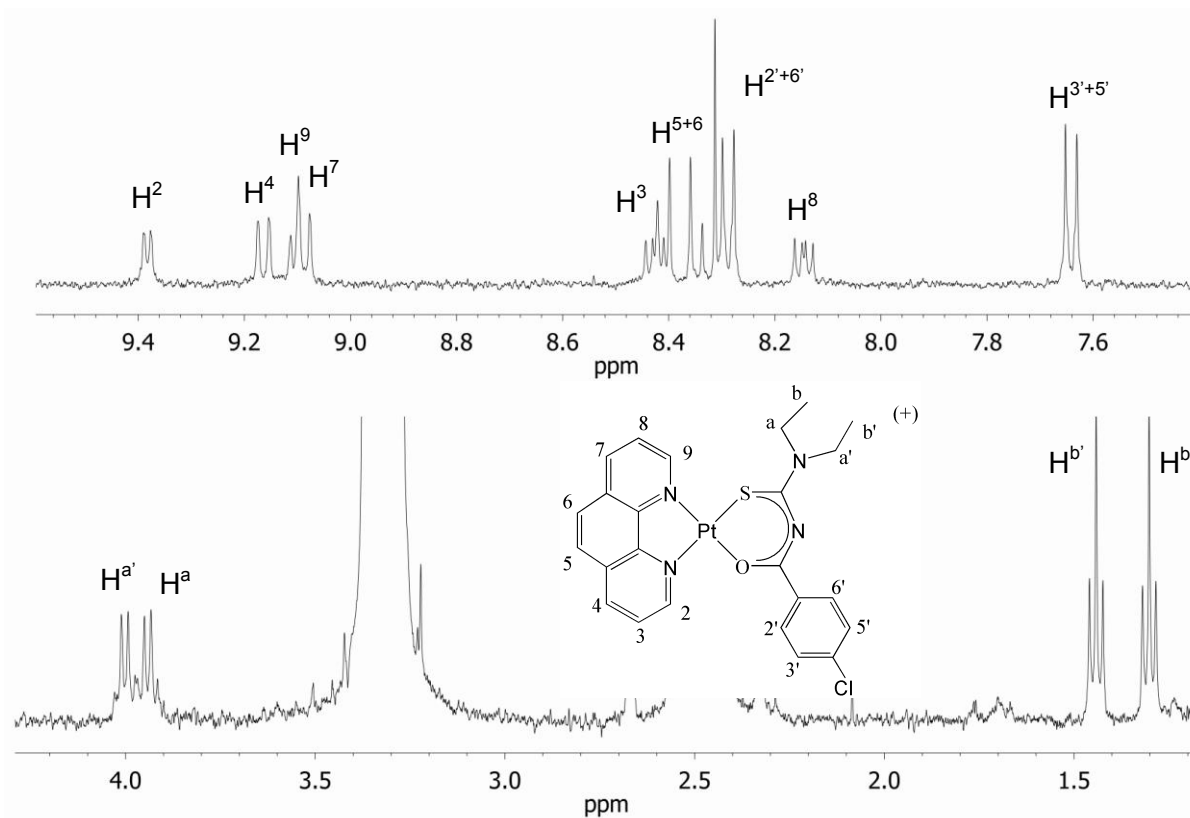


Figure A.4 ^1H NMR spectrum of $[\text{Pt}^{\text{II}}(\text{phen})(\text{L}^5\text{-S},\text{O})]\text{Cl}$ in dimethyl sulfoxide- d_6 at 25°C .

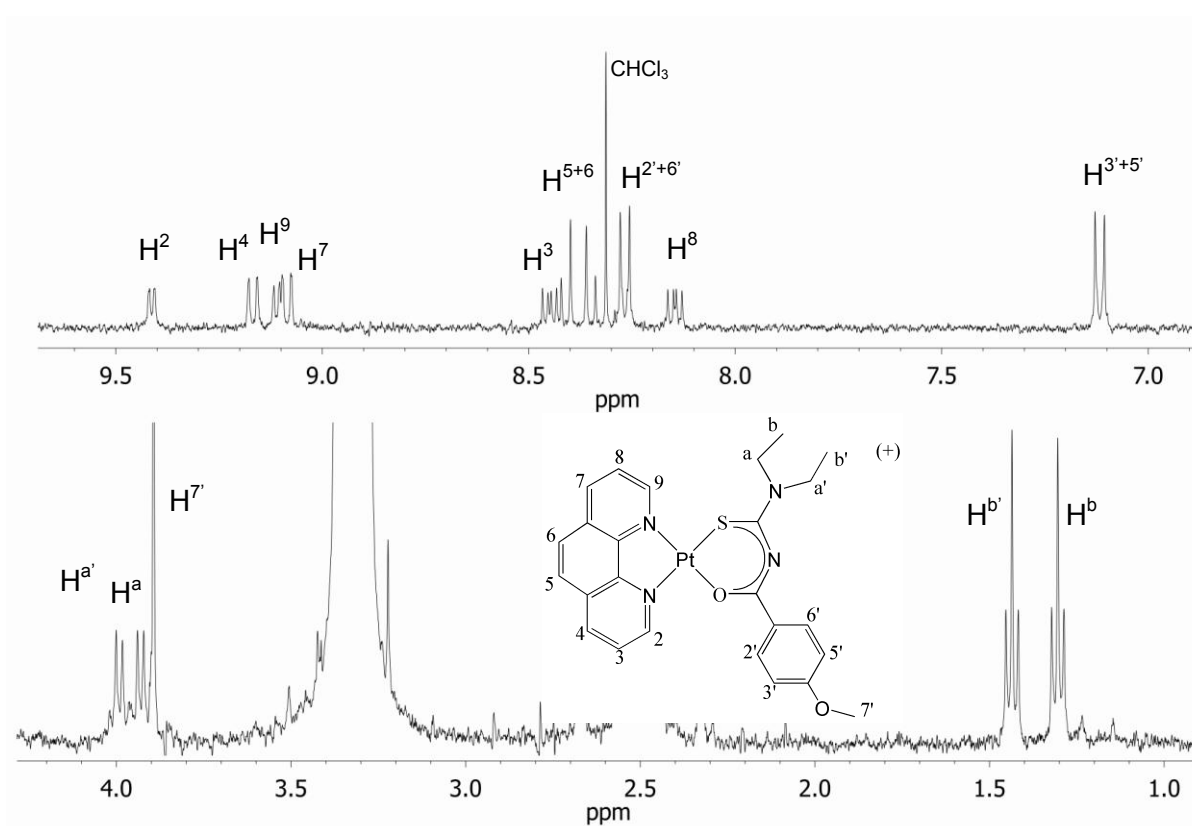


Figure A.5 ^1H NMR .of $[\text{Pt}^{\text{II}}(\text{phen})(\text{L}^6\text{-S,O})]\text{Cl}$ in dimethyl sulfoxide- d_6 at 25°C .

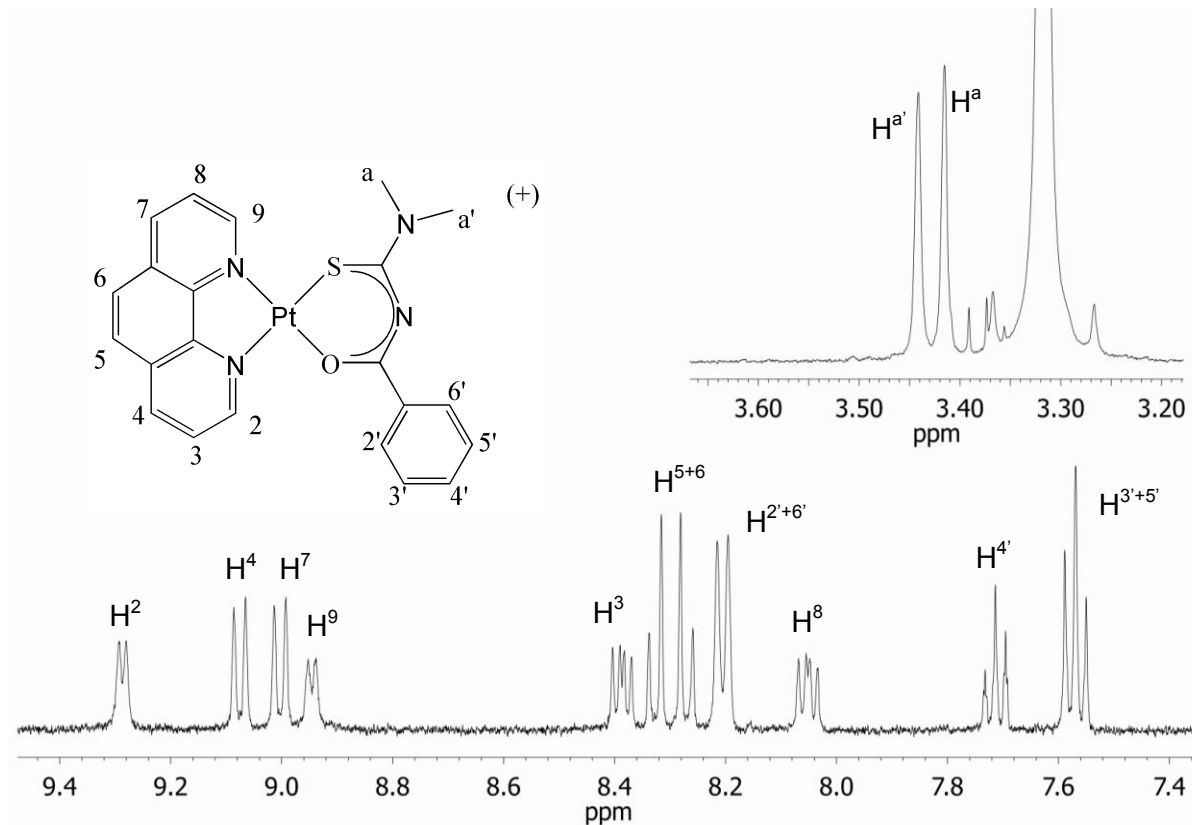


Figure A.6 ^1H NMR spectrum of $[\text{Pt}^{\text{II}}(\text{phen})(\text{L}^7\text{-S,O})]\text{Cl}$ in dimethyl sulfoxide- d_6 at 25°C .

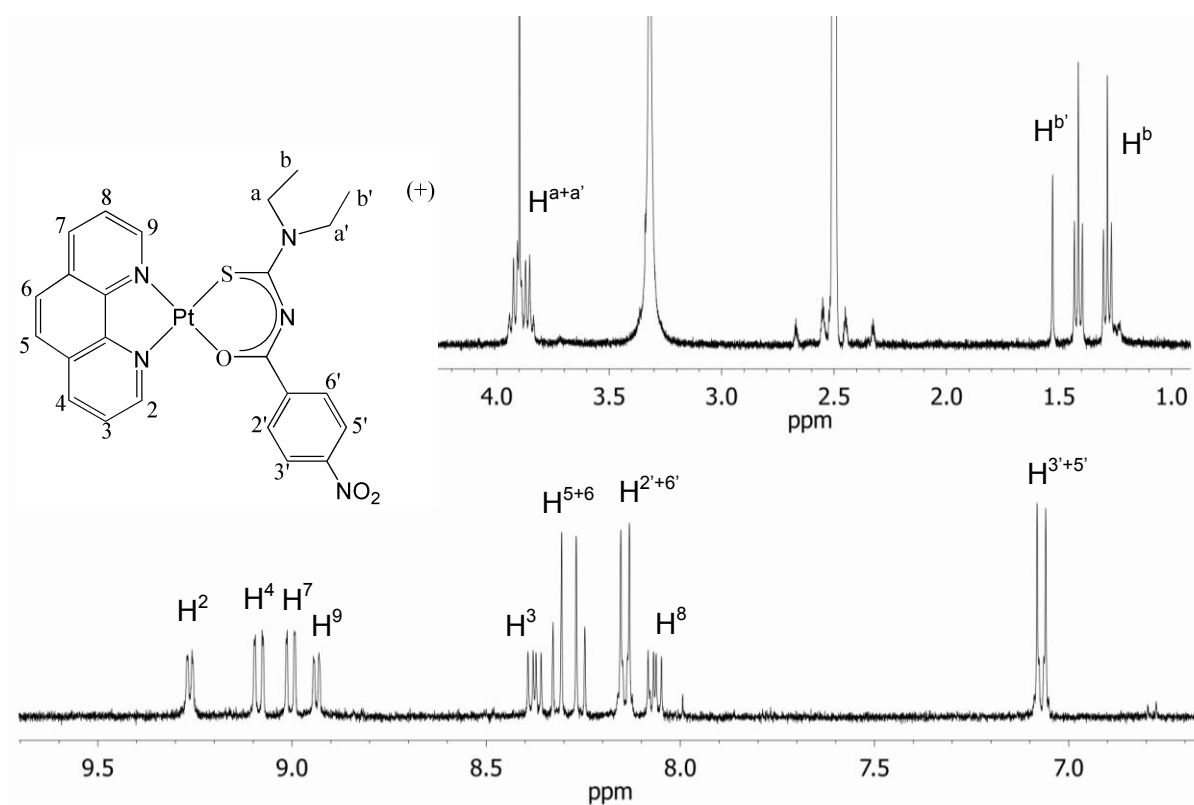


Figure A.7 ^1H NMR spectrum of $[\text{Pt}^{\text{II}}(\text{phen})(\text{L}^8\text{-S,O})]\text{Cl}$ in dimethyl sulfoxide- d_6 at 25°C .

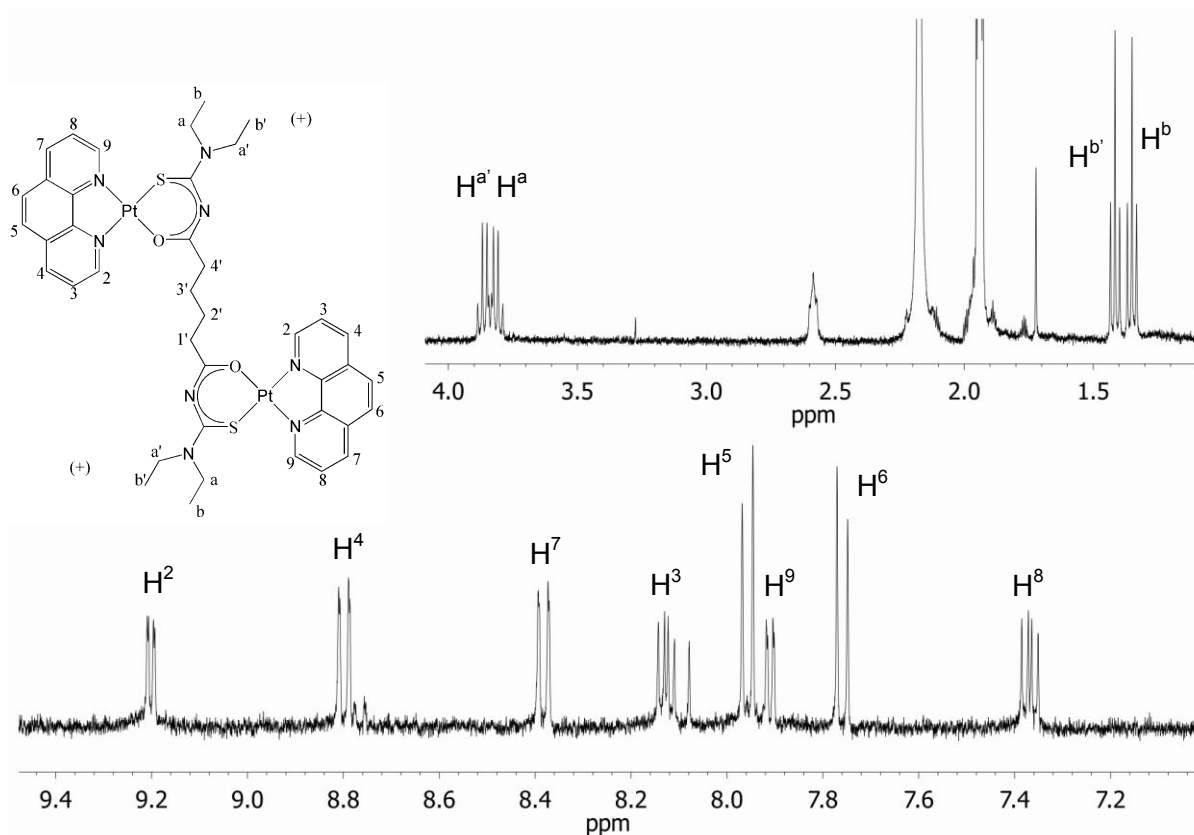


Figure A.8 ^1H NMR spectrum of $[\text{Pt}_2^{\text{II}}(\text{phen})_2(\text{L}^9\text{-S,O})]\text{Cl}_2$ in acetonitrile- d_3 at 25°C .

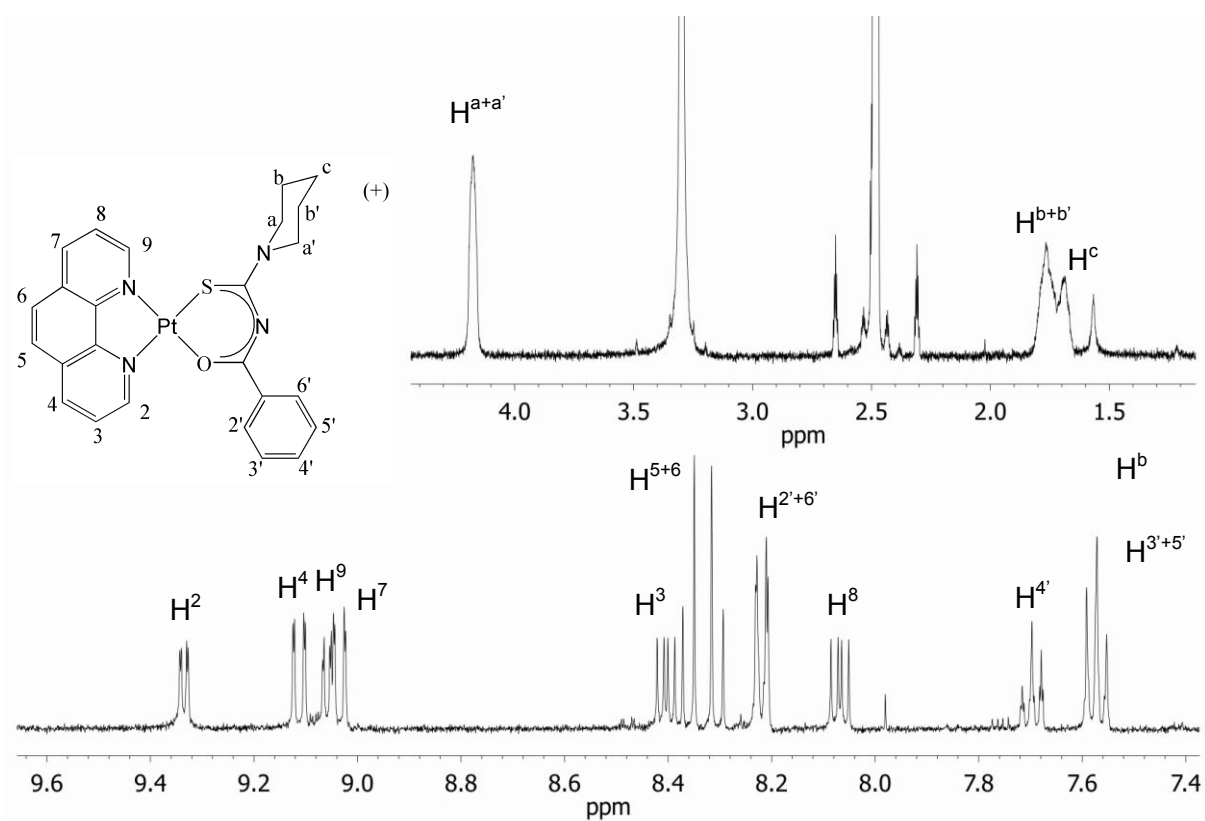


Figure A.9 ^1H NMR spectrum of $[\text{Pt}^{\text{II}}(\text{phen})(\text{L}^{10}\text{-S,O})]\text{Cl}$ in dimethyl sulfoxide- d_6 at 25°C .

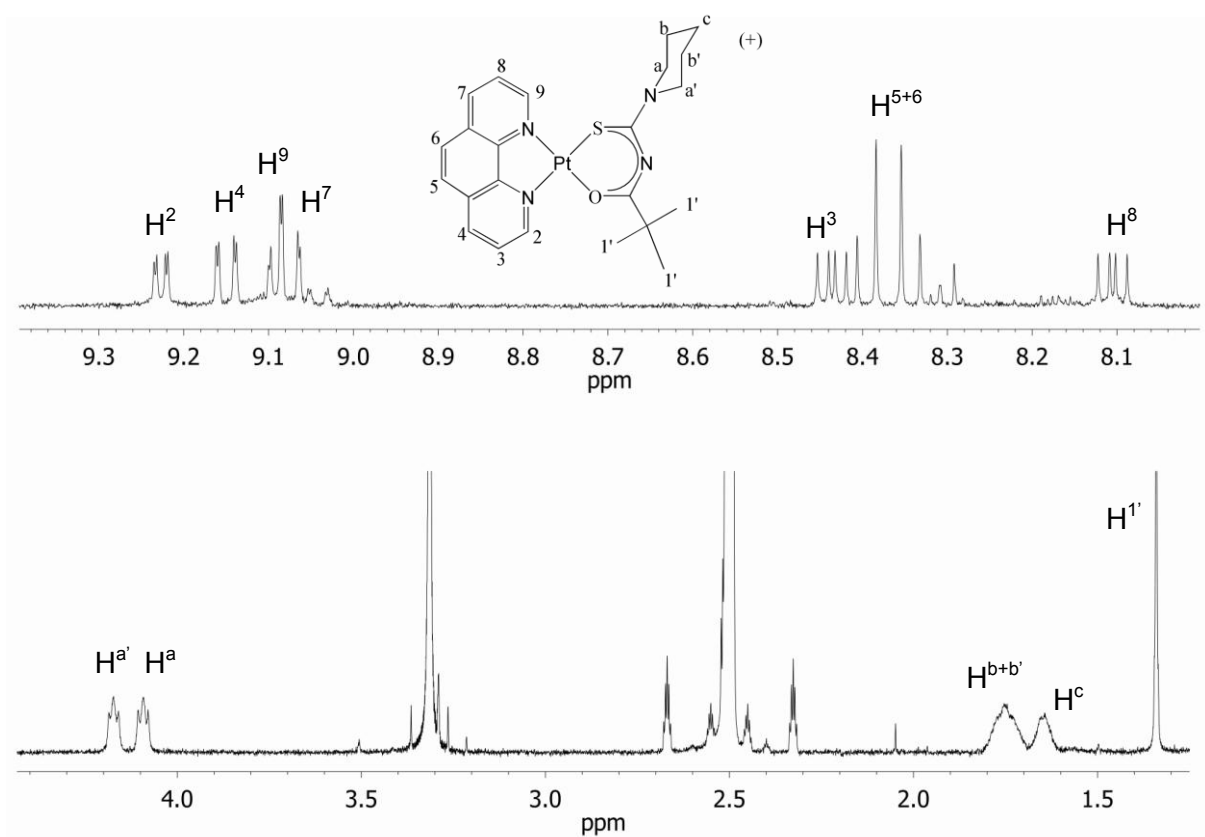


Figure A.10 ^1H NMR spectrum of $[\text{Pt}^{\text{II}}(\text{phen})(\text{L}^{11}\text{-S,O})]\text{Cl}$ in dimethyl sulfoxide- d_6 at 25°C .

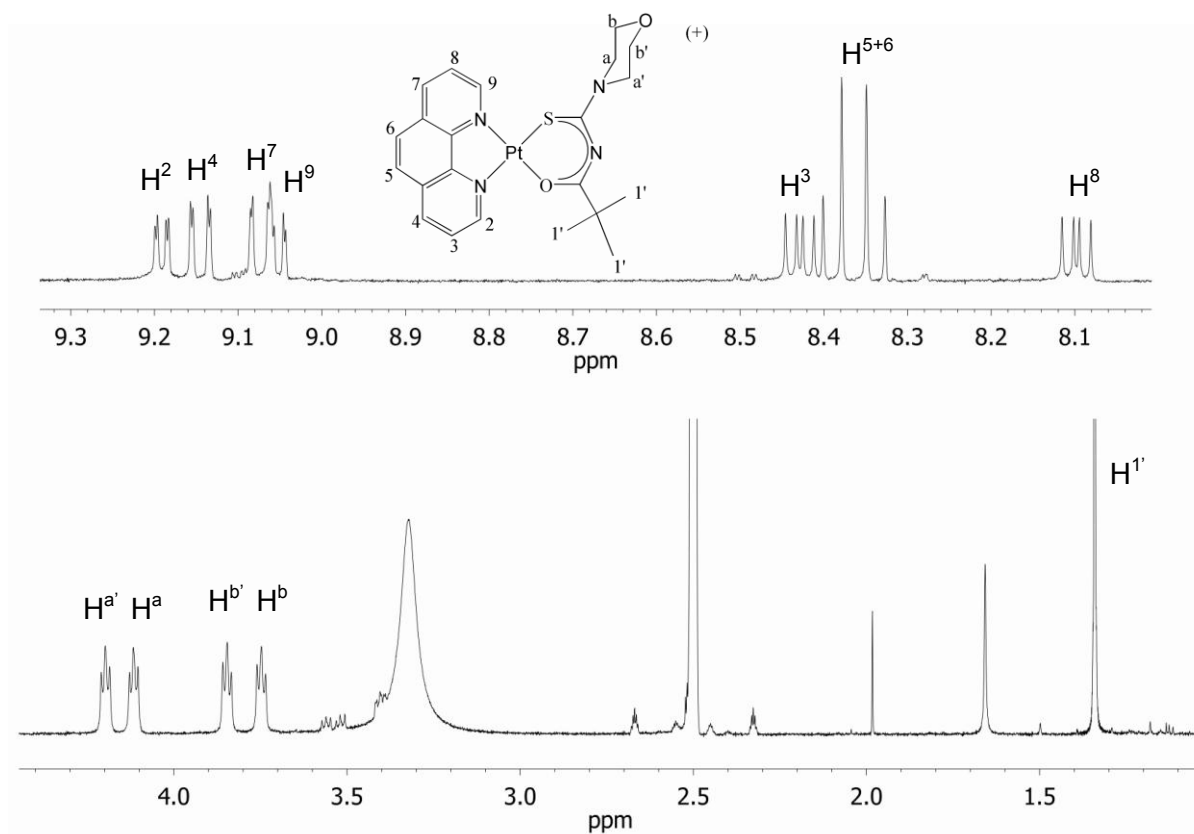


Figure A.11 ^1H NMR spectrum of $[\text{Pt}^{\text{II}}(\text{phen})(\text{L}^{12}\text{-S,O})]\text{Cl}$ in dimethyl sulfoxide- d_6 at 25°C .

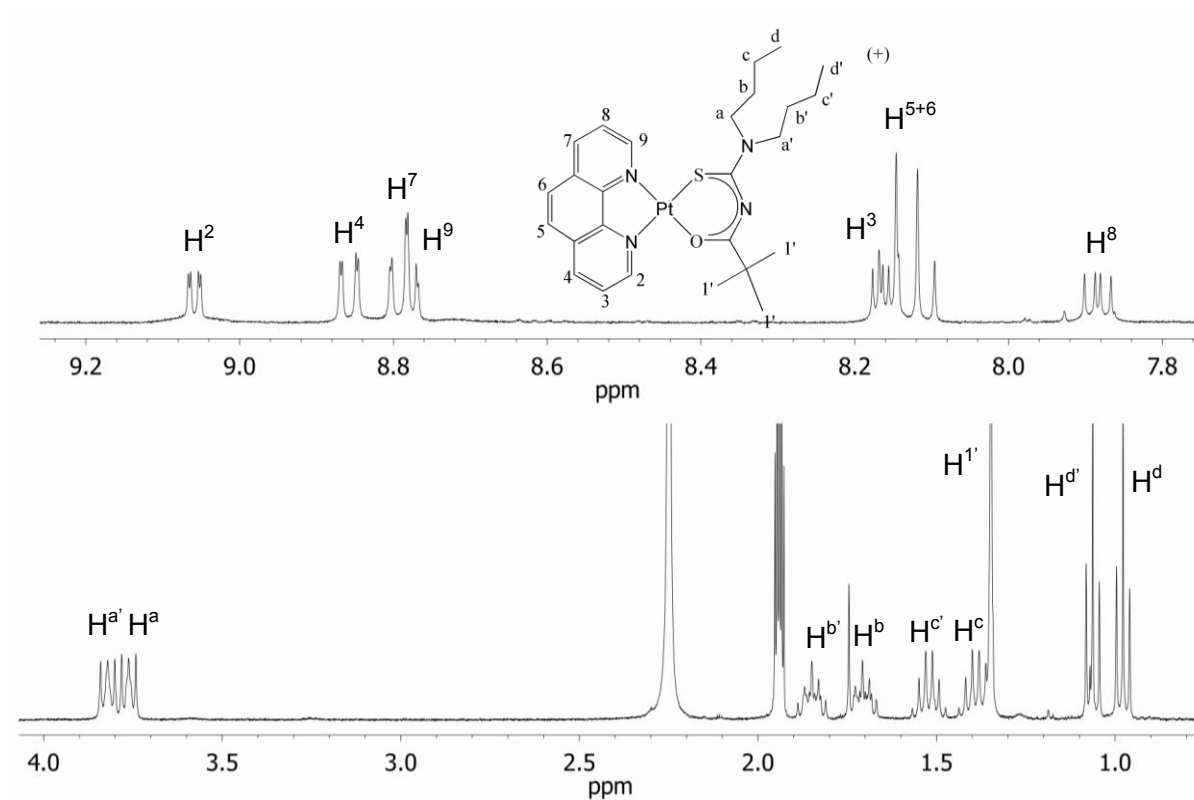


Figure A.12 ^1H NMR spectrum of $[\text{Pt}^{\text{II}}(\text{phen})(\text{L}^{13}\text{-S,O})]\text{Cl}$ in dimethyl sulfoxide- d_6 at 25°C .

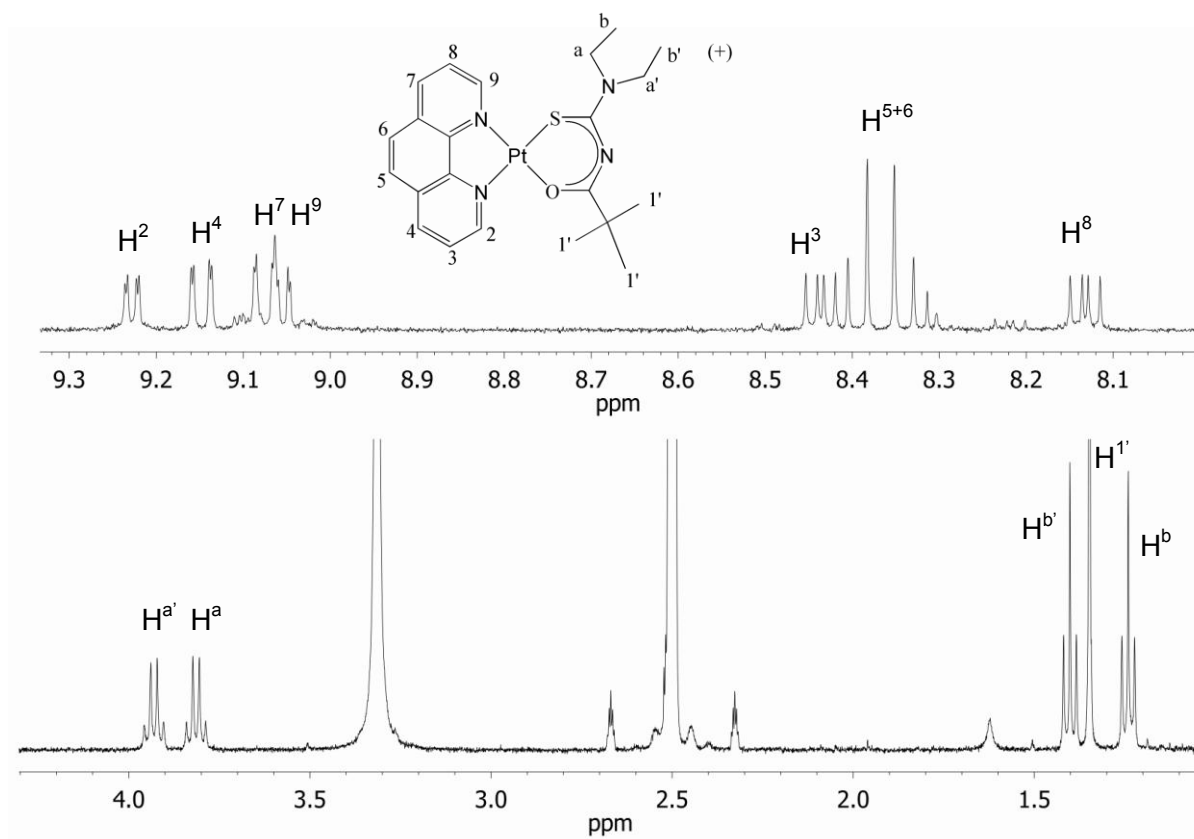


Figure A.13 ^1H NMR spectrum of $[\text{Pt}^{\text{II}}(\text{phen})(\text{L}^{14}\text{-S,O})]\text{Cl}$ in dimethyl sulfoxide- d_6 at 25°C .

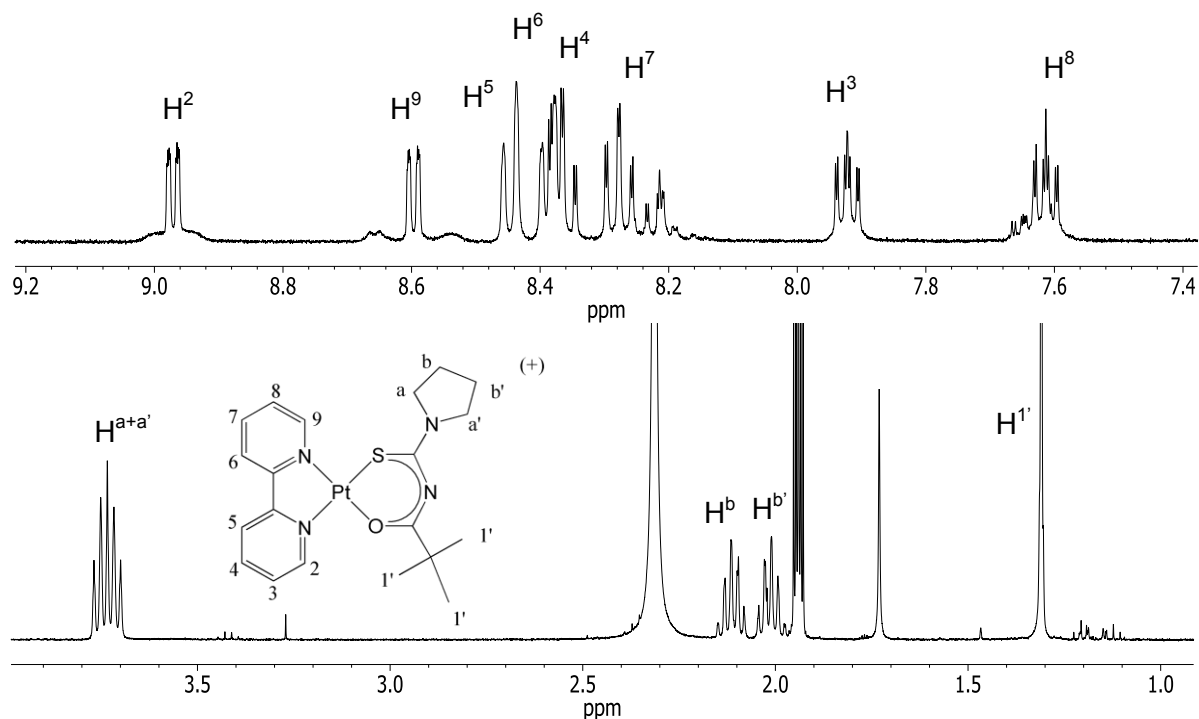


Figure A.14 ^1H NMR spectrum of $[\text{Pt}^{\text{II}}(\text{bipy})(\text{L}^1\text{-S,O})]\text{Cl}$ in acetonitrile- d_3 at 25°C

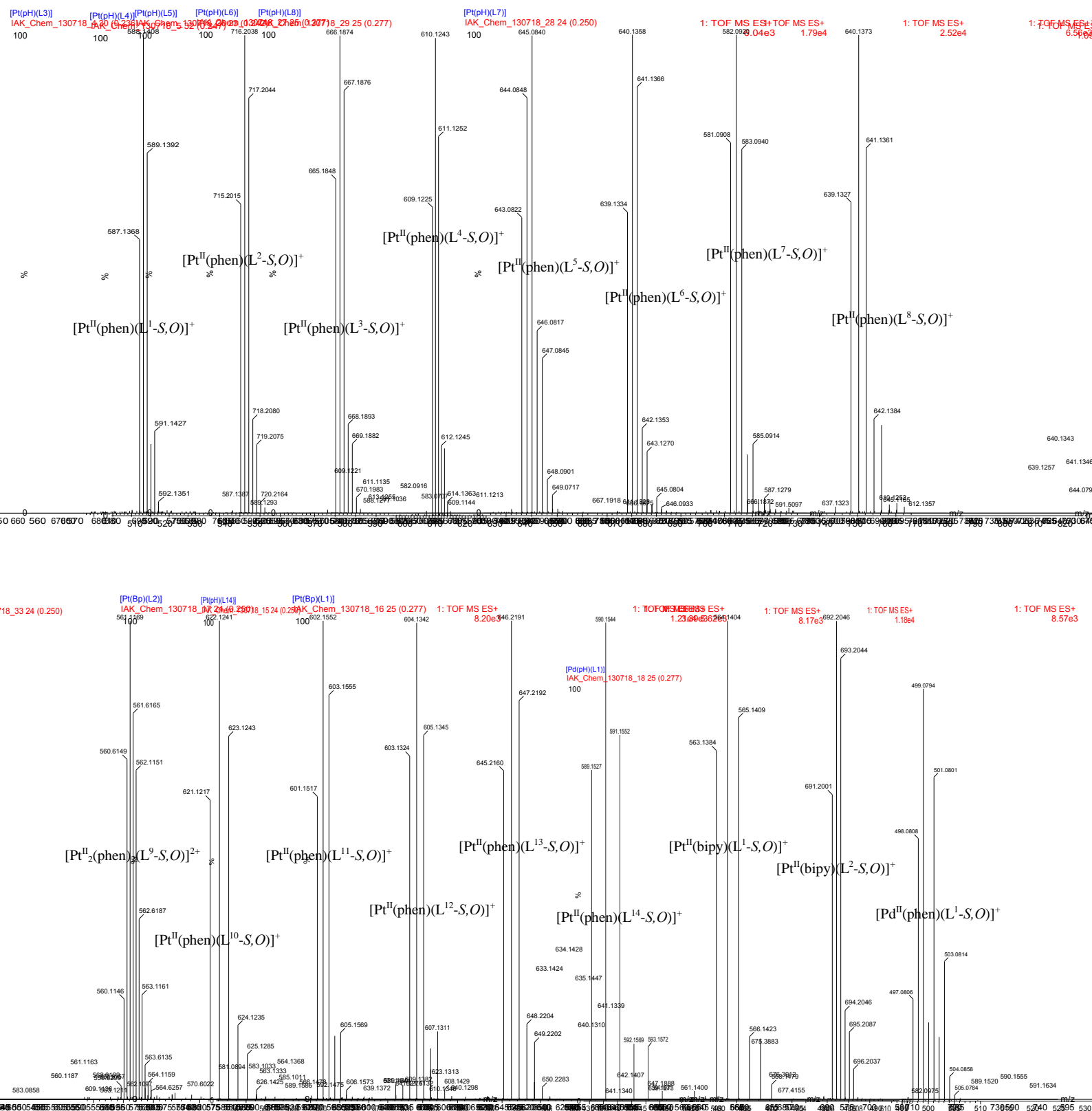
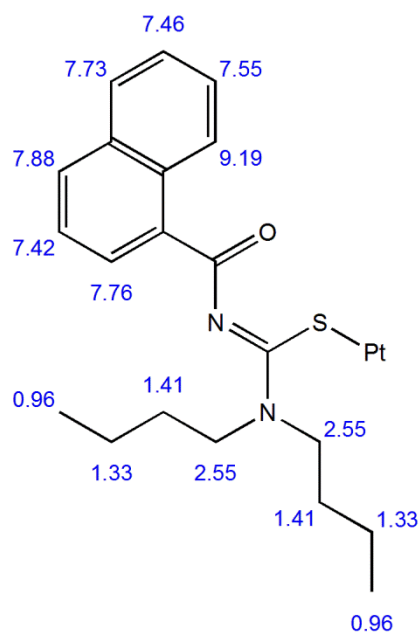


Figure A.15 (+) ESI Mass spectra of $[\text{Pt}^{\text{II}}(\text{phen})(\text{L}^n\text{-S,O})]^+$, $[\text{Pt}^{\text{II}}(\text{bipy})(\text{L}^n\text{-S,O})]^+$ and $[\text{Pd}^{\text{II}}(\text{phen})(\text{L}^1\text{-S,O})]^+$ in methanol with a cone voltage of 15 V.

ChemNMR H-1 Estimation



Estimation Quality: blue = good,
magenta = medium, red = rough

Protocol of the H-1 NMR Prediction:

Node	Shift	Base + Inc.	Comment (ppm rel. to TMS)
CH	7.88	7.67	1-naphthalene
		0.21	1 -C=O
CH	7.42	7.32	1-naphthalene
		0.10	1 -C=O
CH	7.76	7.32	1-naphthalene
		0.44	1 -C=O
CH	9.19	7.67	1-naphthalene
		1.52	1 -C=O
CH	7.55	7.32	1-naphthalene
		0.23	1 -C=O
CH	7.46	7.32	1-naphthalene
		0.14	1 -C=O
CH	7.73	7.67	1-naphthalene
		0.06	1 -C=O
CH2	2.55	1.37	methylene
		1.22	1 alpha -N-C
		-0.04	1 beta -C
CH2	1.41	1.37	methylene
		0.08	1 beta -N-C
		-0.04	1 beta -C
CH2	1.33	1.37	methylene
		0.00	1 alpha -C
		-0.04	1 beta -C
CH3	0.96	0.86	methyl
		0.10	1 beta -C-R
CH2	2.55	1.37	methylene
		1.22	1 alpha -N-C
		-0.04	1 beta -C
CH2	1.41	1.37	methylene
		0.08	1 beta -N-C
		-0.04	1 beta -C
CH2	1.33	1.37	methylene
		0.00	1 alpha -C
		-0.04	1 beta -C
CH3	0.96	0.86	methyl
		0.10	1 beta -C-R

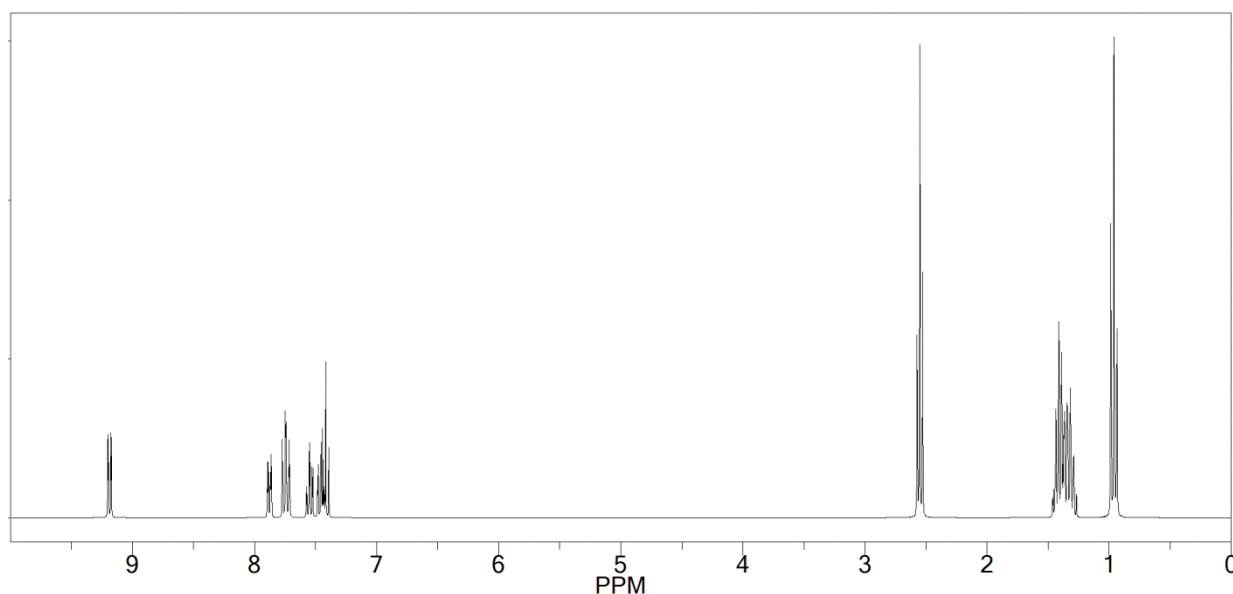


Figure A.16 Calculated ¹H NMR chemical shifts of the relevant section of L² coordinated to the platinum metal centre using the ChemDraw Ultra software package.

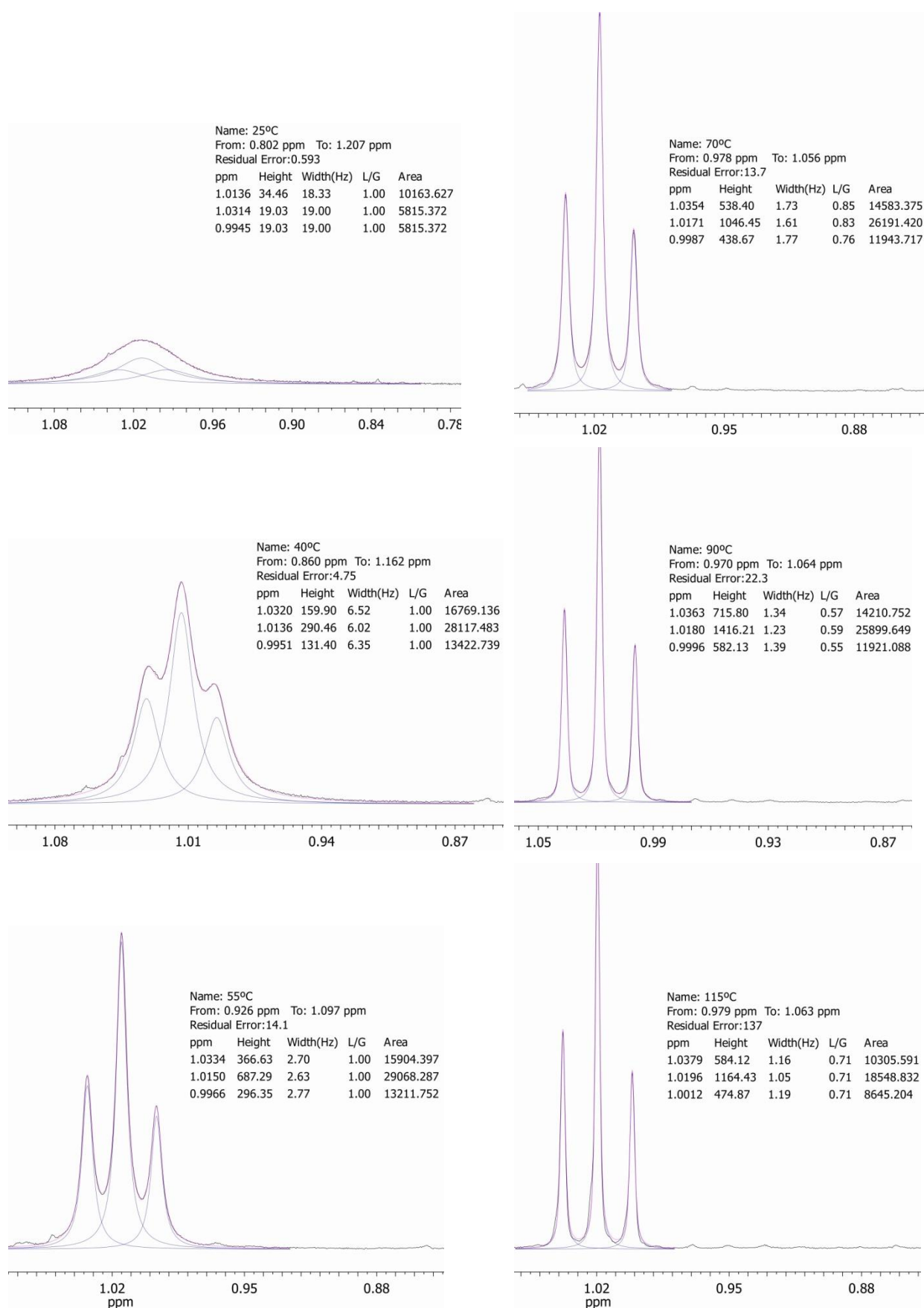


Figure A.17 Line-fits of the ^1H NMR resonance of $\text{H}^{\text{d+d'}}$ of $\text{Pt}^{\text{II}}(\text{phen})(\text{L}^2\text{-S})_2$ at various temperatures.

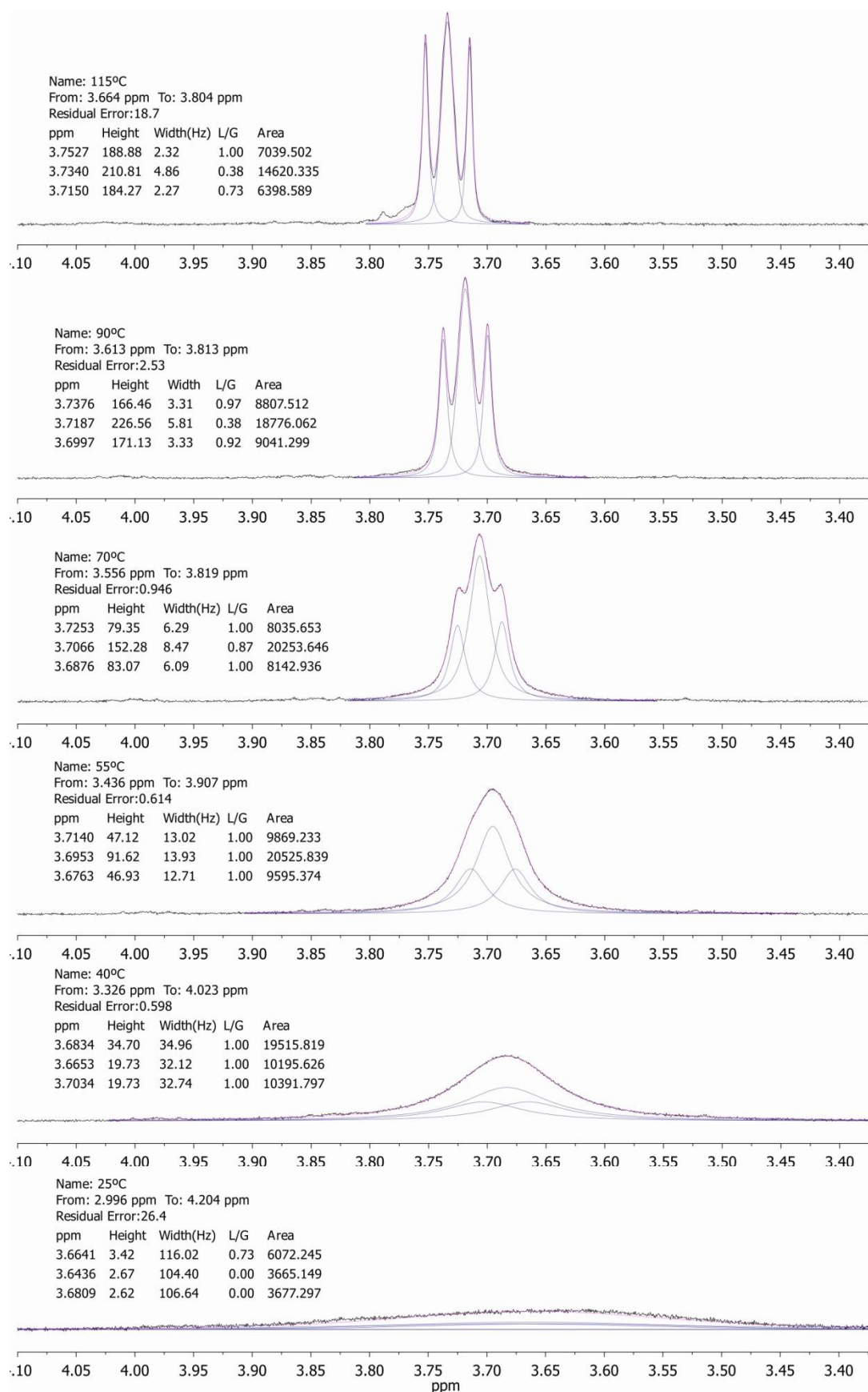


Figure A.18 Line-fits of the ^1H NMR resonance of $\text{H}^{\text{a+a}'}$ of $\text{Pt}^{\text{II}}(\text{phen})(\text{L}^2\text{-S})_2$ at various temperatures.

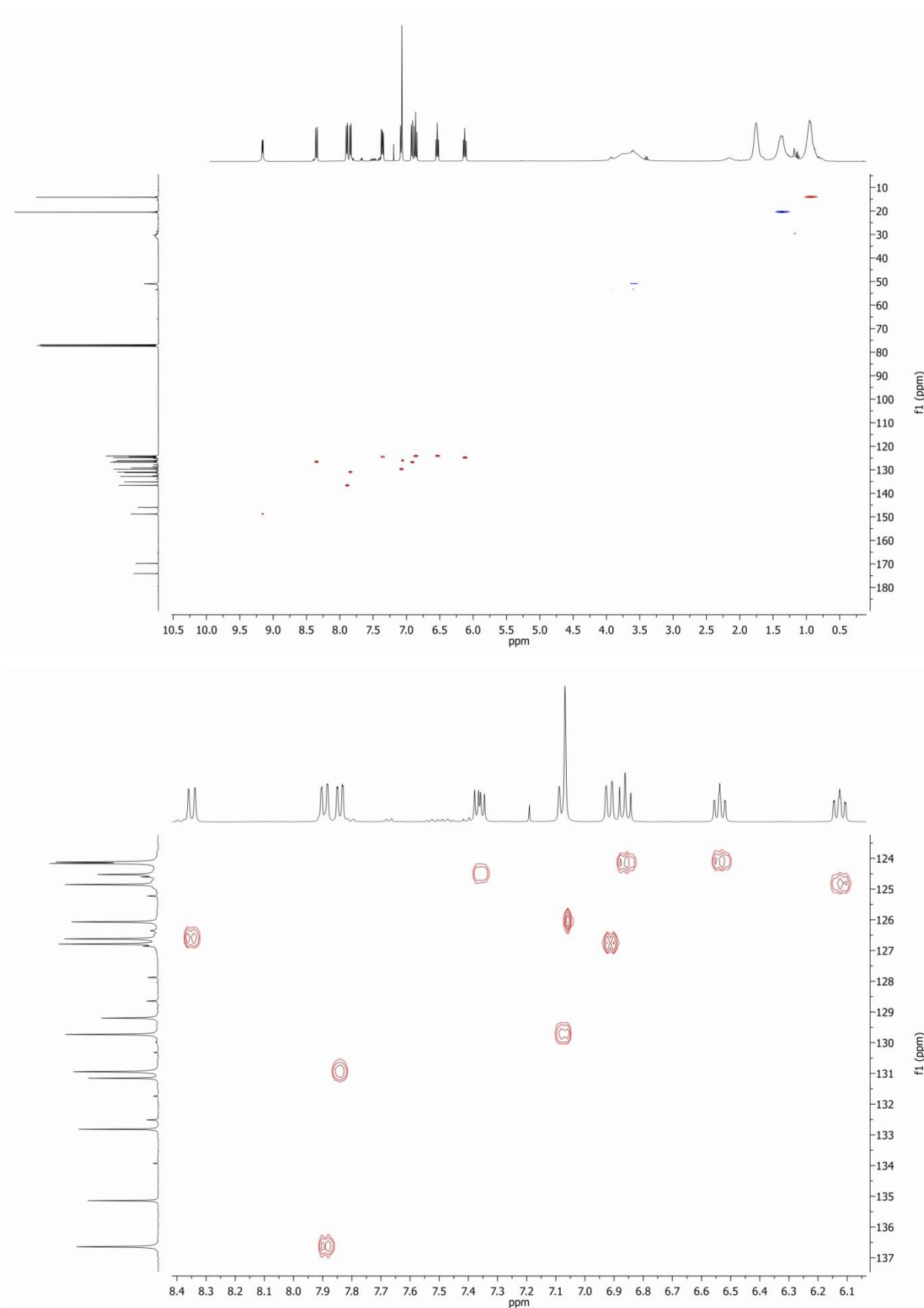


Figure A.19 ^1H , ^{13}C GHSQC plot of $[\text{Pt}^{\text{II}}(\text{phen})(\text{L}^1\text{-S},\text{O})]\text{Cl}$ showing the ^1H and ^{13}C correlations in chloroform- d_1 .

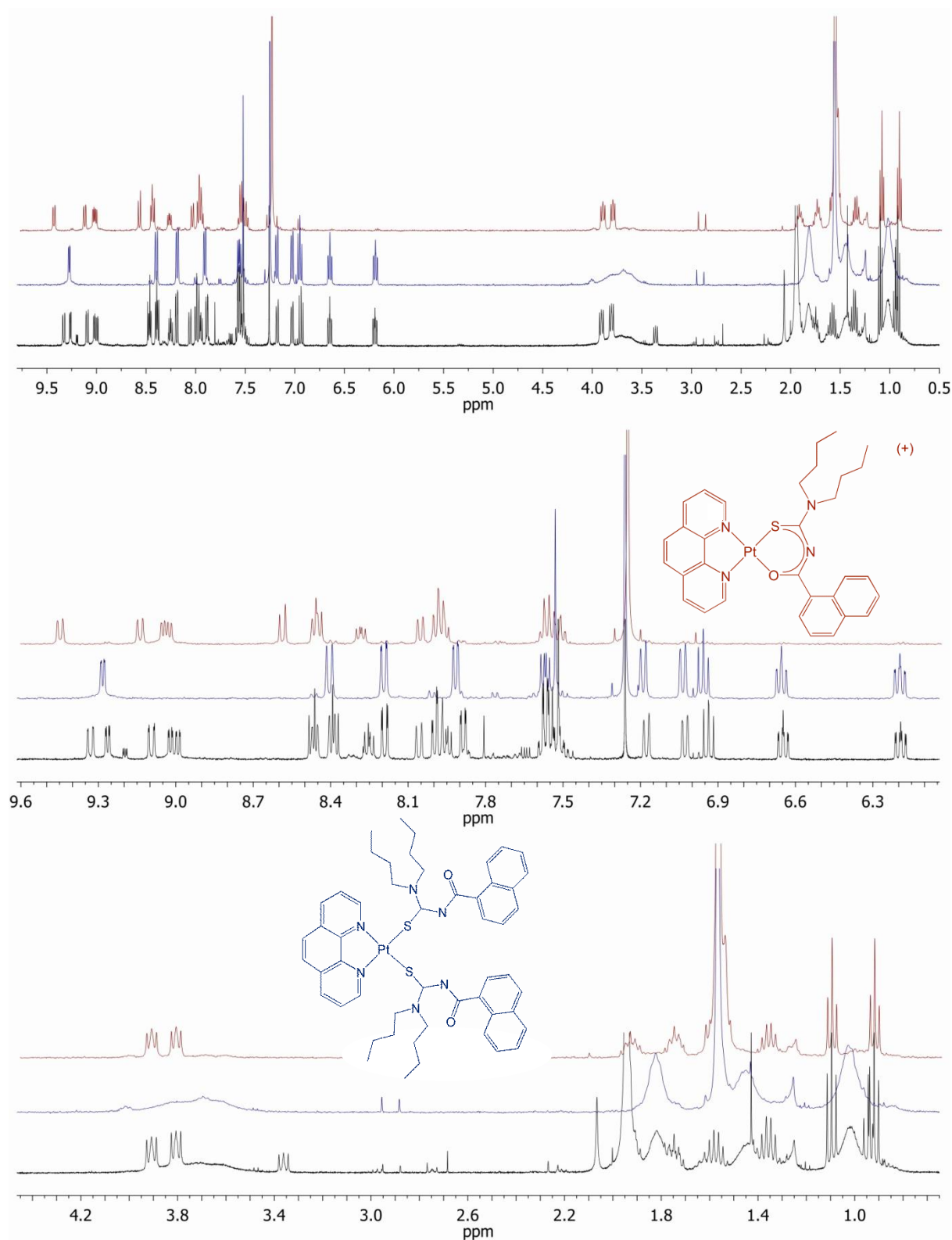


Figure A.20 ^1H NMR spectra of the reaction mixture obtained for the synthesis of $[\text{Pt}^{\text{II}}(\text{phen})(\text{L}^2\text{-S,O})]\text{Cl}$ containing significant amount of the previously 'unknown' $\text{Pt}^{\text{II}}(\text{phen})(\text{L}^2\text{-S})_2$ with the ^1H NMR spectrum of the pure $[\text{Pt}(\text{phen})(\text{L}^2\text{-S,O})]^+$ in red and $\text{Pt}(\text{phen})(\text{L}^2\text{-S})_2$ in blue.

Table A.1 Bond lengths and selected angles, torsion angles, plane angles and distances in the crystal structure of Pt^{II}(phen)(L²-S)₂

<i>Bonds:</i>	Å	<i>Bonds:</i>	Å	<i>Bonds:</i>	Å	<i>Bonds:</i>	Å
PT1-S3	2.2837(2)	C17-C21	1.3812(1)	N26-H26	0.8800(1)	N3-C56	1.4687(2)
PT1-N9	2.0566(2)	C18-N26	1.2962(1)	C27-H27	0.9500(1)	C51-H51A	0.9900(1)
PT1-N10	2.0554(2)	C19-H19	0.9500(1)	C27-C9	1.3591(1)	C51-H51B	0.9900(1)
PT1-S1	2.3002(2)	C19-C33	1.3520(1)	C28-H28	0.9500(1)	C51-C55	1.5170(2)
S3-C18	1.7783(2)	C20-H20	0.9500(1)	C28-C40	1.3665(1)	C53-H53A	0.9900(1)
C2-N10	1.3674(2)	C22-H22A	0.9900(1)	S1-C47	1.7809(2)	C53-H53B	0.9900(1)
C2-C30	1.4216(1)	C22-H22B	0.9900(1)	C1-H11	0.9500(1)	C53-C54	1.5351(2)
C2-C32	1.4171(1)	C22-C25	1.5158(2)	C11-C6	1.4231(1)	C54-H54A	0.9900(1)
C3-O4	1.2246(1)	C23-H23A	0.9900(1)	C11-C39	1.3739(1)	C54-H54B	0.9900(1)
C3-C21	1.5285(2)	C23-H23B	0.9900(1)	C6-C50	1.4344(2)	C54-C8	1.5236(1)
C3-N26	1.3741(2)	C23-C25	1.5230(2)	C9-H9	0.9500(1)	C55-H55A	0.9800(1)
O5-C49	1.2334(1)	C23-C46	1.5288(2)	C10-H10	0.9500(1)	C55-H55B	0.9800(1)
C7-H7	0.9500(1)	C29-C30	1.3981(1)	C39-H39	0.9500(1)	C55-H55C	0.9800(1)
C7-N9	1.3290(1)	C29-C27	1.4330(1)	C39-C44	1.4094(2)	C56-H56A	0.9900(1)
C7-C28	1.3973(1)	C29-C40	1.4032(1)	C40-H40	0.9500(1)	C56-H56B	0.9900(1)
N9-C30	1.3755(1)	C32-C37	1.4023(1)	C41-H41	0.9500(1)	C56-C4	1.5245(2)
N10-C16	1.3280(1)	C32-C9	1.4312(2)	C41-C50	1.4093(1)	C5-H5A	0.9900(1)
C1-H1	0.9500(1)	C33-H33	0.9500(1)	C42-H42	0.9500(1)	C5-H5B	0.9900(1)
C1-C12	1.4184(2)	C33-C42	1.4009(1)	C43-H43A	0.9900(1)	C5-C26	1.5177(2)
C1-C20	1.3644(1)	C34-H34A	0.9900(1)	C43-H43B	0.9900(1)	C5-C4	1.5150(2)
C12-C14	1.4256(2)	C34-H34B	0.9900(1)	C43-C51	1.5339(2)	C8-H8A	0.9900(1)
C12-C19	1.4175(1)	C34-C43	1.5233(2)	C44-H44	0.9500(1)	C8-H8B	0.9900(1)
C13-H13	0.9500(1)	C35-H35	0.9500(1)	C44-C45	1.3562(1)	C8-C58	1.5286(2)
C13-C14	1.4295(2)	C35-C36	1.4098(2)	C45-H45	0.9500(1)	C26-H26A	0.9800(1)
C13-C42	1.3696(1)	C35-C41	1.3611(1)	C45-C50	1.4157(1)	C26-H26B	0.9800(1)
C14-C21	1.4416(1)	C36-H36	0.9500(1)	C46-H46A	0.9800(1)	C26-H26C	0.9800(1)
N8-C18	1.3522(1)	C36-C24	1.3736(1)	C46-H46B	0.9800(1)	C4-H4A	0.9900(1)
N8-C22	1.4688(2)	C37-H37	0.9500(1)	C46-H46C	0.9800(1)	C4-H4B	0.9900(1)
N8-C34	1.4687(2)	C37-C10	1.3629(2)	N1-H1A	0.8800(1)	C58-H58A	0.9800(1)
C16-H16	0.9500(1)	C24-C6	1.4401(2)	N1-C47	1.2874(1)	C58-H58B	0.9800(1)
C16-C10	1.4021(1)	C24-C49	1.520(2)	N1-C49	1.3596(2)	C58-H58C	0.9800(1)
C17-H17	0.9500(1)	C25-H25A	0.9900(1)	C47-N3	1.3623(1)		
C17-C20	1.4096(1)	C25H25B	0.9900(1)	N3-C53	1.4591(2)		

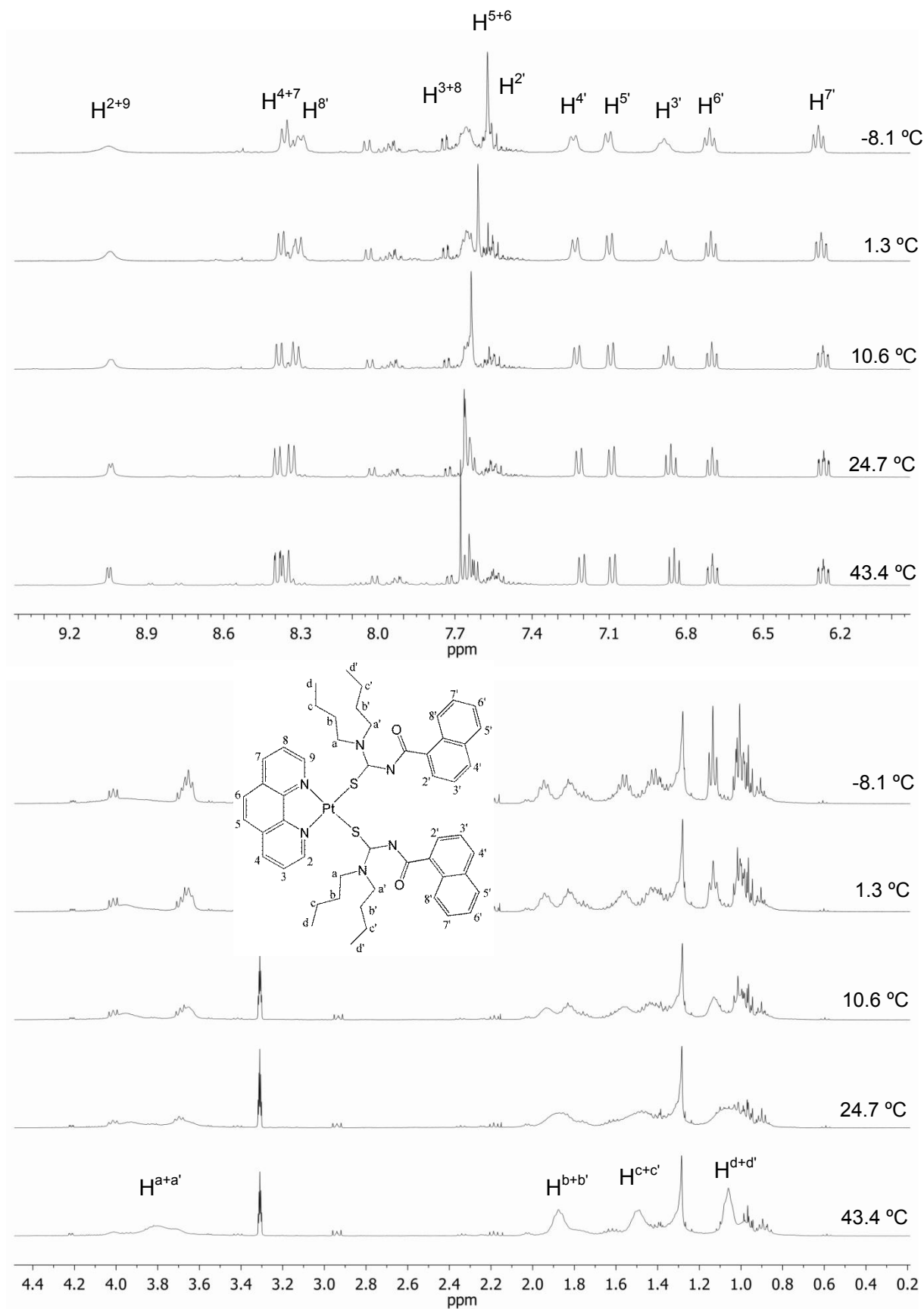


Figure A.21 ^1H NMR temperature dependence of $\text{Pt}^{\text{II}}(\text{phen})(\text{L}^2)_2$ in methanol-d_4 .

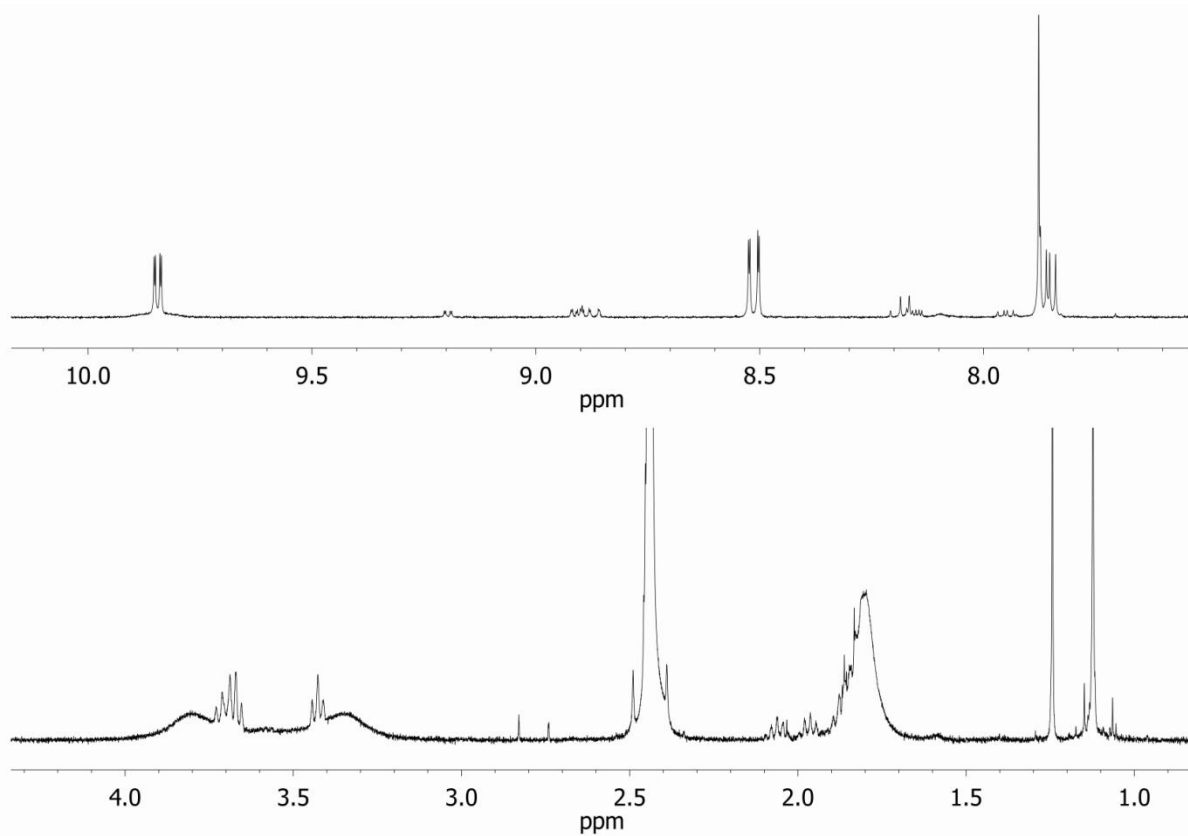


Figure A.22 ^1H NMR of $\text{Pt}^{\text{II}}(\text{phen})(\text{L}^1)_2$ in dimethyl sulfoxide- d_6 .

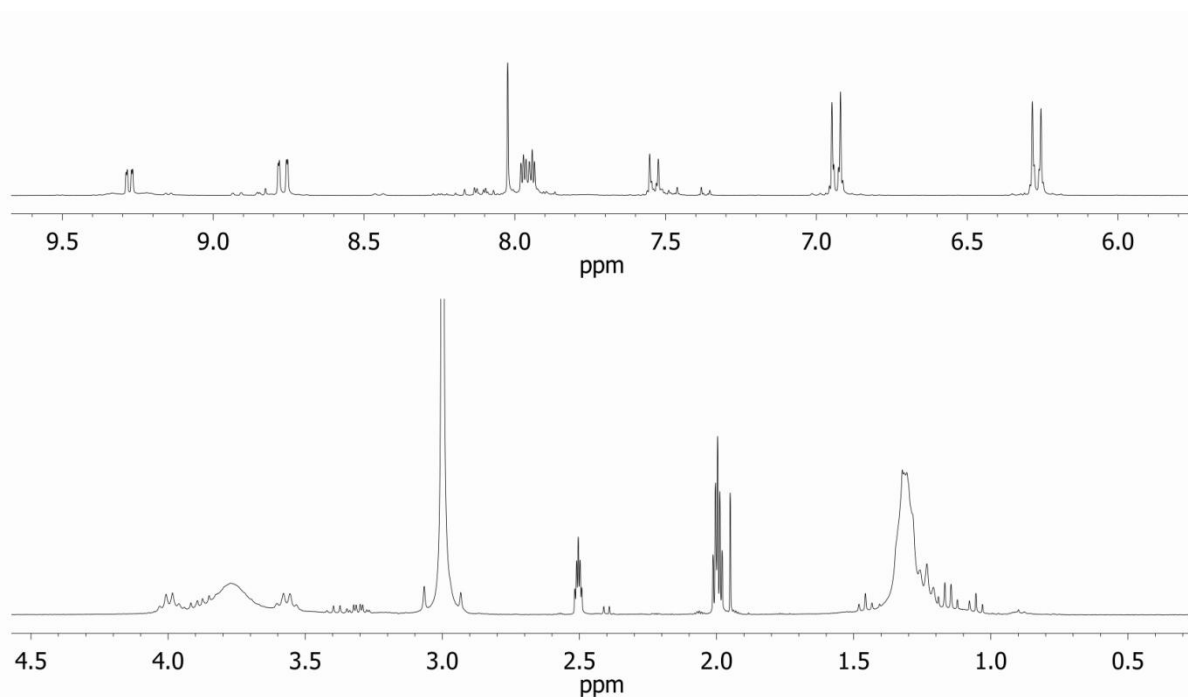


Figure A.23 ^1H NMR of $\text{Pt}^{\text{II}}(\text{phen})(\text{L}^6)_2$ in a mixture of acetonitrile- d_3 and dimethyl sulfoxide- d_6 .

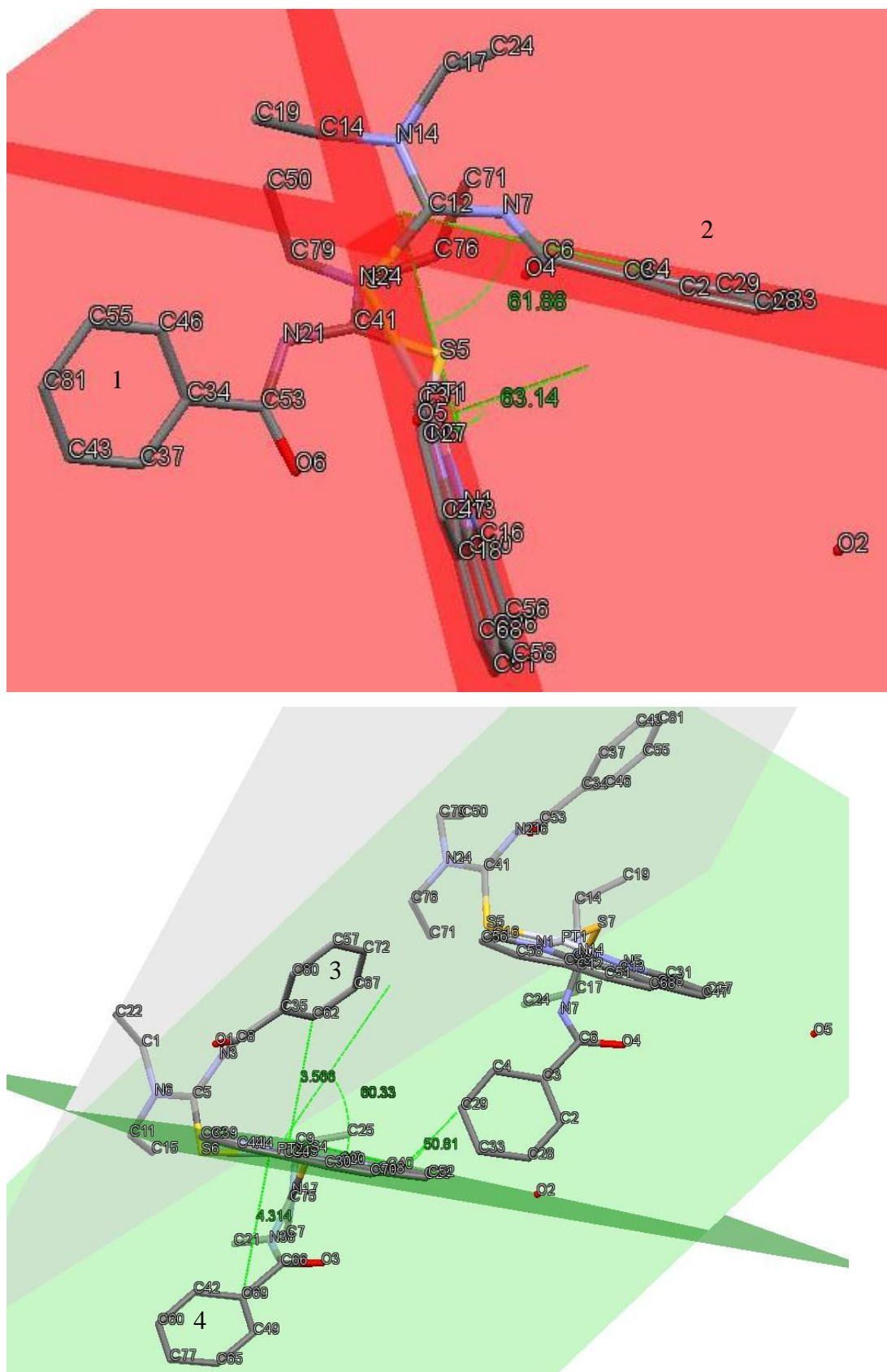


Figure A.24 Plane angles of the phenyl group and the coordinated 1,10-phenanthroline.

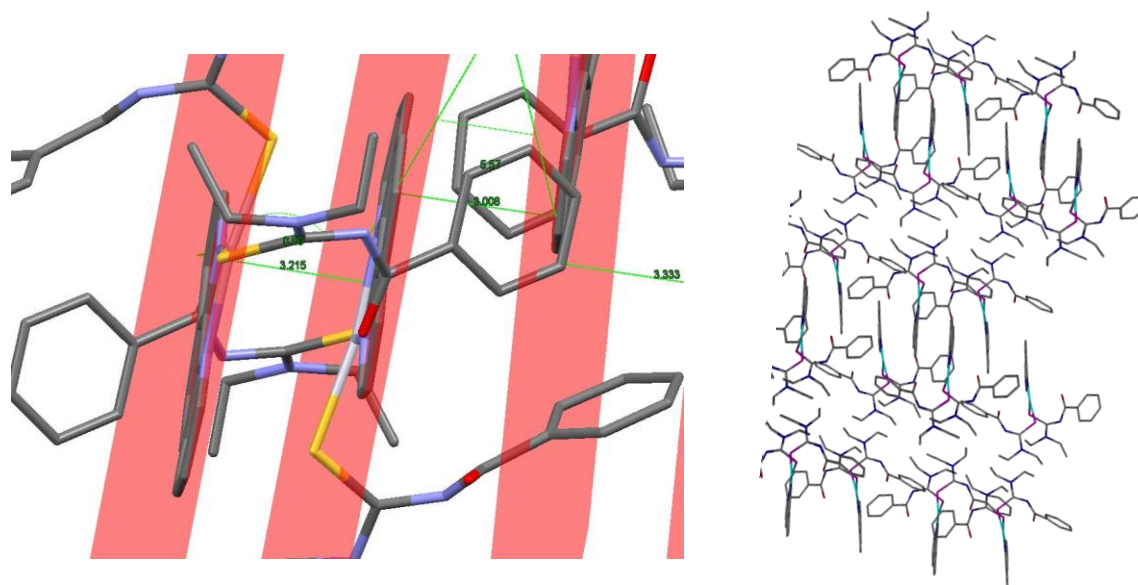


Figure A.25 Distances and angles of the planes created by the coordinated 1,10-phenanthroline moiety.

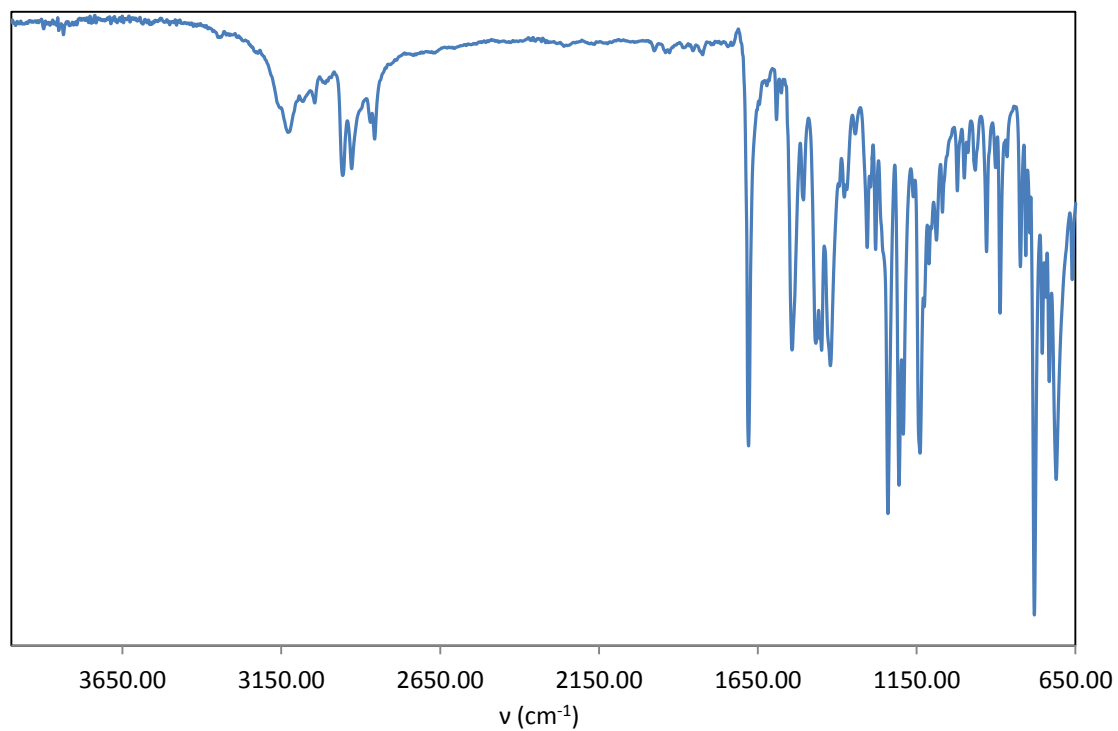


Figure A.26 ATR FTIR of HL^2

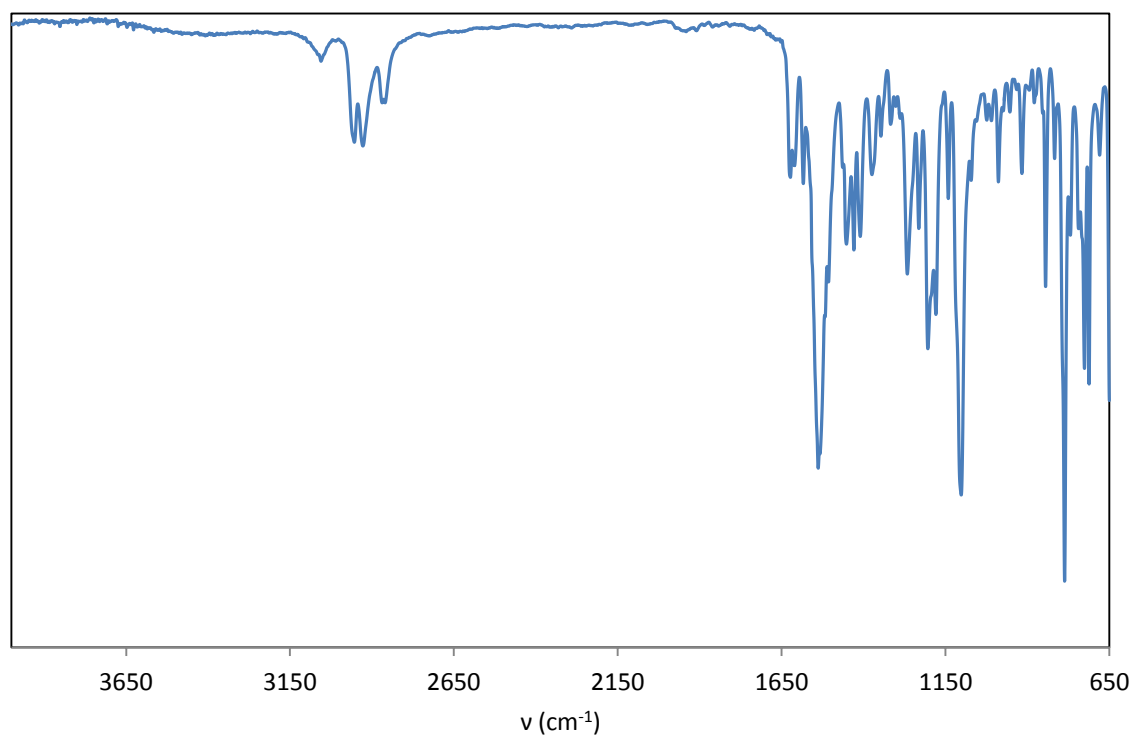


Figure A.27 ATR FTIR of Pt^{II}(phen)(L²-S)₂

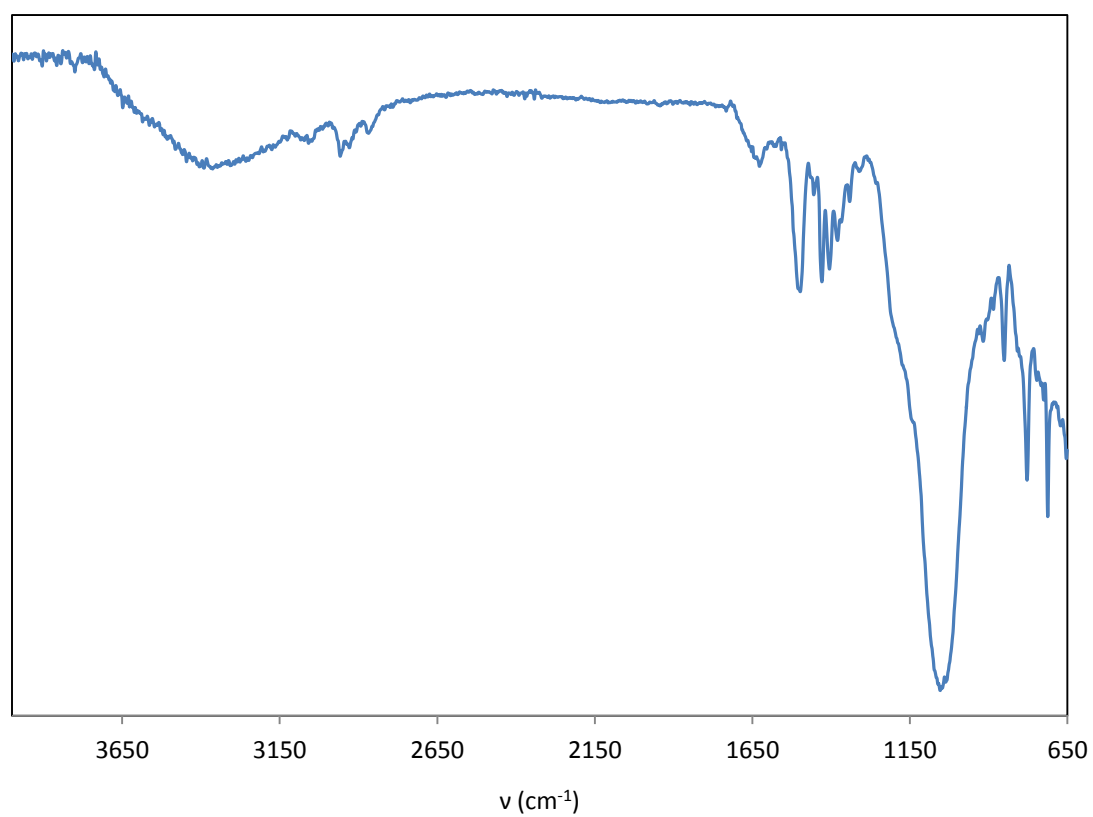


Figure A.28 ATR FTIR of [Pt^{II}(phen)(L²-S,O)]Cl

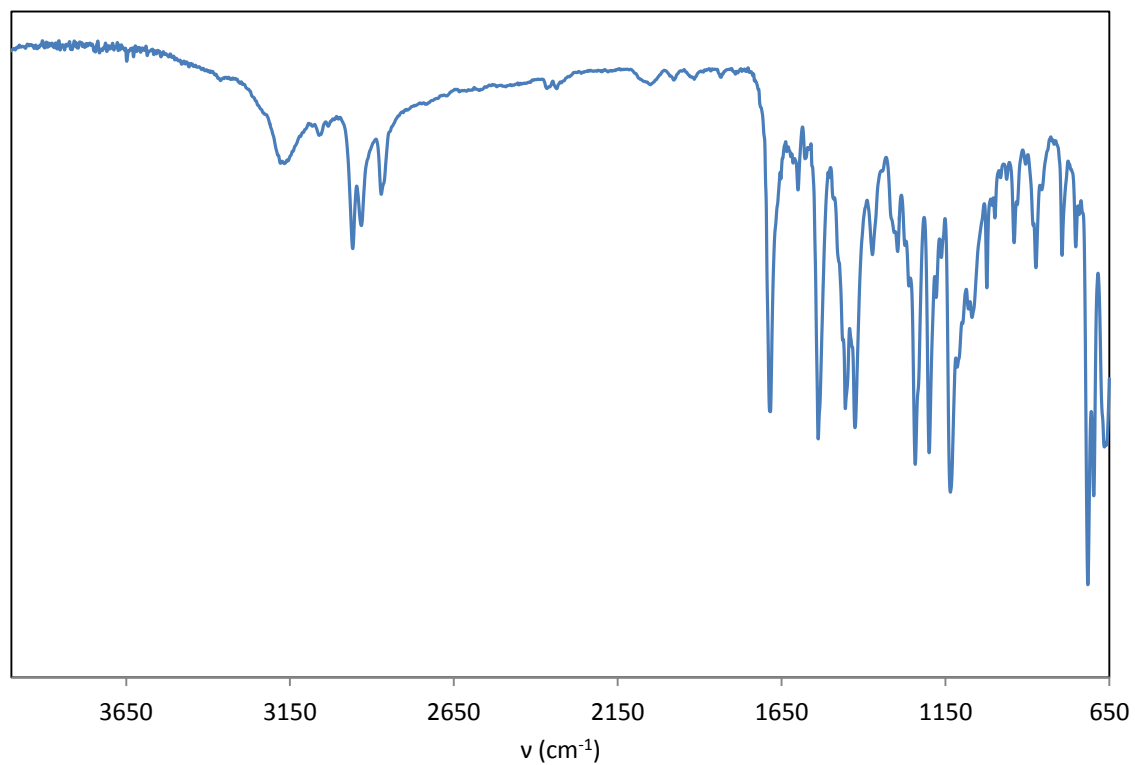


Figure A.29 ATR FTIR of HL³

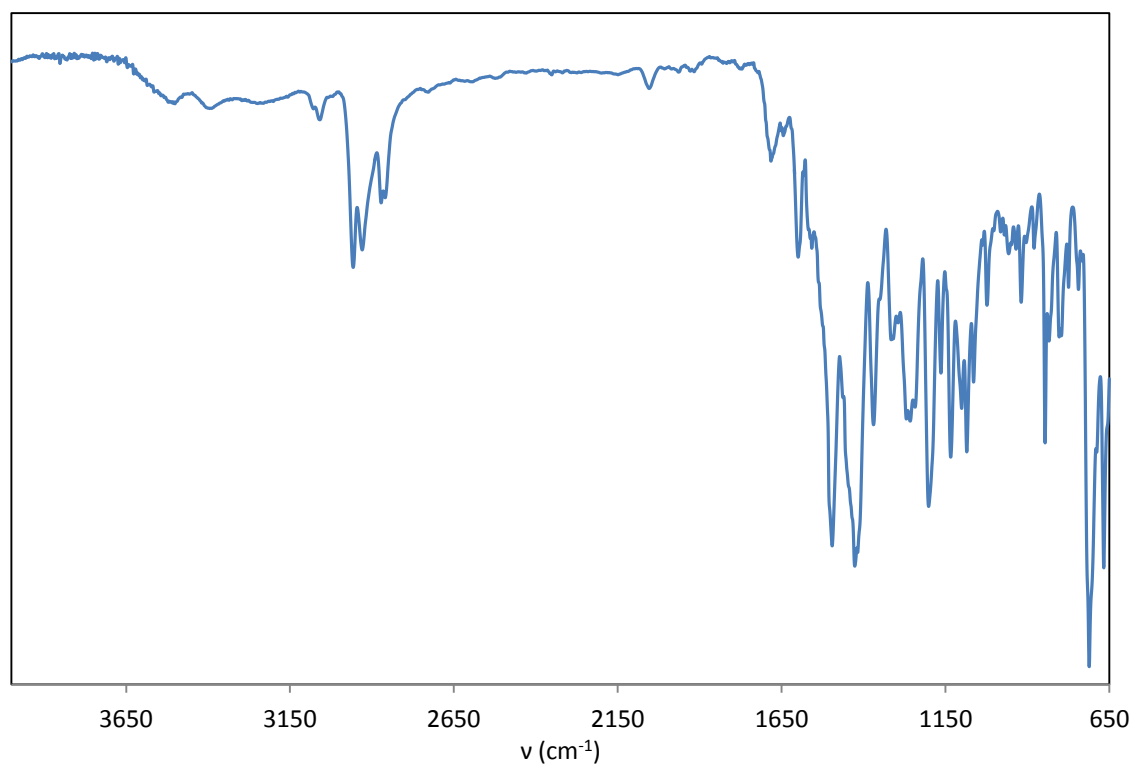


Figure A.30 ATR FTIR of Pt^{II}(phen)(L³-S)₂

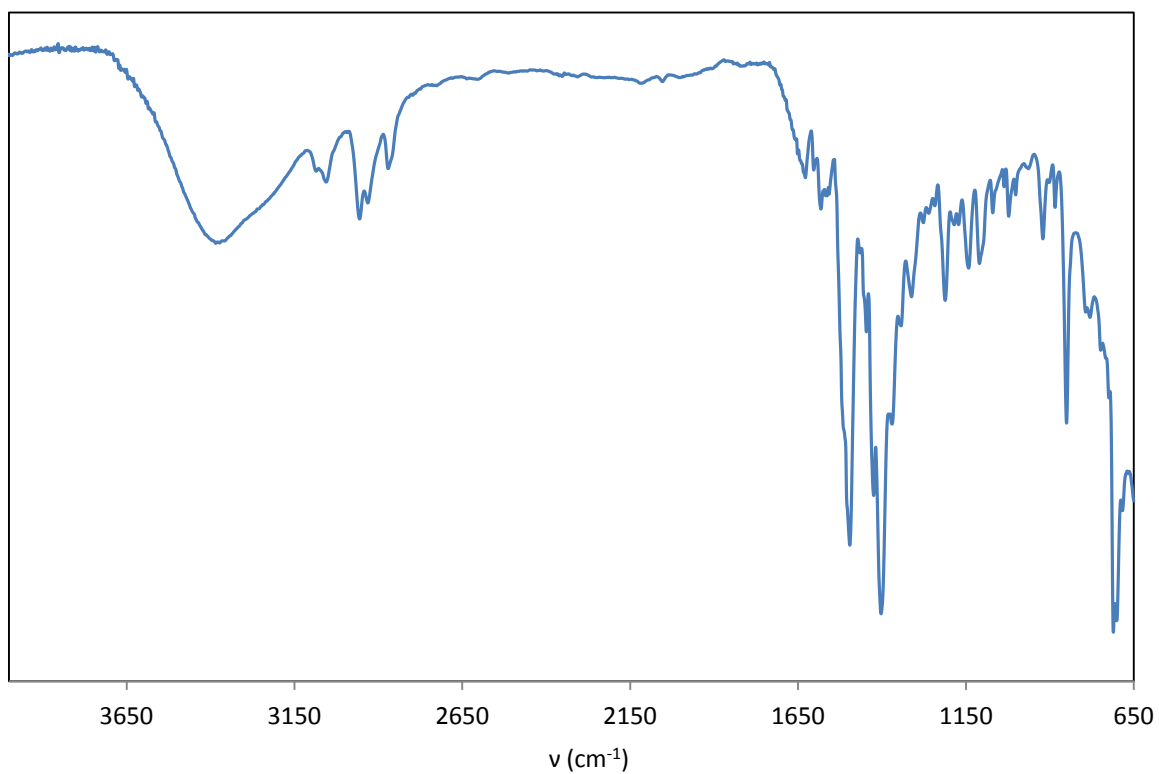


Figure A.31 ATR FTIR of [Pt^{II}(phen)(L³-S,O)]Cl

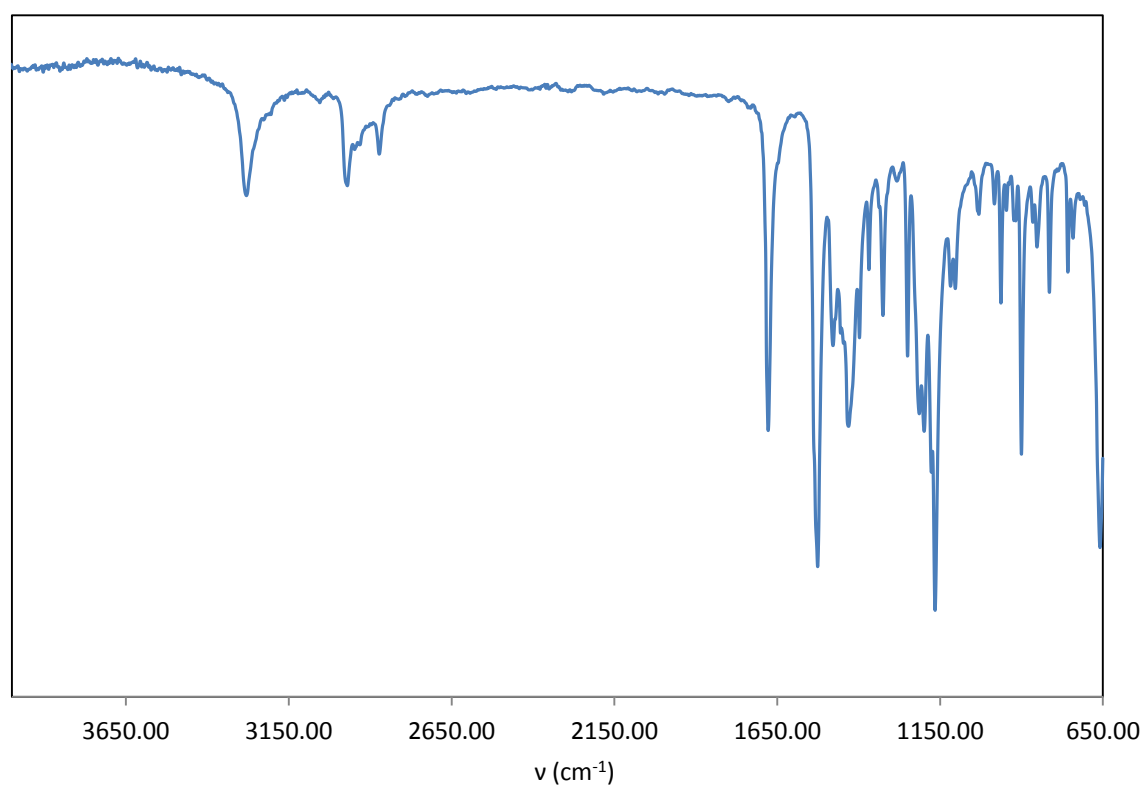


Figure A.32 ATR FTIR of HL¹

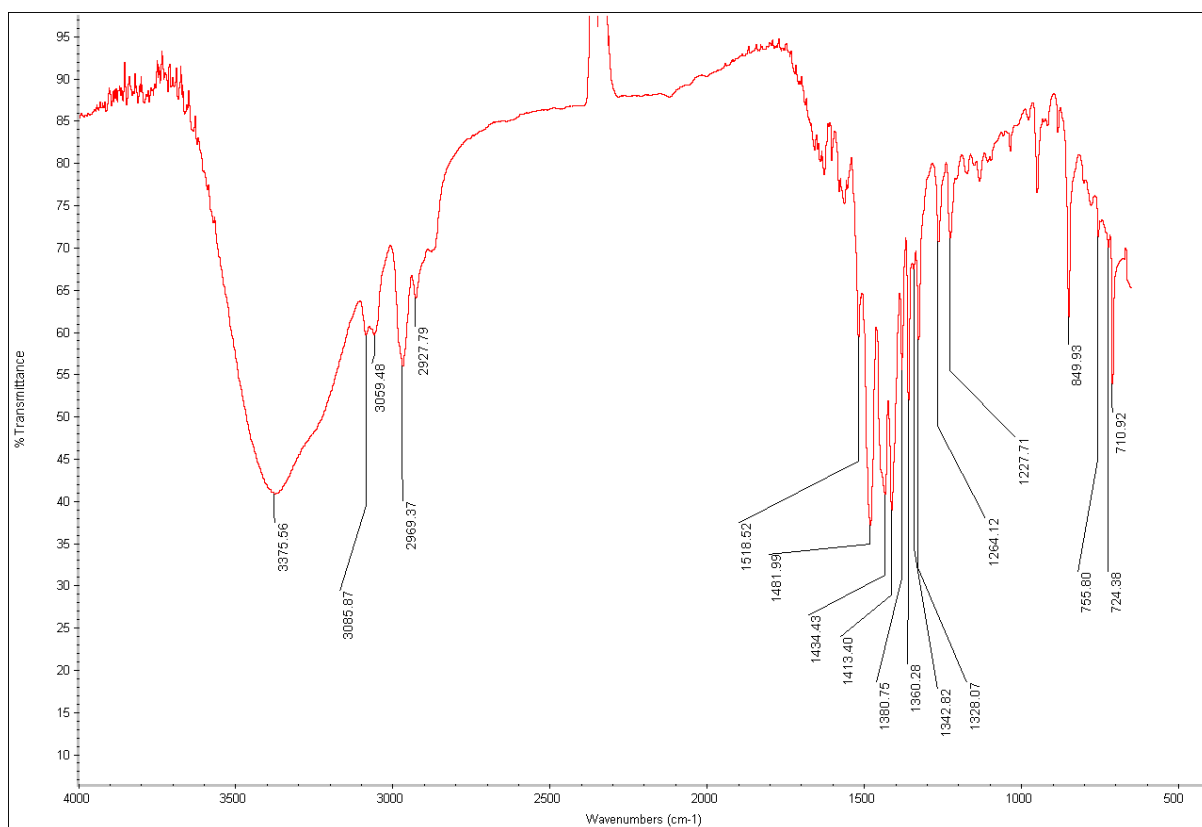


Figure A.33 ATR FTIR of $[\text{Pt}^{\text{II}}(\text{phen})(\text{L}^1\text{-S},\text{O})]\text{Cl}$

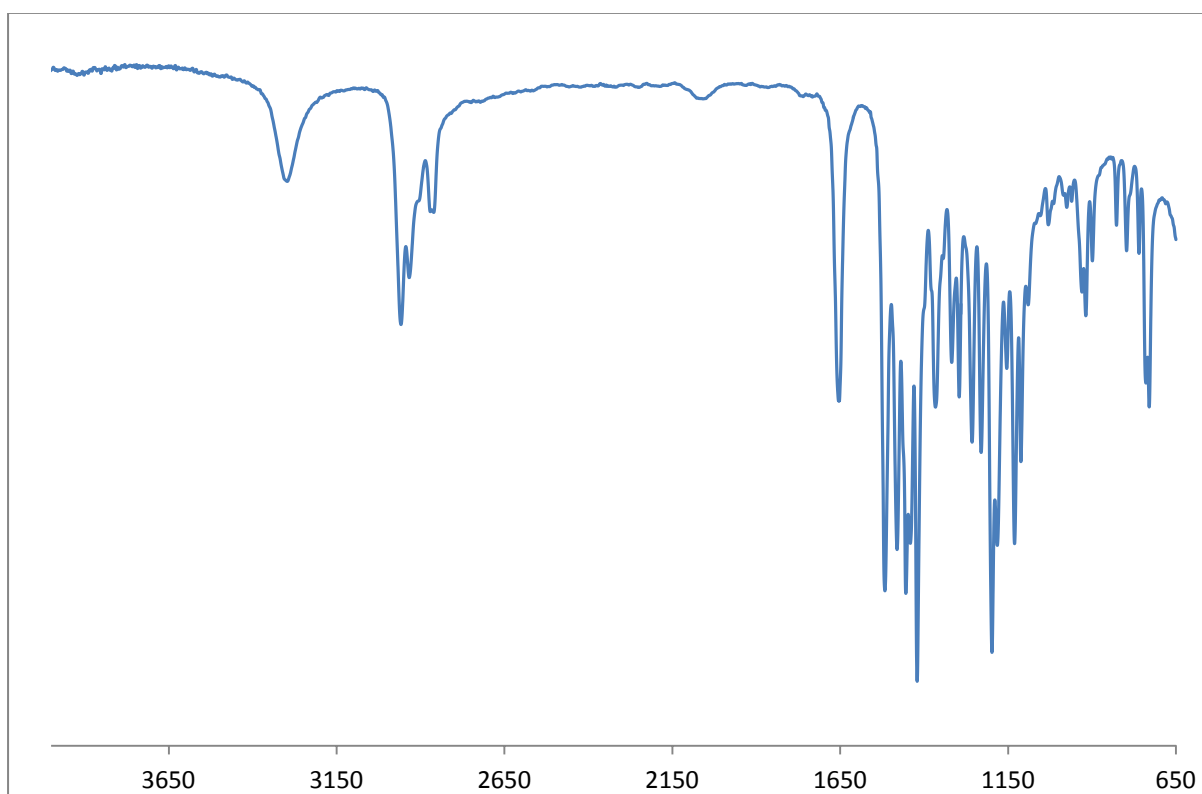


Figure A.34 ATR FTIR of HL^{13}

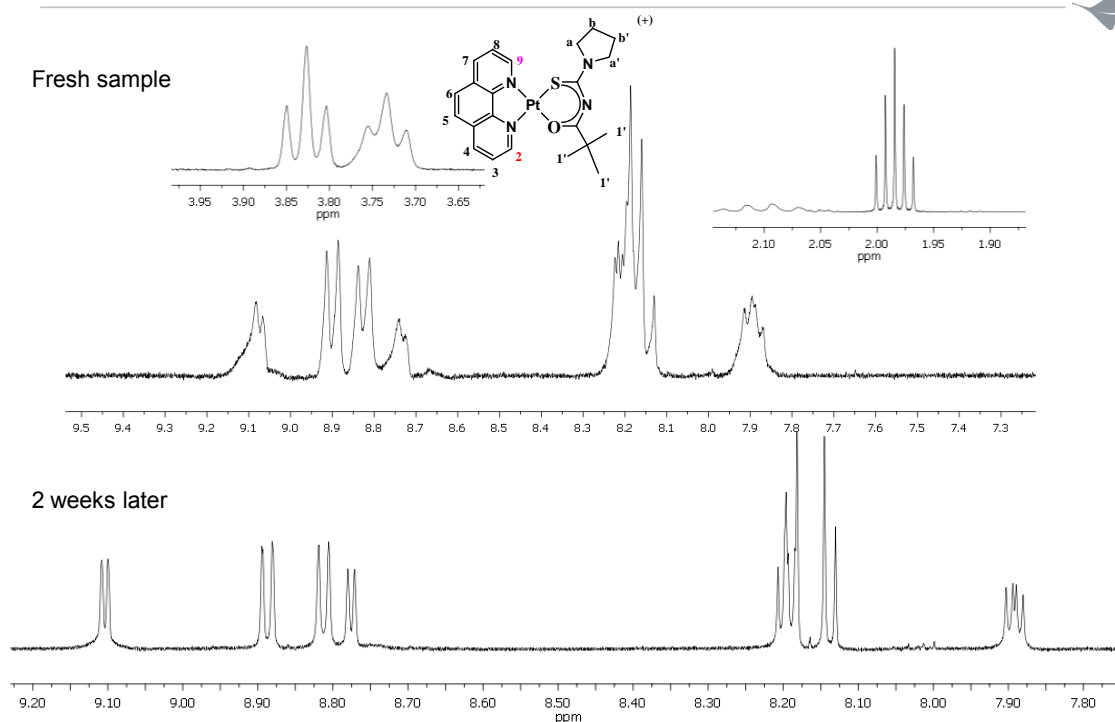
Oriented phase/ insufficient mixing

Figure A.35 Oriented phase observed in the ^1H NMR spectrum as a result of insufficient mixing of $[\text{Pt}^{\text{II}}(\text{phen})(\text{L}^1\text{-S,O})]\text{Cl}$ in acetonitrile- d_3 .

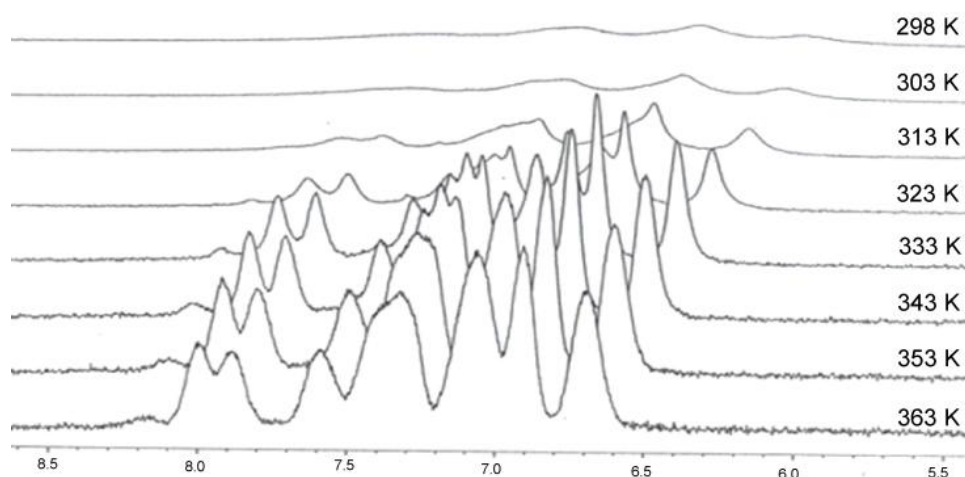


Figure A.36 399.99 MHz ^1H NMR spectra of $[\text{Pt}^{\text{II}}(1,10\text{-phenanthroline})(\text{N,N}\text{-di}(2\text{-hydroxyethyl})\text{-N}'\text{-benzoylthiourea})]\text{Cl}$ as in D_2O a function of temperature.

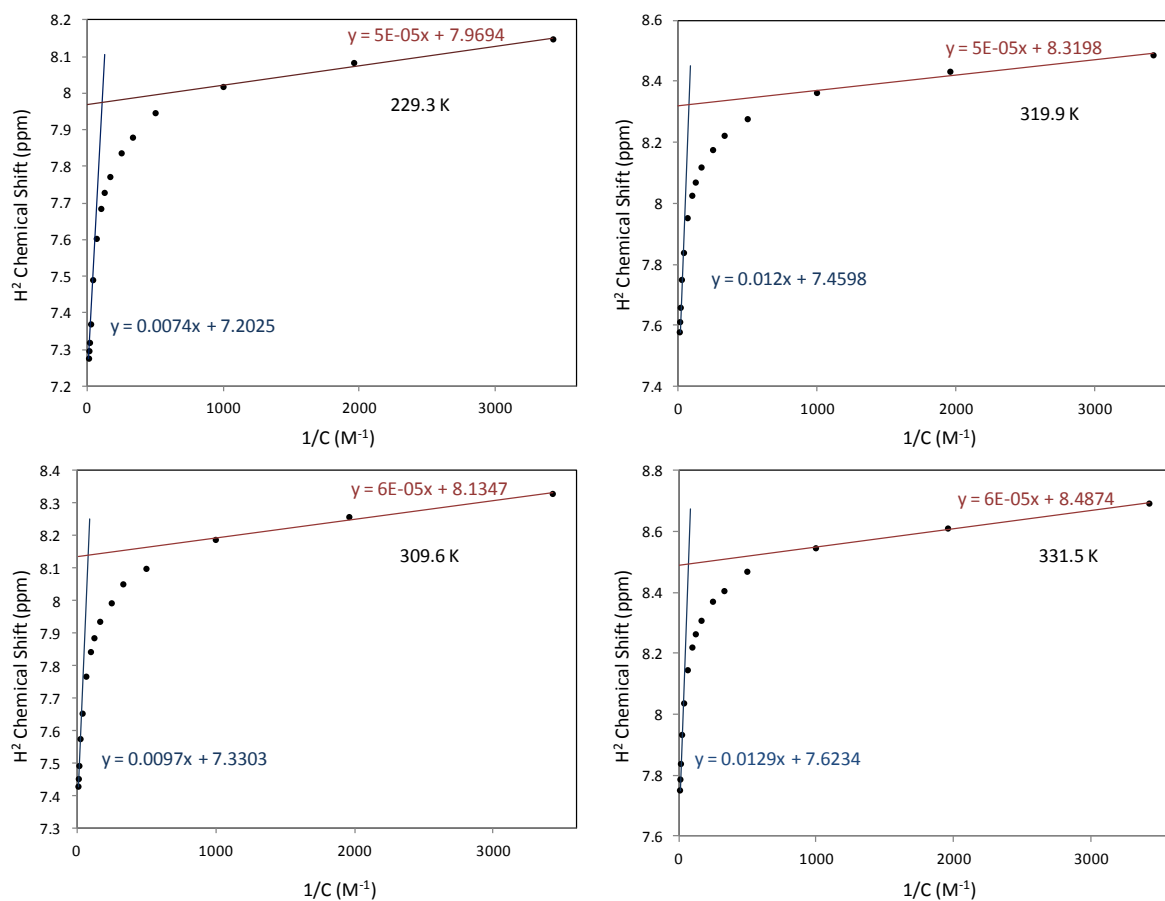


Figure A.37 The observed ^1H chemical shift of H^2 at temperatures 299.3 - 331.5 K against $1/[M]_{\text{T}}$, where $[M]_{\text{T}}$ = Total $[\text{Pt}^{\text{II}}(\text{phen})(\text{L}^1\text{-S},\text{O})]\text{Cl}$ concentration in D_2O .



Figure A.38 TEM image ($\times 73000$) of $[\text{Pt}^{\text{II}}(2,2'\text{-bipyridyl})(\text{N},\text{N}\text{-di}(2\text{-hydroxyethyl})\text{-N}'\text{-benzoylthiourea})]\text{Cl}$ prepared from water and stained with uranyl acetate.

Table A.2 Calculated monomer and dimer chemical shifts (δ_m and δ_d) for solutions 10-30% v/v D₂O:CD₃CN using the dimer model.

Percentage (v/v) D ₂ O:CD ₃ CN	Temperature (K)	δ_m (ppm)	error (+-)	δ_d (ppm)	error (+-)
0	309.6	9.300	0.004	8.118	0.053
	299.3	9.292	0.006	8.123	0.064
	291.6	9.285	0.009	8.105	0.076
	282.6	9.273	0.015	8.087	0.099
20	309.6	9.281	0.006	8.195	0.067
	299.3	9.275	0.007	8.192	0.061
	291.6	9.269	0.023	8.098	0.145
	282.6	9.262	0.02	8.195	0.113
30	309.6	9.264	0.009	8.293	0.053
	299.3	9.26	0.01	8.281	0.048
	291.6	9.253	0.014	8.260	0.055
	282.6	9.246	0.017	8.252	0.054

Table A.3 ^1H $\delta_{\text{obs}}(\text{H}^2)$ and D_{obs} dependence of $[\text{Pt}^{\text{II}}(\text{phen})(\text{L}^1\text{-S},\text{O})]\text{Cl}$ (4.5 mM) on NaCl concentration with corresponding hydrodynamic radii (r_{H}), volumes (V_{H}) and aggregation numbers (N).

$[\text{M}]_{\text{T}}^{-1}$ (M^{-1})	$\delta_{\text{obs}}(\text{H}^2)$ (ppm)			
	299.3 K	309.6 K	319.9K	331.5 K
9.8141	7.275	7.427	7.577	7.750
12.582	7.295	7.451	7.611	7.786
16.691	7.318	7.491	7.658	7.837
25.021	7.368	7.574	7.749	7.932
40.004	7.489	7.652	7.837	8.036
66.673	7.602	7.766	7.951	8.145
100.01	7.684	7.841	8.024	8.219
125.01	7.727	7.884	8.068	8.262
166.68	7.771	7.934	8.117	8.307
250.02	7.835	7.991	8.174	8.369
333.36	7.878	8.050	8.221	8.404
500.05	7.945	8.097	8.275	8.468
1000.1	8.017	8.186	8.361	8.545
1962.4	8.082	8.257	8.431	8.610
3428.9	8.147	8.328	8.485	8.691

B.

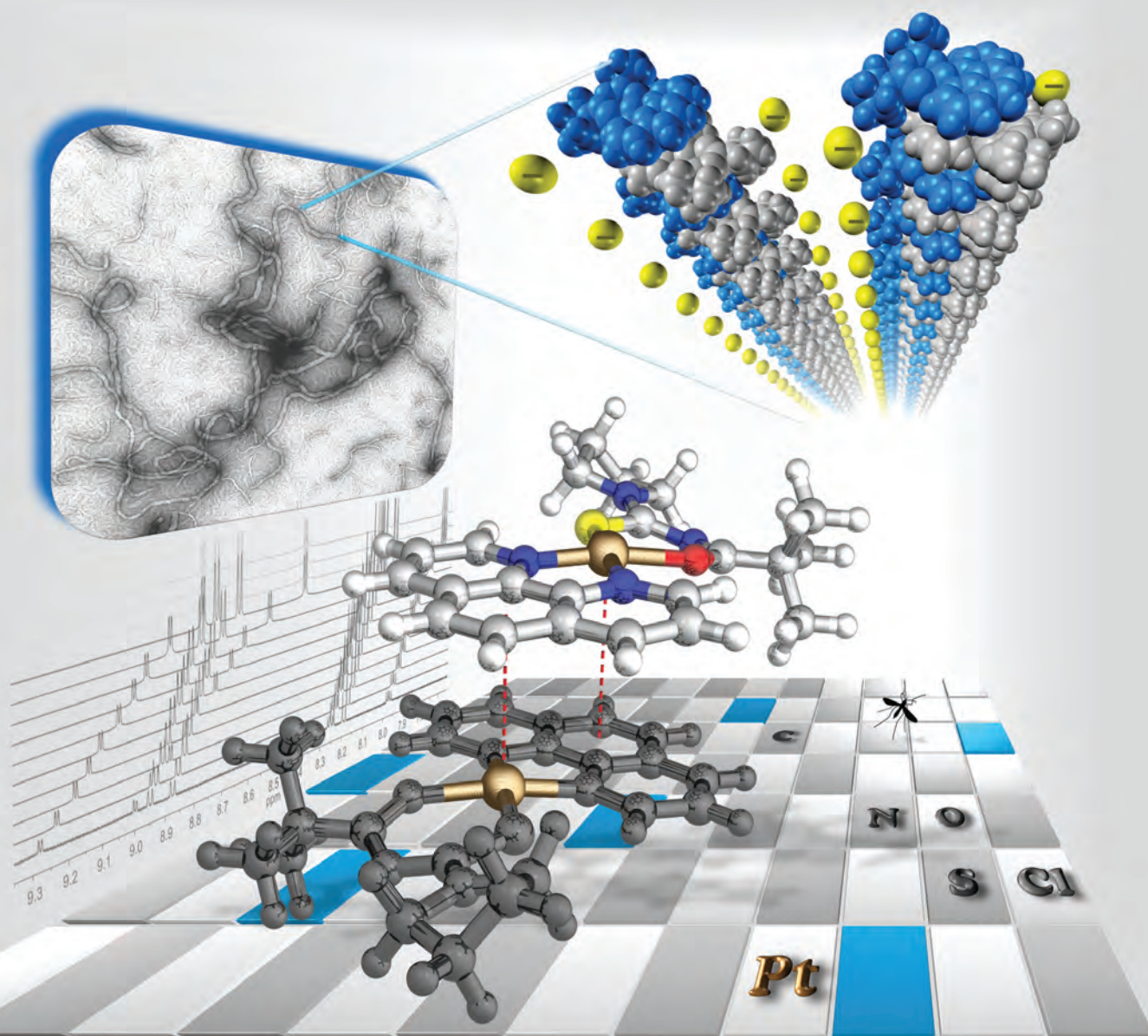
Appendix B - Publications

Dalton Transactions

An international journal of inorganic chemistry

www.rsc.org/dalton

Volume 42 | Number 11 | 21 March 2013 | Pages 3737–4092



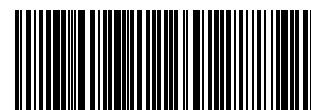
ISSN 1477-9226

RSC Publishing

COVER ARTICLE

Koch *et al.*

Cation- π induced aggregation of water-soluble $[\text{Pt}^{\text{II}}(\text{diimine})(\text{L}^n\text{-S}_2\text{O})]^+$ complexes studied by ^1H DOSY NMR and TEM: from 'dimer aggregates' in acetonitrile to nano-aggregates ('metallogeles') in water



1477-9226 (2013) 42:11;1-S

Cation– π induced aggregation of water-soluble $[\text{Pt}^{\text{II}}(\text{diimine})(\text{L}^n\text{-S,O})]^+$ complexes studied by ^1H DOSY NMR and TEM: from ‘dimer aggregates’ in acetonitrile to nano-aggregates (‘metallogeles’) in water†‡

Cite this: *Dalton Trans.*, 2013, **42**, 3791

Izak A. Kotzé, Wilhelmus J. Gerber, Yu-Shan Wu and Klaus R. Koch*

^1H NMR chemical shift concentration dependence as well as the diffusion coefficients from DOSY NMR of mixed ligand $[\text{Pt}^{\text{II}}(1,10\text{-phenanthroline})(N\text{-pyrrolidyl-}N\text{-(2,2-dimethylpropanoyl)thiourea})]\text{Cl}$ ($[\text{Pt}^{\text{II}}(\text{phen})(\text{L}^1\text{-S,O})]\text{Cl}$) dissolved in mixtures of acetonitrile–water in the range 0–30% (v/v) $\text{D}_2\text{O-CD}_3\text{CN}$ shows that the complex cation ($\text{M}^+ = [\text{Pt}^{\text{II}}(\text{phen})(\text{L}^1\text{-S,O})]^+$) aggregates to form dimers, $2\text{M}^+ \rightleftharpoons [\text{M}^+]_2$, with association constants ranging from $K_{\text{D}}(\text{CD}_3\text{CN}) = 17 \pm 2 \text{ M}^{-1}$ to $K_{\text{D}}(30\% \text{ (v/v) } \text{D}_2\text{O-CD}_3\text{CN}) = 71 \pm 8 \text{ M}^{-1}$ at 299.3 K, presumably *via* non-covalent cation– π interactions. Experimental data are consistent with an ‘offset’ face-to-face cation– π stacking arrangement of the planar cation. However in water-rich solvent mixtures from >30% (v/v) $\text{D}_2\text{O-CD}_3\text{CN}$ to pure D_2O , the extent of aggregation significantly increases until a critical aggregation concentration (CAC) is reached, estimated to be 9.6 and 10.3 mM from ^1H NMR chemical shift concentration dependence and DOSY NMR measurements respectively. Above the CAC the formation of nano-structures formulated as $\{[\text{Pt}^{\text{II}}(\text{phen})(\text{L}^1\text{-S,O})]^+\}_n\text{Cl}^-_y$ ($n, y > 2$) is indicated. DOSY studies show a significant decrease of the average diffusion coefficient D_{obs} as a function of increasing concentration of $[\text{Pt}^{\text{II}}(\text{phen})(\text{L}^1\text{-S,O})]\text{Cl}$ in D_2O . The aggregation number (N) estimated from hydrodynamic volumes of the mononuclear $[\text{Pt}^{\text{II}}(\text{phen})(\text{L}^1\text{-S,O})]^+$ cation (V_{H}^0), and those V_{H} estimated from D_{obs} ($N = V_{\text{H}}/V_{\text{H}}^0$) as a function of total complex concentration, ranges from ~ 2 to ~ 735 in pure D_2O . Above the CAC well defined nano-structures which may be loosely termed “metallogeles” could be characterized by means of transmission electron microscopy. As expected the addition of NaCl appears to increase the extent of aggregate formation, by presumably stabilizing the formation of nano-sized $\{[\text{Pt}^{\text{II}}(\text{phen})(\text{L}^1\text{-S,O})]^+\}_n\text{Cl}^-_y$ aggregates preventing excessive positive electrostatic charge build-up.

Received 5th September 2012,
Accepted 14th November 2012

DOI: 10.1039/c2dt32053c

www.rsc.org/dalton

Introduction

The ‘self-association’ of transition metal complexes, which display biological activity of potential pharmaceutical use, has been the subject of extensive interest in the last decade since their detailed physiochemical behaviour particularly in aqueous solution may have important implications on their mode of action.^{1–5} Our interest in the chemistry of planar, cationic mixed-ligand Pt^{II} complexes of the general type $[\text{Pt}^{\text{II}}(\text{diimine})(\text{L}^n\text{-S,O})]^+$ (where diimine is 2,2-bipyridine or 1,10-

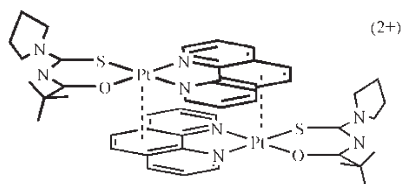
phenanthroline and $\text{HL}^n\text{-S,O}$ are various chelating $N\text{-acyl-}N,N\text{-dialkylthioureas}$) arises from their interesting biological activity ranging from potential anti-malarial activity⁶ to DNA-intercalation and demonstrable *in vivo* activity toward bacterial *E. coli* AB1886 (uvr A) cultures.⁷ Preliminary work also shows that such complexes undergo some interesting DNA-templated ‘biomineralization’.⁸ The *in vitro* anti-malarial activity⁶ of $[\text{Pt}^{\text{II}}(\text{diimine})(\text{L}^n\text{-S,O})]^+$ is postulated to arise from inhibition of β -hematin formation (synthetic hemozoin or malaria pigment) presumably as a result of the cationic planar complex $[\text{Pt}^{\text{II}}(\text{diimine})(\text{L}^n\text{-S,O})]^+$ forming moderately strong outer-sphere aggregates with ferriprotoporphyrin IX, as can be demonstrated in 40% aqueous dimethyl sulfoxide (DMSO) solution, possibly through non-covalent cation– π interactions.⁶ Moreover the ^1H NMR spectra of the series of cationic $[\text{Pt}^{\text{II}}(\text{diimine})(N,N\text{-di}(n\text{-butyl})\text{-}N'\text{-benzoylthiourea})]^+$ complexes (as PF_6^- salts where diimine = 1,10-phenanthroline, 4,7-diphenyl-1,10-phenanthroline, 2,2-bipyridyl, 4,4-di-*tert*-butyl-2,2-bipyridyl and

Platinum Metals Chemistry Research Group, Department of Chemistry and Polymer Science, University of Stellenbosch, P Bag X1, Matieland, 7602, South Africa.

E-mail: krk@sun.ac.za; Fax: +2721 808 2344; Tel: +2721 808 3020

†This paper is dedicated to Professor Stefan Berger (Leipzig University), on the occasion of his retirement.

‡Electronic supplementary information (ESI) available: Consists of tables of all the ^1H and PFGE NMR data and related graphics. See DOI: 10.1039/c2dt32053c



Scheme 1 Postulated 'average' structure of a $\{[Pt^{II}(\text{phen})(L^1-S,O)]^+\}_2$ dimer aggregate in solution based on ^1H NMR shielding trends as a function of concentration.

4,4-dimethyl-2,2-bipyridyl) in acetonitrile at room temperature show significant concentration dependence, consistent with the formation of non-covalent dimer aggregates $2M^+ \rightleftharpoons \{M^+\}_2$ (where $M^+ = [Pt^{II}(\text{diimine})(L^1-S,O)]^+$).⁹ This concentration dependence of the ^1H NMR chemical shifts can be used to estimate the association constants of such an aggregation process, while the relative spatial orientation of the molecules undergoing non-covalent association may be inferred from the extent of the relative changes in ^1H NMR chemical shifts induced as a function of concentration.^{9–12} A recent, detailed study of the water-soluble $[Pt^{II}(1,10\text{-phenanthroline})(N\text{-pyrrolidyl-}N\text{-}(2,2\text{-dimethylpropanoyl})\text{-thiourea})]Cl$ ($[Pt^{II}(\text{phen})(L^1-S,O)]Cl$) in acetonitrile showed that the non-covalent aggregation of the cationic $[Pt^{II}(\text{phen})(L^1-S,O)]^+$ complexes results in dimer aggregates $2M^+ \rightleftharpoons \{M^+\}_2$ in solution (Scheme 1), while the $[Pt^{II}(\text{phen})(L^1-S,O)]^+$ cation certainly forms non-covalent *hetero*-aggregates with aromatic molecules such as fluoranthene (F) corresponding to $M^+ + F \rightleftharpoons M^+F$ in acetonitrile, with an estimated association constant $K_B \sim 67 \pm 7 \text{ M}^{-1}$ at room temperature.¹³ Moreover, in water rich acetonitrile solutions the ^1H NMR spectra of the $[Pt^{II}(\text{phen})(L^1-S,O)]^+$ become progressively broader as the relative amount of water increases. This corresponds to similar unpublished observations of extremely broad, almost featureless ^1H NMR spectra obtained in D_2O at room temperature of the highly water-soluble complex $[Pt^{II}(\text{diimine})(N,N\text{-di}(2\text{-hydroxyethyl})\text{-}N'\text{-benzoylthiourea})]Cl$ (Fig. S1†).¹⁴ These interesting NMR spectra suggest formation of larger nano-scale aggregate structures in water of such cationic complexes,¹⁴ the detailed nature of which has not been established to date.

We here report a study of the non-covalent aggregation behaviour of $[Pt^{II}(\text{phen})(L^1-S,O)]^+$ cations in acetonitrile–water mixtures ranging from pure acetonitrile to pure water by means of the concentration dependence of the ^1H NMR and Diffusion Ordered Spectroscopy (DOSY) techniques, supplemented by transmission electron microscopy to elucidate the nature of these phenomena, and the nano-aggregates which appear to form in water.

^1H diffusion ordered spectroscopy is a suitable technique for studying aggregation behaviour in solution since diffusion coefficients, which are very sensitive towards changes in the molecular/aggregate size, and the number of individual molecules, which constitute an aggregate, may be approximately estimated using the Stokes–Einstein equation.^{15,16} Our aim is to mimic the biological media in which such complex cations

may be active, particularly in the context of their potential anti-malarial activity *in vitro* and/or *in vivo*.¹⁷

Results and discussion

The effect of solvent composition (0–30% (v/v) D_2O – CD_3CN) on aggregation of $[Pt^{II}(\text{phen})(L^1-S,O)]Cl$

In pure acetonitrile, the ^1H NMR chemical shift concentration dependence trends (Fig. 1a) in 10% (v/v) D_2O – CD_3CN , as well as estimated diffusion coefficients by DOSY NMR (*vide infra*), of $[Pt^{II}(\text{phen})(L^1-S,O)]Cl$ can satisfactorily be accounted for by means of an aggregation model resulting in essentially exclusive formation of a $\{[Pt^{II}(\text{diimine})(L^1-S,O)]^+\}_2$, consistent with a non-covalent cation– π association of $[Pt^{II}(\text{phen})(L^1-S,O)]^+$ as demonstrated for related complexes previously.^{9,13} However, by increasing the water content in these solutions, the ^1H NMR resonances as a function of $[Pt^{II}(\text{phen})(L^1-S,O)]Cl$ concentration at 299.3 K become significantly broader as shown for 100% D_2O in Fig. 1b. Moreover, all the ^1H NMR peaks of the diimine moiety of the platinum complex show relatively larger upfield chemical shift displacements in the spectrum (peaks become more shielded) as the water content of the solutions increases, as well as on increasing concentration of the $[Pt^{II}(\text{phen})(L^1-S,O)]^+$ for a given acetonitrile–water mixture. Since only one set of resonance signals is observed in the ^1H NMR spectra for the $[Pt^{II}(\text{phen})(L^1-S,O)]^+$ complex/aggregate under any conditions, this is consistent with fast to intermediate exchange on the NMR timescale for the temperature range of 267.1 to 309.6 K. The relative upfield displacements of the $\delta_{\text{obs}}(\text{H}^2)$ and $\delta_{\text{obs}}(\text{H}^9)$ resonances (δ/ppm) of the diimine moiety of the $[Pt^{II}(\text{phen})(L^1-S,O)]^+$ cation are significantly more pronounced compared to the ^1H NMR signals of the *N*-acyl-*N,N*-dialkylthiourea moiety with increasing concentration (Fig. 1a) and increasing water content of the solvent mixture (Fig. 1b). The relative changes of $\delta_{\text{obs}}(\text{H}^{2/9})/\text{ppm}$ induced as the concentration of $[Pt^{II}(\text{phen})(L^1-S,O)]Cl$ increases from 0.34 to 10.3 mM are significantly larger in pure D_2O compared to acetonitrile ($\Delta^{\text{max}}\delta_{\text{CD}_3\text{CN}} = 0.28 \text{ ppm}$ to $\Delta^{\text{max}}\delta_{\text{D}_2\text{O}} = 0.41 \text{ ppm}$). Similar trends have been reported for the related $[Pt^{II}(\text{diimine})(N,N\text{-di}(n\text{-butyl})\text{-}N'\text{-benzoylthiourea})]Cl$ cation (Fig. S1†).¹⁴ The experimental trends of $\delta_{\text{obs}}(\text{H}^2)$ as a function of $[Pt^{II}(\text{phen})(L^1-S,O)]Cl$ concentration in solutions up to 30% (v/v) D_2O – CD_3CN at various temperatures are shown in Fig. 2. Non-linear least squares fitting of the experimental $\delta_{\text{obs}}(\text{H}^2)$ data to a dimer aggregate model $2M^+ \rightleftharpoons \{M^+\}_2$ ($M^+ = [Pt^{II}(\text{phen})(L^1-S,O)]^+$) results in excellent agreement, allowing for estimated K_D ($\text{RSD}_{\text{max}} < 13\%$) values in 0, 10, 20 and 30% (v/v) D_2O – CD_3CN shown in Table 1 in a temperature range 282.6–309.6 K.

Standard reaction enthalpy ($\Delta_r H^0$) and entropy ($\Delta_r S^0$) values were estimated from the Van't Hoff plots shown in Fig. S2;† the good linear plots of $\ln K_D$ vs. $1/T$ are consistent with only a dimer $2M^+ \rightleftharpoons \{M^+\}_2$ equilibrium and rule out other possible

† The protons H^2 and H^9 of the diimine moiety are most sensitive to changes in concentration and solvent composition.

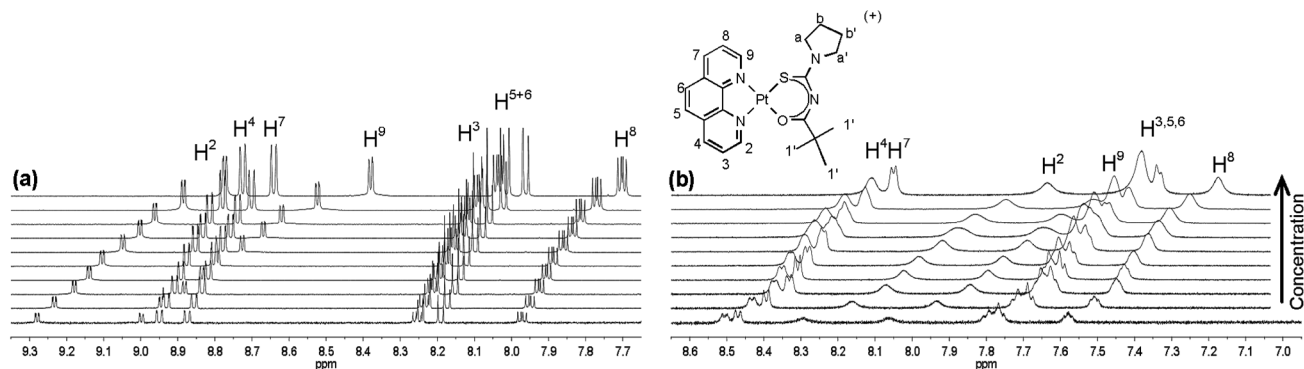


Fig. 1 ^1H NMR spectra (599.99 MHz) of $[\text{Pt}^{\text{II}}(\text{phen})(\text{L}^1\text{-S},\text{O})]^+$ showing the chemical shift dependence of the 1,10-phenanthroline protons on the concentration of $[\text{Pt}^{\text{II}}(\text{phen})(\text{L}^1\text{-S},\text{O})]^+$ in solutions containing (a) 10% (v/v) $\text{D}_2\text{O}-\text{CD}_3\text{CN}$ (0.3–26.4 mM, 299.3 K) and (b) D_2O (0.3–25.0 mM, 309.6 K).

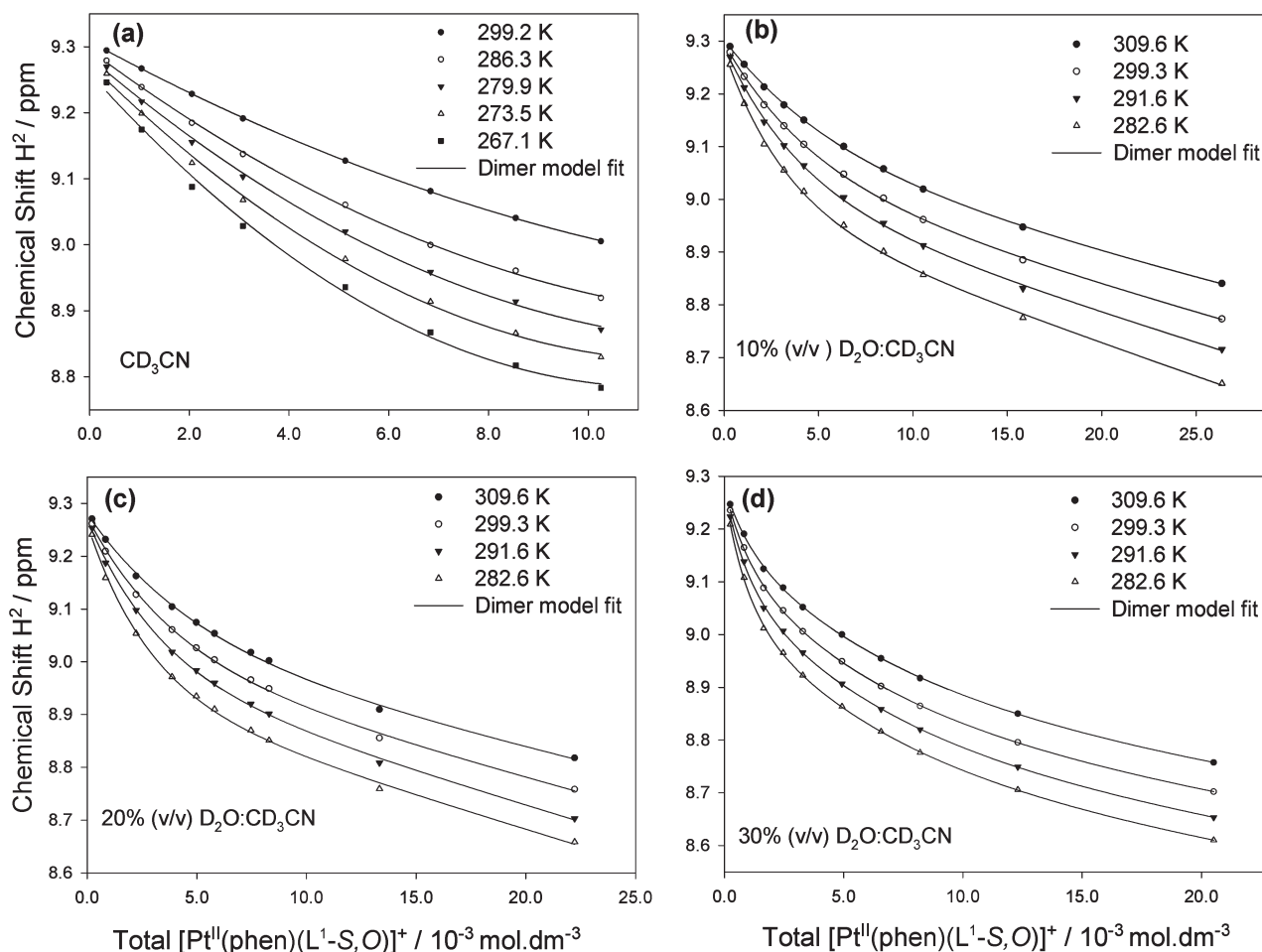


Fig. 2 Excellent agreement between the dimer model least-squares fits and the experimental (symbols) chemical shift dependence of the 1,10-phenanthroline H^2 proton a concentration probe of $[\text{Pt}^{\text{II}}(\text{phen})(\text{L}^1\text{-S},\text{O})\text{Cl}]$ in (a) 0: 100, (b) 10: 90, (c) 20: 80 and (d) 30: 70 (v/v) $\text{D}_2\text{O}-\text{CD}_3\text{CN}$ mixtures. (Calculated monomer and dimer chemical shifts available in the ESI Table S1.†)

competing association processes or equilibria, such as ion-pairing and/or higher order aggregate formation for these solvent compositions ($\leq 30\%$ (v/v) $\text{D}_2\text{O}-\text{CD}_3\text{CN}$).

The increase in K_{D} by a factor of 4–5 when the solvent composition is changed from pure acetonitrile to 30% (v/v)

$\text{D}_2\text{O}-\text{CD}_3\text{CN}$ mixtures indicates that the dimer aggregate $\{[\text{Pt}^{\text{II}}(\text{phen})(\text{L}^1\text{-S},\text{O})]^+\}_2$ is clearly favoured with increasing water (D_2O) content, as might be anticipated due to the expected hydrophobicity of such planar complex cations.

Table 1 Thermodynamic data for the self-association of $[\text{Pt}^{\text{II}}(\text{phen})(\text{L}^1\text{-S},\text{O})]^+$ in 0–30% (v/v) D_2O – CD_3CN solutions as calculated from ^1H NMR chemical shift concentration and temperature dependence

Percentage (v/v) D_2O – CD_3CN	Temperature (K)	K_{D} (M^{-1})	$\Delta_{\text{r}}H^0$ (kJ mol^{-1})	$\Delta_{\text{r}}S^0$ ($\text{J mol}^{-1} \text{K}^{-1}$)	$\Delta_{\text{r}}G^0$ (kJ mol^{-1})
0	309.6	12 (± 1)			
	299.3	17 (± 2)	−25.1 (± 3.1)	−61 (± 11)	−7.0
	291.6	22 (± 2)			
	282.6	29 (± 3)			
309.6	20 (± 2)				
10	299.3	27 (± 3)	−19.7 (± 2.4)	−40 (± 7)	−8.0
	291.6	33 (± 3)			
	282.6	41 (± 5)			
	309.6	29 (± 3)			
20	299.3	39 (± 4)	−20.1 (± 2.5)	−38 (± 7)	−8.6
	291.6	43 (± 4)			
	282.6	64 (± 7)			
	309.6	54 (± 5)			
30	299.3	71 (± 8)	−18.9 (± 2.3)	−27 (± 5)	−10.4
	291.6	87 (± 9)			
	282.6	109 (± 10)			

The process $2\text{M}^+ \rightleftharpoons \{\text{M}^+\}_2$ is evidently enthalpy driven ($\Delta_{\text{r}}H^0 < 0$) while a negative standard reaction entropy ($\Delta_{\text{r}}S^0 < 0$) is consistent with an aggregation/association process.¹⁸ Interestingly the enthalpy of the dimer formation ($\Delta_{\text{r}}H^0$) decreases somewhat on passing from pure acetonitrile ($\Delta_{\text{r}}H^0 = -25.1 \text{ kJ mol}^{-1}$) to a 10% (v/v) D_2O – CD_3CN ($\Delta_{\text{r}}H^0 = -19.7 \text{ kJ mol}^{-1}$) mixture, after which the reaction enthalpy remains essentially constant within experimental error for 20 and 30% (v/v) D_2O – CD_3CN solutions. By contrast the $\Delta_{\text{r}}S^0$ becomes systematically less negative as the D_2O content increases, Table 1. Doty and Myers attributed similar trends in $\Delta\Delta_{\text{r}}S^0$ for dimerization of protein moieties to the dehydration of charged groups upon aggregation, while Kauzmann and Scheraga suggested that this trend may be due to non-covalent hydrophobic bonding of non-polar groups increasing the degree of freedom of the water molecules close to hydrophobic groups.^{19–21} It is thus reasonable to postulate that the trends in $\Delta\Delta_{\text{r}}S^0$ observed in this study may be attributed to the “hydrophobicity” of the coordinated 1,10-phenanthroline moiety, the effects of which become more significant as the solvent polarity increases with increasing water content of the solvent mixture (dielectric constant, $\epsilon_{\text{water}} = 78.5$ and $\epsilon_{\text{acetonitrile}} = 37.5$).^{22,23}

The $\delta(^1\text{H})$ trend differences for ^1H peaks of the 1,10-phenanthroline moiety as compared to butyl and *N*-pyrrolidyl ^1H signals of $[\text{Pt}^{\text{II}}(\text{phen})(\text{L}^1\text{-S},\text{O})]^+$ as a function of concentration and temperature are entirely consistent with a *regiospecific* face-to-face stacking arrangement of the $[\text{Pt}^{\text{II}}(\text{phen})(\text{L}^1\text{-S},\text{O})]^+$ cations in a dimer (Scheme 1) in these solutions up to 30% (v/v) D_2O – CD_3CN as previously postulated in pure acetonitrile.^{9,13} Essentially the two planar complex cations interact with one another through cation– π interactions in a characteristic ‘offset’ stacking configuration consistent with the model proposed by Hunter and Sanders²⁴ in their study on the nature of “ π -stacking interactions” based on porphyrin–porphyrin aggregation.

The observed shielding trends as a function of concentration particularly of the H^2 and H^9 protons of the

coordinated diimine moiety clearly rule out a possible “T-shaped” cation– π interaction in these solutions.²⁴

Aggregation behaviour of $[\text{Pt}^{\text{II}}(\text{phen})(\text{L}^1\text{-S},\text{O})]\text{Cl}$ in water-rich mixtures >30% (v/v) D_2O – CD_3CN

In water-rich acetonitrile >30% (v/v) D_2O – CD_3CN mixtures significantly broader ^1H NMR resonances are observed for all the ^1H peaks associated with the diimine moiety in $[\text{Pt}^{\text{II}}(\text{phen})(\text{L}^1\text{-S},\text{O})]^+$ (Fig. 1b), eventually resulting in poorly resolved ^1H NMR spectra. Additionally, the even more pronounced shielding of the H^2 and H^9 protons of the diimine moiety with increasing $[\text{Pt}^{\text{II}}(\text{phen})(\text{L}^1\text{-S},\text{O})]^+$ concentrations suggests the formation of a larger scale structure/aggregate in solution. Significantly, application of a simple dimer $2\text{M}^+ \rightleftharpoons \{\text{M}^+\}_2$ model to the experimentally observed ^1H NMR shielding trends fails to account for these satisfactorily, particularly as the water content of the solvent increases to pure D_2O .

The significant line-broadening of ^1H NMR peaks in D_2O may be associated with a decrease in the T_2 relaxation times as estimated from ^1H NMR peak width at half-height ($\Delta\nu_{1/2} \propto 1/T_2$) under optimum magnetic field homogeneities.^{25,26} The measured ^1H NMR resonance half-height ($\Delta\nu_{1/2}$) of the $\text{H}^{2/9}$ resonances in $[\text{Pt}^{\text{II}}(\text{phen})(\text{L}^1\text{-S},\text{O})]^+$ increases from 0.9 Hz in pure CD_3CN to 18 Hz in pure D_2O at constant temperature. The extremely pronounced ^1H NMR broadening observed for $[\text{Pt}^{\text{II}}(\text{diimine})(\text{N},\text{N}\text{-di}(2\text{-hydroxyethyl})\text{-N'}\text{-benzoylthiourea})]\text{Cl}$ (Fig. S1†) in D_2O , and an inverse dependence of line-width with temperature¹⁴ undoubtedly indicate that whatever the nature of the aggregate structure(s) formed in solution must have significantly larger average molecular weights.²⁷ We postulate that non-covalent *inter*-molecular interactions associated with the formation of large nano-sized aggregates with high molecular weight D_2O are likely to result in significant shortening of the T_2 relaxation times consistent with larger structures and thus longer molecular correlation/tumbling times τ_c commonly associated with macromolecules.^{26–28} The greater degree of shielding of *inter alia* $\text{H}^{2/9}$ with increasing complex

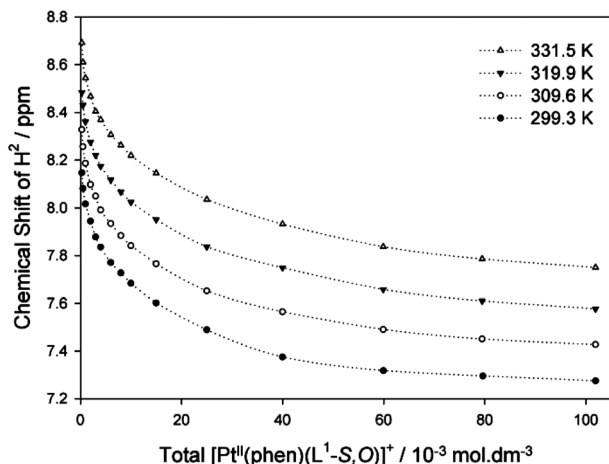


Fig. 3 The ^1H NMR chemical shift dependence of H^2 on $[\text{Pt}^{\text{II}}(\text{phen})(\text{L}^1\text{-S},\text{O})]\text{Cl}$ concentration in D_2O at temperatures 299.3, 309.6, 319.9, and 331.5 K. (Note: the dotted lines are aids for trend visualization.)

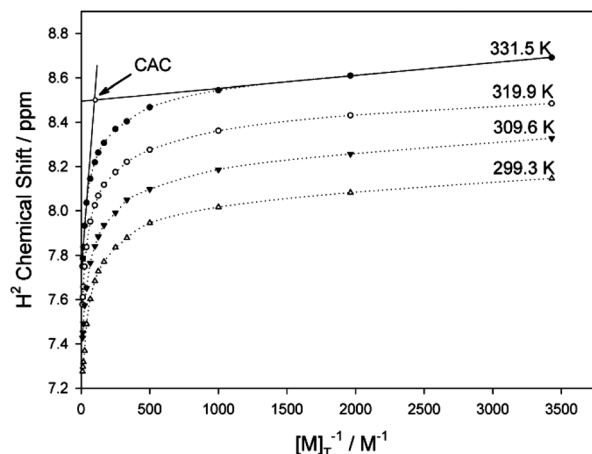
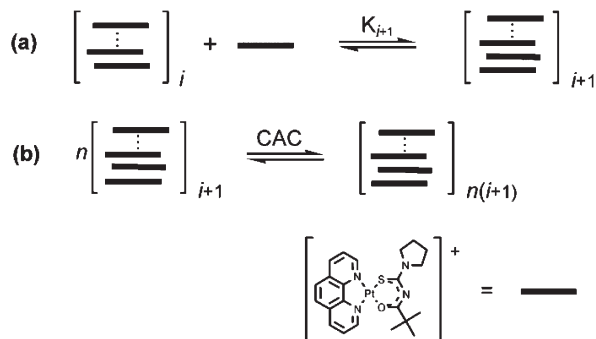


Fig. 4 The observed ^1H chemical shift of H^2 at temperatures 299.3–331.5 K against $1/[\text{M}]_{\text{T}}$ were $[\text{M}]_{\text{T}} = \text{Total } [\text{Pt}^{\text{II}}(\text{phen})(\text{L}^1\text{-S},\text{O})]\text{Cl}$ concentration in D_2O . The expansions and extrapolations of the ^1H NMR chemical shift concentration dependence of all temperatures are displayed in Fig. S3.† (Note: the dotted lines are aids for trend visualization.)



Scheme 2 Postulated aggregation model of $[\text{Pt}^{\text{II}}(\text{phen})(\text{L}^1\text{-S},\text{O})]\text{Cl}$ in aqueous solutions consisting of two major equilibrium processes with (a) an accumulative aggregation with K_i , the respective association constant corresponding to the i th monomer associating to the aggregate and (b) the formation of nano-sized aggregates after a specific critical aggregation concentration (CAC).

concentration in D_2O (due to the chemical shift anisotropy (CSA) phenomenon) illustrated by the data in Fig. 3 for several temperatures is consistent with more extensive cation– π aromatic-ring stacking expected for the planar quasi-aromatic $[\text{Pt}^{\text{II}}(\text{phen})(\text{L}^1\text{-S},\text{O})]^+$ cation. Despite our best efforts, the shielding trends in D_2O and (water rich solutions $> (v/v)$ D_2O – CD_3CN) could also not be satisfactorily accounted for by simple or even higher order aggregation models such as trimer-, tetramer formation, *etc.* We therefore propose a multiple aggregate formation model leading to the formation of structures formulated as $\{[\text{Pt}^{\text{II}}(\text{phen})(\text{L}^1\text{-S},\text{O})]^+\}_n \text{Cl}^-_y$ (n and y variable but >2) similar to a model proposed for procyanidin aggregation in a wine-like medium described by Pianet *et al.*,²⁹ illustrated in Scheme 2.

Our experimental NMR data in D_2O are consistent with a model described in Scheme 2, in which at relatively low total complex concentrations initially, (a) the self-association of $[\text{Pt}^{\text{II}}(\text{phen})(\text{L}^1\text{-S},\text{O})]^+$ cations results in dimer aggregates, which however eventually lead to the formation of $\{[\text{Pt}^{\text{II}}(\text{phen})$

Table 2 Estimated critical aggregation concentrations (CAC) in D_2O from concentration dependence $\delta_{\text{obs}}(\text{H}^2)$ data at various temperatures, as well as diffusion coefficient (D_{obs}) dependence on concentration at 299.3 K

Temp (K)	299.3	309.6	319.9	331.5
δ , CAC mM	9.6 (± 0.6)	12.0 (± 0.7)	13.9 (± 0.9)	14.9 (± 0.9)
D , CAC mM	10.3 (± 1.5)			

$(\text{L}^1\text{-S},\text{O})]^+\}_n \text{Cl}^-_y$ structures *via* an unspecified number of sequential equilibria (K_{i+1}), as the total complex concentration increases; (b) above a certain critical concentration of $[\text{Pt}^{\text{II}}(\text{phen})(\text{L}^1\text{-S},\text{O})]^+$, which may for convenience be termed a ‘critical aggregation concentration’ (CAC), similar to the well-known critical micelle concentration (CMC), larger nano-sized aggregate structures appear to form with concomitant ion-pair formation by Cl^- ions, to offset excessive positive charge build-up as a result of the formation of a charged ‘cation-aggregate’ (Scheme 2b).²⁹

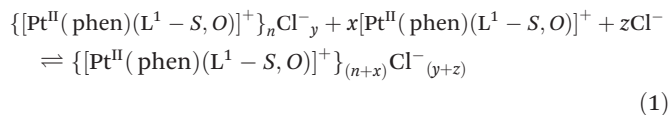
In support of such a CAC model, a plot of $\delta_{\text{obs}}(\text{H}^2)$ of $[\text{Pt}^{\text{II}}(\text{phen})(\text{L}^1\text{-S},\text{O})]^+$ against $1/[\text{M}]_{\text{T}}$ ($[\text{M}]_{\text{T}} = \text{total } [\text{Pt}^{\text{II}}(\text{phen})(\text{L}^1\text{-S},\text{O})]\text{Cl}$ concentration) results in two quasi-linear regions (Fig. 4), the intercept of such lines gives an estimate of the critical aggregation concentration^{30,31} in D_2O for the $[\text{Pt}^{\text{II}}(\text{phen})(\text{L}^1\text{-S},\text{O})]^+$ complex as listed in Table 2. The estimated CAC for $[\text{Pt}^{\text{II}}(\text{phen})(\text{L}^1\text{-S},\text{O})]^+$ increases with temperature as may be expected given that the aggregation process is enthalpy driven ($\Delta_{\text{T}}H^0 < 0$), suggested by data in Table 1.

Effect of chloride ion concentration on $[\text{Pt}^{\text{II}}(\text{phen})(\text{L}^1\text{-S},\text{O})]^+$ aggregation in water

The extent of aggregation of cationic $[\text{Pt}^{\text{II}}(\text{phen})(\text{L}^1\text{-S},\text{O})]^+$ complexes to form dimer $\{\text{M}\}_2^{2+}$ type structures in mainly acetonitrile and in water the postulated nano-scale aggregate structures $\{[\text{Pt}^{\text{II}}(\text{phen})(\text{L}^1\text{-S},\text{O})]^+\}_n$ is likely to lead to

electrostatic positive charge build-up, which is probably partially offset by the chloride ion ion-pairing/association in solution. Thus the effective Cl^- : cation ratio may be expected to stabilize and/or affect the formation of aggregate structures in D_2O . This is confirmed by the significant shielding induced in the $\delta_{\text{obs}}(\text{H}^2)$ peak of the 1,10-moiety of $[\text{Pt}^{\text{II}}(\text{phen})(\text{L}^1\text{-S},\text{O})]^+$ on “titration” of a 4.54 mM solution of $[\text{Pt}^{\text{II}}(\text{phen})(\text{L}^1\text{-S},\text{O})]^+$ below the CAC, with NaCl solution in D_2O increasing the effective $[\text{Cl}^-]$ from 10.5 to 346.7 mM, as illustrated in Fig. S4,† corresponding to a Cl^- : cation ratio of *ca.* 2 to 77. Further increases to a Cl^- : cation ratio to >80 lead to precipitation of a yellow solid from solution. The shielding induced in $\delta_{\text{obs}}(\text{H}^{2/9})$ as a result of increasing the Cl^- : cation ratio cannot be solely due to ionic strength increases, since the corresponding ^1H NMR chemical shifts of the butyl and *N*-pyrrolidyl protons are comparatively small compared to the diimine protons, while the residual solvent peak and any minor impurities in the ^1H NMR spectrum remain essentially unaffected over the titration range. These trends suggest that the overall ‘size’ of the nano-scale aggregate $\{[\text{Pt}^{\text{II}}(\text{phen})(\text{L}^1\text{-S},\text{O})]^+\}_n\text{Cl}^-_y$ appears to grow in size (*n*, *y* increase) or at least be stabilized with increasing Cl^- : cation ratio, until precipitation from solution occurs, akin to the well-known “salting-out” phenomenon.

Thus in water, or at least in water-rich acetonitrile mixtures above 30% (v/v) D_2O - CD_3CN , the proposed positively charged aggregate structures of the $[\text{Pt}^{\text{II}}(\text{phen})(\text{L}^1\text{-S},\text{O})]^+$ complex cation as envisaged in Scheme 2 may be reasonably represented by eqn (1):



Diffusion ordered NMR spectroscopy

A semi-quantitative estimate of the effective number of complex cations (*n*) which may constitute the postulated nano-sized aggregate structure would lend convincing support to this model.

Based on the expectation that the translational diffusion of such aggregates in solution should depend significantly on their effective ‘size’ as suggested by the concentration dependence of ^1H NMR shielding data, ^1H DOSY NMR was used to study this phenomenon in solution. Data from DOSY NMR experiments in the concentration range 0.34–76.08 mM $[\text{Pt}^{\text{II}}(\text{phen})(\text{L}^1\text{-S},\text{O})]^+$ at 299.3 K in D_2O are shown in Fig. 5 and Table 3. Single exponential decay fits the attenuation of the ^1H DOSY NMR data very well, and indicates that the observed diffusion coefficient (D_{obs}) is an average of that of the mononuclear $[\text{Pt}^{\text{II}}(\text{phen})(\text{L}^1\text{-S},\text{O})]^+$ and *all* aggregate species in solution ($D_{\text{obs}} = \alpha_m D_m + \dots + \alpha_i D_i$) in solution. The D_{obs} for the $[\text{Pt}^{\text{II}}(\text{phen})(\text{L}^1\text{-S},\text{O})]^+$ in water shows a significant decrease as a function of concentration (Fig. 5a), consistent with a higher order aggregate formation.

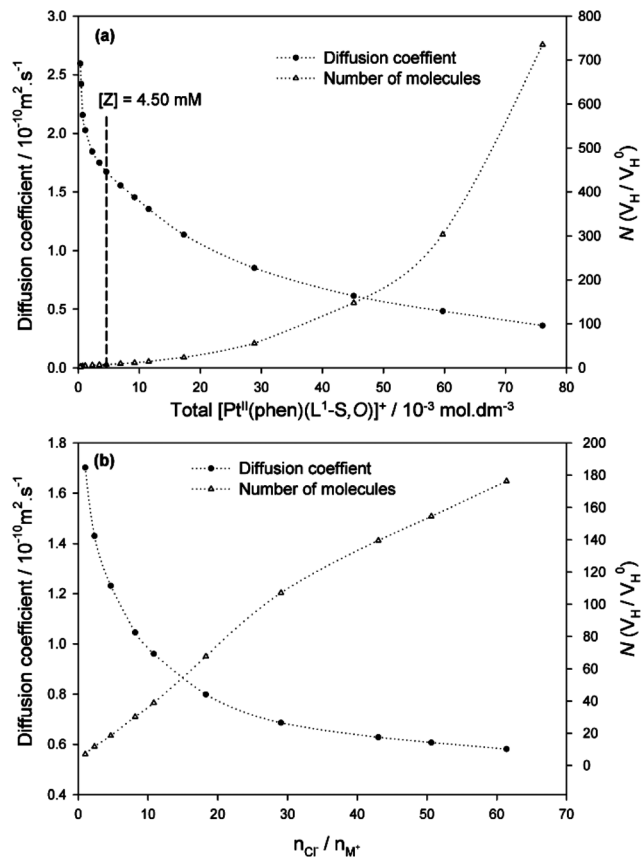


Fig. 5 (a) $[\text{Pt}^{\text{II}}(\text{phen})(\text{L}^1\text{-S},\text{O})]\text{Cl}$ diffusion coefficient (D_{obs}) and average aggregation number (N) ($N = V_{\text{H}}/V_{\text{H}}^0$) as a function of $[\text{Pt}^{\text{II}}(\text{phen})(\text{L}^1\text{-S},\text{O})]\text{Cl}$ concentration in pure D_2O . (b) The effect of Cl^- addition (NaCl) on the diffusion coefficient of $[\text{Pt}^{\text{II}}(\text{phen})(\text{L}^1\text{-S},\text{O})]\text{Cl}$ (concentration indicated as $[Z]$) and the calculated average number of molecules (N) with $n_{\text{Cl}^-}/n_{\text{M}^+}$ the mole ratio of Cl^- over $[\text{Pt}^{\text{II}}(\text{phen})(\text{L}^1\text{-S},\text{O})]^+$ in D_2O .

Table 3 Diffusion coefficient (D) concentration dependence data, calculated hydrodynamic radii (r_{H}) and average aggregation numbers (N), with $N = V_{\text{H}}/V_{\text{H}}^0$ where V_{H} is the volume calculated from r_{H} and V_{H}^0 the estimated volume of a monomer at infinite dilution

Concentration ($10^{-3} \text{ mol dm}^{-3}$)	D ($10^{-10} \text{ m}^2 \text{ s}^{-1}$)	r_{H} (\AA)	V_{H} (\AA^3)	N ($V_{\text{H}}/V_{\text{H}}^0$)
76.08	0.36	56.1	739 692	735
59.72	0.52	39.1	250 561	304
45.14	0.61	32.9	148 577	148
28.84	0.85	23.7	55 532	55.2
17.31	1.14	17.7	23 345	23.2
11.54	1.35	14.9	13 818	13.7
9.230	1.47	13.7	10 708	11.1
6.922	1.55	13.0	9120	9.06
4.615	1.67	12.1	7335	7.29
3.462	1.77	11.4	6182	6.35
2.307	1.84	10.9	5458	5.42
1.154	2.05	9.84	3990	4.08
0.721	2.16	9.34	3415	3.39
0.481	2.42	8.32	2415	2.40
0.337	2.59	7.76	1961	1.95
0 ^a	3.24	6.22	1007	1

^a Extrapolated to infinite dilution using the D_{obs} vs. $1/[\text{M}]_{\text{T}}$ plot.

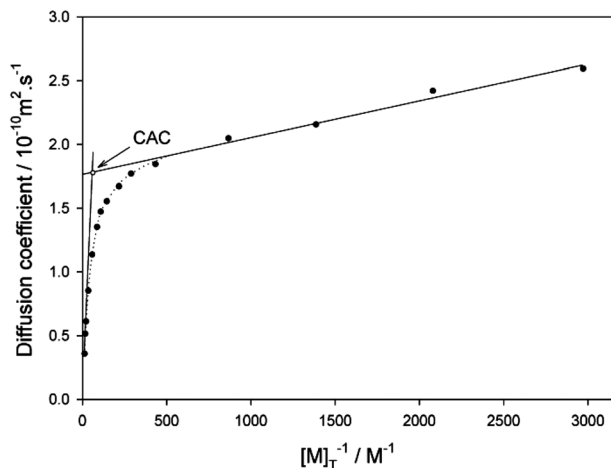


Fig. 6 $[\text{Pt}^{\text{II}}(\text{phen})(\text{L}^1\text{-S,O})]^+$ diffusion coefficient at 299.3 K against $1/[\text{M}]_{\text{T}}$, where $[\text{M}]_{\text{T}}$ = Total $[\text{Pt}^{\text{II}}(\text{phen})(\text{L}^1\text{-S,O})]\text{Cl}$ concentration. (Note: The dotted lines are aids for trend visualization.)

The Stokes–Einstein equation $D = kT/6\pi\eta r_{\text{H}}$ may be used to estimate the hydrodynamic radii of species from the measured diffusion coefficients, where k is the Boltzmann constant, η the solvent viscosity, and r_{H} the hydrodynamic radius. Since the diffusion coefficient obtained for $[\text{Pt}^{\text{II}}(\text{phen})(\text{L}^1\text{-S,O})]^+$ is the average between all species in solution, the r_{H} is an average value. Although the Stokes–Einstein equation is only a crude approximation for estimating the ‘size’ of a square planar $[\text{Pt}^{\text{II}}(\text{phen})(\text{L}^1\text{-S,O})]^+$ complex, the changes in the average r_{H} as a function of concentration may be useful to support the proposed aggregation model herein. The r_{H} of a single monomer (r_{H}^0) has been estimated by extrapolating the D_{obs} to infinite dilution from the plot of D_{obs} vs. $1/[\text{M}]_{\text{T}}$, Fig. 6. An estimate of the CAC at $ca. 10.3 \pm 1.5$ for this complex may also be obtained from this plot, which is in satisfactory agreement with the CAC values obtained by the simple $\delta(\text{H}^2)$ concentration dependence data shown in Table 2.

The extent of aggregation can be estimated by considering the *aggregation number* (N) calculated from the hydrodynamic volumes of the monomer (V_{H}^0) and V_{H} estimated from D_{obs} ($N = V_{\text{H}}/V_{\text{H}}^0$).³² Table 3 lists the data obtained from this system from the ^1H DOSY NMR experiments at 299.3 K. The average aggregate-number in solution increases from $N \sim 1.95$ at the lowest practically measureable concentration by DOSY NMR of 0.34 mM of $[\text{Pt}^{\text{II}}(\text{phen})(\text{L}^1\text{-S,O})]^+$ with an estimated hydrodynamic radius of $ca. 7.8 \text{ \AA}$ and $V_{\text{H}} = 1961 \text{ \AA}^3$, to a maximum $N \sim 735$ ($[\text{M}]_{\text{T}} = 76.1 \text{ mM}$) corresponding to a ‘size’ of $ca. 735 \text{ nm}^3$ for the postulated nano-aggregate structure of $\{[\text{Pt}^{\text{II}}(\text{phen})(\text{L}^1\text{-S,O})]^+\}_n\text{Cl}^-_y$ structure(s) in solution.

Significant changes in D_{obs} are seen in D_2O for a 4.5 mM $[\text{Pt}^{\text{II}}(\text{phen})(\text{L}^1\text{-S,O})]^+$ solution ([Z] dashed line in Fig. 5a) upon increasing the Cl^- :cation ratio by means of ‘titration’ with NaCl. The 4.5 mM concentration was chosen well below the CAC value of 9.6 mM to show the maximum effect. In this way the calculated average aggregation number (N) of $[\text{Pt}^{\text{II}}(\text{phen})(\text{L}^1\text{-S,O})]^+$ increased from 8 to a maximum of $ca. 176$ for the

highest practical Cl^- :cation ratio ($n_{\text{Cl}^-}/n_{\text{M}^+}$), before precipitation occurs (Fig. 5b). The increase in NaCl concentration up to a maximum of $\sim 342 \text{ mM}$ might be expected to increase the viscosity of the solution significantly, although the estimated overall change in viscosity is at most $ca. 0.02 \text{ mPa s}^{-1}$, which results in a difference of only $ca. 1.8\text{--}2\%$ in the calculated diffusion coefficients.³³ These data satisfactorily confirm the effect of increasing the Cl^- :cation ratio on the postulated nano-aggregate (‘metallo-gel’) formation of $\{[\text{Pt}^{\text{II}}(\text{phen})(\text{L}^1\text{-S,O})]^+\}_n\text{Cl}^-_y$ type structures in water, as summarized by the equilibrium (1) above. Such nano-aggregate structures are likely to be well within a size range possibly observable by means of transmission electron microscopy (TEM).

Transmission electron microscopy (TEM)

TEM images obtained from 10–15 mM $[\text{Pt}^{\text{II}}(\text{phen})(\text{L}^1\text{-S,O})]\text{Cl}$ solutions in water and stained with uranyl acetate revealed the presence of well-defined ‘spaghetti-like’ aggregate structures with a diameter of $ca. 20 \text{ nm}$, as shown in Fig. 7a. Similar TEM images have been obtained for the series of related highly water-soluble complexes $[\text{Pt}^{\text{II}}(\text{diimine})(N,N\text{-di}(2\text{-hydroxyethyl})\text{-}N'\text{-benzoyl-thiourea})]\text{Cl}$ from unpublished studies,¹⁴ of which a representative image is shown in ESI (Fig. S5†). The maximum diameter of the spaghetti-like aggregates observed in the TEM images of $[\text{Pt}^{\text{II}}(\text{phen})(\text{L}^1\text{-S,O})]\text{Cl}$ appears to be limited to $ca. 20 \text{ nm}$, with the uranyl acetate stain accumulating at the surface/edges of these aggregates. Images obtained from $[\text{Pt}^{\text{II}}(\text{phen})(\text{L}^1\text{-S,O})]\text{Cl}$ from pure acetonitrile solutions confirm that the extent of aggregation from acetonitrile solutions is significantly less pronounced, resulting in only poorly defined irregular structures of variable and smaller average size (Fig. 7b).

In keeping with the findings of Pianet and co-workers for the self-association of synthetic procyanidins,²⁹ solutions of $[\text{Pt}^{\text{II}}(\text{phen})(\text{L}^1\text{-S,O})]^+$ in water also show a time dependent colloid formation process, resulting in micron-sized structures from solutions of high $[\text{Pt}^{\text{II}}(\text{phen})(\text{L}^1\text{-S,O})]^+$ concentration after aging (>7 days) as observed in TEM images shown in Fig. S6†. Preliminary Tyndall light-scattering experiments also confirm such an aging effect for concentrated solutions. Furthermore Atomic Force Microscopy (AFM) images of a spin-dried droplet of $[\text{Pt}^{\text{II}}(\text{phen})(\text{L}^1\text{-S,O})]\text{Cl}$ dissolved in acetonitrile reveal the presence of micron-sized ‘spaghetti-like’ structures, remarkably similar in overall appearance and morphology to those obtained from TEM images (Fig. S7†).

The possibility of a secondary helical structure was considered since the TEM images of the observed aggregates have a distinct size and shape. High-resolution TEM of samples prepared on a carbon-coated grid immediately after dilution of a solution containing nano-aggregates at concentrations above the CAC shows that the secondary structure appears to form from the agglomeration of ‘strands’ of $\{[\text{Pt}^{\text{II}}(\text{phen})(\text{L}^1\text{-S,O})]^+\}_n\text{Cl}^-_y$ aligned parallel to each other, with a diameter of $ca. 2 \text{ nm}$ (Fig. 7c and S8†). TEM images obtained from samples in diluted solutions left to ‘age’ ($\pm 2 \text{ h}$) do not show any structures in the nano-range as can be obtained from more concentrated freshly prepared samples. Evidently upon

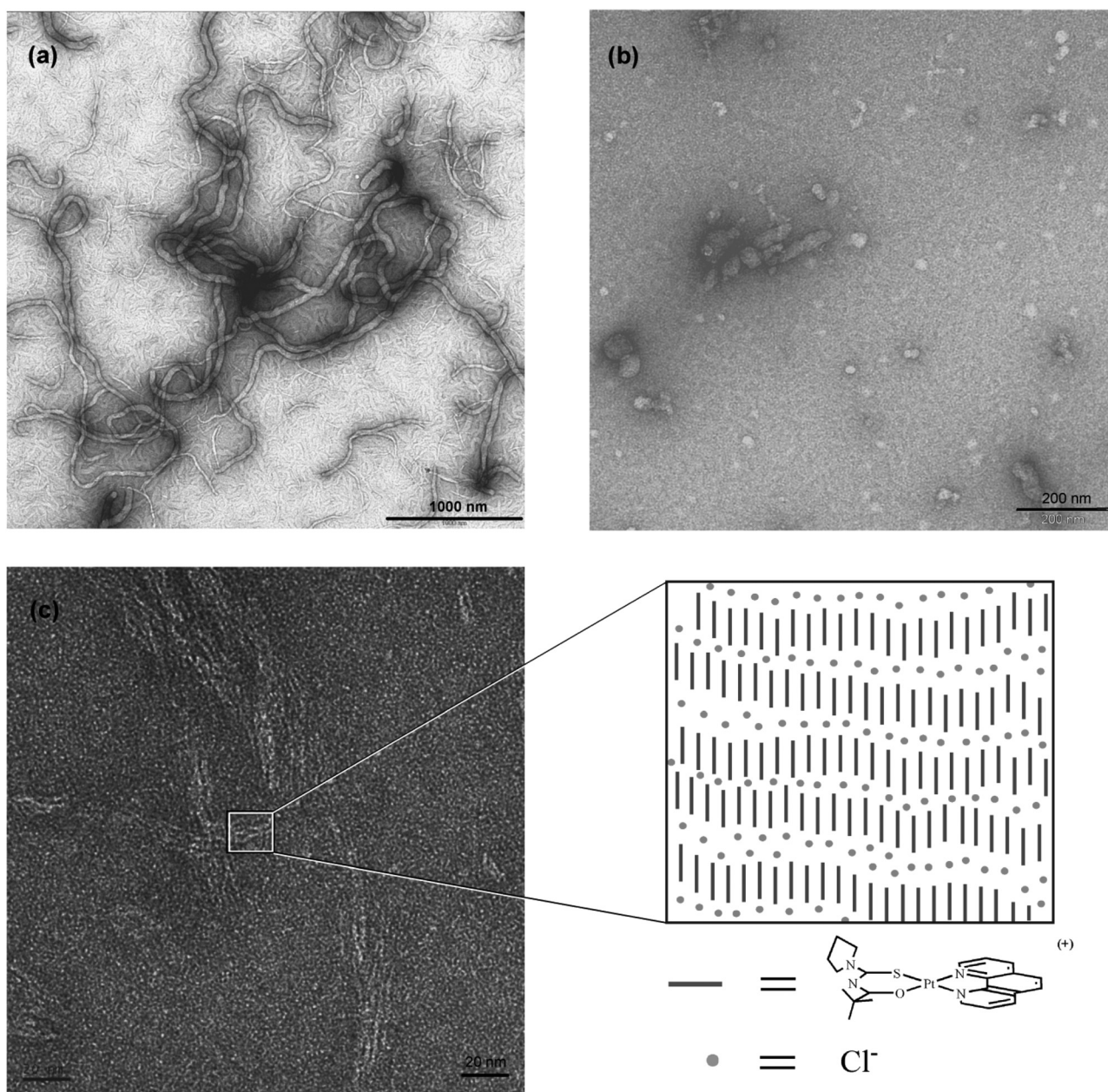


Fig. 7 TEM images of $[\text{Pt}^{\text{II}}(\text{phen})(\text{L}^1\text{-S,O})]\text{Cl}$ in (a) water (b) acetonitrile* and (c) freshly diluted water with uranyl acetate as a stain. *Staining in acetonitrile was done with uranyl acetate in ethanol.

dilution a type of dis-aggregation into presumably monomer and dimer species of $[\text{Pt}^{\text{II}}(\text{phen})(\text{L}^1\text{-S,O})]\text{Cl}$ appears to take place.

On the basis of all the experimental data, it is tempting to postulate a qualitative aggregate growth model for the non-covalent association of $[\text{Pt}^{\text{II}}(\text{phen})(\text{L}^1\text{-S,O})]^+$ in water or water-rich solutions. Our data are consistent with a *region-specific* aggregation process of the hydrophobic planar $[\text{Pt}^{\text{II}}(\text{phen})(\text{L}^1\text{-S,O})]^+$ cations postulated in Scheme 1, strongly indicating a preferred cation- π “stacking” orientation, as found here and as suggested in previous studies with a related compound.^{9,13} The driving force for the self-association or “stacking” of

$[\text{Pt}^{\text{II}}(\text{phen})(\text{L}^1\text{-S,O})]^+$ is most likely to be the result of a combination of cation- π interactions accentuated by hydrophobic effects. Despite numerous efforts we have unfortunately not been able to obtain suitable single crystals for X-ray diffraction analysis.

An estimation of the approximate dimensions of the planar $[\text{Pt}^{\text{II}}(\text{phen})(\text{L}^1\text{-S,O})]^+$ cation from the data obtained from crystal structures of the related $[\text{Pt}^{\text{II}}(\text{en})(\text{phen})]\text{Cl}_2$ ³⁴ and *cis*- $[\text{Pt}^{\text{II}}(\text{L}^1\text{-S,O})_2]$ ³⁵ complexes yields *ca.* 1.5 ± 0.2 nm, suggesting that a single ‘strand’ of $[\text{Pt}^{\text{II}}(\text{phen})(\text{L}^1\text{-S,O})]^+$ in a parallel co-planar stacking arrangement does not completely account for the *ca.* 20 nm nano-sized “spaghetti-like” structures observed in the

TEM images. We thus postulate that the nano-aggregates form by means of agglomeration of single strands of presumably individually stacked $[\text{Pt}^{\text{II}}(\text{phen})(\text{L}^1\text{-S},\text{O})]^+$ cations in an offset cation- π arrangement, most probably stabilized by negatively charged chloride counter ions which may coil into the tube-like super-structures observed in Fig. 7c and S8.† The aggregation of the individual strands of co-planar cation- π stacked complexes may be facilitated by the chloride counter ion layers around the strands to form a positively charged “core” and a negatively charged outer layer of chloride ions to which the next positively charged strand may align due to electrostatic attractions. The overall diameter of the observed tube-like structures in TEM images is limited to ± 20 nm in diameter. The apparent preferred accumulation of the cationic uranyl stain on the outer surface of the nano-structures in the TEM images is consistent with the aggregate formation model postulated here, in which the uranyl cations ion-pair with a negatively charged chloride ‘layer’ on the surface of the stacked cations $[\text{Pt}^{\text{II}}(\text{phen})(\text{L}^1\text{-S},\text{O})]^+$ via π -cation interactions.

Conclusions

$[\text{Pt}^{\text{II}}(\text{phen})(\text{L}^1\text{-S},\text{O})]^+$ cations (M^+) ‘self-associate’ by non-covalent intermolecular cation- π interactions in acetonitrile solutions and water-acetonitrile mixtures of up to 30% (v/v) $\text{D}_2\text{O}-\text{CD}_3\text{CN}$ to form essentially dimer aggregates according to the $2\text{M}^+ \rightleftharpoons \{\text{M}^+\}_2$ model. This process is strongly favored in more polar water-rich solutions ($\Delta_r G_{\text{CD}_3\text{CN}}^0 = -7.0$ kJ mol $^{-1}$; $\Delta_r G_{30\% \text{D}_2\text{O}-\text{CD}_3\text{CN}}^0 = -10.4$ kJ mol $^{-1}$), with the corresponding K_{D} increasing from 17 ± 2 to 72 ± 8 M $^{-1}$ at 299.3 K from acetonitrile to 30% $\text{D}_2\text{O}-\text{CD}_3\text{CN}$ mixtures. The experimental data obtained suggest that the primary driving force for such phenomena is consistent with mainly cation- π stacking interactions, with the increase in the K_{D} attributed to a favorable contribution to a negative $\Delta_r S^0$ as a result of the “hydrophobicity” of the quasi-aromatic nature of these complex cations. Increasing the water content from >30% to 100% (v/v) $\text{D}_2\text{O}-\text{CD}_3\text{CN}$ results in the extent of aggregation significantly increasing as a function of the $[\text{Pt}^{\text{II}}(\text{phen})(\text{L}^1\text{-S},\text{O})]\text{Cl}$ concentration, culminating in the formation of nano-sized structures (“metallogels”) consisting of up to *ca.* 735 mononuclear cations as determined by diffusion coefficients obtained by means of DOSY NMR spectroscopy, above a critical aggregation concentration (9.6–10.3 mM at 299.3 K). Experimental data suggest that in water, excessive positive electrostatic charge build-up in such structures may be partially offset by extensive cation- π interactions as well as by ion-pairing with Cl^- anions. Uranyl acetate stained TEM images form freshly prepared samples of $[\text{Pt}^{\text{II}}(\text{phen})(\text{L}^1\text{-S},\text{O})]\text{Cl}$ and the related $[\text{Pt}^{\text{II}}(\text{diimine})-(N,N\text{-di}(n\text{-butyl})\text{-}N'\text{-benzoylthiourea})]\text{Cl}$ compounds¹⁴ provide convincing visual confirmation of the formation of extensive tube-like structures, *ca.* 20 nm in diameter. Such interesting behavior of $[\text{Pt}^{\text{II}}(\text{phen})(\text{L}^1\text{-S},\text{O})]\text{Cl}$ in aqueous solution may have important implications for the demonstrated bioactivity^{6,7} of these compounds.

Experimental section

Computational methods

Using the average observed chemical shift, δ_{obs} , eqn (2) (where $\delta_i = {}^1\text{H}$ chemical shift, δ_i , and $\alpha_i =$ mole fraction of species i) and the total concentration of reagents, we calculated for the reactions defined in the text the equilibrium constant(s), K_i , and chemical shifts, δ_i , of individual species (monomers, dimer aggregates, trimer aggregates, ion-pairs, *etc.*).

$$\delta_{\text{obs}} = \sum_{i=n} \alpha_i \delta_i \quad (2)$$

This particular type of non-linear least squares optimisation calculation can be solved in several ways.³⁶ We opted to use a program called DIMER- K_{D} , written by us several years ago to fit data with a dimerization model⁹ (the program utilizes the algorithm by Horman and co-workers¹⁰). When dealing with multiple equilibria we used the program called Dynafit version 3.³⁷ However, Dynafit version 3 uses the concentration of the species, c_i , and not mole fraction in the mass balance equations and signal response calculations. This problem was circumvented by multiplying eqn (2) with the total concentration, C_{T} , of the reagent of interest and after grouping terms, eqn (3) is obtained.

$$C_{\text{T}} \delta_{\text{obs}} = \sum_{i=n} c_i \delta_i \quad (3)$$

Analytical instrumentation

${}^1\text{H}$ NMR and DOSY experiments were recorded in 5 mm tubes using a Varian Unity Inova 400 MHz spectrometer operating at 399.95 MHz or a Varian Unity Inova 600 MHz spectrometer equipped with an inverse-detection pulsed field gradient (idpfg) probe operating at 599.99 MHz. ${}^1\text{H}$ NMR chemical shift referencing was done using the corresponding solvent peak with the HDO signal showing no chemical shift changes as a function of complex concentration. Diffusion coefficients were calculated using the Varian vnmrj software (version 2.1b) with a line broadening of 1.0 Hz. Experimental parameters: pulse sequence: Dbppste_cc (Bipolar Pulse Pair Stimulated Echo with Convection Compensation), ${}^1\text{H}$ spectral width: 11 ppm, number of acquisitions varied from sample, recycling delay: 2 s, diffusion delay 50 ms, gradient-pulse duration 3.5 or 4.0 ms, 25 different values of G , the gradient magnitude, varying between 0.0107 and 0.449 Gm $^{-1}$ calibrated using the diffusion coefficient of HDO in D_2O .³⁸ Transmission electron microscopy imaging was done on a Zeiss 912 OMEGA EFTEM with a resolution of 0.35 nm and high resolution images were recorded with a High Resolution FEI/Tecna F20 Cryo TWIN FEGTEM.

Synthesis of complexes

All reagents and solvents were commercially available, and were used without further purification. The general method described by Morgan and Burstall for the synthesis of $\text{Pt}^{\text{II}}(1,10\text{-phenanthroline})\text{Cl}_2$ was used from commercially available

$K_2[PtCl_4]$ and 1,10-phenanthroline monohydrate.³⁹ *N*-Pyrrolidyl-*N*-(2,2-dimethylpropanoyl)thiourea was prepared as described in the literature.³⁵ [*N*-pyrrolidyl-*N*-(2,2-dimethylpropanoyl)-thioureato](1,10-phenanthroline) platinum(II) chloride was prepared as previously described.¹³

Characterization

Previously the NMR characterization of $[Pt^{II}(\text{phen})(L^{1-S,O})]Cl$ was done in acetonitrile- d_3 by 1H , 1H -COSY, $^1H^{15}N$ -HMBC NMR experiments.¹³ 1H NMR assignments to the various protons of $[Pt^{II}(\text{phen})(L^{1-S,O})]Cl$ could be made from the 1H -COSY spectra, although one unambiguous assignment for the $H^{2/9}$ protons was outstanding. Previously the diimine proton of the 1,10-phenanthroline ligand *trans* to the sulphur atom of the coordinated *N*-pyrrolidyl-*N*-(2,2-dimethylpropanoyl)thiourea was assigned based on the expectation of more de-shielded as a result of a more pronounced *trans* effect induced by the sulphur donor atom.⁹ The 1-D NOE spectra (Fig. S9†) showed a positive NOE for the most de-shielded proton of the 1,10-phenanthroline ligand upon excitation of the methyl protons of the *N*-acyl-*N,N*-dialkylthiourea ligand (Fig. S9a†) and *vice versa* (Fig. S9b†). Moreover, upon selective irradiation of the methyl protons $H^{1'}$, NOE's were observed for H^2 and $H^{a'}$ which now allows for the unambiguous assignment of all 1H NMR resonances of the *N*-pyrrolidyl group ($H^{a,b'}$ and $H^{a,b}$), previously tentatively assigned on the basis of the relative magnitude of the relevant ^{195}Pt - ^{13}C coupling constants.³⁵ Hence the unambiguous assignment of the most de-shielded 1,10-phenanthroline proton and methylene protons of the *N*-acyl-*N,N*-dialkylthiourea group could be assigned as H^2 and $H^{a'}$ respectively, Fig. 1.

Acknowledgements

We acknowledge the support of Dr Jacobus Brand for his assistance in NMR and particularly the DOSY spectroscopy. Financial support from Stellenbosch University, the National Research Foundation (bursary to I. Kotzé,) as well as Anglo-platinum Ltd is gratefully acknowledged.

Notes and references

- 1 J. A. A. W. Elemans, A. E. Rowan and R. J. M. Nolte, *J. Am. Chem. Soc.*, 2002, **124**, 1532–1540.
- 2 W. Lu, D. A. Vicic and J. K. Barton, *Inorg. Chem.*, 2005, **44**, 7970–7980.
- 3 A. M. Krause-Heuer, N. J. Wheate, M. J. Tilby, D. G. Pearson, C. J. Ottley and J. R. Aldrich-Wright, *Inorg. Chem.*, 2008, **47**, 6880–6888.
- 4 F. H. Stootman, D. M. Fisher, A. Rodgerc and J. R. Aldrich-Wright, *Analyst*, 2006, **131**, 1145–1151.
- 5 S. Rafique, M. Idrees, A. Nasim, H. Akbar and A. Amin, *Bio-technol. Mol. Biol. Rev.*, 2010, **5**, 38–45.
- 6 T. J. Egan, K. R. Koch, P. L. Swan, C. Clarkson, D. A. Van Schalkwyk and P. J. Smith, *J. Med. Chem.*, 2004, **47**, 2926–2934.
- 7 Y.-S. Wu, K. R. Koch, V. R. Abratt and H. H. Klump, *Arch. Biochem. Biophys.*, 2005, **440**, 28–37.
- 8 H. H. Klump, K. R. Koch and C. T. S. Lin, *Afr. J. Chem.*, 2006, **102**, 264–266.
- 9 K. R. Koch, C. Sacht and C. Lawrence, *J. Chem. Soc., Dalton Trans.*, 1998, 689–695.
- 10 I. Horman and B. Dreux, *Helv. Chim. Acta*, 1984, **67**, 754–764.
- 11 L. Fielding, *Tetrahedron*, 2000, **56**, 6151–6170.
- 12 A. Macchioni, A. Romani, C. Zuccaccia, G. Guglielmetti and C. Querci, *Organometallics*, 2003, **22**, 1526–1533.
- 13 I. A. Kotzé, W. J. Gerber, J. M. Mckenzie and K. R. Koch, *Eur. J. Inorg. Chem.*, 2009, **12**, 1626–1633.
- 14 Y.-S. Wu, *PhD dissertation*, University of Cape Town, 2002.
- 15 P. S. Pregosin, *Prog. Nucl. Magn. Reson. Spectrosc.*, 2006, **19**, 261–288.
- 16 F. Song, S. J. Lancaster, R. D. Cannon, M. Schormann, S. M. Humphrey, C. Zuccaccia, A. Macchioni and M. Bochmann, *Organometallics*, 2005, **24**, 1315–1328.
- 17 T. J. Egan, *Trends Parasitol.*, 2006, **22**, 235–237.
- 18 I. Z. Steinberg and A. H. Scheraga, *J. Biol. Chem.*, 1963, **238**, 172–181.
- 19 P. Doty and G. E. Myers, *Discuss. Faraday Soc.*, 1953, **13**, 51–58.
- 20 W. Kauzmann, C. B. Anfinsen, M. L. Anson, K. Bailey and J. T. Edsall, *Adv. Protein Chem.*, 1959, **14**, 1–63.
- 21 H. A. Scheraga, *J. Phys. Chem.*, 1961, **66**, 1071–1072.
- 22 C. H. Wohlfarth, *Landolt-Börnstein – Group IV Physical Chemistry*, Springer, Berlin Heidelberg, 2008, vol. 17, pp. 117–121.
- 23 H.-J. Schneider, *Angew. Chem., Int. Ed. Engl.*, 1991, **30**, 1417–1436.
- 24 C. A. Hunter and J. K. M. Sanders, *J. Am. Chem. Soc.*, 1990, **112**, 5525–5534.
- 25 T. D. W. Claridge, *High-Resolution NMR Techniques in Organic Chemistry – Tetrahedron Organic Chemistry Series*, Pergamon, Oxford, 1999, 19.
- 26 H. Friebolin, *Basic One- and Two-Dimensional NMR Spectroscopy*, Wiley-VCH, Weinheim, 2005.
- 27 P. J. Hore, *Nuclear Magnetic Resonance*, Oxford, 1995.
- 28 V. I. Bakhmutov, *Practical NMR Relaxation for Chemists*, John Wiley and Sons Ltd., London, 2004.
- 29 I. Pianet, Y. André, M. A. Ducasse, I. Tarascou, J. C. Lartigue, N. Pinaud, E. Fouquet, E. J. Dufourc and M. Laguerre, *Langmuir*, 2008, **24**, 11027–11035.
- 30 L. Luchetti and G. Mancini, *Langmuir*, 2000, **16**, 161–165.
- 31 H. J. Hwang, S. K. Lee, S. Lee and J. W. Park, *J. Chem. Soc., Perkin Trans. 2*, 1999, 1081–1086.
- 32 G. Bellachioma, G. Ciancaleoni, C. Zuccaccia, D. Zuccaccia and A. Macchioni, *Coord. Chem. Rev.*, 2008, **252**, 2224–2238.
- 33 H.-L. Zhang, G.-H. Chen and S.-J. Han, *J. Chem. Eng. Data*, 1997, **42**, 526–530.

- 34 M. Kato and J. Takahashi, *Acta Crystallogr., Sect. C: Cryst. Struct. Commun.*, 1999, **55**, 1809–1812.
- 35 A. N. Mautjana, J. D. S. Miller, A. Gie, S. A. Bourne and K. R. Koch, *Dalton Trans.*, 2003, 1952–1960.
- 36 M. Meloun, J. Havel and E. Högfeltdt, *Computation of Solution Equilibria – A Guide to Methods in Potentiometry, Extraction, and Spectrophotometry*, Ellis Horwood, Chichester, 1987.
- 37 P. Kuzmic, *Anal. Biochem.*, 1996, **237**, 260–273.
- 38 B. Antalek, *Concepts Magn. Reson.*, 2002, **14**, 225–258.
- 39 G. T. Morgan and F. H. Burstall, *J. Chem. Soc.*, 1934, 965–971.